The University Of Sheffield.

Identifying novel secreted effectors of the type VI protein secretion system in *Burkholderia cenocepacia*

By:

Helena L. Spiewak

A thesis submitted in partial fulfilment of the requirements for the degree of

Doctor of Philosophy.

The University of Sheffield

Faculty of Medicine, Dentistry and Health

Department of Infection and Immunity

Supervisors: Dr. Mark S. Thomas and Prof. Phillip C. Wright

14th October 2015

DON’T PANIC.

Abstract

Burkholderia cenocepacia, is a Gram-negative bacterial species belonging to the *Burkholderia cepacia* complex (Bcc), a group of closely related species found ubiquitously in the environment that are also opportunistic human pathogens. *B. cenocepacia* is predicted to be able to secrete proteins through the type six secretion system (T6SS). Characterised in other bacteria, this secretory-apparatus can perforate the cellular membrane in pro- and/or eukaryotic targets, to deliver an arsenal of effector proteins. A cognate immunity protein is required to provide protection against these effectors. Identifying and characterising the T6SS-secreted effectors, their cognate immunity proteins and their molecular targets is key to understanding the role the T6SS plays in the interactions between *B. cenocepacia* and its target organism(s). Here, this study defines a functional role for the *B. cenocepacia* T6SS in bacterial competition. Moreover, this is partly dependent on the phospholipase A_1 activity of a novel evolved TssI, $TssI_{0667}$. The involvement of the *B. cenocepacia* T6SS in pathogenicity in two models of innate immune infection were assessed, but these studies did not demonstrate a contribution from this system to overall virulence. A further putative T6SS-dependent effector, $TanB^H$, was characterised as having nuclease activity but the role of this candidate effector *in vivo* remains unclear. The cognate immunity protein for each effector was identified as Tli6 and $TaaB1^H$, respectively, and demonstrated to form a direct complex with its effector that inhibited the toxic activity of the latter. Therefore, this work has begun to uncover mechanisms used by Bcc bacteria, such as *B. cenocepacia,* that may contribute towards their survival in their natural environment but has not shed any further light on the role of the T6SS in the pathogenic strategies of these bacteria.

Acknowledgements

First and foremost I would like to thank my supervisor Dr. Mark Thomas for his constant support, guidance and feedback throughout my PhD and in the writing of this thesis. I think I have learnt more in the past 3 years than I ever did as an Undergraduate.

Second, a massive thank-you to all of the MST group, past and present, who I have had the pleasure in working with- Jamie, Sayali, Ruyue, Saedaah, Asma, Richard, not forgetting Tom and our new additions. In addition, I would like to thank everyone else in LU103, past and present, for making my time in the lab a lot more entertaining.

I would also like to thank the collaborators who help with aspects of this project, including Prof. Phil Wright and Dr. Caroline Evans, as my second supervisory team, for their advice on mass spectrometry experiments, and Dr. Aurélien Carlier and Dr. Kristy Agnoli for their help with the $H111^{S}$ strain. I would also like to thank the BBSRC for funding my work and The Department of Infection and Immunity, The University of Sheffield for providing the facilities to undertake this work.

Last, I am very grateful to my friends and family who have had to deal with my highs and lows when science' is doing what science' does best- being unpredictable. Thank-you for keeping me sane(ish)… and feeding me biscuits.

In the words of an X-factor finalist "this is for you Gran".

List of Abbreviations

A_{280} – Absorbance at 280 nm
ACD – Actin cross-linking domain
AHL – N-Acyl homoserine lactone
ANK – Ankyrin
ATP – Adenosine triphosphate
Bcc – *Burkholderia cepacia* complex
BcCV – *Burkholderia cenocepacia* containing vesicle
BCESM – Burkholderia cepacia epidemic strain marker
BDSF – cis-2-dodecenoic acid
BHI –Brain heat infusion
bp – base pairs
BSA – Bovine serum albumin
cAMP – cyclic adenosine monophosphate
Cci – Cenocepacia island
CDD – Conserved domain database
CF – Cystic fibrosis
CFU – Colony forming units
cPhe – p-chlorophenylalanine
CRP – Catabolite repressor protein
CTD – C-terminal domain
D-BHI – Dialysed brain heart infusion
Da – Daltons
DMSO – Dimethyl sulfoxide
DNA – Deoxyribonucleic acid
DNase – Deoxyribonuclease
DOC – Sodium deoxycholate
DUF – Domain of unknown function
EAEC – Enteroaggregative *Escherichia coli*
ECL – Enhanced chemiluminescence
EDTA – Ethylenediaminetetraacetic acid,
ET12 – Edinburgh-Toronto 12 lineage
FASP – Filter-aided sample preparation
FHA – Forkhead-associated
FPLC – Fast protein liquid chromatography
g – Grams
GlcNAc – N-acetylglucosamine
GTP - Guanosine-5'-triphosphate
GuHCl – Guanidine hydrochloride
H-NS – Histone-like nucleoid-structuring
Hcp – Haemolysin coregulated protein
His-tag, His6 – Hexahistidine-tag
hpf – hours post-fertilisation
hpi – hours post-infection
HPLC – High-performance liquid chromatography
IMAC – Immobilized metal ion affinity chromatography

IPTG – Isopropyl β-D-1-thiogalactopyranoside
IST – Iso-sensitest
kbp – Kilobase pairs
kDa - Kilodaltons
L – Litres
LB – Lysogeny broth
LPS – Lipopolysaccharide
M – Molar
m – Molecular mass
M.W. – Molecular weight
m/z – Mass-to-charge
Mbp – Megabase pairs
MCS – Multiple cloning site
MERV – Multiple effector translocation VgrG
mg - Milligram
MIX – Marker for type VI effector
mL – Millilitres
mM - Millimolar
MMTS – Methyl methanethiosulfonate
M_r – Relative molecular mass
MS – Mass spectrometry
MS/MS – Tandem mass spectrometry
MurNAc – N-acetylmuramic acid
MWCO – Molecular weight cut-off
ng – Nanogram
NTD – N-terminal domain
OD_{600} – Optical density at 600 nm
OMP – Outer membrane protein
ORF – Open reading frame
PAGE – Polyacrylamide gel electrophoresis
PAI – Pathogenicity island
PBS – Phosphate buffered saline
PCR – Polymerase chain reaction
PheS – Phenylalanine tRNA synthetase
PMF – Proton motive force
PVDF – Polyvinylidene fluoride
RBS – Ribosome binding site
RCF – relative centrifugal force
Rhs – Rearrangement hotspot
RNA – Ribonucleic acid
RNAP – RNA polymerase
RNase – Ribonuclease
ROS – Reactive oxygen species
Rpm – Rotations per minute
SCX – Strong cation exchange
SDS – Sodium dodecyl sulphate
SEC – Size exclusion chromatography

SEC-MALLS – Size Exclusion Chromatography - Multi-Angle Laser Light Scattering
SOE-PCR – Slice overlap extension PCR
T1SS – Type I secretion system
T2SS – Type II secretion system
T3SS – Type III secretion system
T4SS – Type IV secretion system
T5SS – Type V secretion system
T6SS –Type VI secretion system
T7SS – Type VII secretion system
T8SS – Type VIII secretion system
T9SS – Type IX secretion system
Taa – Type VI associate antitoxin
Tae – Type VI amidase effector
Tag – Type VI associated gene
Tai – Type VI amidase immunity protein
Tan – Type VI associate nuclease
TBS – Tris buffered saline
TCA – Trichloroacetic acid
TCEP – Tris(2-carboxyethyl)phosphine)
Tde – Type VI DNase effector
Tdi - Type VI DNase immunity protein
TEAB – Triethylammonium bicarbonate
TFA – Trifluoroacetic acid
Tge – Type VI glycoside hydrolase effector
Tgi – Type VI glycoside hydrolase immunity protein
Tle – Type VI lipase effector
Tli – Type VI lipase immunity protein
TMD – Transmembrane domain
TMED – Tetramethylethylenediamine
Tpe – Type VI peptidoglycan hydrolase effector
TPP – Threonine phosphorylation pathway
TPR – Tetratricopeptide repeat
Tse – Type VI secreted exported
Tss – Type VI secretion system
UPEC- Uropathogenic *Escherichia coli*
UTR – Untranslated region
V – Volts
v/v – volume/volume
VgrG – Valine-Glycine Repeat Protein G
w/v – weight/volume
WT – Wild-type
x *g* – times gravity
X-gal – 5-bromo-4-chloro-3-indolyl-beta-D-galacto-pyranoside
X-gluc – 5-bromo-4-chloro-3-indolyl-beta-D-glucuronic acid
Δ – Deletion
μg – Microgram
μL – Microlitre

Table of Contents

Chapter 1: Introduction

1.1 General introduction

Protein secretion, defined as the process of translocating protein molecules from an intracellular to an extracellular location, is an important feature for both prokaryotic and eukaryotic cells. For bacteria, it is of particular importance for proper functioning and survival of the microorganism within its growth environment. Several bacterial secretion systems have been discerned, including the type VI secretion system (T6SS). This is a multi-subunit, membrane-embedded, protein translocation complex, which is widespread in the genomes of Gram-negative bacteria. These include pathogenic bacteria such as *Vibrio cholerae*, *Pseudomonas aeruginosa* and the *Burkholderia* species (Pukatzki et al., 2006; Mougous et al., 2006; Schell et al., 2007; Shalom et al., 2007). This includes *Burkholderia cenocepacia*, a soil-dwelling organism found ubiquitously in the environment.

The T6SS allows the translocation of specific proteins (effectors) through the inner and outer membrane of the T6SS-containing bacteria using a syringe-like mechanism (Pukatzki et al., 2006; Mougous et al., 2006), injecting effectors into the target host cell, which can be either a eukaryote or another competing bacterium (Hood et al., 2010).

B. cenocepacia is one of twenty closely related bacterial species that make up the *Burkholderia cepacia* complex (Bcc). Unfortunately, many Bcc bacteria are opportunistic pathogens. Notably, Bcc infections pose a significant risk to immuno-compromised people, specifically patients with lung dysfunction, such as those with cystic fibrosis (CF) (Isles et al., 1984). When Bcc colonization occurs in the lungs it can lead to serious life-threatening complications, including pneumonia, chronic lung decline and an often-fatal condition known as cepacia syndrome. The high intrinsic resistance of *B. cenocepacia* to most antibiotics means that these types of infections are difficult to treat effectively. Unfortunately, little is known about the virulence mechanism(s) of the Bcc. It is thought that the Bcc may employ multiple virulence factors to aid in its pathogenesis, some of these include haemolysin production, iron acquisition, protease production, and biofilm formation.

Interestingly, it was found that some T6SSs are virulence determinants in bacterial pathogens including *P. aeruginosa V. cholerae* and highly pathogenic *Burkholderia* species (Pukatzki et al., 2006; Mougous et al., 2006; Schell et al., 2007; Burtnick et al., 2011). However, the main role of the T6SS appears to be in providing the bacteria with a fitness advantage over other competing bacteria within its environment. As a relatively new addition to the bacterial protein secretion scene, the fundamentals of the T6SS are only just beginning to be uncovered.

Despite this, significant discoveries have been made, particularly in the past four years, regarding the identification and characterisation of effector proteins that are secreted by the T6SS. A variety of effectors, that have a range of molecular targets, have been discovered in well-characterised T6SS-containing bacteria, including phospholipases, peptidoglycan hydrolases and nucleases, many of which show toxicity towards other bacteria, and several towards eukaryotes. Yet, there is still a distinct lack of published experimental evidence regarding the role of the T6SS in Bcc bacteria, such as *B. cenocepacia,* and the nature of the effectors it secretes.

1.2 The *Burkholderia cepacia* complex and *B. cenocepacia*

1.2.1 Discovery and classification of the Bcc

The first *Burkholderia* spp. strain was identified in the late 1940's as a Gram-negative soil-dwelling plant pathogen, that was capable of causing disease in onion bulbs (Burkholder, 1950). It was initially thought to belong to the *Pseudomonas* genus (*Pseudomonas cepacia)*. But due to advances in taxonomic identification over the years, in particular, the use of DNA-DNA hybridization and 16S rRNA gene sequence analysis, it was reclassified from the *Pseudomonas* genus to a new genus *Burkholderia*, within the β-proteobacteria class (Yabuuchi et al., 1992). Furthermore, strains of *Burkholderia cepacia* were then found to be genetically diverse leading to division of the genus into several phylogenetically different species, known as genomovars, which were later assigned species designations bases on phenotypic and biochemical tests (Vandamme et al., 1997). These Bcc species include *B. cepacia* (genomovar I), *B. multivorans* (genomovar II)*, B. cenocepacia* (genomovar III)*, B. stabilis* (genomovar IV) *and B. vietnamiensis* (genomovar V). Each of these are phenotypically similar, having a rod-shaped flagella bearing structure, but genetically different. These species live in a range of habitats, including soil, water and the rhizosphere of some plants. It is now thought that the Bcc is made up of at least twenty closely related species, updated as recently as 2015, with two new additions, *Burkholderia stagnalis* and *Burkholderia territorii* (De Smet et al., 2015). Figure 1.1 highlights the biological classification of the Bcc, and the twenty members of this specific cluster of bacteria, some of which have had their complete genome sequenced.

1.2.2 Genetics

All members of the Bcc have large genomes in the 6 to 9 Mbp range, which are generally organised into multiple large replicons. This feature was first recognised in *B. multivorans* ATCC 17616, with 3 large circular replicons of varying size (Cheng and Lessie, 1994). Advances in nucleotide sequencing technology have meant various Bcc species have now had their complete genome sequenced, including clinically important *B. cenocepacia* strains, J2315 (Holden et al., 2009),

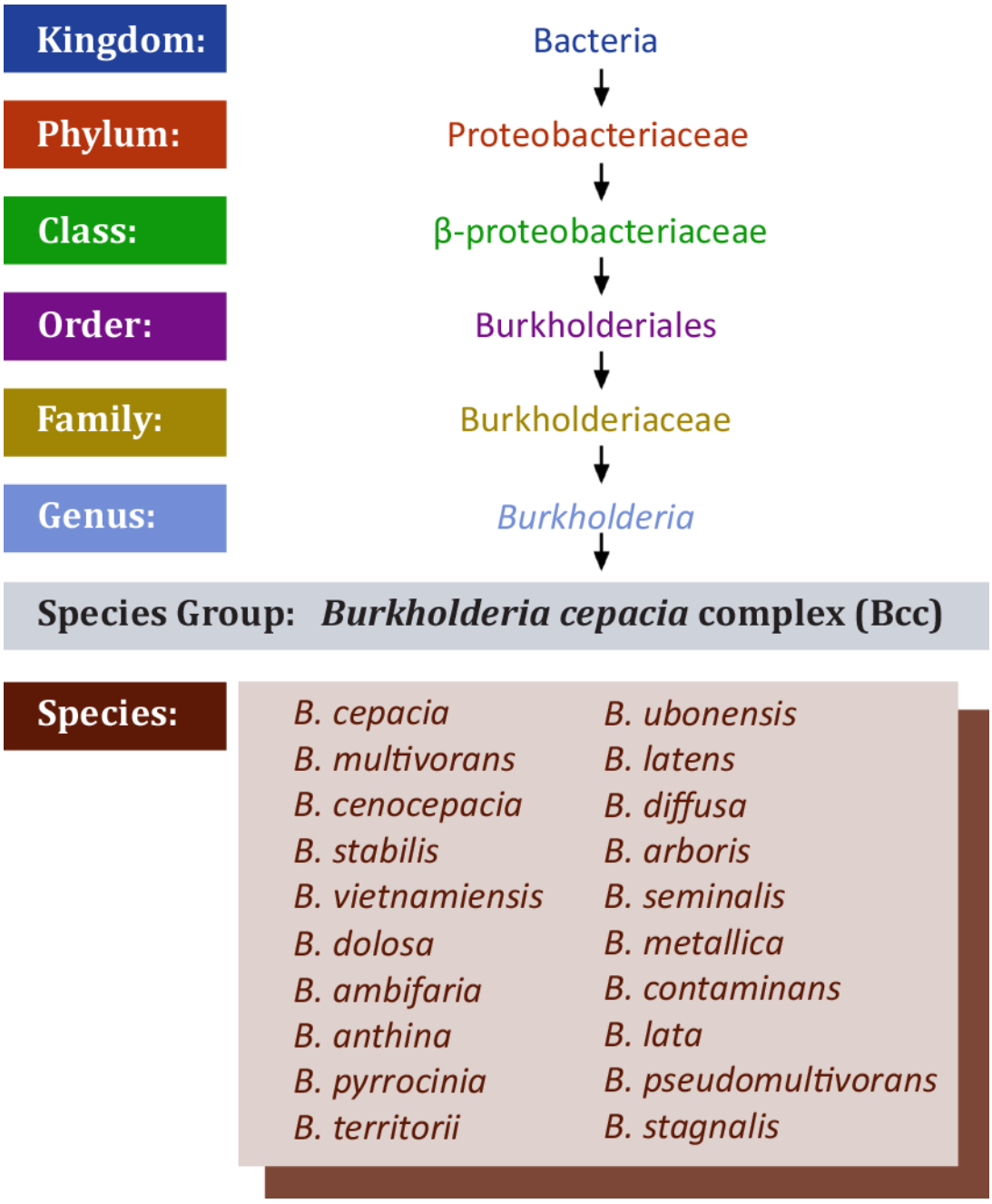

Figure 1.1 Taxonomic classification of the *Burkholderia cepacia* complex. Diagram highlighting the taxonomic ranking of the twenty bacterial species that are members of the *Burkholderia cepacia* complex.

H111 (Carlier et al., 2014), and K56-2 (Varga et al., 2013), and *B. multivorans* ATCC 17616, as well as other animal and plant pathogenic members of the genus such as *B. pseudomallei* K96243 (Holden et al., 2004), *B. thailandensis* E264 (Yu et al., 2006) and *B. glumae* BGR1 (Lim et al., 2009).

B. cenocepacia is a species of particular interest due to its virulent nature as an opportunistic pathogen in humans (Isles et al., 1984). Sequencing of the J2315 multi-drug resistant variant of *B. cenocepacia*, an epidemic lineage strain isolated from a CF-patient (Edinburgh-Toronto-12, ET12), identified just over 8 Mbps of genetic sequence making up its genome, organised in 3 circular chromosomes, of sizes 3.87 Mbp (known as BCAL), 3.22 Mbp (BCAM) and 0.87 Mbp (BCAS), with an additional 93 kbp plasmid, having an average G-C content of approximately 67% (Holden et al., 2009). The genome is estimated to contain 7,365 genes, encoding approximately 7,116 predicted proteins (Holden et al., 2009).

Unexpectedly, the J2315 genome study highlighted two key genomic features, the first being a relatively large number of insertion sequences (Holden et al., 2009). These are small DNA sequences that can move within the genome autonomously, that only encode genes required for insertional events (Mahillon and Chandler, 1998). The second feature was a high prevalence of genomic islands, which are large sequences of genomic DNA that have a foreign origin, probably acquired by horizontal gene transfer during the evolution of the species relatively recently. They were generally identified by differing GC content. Genomic islands may contain clusters of genes that confer a specific function, such as pathogenicity, known as pathogenicity islands (PAIs).

A genomic island identified in the *B. cenocepacia* genome was termed the *B. cenocepacia* island (cci) and encodes virulence and metabolism-associated genes (Baldwin et al., 2004). The cci also encodes a *B. cepacia* epidemic strain marker (BCESM), historically used as a epidemiology marker for virulent *B. cenocepacia* strains isolated from CF-patients (Baldwin et al., 2004). The BCESM marker is present in many but not all CF-isolated *B. cenocepacia* strains and is also present in all ET12 lineage strains (Mahenthiralingam et al., 1997; Mahenthiralingam et al., 2000a; Vandamme et al., 2003). It is clear that the diversity and plasticity of the *B. cenocepacia* genome and the genomes of other members of the Bcc have allowed

them to thrive in their natural environment, as well as adapting to life as opportunistic pathogens.

1.2.3 Environmental importance of the Bcc

Even-though the Bcc can have detrimental effects on plant life, in particular as the cause of sour skin in onions (Burkholder, 1950), many members of the Bcc have now been shown to have a positive impact on the flora present in its ecosystem (Parke and Gurian-Sherman, 2001). For example, Bcc species have been discovered living harmoniously as plant commensals in the rhizospheric soil of many commercially important plants, such as wheat (Viallard et al., 1998) and maize (Nacamulli et al., 2006).

Furthermore, the Bcc has been implicated in preventing the spread of soil-borne plant diseases, such as 'damping-off' disease (Yoshihisa et al., 1989; Bowers, 1993), a condition mainly caused by fungi such as *Pythium,* that damages seeds and seedlings during their development period. Bcc is postulated to do this by producing anti-microbial agents, such as antibiotics like phenylpyrroles (Yoshihisa et al., 1989) or lipopeptides (Kang et al., 1998), that can directly target these pathogenic fungi. Another environmental benefit the Bcc is thought to bring to its habitat is its ability to remove pollutants from the soil, as Bcc bacteria can use a variety of complex carbon sources as an energy supply. For example, some strains can degrade phthalates (Chang and Zylstra, 1998). This means the Bcc can be exploited as a tool for bio-remediation (Parke and Gurian-Sherman, 2001).

1.2.4 Clinical importance of the Bcc

In stark contrast to the predominantly positive impact the Bcc has on its natural environment, the Bcc can have significantly different consequences on a human host. Fortunately, the Bcc does not generally colonise healthy individuals. However, those with certain underlying health-problems and weakened immune systems are susceptible to Bcc infections, with cystic fibrosis patients being the most at risk. The thick, sticky and nutrient-rich secretions produced by the alveolar epithelium of CF-patients creates a breeding ground for infectious bacteria. The

prevalence of Bcc infections in CF patients was first recognised in the mid-1980's, with a Canadian CF clinic recognising up to a 20% Bcc infection rate in patients (Isles et al., 1984). The clinical outcome of these infections were often varied, some patients carried the bacteria with no detrimental effect on their health, while others became chronically infected, resulting in a gradual decline in lung function (Isles et al., 1984). A rare sub-population of Bcc infected individuals reacted adversely to the infection, leading to rapid decline in lung function, septicaemia, necrotizing pneumonia with an often fatal outcome, succumbing to the infection within weeks (Isles et al., 1984), termed 'cepacia syndrome'. All species of Bcc have now been isolated from the sputum of CF-patients, including the new additions *B. stagnalis* and *B. territorii* (De Smet et al., 2015), meaning all strains have the ability to infect humans, although some strains appear more frequently than others.

In particular, *B. cenocepacia* and *B. multivorans* are the most common causative agent of Bcc infections in CF-patients in the USA, Canada and the UK (Drevinek and Mahenthiralingam, 2010; De Soyza et al., 2010), and *B. contaminans* has been identified as commonest recovered species in some CF centres in Argentina and Spain (Martina et al., 2013; Medina-Pascual et al., 2015). A recent publication of a long term epidemiological study of Bcc Infections in CF patients in British Columbia, Canada, indicated a higher incidence of new infections being caused by *B. multivorans* (Zlosnik et al., 2015), yet infection with *B. cenocepacia* still correlate with a poorer prognosis than any of the other Bcc species, as observed previously (Agodi et al., 2001).

Taking into account person-to-person transmissibility, variability in severity of clinical outcomes and the inherent resistance of these organisms to antibiotics, it makes Bcc and *B. cenocepacia* a perturbing pathogen for CF and other immuno-comprised patients. These bacteria appear to have evolved a variety of features that may help Bcc infections to take hold, allowing Bcc bacteria to act as opportunistic pathogens. However, there is still a substantial lack of understanding regarding the virulence mechanisms of the Bcc.

1.2.5 Virulence determinants of the Bcc

Like many other Gram-negative bacteria, Bcc bacteria have certain features that enable them to flourish as opportunistic pathogens. These features are known as virulence determinants/factors. Virulence factors aim to collectively allow the bacteria to colonize a host efficiently, obtaining sufficient energy and nutrients from it, whilst evading and supressing the host's immune system at the same time. Some of the potential virulence determinants of Bcc species include haemolysin production, cell invasion, intracellular survival, iron acquisition, biofilm generation, and protein secretion, including secretion by the type II, type IV and pertinently the type VI secretion systems (Figure 1.2). Some of these virulence factors have been shown to be coordinated by quorum sensing regulatory systems, including acyl-homoserine lactone (AHL)-dependent systems governed by CepIR (Sokol et al., 2003) and CciIR (Baldwin et al., 2004) and an AHL-independent orphan LuxR homologue CepR2 (Malott et al., 2009). A number of these factors will be explored. However, this is not the definitive list of Bcc virulence factors, more have been described in the literature, reviewed in Mahenthiralingam et al. (2005).

1.2.5.1 Haemolysin production

Haemolysis is defined as the rupture of red blood cells caused by damage to its cell membrane integrity. It is a virulence strategy employed by microorganisms to target their host. Both clinical and environmental isolates of Bcc strains have haemolytic abilities, including *B. cenocepacia* (Nakazawa et al. 1987; Vasil et al. 1990). *B. cenocepacia* J2315 was shown to secrete a haemolytic lipopeptide that induces the destruction of mammalian neutrophils and macrophages by inducing apoptosis and degranulation of these cell types (Hutchison et al., 1998). Other haemolysins produced by Bcc strains include cepalycin I and II (Abe and Nakazawa, 1994). A peptide produced by a non-ribosomal synthetase found in select species of the Bcc, *B. vietnamiensis* and *B. ambifaria*, demonstrated haemolytic properties that were required for full virulence in an invertebrate infection model (Thomson and Dennis, 2012).

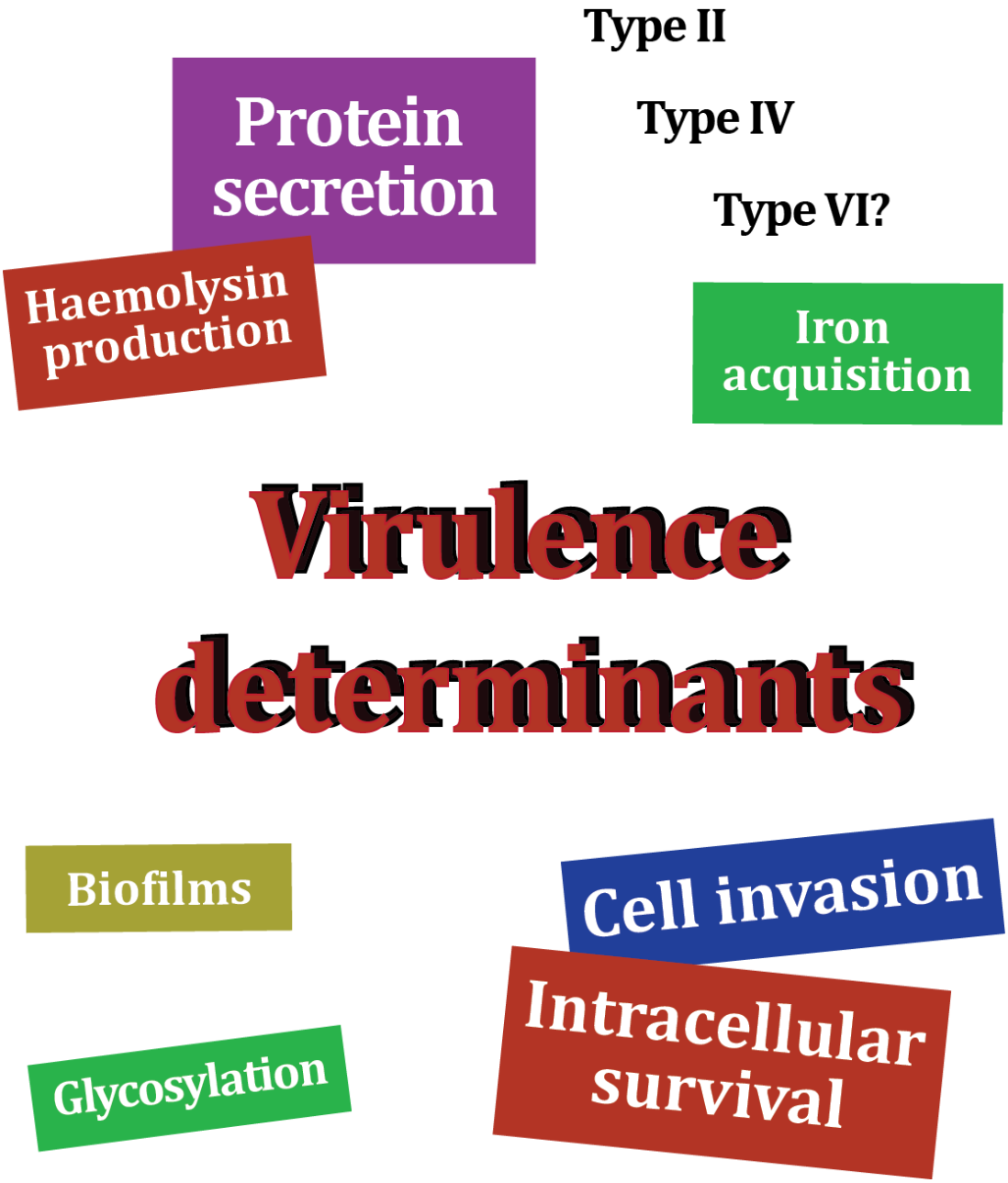

Figure 1.2 Virulence determinants in *Burkholderia cepacia* complex bacteria. A summary diagram showing some of the selected virulence determinants in Bcc bacteria, some of which are discussed further in the text.

1.2.5.2 Invasion and intracellular survival

The immune system plays a vital role in combating infections by foreign bodies. However, tight control over it is required to prevent unnecessarily severe immune responses from occurring, such as those observed in some Bcc infected CF-patients. A trait of the Bcc that may aid in virulence is an ability to invade and survive intracellularly in a variety of cells, evading detection by the immune system. Invasion of mammalian cells by Bcc bacteria has been demonstrated in many cell types. This includes epithelial cell invasion by *B. cenocepacia* (Burns et al., 1996). Here, *B. cenocepacia* were able to invade, survive and replicate intracellularly within A549 human alveolar epithelial cells in *in vitro* tissue culture experiments. This cell line was then further tested with a range of Bcc bacteria to identify particularly invasive strains, it showed that over 70% of *B. cenocepacia* strains tested were invasive in A549 cells (Cieri et al., 2002).

Interestingly, a study observed different invasion routes can be used by different species of the Bcc to infiltrate the human airway epithelium *in vitro* (Schwab et al., 2002). For example, *B. cenocepacia* formed biofilms at the epithelial cell surface, which the bacteria then invaded and destroyed by causing actin rearrangements and damage to the glycoprotein-polysaccharide matrix on the surface of the cells. Whereas, *B. stabilis* infiltrated the area between the epithelial cells (Schwab et al., 2002).

Other examples of the ability of Bcc bacteria to invade the airway epithelium include the demonstration of the invasive capabilities of *B. cenocepacia* and *B. multivorans* into non-CF-phenotype and CF-phenotype lung epithelial cell lines, where the bacterial invasion observed was facilitated by a direct interaction of the invading bacteria with glycosphingolipid receptors on the epithelial cell surface (Mullen et al., 2010). This again suggests an importance of surface glycoproteins on the host cell for invasion. Interestingly, a tyrosine kinase and paired phosphotyrosine phosphatase in the Bcc bacteria *B. contaminans*, of which homologues are found in other Bcc bacteria, has been shown to be important in attachment and invasion of the CF-phenotype lung epithelial cell lines (Ferreira et al., 2015).

Moreover, evidence has shown that *B. cenocepacia* and other Bcc bacteria can invade and survive not only in epithelial cells but also in phagocytic cells such as macrophages and monocytes (Martin and Mohr, 2000; McKeon et al., 2010; Gavrilin et al., 2012), surviving within bacteria-containing membrane vacuoles (*B. cenocepaci*a-containing vacuoles, BcCVs). BcCVs are similar in structure to autophagosomes, but are delayed in their maturation (Lamothe et al., 2007), preventing the bacteria from lysosomal destruction. Infected macrophages show disrupted actin cytoskeletons and BcCV membranes surrounding the bacteria have delayed NADPH oxidase complex formation (Rosales-Reyes et al., 2012b). This results in a delayed production of superoxide anions and thus a delayed production of reaction oxygen species (ROS) (Keith et al., 2009). ROS production is a key bactericidal mechanism for damaging intracellular bacteria in the innate immune response (Lambeth, 2004).

Intracellular sensing of *B. cenocepacia*-infected phagocytes results in caspase-1 activation and production of pro-inflammatory cytokines such as IL-1β from the infected cell eliciting an inflammatory response in the host (Kotrange et al., 2011). This sensing acts via pyrin inflammasome activation (Gavrilin et al., 2012; Xu et al., 2014). Interestingly, the T6SS has been linked to some of the characteristics of the BcCVs in infected macrophages, details of which will be discussed in Section 1.2.5.5.

1.2.5.3 Biofilms

Biofilms are an aggregated complex of microorganisms that develop on a solid surface. This adherent microbial micro-community is predominantly bound together through the production of extracellular molecules, including extracellular proteins, polysaccharides and DNA (reviewed in O'Toole et al. (2000)). This aggregated complex is thought to protect the bacteria from its external environment. Interestingly, the two commonest species found in CF-patients with Bcc infections, *B. cenocepacia* and *B. multivorans*, have demonstrated a greater ability to form biofilms than other Bcc bacteria *in vitro* (Conway et al., 2002), indicating biofilm formation may play a role in virulence in some way, either by allowing the Bcc bacteria to evade the host immune system, or resist antibiotic

agents (Desai et al., 1998). Regulation of the components of *B. cenocepacia* biofilm formation is thought to be controlled by several inter-connecting mechanisms, including c-di-GMP signalling (Huber et al., 2002; Fazli et al., 2011; Fazli et al., 2013), and AHL- and BDSF-dependent quorum sensing systems (Huber et al., 2002; Tomlin et al., 2005; Ryan et al., 2009).

1.2.5.4 Flagellin glycosylation and LPS modifications

A biological role for flagellin glycosylation in host interactions has been suggest in several pathogenic Gram-negative bacterial species, including *Campylobacter jejuni* (Guerry et al., 2006), *P. aeruginosa* (Arora et al., 2005), and some *Aeromonas* species (Gavín et al., 2002; Tabei et al., 2009; Wilhelms et al., 2012). An O-glycosylation flagellin system was recently discovered in *B. cenocepacia* and implicated in virulence (Hanuszkiewicz et al., 2014; Khodai-Kalaki et al., 2015). Specifically, it was shown that epithelial cells exposed to purified glycosylated flagellin showed a reduced inflammatory response through the TLR5-mediated pathway in comparison to non-glycosylated flagellin (Hanuszkiewicz et al., 2014). However, contradictory findings were seen in an *Arabidopsis thaliana* plant model where purified glycosylated flagellin still elicited an innate immune response, demonstrated by production of reactive oxygen species (ROS) and activation of a defence gene (Khodai-Kalaki et al., 2015). Despite this, the study showed that *B. cenocepacia* mutants deficient in key genes required for flagellin glycosylation were attenuated in the *A. thaliana* and *Galleria mellonella* larvae infection models.

Similar results were observed regarding a L-Ara4N modification of the lipid A component of the *B. cenocepacia* lipopolysaccharide layer (Khodai-Kalaki et al., 2015). This LPS modification has been demonstrated to be important for resistance to anti-microbial peptides such as polymyxin B, where it was first described in *Escherichia coli* and *Salmonella typhimurium* and later in *B. cenocepacia* (Nummila et al., 1995; Guo, 1997; Hamad et al., 2012). This modification is essential for *B. cenocepacia* viability (Ortega et al., 2007).

1.2.5.5 Secreted effectors of Bcc bacteria

1.2.5.5.1 T2SS-dependent effectors

Zinc metalloproteases ZmpA and ZmpB (positively regulated by the CepIR quorum sensing system (Sokol et al. 2003)), are two proteins known to be secreted by the type II secretion system (T2SS) in *B. cenocepacia* (McKevitt et al., 1989; Corbett et al., 2003; Kooi et al., 2006). Both of which have been implicated as virulence factors in particular *B. cenocepacia* strains, such as K56-2 (Corbett et al., 2003). ZmpA and ZmpB are zinc-dependent M4 family metallopeptidases that are expressed as larger prepropenzymes before under-going autoproteolysis to generate mature ZmpA and ZmpB. *B. cenocepacia* mutants deficient in these metalloproteases show reduced extracellular protease activity, as determine by casein degradation and are less virulent in a rat lung infection model (Corbett et al., 2003; Kooi et al., 2006). It has been postulated that metalloproteases like these may be responsible for degrading proteinaceous host tissues, such as collagen and fibronectin, allowing greater dissemination within the host and/or degradation of proteinous immune system molecules such as immunoglobulins (Corbett et al., 2003; Kooi et al., 2005). Bcc bacteria can also produce lipases in a T2SS-dependent manner, which may also contribute to virulence. For example, a lipase from *B. cenocepacia* has been shown to contribute to epithelial cell invasion (Mullen et al., 2007).

There is evidence to suggest that a Sec-dependent, low molecular weight, non-functional tyrosine kinase (Dmp), encoded by BCAM028, is involved in delaying maturation of *B. cenocepacia* when infected with ET12 lineage strains of *B. cenocepacia* (Andrade and Valvano, 2014). It is also secreted into the extracellular medium from the periplasm by an undefined mechanism. Secretion systems responsible for the translocation of Sec-dependent proteins over the outer membrane in the final step of their secretion include the T2SS and T5SS.

1.2.5.5.2 T5SS-dependent effectors

T5SS-dependent cell surface proteins, termed trimeric autotransporter adhesins (TAAs), have been implicated in virulence in pathogenic Gram-negative bacteria, including Bcc species (Mil-Homens et al., 2010; Mil-Homens and Fialho,

2011). *B. cenocepacia* J2315 was found to encode several putative TAAs, including those encoded by BCAM0224 and BCAM0223 (Mil-Homens et al., 2010; Mil-Homens and Fialho, 2011). These cell surface TAAs were observed to contribute to adherence of the bacteria to epithelial cells *in vitro*, protecting the bacteria from complement-mediated killing by the host, biofilm formation, and attenuated virulence in an invertebrate infection model (Mil-Homens et al., 2010; Mil-Homens and Fialho, 2012).

1.2.5.5.3 Type VI secretion system

A specific inducible T6SS (T6SS-5) was identified in the non-Bcc *Burkholderia* species *B. pseudomallei* that was expressed upon invasion of macrophages and was required for virulence in a hamster infection model (Shalom et al., 2007; Burtnick et al., 2011). The T6SS-5 in the related *Burkholderia* species *B. mallei* and *B. thailandensis* were required for virulence in similar models (Schell et al., 2007; Schwarz et al., 2010). This virulence is in part due to T6SS-5 dependent intracellular survival and the ability to spread in and between eukaryotic host cells, due to secretion of a specific effector protein, VgrG-5 (Schwarz et al., 2014; Toesca et al., 2014).

A single functional T6SS was identified in *B. cenocepacia* (K56-2) (Aubert et al., 2008). Experimental evidence using an amoeboid host model and macrophage infection model suggested that the *B. cenocepacia* T6SS was responsible for eliciting pathogen-host interactions, particularly in actin remodelling, using a T6SS hypersecreting *B. cenocepacia* mutant (Aubert et al., 2008). Furthermore, using an agar bead rat lung infection model, a random mutagenesis screen identified a large number of mutants that were unable to survive *in vivo* (Hunt et al., 2004). Amongst the mutants, three contained transposon insertions in separate genes within the T6SS cluster, although at the time the function of these genes was unclear.

Recent findings have suggested the T6SS in *B. cenocepacia* may facilitate the escape of T2SS secreted proteins (ZmpA and ZmpB) from BcCVs into the cytoplasm of an infected macrophage host cell (Rosales-Reyes et al., 2012a). This specifically involves the T6SS puncturing the membrane of these vesicles within the phagocytes, leading to leakage of the extracellular metalloprotease proteins

through the perforated BcCV membrane into the macrophage cytoplasm (Rosales-Reyes et al., 2012a).

Further evidence that links the T6SS with intracellular pathogenicity of *B. cenocepacia* includes findings that suggested the T6SS is responsible for manipulating the actin cytoskeleton of macrophages upon infection. It is thought to do this by reducing the amount of the active GTP-bound Rho GTPases, Rac1 and Cdc42, whilst increasing the amount of active GTP-bound RhoA, which impairs normal functioning of the microtubule network, actin polymerisation in particular (Rosales-Reyes et al., 2012b). It was later found that the T6SS in *B. cenocepacia* specifically induces the deamination of RhoA, which actually leads to the activation of innate immune defences, such as programmed cell death and release of pro-inflammatory cytokines, via activation of the pyrin inflammasome and subsequent caspase-1 activation (Gavrilin et al., 2012; Xu et al., 2014). It is unknown whether this specific deamination of RhoA is caused directly by a T6SS secreted effector or by a non-T6SS effector released into the host cell cytoplasm upon puncturing of the BcCV membrane by the T6SS.

1.3 Protein secretion in Gram-negative bacteria

Gram-negative, or diderm, bacteria, have fundamentally different architectures to their cell envelope than Gram-positive, or monoderm, bacteria. Both contain a cytoplasmic membrane, but Gram-negative bacteria have an additional lipid bilayer designated as the outer membrane. There is an inter-membrane region between the inner and outer membrane known as the periplasm. Protein trafficking is important for both Gram-negative and Gram-positive bacteria and generally refers to the translocation of proteins across a membrane and/or insertion of a protein into the membrane. In Gram-negative bacteria secretion is thought of as the translocation of proteins from the cytoplasm across the inner membrane, periplasmic space and outer membrane into the surrounding milieu. They use a variety of protein secretion systems to facilitate this (Figure 1.3). Protein export is defined as the active transport of a protein from the cytoplasm cross the cytoplasmic membrane, meaning translocation of proteins from the cytoplasm into the periplasm in Gram-negative bacteria. But in Gram-positive bacteria, secretion and export are synonymous, due to the absence of the additional lipid bilayer (Desvaux et al., 2009).

1.3.1 Protein export into the periplasm: Sec and Tat systems

Sec, Tat and holin systems in Gram-negative bacteria allow the export of proteins from the cytoplasm into the periplasmic space. Whilst not strictly a bona fide secretion system in Gram-negative bacteria, exported proteins can then be further translocated across the outer membrane using additional secretion systems, such as the T2SS.

Briefly, the Sec export system in Gram-negative bacteria functions by transporting proteins in a unfolded state into the periplasm, either in a co-translational or post-translation manner (reviewed in Pugsley (1993); Natale et al. (2008)). Proteins targeted via this system have an N-terminal signal peptide, which is generally made up of a 15-30 residues that consists a small region of hydrophilic residues followed by of a run of hydrophobic residues. In post-translational export of proteins by the Sec system, a SecB chaperone protein (or

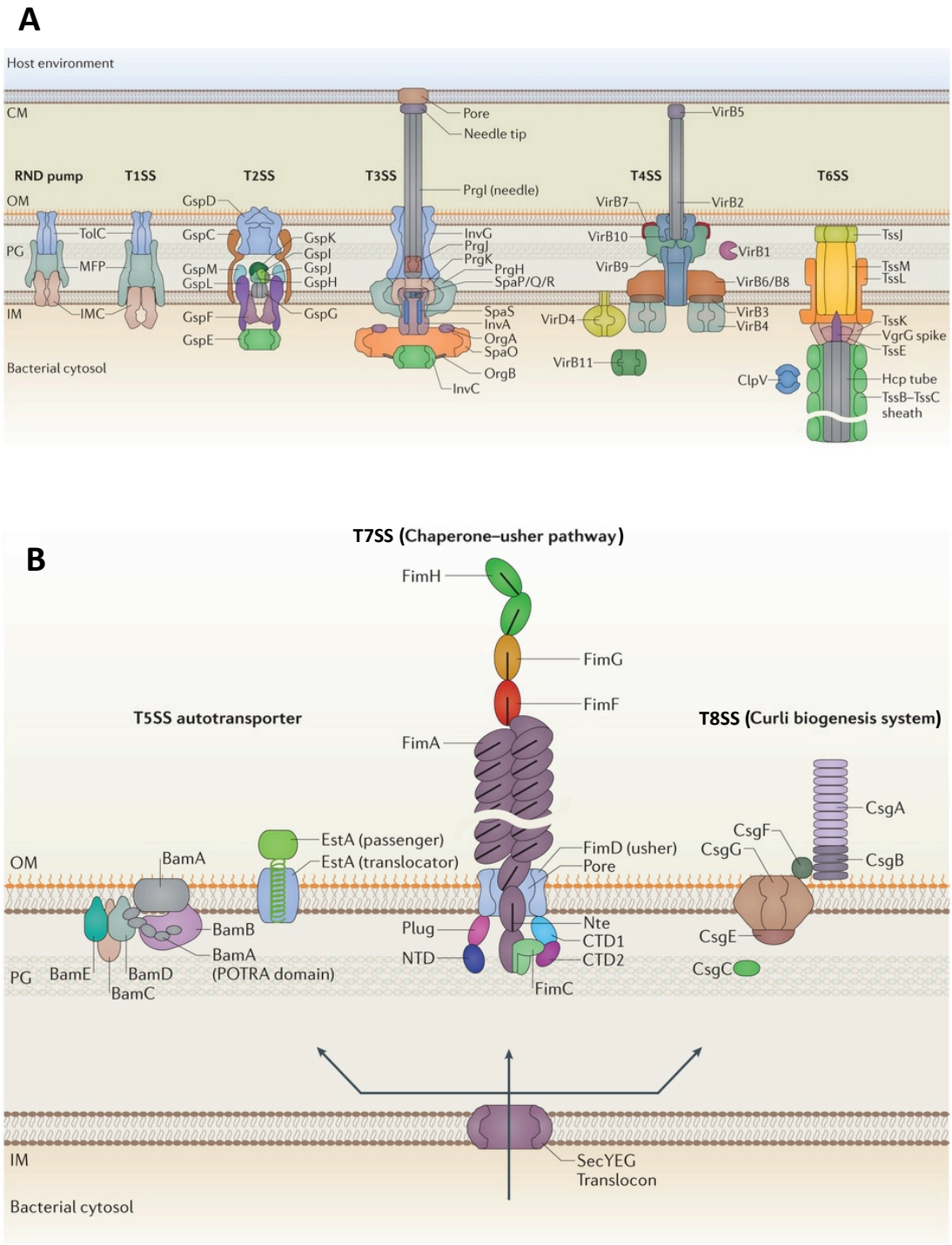

Figure 1.3 Structural overview of secretion systems present in Gram-negative bacteria. There are nine described protein secretion systems in Gram-negative bacteria, eight are depicted in this illustration. (A) Illustration of the secretion systems that span the inner and outer membrane. T1SS, T3SS, T4SS and T6SS do not generally require participation of the Sec or Tat systems. (B) Secretion systems that are located in the outer membrane, T5SS, chaperone-usher system (T7SS) and curli biogenesis system (T8SS). The Sec export system is also depicted. See text for further details. Reprinted by permission from Macmillan Publishers Ltd: Nature Reviews Microbiology (Costa et al., 2015), copyright 2015.

pilot protein) binds to the presecretion protein, maintaining it in an unfolded state to deliver it to a cytoplasmic membrane associated ATPase protein, SecA (Hartl et al., 1990). SecA is associated with a membrane-embedded channel complex, the SecYEG translocon (Brundage et al., 1990; Nishiyama et al., 1994; Douville et al., 1994). In an active process requiring ATP and the proton motif force (PMF), SecA facilitates the threading of the unfolded presecretion protein through a channel created by the SecYEG complex into the periplasm. The N-terminal signal peptide is cleaved by a signal peptidase, such as LepB in *E. coli* (Dalbey and Wickner, 1985). Periplasmic chaperone proteins such as DsbA facilitate further folding into the mature protein by disulphide bond formation in the oxidative periplasmic environment (Bardwell et al., 1991).

Rather than exporting proteins in an unfolded state, the Twin arginine transport system (Tat) functions to translocate folded proteins across the inner membrane into the periplasm in Gram-negative bacteria (Settles, 1997; Sargent et al., 1998), using energy derived from the PMF (review in Palmer & Berks (2012)). Proteins exported by this system have a typical N-terminal signal sequence that contains an RRxFxK motif (the twin arginine motif) preceding a hydrophobic stretch of amino acids, which targets the folded substrate protein to the Tat translocase complex spanning the cytoplasmic membrane. The Tat translocase in proteobacteria is comprised of TatABC membrane embedded subunits. TatBC form a complex that is subsequently bound by the N-terminal portion of the Tat substrate though a recognition site in TatC, which causes a conformational change in the TatBC complex (Bolhuis et al., 2001; Alami et al., 2003). This results in association of the TatBC-substrate complex with TatA subunits within the membrane, causing PMF-dependent polymerisation of TatA, that creating a channel allowing the export of the main body of folded substrate though the membrane (Mori and Cline, 2002; Dabney-Smith et al., 2006; Leake et al., 2008). The N-terminal signal sequence remains affix to the TatBC complex. The signal peptide is cleaved once the protein has been translocated across the membrane (Yahr and Wickner, 2001).

1.3.2 Type I secretion system

The Type I secretion system (T1SS) is a one-step protein translocation mechanism used by Gram-negative bacteria. It contains three essential structural components that are required for the translocation of specific unfolded proteins from the cytoplasm to the exterior of the cell, through a channel that transverses the inner membrane, periplasm and outer membrane (reviewed in Kanonenberg et al. (2013). This structure consists of an inner membrane embedded transporter that contains an ATP-binding cassette (ABC), which hydrolyses ATP to provide energy for this active process. This is in-complex with an inner membrane anchored fusion protein (MFP) that acts as platform linking the inner membrane ABC protein transiently to a trimeric outer membrane channel protein (OMP). This outer membrane protein contains a β-barrel pore structure within the outer membrane and a helical channel structure protruding into the periplasm which can be closed off in a manner similar to an iris diaphragm (Koronakis et al., 2000).

A well characterised substrate of the T1SS is the *E. coli* haemolysin HlyA, which requires the ABC transporter HlyB, MFP HlyD and the OMP TolC (Nicaud et al., 1985; Mackman et al., 1985; Mackman et al., 1986; Wandersman and Delepelaire, 1990). Unfolded substrates have a C- terminal recognition sequence that is recognised by the cytoplasmic portion of the MFP (Balakrishnan et al., 2001; Delepelaire, 2004). This interaction and/or an interaction of the unfold protein with the ABC transporter results in complex formation with the OMP, and triggers opening of the helical channel in the OMP, allowing the unfolded protein to be threaded through the entire channel structure (Bakkes et al., 2010). Once in the exterior, the protein folds into its mature confirmation. Most T1SS substrates have specific ABC and MFS proteins, but some share a common OMP, as in the case of TolC protein which also facilitates the transport bacteriocin colicin V, amongst others (Gilson et al., 1987; Gilson et al., 1990).

1.3.3 Type II secretion system

The type II secretion system (T2SS) is multi-subunit complex involved in the translocation of folded periplasmic proteins across the outer membrane into the

extracellular surroundings in Gram-negative bacteria. It is a two-step process that first requires either translocation of folded proteins into the periplasm by the Tat export system (Voulhoux et al., 2001) or unfolded proteins by the Sec system. Subsequent translocation across the outer-membrane then occurs using the T2SS (also known as the secreton) (reviewed in Korotkov et al. (2012)). Several human pathogens have been shown to use the T2SS for secretion of proteins that act as virulence determinants, such as *P. aeruginosa* and its T2SS substrates ToxA and LasB (elastase) (Woods et al., 1982; Wretlind et al., 1987; Bally et al., 1992), *V. cholerae* with AB_5 cholera toxin (Sandkvist et al., 1997) and *B. cenocepacia* with ZmpA (Corbett et al., 2003).

Using the Gsp nomenclature, the T2SS requires at least twelve different subunits arrange into four subassemblies: an outer membrane complex containing at least GspD (secretin) and GspS, the pseudopilus containing GspG, -H, -I, -J and -K, an inner-membrane complex containing GspC, -F, -L and -M, and a cytoplasmic ATPase (GspE) associated with cytoplasmic regions of the inner-membrane complex (Korotkov et al., 2012). The mode of secretion by this system is not well understood. The current accepted model involves association of the folded periplasmic protein substrate with either the periplasmic portion of GspC and/or the tip region of the pseudopilus. The substrate is then forced through the outer membrane secretin channel, by extension of the pseudopilus structure towards the outer membrane complex. This occurs through polymerisation of pseudopilin subunits in an active process that requires ATP hydrolysis by GspE (Korotkov et al., 2012).

1.3.4 Type III secretion system

The type III (T3SS), also known as the injectisome, is a complex protein secretion system that features in many pathogenic bacteria (reviewed in Cornelis (2006)). This includes *B. pseudomallei,* and its T3SS effector BopA that aids in preventing clearance of the bacteria by autophagosomal action (Cullinane et al., 2008). The T3SS complex uses a hollow needle structure to thread unfolded effector proteins (containing poorly defined signal sequences generally residing in

the N-terminus) through the needle into a eukaryotic target cell, either in to the cytosol or insertion into the cytoplasmic membrane. It does this by using chaperone proteins that unfold and direct the effector to the T3SS complex, which is then thread through the basal body, through the inner rod and then through the needle in an uninterrupted conduit, in an ATP-dependent process (Marlovits et al., 2004; Radics et al., 2014). It is then translocated through to the host cell membrane (Hueck, 1998; Akeda and Galán, 2005).

Contact with the host cell through the needle is the main trigger for protein secretion (Mota et al., 2005). This contacts results in the formation of a ~ 2.3 nm pore in the membrane of the target cell (Mueller et al., 2008). Three additional proteins (translocators) are required for this, two are hydrophobic and one is hydrophilic, termed YopB, YopD, and LcrV in *Yersinia*, respectively (Håkansson et al., 1996; Mueller et al., 2008). YopB and YopD subunits form the translocation pore in the target cell membrane by inserting their hydrophobic structures into it (Blocker et al., 1999), which is facilitated by LcrV, a protein that forms a tip complex at the tip of the T3SS needle (Mueller et al., 2005). The T3SS system is similar in structure to the bacterial flagellum, containing structural homologues to the basal body and hook structures.

1.3.5 Type IV secretion system

Type IV secretion systems (T4SS) involve the one-step translocation of either proteins or DNA from the interior of the cell into a target host cell, which may be another bacterium or a eukaryote. Three categories of T4SS are currently used to define the T4SS. One type is used for the transfer of DNA from cell-to-cell, in the form of an ssDNA-protein conjugative intermediate, which is also known as DNA conjugation. This type of system includes the T4SSs encoded on the R388 and pKM101 conjugative plasmids of *E. coli* (Winans and Walker, 1983; Llosa et al., 1994). Another type is used for the translocation of effector proteins into eukaryotes, such as the T4SS in *Bordetella pertussis* that translocates the A/B pertussis toxin, and the third type is responsible for the release and uptake of DNA in bacteria, such as what occurs in *Helicobacter pylori* (review in Ilangovan et al.

(2015); Costa et al. (2015)). The common architecture of the T4SS system involves core structural proteins termed Vir proteins. In the *E. coli* R388 conjugal apparatus, the current model postulates the structure is arranged into an inner membrane core complex formed by association of VirB8, VirB3 and VirB6 subunits with ATPase subunits VirB11, VirD4 and VirB4. This forms a complex via a stalk structure of unknown composition to an outer membrane core complex, composed of subunits VirB9, ViB7 and VirB10 that form a pore in the outer membrane (Low et al., 2014). A pilus structure that is composed on VirB2 and VirB6 extends into the extracellular space. The exact mechanism for the secretion of unfolded protein substrates or conjugative DNA intermediates after pilus assembly is unknown, but it is thought it may involve a switch between pilus extension and substrate translocation by differential association of the ATPase subunits, once the tip of the pilus has come into contact with a receptor on the target cell (Costa et al., 2015).

1.3.6 Type V secretion system

The Type V secretion system (T5SS), is a two-step protein secretion mechanism that allows the translocation of a Sec-dependent periplasmic protein across the outer membrane through an outer membrane pore structure (reviewed in Henderson et al. (2004); Costa et al. (2015)). Several classes of the T5SS exist, termed T5SSa to T5SSe, none of which require NTPase activity or the PMF for translocation of their substrates. The T5SSa, also known as the autotransporter system, includes the well characterised IgA1 protease from *Neisseria gonorrhoeae* (Pohlner et al., 1987), while T5SSb, referred to as the two-partner secretion pathway (TPS), includes the *B. pertussis* hemagglutinin protein, FHA (Coutte et al., 2001). These two systems are closely related.

Initially, a peptide precursor is targeted into the periplasm by a canonical N-terminal signal peptide using the Sec export system. Periplasmic chaperones may also be utilised by some T5SSs to restrict misfolding of the precursor in the periplasm, to maintained them in a state that can be transported (Ruiz-Perez et al., 2009; Ieva and Bernstein, 2009).

Using IgA1 as an example, the T5SSa functions by utilising an outer membrane translocator domain residing in the C-terminal end of the translocated protein precursor. This inserts in to the outer membrane via the outer membrane Bam complex to form a β-barrel pore structure to facilitate the translocation of its unfolded protease 'passenger' domain out through the outer membrane pore structure into the exterior of the cell (Wu et al., 2005; Ieva and Bernstein, 2009). This is thought to occur by the passenger domain interacting with periplasmic POTRA (polypeptide transport-associated) domains on BamA to aid in transfer of the passenger domain though the β-barrel channel (Pavlova et al., 2013; Noinaj et al., 2013). It has recently been suggested that passenger domain translocation is not solely through the β-barrel structure, but may involve larger membrane assemblies that include Bam and TAM complexes (an alternative outer membrane translocation module) (Selkrig et al., 2012; Pavlova et al., 2013; Gruss et al., 2013). Upon release into the extracellular milieu the protein undergoes maturation to form its fully active protein (Pohlner et al., 1987). The T5SSb (TPS) differs from the T5SSa in that the C-terminal translocation domain of the autotransporter is encoded by a separate protein with which the translocated TPS protein must dock (Mazar and Cotter, 2007).

1.3.7 Type VI secretion system

The type VI secretion system (T6SS) is another secretion system employed by Gram-negative that has subunits associated with the inner and outer membrane, translocating effectors in a one-step manner. This will be discussed in further detail in Section 1.4.

1.3.8 Type VII secretion system

The Gram-negative type VII secretion, also termed the chaperone-usher system, is a further two-step secretory mechanism used for the assembly of pili, fimbriae or other polymeric adhesin structures on the surface of Gram-negative bacteria. A relatively well understood pilus structure, termed the type I pilus, common to the *Enterobacteriaceae* family (Jones et al., 1995), contributes to the

pathogenicity of uropathogenic *E. coli* (UPEC), by direct interaction between the bacterium and host epithelial cells in the bladder via mannose-containing glycoproteins (Abraham et al., 1988; Mulvey et al., 1998). This structure is assembled by a chaperone-usher system that utilises pilin subunits that are exported into the periplasm via the Sec pathway. It specifically uses subunits of FimD, known as the usher, to create a pore in the outer membrane (Klemm and Christiansen, 1990; Thanassi et al., 1998), and a periplasmic chaperone protein, FimC (Lindberg et al., 1989). This chaperone protein associates with the major and minor pilus subunits, FimA, and FimF, -G, and -H, respectively, to facilitate their folding and transport through the periplasm, docking with the outer membrane usher FimD, where pilus assembly occurs extending outwards from the outer membrane to the exterior. The role of the chaperone is three-fold, it prevents misfolding of the pilin subunits, prevents premature assembly of the pilus in the periplasm and stabilises the pilus against proteolysis (Lillington et al., 2014). The minor pilin tip region is assembled first, with FimH at the very tip, preceded by FimG and then FimF, and then extensive major pilin structure made up of FimA subunits.

Note, the Gram-positive ESX secretion system present in mycobacterium, including *Mycobacterium tuberculosis*, is also often referred to as the type VII secretion system (Abdallah et al., 2007), but is unrelated to the system present in Gram-negative bacteria.

1.3.9 Type VIII secretion system

The type VIII secretion system (T8SS), also termed the extracellular nucleation-precipitation secretion pathway (Desvaux et al., 2009) has a similar purpose as the T7SS, to function to append surface adhesins on Gram-negative bacteria. But rather than pilin structures, the T8SS is involved in the appendage of curli amyloid fibres extending from the bacterial outer membrane (Olsén et al., 1989; Chapman et al., 2002), (reviewed in Barnhart & Chapman (2006); Costa et al. (2015)). It is thought to be involved in cell surface adhesion, aggregation and aid in the formation of biofilms (Kikuchi et al., 2005).

The common nomenclature used to designate the subunit components of this system is Csg (Olsén et al., 1993). All subunits required for this system are transported into the periplasm in a Sec-dependent manner. Assembly and secretion of the curli fibre, comprised mainly of CsgA (Olsén et al., 1989; Olsén et al., 1993), is thought to involve an outer membrane-spanning complex comprised of oligomeric CsgG lipoprotein subunits that contain a hollow periplasmic region, which associates with the periplasmic CsgE subunit (Nenninger et al., 2011). This acts as a stopper, forming a structure likened to a vestibule/chamber (Goyal et al., 2014). The major curli subunit, CsgA, and an additional minor curli subunit, CsgB, are translocated in an unfolded state through the narrow channel in CsgG. A current model suggests polypeptides of CsgA become trapped within the CsgG-CsgE chamber structure, and their translocation out to the exterior through the CsgG pore is due to an entropy-gradient rather than an active mechanism (Goyal et al., 2014). CsgB functions to nucleate the polymerization of CsgA into fibres (Hammer et al., 2007).

1.3.10 Type IX secretion system

The final known Gram-negative secretion system is the type IX secretion system (T9SS), also known as the Por secretion system. This is a recently discovered secretion system restricted to species of the *Bacteroidetes* phylum (review in Nakayama (2015)). It is required for *Flavobacterium johnsoniae* gliding motility across a surface (Nelson et al., 2007; Sato et al., 2010; Shrivastava et al., 2013) and has been implicate in the secretion of virulence factors, such as extracellular proteases termed gingipains, including Kgp and Rgp, in the human periodontal pathogen *Porphyromonas gingivalis.* Many of these proteins have similar C-terminal motifs that are postulated to be an identifier for secretion by the T9SS (Nakayama et al., 1995; Saiki and Konishi, 2007; Sato et al., 2013).

Secretion by this system in *P. gingivalis* involves a collection of at least ten protein subunits, including Sov, PorK, -L, -N, -M, -P, -Q, -T, -U, -W, -X and –Y (Sato et al., 2010) of which the structural complex arrangement is unknown. However, it has been observed that PorK, -N and -P associate with the outer membrane and PorL

and PorM with the inner membrane (Saiki and Konishi, 2007; Glew et al., 2014), there is debate over whether PorT is an inner or outer membrane protein (Nguyen et al., 2009; Nakayama, 2015). The basic model of secretion involves Sec-dependent export of the effector proteins and then translocation across the outer membrane through the T9SS complex.

1.4 Type VI secretion system

1.4.1 Structure and mode of action of the T6SS

The type VI secretion system (T6SS) has multiple subunits making up its large and complex structure, thought to be organised into a needle-like structure containing two distinct interacting subassemblies, a phage tail-like structure and a channel/chamber structure that spans the inner membrane, periplasm and the outer membrane. It is proposed to require the products of approximately thirteen genes (*tssA* through to *tssM*) organised into a T6SS gene cluster (Shalom et al., 2007; Cascales, 2008; Aschtgen et al., 2008). These protein products either act as structural proteins and/or secreted products (Zheng and Leung, 2007; Bingle et al., 2008). Some systems require an additional protein (TagL, TagN, TagP or TagW, dependent on the system) containing a peptidoglycan-binding domain that anchors the T6SS to the cell envelope (Aschtgen et al., 2010b). These occur in systems in which the TssL subunit lacks such a domain. The consensus idea is that the T6SS forms a needle-like structure extending from the cytoplasm, which uses a crossbow-like action to fire the tubular structure through the inner membrane, periplasm and outer membrane of a T6SS-containing bacterium to then perforate the cellular membrane of a target host cell, as shown in Figure 1.4.

1.4.1.1 Phage tail-like complex

The mechanism of the T6SS involves penetrating the target cell membrane in a manner similar to that of bacteriophage T4, which punctures and injects its DNA into a susceptible bacterium. Several subunits of the T6SS share homology to proteins that make up the T4 bacteriophage contractile tail. Firstly, a trimeric secreted protein, TssI (also referred to as VgrG), has structural similarities to the phage tail T4 spike proteins gp5 and gp27, which similarly form a $(gp5\text{-}gp27)_3$ complex responsible for puncturing the bacterial outer membrane (Pukatzki et al., 2007; Leiman et al., 2009).

Recent work has suggested the TssI spike may be further sharpened by PAAR (Pro, Ala, Ala, Arg) proteins, some of which may interact with, or contain additional effector domains, to allow several effectors to be delivered by the

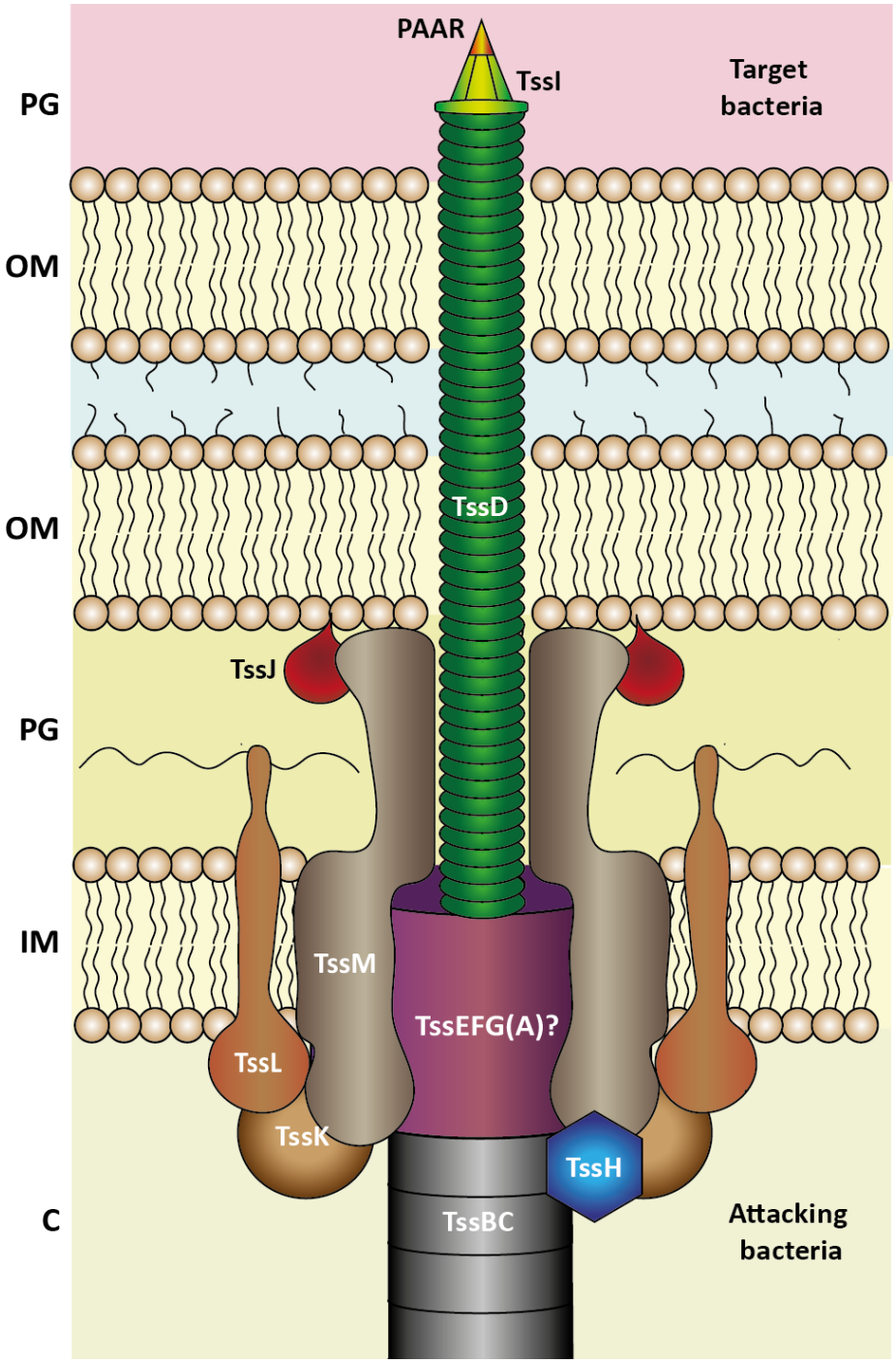

Figure 1.4 Model of the Type VI secretion apparatus. A spike-like protein TssI is located at the tip of a tube structure comprised of stacked units of TssD. PAAR proteins sharpen the tip of TssI. The system contains a baseplate complex of unknown composition, but probably includes TssE, TssF, TssG and TssA. The TssD tail tube is surrounded by a sheath of TssB and TssC units, which in an extended state readies the tube complex to be fired through the cell envelope (IM, PG, and OM) into the host cell membrane. TssH disassembles contracted TssBC complexes. TssM, TssL and TssJ interact to form a cell-enveloped embedded sub-complex. TssK links the TssJLM sub-complex to the phage-like components, interacting with TssM and TssL, and TssGF. Subunits as indicated with labels.

system (Shneider et al., 2013). The PAAR protein is similar to the apex domain of phage spike proteins gpV and gp138 in bacteriophages P2 and φ92. All show a tapered structure containing a co-ordinated metal iron for stability, an iron ion in gpV and gp138 and a zinc ion in PAAR (Browning et al., 2012; Shneider et al., 2013). Bacteriophages P2 gpV and φ92 gp138 are also homologous to the gp5 spike protein of bacteriophage T4. Although, gp5 does not contain an apex domain (Kanamaru et al., 2002), but instead it is thought it uses a PAAR-like protein gp5.4 to sharpen its tip in a similar manner (Kostyuchenko et al., 2003; Shneider et al., 2013).

Accordingly, the TssI-PAAR complex is proposed to act as a spike protein sitting at the top of a long syringe-like structure with an inner tube structure made from the stacking of hollow rings of a small T6SS protein known as TssD (Hcp) (Mougous et al., 2006; Leiman et al., 2009; Pell et al., 2009), which has structural similarities to the T4 bacteriophage tail protein gp19 (Leiman et al., 2009) and λ phage tail protein gpV (Pell et al., 2009). Six TssD monomers come together to form the ring structure that measures 80-90 Å in diameter, with an internal diameter of 35-40 Å (Mougous et al., 2006), proposed to be wide enough to allow the translocation of unfolded proteins as well as small folded proteins (Cascales and Cambillau, 2012). In the current T6SS model, TssD rings are added to the TssD unit nearest the inner membrane, allowing TssD polymerisation and extension into the cytoplasm (Basler et al., 2012), with the TssI tail spike located at the tip of the tube, which also controls the TssD polymerisation process (Brunet et al., 2014). This syringe-like spike complex penetrates the target cell membrane allowing effector molecules to be transported into the target cell (Leiman et al., 2009).

The force used to push out the TssD tube structure is likely to be generated by the contraction of a tail sheath-like structure comprised of polymerized TssB (VipA) and TssC (VipB) subunits that surrounds the TssD tube (Bönemann et al., 2009; Leiman et al., 2009; Basler et al., 2012; Brunet et al., 2014). An EM structure of the contracted TssBC sheath structure has recently been observed. It was found to share structural fold similarities with the phage sheath, particular in regards to an inner and middle region within the structure (Kudryashev et al., 2015; Clemens

et al., 2015). However, the T6SS sheath has a different outer region which Kudryashev and co-workers suggested formed the basis of an interaction with the TssH subunit that allowed disassembly of the contract sheath, something that does not occur with phage sheaths (Kudryashev et al., 2015).

TssH (ClpV), an AAA+ family ATPase able to generate mechanical force from ATP hydrolysis, is able to interact with and disassemble the TssBC units that form the sheath structure around the inner TssD tube (Bönemann et al., 2009). In certain systems TssH mutants still retain some T6SS activity, but are significantly less efficient (Zheng et al., 2011; Basler et al., 2012). This led to the idea that the ATP-dependent activity of TssH is required for the removal of the contracted TssBC subunits by disassembly of the components, which are then recycled, increasing the efficiency of the system (Basler et al., 2012; Basler and Mekalanos, 2012; Zoued et al., 2014). TssB and TssC are also prevented from forming aggregates within the cytoplasm by TssH, thus preventing the cell from being overladen with contracted sheaths (Kapitein et al., 2013). The interaction between TssH and the contracted sheath is facilitated through a specific region located at the N-terminus of TssH that interacts with an exposed region of an α-helix located at the N-terminus of TssC, which is only available in the contracted form of the TssBC sheath (Pietrosiuk et al., 2011; Zoued et al., 2014).

The T6SS is proposed to contain a baseplate complex, similar in function and structure to that of a bacteriophage baseplate. The bacteriophage baseplate aids in membrane recognition and attachment, but more importantly it undergoes structural changes that lead to contraction of the tail sheath, to propel the tail tube forward through the centre of the baseplate (Kostyuchenko et al., 2003). During tail tube injection the bacteriophage T4 baseplate undergoes goes a conformational change from a hexagon shape to a 6-pointed star (Kostyuchenko et al., 2003). A similar mechanism is envisaged for the T6SS complex, where contraction of the TssBC sheath, and thus propulsion of the TssD tail tube, is caused by a conformational change in the T6SS baseplate (Basler et al., 2012).

The components of the T6SS baseplate are not yet established. TssE, which is homologous to the T4 baseplate wedge protein gp25 (Leiman et al., 2009), is a

candidate baseplate protein, along with a suggested cytoplasmic inner membrane associated sub-complex formed between TssK, TssG and TssF (English et al., 2014), all of which are essential for T6SS activity. A further uncharacterised essential cytoplasmic subunit, TssA, has also been suggested to form part of the baseplate complex (Zoued et al., 2013; English et al., 2014).

1.4.1.2 Transmembrane sub-complex

A cell envelope-embedded sub-complex is needed to hold the phage-like subassembly of the T6SS in place, comprised of TssJ, TssL and TssM (Zheng and Leung, 2007; Ma et al., 2009b; Aschtgen et al., 2010a; Durand et al., 2012; Durand et al., 2015). TssK is also thought to facilitate a link between these two sub-complexes (Zoued et al., 2013). TssM and TssL make up an inner membrane-embedded complex (Ma et al., 2009b; Durand et al., 2012), which is then connected to the outer membrane via the C-terminal periplasmic region of TssM interacting with the outer membrane-anchored lipoprotein TssJ, forming a transenvelope chamber (Aschtgen et al., 2008; Felisberto-Rodrigues et al., 2011; Durand et al., 2015). Recent data has suggested that the assembly of the TssJLM complex is the first step in T6SS complex formation, requiring sequential addition of TssJ, TssM and then TssL (Durand et al., 2015).

Many TssL orthologues contain a peptidoglycan (PG)-binding domain that is thought to stabilize the T6SS complex in the cell envelope, and/or provide a mechanism of targeting the T6SS to particular locations in the membrane (Aschtgen et al., 2010b). If the PG-binding domain is absent from TssL then the T6SS will usually incorporate a PG-binding Tag protein that serves a similar purpose, such as TagL (Aschtgen et al., 2010a).

Most TssM subunits contain a large N-terminal cytoplasmic domain between its second and third transmembrane domain. This cytoplasmic region often contains Walker A and Walker B motifs, that bind and hydrolyse ATP or GTP (Ma et al. 2009). These motifs are required for proper functioning of some T6SSs (Ma et al. 2009), but not all (Zheng and Leung, 2007). Recent evidence suggests that in some T6SSs the ATP hydrolysis activity of TssM is needed to allow formation of a complex between the TssM-TssL inner membrane complex and periplasmic hexameric TssD,

where the periplasmic domain of TssL and TssD directly interact (Ma et al., 2012). But this may only be in specific T6SSs, such as *Agrobacterium tumefaciens* used in the Ma et al. study, and is probably not relevant for TssL proteins that lack PG-binding domains, as their periplasmic domain is then subsequently only very small.

1.4.2 Biological functions of the T6SS

When first discovered, the major role of the T6SS was thought to be in virulence (Pukatzki et al., 2006; Schell et al., 2007; Aubert et al., 2008). However, subsequent investigations have implicated several alternative roles for the T6SS, the foremost being its importance in interactions between bacteria, including a major role in bacterial competition (Schwarz et al., 2010; Hood et al., 2010; MacIntyre et al., 2010), biofilm formation (Enos-Berlage et al., 2005; Aschtgen et al., 2008), and quorum sensing (Weber et al., 2008), as well as stress sensing and environmental adaption (Ishikawa et al., 2012; Salomon et al., 2013).

1.4.2.1 Bacterial competition

The involvement of the T6SS in bacterial interactions has been widely documented. The first described instance was the identification of several anti-bacterial T6SS effectors, Tse1-3, secreted by the H1-T6SS in *P. aeruginosa* (Hood et al., 2010). Identification of a variety of other Gram-negative bacteria that used a T6SS to target anti-bacterial effectors quickly ensued, including *V. cholerae* (MacIntyre et al., 2010), *Serratia marcescens* (Murdoch et al., 2011), the T6SS-1 of *B. thailandensis* (Schwarz et al., 2010) *Pseudomonas fluorescens* (Decoin et al., 2014), *Vibrio parahaemolyticus* (Salomon et al., 2013) and *A. tumefaciens* (Ma et al., 2014).

Furthermore, fluorescent microscopy has been used to visualize the T6SS induced attack between bacterial cells *in vivo* (Basler and Mekalanos, 2012; Leroux et al., 2012; Gerc et al., 2015). The ability of the T6SS to target bacterial cells of the same species has also been highlighted (Dong et al., 2013; Unterweger et al., 2014; Whitney et al., 2014; Diniz and Coulthurst, 2015). Overall, there is clear evidence that many T6SSs have a role to play in bacterial interactions, particularly in regards

to providing a growth survival advantage, using the T6SS as key weapon to attack and out-compete other bacteria in their surroundings.

1.4.2.2 Pathogenesis

Specific T6SSs of several human pathogens and their anti-eukaryotic effectors have been linked to eukaryotic virulence. T6SS contact-dependent cytotoxicity towards *Dictyostelium* and macrophages was first observed in *V. cholerae* (Pukatzki et al., 2006). It was later demonstrated to be caused by a modified VgrG (TssI) spike protein with a C-terminal actin cross-linking domain (ACD), VgrG-1, whose ACD was delivered to the cytosol of the macrophage host cell, where it targeted its substrate G-actin (Pukatzki et al., 2007). The T6SS-5 of two related *Burkholderia* species, *B. mallei* and *B. pseudomallei,* was found to be fundamental for eukaryotic virulence (Schell et al., 2007; Burtnick et al., 2011). The H2-T6SS of *P. aeruginosa* has also been implicated in its ability to invade epithelial cells *in vivo* in addition to having anti-bacterial activity (Sana et al., 2012; Russell et al., 2013). This may occur through delivery of trans-kingdom effectors that are able to target both prokaryotes and eukaryotes, including a phospholipase D effector termed $Tle5^{PA}$ (Russell et al., 2013; Jiang et al., 2014).

1.4.3 Regulation of the T6SS

Various methods have been proposed to regulate expression/or activity of the T6SS at a transcriptional, post-transcription or post-translation level, summarised in Figure 1.5.

1.4.3.1 Transcriptional and post-transcriptional regulation of the T6SS

The T6SS gene clusters in various bacteria have been demonstrated to be controlled in part at a transcriptional and/or post-transcriptional level by diverse regulatory mechanisms (reviewed in Bernard et al. (2010)). This includes alternative sigma factor σ^{54}-dependent transcriptional regulation, such as in *V. cholerae*. This bacteria uses the enhancer binding protein VasH to promote transcription from σ^{54}-dependent promoters within the T6SS cluster (Pukatzki et al., 2006; Ishikawa et al., 2009). Two-component-dependent regulation is also common, including the VirA-

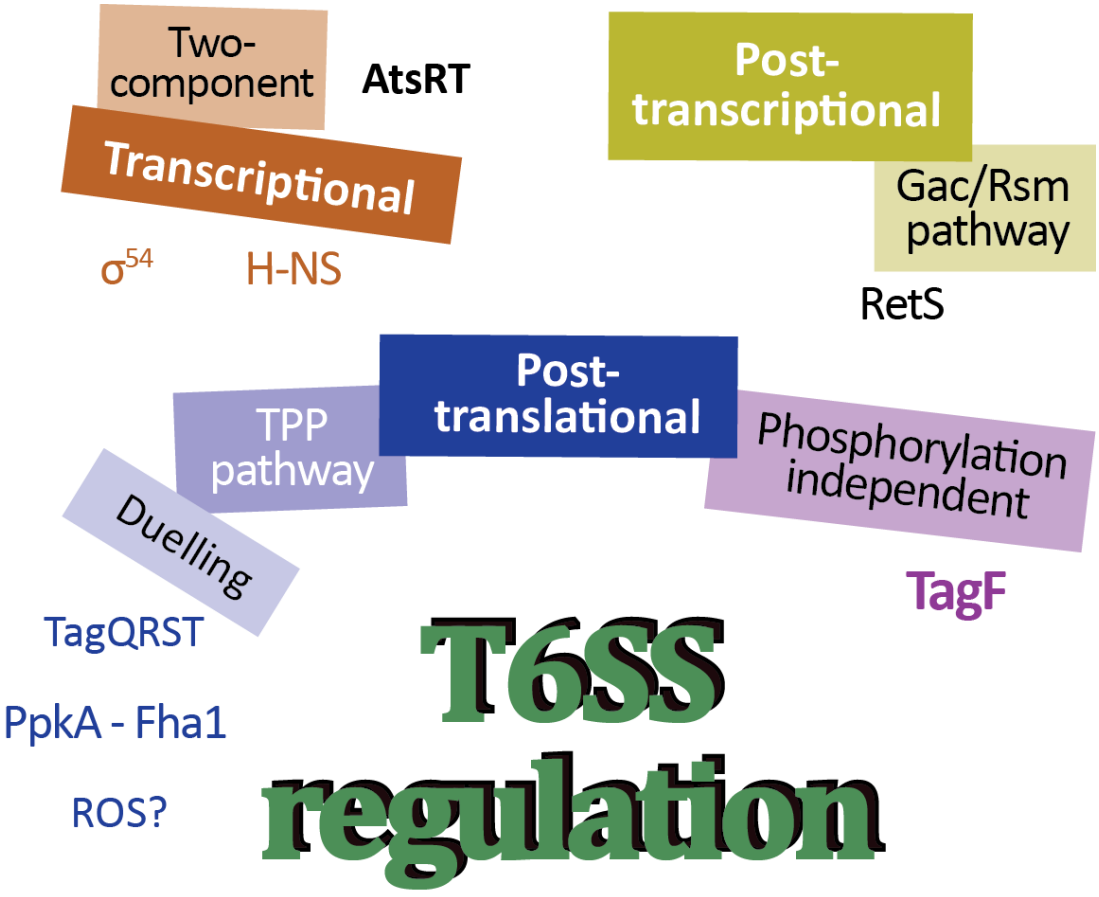

Figure 1.5 Mechanisms of T6SS regulation. Summary diagram showing selected mechanisms used to regulate the T6SS system in various bacteria. See text for further details.

VirG sensor kinase and response-regulator pair, which regulates the T6SS-5 cluster in *B. mallei* and its relatives (Schell et al., 2007). Another example is the global two-component regulatory system AtsR-AtsT in *B. cenocepacia* (Aubert et al., 2008; Khodai-Kalaki et al., 2013).

Another mechanism of transcriptional regulation is by histone-nucleoid structuring-like proteins (H-NS) that specifically bind to and repress transcription from regions of DNA that are AT-rich, including some genes within T6SS clusters. For example, MvaT, a H-NS-like protein in *P. aeruginosa* represses transcription of H2-T6SS and H3-T6SS (Castang et al., 2008). Recently an H-NS protein has been discovered to regulate the T6SS in *V. parahaemolyticus* (Salomon et al., 2014b).

Global virulence regulator RetS, of *P. aeruginosa*, post-transcriptionally suppresses the H1-T6SS through negative regulation of the Gac/Rsm pathway (Goodman et al., 2004; Mougous et al., 2006). Here, RetS is able to inhibit the GacS/GacA/rsmZ signalling pathway leading to elevated levels of free RsmA, which is a post-transcriptional regulatory protein that can bind to and negatively regulate mRNA transcripts from genes within the H1-T6SS cluster (Brencic and Lory, 2009). RsmA does this by binding to small exposed motifs in the 5' leader sequence of its target mRNA transcripts. Thus, preventing ribosome binding (30S subunit) to the RBS, and stopping subsequent translation initiation, which ultimately results in the degradation of the mRNA (Brencic and Lory, 2009).

1.4.3.2 Post-translational regulation of the T6SS

1.4.3.2.1 T6SS 'duelling'

Due to the complex structural features of the T6SS and a rapid response needed from the system, it may be expected that the complex is post-translationally regulated (Bernard et al., 2010). Specific environmental signals may result in assembly and firing of the complex to deliver its effectors or simply trigger a pre-assembled complex. Such post-translational regulation has been described in the H1-T6SS of *P. aeruginosa*. In particular, a threonine phosphorylation pathway (TPP) was identified that is thought to use surface growth as a stimulus for activation. Here, the dimerization and auto-phosphorylation of PpkA, a cytoplasmic

membrane-anchored threonine protein kinase, phosphorylates a cytoplasmic FHA-domain protein (Fha1) (Mougous et al., 2007), that acts as a T6SS scaffold protein.

The current model suggests that Fha1 may complex with TssH and other components of the T6SS (Hsu et al., 2009). It has been suggested that Fha1 phosphorylation localizes the Fha1 to other structural T6SS components and may be required for proper assembly of the T6SS machinery (Mougous et al., 2007). This would result in correct firing of the complex and allow contraction of the sheath. Whereby TssH can then disassemble the contracted sheath subunits, and recycle them, increasing the efficiency of the system (Bönemann et al., 2009; Basler and Mekalanos, 2012; Kapitein et al., 2013). PppA is a phosphatase responsible for dephosphorylating phosphorylated Fha1 (Mougous et al., 2007) (Figure 1.6).

It has also been suggested that a different T6SS, in *A. tumefaciens*, uses PpkA to phosphorylate a residue on the cytoplasmic face of TssL rather than phosphorylate Fha1. This phosphorylation event facilitates an interaction between this region and Fha1, activating T6SS in *A. tumefaciens* (Lin et al., 2014). It is unclear how applicable this is to other T6SSs.

Studies have indicated the participation of non-conserved Tag proteins in signal detection and transmission through the TPP in *P. aeruginosa*. TagQ, an OM-associated lipoprotein, is suggested to localise the periplasmic protein TagR to the OM (Casabona et al., 2013), where TagR promotes PpkA auto-phosphorylation by interacting with the periplasmic domain of PpkA (Hsu et al., 2009). An inner membrane ABC transporter TagT-TagS may also be involved in this process (Casabona et al., 2013) (Figure 1.6).

Later, time-lapsed fluorescence microscopy suggested the H1-T6SS in *P. aeruginosa* may be activated upon attack by another T6SS-containing bacterium, termed T6SS 'duelling' (Basler et al., 2013). Basler and colleges suggested the TagQRST system is responsible for the transmission of an unknown signal, produced upon attack of *P. aeruginosa* by another T6SS bacterium, through the TPP, which is facilitated by surface growth (Figure 1.6). Thereby stimulating H1-T6SS activity and mounting a T6SS response, which occurs at the initial point of contact initiated by the attacking bacterium (Basler et al., 2013). The authors go on to suggest that the

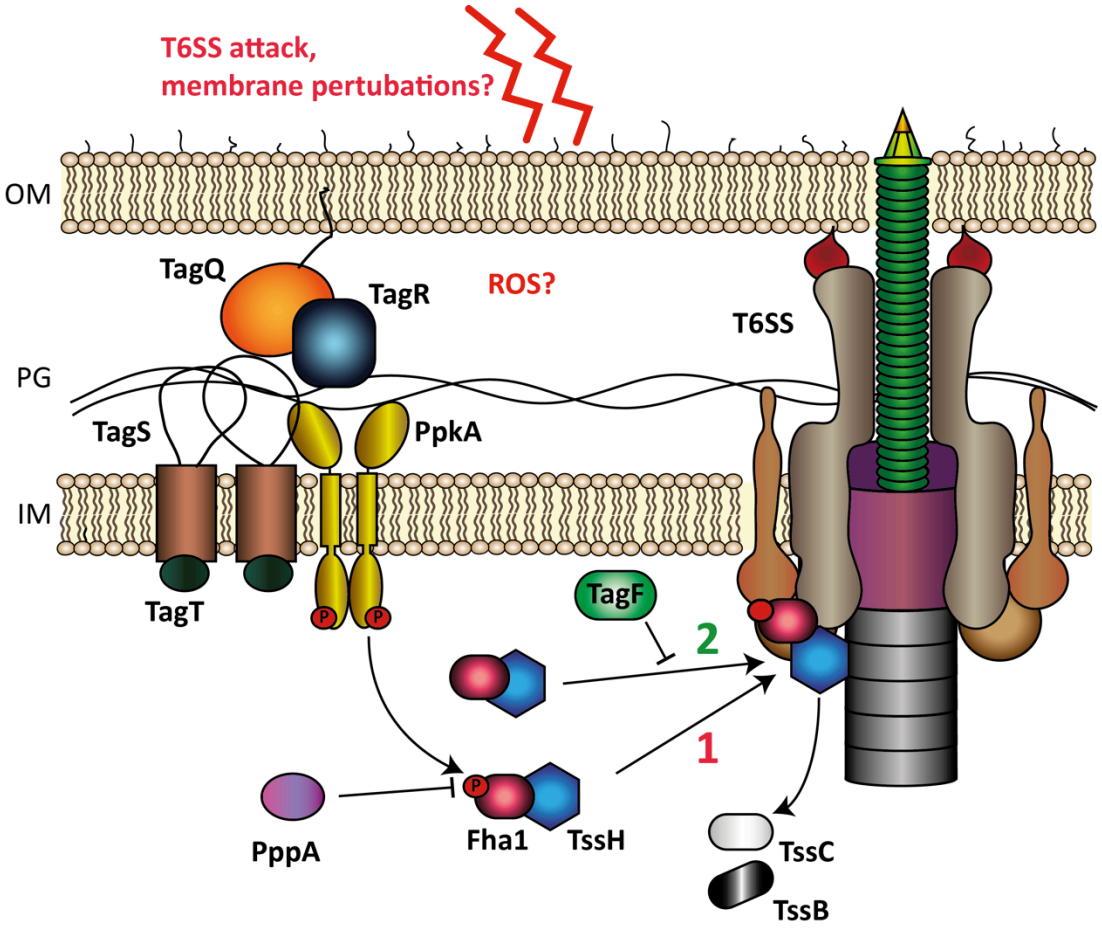

Figure 1.6 Overview of the proposed post-translational regulatory mechanisms of the T6SS in *P. aeruginosa*. (1) Surface-growth induced (duelling) activation of the tyrosine phosphate pathway (TPP) and TagQRST system. Activation of this pathway may occur through membrane perturbations/or ROS production. This pathway results in the phosphorylation of Fha1 and complex formation with TssH, where the complex is then localised to the T6SS complex to positively regulate T6SS activity. See text for further details. (2) Phosphorylation independent post-translational regulation of T6SS activity via the cytoplasmic protein TagF (non-duelling). TagF negatively regulates the recruitment of unphosphorylated Fha1 in complex with TssH to the T6SS apparatus, either directly or indirectly in an unknown manner. See text for further details. IM, inner membrane; PG, peptidoglycan/periplasm; OM, outer membrane; ROS, reactive oxygen species.

TagQRST system may directly sense disruptions to the cell envelope as a result of an attack by another T6SS-containing bacterium (Basler et al., 2013) (Figure 1.6).

However, genes encoding essential components of the TPP (*ppkA*, *pppA* and *fha1)* are absent from many T6SS clusters, including the T6SS cluster in *B. cenocepacia*, suggesting that they do not employ the TTP as a mode of regulation.

Interestingly, membrane perturbations caused by mating pair formation pilus (a type of T4SS) can also induce the assembly and firing of the H1-T6SS in *P. aeruginosa* at the site of contact, as well as artificial modulation of the outer membrane/or LPS by the anti-microbial peptide polymyxin B (Ho et al., 2013). Recent evidence has suggested that production of reactive oxygen species (ROS) can be induced in *E. coli,* as a consequence of membrane perturbations or cell wall damage caused by the T6SS of *V. cholerae* and its effector VgrG3, as well as T6SS-mediated attacks by *Acinetobacter baylyi* and *P. aeruginosa* (Dong et al., 2015). T6SS-independent methods including polymyxin B challenge can also induced ROS (Dong et al., 2015). ROS are sensed by the regulatory protein SoxR which activates transcription of *soxS*, encoding a transcriptional activator, that in-turn regulates genes involved in redox stress response (Greenberg et al., 1990; Amábile-Cuevas and Demple, 1991; Nunoshiba et al., 1992). It has been suggested that ROS production may trigger activation of the T6SS in some species (Dong et al., 2015).

1.4.3.2.2 Non-duelling

The duelling mechanism observed in *P. aeruginosa* does not hold true for all T6SSs. Recent evidence in *S. marcescens* has observed that the T6SS in this bacterium is fired indiscriminately without being triggered by a T6SS-induced attack from a surrounding bacterium (Gerc et al., 2015). PpkA is also important for T6SS activity in *S. marcescens* (Fritsch et al., 2013), but it has been suggested that rather than PpkA controlling the induction of the system (i.e. an on state), it is instead used as an control measure to prevent the system from firing (i.e. an off state) (Gerc et al., 2015). A similar situation has been described for *V. cholerae*, which again does not required attack from a surrounding bacteria to elicit a T6SS attack (Basler and Mekalanos, 2012).

Furthermore, a relatively conserved cytosolic Tag protein, TagF, encoded by many T6SS gene clusters, including the *Burkholderia* T6SS-1, was found to be a negative post-translational regulator of H1-T6SS in *P. aeruginosa*. It acts independently of the PpkA-Fha1 phosphorylation pathway, and does not respond to surface growth stimuli (Silverman et al., 2011). Even though TagF is not involved in the TPP, the two regulatory processes converge on recruitment of TssH to the T6SS assembly. This recruitment requires Fha1, in which unphosphorylated Fha1 forms a complex with TssH (Silverman et al., 2011) (Figure 1.6). The other regulatory components of the TagF-dependent pathway in *P. aeruginosa* are unknown.

1.5 T6SS-dependent effectors

The general lack of understanding regarding the signals that cause activation of the T6SS originally hampered efforts at identifying the secreted products of the T6SS. However, insights into the regulatory mechanisms of particular T6SS clusters and advances in detection methods have opened up a new era for effector identification. A variety of T6SS-dependent effectors have now been described. Many of which target other bacteria, either via their peptidoglycan layer, phospholipid membranes or cytoplasmic targets. A select few anti-eukaryotic effectors have also been described. A summary of the molecular targets of anti-bacterial T6SS-dependent effectors is depicted in Figure 1.7.

1.5.1 Evolved TssI effectors

Early findings suggested some T6SS effectors might be variants of the TssI protein (TssI-related effectors). Several variants of TssI with C-terminal extensions possessing obvious effector activity were identified. These extensions included a peptidoglycan-binding domain and an actin-cross linking domain (ACD) in TssI proteins of *V. cholerae,* VgrG-3 and VgrG-1, respectively (Pukatzki et al., 2007; Pukatzki et al., 2009) and a metalloprotease domain in VgrG2b of *P. aeruginosa* (Sana et al., 2015). The term 'evolved TssI' has been used to describe these effector domain-containing TssIs (Pukatzki et al., 2007).

Subsequent work experimentally validated VgrG-1 as an anti-eukaryotic effector, by demonstrating *in vivo* and *in vitro* inhibition of actin-cross linking activity in a *vgrG-1* mutant. This ACD was thought to be responsible for a particular round cell morphology seen in macrophage cells infected with *V. cholerae* (Pukatzki et al., 2007). The peptidoglycan activity of the *V. cholerae* VgrG-3 CTD was also experimentally determined, and the effector was implicated as having anti-bacterial properties (Brooks et al., 2013).

Similarly, the C-terminal region of VgrG2b of the *P. aeruginosa* H2-T6SS has been linked to anti-eukaryotic virulence, by specifically inducing internalisation of *P. aeruginosa* within epithelial cells as a result of an interaction between VgrG2b and

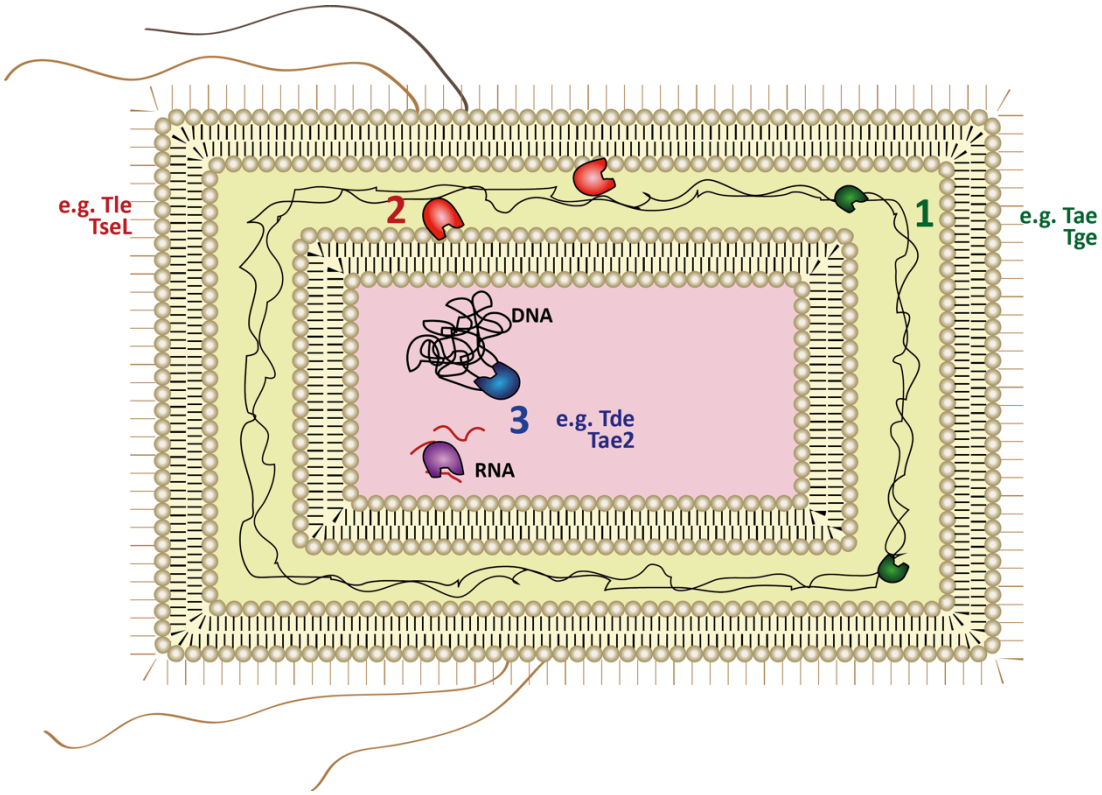

Figure 1.7 An overview of the molecular targets for anti-bacterial T6SS-dependent effectors. Illustration shows potential molecular targets of T6SS dependent anti-bacterial effectors, (1) the peptidoglycan layer, (2) phospholipid bilayers and (3) cytoplasmic targets, such as DNA or RNA. Two examples of known T6SS effectors are given for each target indicated (see text for details).

the γ-tubulin ring complex (γTuRC), a component of the host cell's microtubule machinery (Sana et al., 2015). A further example of a characterised evolved TssI is VgrG-1 in *Aeromonas hydrophila* (AHA_1119) that has an ADP- ribosyltransferase domain, which is able to induce actin dysfunction that results in apoptosis of eukaryotic cells (Pukatzki et al., 2009; Suarez et al., 2010).

1.5.2 Peptidoglycan-targeting effectors

Advances in proteomics has made a major contribution to the progression in T6SS-dependent effector identification as it has allowed identification of non-TssI effectors which would have been more difficult to identify bioinformatically than TssI derivatives. Taking a shotgun proteomics approach Hood and co-workers were the first to demonstrate that H1-T6SS in *P. aeruginosa* was able to export anti-bacterial effectors, which were termed Tse1-3 (Hood et al., 2010). These effectors were paired with corresponding immunity proteins to prevent self-toxicity. Tse1 and Tse3 were later shown to have peptidoglycan-degrading activity when injected into the periplasm of a recipient bacterial cell by the T6SS (Russell et al., 2011).

Peptidoglycan in Gram-negative bacteria is composed of a glycan backbone structure of alternating subunits of *N*-acetylglucosamine (Glc*N*Ac) and *N*-acetylmuramic acid (Mur*N*Ac) linked by a β-(1,4)-glycosidic bond. A short peptide of differing length, but usually consist of L-Ala-D-Glu-*m*-DAP-D-Ala-(D-Ala), is attached to the lactyl ether group on the 3-carbon of Mur*N*Ac (reviewed in Vollmer et al. (2008)). Amide crosslinks are formed between the peptides on different glycan strands, specifically between D-Ala and *m*-DAP, through their free carboxyl and amino groups, respectively (Figure 1.8).

It is now evident that there are superfamilies of small periplasmic peptidoglycan-degrading effectors (and families of immunity proteins) prevalent in many T6SS-containing species that are anti-bacterial. This includes a superfamily of amidase effector-immunity pairs that are responsible for the hydrolysis of amide bonds in the peptide crosslinks, Tae-Tai (for type VI amidase effector/immunity). The Tae1 and Tae4 family of effectors hydrolyse the amide bond between D-Glu and *m*-DAP in the stem of the peptide extension, and Tae2 and Tae3 families

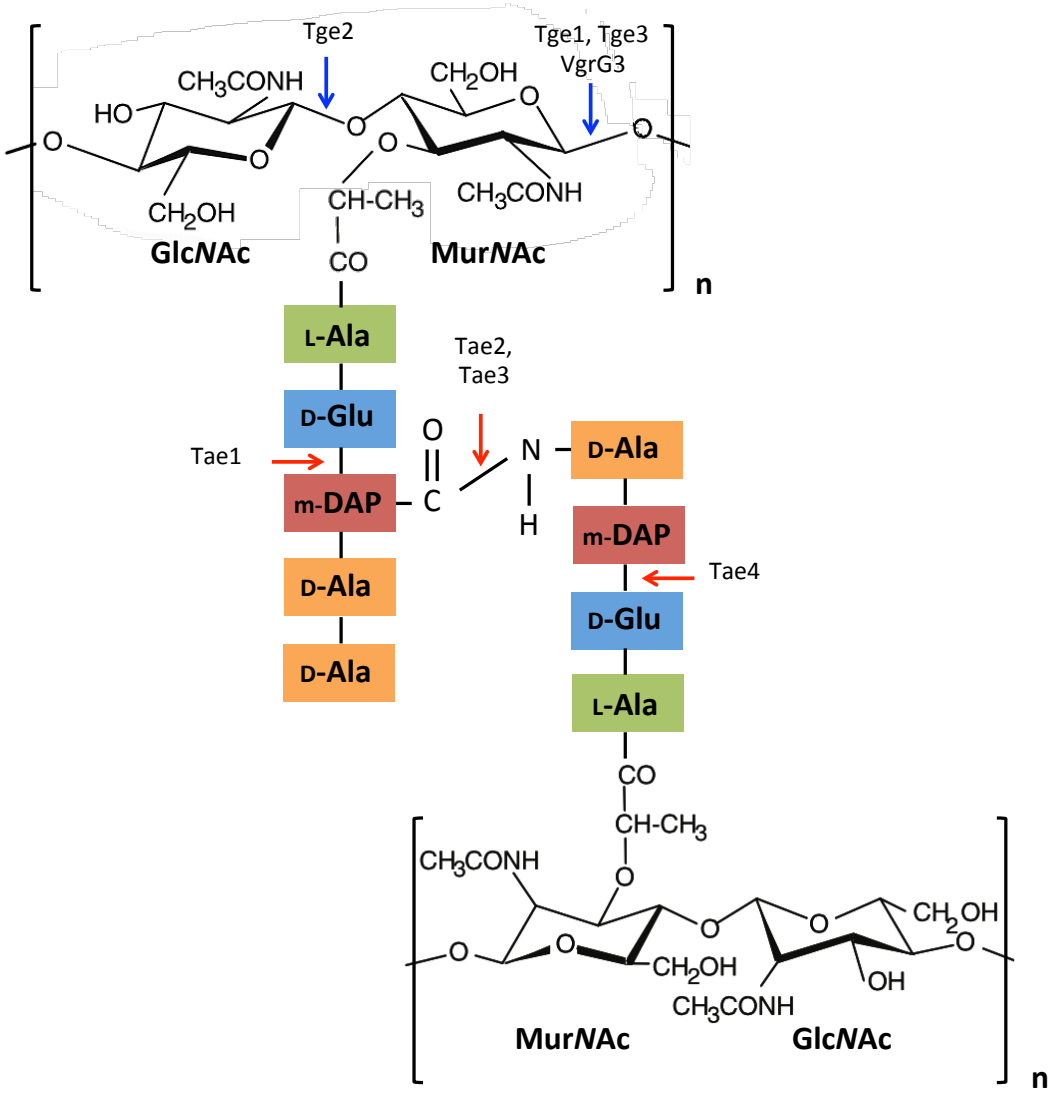

Figure 1.8 Bond cleavage specificity of the peptidoglycan-degrading T6SS-dependent effectors. Diagram shows the simplified structure of Gram-negative peptidoglycan along with the bond specificities of peptidoglycan hydrolase T6SS effectors. The effectors of the Tae superfamily are amidases that hydrolyse amide bonds between and within peptide crosslinks (red arrows), as indicated. The Tge effector superfamily and the CTD of VgrG-3 are glycoside hydrolases effectors that hydrolyse the β-(1,4)-glycosidic bond between *N*-acetylglucosamine (Glc*N*Ac) and *N*-acetylmuramic acid (Mur*N*Ac) (blue arrows). See text for further details.

between crosslinking *m*-DAP and D-Ala residues (Russell et al., 2012) (Figure 1.7).

Another peptidoglycan hydrolysing superfamily is the glycoside hydrolase effector-immunity pairs, Tge-Tgi (for type VI glycoside effector/immunity). These effectors hydrolyse β-(1,4)-glycosidic bonds between GlcNAc and MurNAc. The Tge1, and possibly Tge3, family of effectors act as muramidases, whereas the Tge2 family are suggested to be glucosaminidases (Figure 1.7) (Whitney et al., 2013).

Some of these peptidoglycan degrading effectors have been experimentally confirmed, including the family 1 Tae effector Tse1 ($Tae1^{PA}$) in *P. aeruginosa* (Hood et al., 2010; Russell et al., 2011), family 2 Tae effector $Tae2^{BT}$ in *B. thailandensis* (Russell et al., 2012), and family 4 Tae effectors Ssp1 ($Tae4.1^{SM}$) and Ssp2 ($Tae4.2^{SM}$) in *S. marcescens* (Murdoch et al., 2011; Fritsch et al., 2013). The family 1 Tge effector Tse3 ($Tge1^{PA}$) in *P. aeruginosa* and the family 2 Tge effector $Tge2^{PP}$ in *P. protegens* have also been experimentally confirmed (Hood et al., 2010; Whitney et al., 2013).

Recently, additional anti-bacterial periplasmic targeting H1-T6SS-dependent effectors have been described in *P. aeruginosa*, Tse4 and Tse5, but their specific targets molecular are unknown (Whitney et al., 2014). The CTD of the evolved TssI in *V. cholerae*, VgrG-3, has also been classified as a muramidase enzyme, but not a member of the Tge superfamily (Russell et al., 2014).

1.5.3 Membrane-targeting effectors

1.5.3.1 Lipases and phospholipases

Phospholipases are a subset of lipase enzyme, which are a type of esterase. Other esterases include endo- and exo-nucleases, phosphatases and sulphatases, all are responsible for catalysing a fundamental reaction that involves the splitting of an ester bond by water (hydrolysis) to produce an acid and alcohol (Figure 1.9). Lipases specifically catalyse the hydrolysis of ester bonds in lipid molecules in a base catalysed hydrolysis reaction. A variety of lipid molecules occur in nature, including phospholipids, mono-, di- and triglycerides, fatty acids, sphingolipids and sterol lipids. Therefore, lipases are required to show substrate specificity.

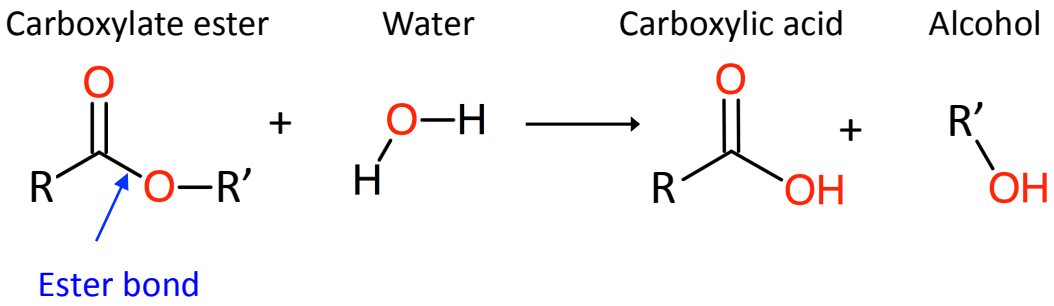

Figure 1.9 Hydrolysis of an ester bond. Diagram showing a simplified esterase reaction where an ester bond is split by water in a hydrolysis reaction that produces an acid and an alcohol as products. R and R’ groups present alkyl groups.

Nevertheless, it appears many lipases use a hydrolysis mechanism that involves a catalytic triad of serine, histidine, aspartate residues, including human pancreatic lipases (Winkler et al., 1990), fungal lipases (Brady et al., 1990) and bacterial lipases, such as the LipA lipase from *B. glumae* (Noble et al., 1993) and the *B. cepacia* lipase (Kim et al., 1997). The catalytic triad of many of these enzymes is located in a structural fold that is found in a diverse range of hydrolytic enzymes, the α/β-hydrolase fold (Ollis et al., 1992). Some other hydrolytic enzymes, including serine proteases (such as trypsin), also use the same three residues in this catalytic triad, as a basis for their catalytic action (Hedstrom, 2002).

1.5.3.2 Catalytic triad mechanism of a lipase

The general accepted principle of the hydrolysis of an ester bond using a catalytic triad of serine, histidine and aspartate residues involves the following covalent catalysis mechanism (reviewed in Dodson (1998)). To begin, the acidic side chain of the aspartate residue causes alignment and polarisation of the imidazole side chain of the histidine residue due to hydrogen bond formation, such that the imidazole moiety is able to act a strong general base that deprotonates the hydroxyl group of the serine side-chain, thereby activating the nucleophile. The serine sidechain oxygen in this state is able to perform a nucleophilic attack on the carbon in an ester carbonyl group in the substrate (Figure 1.10A). This results in the formation of a tetrahedral intermediate, where the oxygen atom of the carbonyl group has gained an electron. This negatively charged intermediate is thought to be stabilised by an oxyanion hole located in the active site. A carbonyl group is quickly re-established in this intermediate by a proton donated by the protonated histidine residue to facilitate the first leaving group (Figure 1.10B). Thus, the alcohol component of the ester is expelled, leaving the acid moiety as an acyl-enzyme intermediate. The carbonyl carbon of the intermediate is then subjected to another nucleophilic attack, this time by an activated water molecule (hydroxyl anion) generated by proton transfer from the water molecule to the histidine residue (Figure 1.10C). Again this creates a tetrahedral intermediate. The final step in the reaction is the re-generation of the carbonyl group by donation of a proton by the histidine residue to facilitate the second leaving group, the carboxylic acid

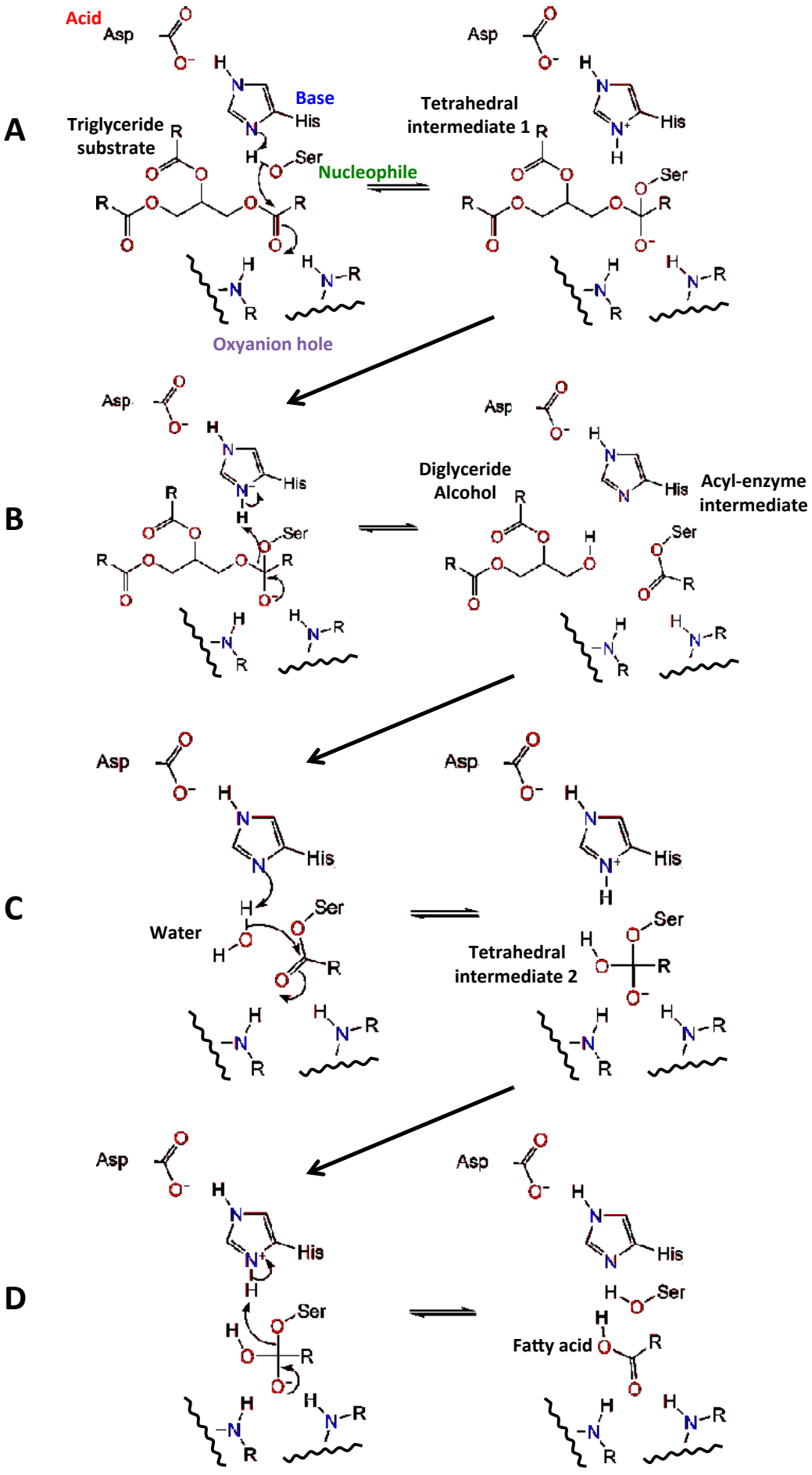
A
Acid
Asp
Base
His
Triglyceride substrate
Ser
Nucleophile
Tetrahedral intermediate 1
Oxyanion hole
B
Diglyceride Alcohol
Acyl-enzyme intermediate
C
Water
Tetrahedral intermediate 2
D
Fatty acid

Figure 1.10 Catalytic mechanism of the lipase catalytic triad. Diagrammatic presentation (above) of the reaction mechanism involved in the hydrolysis of a *sn*-1 ester bond in a triglyceride (triacyl glycerol) by the conserved serine, histidine, aspartate catalytic triad. For details of each step involved in (A) to (D) see text.

(Figure 1.10D). Thus, the serine residue in the active site is regenerated, and the fatty acid is expelled from the active site.

1.5.3.3 Types of phospholipases

There are several different classes of phospholipase enzymes, each of which hydrolyse the phospholipid substrate at specific ester bond positions (Figure 1.11) (reviewed in Richmond and Smith (2011)). This includes the acyl hydrolases phospholipase A_1 (PLA_1), which hydrolyses the ester bond at the *sn*-1 carbon position in a phospholipid, phospholipase A_2 (PLA_2), which cleaves at the *sn*-2 carbon position (Haas et al., 1962) and phospholipase B that cleaves at both *sn*-1 and *sn*-2 positions. There are also the phosphodiesterases, phospholipase C, that cleave the phosphodiester bond between the *sn-3* carbon and the phosphoryl head group just before the phosphate, and phospholipase D, which is responsible for the cleavage of the *sn*-3 phosphodiester bond at the other side of the phosphate. Most phospholipases are also capable of hydrolyzing ester bonds of other lipid structures.

1.5.3.4 Superfamily of phospholipase effectors

A T6SS-dependent lipase effector superfamily has recently been identified that encompassed effectors that possess phospholipase A_1, phospholipase A_2, or phospholipase D activity (Russell et al., 2013). These are termed type VI lipase effectors (Tle), which appear to have anti-bacterial properties and specifically target membrane phospholipids. These effectors are further split into 5 families, Tle1-Tle5 based on conserved amino acid sequences within and neighbouring the predicted active site of the enzyme. Tle1-Tle4 family members contain a conserved GxSxG motif in the active site, including the experimentally characterised $Tle1^{BT}$ anti-bacterial effector encoded by BH_I2698 in *B. thailandensis,* which is a substrate of T6SS-1 (Russell et al., 2012; Russell et al., 2013).

Tle5 family members contain two separated HxKxxxxD motifs, which includes a previously identified *P. aeruginosa* phospholipase D enzyme termed PldA, renamed $Tle5^{PA}$, which was also shown to have anti-bacterial activity and is secreted by the H2-T6SS. Interestingly, $Tle5^{PA}$ has also been noted to have anti-eukaryotic activity, suggesting it functions as a transkingdom effector similar to

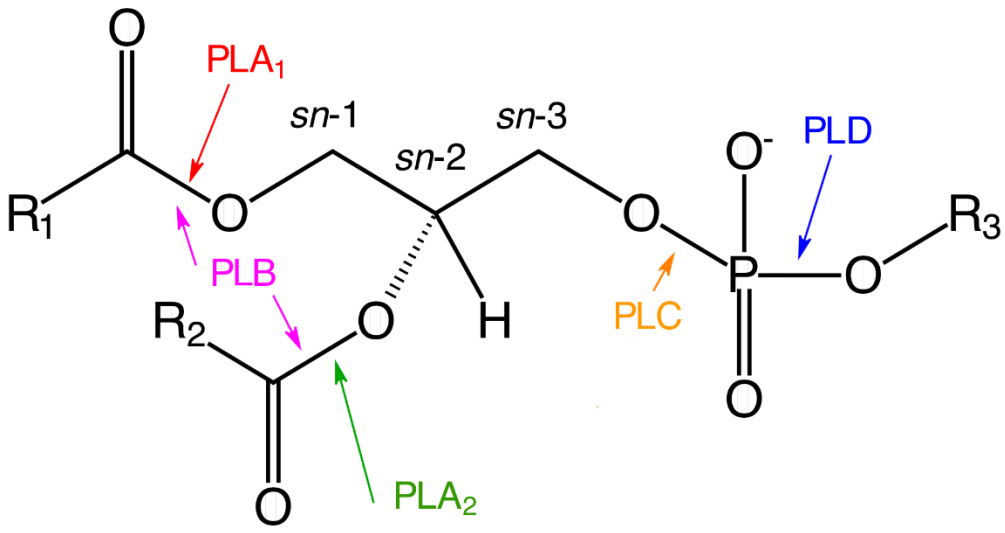

Figure 1.11 Overview of the specificity of classes of phospholipase enzymes. Illustration of the specific ester bonds within a phospholipid molecule that are cleaved by particular classes of phospholipase, including phospholipase A_1 (PLA_1), phospholipase A_2 (PLA_2), phospholipase B (PLB), phospholipase C (PLC) and phospholipase D. The bonds that are cleaved are indicated by labelled arrows.

another *P. aeruginosa* transkingdom phospholipase D enzyme, PldB, secreted by the H3-T6SS. Both of these effectors activate the PI3K/Akt signalling pathway in a eukaryotic host to enhance bacterial internalisation (Jiang et al., 2014).

A further Tle lipase effector, $Tle2^{VC}$ in *V. cholerae* (also known as TseL), was found to have anti-bacterial activity dependent on it lipase activity, as well as a role in anti-eukaryotic predation (Dong et al., 2013). Note however, all of these effectors appear too large to be directly transported through the hollow TssD tube, unlike the small peptidoglycan-degrading Tae effectors.

As with the peptidoglycan-targeting effectors, the membrane-targeting effectors are paired with corresponding immunity proteins that possess Sec-dependent signal sequences. Thus, members of the Tle1-Tle5 families of effectors are encoded adjacent to corresponding *tli* genes.

1.5.3.5 Pore-forming effectors

Further membrane targeting effectors include a pore forming colicin-like effector of *V. cholerae*, VasX, that was found to exhibit anti-amoeboid properties and whose expression is regulated by a σ^{54}-dependent activator, VasH (Miyata et al., 2011). It was characterised as targeting the inner membrane of target bacterial cells from the periplasm with the aid of an accessory protein VasW (Miyata et al., 2013). BTH_I2691, a substrate of the T6SS-1 of *B. thailandensis*, is also predicated to have a colicin-like structure, indicating a mechanism of action similar to that of VasX (Russell et al., 2012). As expected both of these effectors have cognate immunity proteins (Russell et al., 2012; Miyata et al., 2013). Recently, both VasX and BTH_12691 were found to contain a similar N-terminal motif that is present in a variety of proteins that are located within the vicinity of T6SS clusters or T6SS-related genes, such as *tssI*. This motif was term MIX (marker for type VI effectors) and was suggested to act as an identifier for a subset of T6SS substrates (Salomon et al., 2014a).

1.5.4 Cytoplasmic targeting effectors

Several cytoplasmic targeting effectors have been described, the first, Tse2, is specified by the *P. aeruginosa* H1-T6SS. This effector demonstrated toxicity when ectopically expressed in the cytoplasm of bacterial and eukaryotic cells (Hood et al., 2010), but only displayed growth inhibiting properties towards other bacterial cells and not eukaryotes when delivered by the H1-T6SS (Li et al., 2012). However, the bacteriostatic activity was manifested against sister *P. aeruginosa* cells (Hood et al., 2010) and not towards other competing bacterial species, such as *B. thailandensis* (Leroux et al., 2012). The molecular target of Tse2 is unknown, however, is has been suggested that it may function as a nuclease effector, although experimental evidence is lacking (Li et al., 2012).

1.5.4.1 Nuclease effectors

Following on from this, a superfamily of DNase effectors has been described, termed Tde effectors (type VI DNase effector). The main characterised examples occur in the plant pathogen *A. tumefaciens* (Ma et al., 2014). They contain a C-terminal toxin_43 domain with a conserved HxxD motif that is required for catalysis. This domain was initially thought to specify RNase activity (Zhang et al., 2012). However, Ma and co-workers found that effectors containing this domain actually exerted DNase activity (Ma et al., 2014). The superfamily is split into seven families based on the domain architecture of the N-terminus of the proteins. Some of which contain specific 'domain of unknown functions', such as DUF4150, or PAAR domains. Interestingly, Tde1 and Tde2 from *A. tumefaciens* aided inter-bacterial competition by the producing organism but only *in planta*, suggesting these effectors are required for growth advantages in specialised niches.

1.5.4.1.1 Catalytic mechanism of endonucleases

Using the ββα-Me-finger endonuclease of *S. pyogenes* Spd1 as an example, the following catalytic mechanism is typical of endonucleases. The active site is arranged in such a way that a histidine residue is central to catalysis by acting as general base that causes the deprotonation of a nearby water molecule. This in turn results in a nucleophilic attack on the scissile phosphate group within the

phosphodiester bond between two nucleotides (Korczynska et al., 2012). This is facilitated by the metal ion acting as a Lewis acid, thereby accepting electrons to stabilise the negatively charge phosphate transition state and the leaving group. The metal ion is coordinated in a metal cluster by two other essential residues. For Spd1, this is an asparagine residue that coordinates the Mg^{2+} directly, and indirectly through a glutamate residue. The glutamate is proposed to coordinate two water molecules to bridge with the metal ion, and the further essential arginine residue is required for stabilisation of the catalytic product to limit a reverse reaction between transition states (Korczynska et al., 2012).

1.5.4.1.2 Roles of extracellular nucleases and nuclease toxins

A wide variety of roles have been proposed for extracellular nucleases. *S. marcescens* extracellular endonuclease (Sm_2) has been postulated to be involved in scavenging under nutrient-limiting conditions, using the ribose components of the nucleotide monomers as a carbon source or recycling the nucleotides for its own DNA/RNA synthesis (Beliaeva et al., 1976; Benedik and Strych, 1998). However, experimental evidence is lacking for this. Other secreted endonucleases, including the *V. cholerae* nuclease Dns, an EndA type nuclease, may be involved in resisting natural transformation events from exogenous DNA, as well as modulating extracellular DNA, an important component of bio-films structures (Focareta and Manning, 1991; Blokesch and Schoolnik, 2008; Seper et al., 2011).

Pertinently, a wide array of nuclease proteins produced by both prokaryotes and eukaryotes are known to be toxins. This includes the highly specific fungal nuclease, α-sarcin, produced by *Aspergillus giganteus* that acts as an RNase enzyme to cleave a single phosphodiester bond in 28S rRNA (Korennykh et al., 2007) and a DNase toxin in the snake venom of *Bothrops atrox* (Georgatsos and Laskowski, 1962).

It appears that bacteria harbour the largest reservoir of nucleic acid targeting toxins, many of which target other bacteria in a competitive growth environment, termed bacteriocins. These include colicin toxins in *E. coli*, such as Colicin E2 (Cascales et al., 2007) and the variable C-terminal domains of the CdiA protein contact-dependent growth inhibition system (CDI) (Poole et al., 2011).

Some nucleases are involved in host DNA damage in toxin-antitoxin systems (TA) that ultimately result in cell death for the toxin-producing bacterium, which is usually promoted under stress conditions (Yamaguchi et al., 2011). Moreover, T6SS-dependent DNase effectors have been described that are important for inter- and intraspecies bacterial competition, including Rhs-related effectors (Zhang et al., 2012; Koskiniemi et al., 2013; Hachani et al., 2014; Diniz and Coulthurst, 2015) and a superfamily of DNase effectors that are important for *in planta* interspecies competition in *A. tumefaciens* (Ma et al., 2014).

1.5.4.2 Rhs effectors

Other cytoplasmic targeting effectors are components of Rhs (rearrangement hot-spot) elements. Rhs proteins are generally large filamentous proteins that contain an N-terminus with a PAAR domain, RHS sequence repeats (GxxxRYxYDxxGRl(I/T)), an RHS repeat-associated core that contains a self-cleavage site and then C-terminal toxin domain that is highly variable (Wang et al., 1998; Zhang et al., 2012; Busby et al., 2013). This latter feature defines them as polymorphic toxins (Jamet and Nassif, 2015). The recent structure of an Rhs protein, 'C protein' from the tripartite ABC insecticidal toxin from entomopathogen *Yersinia entomophaga*, observed that the N-terminal RHS repeat region forms as extended β-sheet-containing protective shell around the C-terminal toxin domain (Busby et al., 2013). This structure leaves the RHS-associate core region exposed, allowing cleavage and release of the toxin when required (Busby et al., 2013). Each RHS repeat motif was shown to correspond to a β-strand-turn-β-strand structural motif and it was proposed that all Rhs proteins would be structurally arranged in this way (Busby et al., 2013). The common YD repeat motif was also suggested to form this same structural motif.

Some Rhs proteins have nuclease domains located at the C-terminus. These include RhsA and RhsB in *Dickeya dadantii.* RhsB possess a C-terminal domain with an HNH endonuclease motif that confers a competition advantage over other bacterial species in a T6SS-dependent manner (Koskiniemi et al., 2013). Other examples of similar characterised effectors include Rhs1 and Rhs2 in *S. marcescens* which are mostly important for T6SS-dependent intraspecies bacterial competition

(Fritsch et al., 2013; Diniz and Coulthurst, 2015). Interestingly, the C-terminal domain of Rhs2 was noted to have homology to the HNH endonuclease motif and as expected conferred DNase activity, whereas Rhs1 did not exhibit either of these characteristics. Its cytoplasmic molecular target remains unknown.

Three *tssI* linked genes in *P. aeruginosa* encode anti-bacterial effectors that act on cytoplasmic targets. Each of the gene products contains either a RHS-repeat region or PAAR motif with a toxic C-terminal domain. One of these, PA0099, was predicted to possess nuclease activity, due to the presence of a GHH signature-containing HNH/endonuclease VII superfamily domain (Hachani et al., 2014).

1.5.5 Effector delivery

The method of T6SS-dependent effector delivery is an area of research that still remains to be fully understood. There is evidence to suggest the T6SS may use several methods to translocate effector proteins from out of the bacterial cytoplasm and into its target host cell, summarised in Figure 1.12. It is possible several mechanisms may be used in one firing action of the system, delivering several different effectors at one time (Shneider et al., 2013). Two broad mechanisms have been suggested, where the effectors secreted by each of these mechanisms are classified as either cargo effectors or specialised effectors, and typically encoded close to cognate *tssI* or *tssD* genes (reviewed in Durand et al. (2014)). Small effector proteins may be translocated through/with the TssD inner tube, whilst larger effectors may delivered by association with/as a TssI spike protein, as proposed by the model termed MERV, multiple effector translocation VgrG (Shneider et al., 2013).

1.5.5.1 TssD-mediated effector delivery

Upon initial discovery of the T6SS, is was postulated the system may use the TssD tubular structure as a conduit to translocate small folded effector proteins or unfolded (or partially folded) effectors (Mougous et al., 2006). However, rather than travel through the tubular structure there is now evidence to suggest that some small folded proteins, such as the Tse1-Tse4 secreted by the H1-T6SS in *P. aeruginosa* (two of which are confirmed PG hydrolases), can interact with

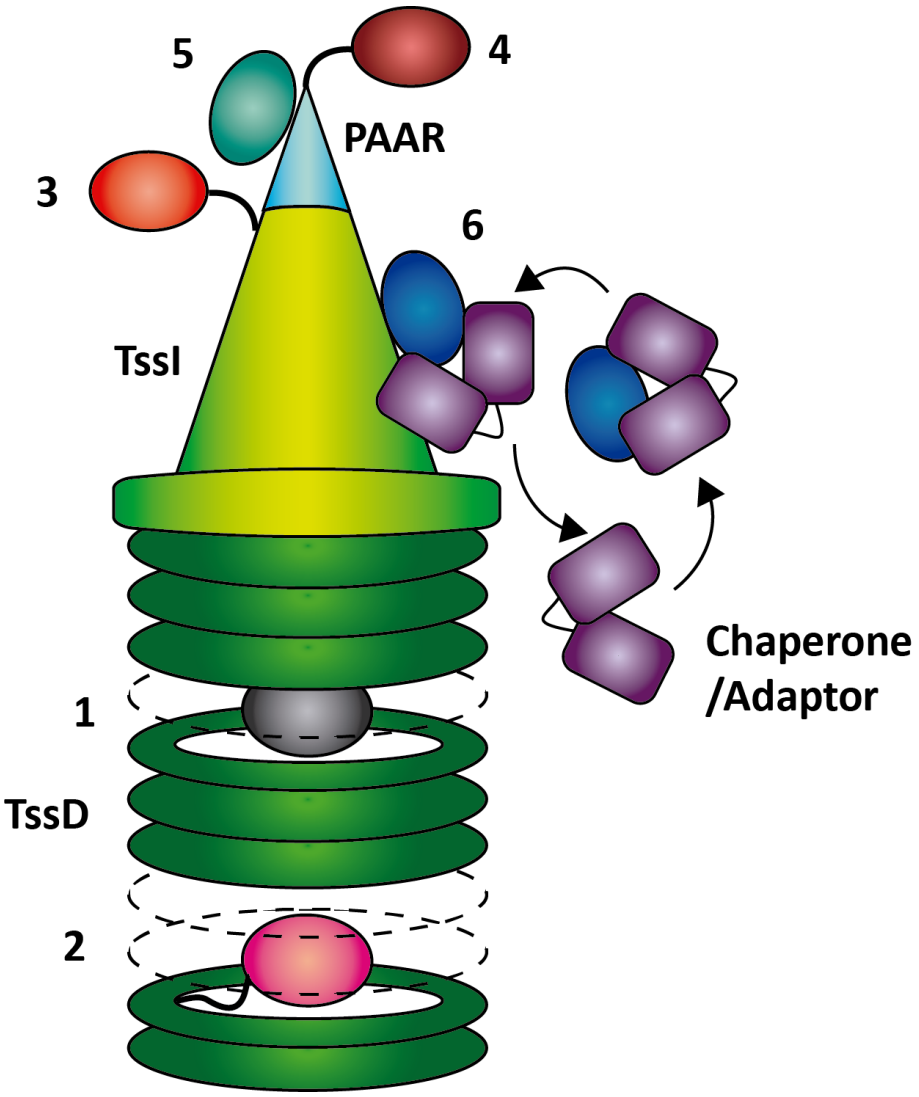

Figure 1.12 General model for T6SS effector delivery. Diagram showing the current models suggested for how T6SS effectors are delivered by the system. (1) and (2) are TssD-mediated delivery methods, either by TssD entrapping the effector within its lumen (1), or specialised evolved TssD proteins with C-terminal effector-like domains (2). (3)-(6) use TssI as a mediator for effector delivery, known as the MERV model. Effectors delivered by (3) are TssI proteins with C-terminal effector extensions, (4) are specialised PAAR proteins that have C- or N-terminal extensions, (5) are cargo effectors that can interact with either a PAAR protein or the extension domain on a specialised PAAR protein and finally (6) are proteins that can directly interact with TssI or an extension domain on TssI, forming a complex that is secreted. Evidence suggests that effectors of type (6) may use chaperone proteins to facilitate their secretion by stabilising the effector and docking it onto the TssI protein. Chaperones may not be secreted. See text for further details.

the inner face of TssD ring structures to stabilise the effectors. Thus, acting as a chaperone-like protein whilst also entrapping the cargo within the internal 40 Å lumen of the structure (Silverman et al., 2013; Whitney et al., 2014) (1 in Figure 1.12). The effector cargo is released when TssD is secreted into its target location. Other small effectors such as EvpP in *Edwardsiella tarda* have been implicated to be translocated by this method (Lin et al., 2013). This method ensures that such effectors are only secreted by a particular T6SS.

Another TssD-mediated method may occur by specialised forms of TssD, 'evolved TssDs', which contain C-terminal enzymatic domains (2 in Figure 1.12), such as that discovered in *Salmonella enterica subsp. Arizonae*. This TssD is fused to a pyocin and a HNH endonuclease domain (Blondel et al., 2009). However, no experimental evidence has been presented to verify this, or any another evolved TssD, as being a functional subunit of the T6SS.

1.5.5.2 TssI-mediated effector delivery

The second broad mechanism for T6SS effector secretion is by TssI-mediated delivery. This includes specialised evolved TssI proteins with C-terminal extension domains (number 3 in Figure 1.12), as previously discussed in Section 1.5.1. Moreover, it may also include additional proteins that can bind to TssI proteins to allow effector secretion. This includes the use of PAAR repeat proteins, that are thought to interact with and sharpen the tip of TssI proteins, which is essential for T6SS secretion and function (Shneider et al., 2013).

The PAAR domain proteins form part of a superfamily, which also contains PF05488, COG4104 and DUF4150 family proteins (Shneider et al., 2013). There are several classes of PAAR protein that contain additional N- or C-terminal extensions, some with predicted enzymatic activity, e.g. nuclease activity, that may be further specialised effectors (4 in Figure 1.12). These extended PAAR proteins include Rhs proteins. Some extension domains may be involved in protein-protein interactions, e.g. the transerythrin domain (Shneider et al., 2013). It was suggested some effector proteins might be able to bind to 'core' PAAR proteins or PAAR proteins with N- or C-terminal extensions via the extension region to fix them indirectly onto

TssI spike proteins (5 in Figure 1.12). However, there is no direct evidence for a PAAR protein-effector interaction.

Recent findings have provided evidence for a superfamily of additional adaptor or chaperone proteins that works independently of PAAR-containing proteins. This superfamily contains a domain of unknown function, DUF4123, and is generally encoded directly upstream of its cognate effector gene. Representatives of this superfamily were termed TEC proteins (T6SS effector chaperone) or Tap (T6SS accessory protein). An exemplar TEC/Tap protein is in *V. cholerae* encoded by VC1417, which is required for the secretion and effector-mediated bacterial killing of the T6SS effector, $Tle2^{VC}$ (TseL) (Liang et al., 2015; Unterweger et al., 2015). A direct interaction between the VC1417-encoded TEC protein and its $Tle2^{VC}$ effector protein, and between this TEC and the TssI protein encoded in the vicinity of these genes (VgrG-1), and an interaction between $Tle2^{VC}$ and VgrG-1 were all demonstrated (Liang et al., 2015; Unterweger et al., 2015). However, the chaperone protein is not secreted, implying that the chaperone is required for mediating an interaction with the TssI protein, but once the effector has been docked the chaperone is released (Unterweger et al., 2015) (6 in Figure 1.12).

A further accessory protein specific for Rhs1 in *S. marcescens* has also been suggested, termed EagR1 (effector accessory gene, with Rhs1), which was required for the secretion and effector-mediated anti-bacterial activity of Rhs1 (Diniz and Coulthurst, 2015). This adaptor is homologous to other proteins encoded in similar locations. These include genes encoded upstream of genes encoding Rhs- and PAAR-containing T6SS effectors, including PA0094 located upstream from a gene encoding the anti-bacterial PAAR-containing T6SS-dependent protein PA0093 of *P. aeruginosa* (Hachani et al., 2014) and cytotoxic Rhs proteins RhsA and RhsB of *D. dadantii* (Koskiniemi et al., 2013).

1.6 Hypotheses

Using evidence provided in the literature regarding the T6SS, its role and the types of effectors it secretes in other Gram-negative bacteria, as well as work previously undertaken in our laboratory, the following hypotheses may be proposed:

1. Bcc bacteria, including *B. cenocepacia* use its ancestral T6SS-1 to target other bacteria and/or eukaryotes, which it does by secreting T6SS-dependent effectors that have specific molecular targets.
2. In addition to transcriptional regulation, *B. cenocepacia* may regulate its T6SS using putative post-transcriptional regulators. These may be exploited for the discovery of novel effector proteins.
3. Proteins with predicted enzymatic domains encoded within *tssI* clusters in the *B. cenocepacia* genome may function as T6SS-dependent effectors. This may include effectors with phospholipase activity, nuclease activity or peptidoglycan hydrolase activity.
4. Each of these effectors will have a corresponding immunity protein/antitoxin that provides protection to the producing bacterium against the enzymatic activity of the putative effector protein.

1.7 Aims and objectives:

To test the hypotheses proposed in Section 1.6, this work centres on the following aims and objectives:

1. Evaluate the anti-bacterial and/or anti-eukaryotic role of the T6SS in the Bcc bacterium *B. cenocepacia* using bacterial competition assays and eukaryotic infection models.
2. Investigate mechanisms for T6SS-1 regulation with the aim of increasing the activity of the T6SS for novel effector discovery. This will be carried out by genetic inactivation of putative regulators identified by bioinformatic analysis and evaluation of their effects on T6SS activity in *B. cenocepacia*.
3. Identify putative T6SS-dependent effectors and their cognate immunity proteins in *B. cenocepacia* by bioinformatic analysis and mass spectrometry.
4. Characterise the enzymatic properties, function and secretion of selected putative T6SS-dependent effectors identified in *B. cenocepacia*. Verify the identified immunity proteins/antitoxins for these putative effectors. This will be carried out by enzymatic studies, ectopic expression, interaction studies and *B. cenocepacia* mutant generation.

Chapter 2: Materials and methods

2.1 Bacteriological techniques

2.1.1 Bacterial strains, maintenance and growth conditions

The bacterial strains used in this study (Table 2.1) were routinely cultured from -80°C glycerol stocks (15% (v/v) glycerol) on appropriate agar plates and grown at temperatures between 25°C and 37°C for 16 to 72 hours dependent on optimal culturing conditions for the species, as indicated (Table 2.2). Plates were sealed with parafilm and stored in the dark at room temperature for *B. cenocepacia* strains or 4°C for all other bacterial strains for further strain maintenance. The viability of *B. cenocepacia* is reduced if stored at 4°C.

Table 2.1 Bacterial strains used in this study.

Strain	Genotype/Description	Source/Reference
***Burkholderia cenocepacia* strains**		
H111	CF isolate from patient at Medizinische Hochschule, Hannover (1993), serum-resistant.	(Römling et al., 1994)
H111^{S}	Spontaneous chromosome 3 deficient derivative of strain H111, serum sensitive.	Thomas, unpublished.
H111Δc3	Engineered chromosome 3 deletion derivative of strain H111.	(Agnoli et al., 2012)
Pc715j	CF isolate from patient at Rainbow Babies and Children's Hospital, Ohio, ET12 lineage.	(McKevitt et al., 1989)
K56-2^{vir}	CF isolate from patient at Hospital for Sick Children, Toronto, Canada, ET12 lineage.	L. Eberl, University of Zurich. (Mahenthiralingam et al., 2000b).
K56-2^{att}	As K56-2^{vir}, but a virulent in Zebrafish infection model, SHV^{-}.	Lab stock.
H111-*tssA*::Tp	H111 mutant with *dfr* cassette inserted into tssA gene in reverse orientation to *tssA*.	(Shastri, 2011)
H111-*tssK*::Tp	H111 mutant with *dfr* cassette inserted into *tssK* gene in same orientation to *tssK*.	(Shastri, 2011)
H111-*tssM*::Tp	H111 mutant with *dfr* cassette inserted into *tssM* gene in reverse orientation to *tssM*.	This study.
H111-Δ*tssM*	H111 mutant with in-frame deletion of internal XhoI fragment of *tssM*.	This study.
H111-*tagX*::Tp	H111 mutant with *dfr* cassette inserted into *tagX* gene in same	This study.

	orientation to *tagX*.	
H111^{S}-*tagF*::Km	H111^{S} mutant with *nptII* cassette inserted into *tagF* gene in reverse orientation to *tagF*.	Bull and Thomas, unpublished.
H111-*tagF*::Km	H111 mutant with *nptII* cassette inserted into *tagF* gene in reverse orientation to *tagF*.	This study.
H111Δc3-*tagF*::Km	H111Δc3 mutant with *nptII* cassette inserted into *tagF* gene in reverse orientation to *tagF*.	This study.
H111^{S}Rif	Spontaneous c3^{-} mutant, serum sensitive and spontaneous rifampicin resistance.	This study.
H111-pC3::*gabD*	H111 containing mobilisation element as pSHAFT2 suicide vector inserted into *gabD* on chromosome 3 to be used as pC3 donor strain, (Cm^{r}).	Agnoli, unpublished.
H111^{S}Rif/pC3	H111^{S}Rif with reintroduced chromosome 3, as pC3-*gabD*::pSHAFT2 element, (Cm^{r}).	This study.
H111^{S}Rif-*tagF*::Km/pC3	H111sRif/pC3 mutant with *nptII* cassette inserted into *tagF* gene in reverse orientation to *tagF.*	This study.
H111-ΔBCAS0667	H111 mutant with in-frame deletion of BCAS0667.	This study.
H111-Δ*atsR*	H111 mutant with in-frame deletion of *atsR*.	This study.
H111-Δ*tanB^{H}*	H111 mutant with in-frame deletion of *tanB^{H}*.	This study.
H111-Δ*tanB^{H}*-*taaB1^{H}*	H111 mutant with in-frame deletion of *tanB^{H}* and *taaB1^{H}* region.	This study.
Pc715j-*tssA*::Tp	Pc715j mutant with *dfr* cassette inserted into *tssA* gene in reverse orientation to *tssA*.	(Shastri, 2011)
Pc715j-*tssK*::Tp	Pc715j mutant with *dfr* cassette inserted into *tssK* gene in same orientation to *tssK*.	(Shastri, 2011)
Pc715j-*tssM*::Tp	Pc715j mutant with *dfr* cassette inserted into *tssM* gene in reverse orientation to *tssM*.	(Shastri, 2011)
K56-2^{att}-*tssA*::Tp	K56-2^{att} mutant with *dfr* cassette inserted into *tssA* gene in reverse orientation to *tssA*.	This study.
K56-2^{att}-*tssM*::Tp	K56-2^{att} mutant with *dfr* cassette inserted into *tssM* gene in reverse orientation to *tssM*.	This study.
K56-2-*tssA*::Tp	K56-2^{vir} mutant with *dfr* cassette inserted into *tssA* gene in reverse orientation to *tssA*.	This study.

K56-2-*tssM*::Tp	K56-2^{vir} mutant with *dfr* cassette inserted into *tssM* gene in reverse orientation to *tssM*.	This study.
***Escherichia coli* strains**		
JM83	F$^-$ *ara* Δ(*lac-proAB*) *rpsL* [Φ80, *lacZ*ΔM15] *thi* (Sm^r)	(Yanisch-Perron et al., 1985)
MC1061	*hsdR araD139* Δ(*ara-leu*)7697 Δ*lacX74 galU galK rpsL* (Sm^r)	(Casadaban and Cohen, 1980)
XL1-blue	*recA1 endA1 gyrA96 thi-1 hsdR17* (r_K–m_K^+) *supE44 relA1 lac* F'[*proAB*$^+$ *lac*I^q ZΔM15::Tn10(Tc^r)]	Stratagene
CC118(λpir)	*araD139* Δ(*ara-leu*)$_{7697}$ Δ*lacX74 galE galK phoA20 thi-1 rpsE argE*(am) *recA1* λpir *rpoB* (Rf^r)	(Herrero et al., 1990)
S17-1(λpir)	*thi proA hsdR recA* RP4-2-*tet*::Mu-1 *kan*::Tn*7* λpir (Tp^r Sm^r)	(Simon et al., 1983)
SM10(λpir)	*thi thr leu tonA lacY supE recA*::RP4-2-Tc::Mu λpir. (Km^r)	(Simon et al., 1983)
BTH101	F- *cya-99 araD139 galE15 galK16 hsdR2 mcrA1 mcrB1 rpsL1* (Sm^r)	(Karimova et al., 1998)
BL21(DE3)	F$^-$ *ompT gal dcm lon hsdS*$_B$(r_B^- m_B^-) λ(DE3 [*lacI lacUV5*-T7 gene 1 *ind1 sam7 nin5*])	(Studier and Moffatt, 1986)
BL21(DE3)/pLysS	F$^-$ *ompT gal dcm lon hsdS*$_B$(r_B^- m_B^-) λ(DE3) pLysS (Cm^r)	(Moffatt and Studier, 1987)
Other bacterial species		
Acinetobacter baylyi ADP1	Unencapsulated mutant derived from soil isolate BD4.	(Juni and Janik, 1969)
Burkholderia lata 383	Soil isolate from Trinidad and Tobago (1958), prototroph.	BCCM/LMG Bacteria Collection
Burkholderia multivorans C1961	Brain abscess isolate from patient at Aberdeen Royal Infirmary, UK (1995).	(Hobson et al., 1995)
Burkholderia thailandensis E264	Rice field soil isolate from Thailand (1995).	(Smith et al., 1995)
Serratia marcescens Db10	Moribund *Drosophila* flies isolate, non-pigmented.	(Flyg et al., 1980)
Pseudomonas aeruginosa PA01	Wound isolate from patient in Melbourne.	(Holloway, 1955)
Pseudomonas putida KT2440	Spontaneous r- derivative of strain mt-2.	(Bagdasarian et al., 1981)
Pseudomonas fluorescens ATCC 17571	Strain PJ 682, biotype C, group IV. Isolated from polluted seawater, Oresund, Denmark.	(Jessen, 1965; Stanier et al., 1966)
Pseudomonas fluorescens HLS1	Spontaneous rifampicin-resistant derivative of wild-type ATCC 17571.	This study.

Abbreviations: Cm^r, chloramphenicol-resistant; Km^r, kanamycin-resistant; Sm^r, streptomycin-resistant; Rf^r, rifampicin-resistant; Tc^r, tetracycline-resistant; Tp^r, trimethoprim-resistant.

Table 2.2 Optimal culturing conditions for bacterial species from glycerol stocks used in this study.

Bacterial species	Agar plate type	Incubation temperature	Incubation period (hours)
B. cenocepacia H111, Pc715j, K56-2	M9 minimal, 0.5% glucose	37°C	64 - 72
B. thailandensis	M9 minimal, 0.5% glucose	37°C	64 - 72
B. lata	M9 minimal, 0.5% glucose	37°C	64 - 72
E. coli	LB	37°C	16
P. aeruginosa	M9 minimal, 0.5% glucose	37°C	36 - 48
P. fluorescens	LB	25°C	48 - 64
P. putida	LB	30°C	24
S. marcescens	LB	30°C	24
B. multivorans	M9 minimal, 0.5% glucose	37°C	64 - 72
A. baylyi	LB	37°C	16 - 24

2.1.2 Bacteriological media

Brain-Heart Infusion (BHI)

37 grams (g) Brain-Heart infusion (BD) was dissolved in 1 litre (L) ddH_2O, and sterilised by autoclaving at 121°C at 15 psi for 20 minutes. BHI agar was made as above with addition of 1.5% (w/v) bacteriological agar (VWR International). Once cooled to ~55°C approximately 25 millilitres (mL) of the agar was poured into standard 90mm plastic petri dishes (Thermo Scientific) and left to solidify. After solidification, agar plates were dried at 42°C for 30 minutes before use.

Dialysed Brain-Heart Infusion (D-BHI)

To reduce the interference of larger M.W. proteins present in BHI on the analysis of proteins in spent culture supernatants, dialysed-BHI (D-BHI) was employed. For 500 mL of D-BHI, 9.25 g BHI was made up to 25 mL with ddH_2O, this was then dialysed against 500 mL ddH_2O overnight at 4°C using 12000-14000 MWCO dialysis tubing. The dialysate solution was sterilised by autoclaving.

Iso-Sensitest broth (IST)

Iso-Sensitest medium was required when selecting for trimethoprim-resistance in *E. coli*, as LB agar contains small amounts of thymidine that can interfere with trimethoprim selection if low levels of the antibiotic are used. 23.4 g Iso-Sensitest broth (Oxoid) was dissolved in 1 L ddH_2O, and sterilised by autoclaving. Iso-Sensitest agar was made as above with addition of 1.5% (w/v) bacteriological agar. Antibiotics were added after cooling to ~55°C.

Lennox broth agar

For improved selection of kanamycin-resistance in *B. cenocepacia,* Lennox broth agar was employed. 10 g tryptone (BD), 5 g yeast extract (Oxoid), 5 g NaCl (Fisher Scientific) and 1.5% (w/v) bacteriological agar was dissolved in 1 L ddH_2O and sterilised by autoclaving. Antibiotics were added after cooling to ~55°C.

Lysogeny broth (LB)

10 g tryptone, 5 g yeast extract, 10 g NaCl was dissolved in 1 L ddH_2O and sterilised by autoclaving. LB agar was made as above with addition of 1.5% (w/v) bacteriological agar before autoclaving. Antibiotics were added after cooling to ~55°C.

King's B agar

For distinction between fluorescent and non-fluorescent pseudomonads King's B agar was used. For 200 mL of medium, 2 g proteose peptone #2/#3 (Difco), 0.3 g anhydrous K_2HPO_4, and 1.5% (w/v) bacteriological agar were dissolved in 196 mL ddH_2O and sterilised by autoclaving. After cooling 3 mL of sterile 50% glycerol solution and 1 mL 1M $MgSO_4$ were added and plates poured. Fluorescent bacteria were identified by visualisation on a UV 302nm transluminator (UVP).

MacConkey-Lactose agar

40 g MacConkey agar base (BD) was dissolved in 900 mL ddH_2O and sterilised by autoclaving. After cooling to 55°C, 100 mL of 10% maltose solution (10

g solid maltose (Fisher Scientific) dissolved in 100 mL ddH_2O, filter sterilised) was added, gently mixed and then poured.

M9 Minimal agar

5 g D-glucose (VWR International) and 1.5% (w/v) bacteriological agar no. 1 (Oxoid) were added to 900 mL ddH_2O, and sterilised by autoclaving. After cooling, 100 mL of 10X M9 salts were added to give a final concentration of 1X M9 salts, and filter-sterilised 100 mM $CaCl_2$ and 1 M $MgSO_4$ solutions were added to give a final concentration of 100 μM and 1 mM, respectively.

M9 Minimal agar for pEX18Tp-based plasmids

M9 minimal salts agar containing glycerol, casamino acids, thiamine, X-gal, IPTG and trimethoprim were used for selection of *E. coli* transformants containing pEX18Tp-*pheS* and pEX18TpTer-*pheS*-based plasmids. For 200 mL of medium, 2 g casamino acids (BD) (final concentration 1%) and 1.5% (w/v) bacteriological agar were combined and added to 178 mL of ddH_2O, and sterilised by autoclaving. After cooling, 20 mL of 10X M9 salts was added to give a final concentration of 1X M9 salts. Sterile solutions of 50% glycerol, freshly prepared 1% thiamine, 100 mM $CaCl_2$ and 1 M $MgSO_4$ were then added to give a final concentration of 0.5%, 0.0005%, 100μM and 1mM, respectively. Following which, IPTG and X-gal stock solutions were added to give final concentrations of 100μM and 40μg/mL, respectively. Antibiotics were added after cooling to ~55°C.

10X M9 salts

Stock 10X M9 salts were prepared by combining 60 g Na_2HPO_4, 30 g KH_2PO_4, 5 g NaCl and 10 g NH_4Cl in 1 L ddH_2O, and sterilised by autoclaving.

2.1.3 Antibiotics

The appropriate antibiotics were added to the culture media at the relevant concentration for selection (Table 2.3). Antibiotics were made at the stated stock concentrations, filter sterilised if dissolved in ddH_2O and stored at -20°C.

Table 2.3 Standard antibiotic concentrations used in this study.

Antibiotic	Stock concentration (mg/mL)	Final concentration (µg/mL)	
		E. coli	***B. cenocepacia***
Ampicillin	100 in ddH_2O	100	n/a
Chloramphenicol	25 in 100% ethanol	25	50
Carbenicillin	100 in ddH_2O	200-500 (BHI)[a]	
Kanamycin	50 in ddH_2O	50	50-100
Rifampicin	50 in 100% methanol	100	100
Streptomycin	75 in ddH_2O	75	n/a
Tetracycline	10 in 50% ethanol	10	n/a
Trimethoprim	25 in DMSO	25 (IST/M9)[a] 200 (LB/BHI)[a]	25 (H111)[b] 100 (K56-2)[b]

[a]indicates the media used in conjunction with stated antibiotic concentration.
[b]indicates which *B. cenocepacia* strain the stated antibiotic concentration is applicable to.
n/a, not applicable.

2.1.4 Additional media supplements

Additional media supplements were made as stock solutions at the indicated concentration, filter sterilised if applicable and added to the appropriate media when required (Table 2.4).

Table 2.4 Additional media supplements used in this study.

Supplement	Stock concentration	Final concentration	Supplier
$CaCl_2$	100 mM in ddH_2O	100 µM	BD Biosciences
DL-4-Chlorophenylalanine (cPhe)	n/a	1 mg/mL	Acros Organics
Glucose solution	20% (w/v) in ddH_2O	1% (v/v)	Fisher Scientific
Glycerol solution	50% (v/v) in ddH_2O	0.5 to 1.5% (v/v)[a]	Fischer Scientific
Isopropyl β-D-1-thiogalactopyranoside (IPTG)	1 M in ddH_2O	100 µM to 1 mM[a]	Melford Laboratories
$MgSO_4$	1 M in ddH_2O	1 mM	BD Biosciences
Thiamine	10 mg/mL in ddH_2O	0.005 mg/mL	Sigma
5-bromo-4-chloro-3-indolyl-β-D-galactopyranoside (X-gal)	20 mg/mL in DMSO	40 µg/mL	Melford Laboratories

[a] concentration used dependent on the procedure undertaken.

2.2 Recombinant DNA techniques

2.2.1 Plasmids

The following plasmids were in this study (Table 2.5).

Table 2.5 Plasmids used in this study.

Plasmid	Features	Source/ Reference
Vector backbones		
pBluescriptII KS (+)	General cloning vector, ColE1-derived phagemid, *lacZα* MCS. (Ap^r)	(Alting-Mees and Short, 1989)
pETDuet-1	*E. coli* T7 expression vector, pBR322-derived ColE1 replicon, two T7 promoter/lac operator regions proceeding two MCS, *lacI.* (Ap^r)	Novagen.
pET-14b	*E. coli* T7 expression vector, pBR322-derived replicon, N-terminal His-tag with thrombin cleavage site. (Ap^r)	Novagen.
pET-22b(+)	*E. coli* T7 expression vector, pBR322-derived replicon, N-terminal *pelB* signal sequence for periplasmic localisation, *lacI*. (Ap^r)	Novagen.
pET-28a(+)	*E. coli* T7 expression vector, pBR322-derived replicon, N and C-terminal His-tag, thrombin cleavage site and T7-tag, *lacI.* (Km^r)	Novagen.
pBBR1MCS-1	Broad-host range cloning vector, pBBR1-replicon, *lacZα* MCS. (Cm^r)	(Kovach et al., 1994)
pBBR1MCS-2	As pBBR1MCS-1 with kanamycin resistant cassette. (Km^r)	(Kovach et al., 1995)
pSCrhaB2	Broad-host range expression vector, rhamnose inducible promoter, pBBR1-replicon, *rhaR*, *rhaS*, mob^+. (Tp^r)	(Cardona and Valvano, 2005)
pIN29	Broad-host range expression vector, *dsRed*, mob^-. (Cm^r)	(Vergunst et al., 2010)
pSHAFT2	Suicide vector derived from pUTmini-Tn*5*Cm, R6K-derived replicon, $oriT^+$. (Ap^r, Cm^r)	(Shastri, 2011)
pEX18Tp-*pheS*	Gene replacement vector with ColE1-derived replicon, $oriT^+$, mob^+ and mutated α-subunit of phenylalanyl tRNA synthase, *pheS*, for cPhe counter-selection. (Tp^r)	(Barrett et al., 2008)
pEX18Tp-*pheS*ΔrrnBT1T2	pEX18Tp-*pheS* derivative with AfeI-BsaI restriction fragment removed.	This study.
pEX18TpTer-*pheS*	pEX18Tp-*pheS*ΔrrnBT1T2 derivative with a *dfr* gene with a rrnT1T2 terminator in replacement of SpeI-EcoRV restriction fragment.	This study.

pEX18TpTer-*pheS*-Cm	pEX18TpTer-*pheS* derivative containing filled-in EcoRI *cat* gene fragment from p34E-Cm2, cloned into the ScaI site. (Tp^r, Cm^r)	This study.
p34E-Tp	p34E containing *dfr* cassette. (Ap^r, Tp^r)	(DeShazer and Woods, 1996)
p34E-TpTer	p34E-Km derivative containing TpTer StuI fragment of pUC19-TpTer cloned between Klenow-filled EcoRI. (Ap^r, Tp^r)	(Shastri, 2011)
p34E-Cm2	p34E-Km derivative containing cat gene with synthetic promoter cloned between EcoRI sites. (Ap^r, Cm^r)	(Shastri, 2011)
pKT25	Low copy BACTH vector encoding T25 domain of CyaA from *B. pertussis,* where gene of interest is fusion to C-terminus of T25. (Km^r)	(Karimova et al., 1998)
pKNT25	Low copy BACTH vector encoding T25 domain of CyaA from *B. pertussis,* where gene of interest is fusion to N-terminus of T25. (Km^r)	(Karimova et al., 1998)
pUT18C	High copy BACTH vector encoding T18 domain of CyaA from *B. pertussis,* where gene of interest is fusion to C-terminus of T18. (Ap^r)	(Karimova et al., 1998)
pUT18	High copy BACTH vector encoding T18 domain of CyaA from *B. pertussis,* where gene of interest is fusion to N-terminus of T18. (Ap^r)	(Karimova et al., 1998)
pAS8	Yeast expression vector under control of GAL1 promoter and pgk1 terminator, containing URA3, ARS1 CEN4, and ColE1-*ori* for replication in *E. coli.* (Ap^r)	E. Hettema, University of Sheffield.
T6SS gene replacement, complementation vectors and others		
pBBR1-*tssA*	pBBR1MCS-1 containing *tssA* from *B. cenocepacia* H111 between HindIII and BamHI sites, orientated in same direction as *lac* promoter.	(Shastri, 2011)
pBBR2-*tssA*	As pBBR1-*tssA* but with pBBR1MCS-2 backbone.	This study.
pBBR1-*tssM*	pBBR1MCS-1 containing *tssM* from *B. cenocepacia* H111 cloned between Acc65I and XbaI sites, orientation in same direction as lac promoter.	This study.
pBBR2-*tssM*	As pBBR1MCS-1-*tssM* but with pBBR1MCS-2 backbone.	This study.
pET-14b-His_6.*tssD*	pET-14b containing *tssD* from *B. cenocepacia,* incorporating a N-terminal His-tag. (Ap^r)	(Shastri, 2011)
pHLS22	As pET-14b-His_6.*tssD*, with an excised NdeI fragment.	This study.

pSHAFT-*tagF::Km*	pSHAFT containing *tagF* fragment disrupted by *kan* cassette in same orientation as *tagF*. (Ap^r, Cm^r, Km^r)	Bull and Thomas, unpublished.
pSHAFT2-*tssM*::Tp(rev)	pSHAFT2 containing *tssM* fragment disrupted by *dfr* cassette in reverse orientation between SalI and NotI sites. (Ap^r, Cm^r, Tp^r)	(Shastri, 2011)
pBluescriptII-*tagX*	pBluescriptII containing *tagX* between BamHI and XhoI sites.	This study.
pBBR1MCS-t*ssM*ΔXhoI	pBBR1MCS-1 containing deleted allele of *tssM* with XhoI restriction fragment removed.	(Shastri and Thomas, unpublished)
pEX18Tp-*pheS*-Δ*tssM*	pEX18Tp-*pheS* containing in-frame *tssM* deletion fragment between XbaI and KpnI sites.	This study.
pEX18TpTer-*pheS*-Δ*tssM*	As pEX18Tp-*pheS*-Δ*tssM* but with pEX18TpTer-*pheS.*	This study.
pBluescriptII-*tagX::Tp*	pBluescriptII-*tagX* with *dfr* cassette inserted in ZraI site of *tagX* in same orientation as *tagX*. (Ap^r, Tp^r)	This study.
pSHAFT2-*tagX::Tp*	pSHAFT2 containing *tagX*::Tp allele from pBluescriptII-*tagX*::Tp disrupted between SalI and XbaI sites. (Ap^r, Cm^r, Tp^r)	This study.
pEX18TpTer-*pheS*-Δ*atsR*	pEX18TpTer-*pheS* containing deletion fragment of *atsR* and 500 bp flanking regions from H111 between XbaI and HindIII sites.	This study.
***tanB^H, taaB1^H, taaB2^H* vectors**		
pHLS1	pETDuet-1 containing *taaB1^H* from *B. cenocepacia* H111 cloned between NdeI and Acc65I sites.	This study.
pHLS2	pETDuet-1 containing *taaB2^H* from H111 cloned between NdeI and Acc65I sites.	This study.
pHLS3	pETDuet-1 containing *tanB^H* cloned between BamHI and HindIII incorporating N-terminal His-tag, and *taaB1^H* cloned between NdeI and Acc65I sites, for dual expression.	This study.
pHLS4	pETDuet-1 containing *tanB^H.CTD* (C-terminal 139 codons) cloned between BamHI and HindIII incorporating N-terminal His-tag, and *taaB1^H* cloned between NdeI and Acc65I sites, for dual expression.	This study.
pHLS5	pETDuet-1 containing *tanB^H-taaB1^H* cloned between BamHI and Acc65I, incorporating N-terminal His-tag.	This study.
pHLS6	pSCrhaB2 containing *taaB1^H* cloned between NdeI and Acc65I sites.	This study.

pHLS7	pETDuet-1 containing *tanB*^{H} with glycine to aspartic acid mutation at amino acid 276 cloned between BamHI and HindIII incorporating N-terminal His-tag.	This study.
pHLS8	As pHLS1 but incorporating a C-terminally FLAG tagged version of *taaB1*^{H}.	This study.
pHLS9	As pHLS3 but containing C-terminally FLAG tagged version of *taaB1*^{H}.	This study.
pHLS10	As pHLS4 but containing C-terminally FLAG tagged version of *taaB1*^{H}.	This study.
pHLS11	pSCrhaB2 containing *tanB*^{H} from *B. cenocepacia* H111 containing G276D mutation and N-terminal His tag cloned between XbaI and HindIII sites.	This study.
pEX18TpTer-*pheS*-Δ*tanB*^{H}	pEX18TpTer-*pheS* containing Δ*tanB*^{H} deletion fragment cloned between XbaI and HindIII.	This study.
pEX18TpTer-*pheS*-Δ*tanB*^{H}-*taaB1*^{H}	pEX18TpTer-*pheS* containing Δ*tanB*^{H}-*taaB1*^{H} deletion fragment cloned between XbaI and HindIII.	This study.
pKT25-*tanB*^{H}	pKT25 containing *tanB*^{H} from *B. cenocepacia* H111 containing G276D mutation fused to C-terminus of *cyaA* T25 fragment, cloned between BamHI and Acc65I sites.	This study.
pKTN25-*tanB*^{H}	pKNT25 containing *tanB*^{H} with G276D mutation fused to N-terminus of *cyaA* T25 fragment, cloned between BamHI and Acc65I sites.	This study.
pUT18C-*tanB*^{H}	pUT18C containing *tanB*^{H} with G276D mutation fused to C-terminus of *cyaA* T18 fragment, cloned between BamHI and Acc65I sites.	This study.
pUT18-*tanB*^{H}	pUT18 containing *tanB*^{H} with G276D mutation fused to N-terminus of *cyaA* T18 fragment, cloned between BamHI and Acc65I sites.	This study.
pKT25-*tanB*^{H}*.CTD*	pKT25 containing *tanB*^{H}*.CTD* from *B. cenocepacia* H111 with G276D mutation fused to C-terminus of *cyaA* T25 fragment, cloned between BamHI and Acc65I sites.	This study.
pKTN25-*tanB*^{H}*.CTD*	pKNT25 containing *tanB*^{H}*.CTD* with G276D mutation fused to N-terminus of *cyaA* T25 fragment, cloned between BamHI and Acc65I sites.	This study.
pUT18C-*tanB*^{H}.CTD	pUT18C containing *tanB*^{H}*.CTD* with G276D mutation fused to C-terminus of *cyaA* T18 fragment, cloned between	This study.

	BamHI and Acc65I sites.	
pUT18-*tanB^{H}.CTD*	pUT18 containing *tanB^{H}.CTD* with G276D mutation fused to N-terminus of *cyaA* T18 fragment, cloned between BamHI and Acc65I sites.	This study.
pKT25-*taaB1^{H}*	pKT25 containing *taaB1^{H}* from *B. cenocepacia* H111 fused to C-terminus of *cyaA* T25 fragment, cloned between BamHI and Acc65I sites.	This study.
pKTN25-*taaB1^{H}*	pKNT25 containing *taaB1^{H}* fused to N-terminus of *cyaA* T25 fragment, cloned between BamHI and *Acc65I* sites.	This study.
pUT18C-*taaB1^{H}*	pUT18C containing *taaB1^{H}* fused to C-terminus of *cyaA* T18 fragment, cloned between BamHI and Acc65I sites.	This study.
pUT18-*taaB1^{H}*	pUT18 containing *taaB1^{H}* fused to N-terminus of *cyaA* T18 fragment, cloned between BamHI and Acc65I sites.	This study.
***tpe1* vectors**		
pHLS19	pETDuet-1 containing *tpe1* from *B. cenocepacia* H111 cloned between NcoI and XhoI sites, with an N-terminal His-tag.	This study.
pHLS20	pETDuet-1 containing NTD of *tpe1* from H111 cloned between BamHI and HindIII, with an N-terminal His-tag.	This study.
pHLS21	pETDuet-1 containing CTD of *tpe1* from H111 cloned between BamHI and XhoI, with an N-terminal His-tag.	This study.
BCAS0667 and BCAS0666 vectors		
pHLS12	pET-22b(+) containing BCAS0667.CTD (C-terminal 265 codons) from H111 cloned between NcoI and XhoI sites, incorporating N-terminal pelB leader sequence for periplasmic localisation.	This study.
pHLS13	pET-22(b)+ containing BCAS0667.CTD (C-terminal 258 codons) cloned NcoI and HindIII restriction fragment, incorporating N-terminal *pelB* leader sequence for periplasmic localisation.	This study.
pHLS14	As pHLS13 but with S879A mutation.	This study.
pHLS16	pETDuet-1 containing BCAS0667.CTD (C-terminal 258 codons) from H111, cloned into BamHI and SalI sites, incorporating an N-terminal His tag.	This study.
pHLS18	As pHLS16 but BCAS0666 from H111 without signal sequence, cloned between NdeI and Acc65I sites, incorporating a C-terminal 3xFLAG tag.	This study.

pSH1	pETDuet-1 containing BCAS0667.CTD (C-terminal 267 codons) from H111 and BCAS0666 without its signal sequence in MCS2.	Hedayat and Thomas, unpublished.
pET28a-*tssI*$_{0667}$ 258	pET-28a containing BCAS0667.CTD (C-terminal 258 codons) clone between NdeI and BglII sites, for intracellular expression.	(Jones, 2012)
pET28a- *tssI*$_{0667}$ 258 ΔS	As pET28a-*tssI*$_{0667}$ 258 but with mutated S879A site.	(Jones, 2012)
pBBR2-BCAS0667	pBBR1MCS-2 containing BCAS0667 from *B. cenocepacia* H111 cloned between Acc65I and XbaI sites, orientated in same direction as *lac* promoter.	This study.
pAS8-BCAS0667.CTD	pAS8 containing BCAS0667.CTD (C-terminal 258 codons) from *B. cenocepacia* H111 cloned between Eco53kI and SalI sites.	This study.
pHLS15	pSCrhaB2 containing the entire BCAS0666 cloned between NdeI and XbaI sites.	This study.
pHLS17	pETDuet-1 containing BCAS0666 without its signal sequence cloned between NdeI and Acc65I sites.	This study.
pEX18TpTer-*pheS*-ΔBCAS0667	pEX18TpTer-*pheS* containing ΔBCAS0667 deletion fragment cloned between BamHI and HindIII sites.	This study.
pEX18TpTer-*pheS*-ΔBCAS0667-0666	pEX18TpTer-*pheS* containing ΔBCAS0667-0666 deletion fragment cloned between BamHI and HindIII sites.	This study.
Other bacterial adenylate cyclase two-hybrid constructs		
pKT25-*tssI*$_{1294}$	pKT25 containing *tssI*$_{1294}$ from *B. cenocepacia* H111 fused to C-terminus of *cyaA* T25 fragment.	(Jones, 2012)
pKTN25-*tssI*$_{1294}$	pKNT25 containing *tssI*$_{1294}$ fused to N-terminus of *cyaA* T25 fragment.	(Jones, 2012)
pUT18C-*tssI*$_{1294}$	pUT18C containing *tssI*$_{1294}$ fused to C-terminus of *cyaA* T18 fragment.	(Jones, 2012)
pUT18-*tssI*$_{1294}$	pUT18 containing *tssI*$_{1294}$ fused to N-terminus of *cyaA* T18 fragment.	(Jones, 2012)
pKT25-*tagA*	pKT25 containing *tagA* from *B. cenocepacia* H111 fused to C-terminus of *cyaA* T25 fragment.	(Jones, 2012)
pKTN25-*tagA*	pKNT25 containing *tagA* fused to N-terminus of *cyaA* T25 fragment.	(Jones, 2012)
pUT18C-*tagA*	pUT18C containing *tagA* fused to C-terminus of *cyaA* T18 fragment.	(Jones, 2012)
pUT18-*tagA*	pUT18 containing *tagA* fused to N-terminus of *cyaA* T18 fragment.	(Jones, 2012)

pKT25-*tssI*$_{0148}$	pKT25 containing *tssI*$_{0148}$ from *B. cenocepacia* H111 fused to C-terminus of *cyaA* T25 fragment.	(Jones, 2012)
pKTN25-*tssI*$_{0148}$	pKNT25 containing *tssI*$_{0148}$ fused to N-terminus of *cyaA* T25 fragment.	(Jones, 2012)
pUT18C-*tssI*$_{0148}$	pUT18C containing *tssI*$_{0148}$ fused to C-terminus of *cyaA* T18 fragment.	(Jones, 2012)
pUT18-*tssI*$_{0148}$	pUT18 containing *tssI*$_{0148}$ fused to N-terminus of *cyaA* T18 fragment.	(Jones, 2012)

Abbreviations: Ap^r, ampicillin-resistant; Cm^r, chloramphenicol-resistant; Km^r, kanamycin-resistant; Tp^r, trimethoprim-resistant.

2.2.2 PCR primers

For amplification of specific genes or gene fragments, primers were designed to anneal to specific regions of the gene. Primers used for cloning purposes had restriction sites and a GC-clamp incorporated into the 5' ends of the primers. See Table 2.6 for primers used in this study. All primers were manufactured by Eurogentec, Belgium.

Table 2.6 Primers used in this study.

Primer ID	Sequence	Restriction site
Screening/sequencing primers		
M13 Forward	5'-TGTAAAACGACGGCCAGT-3'	-
M13 Reverse	5'-CAGGAAACAGCTATGACC-3'	-
M13revBACTH	5'-GTGTGGAATTGTGAGCGGAT-3'	-
T7 forward	5'-TAATACGACTCACTATAGGG-3'	-
T7 rev	5'-GCTAGTTATTGCTCAGCGGT-3'	-
T7 terminator	5'-GCTAGTTATTGCTCAGCGG-3'	-
pETDuet-T71for	5'-ATGCGTCCGGCGTAGA-3'	-
pACYCDuet-T7-1rev	5'-GATTATGCGGCCGTGTACAA-3'	-
pACYC-T7-2for	5'-TTGTACACGGCCGCATAATC-3'	-
pEX18Tpfor	5'-GAAGCCAGTTACCTTCGGA-3'	-
pEX18Tprev	5'-TTGTCGGTGAACGCTCTCCT-3'	-
pSCrhaB2for	5'-TCAGTAACGAGAAGGTCGCG-3'	-
pSCrhaB2rev	5'-TACTGCCGCCAGGCAAATTC-3'	-
T6SS gene replacement and complementation primers		
tssA-OPFor	5'-GCGCAAGCTTCACGCGACATCTCATGCATC-3'	HindIII

tssA-OPRev (Rev2)	5’-ATCACGAAGAGCATTCCGCC-3’	-
tssMForAcc65I	5’-GCGCGGTACCTTAAAATCGCACCGGAACCTGAAC-3’	Acc65I
tssMrevXbaI	5’-GCGCTCTAGAATTTGCGCCTGTACGGTTTG-3’	XbaI
tssMFor	5’-GCGCTCTAGAGGAACCTGAACGTCCTATGC-3’	XbaI
tssMRev	5’-GCGCCTCGAGCTGTTGGTTTCGCCTTCCTG-3’	XhoI
tssM-OPFor	5’- TCATCCCGTTTGACAGCATG -3’	-
tssM-OPRev	5’- AGAAGCCGTTCTTCGAGAAC -3’	-
tssMrev-OP2	5’-ATCTTGCCGAAGTAGGCGATTT-3’	-
tagFfor		
tagFrev	5’-GCGCAAGCTTTCGAGGTAGCTGACGAGCTT-3’	HindIII
H111tagFfor	5’-TGAACGTGTCGGTGACGAT-3’	
H111tagFrev	5’-CCTGAATCGTGCGATGCAT-3’	
BCAL0353For	5’-GCGCCTCGAGTAAAGTGCGCCGGAAAATTCAAA-3’	XhoI
BCAL0353Rev	5’-GCGCGGATCCCAGTGTCACGCGACATCATA-3’	BamHI
BCAL0353CompFor-OP	5’-GCGCTCTAGAATCCCCGGAAATTGGAATTG-3’	XbaI
BCAL0353CompRev-OP	5’-GCGCAAGCTTGGTAAGGAAAGGAGACGTAT-3’	HindIII
AtsRForAXbaI	5’-GCGCTCTAGAGAAGCGAGCGAGGACGAGAT-3’	XbaI
AtsRRevIP-B	5’-TCAGGCGAGCAGTGTCTCGACCGAGCCGAGGACCAGGATGAT -3’	-
AtsRForIP-C	5’-ATCATCCTGGTCCTCGGCTCGGTCGAGACACTGCTCGCCTGA -3’	-
AtsRRevDHindIII	5’-GCGCAAGCTTTCGAATTCGGCGCGAACTGG -3’	HindIII
AtsRFor-OP	5’-ACATCCTCGACTGGATGCTCGG-3’	-
AtsRRev-OP	5’-TGATGGACACCGAGCAACGCTA-3’	-
tanB^{H}, taaB1^{H}, taaB2^{H} **primers**		
BCAL1298ForNtermHisBamHI	5’-GCGCGGATCCAATGGGTGACAAGGGCAATAC-3’	BamHI
BCAL1298RevHindIII	5’-GCGCAAGCTTACTCTCAATTAAGTTTCCCACC-3’	HindIII
BCAL1298RevAcc65I	5’-GCGCGGTACCACTCTCAATTAAGTTTCCCACC-3’	Acc65I
BCAL1298Rev2Acc65I	5’-GCGCGGTACCCGATTAAGTTTCCCACCAATGT-3’	Acc65I
BCAL1298CTDForNtermHisBamHI	5’-GCGCGGATCCAATACTGCGCAATGGCTATTC-3’	BamHI
BCAL1299ForNdeI	5’-GCGCCATATGAATCAAGAAATTATTGCTGG-3’	NdeI
BCAL1299ForBamHI	5’-GCGCGGATCCGATGAATCAAGAAATTATTGCTGG-3’	BamHI
BCAL1299RevAcc65I	5’-GCGCGGTACCGATTTTTCCTTCCCCGTTA-3’	Acc65I
BCAL1299Rev2Acc65I	5’-GCGCGGTACCCGTCGCCAGTCGATTGCCGGAT-3’	Acc65I

BCAL1299RevFLAGAcc65I	5’-GCGCGGTACCTTACTTATCGTCGTCATCCTTGTAATCTCGCCAGTCGATTGCCGG-3’	Acc65I
BCAL1300ForNdeI	5’-GCGCCATATGTTCTATCTGTCCAGC-3’	NdeI
BCAL1300RevAcc65I	5’-GCGCGGTACCCTTCATGGAAGATTGTGAGG-3’	Acc65I
BCAL1298ForA	5’-GCGCTCTAGAGCGATGTACTTCGCGATCAC-3’	XbaI
BCAL1298revIP-B	5’-ACCAATGTTGTTCCCGAACTTCTGACCGTACAATCTGCCGAC-3’	-
BCAL1298ForIP-C	5’-GTCGGCAGATTGTACGGTCAGAAGTTCGGGAACAACATTGGT-3’	-
BCAL1298revD	5’-GCGCAAGCTTTCCAACTCGTCCAAAGTGCT-3’	HindIII
BCAL1298ForOP	5’-TGACGTTGCTTTGGTTTGCCAT-3’	-
BCAL1298RevOP	5’-CGCAGGAAGGTCATGGTAGAAC-3’	-
BCAL1299ForA	5’-GCGCTCTAGAGTGCTTAAGACTGAAGGGGC -3’	XbaI
BCAL1299RevIP-B	5’-CTCATTTCCCGTTCCATCGATCGGGTAAATGTCATCTGCACC-3’	-
BCAL1299ForIP-C	5’-GGTGCAGATGACATTTACCCGATCGATGGAACGGGAAATGAG-3’	-
BCAL1299RevD	5’-GCGCAAGCTTGCAAGTAACTCGCTCGGATC-3’	HindIII
BCAL1299revOP	5’-CGCCATGTATCCATCATTACCG-3’	-
BCAL1298-99revIP-B	5’-CTCATTTCCCGTTCCATCGATCTGACCGTACAATCTGCCGAC-3’	-
BCAL128-99ForIP-C	5’-GTCGGCAGATTGTACGGTCAGATCGATGGAACGGGAAATGAG -3’	-
***tpe1* primers**		
BCAL1166NTDForNtermHisBglII	5’-GCGCAGATCTAATGATCATCAGCCCTCCCTT-3’	BglII
BCAL1166CTDForNtermHisBamHI	5’-GCGCGGATCCGGCTTCATCTTTGCTCGATAG-3’	BamHI
BCAL1166NTDRev HindIII	5’-GCGCAAGCTTTTAATCCTGTGGACCCTTAATAATG-3’	HindIII
BCAL1166CTDRevXhoI	5’-GCGCCTCGAGTTTCTCACGACAACTTCCGC-3’	XhoI
BCAL1166ForNtermHis NcoI	5’-GCGCCATGGGCAGCAGCCATCACCATCATCACCACAGCATGATCATCAGCCCTCCCT-3’	NcoI
BCAS0667 and BCAS0666 primers		
BCAS0667PLAForNcoI	5’-GCGCCATGGCCAAGGGGCTTGCGAGCCCCGA-3’	NcoI
BCAS0667PLAFor BamHI	5’-GCGCGGATCCGGCGACGCGCGCGGC-3’	BamHI
BCAS0667ForATG1 Acc65I	5’-GCGCGCGGTACCTTAAGGGCAGAACCTGAGACGAAA-3’	Acc65I
BCAS0667ForYeast	5’-AAAATGCCGGCGACGCGCGCGGCG-3’	-
BCAS0667PLAFor2NcoI	5’-GCGCCATGGACCCGGCGACGCGCGCGGCGGC-3’	NcoI
BCAS0667PLARevXhoI	5’-GCGCCTCGAGCGCGCCGGCGGTTATCGCTT-3’	XhoI
BCAS0667RevXbaI	5’-GCGCTCTAGACGGCGGTTATCGCTTTTTTG-3’	XbaI

BCAS0666ForNdeI	5’-GCGCCATATGCGATACAAAAAAGCGAT-3’	NdeI
BCAS0666For2NdeI	5’-GCGCATATGCAAGGGACGAACATGACTGGCTT-3’	NdeI
BCAS0666RevXbaI	5’-GCGCTCTAGAAAACGTTCATCATTTCCCG-3’	XbaI
BCAS0666Rev3xFLAG Acc65I	5’-GCGCGGTACCCTACTTGTCATCGTCATCCTTGTAGTCGATGTCATGATCTTTATAATCACCGTCATGGTCTTTGTAGTCATCCGTCTGGCCGGCCGG -3’	Acc65I
0667ΔforA	5’-GCGCGGATCCATCAGCCCAGTGCAAGTCCC-3’	BamHI
0667ΔIPrevB	5’-TTGATCCTTCGCGACCTGCTGCAACAGATTCCCGCCGGAACC-3’	-
0667ΔIPforC	5’-GGTTCCGGCGGGAATCTGTTGCAGCAGGTCGCGAAGGATCAA-3’	-
0667ΔrevD	5’- GCGCAAGCTTACGTTCGCCTTGTGCTCAAC -3’	HindIII
0667-0666ΔIPRevB	5’-CGTTACGATCTTGCGGCGAATCAACAGATTCCCGCCGGAACC-3’	-
0667-0666ΔIPforC	5’-GGTTCCGGCGGGAATCTGTTGATTCGCCGCAAGATCGTAACG-3’	-
0667-0666ΔrevD	5’-GCGCAAGCTTTAAATCAGCGTCTACACGCGC-3’	HindIII
0667for-OP	5’-CAAATGGCAACCTGGCGGACAT-3’	-
0667rev-OP	5’-CGCCTCGAAAAGTGCCGTCTTT-3’	-
0666rev-OP	5’- GCCTTCGTGAATCCGGATACGG -3’	-

2.2.3 Genomic DNA isolation

For the isolation of bacterial DNA to be used as the DNA template for PCR reactions, several colonies were selected from a freshly cultured bacterial plate and resuspended in 200 μL TE buffer (10 mM Tris-HCl, 1 mM EDTA, pH 8.0). This was then boiled at 100°C in a water bath for 10 minutes followed by centrifugation for 5 minutes at 15,000 x *g* to isolate the cell debris. The supernatant was then removed and transferred to a clean microcentrifuge tube for use and the bacterial pellet was discarded.

2.2.4 Plasmid isolation: kit minipreparation

Overnight cultures of transformants containing the desired plasmid were grown by inoculating 3 mL of antibiotic-supplemented liquid broth and incubated overnight at 37°C with shaking. 1.5 mL of overnight culture was transferred into a microcentrifuge tube and centrifuged at 15,000 x *g* for 3 minutes to recover the

bacteria, the supernatant was discarded. The plasmid was extracted using a GeneJet mini prep kit (Thermo Scientific) according to manufacturer's instructions with the following modifications. After binding of DNA to the silica columns, 500 μL of buffer PB (Qiagen) was added, the column was centrifuged and the flow-through discarded. Bound DNA was then washed and eluted as manufacturer's instructions. Plasmids preparations extracted by this method were suitable for DNA sequencing and other downstream applications.

2.2.5 Plasmid isolation: recycled column minipreparation

For a quick but crude method of plasmid extraction bacteria were cultured and pelleted as Section 2.2.4 and then the plasmid extracted as follows. Bacteria were gently resuspended in 100 μL solution I (50 mM Tris-HCl pH 8.0, 10 mM EDTA, 100 μg/ml RNaseA), and then lysed with addition of 150 μL solution II (200 mM NaOH, 1% SDS) followed by immediate inversion of the tube. The solution was then neutralised and proteins precipitated by adding 200 μL solution N3 (4.2 M GuHCl, 0.9 M Potassium acetate, pH 4.8) and inverting. Precipitates were pelleted by centrifugation at 16,000 x *g* for 10 minutes. 700 μL of the cleared solution was applied to a recycled acid/alkali washed DNA spin column (Thermo Scientific/Dutscher Scientific) and centrifuged for 1 minute for the solution to pass through the column, allowing the DNA to bind to the silica membrane. The column was dried by centrifugation for 2 minutes, transferred to a clean microcentrifuge tube and then bound DNA was eluted with addition of 20-40 μL buffer EB (Qiagen). This was incubated for 5 minutes at room temperature and centrifuged for 1 minute to collect the DNA eluate. Plasmids extracted via this method were only suitable for size analysis by DNA gel electrophoresis and not DNA sequencing.

2.2.6 Plasmid isolation: manual minipreparation

An alternative crude plasmid extraction was as follows. Bacteria were cultured and harvested as Section 2.2.4. The supernatant was discarded and bacteria resuspended in 100 μL of solution I (Section 2.2.5) and incubated on ice for

5-10 minutes. 150 μL solution II was added, the mixture inverted immediately and incubated on ice for 5 mins. Following this 150 μL of solution III (3 M potassium acetate, 2 M acetic acid) was added, the solution inverted and then incubated on ice for 5 minutes. Supernatants were transferred to clean microcentrifuge tubes and ethanol precipitated as follows. 2 volumes of 100% ethanol (~800 μL) was added and vortex. The solution was left to precipitate for 15 minutes on ice. The precipitate was collected by centrifugation at 15,000 x *g* for 5 minutes, the supernatant removed and discarded. Following this the pellet was washed with 1 mL of 70% ethanol, centrifuged again and the supernatant removed thoroughly. The precipitate was left to air-dry for 30 minutes and then finally resuspended in 30-50 μL sterile ddH_2O. Plasmids extracted via this method were only suitable for size analysis by DNA gel electrophoresis and not DNA sequencing.

2.2.7 DNA electrophoresis

All DNA samples were analysed by gel electrophoresis to determine the DNA fragment size and concentration. 5 μL of sample was combined with 5 μL 2X DNA loading dye (4.2 mg/ml bromophenol blue, 5.5% (v/v) glycerol final conc.) and loaded onto a 0.8% or 1.0% agarose gel (Fisher) in 1x TAE (40 mM Tris, 20 mM acetic acid, and 1 mM EDTA) as standard protocol. Appropriate DNA ladders were included, 5 μL of pre-stained DNA ladder mix (Thermo Scientific/York biosciences) for linear DNA, or 1 μL supercoiled DNA ladder (New England Biolabs) for plasmid DNA. Gels were then visualized by post-electrophoresis ethidium bromide staining (0.5 mg/L ethidium bromide in ddH_2O) using a UV transluminator (UVP). Images were captured using a Kodak EDAS 290 gel documentation system.

2.2.8 PCR for cloning

Genomic DNA (Section 2.2.3) was used as template DNA to amplify specific DNA fragments in a PCR reaction using Hot-start KOD DNA polymerase (Merck Millipore), in a total reaction volume of 50 μL as manufacturer's instructions. Briefly, each reaction comprised of: 1 X KOD buffer, 2 mM $MgSO_4$, 0.2 mM dNTP mix

(final concentration), 0.6 mM forward and reverse primers, 2.5 µL DMSO per reaction (for GC-rich DNA) and 0.5 U KOD DNA polymerase. Using a G-STORM GS1 thermal cycler (Gene technologies), samples underwent a 5 minute 95°C hot-start step, and then 30 cycles of the following temperature steps to ensure full amplification of the DNA. DNA denaturation for 30 seconds at 95°C; primer annealing for 30 seconds at a calculated annealing temperature (this temperature varied due to primer length and G+C content, using the formula [2(A+T) + 4(G+C)]-5°C or NEB online T_m calculator) and finally, elongation at 72°C for 1 minute per 1000 bp. PCR products were analysed by DNA agarose gel electrophoresis (Section 2.2.7).

2.2.9 Colony PCR screening

Transformant colonies were screened by colony PCR to identify which transformants contained correctly sized DNA inserts within the plasmid of interest. The PCR method was as described in Section 2.2.8 with the following modifications. DNA to be amplified was obtained by selecting a transformant colony and smearing it on the inside of a PCR tube, then patching the colony onto an appropriate selection plate. GoTaq Flexi G2 DNA polymerase (Promega) replaced KOD DNA polymerase, and was used as manufacturer's protocol in a total reaction volume of 25 µL.

2.2.10 DNA clean up

To remove interring enzymes and buffers resulting from DNA manipulation techniques, such as PCR or restriction digestion, DNA samples were purified using a spin-column-based purification kit as manufacturer's instructions (Thermo Scientific/Qiagen/Macherey-Nagel). DNA was eluted in an appropriate volume and analysed by DNA gel electrophoresis (Section 2.2.7).

2.2.11 DNA gel extraction

To purify the corrected sized DNA fragment from a mixture of differently sizes DNA fragments, the entire sample was separated by DNA agarose gel electrophoresis. The desired band corresponding to the DNA fragment of interest was then excised from the gel using a sterile scalpel. DNA was then purified using a spin-column based gel extraction kit (Qiagen/Macherey-Nagel) according to the manufacturer's instructions. UPrep or GeneJet spin columns replaced Qiagen columns where appropriate.

2.2.12 DNA restriction digestion

At least 200 ng of PCR fragment and plasmid DNA were subjected to restriction digestion by the appropriate restriction enzyme (Promega/New England Biolabs) in a 50 μL reaction volume as manufacturer's instructions for 2 hours at the recommended temperature from the restriction enzyme. The digested DNA was then purified as Section 2.2.10.

For diagnostic restriction digestions of plasmid clones, 5 μL of plasmid DNA was digested with the appropriate restriction enzyme in a 25 μL total reaction volume for 1 hour at the recommended temperature. 5 μL 6X DNA loading dye was added to the reaction and 15 μL ran directly on a DNA agarose gel.

2.2.13 Blunting of DNA

To fill in a 5' overhang to generate a blunt ended fragment, DNA polymerase I large (Klenow) fragment (Promega) was employed. 1-4 μg of DNA was combined with 3 μL 10 X DNA polymerase buffer, 0.3 μL BSA, 1.2 μL 1mM dNTP mix (Thermo), 2 μL Klenow fragment enzyme and sterile ddH_2O up to total reaction volume of 30 μL. The reaction was incubated for 15 minutes at room temperature. To stop the reaction DNA was purified as Section 2.2.10. For the blunting of 3' overhangs, T4 DNA polymerase was used according to manufacturer's instructions.

2.2.14 DNA ligation

To insert a DNA fragment into a vector, digested DNA fragments and cut plasmids were combined in 3:1 or 5:1 molar ratio of insert:vector (for directional or blunt cloning, respectively) and ligated using T4 DNA ligase (1 U/µL) (Promega) as manufacturer's protocol, in a total reaction volume of 30 µL. Ligation reactions were incubated at room temperature for 6 hours or overnight. Ligation reactions using cut vector with no insert DNA and with and without T4 DNA ligase were also included to act as ligation and vector controls, respectively.

2.2.15 DNA sequencing

All DNA sequencing was performed by the Genetic Core Facility at The University of Sheffield.

2.2.16 Plasmid transfer techniques

Chemically-competent cell preparation

Chemically competent *E. coli* cells were prepared according to Hanahan's method (Hanahan, 1983). Briefly, 50 mL LB culture was inoculated with 0.5 mL of overnight starter culture, and incubated at 37°C with shaking until an OD_{600} of 0.3-0.5 was achieved. Upon reaching the appropriate cell density, the culture was chilled on ice for 15 minutes then pelleted by centrifugation at 3,400 x g for 10 minutes at 4°C in an Allegra X-22R benchtop refrigerated centrifuge (Beckman Coulter). The bacterial pellet was resuspended in 16 mL of filter-sterilised RF1 solution (100 mM KCl, 50 mM $MnCl_24H_2O$, 30 mM CH_3COOK, 10 mM $CaCl_22H_2O$, 15% (v/v) glycerol, pH 5.8 with 0.2M CH_3COOH) by moderate vortexing, chilled on ice for 30 minutes and then pelleted by centrifugation as previously. A fresh working solution of RF2 was made by combining 0.5 mL RF2A (0.5 M MOPS, pH 6.8) with 9.8 mL RF2B (75 mM $CaCl_22H_2O$, 10 mM KCl, 15% (v/v) glycerol), and then filter-sterilised. The chilled bacterial pellet was resuspended in 4 mL of RF2 and incubated for a further 15 minutes on ice. The bacterial suspension was then

aliquoted into chilled sterile 1.5 mL microcentrifuge tubes in 200-400 µL aliquots. Cells where then froze at -80°C immediately for long-term storage.

Heat-shock assisted transformation

Appropriate *E.coli* competent cells (made competent by Hanahan's method (Hanahan, 1983) (see above) were thawed on ice. 100 µL of competent cells were added to 15 µL of a ligation reaction or 1 µL of plasmid DNA and kept on ice for 30 minutes with periodic agitation of the suspension every 10 minutes. Cells were then subjected to a heat shock at 42°C for 2.5 minutes, then returned to ice for 5 minutes. 1 mL of liquid broth was then added and the bacterial suspension was incubated for 1 hour at 37°C to allow plasmid replication and expression of antibiotic resistance genes. 100 µL was spread onto an agar plate supplemented with the appropriate antibiotics.

Electroporation assisted transformation

Electro-competent *B. cenocepacia* cells were prepared as follows. 6 mL LB was inoculated and grown overnight at 37°C. Cultures were harvested by centrifugation at 3,500 x *g* in an Allegra X-22R benchtop refrigerated centrifuge for 10 minutes at room temp. The supernatant was removed and bacteria resuspended in 6 mL chilled 300 mM sterile sucrose solution, and then re-centrifuged for 10 mins. The supernatant was discarded and the 300 mM sucrose wash was repeated. Bacteria were then resuspended in 100 µL 300 mM sucrose. 500 ng vector DNA (prepared by kit plasmid minipreparation) was combined with 100 µL electro-competent cells and transferred to a sterile 2 mm electroporation cuvette (with longer electrode design) (Geneflow) and subjected to an electric pulse using Gene Pulser Xcell (BioRad) set at 25 µF, 200 Ω, 2.5 kV. 1 mL LB was added and the suspension was transferred to a 25 mL universal tube and incubated at 37°C for 2 hours to allow cells to recover. Cultures were transferred to a sterile micro-centrifuge tube, centrifuged at 16,000 x *g* for 1min and concentrated into 200 µL LB. 100 µL was plated onto appropriate selection plates and incubated at 37°C. 10^{-1} to 10^{-3} dilutions were also plated.

Conjugation

3ml LB cultures were inoculated with the recipient *B. cenocepacia* strain and *E. coli* donor strain and grown overnight at 37°C. 1 mL of each culture was harvested by centrifugation for 2 minutes at 16, 000 x *g*. The supernatant was discarded and the pellets resuspended in 100 µL 0.85% (w/v) sterile saline. 25 µL of donor and recipient cultures were combined in a microcentrifuge tube and then spread over a 0.45 µm nitrocellulose filter membrane (Millipore) placed on a LB or BHI agar plate. Plates were incubated at 37°C for 8-16 hours. Donor and recipient strains were also incubated on filters membranes, as above, to act as controls, where 25 µL of each culture was combined with 25 µL saline. Conjugation filters were harvested by vortexing in 3 mL saline to resuspend the bacteria. 100 µL of the cultures were plated on appropriate selection plates and incubated at 37°C for 48-72 hours. 10^{-1}, 10^{-2} and 10^{-3} dilutions were also plated if appropriate.

2.3 Recombinant protein overproduction and purification techniques

2.3.1 Small-scale test expression

To determine whether recombinant proteins of interest were overproduced by an expression plasmid, the plasmid was introduced into an *E. coli* expression host strain, such as BL21(DE3) or BL21(DE3)/pLysS by transformation. A single CFU was used to inoculate 8 mL BHI broth (with appropriate antibiotics) and cultured at 37°C until a mid-log growth phase was reached (OD_{600} 0.3-0.5). The culture was then divided into two separate sterile culture tubes to allow half of the culture to be induced and the remainder left uninduced. For induction of protein synthesis from T7 based expression systems, such as the pET vector series, 1 M IPTG was added to give a final concentration of 1 mM. For rhamnose-inducible expression systems, such as pSCrhaB2, 10% (w/v) rhamnose was added to give a final concentration of 0.1% (w/v). Cultures there then incubated for a further 4 hours at 37°C or 30°C to allow protein synthesis from the induced expression plasmids. 200 µL aliquots of the uninduced and induced samples were taken and centrifuged at 16,000 x *g* to isolate the bacteria. The pellet was then resuspended in 50 µL of 2X SDS-PAGE sample buffer (250 mM Tris-HCl, 10% SDS, 20% glycerol, 10% β-mercaptoethanol, 0.01% bromophenol blue) and boiled for 10 minutes to lyse the cells, giving whole cell samples. Samples were the analysed by SDS-PAGE (Section 2.5.2).

2.3.2 Determination of solubility of recombinant proteins

Recombinant proteins may be soluble or insoluble when overproduced, the former being the ideal form. To determine the solubility of an overproduced protein of interest, 50 mL BHI was inoculated, grown and protein synthesis induced as Section 2.3.1 with minor alterations. Rather than dividing the culture before induction, a 200 µL aliquot of the culture was taken and the remaining culture induced with 1 mM IPTG. After induction, the culture was pelleted by centrifugation at 3,500 x *g*, the supernatant removed and cells resuspended in 25 mL of wash buffer (25 mM Tris-HCl (pH 7.5), 150 mM NaCl, and 2mM EDTA). The suspension

was centrifuged again and the supernatant removed. The bacterial pellet was weighed and then frozen at -20°C overnight. After thawing on ice, 5 mL per 1g of bacterial pellet of lysis buffer (50 mM Tris-HCl (pH 8.0), 2 mM EDTA, 200 mM NaCl, and 5% glycerol) was used to resuspend the cells. A fresh stock solution of 10 mg/mL lysozyme (Sigma) was made up in ddH_2O and added to the resuspended pellet to a give a final concentration 200 µg/mL and incubated at 4°C on a rolling mixer for 30 minutes. A fresh stock of serine protease inhibitor was made by dissolving 25 mg/mL, phenylmethylsulfonyl fluoride (PMSF) (Applichem) in 100% ethanol, and added to the bacterial cells at a final concentration of 25 µg/mL. Freshly prepared sodium deoxycholate (Sigma), at a final concentration of 500 µg/mL, was added to the lysing cells, and mixed for a further 30 minutes at 4°C. Sonication was then performed on the cell suspension using a SONICS Vibracell VCX750 Ultrasonic Cell Disrupter with a micro-tip probe. This was performed at an amplitude of 22% in 30-second bursts, followed by a 2-minute incubation on ice, until the viscosity of the solution was reduced and the cells fully disrupted. 50 µL crude sample was taken of the sonicated sample and combined with 50 µL 2X SDS-PAGE sample buffer, to give the total protein fraction. The remainder of the lysed sample was then centrifuged at ≥19,000 x *g* for 30 minutes at 4°C in an Avanti J-26 XP High Performance centrifuge (Beckman Coulter) or a Universal 320R refrigerated bench-top centrifuge (Hettich) to isolate cell debris and insoluble fractions. A 50 µL aliquot of the supernatant was removed and combined with 2X SDS-PAGE sample buffer to give the soluble protein fraction. A 10 µL pipette tip was used to remove a sample of the pellet and re-suspended in 25µL 2X SDS-PAGE sample buffer, to give the insoluble pellet fraction. Uninduced and induced whole cell samples, total, soluble and insoluble samples were analysed by SDS-PAGE (Section 2.5.2). Overproduced proteins present in the supernatant of the cleared lysate were considered soluble, where-as proteins present in only the total and insoluble pellet samples were considered insoluble.

2.3.3 Large-scale recombinant protein expression

To produce greater quantities of recombinant protein for purification by nickel affinity chromatography, 500 mL to 1 L cultures were induced and samples lysed as described in Section 2.3.2 with minor alterations. EDTA was omitted from the lysis buffer and replaced with 10 mM imidazole (Fisher Scientific). After clarification of the lysate by centrifugation the supernatant containing the soluble overproduced recombinant proteins was ready to be subjected to nickel affinity chromatography (Section 2.3.4 and 2.3.5).

2.3.4 Small-scale nickel affinity chromatography using a batch chromatography method

For small-scale nickel affinity purification a batch chromatograph methodology was undertaken as follows. 100 μL charged His-Buster Nickel Affinity Gel (Amocol Bioprocedure) was aliquoted into a micro-centrifuge tube and centrifuged at 700 x *g* for 1 minute to isolate the resin, the supernatant was discarded. The resin was then resuspended in 500 μL ddH_2O to wash the resin, centrifuged and the supernatant was removed as above. For equilibration, the previous step was repeated three times but used 500 μL of equilibration buffer (50 mM Tris-HCl (pH 8.0), 200 mM NaCl, 10 mM imidazole and 5% glycerol) rather than ddH_2O. After this, 200 μL of protein lysate was added to the equilibrated resin and gently resuspended. The resin and lysate suspension was then incubated at room temperature with inversion on a rotary mixer (22rpm) for 30 minutes to allow the His-tagged proteins to bind to the nickel resin. After incubation, the resin was pelleted by centrifugation and the supernatant removed and retained as the flow-through sample. To wash the resin to remove non-specifically bound proteins 500μL of the appropriate wash buffer (50mM Tris-HCl (pH 8.0), 200mM NaCl, 10mM imidazole and 5% glycerol as standard) was added to the resin and vortexed. This was followed by centrifugation. The supernatant was removed and retained. This process was repeated twice more.

Bound proteins were then eluted in one of two ways, dependent on downstream applications. In the first method proteins were eluted by displacement

of the Histidine-Ni^{2+} complex with an excess of imidazole acting as a metal ion ligand for the Ni^{2+}, by the addition of 200 µL elution buffer (50 mM Tris-HCl (pH 8.0), 200 mM NaCl, ≥150mM imidazole, 5% glycerol). This was followed by incubation at room temperature with inversion for 30 minutes. An alternative method for elution was to re-suspend the resin directly in 100 µL 2X SDS-PAGE sample buffer and boil at 100°C for 5 minutes in a heat block. This resin-SDS-PAGE sample buffer suspension was then collected by centrifugation at 700 x *g* for 5 minutes. Load, flow-through, wash fractions and imidazole-eluted samples were all analysed by SDS-PAGE (Section 2.5.2).

2.3.5 Large-scale nickel affinity chromatography using a FPLC protein purification system

For large-scale His-tagged protein purification the following protocol was undertaken. A charged 1 mL HisTrap HP pre-packed nickel sepharose column (GE Healthcare) was manually washed with 10 mL ddH_2O using a syringe and female connector, at a flow rate of 1 mL/minute, ensuring not to introduce air bubbles into the column. The column was then equilibrated in 10 mL of the appropriate equilibration buffer (50 mM Tris-HCl (pH 8.0), 200 mM NaCl, 10 mM imidazole and 5% glycerol as standard) at a flow rate of 1 mL/min. The clarified protein lysate was passed through a syringe driven 0.22 µM filter unit (Millipore) and manually loaded onto the column at a flow rate of 1 mL/min. The flow-through was retained. Any unbound or non-specific bound proteins were then remove by washing the column with 10 mL wash buffer ((50 mM Tris-HCl (pH 8.0), 200 mM NaCl, 10 mM imidazole and 5% glycerol as standard), where the wash buffer was retained for analysis.

The loaded HisTrap column was attached to an ÄKTA purifier 10 FLPC purification system (GE Healthcare) controlled by UNICORN control software (GE Healthcare). The ÄKTA purifier was pre-equilibrated with a low imidazole buffer (50 mM Tris-HCl (pH 8.0), 200 mM NaCl, 10 mM imidazole and 5% glycerol) in pump A and high imidazole buffer (50 mM Tris-HCl (pH 8.0), 200 mM NaCl, 500 mM imidazole and 5% glycerol) in pump B. Bound protein where then eluted by applying an imidazole gradient over the column, starting at 10 mM imidazole and finishing at

500 mM imidazole over a 30 minute time period, at a flow rate of 1 mL/min. Eluted fractions where collected in 1mL aliquots automatically using a fraction collector Frac-950 (GE Healthcare). UV absorption at 280 nm (A_{280}) of the flow path was monitored by a Monitor UV-900 (GE healthcare) to act as a guide to identify which fractions contained eluted proteins. Load, flow-through, wash, and imidazole-eluted fractions were analysed by SDS-PAGE (Section 2.5.2).

2.3.6 Nickel affinity chromatography under denaturing conditions

For proteins that had to be purified under denaturing conditions, e.g. His-tagged proteins purified away from a protein-protein complex, the protocol described in Section 2.3.5 was used with alterations. Before loading, strong denaturants were added to the clarified cell lysate, either urea (Fisher Scientific) or guanidine hydrochloride (GuHCl) (Acros Organics) at a final concentration of 4-6 M or 2-4 M, respectively. The denaturant-containing lysate was then incubated for 15 minutes to promote protein denaturation and complex dissociation. This lysate was then loaded on a 1 mL HisTrap column, and washed and eluted as previously described in Section 2.3.5, but with buffers that also contained the denaturant used in the lysate sample (i.e. 2-4 M GuHCl).

2.3.7 Size exclusion chromatography by gel filtration

Size exclusion chromatography can be used to separate molecules based on their molecular size and allows the estimation of the molecular weight (M.W.) of proteins when calibrated with molecular standards. For separation of molecular weights from 1000 to 300000 a Superose 12 10/300 GL pre-packed column (GE Healthcare) was employed, and for separation between 5000 and 5000000 a Superose 6 HR 10/300 GL pre-packed column (GE Healthcare) was used. Both columns were used with an ÄKTA FPLC purifier 100 as follows. The column was washed with one column volume of ddH_2O to remove the ethanol storage buffer at flow rate of 0.5 mL/min for Superose 12 (max. pressure 2.4 MPa), and 0.2 mL/min for Superose 6 (max. pressure 1.2 MPa). 2 column volumes of equilibration buffer (50 mM Tris-HCl, 200 mM NaCl) was used to equilibrate the column at a flow rate of

0.5 mL/min for Superose 12 and 0.3-0.5 mL/min for Superose 6. A protein sample was then injected onto the column using a 100 μL or 1 mL sample loop (dependent on the application) and the flow rate maintained at 0.5 mL/min for Superose 12 or 0.3-0.5 mL/ml for Superose 6. A_{280} of the flow path was monitored to identify at which point proteins where eluted from the column.

If the molecular weight (M.W.) was being analysed the gel filtration column was calibrated with proteins standards of a known M.W. from a low or high M.W. calibration kit (GE Healthcare) as manufacturer's instructions with alterations. Briefly, standards were combined and dissolved in 1 mL equilibration buffer at a concentration of 1 mg/mL. This sample was further concentrated into 500 μL using a 10000 MWCO Amicon Ultra-4 centrifugal filter unit (Millipore). 100 μL of the sample was injected onto the equilibrated Superose column and UV absorbance of eluates monitored to determine the elution volume (V_e) after injection for all the standards. This was repeated to give an average V_e for each standard. 100 μL of Blue Dextran 2000 (1 mg/mL) was injected onto the column to determine the column void volume (V_o). This data was then used to calculate the K_{av} value for each standard using the equation $K_{av} = (V_e-V_o)/(V_c-V_o)$, where V_c = geometric column volume. A calibration curve was then generated by plotting K_{av} values (x axis) against relative molecular mass (M_r) (y axis) on a log scale. A semi-log regression curve was fitted to the data points using GraphPad Prism, resulting in a line equation of y=10^(mx + c), where m equals the gradient of the line and c is the y intercept. The average elution volume (V_e) of a protein of interest was experimentally determined and used to calculate its K_{av} value. Using the line equation generated from the calibration curve this K_{av} value could then be used to estimate the M_r and molecular mass *m* in Daltons (Da) using the calibration curve.

2.3.8 Buffer exchange

To remove interfering buffer components (such as NaCl or imidazole) after protein purification, appropriate protein fractions were pooled and the buffer was exchanged by dialysis against a more suitable buffer (50 mM Tris-HCl (pH 8.0) as standard). Specifically, dialysis tubing (3000 MWCO) was cut to the appropriate

size, thoroughly washed in ddH_2O and then equilibrated in dialysis buffer. Pooled protein fractions were transferred into the dialysis tubing and secured using dialysis clips. The sample was dialysed against a volume of buffer at least 100 times greater than the sample volume for ≥8hours at 4°C with stirring, with 3 changes of the buffer.

2.3.9 Protein storage

For short-term storage of purified proteins, proteins were stored at 4°C. For longer-term storage, sterile glycerol was added to the purified proteins to give a final concentration of 15% (v/v) and froze at -20°C for mid-term storage or -80°C for long-term storage. Samples containing 50% glycerol (final conc.) were also stored at -20°C.

2.4 Native protein extraction and purification techniques

2.4.1 Secreted protein extraction from broth cultures

To extract proteins present in the liquid culture supernatant, 15-40 mL D-BHI broth was inoculated with an overnight culture to give an initial starting OD_{600} 0.03 and incubated at 37°C with shaking until an OD_{600} of ~1.0 was reached. Cultures were centrifuged at 3,400 x *g* in an Allegra X-22R benchtop refrigerated centrifuge for 20 minutes at 4°C to harvest the bacteria. The supernatant was then filter sterilised through a 0.22 μm syringe driven filter unit (Millipore). Proteins present in the supernatant were precipitated by DOC-TCA (Section 2.4.3).

For cell-associated protein fractions, the subsequent cell pellet recovered from the above procedure was gently resuspended in 1 mL of PBS for every 20 mL of culture centrifuged. 25 μL of this cell suspension was then taken, combined with an equal volume of 2x SDS-sample buffer and boiled for 10 minutes in a heat block to lyse the cells. Samples were then analysed by SDS-PAGE (Section 2.5.2).

2.4.2 Secreted protein extraction from solid medium grown cultures

To extract proteins secreted when cultured on a solid surface, the following protocol was carried out. Sterile dialysis membranes were prepared by cutting dialysis tubing (12000-14000 MWCO) into 40 mm diameter discs and soaked in ddH_2O for 1 hour with agitation. The membranes were then placed between filter paper soaked in 1% glycerol, and sterilised by autoclaving in a glass petri dish for 15 minutes. 3 mL LB or BHI broth was inoculated with a single CFU and incubated at 37°C until OD_{600} of 0.5. A sterile dialysis membrane was placed onto a LB or BHI agar plate and 100 μL of the culture spread over it using a p200 tip. The plates where then incubated at 37°C for 16 hours. After incubation, the dialysis membrane was removed, transferred into a universal tube containing 1 mL sterile PBS, and gently vortex to resuspend the bacteria. Cultures where then centrifuged for 10 minutes at 3,400 x *g* to isolate the bacteria. Culture supernatants were carefully removed, filter sterilised using a 0.22 μM syringe driven filter unit and DOC-TCA precipitated (Section 2.4.3).

2.4.3 DOC-TCA protein precipitation

For protein precipitation of samples with low protein content the following protocol was employed, according to Bensadoun and Weinstein (1976), with alternations. A 20 mg/mL sodium deoxycholate (DOC) (Sigma) solution was made up in ddH_2O, added to the filter sterilised supernatant at a final concentration 0.2 mg/mL and chilled on ice for 30 minutes. 100% chilled trichloroacetic acid (TCA) solution (w/v) (Sigma) was added to a final concentration of 10% (v/v) and the solution was incubated at -20°C overnight. For large volumes of supernatant, the frozen supernatant-DOC-TCA-solution was thawed on ice and aliquoted into four 1.5 mL microcentrifuge tubes. Proteins were pelleted by centrifugation at 18,000 x *g* for 10 minutes at 4°C in a Universal 320R refrigerated benchtop centrifuge (Hettich). The supernatant was carefully removed. This process was repeated several times using the same microcentrifuge tubes to process the entire sample volume. 1 mL ice-cold acetone (Sigma) was added to each pellet, vortexed and incubated at -20°C for 1 hour. Samples were then centrifuged at 19,000 x *g* at 4°C for 15 minutes. Following which, the supernatant was removed and pellets air-dried at room temperature for 30 minutes to remove residual acetone. The protein pellet was then solubilized in solubilisation buffer at a final volume of 1000-fold less than the initial culture supernatant volume (e.g. 20 µL for 20 mL culture supernatant). The solubilisation buffer either contained fresh 6 M urea (Sigma) and 25 mM ammonium bicarbonate (Sigma) or PBS containing 0.05% (w/v) SDS and 0.1% Triton X-100. An equal volume of 2X SDS-PAGE sample buffer was added to each sample, and analysed by SDS-PAGE (Section 2.5.2).

For small volumes of supernatant (e.g. from solid surface grown cultures), the precipitated solution was thawed and centrifuged in its original microcentrifuge tube and processed as above. The protein pellet was then resuspended in 20 µL of urea solubilisation buffer.

2.5 Protein quantification and separation techniques

2.5.1 Protein quantification assay

To quantify the concentration of protein in a solution, a modified Bradford assay was performed using a Bio-Rad protein assay kit I (Bio-Rad) as manufacturer's instructions, with minor alterations. Briefly, 1.0 mg/mL to 0.2 mg/mL protein standards were made using a 10 mg/mL BSA stock solution (Promega) diluted in an appropriate buffer (e.g. 50 mM Tris-HCl pH 8.0). The protein sample to be quantified was also diluted in appropriate buffer, at 1:1, or 1:3 dilution in a final volume of 50 µL. 1 part protein assay dye reagent concentrate (Bio-Rad) was combined with 4 parts ddH_2O, and filter sterilised using 0.22 µM syringe driven filter unit. 20 µL of protein standard and 20µL of protein sample were transferred into separate 1 mL semi-micro disposable cuvettes (Fisher Scientific) in duplicate. 1 mL diluted protein dye reagent was added, mixed and incubated for 5 minutes at room temperature. Absorbance at 595nm (OD_{595}) was measured using a spectrophotometer blanked with 1 mL diluted protein dye reagent. Protein samples with an OD_{595} over the range of the spectrophotometer (>0.9) where further diluted and re-tested with fresh reagent. A standard curve was generated by plotting the average absorbance obtained from the protein standards against their protein concentration (in mg/mL). Using this standard curve, the protein concentration of the unknown sample was then estimated using the average absorbance of the solution, taking into consideration the initial dilution factor of the sample.

2.5.2 Sodium dodecyl sulphate- polyacrylamide gel electrophoresis (SDS-PAGE)

An appropriate percentage Tris-glycine SDS-PAGE gel (0.75 mm, 10-well) was cast (typically 15%) as standard protocol (Laemmli, 1970) using a Mini-PROTEAN-II or Tetra Cell system (Bio-Rad) with 30% acrylamide/Bis-acrylamide solution (Fisher). For sample loading, an equal volume of 2X SDS-PAGE sample buffer (250 mM Tris-HCl, 10% SDS, 20% glycerol, 10% β-mercaptoethanol, 0.01% bromophenol blue) was combined with the protein sample, boiled at 100°C for 10

minutes to denature the proteins, and then centrifuged at 16,000 x *g* for 10 minutes. Samples were then loaded onto the gel and run at 120V for 1-1.5 hours in Tris-glycine SDS-PAGE running buffer (25 mM Tris, 192 mM Glycine, 0.1% SDS). 5 µL E.Z-Run unstained/pre-stained *Rec* protein ladder (Fisher) was also loaded as a protein marker. Gels were then stained with Coomassie blue solution (50% (v/v) methanol, 10% (v/v) acetic acid, 2.5 g/L Coomassie Brilliant Blue R-250) and destained with destain solution (40% (v/v) methanol, 10% (v/v) acetic acid) to visualise proteins. An image of the stained gel was captured using a light-box and Kodak EDAS 290 electrophoresis documentation system (Kodak).

2.5.3 Western blotting

SDS-PAGE gels were electro-blotted onto 0.45 µm PVDF membranes (Millipore), using a Mini-trans blot cell (BioRad), at 100 V for 1 hour or overnight at 30 V according to manufacturer's instructions or using a Trans-Blot Turbo semi dry blotter (BioRad) according to manufacturer's instructions. After transfer, the membrane was washed in Tris-buffer saline (TBS) (137 mM NaCl, 25 mM Tris base and 3 mM KCl, pH 8.0) for 1 minute to remove traces of transfer buffer and then blocked by incubation with blocking solution containing 5% (w/v) non-fat dry milk powder (Marvel, Premier foods) in TBS-Tween (TBS-T) (137 mM NaCl, 25 mM Tris base and 3 mM KCl, 0.05% Tween-20, pH 8.0) for 1 hour at room temperature. The membrane was then incubated with the appropriate primary antibody diluted in 5 mL blocking solution at 4°C overnight on a rolling mixer, or 2 hours at room temperature. The membrane were subjected to three 10-minute washes in TBS-T, and then incubated for 1 hour at room temperature with an appropriate HRP-conjugated secondary antibody diluted in 5 mL blocking solution. This was followed by three 10-minute washes in TBS-T, and a final wash in TBS. Detection of horseradish peroxidase (HRP) activity was achieved by the addition of a luminol-based enhanced chemiluminescence substrate, EZ-ECL (Biological Industries), as manufacturer's instructions. Chemiluminescence was detected using a ChemiDoc XRS+ system imager and Image Lab software (Bio-Rad).

2.5.4 Antibodies

Table 2.7 indicates the primary and secondary antibodies used in this study and dilutions they were used at.

Table 2.7 Antibodies used in this study.

Primary antibody (Source)	Type	Dilution	Secondary antibody (Source)
Anti-TssD (University of Sheffield Biological Services)	Custom polyclonal in rat	1:1000-1:2000	Goat anti-rat HRP at 1:5000 (SouthernBiotech)
Anti-TssD (York Biosciences)	Custom polyclonal in rabbit	1:10000-1:15000	Goat anti-rabbit HRP at 1:20000 (Vector Laboratories)
Anti-BCAS0667 CTD (University of Sheffield Biological Services)	Custom polyclonal in rat	1:500-1:1000	Goat anti-rat HRP at 1:5000
Anti-hexa-histidine tag (Berkeley Antibody Company)	Monoclonal in mouse	1:1000-2500	Rabbit anti-mouse HRP at 1:4000 (Thermo scientific)
Anti-FLAG (Sigma)	Polyclonal affinity isolate in rabbit	1:2500	Goat anti-rabbit HRP at 1:5000.
Anti- β subunit of *E. coli* RNA polymerase (Neoclone)	Monoclonal in mouse	1:2000	Rabbit anti-mouse HRP at 1:5000

2.5.4.1 Custom antibody production

Custom polyclonal antibodies were raised against a purified protein antigen in rat using a standard 90-day protocol by the Biological Services Department at The University of Sheffield. This protocol involved 4 intravenous injections of the antigen, with antibody titre of the immunised rats determined after the third antigen injection.

2.5.4.2 Analysis of antibody titre

Sample bleeds were taken from immunised rats after a third antigen injection to determine the antibody titre. Western blotting was used to estimate the maximum dilution of purified antigen that was detectable with a 1:1000 and 1:5000 dilution of anti-sera from the immunised rats. Then was then used to make an informed decision on if to proceed with a final antigen injection and the taking of terminal bleeds ten days later.

2.6 Mass spectroscopy techniques

2.6.1 In-solution digestion

First, DOC-TCA precipitated proteins from culture supernatants were resuspended in solubilisation buffer containing PBS, 0.05% (w/v) SDS and 0.1% (v/v) Triton X-100 (Section 2.4.1 and 2.4.3) and then transferred to Lo-bind microcentrifuge tubes (Eppendorf). Samples were reduced by the addition of 50 mM tris(2-carboxyethyl) phosphine (TCEP) to give a final concentration of 5 mM and heated at 65°C for 1 hour. Following this, 200 mM methyl methanethiosulfonate (MMTS) was added to give a final concentration of 10 mM and incubated for 10 mins at room temperature to alkylate the samples. Trypsin (MS grade, Sigma) was then added to the samples at a 1:25 ratio and incubated overnight at room temperature to digest the proteins into peptides. The resulting peptides were dried using a vacuum concentrator (Eppendorf) and then resuspended in 50 μL 1 M triethylammonium bicarbonate buffer (TEAB) (pH 8.5) (Sigma).

2.6.2 Detergent removal

Due to incompatible of the sample from Section 2.6.1 with mass spec analysis, the samples were subjected to detergent removal using a HiPPR™ Detergent Removal Spin Column Kit (Thermo Fisher Scientific) as manufacturer's instructions. HiPPR™ Detergent Removal resin, 0.8 mL spin columns provided in the kit and 1 M TEAB equilibration buffer were used. The detergent-free sample was eluted into Lo-Bind microcentrifuge tubes and then dried to completeness using a vacuum concentrator.

2.6.3 Desalting and concentration using C18 resin

For sample desalting and concentration prior to MS analysis, samples were dried after detergent removal, resuspended in 100 μL of buffer C (3% (v/v) acetonitrile, 0.1% (v/v) trifluoroacetic acid (TFA) in HPLC grade H_2O) and then subjected to C18 resin clean up. To do this, a C18 spin tip was fitted to a 2mL

collection tube and conditioned by the addition of 100 μL 100% acetonitrile (Sigma). The spin tip and collection tube assembly was centrifuged at 1000 x *g* for 30 seconds and the flow-through discarded. 100 μL of HPLC grade H_2O was then added to the spin tip, span as before and the flow-through discarded. The tip was then equilibrated with the addition of 100 μL buffer C, centrifuged and the resulting flow-through discarded. The peptide sample was then carefully loaded onto the resin, ensuring not to introduce any air bubbles, and centrifuged as above to pass the sample through the resin. Peptides were expected to bind to the C18 resin. The flow-through was retained as a precautionary measure in case the peptides did not bind. The resin was washed to remove salts by adding 100 μL of buffer A (3% (v/v) acetonitrile, 0.1% (v/v) formic acid in HPLC grade H_2O) to the spin tip, centrifuged as before and the flow-through discarded. This was repeated thrice more. After the final wash step peptides were eluted by the addition of 100 μL buffer B (97% acetonitrile, 0.1% formic acid in HPLC grade H_2O), and centrifuged as above into clean Lo-Bind microcentrifuge tubes. Samples where then subjected to concentration using a vacuum concentrator to reduce the sample volume before fractionation.

2.7 Techniques for analysis of protein–protein interactions

2.7.1 Pull-down assay

The following pull-down assay is based on the principle of immobilising a His-tagged 'bait' protein onto a nickel matrix, adding a labelled 'prey' protein which is thought to interact with the bait protein, and then elution of the His-tagged protein from the matrix. If the two proteins interact to form a complex then the prey protein should be present in the sample after elution of the His-tagged protein, by being 'pulled-down'.

Two pull-down methods were undertaken, either co-overproduction of both prey and bait together from a dual expression plasmid, or the classical method of separate overproduction of the two proteins of interest and then sequential addition of the lysates to the affinity resin. The protocol used in each method was based on the 'small-scale batch chromatography method' (Section 2.3.4), with minor alterations. For co-production lysates, the lysate was bound to nickel affinity resin, washed and eluted as standard procedure (Section 2.3.4). For the classical pull-down method, the His-tagged bait protein was immobilised onto nickel resin and washed as Section 2.3.4. Following this, 100 μL of lysate containing the tagged-prey protein (either FLAG or 3xFLAG epitopes) was then added to the resin containing the immobilised bait protein and subjected to gentle inversion on a rotary mixer (at 22rpm) for 30 minutes at room temperature. The sample was then centrifuged at 700 x *g* for 1 minute to isolate the resin. The supernatant was removed and retained as flow-through. The resin was then washed with 500 μL wash buffer (50mM Tris-HCl (pH 8.0), 200mM NaCl, 10mM imidazole and 5% glycerol), span down to collect the resin and the supernatant removed and retained. This processed was repeated twice more. After the final wash step bound proteins were eluted as described in Section 2.3.4 by the addition of elution buffer containing 150-500 mM imidazole. A negative control reaction was undertaken where the prey protein was incubated with resin that did not contain immobilised bait protein. This was to ensure that the prey protein was unable to bind non-specifically to the resin. A positive control was included were the His-tagged bait protein was bound to the resin on its own.

All samples including the load, flow-through, wash and imidazole elution samples were combined with 2X SDS-loading buffer and subjected to SDS-PAGE on appropriate percentage SDS-PA gels (12-15%) (Section 2.5.2). Corresponding samples were also subjected to separation by SDS-PAGE, electro-blotting onto PVDF membrane in duplicate and analysis by western blotting, using antibodies against each tagged protein on separate blots (e.g. anti-His6 and anti-FLAG) (Section 2.5.3).

2.7.2 Bacterial two-hybrid assay (BACTH)

The bacterial adenylate cyclase two-hybrid system (BACTH) (Euromedex) allows analysis of protein-protein interactions *in vivo*. This method is based upon restoration of adenylate cyclase activity (cyclic AMP (cAMP) production from ATP) in a Δ*cyaA E. coli* strain by the formation of an active adenylate cyclase domain from *Bordetella pertussis* (CyaA). This occurs by a interaction between the complementary T25 and T18 fragments of CyaA (Karimova et al., 1998). The coding sequencing of the genes that encode the proteins of interest (i.e. that are hypothesised to interact) are fused to the C- or N-terminus of coding sequences of T25 and T18 fragments by cloning into the BACTH vectors pUT18, pUT18C, pKT25 and pKNT25. If the hybrid fusion proteins interact, the T25 and T18 fragments are brought together, restoring activity of CyaA. This results in cAMP production. cAMP can then go on to form a complex with dimeric CRP, the cAMP receptor protein. This complex acts as an activator of gene transcription, including the activation of genes within operons involved in catabolism of lactose and maltose. This leads to the bacteria being able to use maltose or lactose as their sole carbon source, which can be discerned by using indicator media, such as MacConkey agar.

The coding sequence of the genes of interest were cloned in-frame into the MCS of vectors pUT18 and pUT18C, and pKT25 and pKNT25 by standard molecular biology techniques, using *E. coli* XL1-blue as the host strain. Compatible pUT18, pUT18C and pKT25 and pKNT25 plasmids were then co-introduced into chemically competent *E. coli* BTH101 cells by transformation. The resulting transformants were plated onto MacConkey agar containing 1% maltose, ampicillin and kanamycin, to give 100-200 CFU per plate. The plates were incubated at 30°C for up to 7 days,

and colony colour monitored for Mal^+ phenotype (purple appearance) after 72 hours. A positive control was included which involved co-introducing pUT18C-zip and pKT25-zip plasmids into BTH101, which should have given a strong positive Mal^+ phenotype. Mal^+ phenotype was scored as indicated in Table 2.8.

Table 2.8 Scoring system used to describe Mal^+ phenotype in BACTH assay.

Colony appearance	Score[a]
Very strong Mal^+ phenotype, deep purple after 72 hours, more than zip control.	+++++
Strong Mal^+ phenotype, deep purple after 72 hours, as zip control.	++++
Mal^+ phenotype, red/purple after 72 hours	+++
Weaker Mal^+ phenotype red/pink after 72 hours	++
Weak Mal^+ phenotype red/pink after 84 hours	+
Negative Mal phenotype, pale pink	-
Patchy, non-uniform colouration	P

[a] phenotype observed and scored after incubation on MacConkey agar containing 1% maltose (w/v) at 30°C for at least 72 hours.

2.8 Techniques for analysis of nuclease activity

2.8.1 Substrate-gel zymography

To analyse DNase activity of recombinant proteins DNA substrate zymography was performed as follows. Protein samples were combined with an equal volume of 2X SDS-PAGE sample buffer without β-mercaptoethanol, and loaded directly onto a DNA substrate gel. This gel was made by co-polymerising 12-15% SDS-polyacrylamide with 30 µg/mL sheared salmon testis DNA (Fluka). Samples were not subject to heat treatment prior to loading. Sample were run at 120 V for ~1.5 hours. After separation, the gel was washed in wash buffer containing 40 mM Tris-HCl, pH 7.6 for 30 minutes with agitation at room temperature to help remove SDS. The gel was then incubated in renaturation buffer (50 mM Tris-HCl, pH 7.5, 5 mM $MgCl_2$, and 20% 2-propanol) for 1 hour with gentle rocking at room temperature, with two changes of buffer. The gel was transferred to a reaction buffer (50 mM Tris-HCl, pH 7.5, 5 mM $MgCl_2$, 2 mM $CaCl_2$, and 0.1% Triton X-100) and incubated at 37°C for 2 hours. The buffer was removed and replaced with reaction buffer containing ethidium bromide at a final concentration of 2 µg/mL, and left for a further 30 minutes. Gels were visualised under a UV transluminator using a ChemiDoc XRS+ imaging system (Bio-Rad).

2.8.2 In-solution DNA degradation assay

To determine if purified proteins were able to degrade DNA in-solution the following was undertaken. 100 ng of supercoiled plasmid DNA (pBluescriptII) was incubated with 2 µL of purified enzyme in a reaction buffer containing 10 mM Tris-HCl (pH 7.5) with or without 2.5 mM $MgCl_2$, 0.5 mM $CaCl_2$ in total reaction volume of 10 µL. The ability of EDTA to act as an inhibitor of DNase activity was also performed by addition of 20 mM EDTA to the reaction buffer. Control reactions were included to test the DNase activity of the enzyme in each buffer component separately, and a negative reaction lacking the addition of the enzyme. DNase I (Qiagen) was used as a positive control to demonstrate degradation of DNA in solution. Samples were incubation at 37°C for 2 hours in a heated water bath.

Following this, 2 µL 6X DNA loading dye was added to each reaction, and the entire sample ran on a 0.8-1.0% DNA agarose gel to visualise the integrity of the DNA.

Linearised plasmid DNA (linearised by restriction digestion and DNA clean up) and M13mp18 single-stranded DNA (ssDNA) (New England BioLabs) were also used as DNA substrates as above, to test the DNase activity of purified enzymes on different DNA substrates.

2.9 Techniques for analysing bacterial toxicity

2.9.1 Bacterial competition assay

4 mL LB-broth cultures were inoculated with a single colony from a freshly cultured LB/BHI agar plate of the predator (*B. cenocepacia*) and prey (e.g. *P. putida*, *E. coli* CC118(λpir)) strains and grown overnight at 37°C. OD_{600} was determined for each culture. An aliquot of each strain was taken and normalised to give a 1 mL bacterial suspension of OD_{600} of 0.5. Bacterial suspensions were combined in a 5:1 ratio of predator:prey in a total volume of 60 µL. For example, 50 µL *B. cenocepacia* was combined with 10µL *P. putida*. Monoculture controls of prey and predator strains were also included by combining cultures with sterile LB in the appropriate ratio, e.g. 50µL sterile LB to 10µL *P. putida*. 25 µL of each co-culture and control culture were then spread over a 0.45 µm nitrocellulose filter membrane placed on a pre-warmed LB agar plate, left to soak in and then incubated at 30°C for 4 hours. After incubation, bacterial growths were harvested from the filter membranes by transferring the membranes into separate universal tubes containing 1 mL sterile LB and vortexed for 1 minute to ensure filter membranes were fully coated in medium. 10^{-1} to 10^{-5} serial dilutions in LB were made from the re-suspended cultures. 10 µL of each dilution was spotted onto two separate selection plates in triplicate using the surface viable count method (Miles et al., 1938). Plates were incubated at either 37°C or 30°C overnight, dependent on the strain. The number of viable CFU were counted and used to calculate the CFU/mL for each co-culture or control culture tested. Data was represented as a grouped scatter plot.

2.9.2 Ectopic expression toxicity assay

To determine whether ectopic production of a candidate effector protein had a detrimental effect on the culture the following protocol was undertaken. For periplasmic ectopic overproduction from pET-22b(+) based vectors, plasmids were first introduced into *E. coli* BL21(DE3)/pLysS. A single colony was then used to inoculate 2 mL of BHI-broth containing 200 µg/mL carbenicillin and 25 µg/mL chloramphenicol. Cultures were grown at 37°C with shaking until an OD_{600} of ~0.4 was reached, as measured by a spectrophotometer. 1 mL of culture was taken and

centrifuged at 5000 x *g* for 2 minutes to isolate the bacteria. The supernatant was removed and 1 mL fresh sterile BHI was used to resuspend the bacteria. The resulting bacterial suspension was then used to inoculate 8 mL of BHI-broth containing 500 μg/mL carbenicillin and 25 μg/mL chloramphenicol to give an OD_{600} of 0.03, in duplicate. Cultures were then grown at 37°C with shaking until an OD_{600} of ~0.8. One of the duplicate cultures was then induced by the addition of 1 mM IPTG (final concentration), whilst the other remained uninduced. Both cultures were transferred to 30°C for 3 hours where the culture optical density was then monitored at 30-minute intervals after induction. After the final 3-hour time-point 1 mL of the remaining culture was centrifuged to isolate the bacteria, resuspended in 100 μL 2X SDS-PAGE sample buffer and then boiled for 5 minutes to lyse the cells.

The resulting culture optical densities measured over the course of the induction (from time 0 when the induced was added) were compared between uninduced and induced samples and between wild-type and a catalytically inactive mutant. Data was represented as a line chart, plotting the OD_{600} value (y axis) against the time after induction that the value was taken (x axis).

Induced and uninduced samples were also subjected to SDS-PAGE and western blot analysis to verify protein production.

For co-expression experiments using pET-22b(+) and pSCrhaB2 derived plasmids the same protocol was undertaken with minor alterations. This involved addition of 100 μg/mL trimethoprim in all culture media and induction with both 1 mM IPTG and 0.1% rhamnose (final concentration).

2.10 Techniques for analysis of eukaryotic virulence *in vivo*

2.10.1 Zebrafish embryo infection assay

Zebrafish embryo infection was performed as described in (Vergunst et al., 2010). Briefly, a plasmid encoding DsRed, pIN29, was transferred into *B. cenocepacia* strains by electroporation (Section 2.2.16). Bacteria were then grown overnight in LB containing the appropriate antibiotics. In preparation for injection into embryos, overnight bacterial cultures were harvested by centrifugation, resuspended in PBS and diluted to give approximate bacterial concentration of $5x10^7$ CFU/mL. 30 hours post-fertilisation zebrafish embryos were dechorionated and anesthetized in E3 medium with 0.02% buffered tricaine methanesulfonate (MS222, Sigma) ready for infection. Embryos were then microinjected with 200-300 CFU of DsRed-labelled bacteria directly into the blood circulation and maintained in E3 medium at 28°C for 48 hours. 20 embryos were infected per bacterial strain tested and the experiment performed in duplicate. Embryo survival was monitored at regular intervals, were dead embryos scored as those without a heartbeat. Percentage embryo survival was then represented using a Kaplan-Meier plot.

Bacterial replication within the embryos was assayed by injection of bacteria as described above. 5 infected embryos per treatment group were taken at 0, 24 and 48 hours post-infection and subjected to bacterial enumeration as described in (Vergunst et al., 2010). Briefly, individual embryos were washed in 1 mL sterile PBS and anesthetized with 0.02% tricaine methanesulfonate. Following this, each embryo was transferred into a microcentrifuge tube, incubated with 50 μL Trypsin-EDTA solution (0.25% trypsin, 1 mM EDTA in PBS) and then disrupted by pipetting repeatedly. For further disruption, 50 μL Triton X-100 solution (2% Triton X-100 in PBS) was added to give a final conc. 1% Triton X-10 and left to incubate at room temperature for 20 minutes. This was then followed by repeated pipetting. Serial dilutions were made of the resulting suspensions in PBS. Bacteria were enumerated by spotting 10 μL of each dilution in triplicate on LB agar containing 100 μg/mL chloramphenicol using the surface viable count method described in (Miles et al., 1938) and cultured at 37°C for 24-48 hours. These counts were used to calculate

the CFU/mL at each time-point during the infection and the data was represented as a grouped scatter plot.

2.10.2 *Galleria mellonella* larvae infection assay

Final-instar *Galleria mellonella larvae* were purchased fresh from Livefoods UK and maintained at 4°C before infection. For preparation of bacteria for injection, *B. cenocepacia* K56-2 strains were cultured from -80°C glycerol stocks onto BHI agar. A single colony was then used to inoculate 5 mL BHI-broth and incubated at 37°C with shaking for ~5-6 hours until an OD_{600} of 0.6 was reached. The bacteria were centrifuged at 5000 x *g* for 2 mins and resuspended in PBS to give an approx. OD_{600} of 0.5, equating to approximately $4x10^8$ CFU/mL.

For optimization of bacterial dosage, serial dilutions of the bacteria were made in PBS to give of $4x10^6$ to $4x10^2$ CFU/mL. 10 μL of each dilution was then injected into the hindmost left proleg of the larva using a 25 μL Hamilton syringe (702N series, 22s gauge fixed needle, point style 2) or semi-automatically using a PB-600-1 Repeating Dispenser (Hamilton) affix to a Gastight 500 μL Hamilton syringe (Model 1750 RN (large hub) SYR, with a 22 gauge, large hub RN NDL, 2 inch, point style 2 needle). 20 larvae were infected per treatment group. Control treatment groups were injected with 10 μL of sterile PBS, or 10 μL heat killed bacteria (the lowest dilution of the bacterial culture used boiled at 100°C for 10 minutes). An additional group of larvae were left untreated. Larvae where incubated at 37°C for 48 hours in sterile plastic petri dishes lined with filter paper discs. The numbers of alive/dead larvae were assessed for each treatment group at 18, 24, 40 and 48 hours post-treatment. Dead larvae were classed as those that were stationary and no longer responded to touch. Percentage larval survival for each treatment group over-time was presented as a line chart, or the percentage larval survival relative to the bacterial inoculum was presented as a kill curve.

For determination of virulence of strains, larvae were infected as above with minor alterations. 30 larvae per treatment group were infected with $4x10^4$ and $4x10^2$ CFU/larvae of wild-type or mutant strains, separately. Larval survival was

monitor from 16 hours to 26 hours post-infection at 2-hour intervals. Percentage larval survival after infection was represented as a line chart.

To approximate the initial bacterial load 10^{0} to 10^{-8} serial dilutions were made from each bacterial suspension used. 10 μL of each dilution were then spotted onto LB agar contain 10 μg/mL tetracycline in triplicate using the surface viability method (Miles et al., 1938). A 10 μL spot of heat-killed bacterial suspension was also plated to verify the effectiveness of heat killing of the control. Plates were incubated at 37°C for 48 hours and then the colonies were counted to give an estimation of the CFU/mL of each inoculum.

Chapter 3: Bioinformatic analysis of T6SS gene clusters and putative effectors in *B. cenocepacia* J2315

3.1 T6SS gene clusters in *B. cenocepacia*

3.1.1 Ancestral T6SS cluster, T6SS-1

Many T6SS-containing bacteria have multiple T6SSs encoded within their genome, including some of the *Burkholderia* species. *B. pseudomallei* for example has six T6SS clusters (Shalom et al., 2007) while *B. lata* has three (M. S. Thomas, personal communication). However, most members of the Bcc, including *B.cenocepacia* J2315 and K56-2*,* have just one T6SS, which is referred to as the ancestral T6SS or T6SS-1, as it is the most prevalent in the *Burkholderia* spp. and is particularly conserved in two groups of *Burkholderia*, the Bcc and the pseudomallei group (Angus et al., 2014). Moreover, in almost all species of *Burkholderia* for which genomes sequences are available, T6SS-1 (when present) is located on chromomsome 1, whereas additional T6SS clusters (where present) are generally located on chromosome 2. For example, T6SS-1 is encoded on chromosome 1 in *B. pseudomallei*, whereas T6SS-2 to T6SS-6 are encoded by chromosome 2 (Shalom et al., 2007). In *B. cenocepacia* J2315 the T6SS-1 cluster is found on chromosome 1 at the BCAL0337-BCAL0353 locus, and the T6SS-1 homologous cluster in *B. cenocepacia* H111 is similarly located on chromosome 1 at the I35_0328-I35_0344 locus. This ancestral cluster has a similar genetic organisation in not only the *Burkholderia* spp., but other related proteobacteria such as the plant pathogen *Ralstonia solanacearum* and the water-dwelling photoheterotrophic *Rubrivivax gelatinosus*. It is also present in the ϒ-proteobacteria species *Xanthamonas oryzae*, an important environmental pathogen that causes bacterial blight in rice plants.

Most clusters contain the core *tss* gene orthologues *tssA-tssM* on closely linked transciptional units, although in some members of the Bcc a *tssI* gene is not present at this locus (Figure 3.1). At least two pairs of putative divergent promoters are present in the *Burkholderia* T6SS-1, between *tssJ* and a type VI associated gene, *tagM* (Shalom et al., 2007), which have been experimentally confirmed (Shastri, 2011) and between two additional *tag* genes, *tagV* and *tagX*, located upstream of *tssM,* neither of which have been confirmed. In *B. cenocepacia,* a *tssI* gene is not found in the cluster, but at least 10 different *tssI* genes are located elsewehere

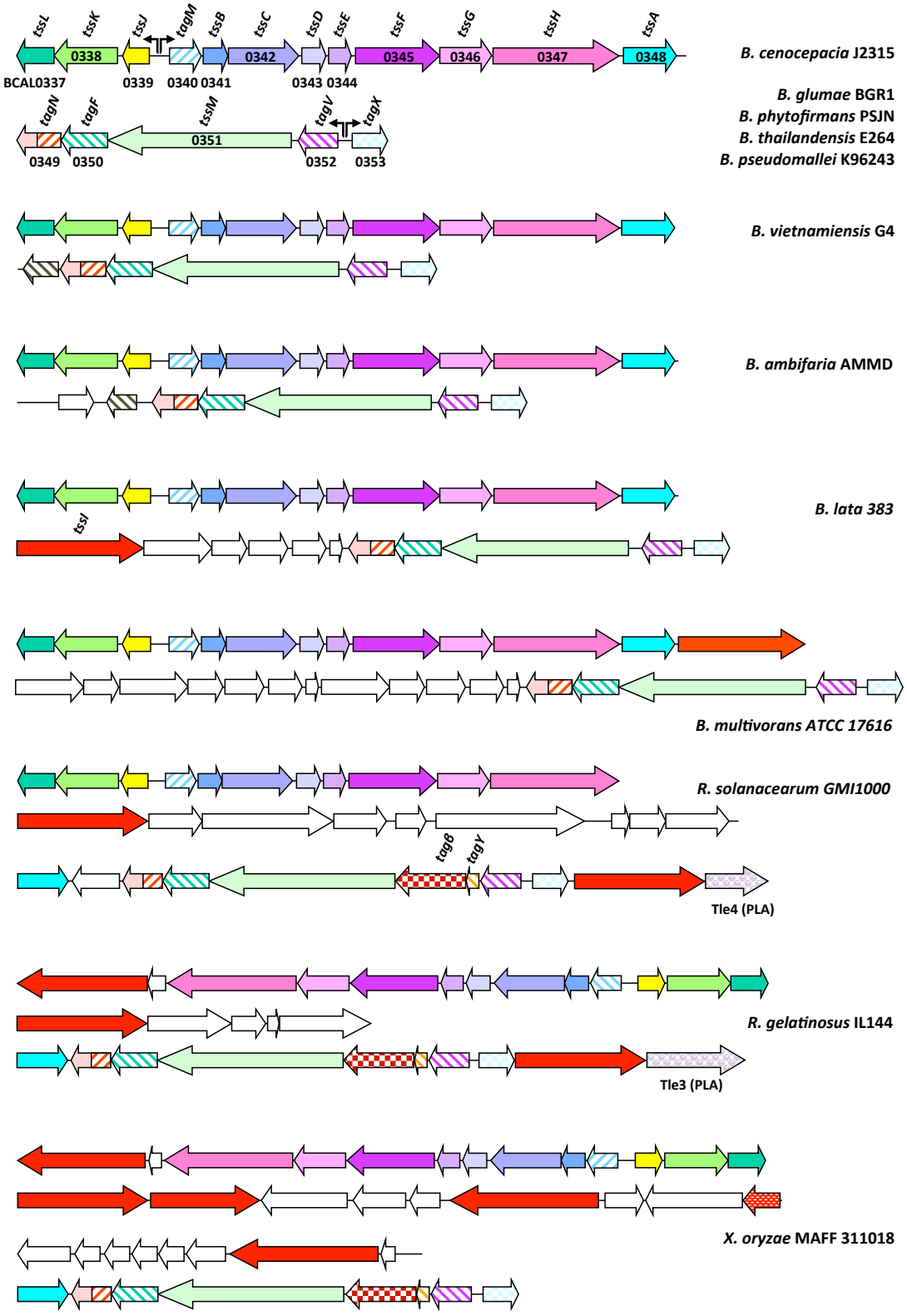

Figure 3.1 The ancestral *Burkholderia* T6SS gene cluster (T6SS-1) and orthologous T6SS gene clusters. Illustration of the genetic arrangement of the ancestral *Burkholderia* T6SS-1 cluster, containing *tssA* through to *tssM*, along with the conserved *tag* genes, *tagM, tagN, tagF, tagV* and *tagX*, and less conserved *tag* genes *tagY and tagβ*. Standard T6SS nomenclature is indicated in black font above the arrows. Orthologous T6SS subunit genes

between clusters are depicted in the same uniform colour, while *tag* genes are hatched or chequered. Predicted non-*tssI* effector genes are filled in purple bubbles. Genes shown in white are of unknown function and are not conserved in T6SS-1 gene clusters. The bacterial species containing each cluster is indicated on the right. Numbering within or below arrows of the first cluster shown indicate the genetic loci from *B. cenocepacia* J2315, BCAL0337 – BCAL0353. Not to scale.

throughout the genome.

3.1.2 T6SS associated genes (*tag*)

In total there are 5 conserved *tag* genes in the ancestral *Burkholderia* T6SS-1 cluster: *tagF*, *tagM*, *tagN, tagX*, and *tagV*, whose products may to be involved in function or regulation of the system. Figure 3.1 also illustrates the presence of these conserved *tag* genes in T6SS-1-like clusters in other Gram-negative bacteria. Figure 3.2 illustrates the predicted topological arrangement of the conserved Tag proteins in relation to other T6SS subunits.

TagN has a peptidoglycan-binding domain, that is proposed to act structurally to anchor the T6SS to the cell envelope (Aschtgen et al., 2010b). This is consistant with the fact that the TssL encoded by T6SS-1 lacks a peptidoglycan-binding C-terminal domain. The presence of a cytoplasmic TagF-like protein (BCAL0350 in J2315), suggesting a mechanism similar to that seen in *P. aeruginosa*, as a TPP-independent negative post-translation regulator (Section 1.4.3) (Silverman et al., 2011). An additional conserved Tag protein, TagM (BCAL0340 in J2315), contains an N-terminal Sec-dependent signal peptide and is predicted to be an outer membrane-anchored lipoprotein. TagM may be involved in post-translational regulation of the T6SS encoded by T6SS-1. This protein also contains two periplasmically located TPR repeat domains that may be important for protein-protein interactions. A Δ*tagM* mutant in *B. cenocepacia* K56-2 has been observed to show increased intracellular bacterial replication in a macrophages host, but it is unclear whether this feature is related to the T6SS (Tolman and Valvano, 2012).

A further potential post-translational regulator is the uncharacterized conserved hypothetical protein TagX (BCAL0353 in J2315). *tagX* is, without exception, located upstream, but in the opposite orientation to *tagV*. *tagV* encodes a putative Sec-dependent membrane-anchored VanY-like D-alanyl-D-alanine carboxypeptidase, therefore may specify peptidoglycan hydrolase activity (Wright et al., 1992). It is likely to be anchored into the cytoplasmic membrane, with the enzymatic domain in the periplasm, which is consistent with its predicted peptido-

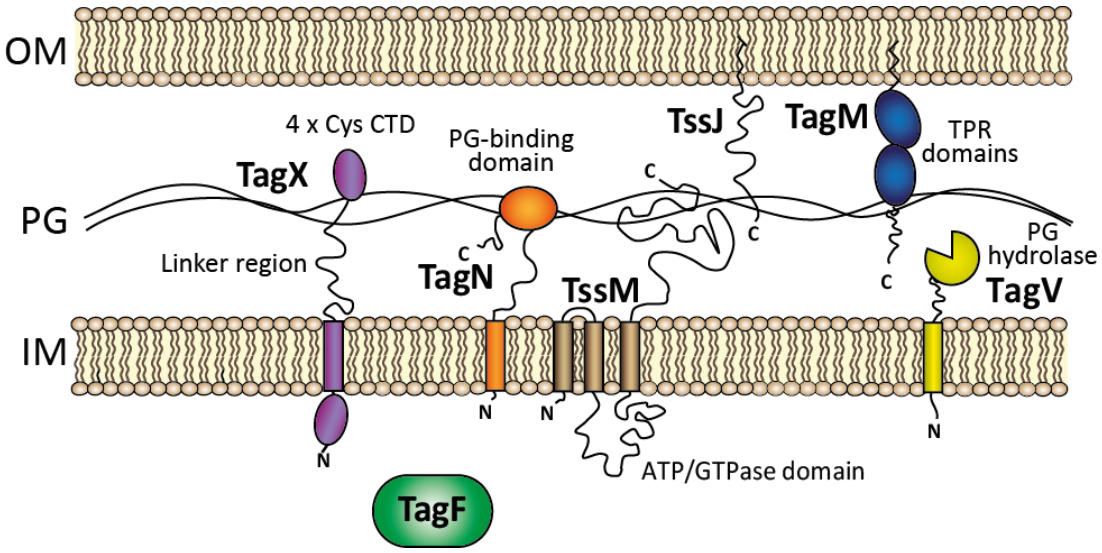

Figure 3.2 Predicted structural organisation of conserved Tag proteins in the ancestral *Burkholderia* T6SS. TagF, TagM and TagX are candidate post-translation regulators of the T6SS in *B. cenocepacia*. Also shown are the two T6SS core subunits that are largely located in the periplasmic space, where TssM contacts TssJ. TagF may be a cytoplasmic negative post-translational regulator, possibly acting on TssM. TagX is predicted to contain a TMD, and a long linker region extending into the periplasm with a CTD containing four conserved cysteine residues. TagN is an inner membrane-bound protein, containing a peptidoglycan-binding domain, probably anchoring the complex to the peptidoglycan. TagV is a putative Sec-dependent peptidoglycan hydrolase/endolysin, which is also likely to be anchored to the inner membrane. Zigzag motifs represent acyl moiety at the N-terminus of OM-anchored lipoproteins. Cylindrical motifs in the inner membrane represent TMDs. OM, outer membrane; PG, peptidoglycan/periplasm; IM, inner membrane; CTD, C-terminal domain; TPR, tetratricopeptide repeat; N, N-terminus; C, C-terminus.

glycan hydrolase activity. TagV may be involved in assembly or stability of the T6SS within the cell envelope.

In regard to *tagX*, bioinformatic analysis of the encoded protein has highlighted some interesting features, discussed in Section 5.2. These include a putative cytoplasmic N-terminal domain, followed by transmembrane a domain, and a periplasmic linker connecting the transmembrane domain to a C-terminal domain. Notably, this C-terminal domain contains four conserved cysteine residues. This arrangement is common in iron-sulphur cluster proteins that act as redox or metal ion sensors (Lill, 2009), such as the superoxide and NO sensor SoxR in *E. coli* (Nunoshiba et al., 1992; Ding and Demple, 2000), hence the designation of TagX as a putative regulatory protein (Section 5.2 for more details).

Further Tag proteins, including those encoded by the *tagY* and *tag*β genes, are present in some T6SS-1 gene clusters and where they are absent they are linked to *tssI* (*vgrG*) gene clusters. TagY is likely to be a type of PAAR protein, as many contain homology to the pfam05488 PAAR_motif of the PAAR-superfamily (CL15808) (Shneider et al., 2013). Tagβ is predicted to be a cytoplasmic membrane-anchored protein containing three transmembrane domains and a large cytoplasmic domain. Its function is unknown.

3.1.3 An additional T6SS cluster in *B. cenocepacia* H111

Inerestingly, a second unidentified T6SS cluster is present in the H111 strain of *B. cenoepacia*, located on chromosome 2 at the I35_4151-I35_4168 locus (Figure 3.3) (our unpublished observations). It contains homologues of all the core T6SS genes, *tssA*-*tssM*, and unlike the T6SS-1 cluster this cluster does contain its own *tssI* gene. This cluster is homologous to a T6SS cluster found in related environmental and plant-associated bacterial species, which includes *Cupriavidus metallidurans* of the *Burkholderiaceae* family and one of three intact T6SSs found in *B. glumae*, a plant pathogen (Figure 3.3). The cluster is defined as a new clade of T6SS cluster in *Burkholderia* species due to its unique gene arrangement, termed T6SS-a (Angus et al., 2014). For simplicity the second T6SS cluster of *B. cenocepacia* H111 will be

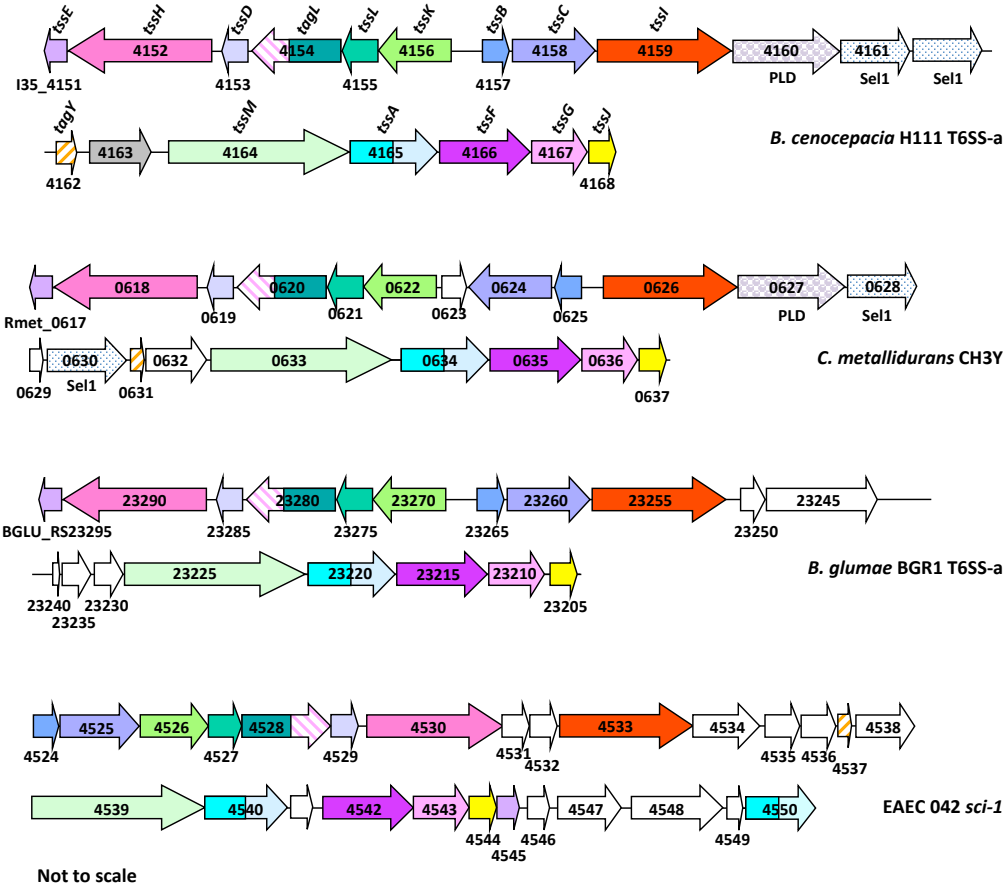

Figure 3.3 The T6SS-a gene cluster of *B. cenocepacia* H111 and similar clusters in other bacteria. Illustration of the genetic arrangement of *B. cenocepacia* H111 additional T6SS cluster, T6SS-a, found on chromosome 2 at I35_4151-I35_4168. Standard T6SS nomenclature gene names are indicated in black font above the genes (block arrows). Orthologous T6SS subunit genes between clusters are depicted in the same uniform colour, while *tag* genes are hatched or chequered. Predicted non-*tssI* effector genes are filled in purple bubbles. Genes shown in white are of unknown function and are not conserved in T6SS-a gene clusters. Gene loci indicated within or below arrows. Two homologous T6SS clusters are shown from *C. metallidurans* CH3Y and *B. glumae* BGR1. A similar T6SS cluster, the Sci-1 cluster from Enteroaggregative *Escherichia coli* 042 (EAEC) is also shown. Not to scale. PLD, predicted phospholipase lipase D enyzme.

referred to as T6SS-a.

Note, several genes within the *B. cenocepacia* H111 T6SS-a are likely to have missannotated translation inititation sites, including *tssM-a* located at I35_4164. The start codon is probably located approximately 237 bp upstream, meaning a further 79 codons are present. By using this earlier start site, TssM-a would then contain two additional transmembrane helices, bringing the total to three rather than one. This encoded TssM-a also lacks the Walker A motif found in most TssM orthologues, including that encoded by T6SS-1.

Interestingly, genetic organisation of the H111 T6SS-a is also similar but not identifical to the arrangement of the Sci-1 T6SS cluster of enteroaggregative *E. coli* (EAEC) located on a pathogenicity island (PAI) (Dudley et al., 2006). The Sci-1 T6SS is constitutively expressed under standard laboratory conditions (Dudley et al., 2006; Aschtgen et al., 2010a), but is thought to be controlled at a transcriptional level by the AraC-type global positive regulator, AggR (Dudley et al., 2006). It is also fine-tuned by Fur-dependent regulation of the Sci-1 T6SS promoter, which in turn is susceptible to DNA methylation of sites within the Sci-1 promoter, where DNA methylation reduces the ability of Fur to bind to its specific binding region (Brunet et al., 2011). In H111 T6SS-a there is a pair of putative divergent promoters between *tssB-a* and *tssK-a*, neither of which contain potential Fur binding sites ('Fur boxes'), so T6SS-a is probably not regulated by Fur. However, transcription of the cluster could still be regulated by an unknown global transcriptional regulator, as observed for Sci-1 T6SS and AggR in EAEC.

3.2 Survey of *tssI* genes in *B. cenocepacia* J2315 and H111

Genes encoding proteins that are homologous to the TssI subunit found in other T6SS-containing bacteria have been identified in the *B. cenocepacia* genome (Aubert et al., 2008). There are eleven *tssI* orthologues in the *B. cenocepacia* J2315 genome, although only nine of them are intact. A BLASTP search of the *B. cenocepacia* H111 genome using the TssI encoded by BCAM0148 identified twelve genes encoding TssI orthologues. Table 3.1 shows the *tssI* gene loci identified in H111 and indicates the corresponding gene in J2315. Note, that an orthologue of the disrupted *tssI* gene BCAL2503 is not present in H111, and two additional *tssI* genes are found in H111 that are not present at the same genomic location in J2315. The encoded products do however, share homology with TssI proteins found in J2315. One is encoded by I35_7565, found on chromosome three, which is similar to the TssI encoded by BCAL1359, and the other is I35_4159, found on chromosome 2, which is similar to BCAM0148. The latter is located in the T6SS-a gene cluster (Section 3.1.3).

All of these TssI protein, bar that encoded by BCAL2503, contain the core gp27-gp5-like region common to all TssI proteins (Pukatzki et al., 2007; Leiman et al., 2009) (Figure 3.4). Interestingly, all but four contain a C-terminal DUF2345 domain, which is hypothesised to act as an adaptor domain for interactions with specific T6SS-dependent effectors to allow their export (M.S. Thomas, personal communication). The DUF2345 domain is present at the C-terminus of TssI proteins in a wide range of bacteria, including VgrG2b encoded within the H2-T6SS of *P. aeruginosa* (Sana et al., 2015).

Table 3.1 *tssI* genes in *B. cenocepacia* J2315 and H111

J2315 gene locus[a]	H111 orthologues	Protein designation[b]
BCAL1165	I35_5787	$TssI_{1165}$
BCAL1294	I35_1208	$TssI_{1294}$
BCAL1355	I35_1250	$TssI_{1355}$
BCAL1359[c]	I35_1254	$TssI_{1359A}$
	I35_7565	$TssI_{1359B}$
BCAL1362	I35_1256	$TssI_{1362}$
BCAL2279*	I35_2205	$TssI_{2279}$
BCAL2503*	-	$TssI_{2503}$
BCAM0043	I35_4043	$TssI_{0043}$
BCAM0148[c]	I35_4131	$TssI_{0148A}$
	I35_4159	$TssI_{0148B}$
BCAM2254	I35_6147	$TssI_{2254}$
BCAS0667	I35_7843	$TssI_{0667}$

[a] TssI orthologues encoded by genes at specified loci in *B. cenocepacia* J2315.
[b] Terminology used in this study.
[c] Two orthologues of the encoded protein of this gene are found in *B. cenocepacia* H111, as indicated in the adjacent column.
- indicates no corresponding orthologue found.
* indicates *tssI* gene is disrupted. BCAL2503 is very likely to be non-functional as the encoded product is truncated at the N-terminus and fused to a TssF orthologue. The DUF2345-coding segment of BCAL2279 is disrupted by an IS1356 tnpase.

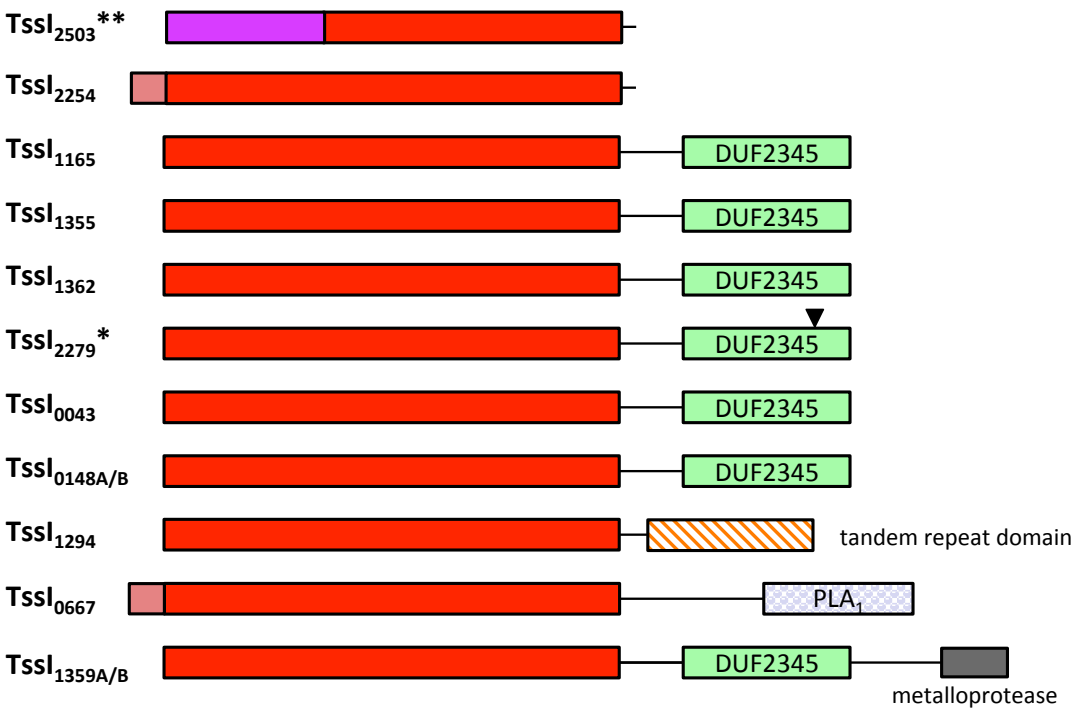

Figure 3.4 Domain organisation of TssI orthologues present in *B. cenocepacia*. Schematic representation of TssI orthologues present in *B. cenocepacia* J2315 and H111. Central gp27-gp5-like region is depicted in red and DUF2345 domain is shown in green. Evolved TssI proteins are shown with additional C-terminal extension domains as indicated. An N-terminal extension of 65 amino acids is present in two non-DUF2345 containing TssI orthologues, depicted in pink. A TssF fusion is indicated in purple, and the black triangular marker indicates IS1356 tnpase disrupted region. *, indicates orthologue is disrupted; **, indicates orthologue is disrupted and not present in strain H111. The corresponding designated protein name is indicated on the left.

3.3 Evolved TssI proteins as putative T6SS-dependent effectors in *B. cenocepacia*

Most of the TssI proteins encoded within the *B. cenocepacia* genome are evolved TssIs (discussed in Section 1.5.1) as they contain C-terminal extension domains, although, possibly not all of these domains have effector-like functions. Only two TssIs encoded by the J2315 genome ($TssI_{1359A}$ and $TssI_{0667}$) and an additional TssI encoded by H111 ($TssI_{1359B}$) could be predicted with any definite certainty to possess effector function. These are reviewed below.

3.3.1 $TssI_{1359A}$ and $TssI_{1359B}$ as evolved TssI proteins with a putative metalloprotease domain

An evolved TssI protein identified in *B. cenocepacia* strains J2315 and H111 is $TssI_{1359A}$, which is encoded by BCAL1359 in J2315 and I35_1254 in H111. This evolved TssI has a M6 family metalloprotease domain (TIGR03296) at its C-terminus (Figure 3.5A). The M6 family metalloproteases include the experimentally characterised immune inhibitor A from *Bacillus thuringiensis*, which has been shown to require a conserved HExxH motif for catalytic activity that is common in many zinc metalloproteases. It is thought that both conserved histidine residues are required for zinc ligand binding and the conserved glutamate residue is an active site residue (Lovgren et al., 1990). $TssI_{1359A}$ contains this catalytic HExxH motif, and additional conserved residues surrounding this motif. In particular, both contain a conserved alanine residue before the first histidine residue, a conserved glycine residue before the second histidine residue and then a PDEY motif located five amino acids C-terminal to the HExxH motif, giving a consensus motif of AHExGHxxgxPDEY.

$TssI_{1359B}$ encoded by I35_7665 also contains a C-terminal M6 family metalloprotease domain at its C-terminus. The catalytic motif of this protein partially follows the consensus AHExGHxxgxPDEY found in $TssI_{1359A}$ with one amino acid difference. Rather than a second relatively conserved glycine residue located two amino acids N-terminus to the PDEY motif (g), Tss_{1359B} contains an asparagine residue instead.

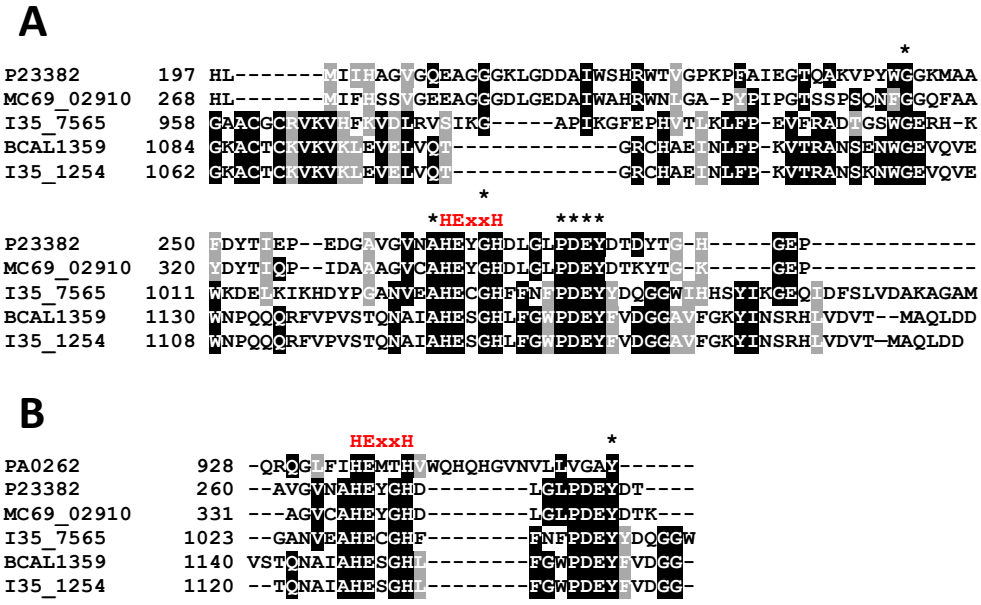

Figure 3.5 Alignment of C-terminal domains of $TssI_{1359A}$ and $TssI_{1359B}$ from *B. cenocepacia* J2315 and H111 with other metalloproteases. (A) The C-terminal amino acid sequence of $TssI_{1359A}$ in *B. cenocepacia* J2315 and H111 (BCAL1359 and I35_1254, respectively), and $TssI_{1395B}$ in *B. cenocepacia* H111 (I35_7565) were aligned with characterised M6 metalloprotease protein immune inhibitor A from *B. thuringiensis* (P23382), and an additional M6 metalloprotease encoded by MC69_02910 in *A. hydrophila* using Clustal Omega. (B) The HExxH region of proteins in (A) were aligned with the corresponding region of the experimentally characterised evolved VgrG2b protein encoded by PA0262 in *P. aeruginosa*. The conserved motif indicated in red above the alignment. Black shading indicates identical residues at the corresponding position in 50% of sequences, grey shading indicates similar residues at the corresponding position in 50% of sequences. Identical residues in 100% of sequences are indicated with an asterisk above the alignment. The designated gene locus is indicated on the left.

Interestingly, a metalloprotease domain-containing evolved TssI secreted by the H2-T6SS in *P. aeruginosa,* termed VgrG2b (Mougous et al., 2006; Barret et al., 2011; Sana et al., 2012; Sana et al., 2015), has been shown to be important for the internalisation of bacteria into epithelial cells (Sana et al., 2012). The C-terminal extension domain of VgrG2b contains the conserved HExxH metalloprotease motif, but not within the AHExGHxxgxPDEY motif seen in the M6 family metalloproteases (Figure 3.5B). Rather, it is defined as a PS00142 zinc-dependent metalloprotease. This evolved TssI is one of only a few T6SS-dependent effectors that have been shown to target eukaryotic cells rather than other bacterial species.

VgrG2b is thought to interact with key components of the host cell's microtubule structure, through the γ-tubulin ring complex, which aids in bacterial internalisation (Sana et al., 2015). Sana and colleagues postulated that the C-terminal metalloprotease domain is critical for this, as they demonstrated that a truncated TssI derivative, lacking the C-terminal metalloprotease domain, was unable to interact with the γ-tubulin ring complex, nor promote bacterial internalisation. Thus, it is possible that the metalloprotease-containing $TssI_{1359A}$ or $TssI_{1359B}$ proteins of *B. cenocepacia* may also be involved in similar interactions with the cytoskeletal network of eukaryotic host cells, which is consistent with the implied role of the T6SS system in actin arrangements in macrophages that have internalised *B. cenocepacia* (Rosales-Reyes et al., 2012b).

3.3.2 $TssI_{0667}$ as an evolved TssI protein

$TssI_{0667}$ is encoded by the BCAS0667 gene in *B. cenocepacia* J2315 and I35_7843 gene in H111, both of which are located on chromosome 3. Amino acid sequence analysis of $TssI_{0667}$ from both J2315 and H111 indicated that the two orthologues are nearly identical. In line with other TssI proteins, $TssI_{0667}$ contains an N-terminal gp27-gp5-like region, but it does not contain the DUF2345 region present in several other TssI proteins encoded by *B. cenocepacia*. The coding region for the BCAS0667 gene has an ambiguous translational initiation site, as there are two putative ATG start codons separated by 64 codons. Analysis of DNA sequences upstream of each of these ATG codons indicated a more fitting Shine-Dalgarno site

upstream from the first ATG codon (Figure 3.6). However, translation from this codon results in a 65 amino acid N-terminal extension that is not common to other TssI orthologues. Although, one other TssI orthologue present in *B. cenocepacia* that lacks a DUF2345 domain, $TssI_{2254}$, also has this N-terminal 65 amino acid extension that is nearly identical to one present in $TssI_{0667}$. Instead of a DUF2345 domain, $TssI_{0667}$ contains a long linker region of approximately 60 amino acids that is predominately composed of valine and proline residues, which connects the core TssI region to a C-terminal domain.

3.3.3 C terminal-domain of $TssI_{0667}$ as a phospholipase

A BLASTP search using the amino acid sequence of the $TssI_{0667}$ C-terminal domain as the query indicated homology to phospholipase enzymes, specifically to phospholipase A enzymes, including the secreted phospholipase A_1 enzymes, PlhA and PhaA, from *S. marcescens* (Givskov et al., 1988; Givskov and Molin, 1993; Song et al., 1999; Shimuta et al., 2009), the characterised T3SS substrate YplA in *Yersinia enterocolitica*, which is a phospholipase A_2 (Schmiel et al., 1998; Young et al., 1999; Hatic et al., 2002) and the phospholipase A_1 produced by *Trypanosoma brucei*, $TbPLA_1$ (Richmond and Smith, 2007) (Figure 3.7). All of which contain a conserved lipase specific motif of GxSxG or GxSxxG and align well with an experimentally confirmed catalytic triad in the *T. brucei* $TbPLA_1$ enzyme of Ser131, His234 and Asp183 (Richmond and Smith, 2007). This indicated the catalytic triad in BCAS0667 was likely to be located at Ser879, His971 and Asp929.

3.3.4 Enzymatic characterisation of the C-terminal domain of $TssI_{0667}$

Work previously performed in our lab has focused on the characterisation of the enzymatic features of the C-terminal domain of $TssI_{0667}$ (Jones, 2012). It was found that the shortest active region of the CTD contained the final 258 amino acids of $TssI_{0667}$, and showed specificity toward phospholipase A_1 substrates, as it was capable of cleaving *sn*-1 specific fluorogenic substrates but not analogous phospholipase A_2 substrates. It was also was able to hydrolyse ester bonds of non-phospholipid substrates, where it showed esterase activity towards long chain fatty

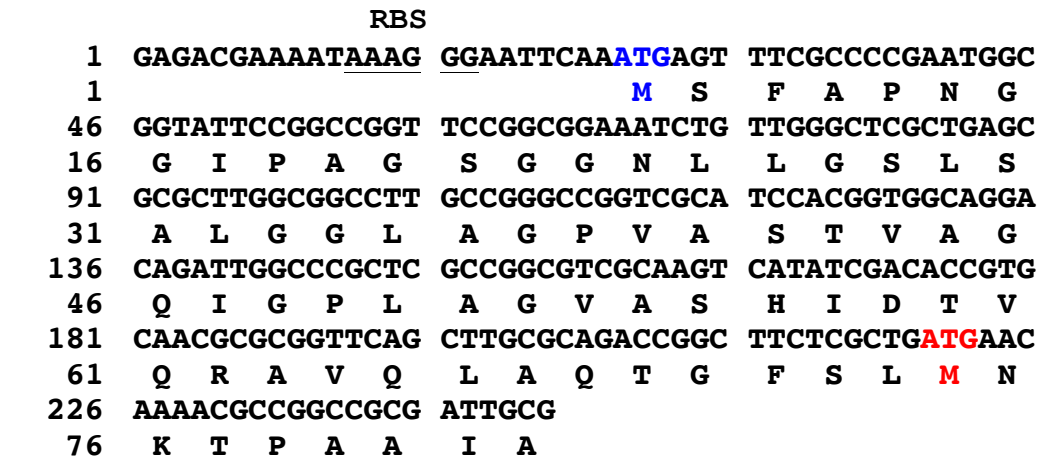

Figure 3.6 Presence of two putative translation initiation sites in BCAS0667. Analysis of the DNA sequence of BCAS0667 identified two potential initiation sites for BCAS0667 translational, as indicated in blue and red font. The underlined sequence indicates a putative Shine-Dalgarno sequence for ribosomal binding (RBS) to mRNA located upstream of the first initiation codon. The translated amino acid is indicated under each codon. Only the first 82 codons of BCAS0667 (numbered from the first ATG) are shown. DNA and amino acid positions are stated on the left.

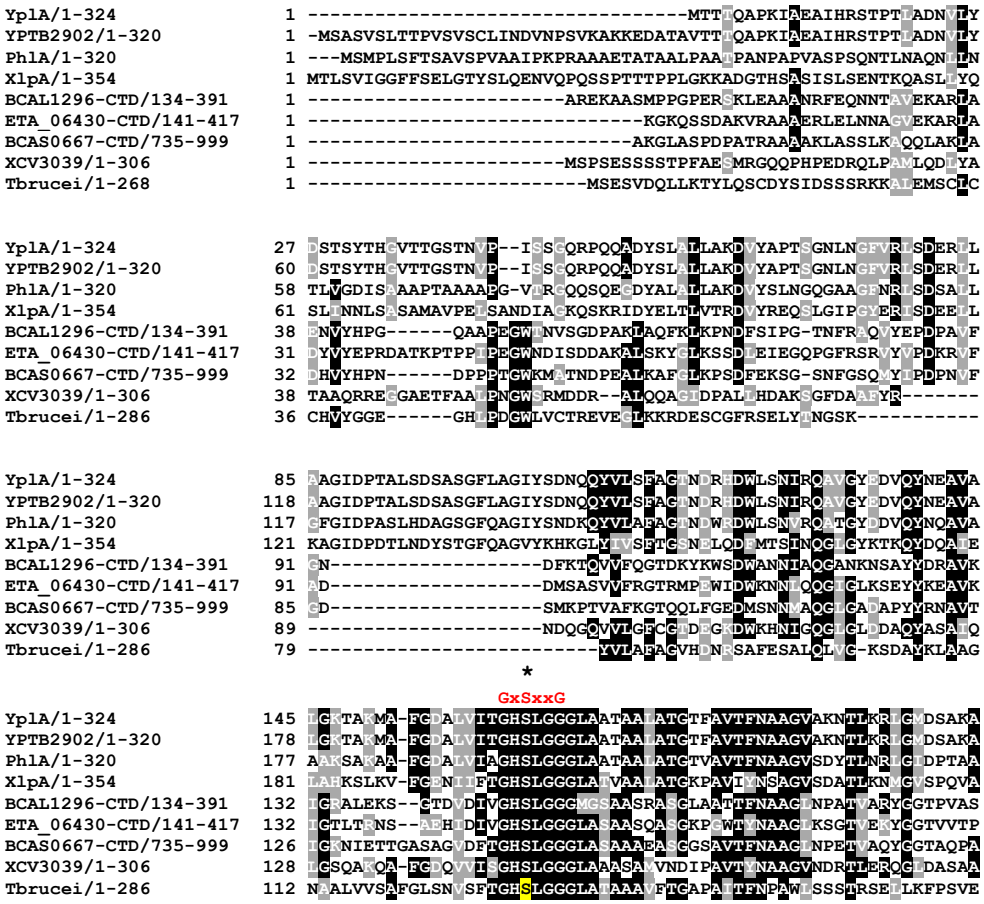

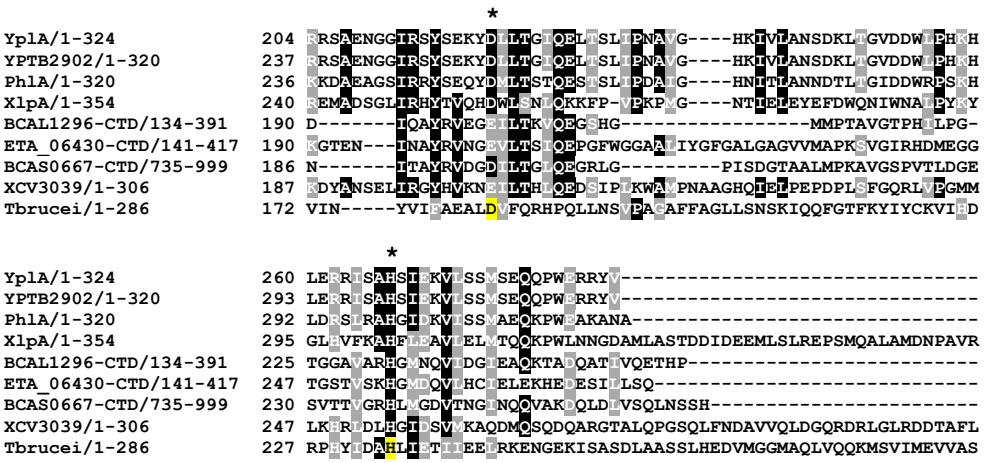

Figure 3.7 Alignment of the C-terminal domain of proteins encoded by BCAS0667 and BCAL1296 with other phospholipase A_1 and A_2 enzymes. The amino acid sequence of the phospholipase domain encoded by BCAS0667 and BCAL1296 were aligned with other putative and experimentally confirmed phospholipase A_1 and A_2 proteins using Clustal Omega. The conserved lipase motif is indicated in red font above the sequence. The confirmed *T. brucei* Ser-His-Asp catalytic triad residues are highlighted in yellow, and the corresponding conserved residues are indicated with an asterisk above the sequence. Black shading indicates identical residues at the corresponding position in 50% of sequences, grey shading indicates similar residues at the corresponding position in 50% of sequences. The designated gene locus or protein name followed by corresponding amino acid positions are indicated to the left.

acid-containing substrates such as polysorbate 80 and a fatty acyl ester of 4-nitrophenyl, 4-nitrophenol palmitate. Interestingly, it was also observed that the domain was its most active at 10°C, indicating psychrophilic properties.

Furthermore, the catalytic triad region was defined as residues Ser879, Asp929 and His971 by enzymatic analysis of point-mutation variants at these specific residues. However, key questions regarding this evolved TssI remained to be answered, as the work by Jones did not look to verify the secretion of $TssI_{0667}$ by the T6SS nor investigate the role this evolved TssI may play in *B. cenocepacia.*

3.3.5 $TssI_{0667}$ and the T6SS-dependent phospholipase effector superfamily

A superfamily of freestanding anti-bacterial T6SS-dependent phospholipase A_1 and A_2 effectors have been described, termed Tle effectors, that are found in a wide range of T6SS-containing bacteria (Russell et al., 2013). This superfamily has four subfamilies, Tle1- Tle4, that are based on a specific GxSxG motif and the flanking motifs surrounding it (Section 1.5.3). Alignment of the phospholipase domain of $TssI_{0667}$ and members of the Tle2 family indicates conservation of the GxSxG motif, yet $TssI_{0667}$.CTD lacks similarity in the regions flanking this motif (Figure 3.8). Therefore, the creation of an additional Tle family, Tle6, to encompass the CTD domain of $TssI_{0667}$ and any other T6SS-dependent PLA_1 that shares significant homology to this domain would be suitable. This includes a putative non-*tssI* effector encoded by BCAL1296 in *B. cenocepacia* (discussed in Section 3.4.2).

3.3.6 Putative $TssI_{0667}$ immunity protein encoded by BCAS0666

Immediately downstream of BCAS0667 is a gene that encodes a 289 amino acid protein, BCAS0666. Upon a BLASTP search using the amino acid sequence of the BCAS0666 gene product, it was found to contain four ankyrin repeat motifs (cd00204) located between residues 80-210. This structural motif consists of a relatively loosely conserved sequence of 33 amino acids that is usually repeated and forms a structure that functions wholly in protein-protein interactions

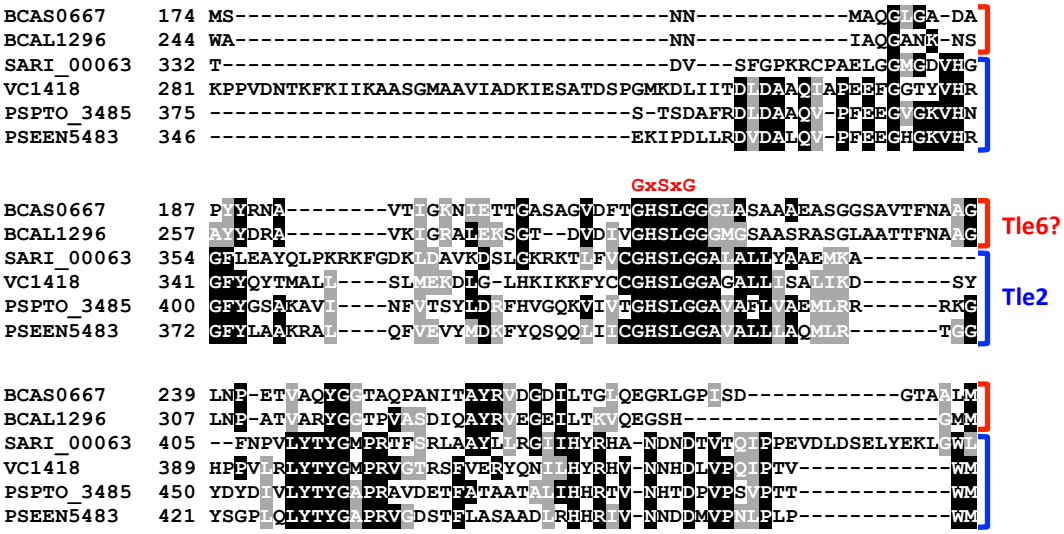

Figure 3.8 Amino acid sequence alignment of the C-terminal phospholipases domains of $TssI_{0667}$ and BCAL1296 with Tle2 family proteins. The amino acid sequences of the C-terminal predicted phospholipase regions of $TssI_{0667}$ and BCAL1296 were aligned with Tle2 family proteins (Russell et al., 2013). The conserved phospholipase signature motif is indicated in red font above the sequences. The red line indicates sequences from proteins that form part of a new Tle6 family, and the blue line indicates those from Tle2 family proteins. Black shading indicates identical residues at the corresponding position in 50% of sequences, grey shading indicates similar residues at the corresponding position in 50% of sequences. The designated gene locus is indicated on the left.

(Davis et al., 1991; Bork, 1993; Kohl et al., 2003) (Figure 3.9). Each ankyrin repeat forms a helix-turn-helix structure, where repeats stack in a super helical bundle (Gorina and Pavletich, 1996).

Alignment of the protein encoded by BCAS0666 and proteins encoded downstream of other $TssI_{0667}$ CTD-like phospholipase effectors genes, including the experimentally confirmed accessory proteins, YplB and PhlB, of the *Yersinia* and *Serratia* spp. phospholipases, YplA and PhlA, highlights the conservation of the four ankyrin repeat motifs amongst these proteins. Both YplB and PhlB have been found to form a complex with YplA and PhlA, respectively, that inactivates their enzymatic activity (Givskov and Molin, 1993; Schmiel et al., 1998). This suggests that these proteins, including that encoded by BCAS0666, are likely to form similar super helical bundles based on the helix-turn-helix structures of the ankyrin repeat motif, which mediates a direct interaction between the effector-immunity protein pair. Due to the designation of the C-terminal domain of $TssI_{0667}$ as a Tle6 family member it is appropriate to name the cognate immunity/accessory proteins corresponding to this family as Tli6. Accordingly, Tli6 orthologues are not homologous to Tli2 (data not shown).

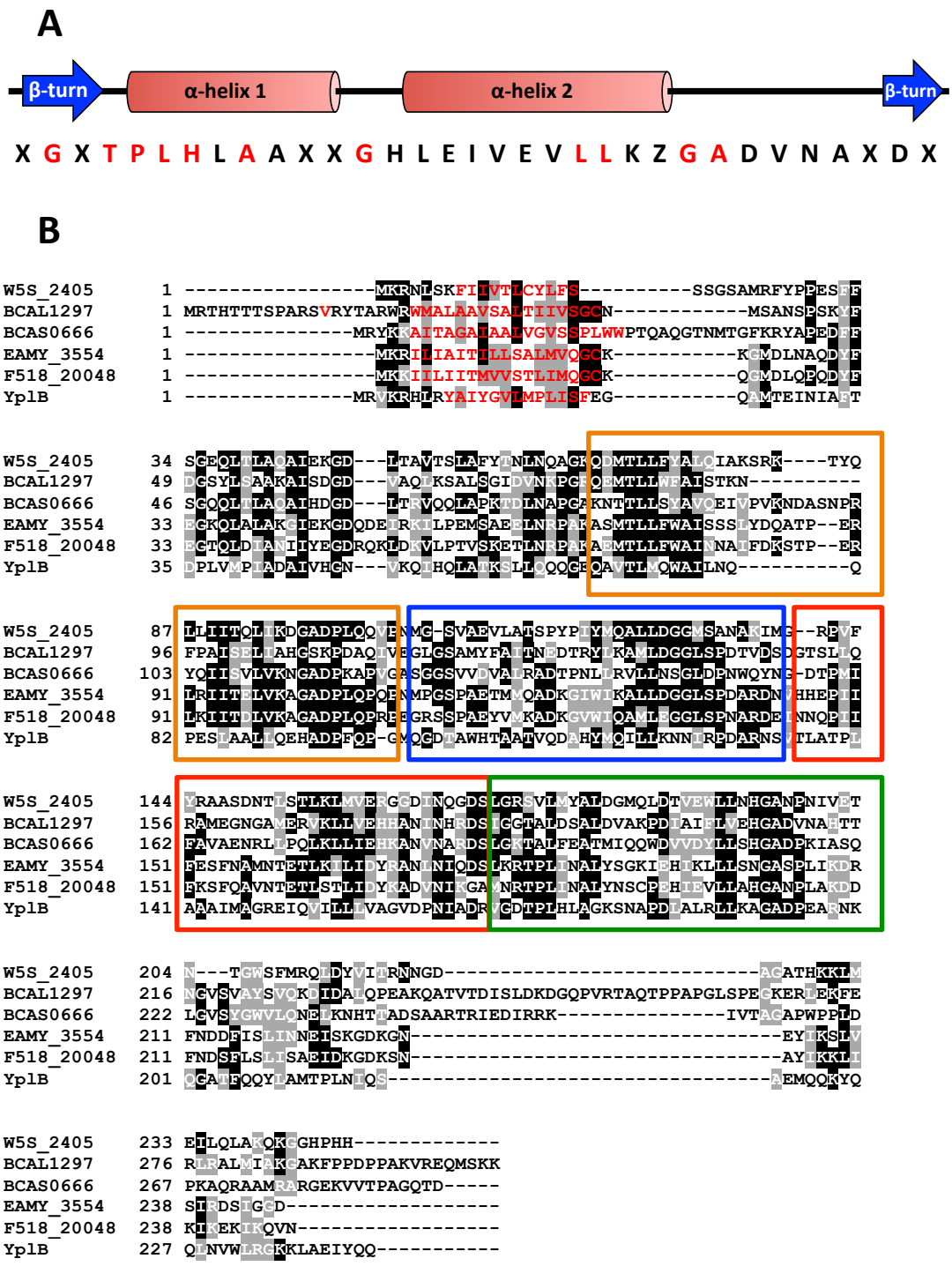

Figure 3.9 Putative immunity proteins encoded by BCAS0666 and BCAL1297 contain ankyrin repeat motifs. (A) Schematic representation of ankyrin structural motif showing α-helices and β-turns in relation to the conserved 33-residue sequence. Red letters indicate highly conserved residues. (B) An alignment of amino acid sequences of putative immunity proteins encoded by BCAS0666 and BCAL1297 with other ankyrin-containing proteins downstream of genes encoding Tle6-like proteins. Coloured boxes indicate the four individual ankyrin repeat motifs. Black shading indicates identical residues at the corresponding position in 50% of sequences, grey shading indicates similar residues at the corresponding position in 50% of sequences. The designated gene locus is indicated on the left. Red font indicates putative signal sequence.

3.4 Putative T6SS-dependent effectors in *B. cenocepacia* localised to *tssI* gene clusters

Several characterised T6SS effectors have been shown to belong to superfamilies of effectors, including those based on their: predicted enzymatic function, such as the Tae effectors with muramidase activity (Hood et al., 2010; Russell et al., 2011); localisation of their genes with *tssI* or *tssD* genes of the T6SS and associated accessory proteins (Hachani et al., 2014; Liang et al., 2015); or presence of conserved motifs identifying them as T6SS effectors, such as the N-terminal MIX motif (Salomon et al., 2014a). Here, using what is known about previously characterised T6SS-dependent effectors, coupled with bioinformatic tools it was sought to identify putative T6SS-dependent non-*tssI* effectors encoded by the *B. cenocepacia* strain J2315 *in silico*, specifically those located within close proximity to intact *tssI* gene clusters that may act as T6SS-dependent effectors. An overview of the effectors identified is depicted in Figure 3.10.

3.4.1 The BCAL1165 *tssI* cluster

3.4.1.1 Putative peptidoglycan hydrolase effector encoded by BCAL1166

A brief analysis of the *tssI* cluster located at BCAL1165 indicated a 960 amino acid protein encoded by the gene located directly downstream of BCAL1165 as a potential effector, the gene BCAL1166 (Figure 3.10A). A BLASTP alignment suggested that the protein encoded by BCAL1166 contains an N-terminal M23 peptidase-like region (residues 73-134, 172-191, and 407-413) that was interrupted by a SH3 domain (located between the first M23 homology regions at aa 283-326) and a putative linker sequence. It also contained a DUF domain between residues 680-747 that was also present in a homologous protein encoded by the H111 gene I35_5786. This was followed by a lysozyme-like domain (cl00222) located at the C-terminus (Figure 3.11). The M23 peptidase domain specifies amidase/peptidase activity, so may hydrolyse amide bonds within and between the peptide crosslinks in peptidoglycan (Figure 1.8, Section 1.5.2) (Firczuk et al., 2005). The lysozyme-like domain specifies glycoside hydrolase, therefore hydrolyses the β-(1,4)-glycosidic bond between GlcNAc and MurNAc in the peptidoglycan structure.

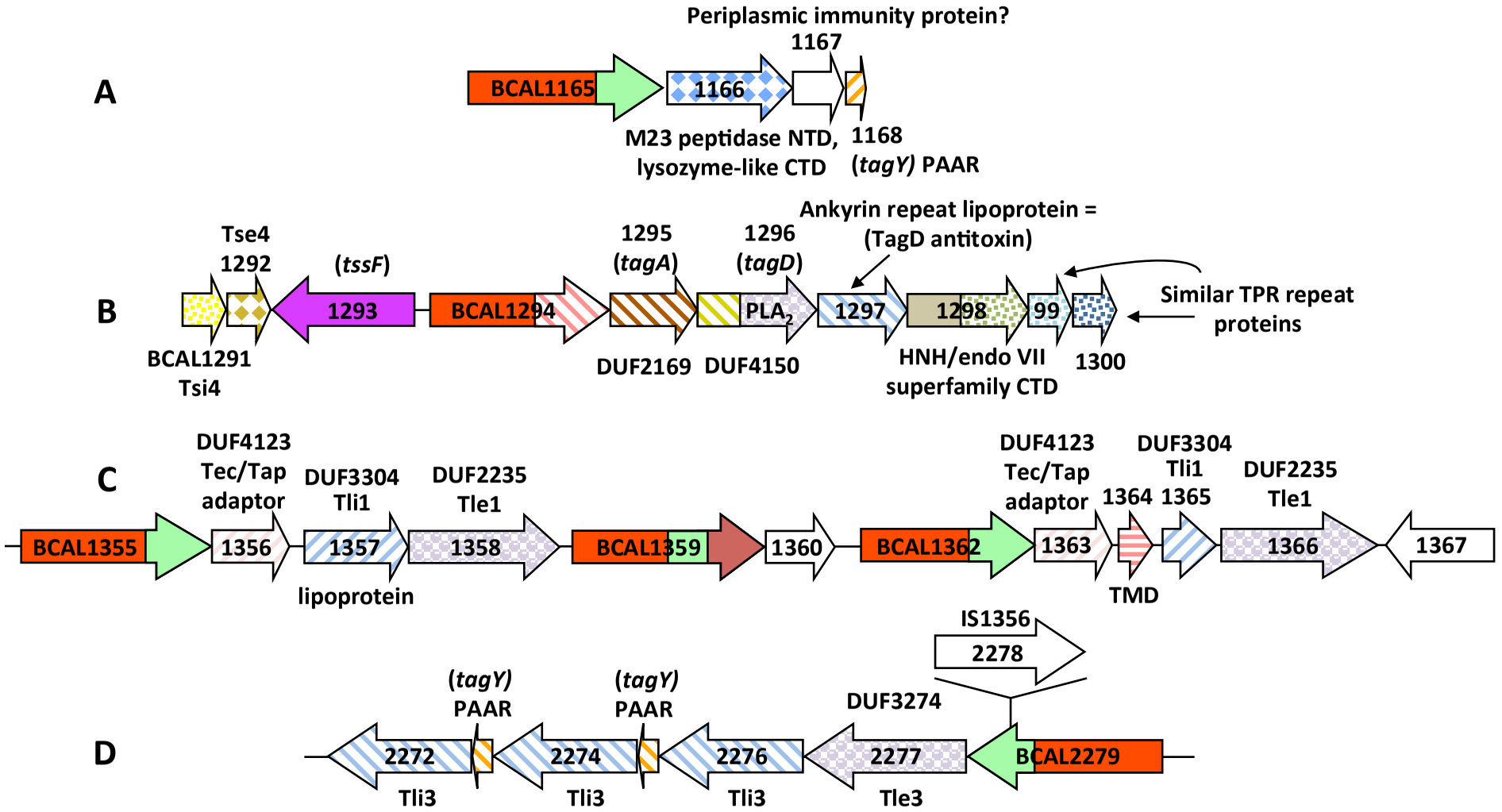
A
Periplasmic immunity protein?
1167
BCAL1165
1166
M23 peptidase NTD,
lysozyme-like CTD
1168
(tagY) PAAR
B
Tse4
1292
(tssF)
1293
BCAL1294
1295
(tagA)
1296
(tagD)
Ankyrin repeat lipoprotein =
(TagD antitoxin)
PLA2
1297
1298
99
1300
Similar TPR repeat
proteins
BCAL1291
Tsi4
DUF2169
DUF4150
HNH/endo VII
superfamily CTD
C
DUF4123
Tec/Tap
adaptor
DUF3304
Tli1
DUF2235
Tle1
BCAL1355
1356
1357
1358
BCAL1359
1360
BCAL1362
1363
1364
1365
1366
1367
lipoprotein
TMD
D
IS1356
2278
(tagY)
PAAR
(tagY)
PAAR
DUF3274
2272
2274
2276
2277
BCAL2279
Tli3
Tli3
Tli3
Tle3

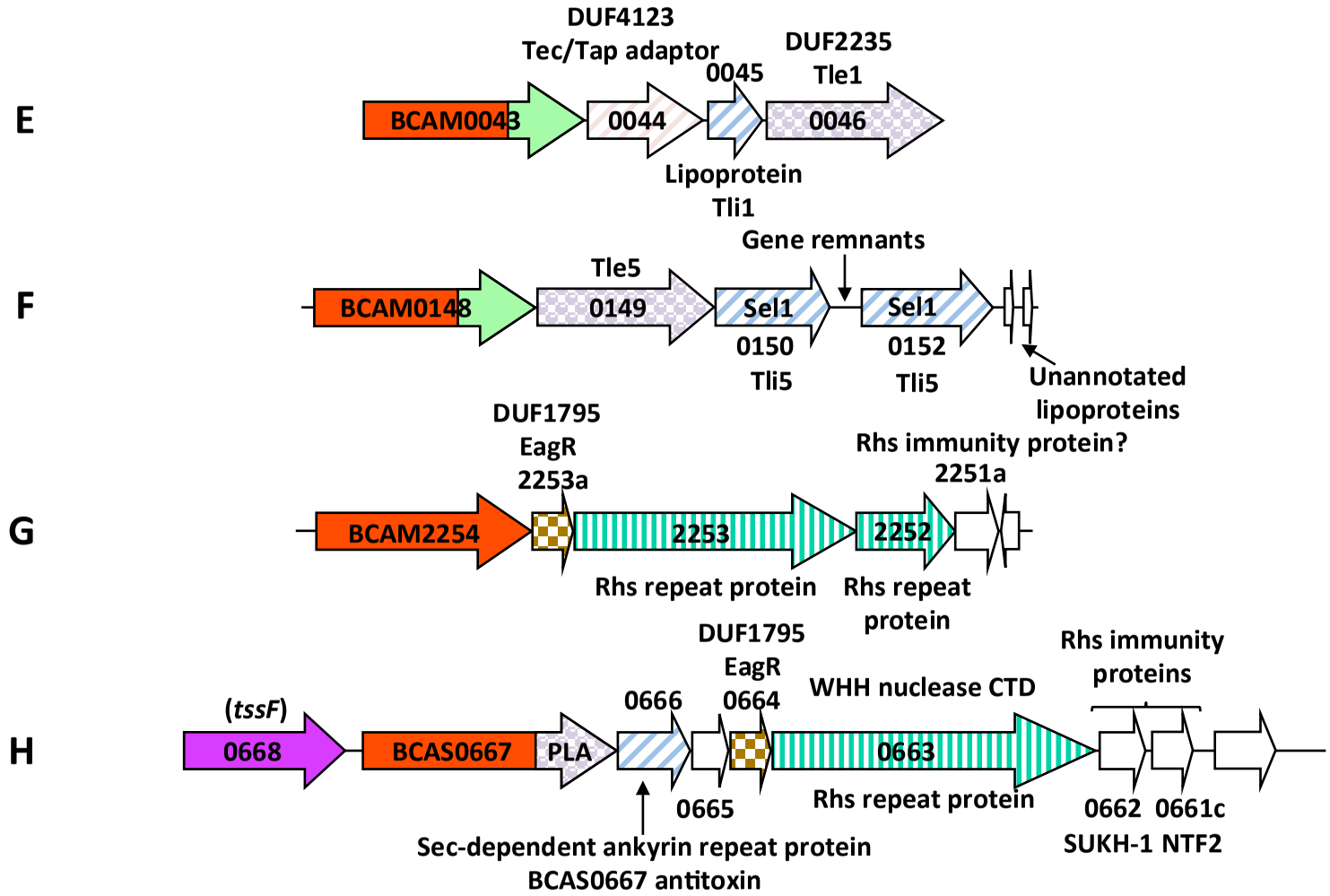

Figure 3.10 Putative T6SS-dependent effector genes located in the *tssI* gene clusters of *B. cenocepacia* J2315. (A-H) Schematic representation showing the putative T6SS-dependent effector genes encoded within eight of the nine intact *tssI* gene clusters of *B. cenocepacia* J2315. BCAL2503 *tssI* cluster is omitted as the encode TssI product is truncated at the N-terminus and fused to a TssF orthologue so it is unlikely to be expressed or functional. Features of each candidate effector, such as DUF or homology with other known T6SS effectors are indicated above or below each effector gene.

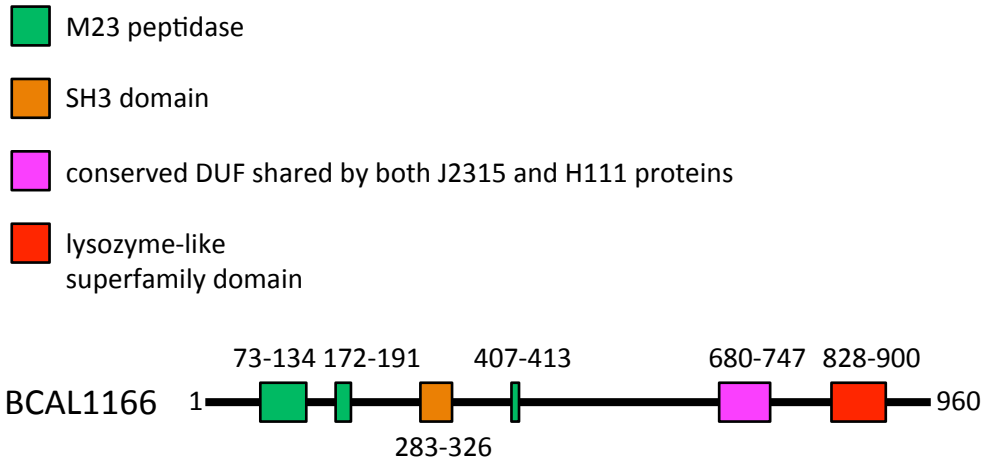

Figure 3.11 Domain organisation of a putative T6SS-dependent effector encoded by BCAL1166. Diagrammatic representation of the conserved domains identified in the protein encoded by BCAL1166 using a BLASTP search and alignment of homologous proteins using Clustal Omega. Conserved domains are represented by coloured boxes. The key above the figure indicates domains represented by block colours. The location of each domain in the amino acid sequence of the protein is indicated above each domain

Taking together these observations, it is hypothesised that the protein encoded by BCAL1166 may specify peptidoglycan hydrolase activity, with both muramidase activity and amidase activity, hence is a strong candidate as an anti-bacterial effector. Analysis of the protein encoded directly down-stream of BCAL1166, BCAL1167, identified an N-terminal Sec-dependent signal sequence, indicating periplasmic localisation of this protein, suggesting it may be the immunity protein for BCAL11666, and further strengthens the idea of a periplasmic target for the putative effector encoded by BCAL1166.

3.4.2 The BCAL1294 *tssI* cluster

3.4.2.1 Tse family protein encoded by BCAL1292

Several potential T6SS-dependent effectors are present in the BCAL1294 cluster (Figure 3.10B). A BLASTP search of the product of the BCAL1292 gene suggested that it encodes a Tse4 family effector (periplasmic-targeting effectors), with significant homology to the *P. aeruginosa* Tse4 encoded by PA2777 (Whitney et al., 2014). This search also highlighted an additional Tse4-like protein encoded by BCAL2504 in *B. cenocepacia* J2315 that is located adjacent to the truncated *tssI* gene BCAL2503 (Figure 3.12). Located directly downstream of BCAL1292 is BCAL1291. An alignment of the protein encoded by BCAL1291 and the immunity protein of the *P. aeruginosa* Tse4, Tsi4 (PA2776), demonstrated significant homology between the pair. Two further Tsi4 proteins were found encoded within the J2315 genome by a BLASTP analysis searching for orthologues of Tsi4 proteins. This identified the protein encoded downstream of the Tse4 encoded by BCAL2504, and an orphan Tsi4 protein encoded by BCAM1200 that was not linked to a Tse4 effector (Figure 3.13).

3.4.2.2 Phospholipase A encoded by BCAL1296

A further putative effector identified as being encoded in the BCAL1294 cluster was the product of BCAL1296. BLASTP search using the 391 amino acid sequence encoded by BCAL1296 as the query indicated a DUF4150 domain, between residues 10-117 spanning its N-terminal region. This domain is a member of the PAAR-like superfamily (CL21497), and is proposed to sharpen the tip of the

Figure 3.12 Alignment of putative Tse4 proteins from *B. cenocepacia* J2315. Amino acid sequences encoded by BCAL1292 and BCAL2504 from *B. cenocepacia* J2315 and a known Tse4 protein encoded by PA2774 in *P. aeruginosa* PAO1 were aligned using Clustal Omega. Black shading indicates identical residues at the corresponding position in 50% of sequences, grey shading indicates similar residues at the corresponding position in 50% of sequences. The gene locus designations are indicated on the left.

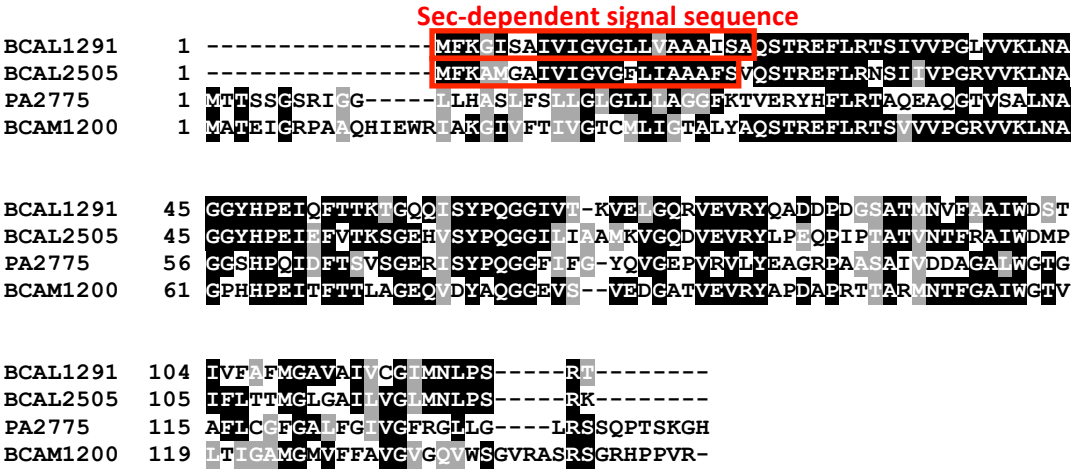

Figure 3.13 Alignment of putative Tsi4 proteins from *B. cenocepacia* J2315. Amino acid sequences encoded by BCAL1291, BCAL2505 and BCAM1200 from *B. cenocepacia* J2315 and a known Tsi4 protein encoded by PA2775 in *P. aeruginosa* PAO1 were aligned using Clustal Omega. Black shading indicates identical residues at the corresponding position in 50% of sequences, grey shading indicates similar residues at the corresponding position in 50% of sequences. The sequence boxed in red indicates Sec-dependent signal sequences. The gene locus designations are indicated on the left.

TssI spike and may also act as a module to facilitate binding of effectors to the spike (Shneider et al., 2013). In the case of evolved PAAR proteins, such as BCAL1296, effector domains may also be present on the N- or C-terminus that are also attached to the TssI spike when the PAAR domain interacts with its TssI substrate (Shneider et al., 2013). DUF4150-containing proteins have been previously designated as TagD proteins (Shalom et al., 2007). Functional DUF4150-containing effectors have been described elsewhere, this includes the product of PA0099 in *P. aeruginosa*, which acts as an anti-bacterial DNase effector requiring the VgrG1b protein for export (Hachani et al., 2014).

Rather than a DNase domain, BCAL1296 was identified as containing a C-terminal extension incorporating an esterase/lipase superfamily domain according to the CDD database. Lipases hydrolyse ester bonds within lipid molecules (discussed in Section 1.5.3). Further investigation of this region indicted that the CTD region shared similar features to the phospholipase domain of the protein encoded by BCAS0667, and with other predicted phospholipases, including those encoded by ETA_0640 from *Erwinia tasmaniensis*, YE1005 from *Y. enterocolitica* and XCV3039 from *Xanthomonas euvesicatoria*, containing the conserved lipase motif of GxSxG or GxSxxG (Figure 3.8, Section 3.3.5). Notably, the product of BCAL1296 contained a catalytic triad, but instead of a serine-aspartate-histidine triad, a glutamate residue replaces the aspartate. These two amino acids have similarly charged sides and differ by only an extra carbon, therefore the product of BCAL1296 may still exhibited enzymatic activity.

3.4.2.3 A putative endonuclease encoded by BCAL1298

3.4.2.3.1 Homology to the protein product of BCAL1298

An additional putative candidate effector encoded within the BCAL1294 gene cluster is the protein encoded by BCAL1298. A BLASTP search using the 349 amino acid sequence encoded by BCAL1298 as a query indicated a C-terminal domain of the GH-E HNH/ENDO VII nuclease superfamily, spanning residues 272-339. Only one protein was found to have regions of homology to that encoded by BCAL1298, which covered the entire length of the protein, encoded by X976_1941 in *B. pseudomallei* MSHR7500. Homologous proteins in other *B. cenocepacia* strains

were not identified. However, several proteins were identified that showed homology to the N-terminus of the product of BCAL1298, including AK36_2612 from *B. vietnamiensis*, DO62_782 from *B. pseudomallei* BDD and a PAAR motif containing protein encoded by *Herbaspirillum rubrisubalbicans* (C798_RS0113785). Proteins with homology to just the C-terminus were also identified, corresponding to other putative GH-E superfamily-domain proteins, including a PAAR motif-containing protein encoded by EOS_31360 in *B. glathei,* a DUF4150 and PAAR-motif containing protein encoded by ON18_RS05025 *in the bacteria Pusillimonas noertemannii (*of the Burkholderiales order) and NR99_RS29435 in a *P. aeruginosa* strain.

3.4.2.3.2 Putative GH-E HNH/Endo VII superfamily domain encoded by BCAL1298

Nucleases function as esterases to catalyse the cleavage of the phosphodiester link between the 3' carbon and 5' carbon of two pentose molecules in adjacent nucleotides by a base catalysed hydrolysis reaction. Endonucleases target phosphodiester bonds between nucleotides within a polynucleotide chain, whereas exonucleases target the bond between two nucleotides that lay at either the 3' or 5 end of a DNA fragment, thereby requiring free 3' or 5' hydroxyl groups for breakage of the bond. Endonuclease can be sequence (restriction endonuclease) or structure (Flap endonuclease (FENS)) specific and can have a preference for single stranded or double stranded DNA, RNA, or be fairly non-specific regarding the nature of the polynucleotide substrate. Endonucleases can also have exonuclease activity. Nucleases are fundamental to all living organisms. Endo- (and exo-) nucleases play a pivotal role in processes such as DNA repair, DNA replication and recombination.

The GH-E HNH/Endo VII superfamily is a type of endonuclease that belongs to the ββα-Metal(Me)-finger nucleases clan, meaning they contain a structural motif made up an anti-parallel β-hairpin followed an α-helix (Scholz et al., 2003). This structure harbours essential residues required for catalysis and metal ion coordination. Well studied endonucleases that contain this common ββα-Me-finger motif include the bacteriophage T4 endonuclease VII (Biertümpfel et al., 2007),

Serratia endonuclease (Nestle and Roberts, 1969; Kühlmann et al., 1999), *Streptococcus pyogenes* Spd1 endonuclease (Korczynska et al., 2012), the periplasmic Endo I nuclease encoded by *endA* in *E. coli* (Cordonnier and Bernardi, 1965; Jekel and Wackernagel, 1995) and eukaryotic endonucleases, such as Nuc1 of *Saccharomyces cerevisiae* (Vincent et al., 1988) and the mammalian endonuclease G, which are involved in mitochondria DNA replication and repair (Côté and Ruiz-Carrillo, 1993).

These enzymes typically require a metal ion (usually Mg^{2+}) and essential aspartate, histidine, and asparagine residues for catalysis (Giraud-Panis and Lilley, 1996; Golz et al., 1997). The conserved histidine residue is essential for the de-protonation of a water molecule for nucleophilic attack of the phosphate in the phosphodiester bond between two nucleotides, and the aspartate and asparagine residues are required for co-ordinating the metal ion (Biertümpfel et al., 2007). Further refinement of HNH/Endo VII nucleases by sequence alignments, generated the GH-E HNH/Endo VII superfamily (Zhang et al., 2011). Here, additional conserved residues associated with the active site were assigned, including a glycine residue preceding the catalytic histidine and glutamate residue further downstream. However no GH-E HNH/Endo VII proteins have yet to be experimentally characterised.

Alignment of the C-terminal domain of the protein encoded by BCAL1298 with other GH-E HNH/Endo VII containing proteins identified potential catalytic aspartate, histidine and asparagine residues at positions 290, 293 and 333, respectively, that corresponded to a similar experimentally characterised class of nucleases, Endo VII (Figure 3.14). Yet the conserved residues defined by Zhang and colleagues were not present in the product of BCAL1298, these residues are indicated by blue circles in Figure 3.14.

3.4.2.4 Product of BCAL1295, a non-evolved TagA protein

The product of BCAL1298 also contains a N-terminal region (residue 1- 232) that is homologous to other predicted proteins located in close proximity to T6SS clusters, including C798_RS0113785 from *H. rubrisubalbicans* and AK36_2612 from *B. vietnamiensis* (see Figure 6.2, Section 6.1). Some of which are also located

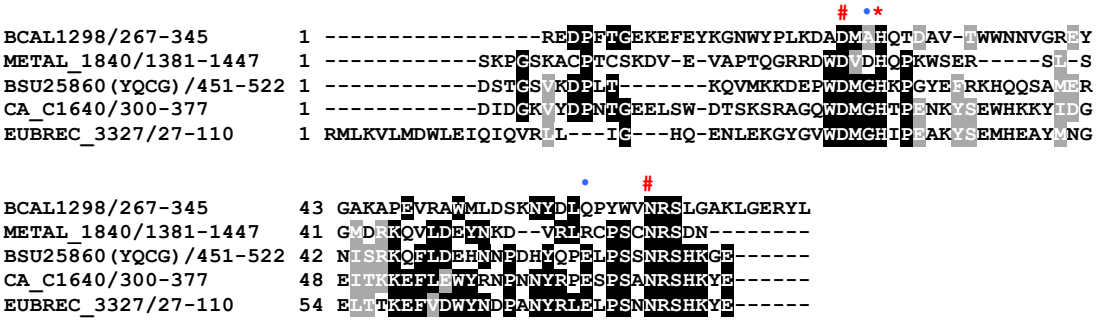

Figure 3.14 Alignment of the C-terminal domain of the protein encoded by BCAL1298 with members of the GH-E HNH/ENDO VII nuclease superfamily. The C-terminal amino acid sequence encoded by BCAL1298 from *B. cenocepacia* J2315 was aligned with other proteins containing a GH-E HNH/ENDO VII nuclease superfamily domain, from both Gram-negative and Gram-positive bacteria, using Clustal Omega. Black shading indicates identical residues at the corresponding position in 50% of sequences, grey shading indicates similar residues at the corresponding position in 50% of sequences. The asterisk indicates a conserved histidine needed for activation of a water molecule for hydrolysis, red hashes indicate conserved aspartate and asparagine metal ion coordinating residues, blue circles indicate important glycine and glutamate residues proposed by Zhang et al. (2011). Gene locus designations followed by the corresponding amino acid positions are indicated on the left.

directly downstream of a gene that is similar to BCAL1295 (and its orthologous gene in *B. cenocepacia* H111, I35_1209). All of these genes encode DUF2169-containing proteins. The DUF2169-containing proteins in Figure 3.15 show homology particularly at the N- and C-terminus. Proteins containing this domain that are encoded with T6SS subunit genes have previously been designated as TagA proteins (Shalom et al., 2007). In some cases, TagA proteins contain a C-terminal extension harbouring pentapeptide repeats (evolved TagA) (Shalom et al., 2007). These observations may suggest that TagA acts as an adaptor or chaperone protein to facilitate the secretion of downstream effectors by the T6SS, similar to TEC and EagR1 chaperones recently described (Liang et al., 2015; Diniz and Coulthurst, 2015; Unterweger et al., 2015).

3.4.2.5 Putative endonuclease immunity proteins encoded by BCAL1299 and BCAL1300

Located immediately downstream of BCAL1298 are two genes encoding small 148 and 144 amino acid proteins, that share homology with each other. Both proteins contain three tetratricopeptide repeat (TPR) structural motifs, each consisting of 34 amino acid sequences that form two α-helical domains, approximately located at residues 15-48, 56-89 and 94-127 in the protein encoded by BCAL1299 (Figure 3.16). These structures are thought to participate in protein-protein interactions (Blatch and Lässle, 1999). Therefore, it is likely that the proteins encoded by BCAL1299 and BCAL1300 are immunity proteins for the C-terminal nuclease domain of the product of BCAL1298.

3.4.3 The BCAL1355, BCAL1359, BCAL1362 *tssI* cluster

3.4.3.1 Tle1 phospholipase effector encoded by BCAL1358

The cluster containing the *tssI* genes BCAL1355, BCAL1359 and BCAL1362 is particularly interesting (Figure 3.10C). A survey of this cluster indicted that the gene encoded directly downstream of BCAL1355, BCAL1356, codes for a protein containing a DUF4123-region. Proteins containing this domain have been identified as T6SS effector chaperone proteins by two separate groups, known as TEC or Tap (Liang et al., 2015; Unterweger et al., 2015). TEC/Tap proteins are thought to

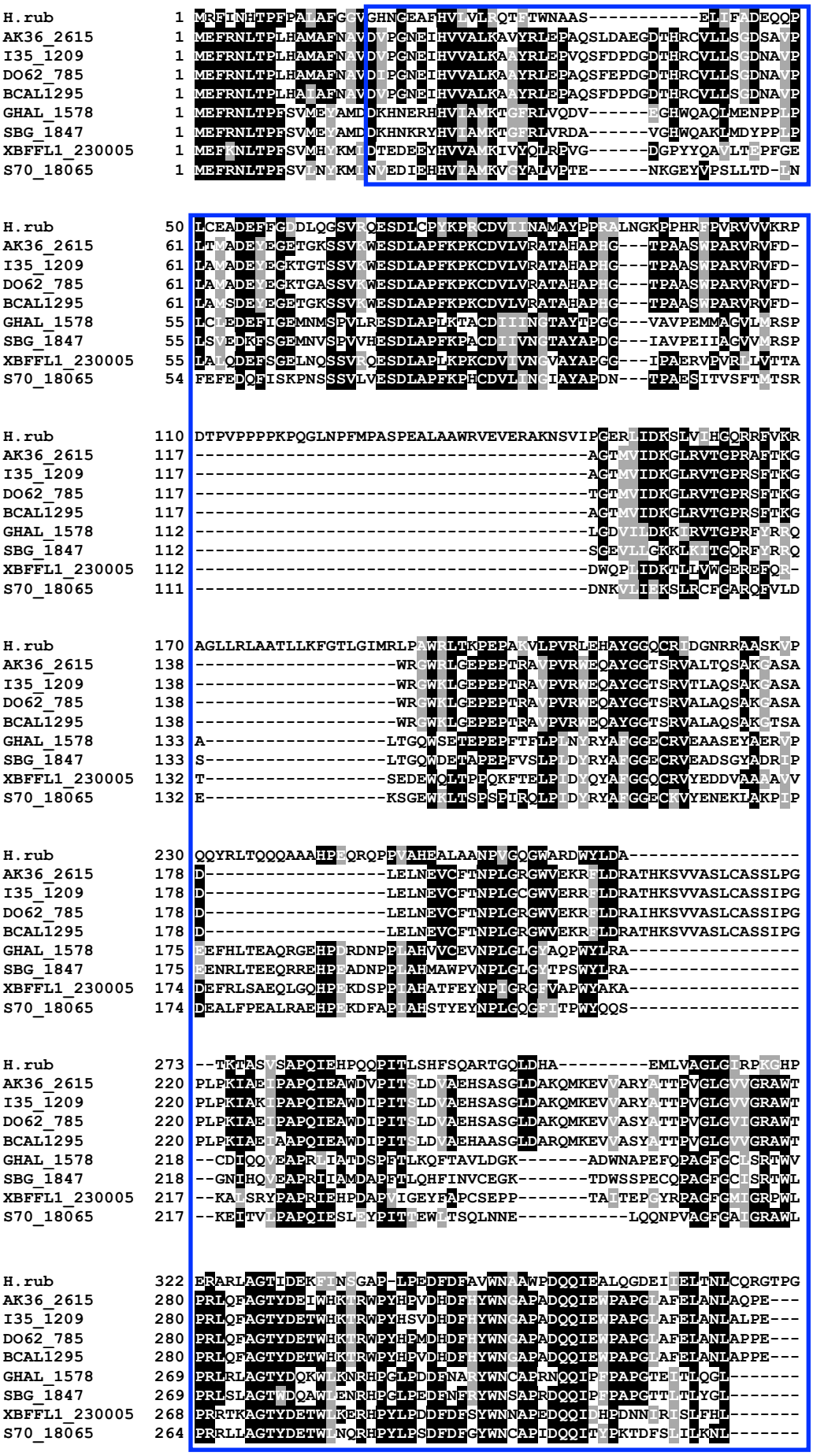
H.rub
AK36_2615
I35_1209
DO62_785
BCAL1295
GHAL_1578
SBG_1847
XBFFL1_230005
S70_18065

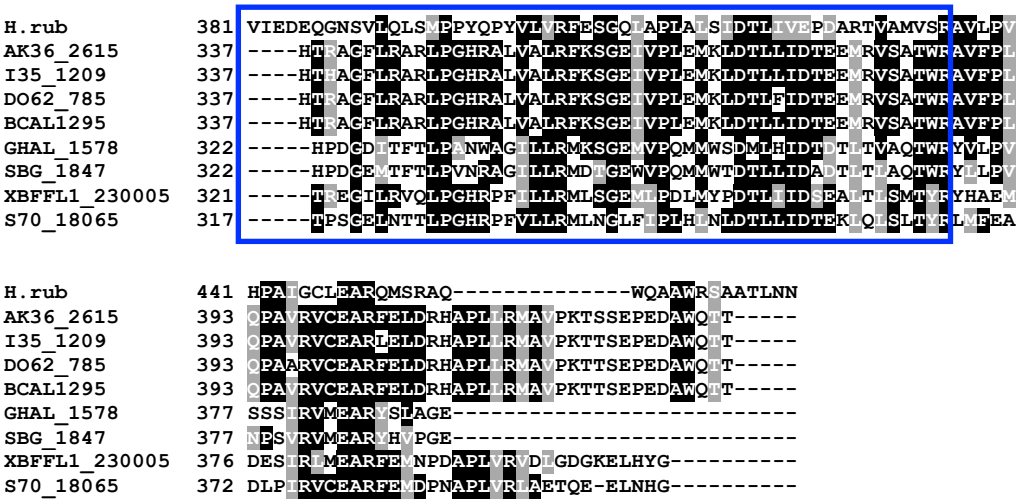

Figure 3.15 Alignment of the protein encoded by BCAL1295 with other DUF2169-containing proteins. Amino acid sequences encoded by BCAL1295 and I35_1209 from *B. cenocepacia* J2315 and *B. cenocepacia* H111, respectively, and other identified DUF2169-containing proteins were aligned using Clustal Omega. The proteins used in the alignment are encoded by genes that are located in a similar position as BCAL1295, in that they are located upstream from a gene encoding a product whose NTD shows homology to the NTD of the protein encoded by BCAL1298. Black shading indicates identical residues at the corresponding position in 50% of sequences, grey shading indicates similar residues at the corresponding position in 50% of sequences. Sequences boxed in blue correspond to the DUF2169 region. The gene locus designations are indicated on the left.

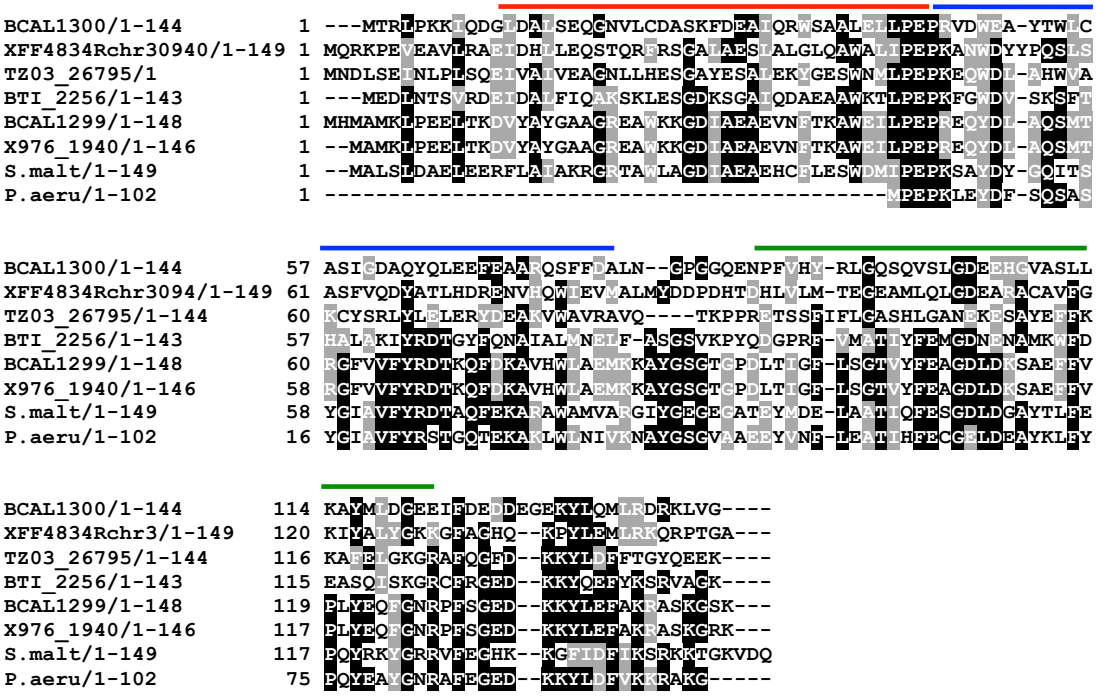

Figure 3.16 Alignment of TPR-repeat containing proteins encoded by BCAL1299 and BCAL1300 from *B. cenocepacia* J2315. Amino acid sequences encoded by BCAL1299 and BCAL1300 from *B. cenocepacia* J2315 and other proteins containing TPR repeat regions from both Gram-negative and Gram-positive bacteria were aligned using Clustal Omega. Coloured overline indicates 34 amino acid sequence corresponding to TPR predicted regions according to the CDD database and consensus sequence in Blatch and Lässle (1999). Black shading indicates identical residues at the corresponding position in 50% of sequences, grey shading indicates similar residues at the corresponding position in 50% of sequences. Gene locus designations followed by corresponding amino acid positions are indicated on the left.

facilitate the binding of a cognate effector protein to the TssI subunit encoded within the vicinity of the adaptor and effector genes. A candidate effector protein for the putative chaperone encoded by BCAL1356 is the protein encoded by BCAL1358. This contains a DUF2235 domain, which has been linked to T6SS-dependent antibacterial effectors. This includes the experimentally confirmed T6SS-dependent substrate BTH_I2698 that was identified in a mass spectrometry secretome analysis of *B. thailandensis* (Russell et al., 2012) and a protein containing a C-terminal DUF2235 region encoded by v12G01_02265 in *Vibrio alginolyticus* (Salomon et al., 2014a). Moreover, the DUF2235-containing protein encoded by BCAL1358 shares amino acid sequence homology to the catalytic region in Tle1 phospholipase A_2 effectors, of which BTH_12698 ($Tle1^{BT}$) is a member of (Russell et al., 2013). In fact, it is the DUF2235 region of BCAL1358 that contains the strongly conserved Tle1 motif catalytic site (it contains the conserved GxSxG lipase motif at residues 373-379 and is flanked by the motifs that define the Tle1 class) (Figure 3.17). This suggests that DUF2235-containing proteins are Tle1 proteins.

Similar to other Tle1 effectors, BCAL1358 has a predicted DUF3304-containing lipoprotein encode upstream of the effector (BCAL1357), which is likely to be the effector's cognate immunity protein, Tli1. A DUF3304-containing lipoprotein encoded upstream of a *tle1* gene in *B. thailandensis* (encoded by BTH_ I2699) has been experimentally verified as the Tle1 effector immunity protein (Russell et al., 2013), with which BCAL1357 has sequence homology to (Figure 3.18).

3.4.3.2 A DUF4123 domain protein encoded by BCAL1363

Interestingly, the BCAL1363 gene located immediately downstream of the other non-evolved *tssI* gene in this cluster, BCAL1362, also encodes a DUF4123-containing TEC/Tap adaptor protein, as noted by Unterweger et al. (2015) , similar to the product of BCAL1356. Again there is a DUF2235-containing protein encoded by BCAL1366 downstream of the adaptor (Figure 3.10C). Conversely, it is lacking the conserved G.xS.xG motif, instead it has a G.xVx.G motif at residues 380-386 and thereby lacks the essential serine residue of the catalytic triad. However, but it still flanked by conserved amino acid sequence motifs found in Tle1 (Figure 3.17).

Furthermore, BCAL1366 is located adjacent to a gene encoding a DUF3304-

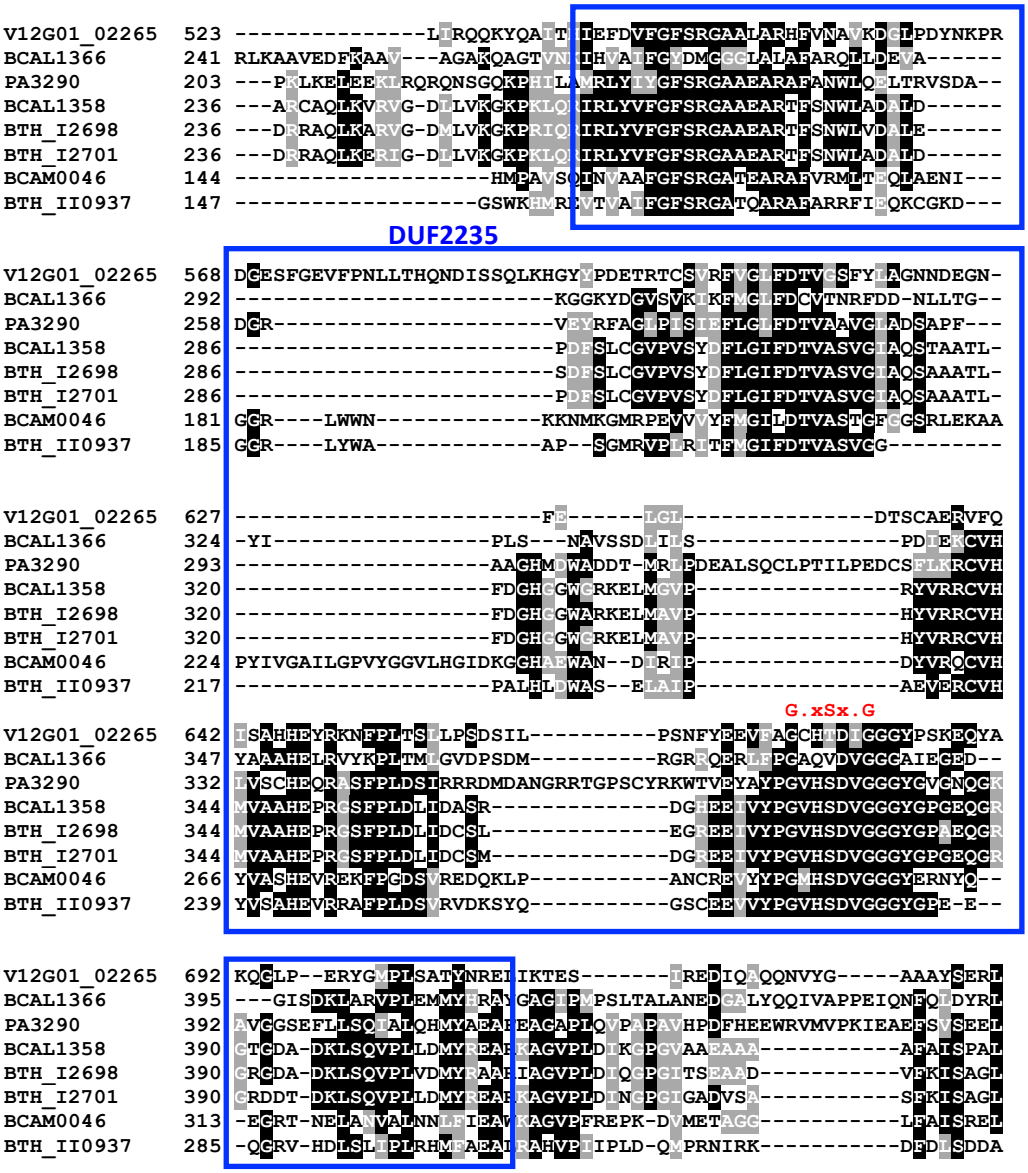

Figure 3.17 Alignment of proteins encoded by BCAL1358, BCAL1366 and BCAM0046 with other DUF2235-containing proteins. Amino acid sequences encoded by BCAL1358, BCAL1366 and BCAM0046 from *B. cenocepacia* J2315 were aligned with a experimentally characterised DUF2235-containing Tle1 phospholipase A_2 T6SS-dependent effector from *B. thailandensis* (BTH_I2698, and its gene duplicate BTH_I2701), as well as an identified Tle1 of *P. aeruginosa* (PA3290), an experimentally characterized DUF2235-containing protein encoded by V12G01_02265 in *V. alginolyticus* and a further Tle1 effector in *B. thailandensis* encoded by BTH_II0937. Black shading indicates identical residues at the corresponding position in 50% of sequences, grey shading indicates similar residues at the corresponding position in 50% of sequences. The conserved Tle1 motif is indicated in red, and regions corresponding to the DUF2235 domain are boxed in blue. The gene locus designations are indicated on the left.

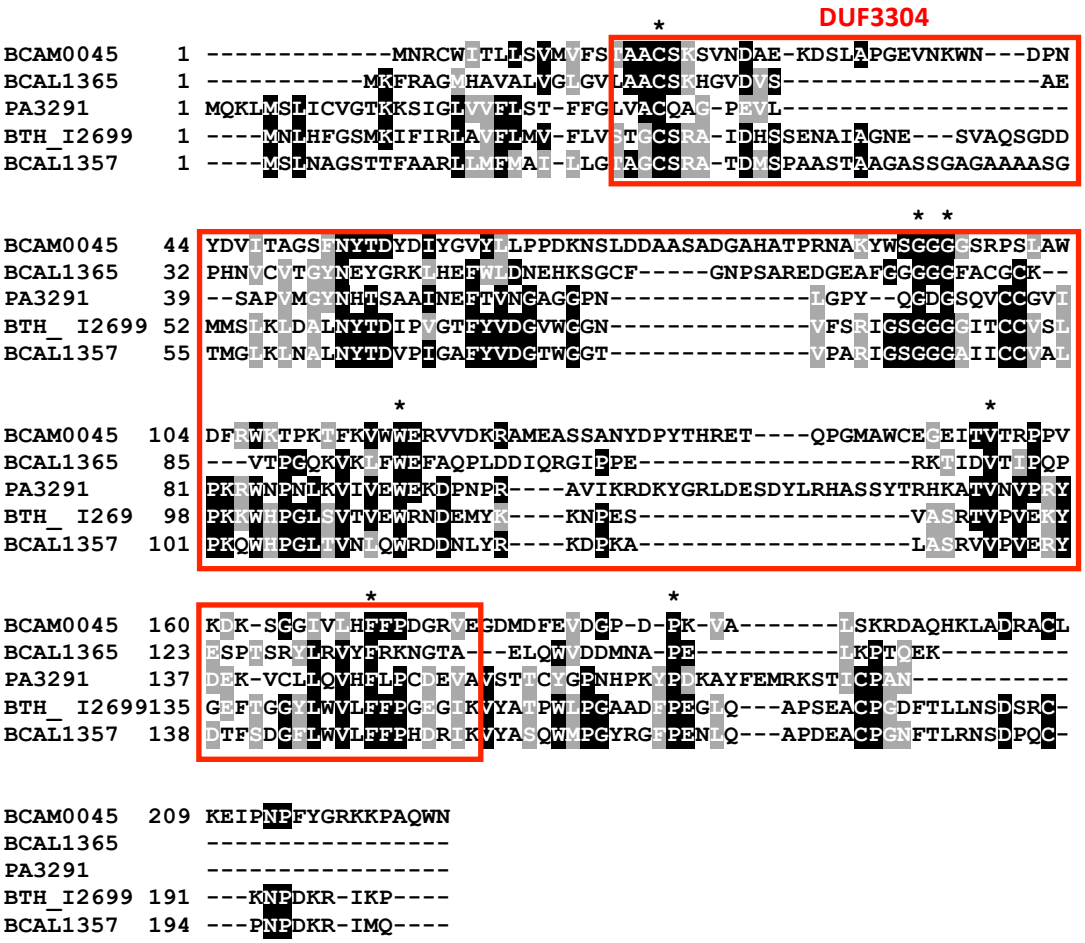

Figure 3.18 Alignment of proteins encoded by BCAL1357, BCAL1365 and BCAM0045 with Tli1 immunity proteins. Amino acid sequences encoded by BCAL1357, BCAL1365 and BCAM0045 from *B. cenocepacia* J2515 were aligned with an experimentally characterised Tli1 immunity proteins from *B. thailandensis* (BTH_1266), and a Tli1 in *P. aeruginosa* (PA3291) using Clustal Omega. Corresponding DUF3304-regions are boxed in red. Black shading indicates identical residues at the corresponding position in 50% of sequences, grey shading indicates similar residues at the corresponding position in 50% of sequences. Asterisks indicate identical residues in 100% sequences. The gene locus designations are indicated on the left.

lipoprotein that shares homology with Tli1 immunity proteins Figure 3.18). Therefore it is likely to be the immunity protein of the BCAL1366. Whether the Tle1-like BCAL1366 gene product actually exhibits PLA_2 activity awaits experimental investigation.

3.4.4 The BCAL2279 *tssI* cluster

3.4.4.1 Tle3 phospholipase effector encoded by BCAL2277

Within the BCAL2279 *tssI* cluster there is a predicted Tle3 class of phospholipase effector encoded by BCAL2277 that is located directly downstream of the *tssI* gene (Figure 3.10D). The BCAL2277 gene product is homologous to the identified Tle3 effector of *B. cenocepacia* PC184 (ZP_04941041) (Russell et al., 2013), and also homologous to the experimentally verified anti-bacterial T6SS-dependent substrates of *B. thailandensis*, encoded by BTH_II0090 and BTH_II3226 (Russell et al., 2012). Alignment of the protein encoded by BCAL2277 (residues 203-283) with other Tle3 phospholipases indicated that the protein contained a similar GxSxG-like motif at residues 235-239, but which contained a cysteine in place of the first glycine residue (Figure 3.19). It did however have similar flanking motifs as those contained within Tle3 class phospholipases. Many Tle3 orthologues also contain a C-terminal DUF3274 domain of unknown function.

Analysis of the BCAL2272, BCAL2274 and BCAL2276 genes located downstream of BCAL2277 suggested their products shared sequence homology with each other and with two Tli3 proteins encoded downstream from the experimentally verified BTH_II0091 and BTH_I3227 Tle3 effector genes of *B. thailandensis* (Russell et al., 2012) (Figure 3.20). The two Tli3 proteins from *B. thailandensis* are identified as containing DUF2875 domains. However, the putative Tli proteins encoded by the *B. cenocepacia* J2315 BCAL2279 *tssI* gene cluster are not identified as having this domain. Nevertheless, upon alignment of these proteins there were short regions of amino acid conservation between the DUF2875 region of BTH_II0091 and BTH_I3227 and the three putative Tli3 proteins. Note that a Sec-dependent sequence is not detected for BCAL2276 until a variant of the protein that starts with the methionine residue at position 43 is used in a Signal

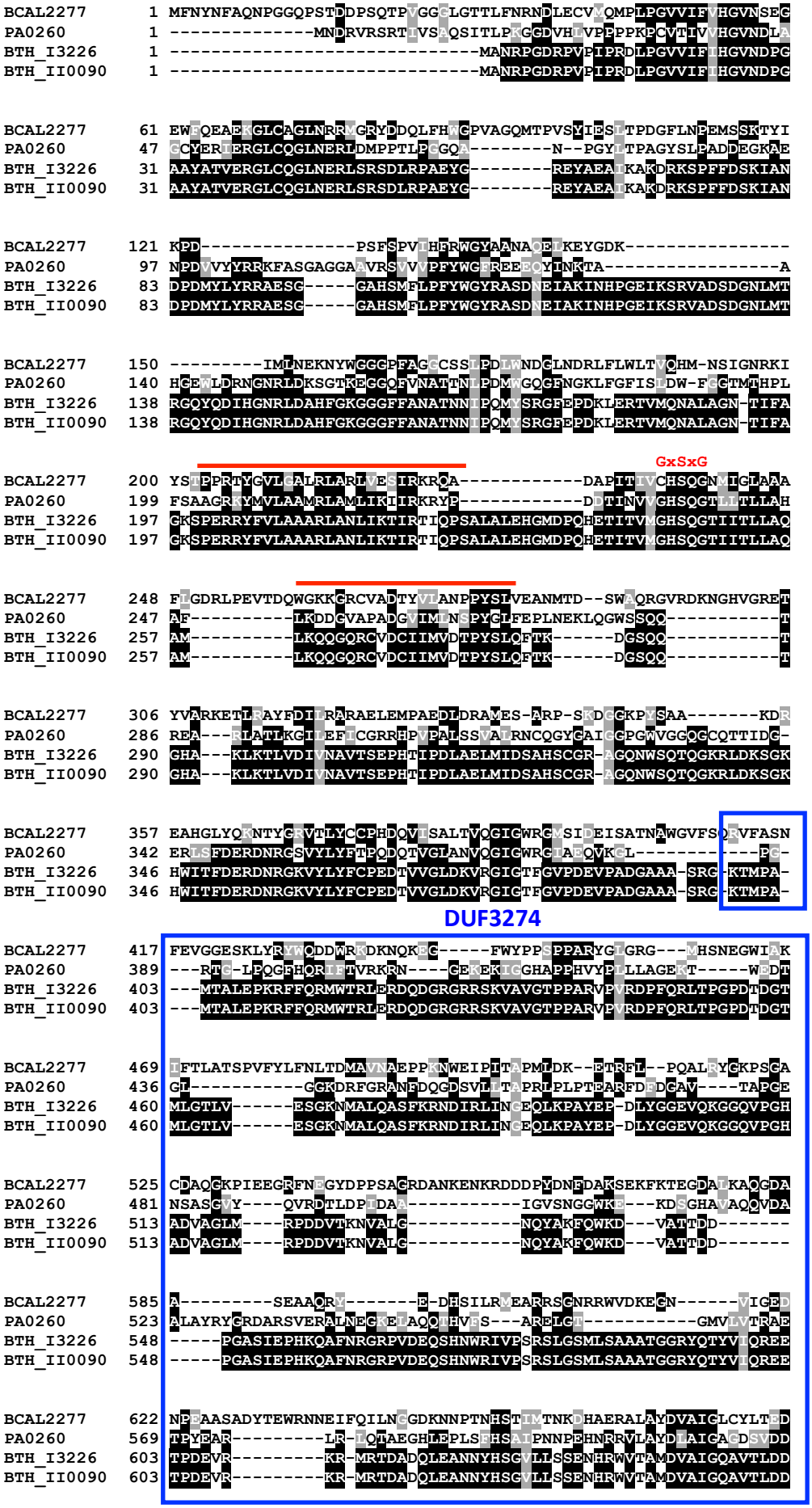
GxSxG
DUF3274

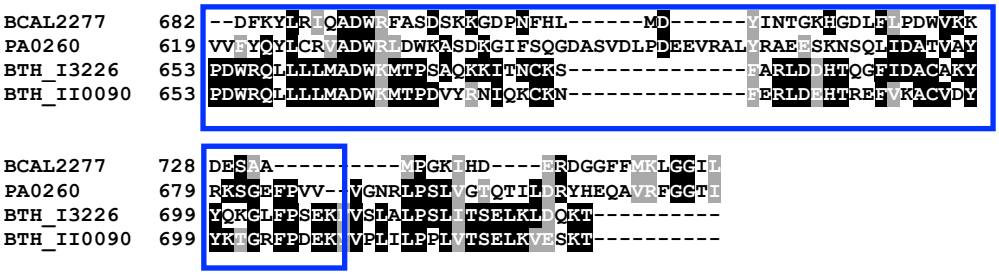

Figure 3.19 Alignment of the BCAL2277 protein product with characterised and putative Tle3 effectors. Amino acid sequences encoded by BCAL2277 from *B. cenocepacia* J2315 was aligned with an experimentally characterised T6SS-dependent Tle3 phospholipase A effectors from *B. thailandensis* (BTH_I3266 and BTH_II0090), as well as an identified Tle3 of *P. aeruginosa* (PA0260). Black shading indicates identical residues at the corresponding position in 50% of sequences, grey shading indicates similar residues at the corresponding position in 50% of sequences. The conserved Tle3 motif is indicated in red, the red overlines indicate conserved flanking regions surrounding this motif. The regions corresponding to the DUF3274 domain are boxed in blue. The gene locus designations are indicated on the left.

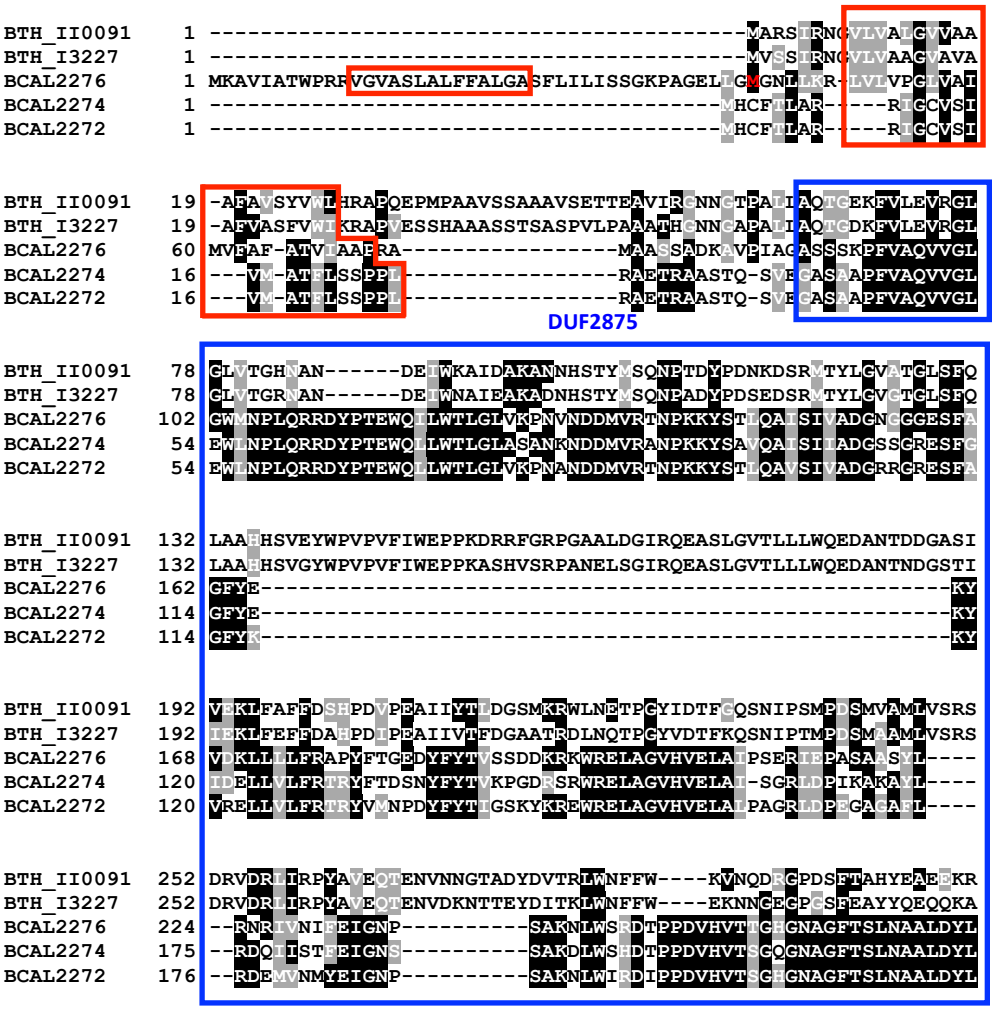

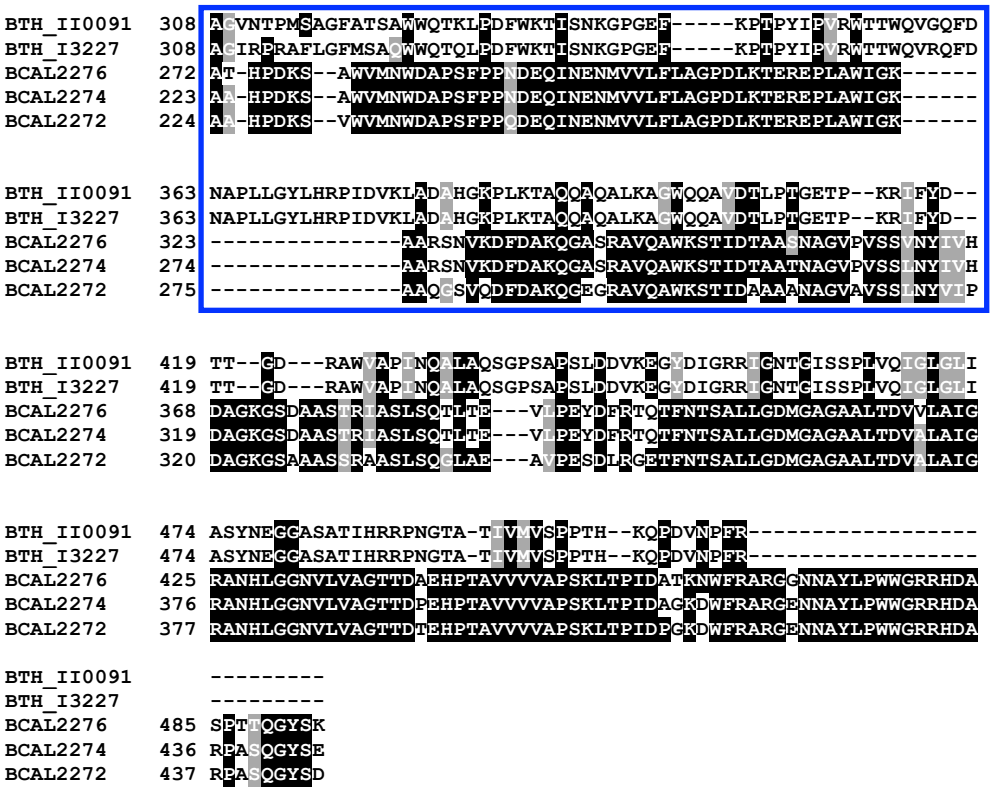

Figure 3.20 Alignment of the BCAL2276, BCAL2274 and BCAL2272 protein products with characterised Tle3 immunity proteins. Amino acid sequences encoded by BCAL2276, BCAL2274 and BCAL2272 from *B. cenocepacia* J2315 were aligned with the confirmed Tli3 proteins from *B. thailandensis,* encoded by BTH_II0091 and BTH_I3227. Black shading indicates identical residues at the corresponding position in 50% of sequences, grey shading indicates similar residues at the corresponding position in 50% of sequences. Regions corresponding to the DUF2875 domain are boxed in blue. Regions boxed in red may be Sec-dependent signal sequences. The gene locus designations are indicated on the left.

P search. However, there is a putative Sec-dependent signal sequence located upstream from the Signal P detected sequence that was identified manually (Figure 3.20).

3.4.5 The BCAM0043 *tssI* cluster

3.4.5.1 An additional Tle1 phospholipase effector encoded by BCAM0046

The product of the BCAM0046 gene located several genes downstream of the BCAM0043 *tssI* gene (Figure 3.10E) has previously been identified as an anti-bacterial Tle1 phospholipase by bioinformatic analysis (Russell et al., 2013). Alignment of the protein encoded by this gene with the experimentally characterised Tle1 protein encoded by BTH_2698 in *B. thailandensis* further confirmed it as a Tle1 phospholipases A_2 (Figure 3.17). As with other Tle1 proteins it contains a conserved G.xSx.G motif (residues 298-304), with the conserved flanking regions characteristic of the Tle1 class of phospholipases, and also corresponds to a DUF2235 domain at residues 48-331.

Similar to other Tle1 effectors, the protein encoded by the gene upstream of BCAM0046, BCAM0045, is a predicted periplasmic lipoprotein that contains a DUF3304 region. Therefore this protein likely to be the Tli1 immunity protein for the Tle1 encoded by BCAM0046 (Figure 3.18).

3.4.6 The BCAM0148 *tssI* cluster

3.4.6.1 Tle5 phospholipase effector encoded by BCAM0149

The BCAM0148 *tssI* gene cluster contains a gene encoding a putative T6SS effector located immediately downstream of BCAM0148 (Figure 3.10E). The protein encoded by this gene, BCAM0149, is homologous to Tle5 family member proteins identified in *B. cenocepacia* H111 and AU1054, which are phospholipase D (PLD) enzymes (Russell et al., 2013). Alignment of the BCAM0149 gene product highlights the presence of two conserved HxKxxxxD motifs (residues 263-270 and 581-588), characteristic of the Tle5 family (Figure 3.21). Tle5 of *P. aeruginosa,* PA3487, was shown to be an anti-bacterial effector capable of degrading phosphatidylethanol-

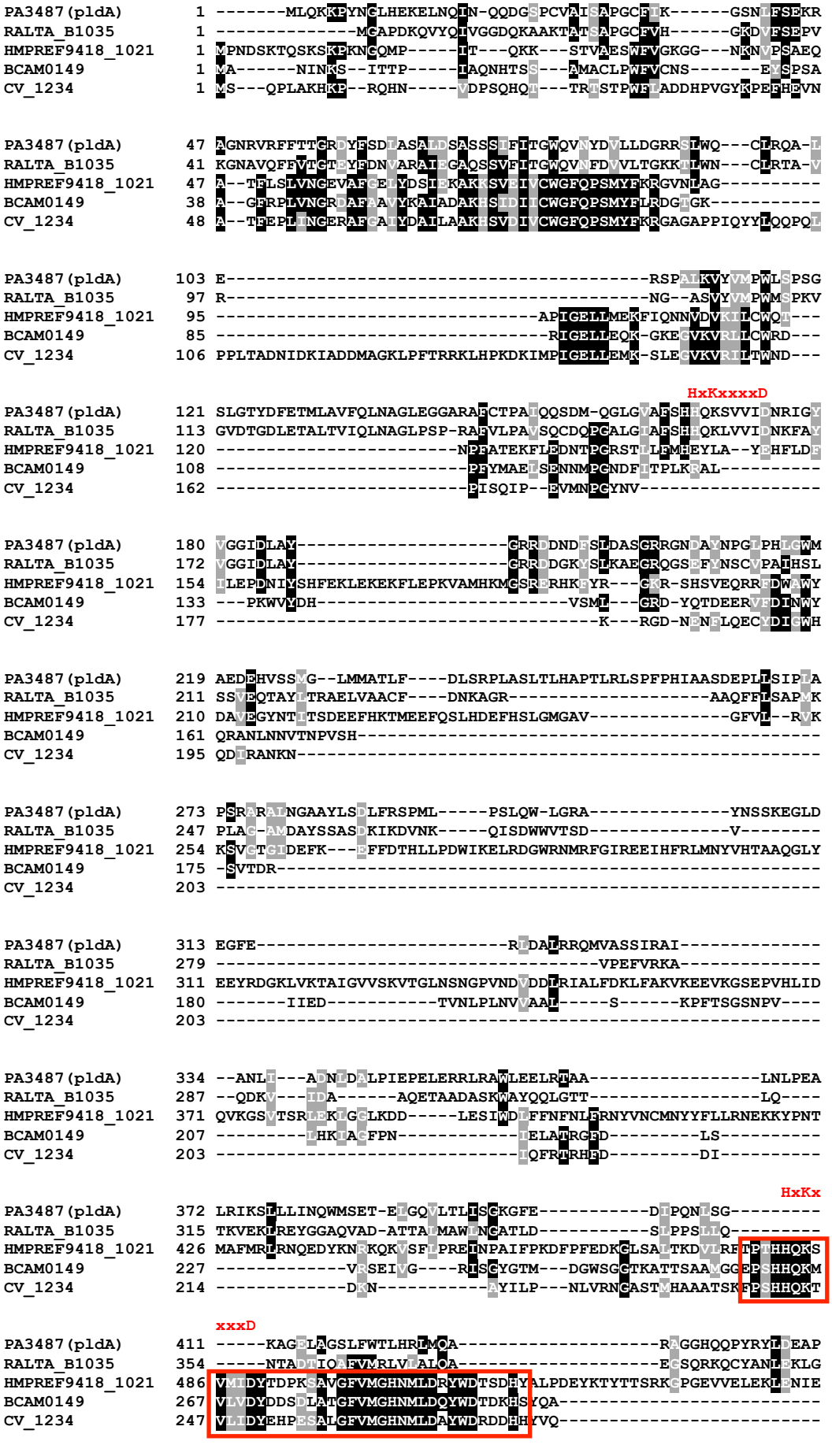
HxKxxxxD
HxKx
xxxD

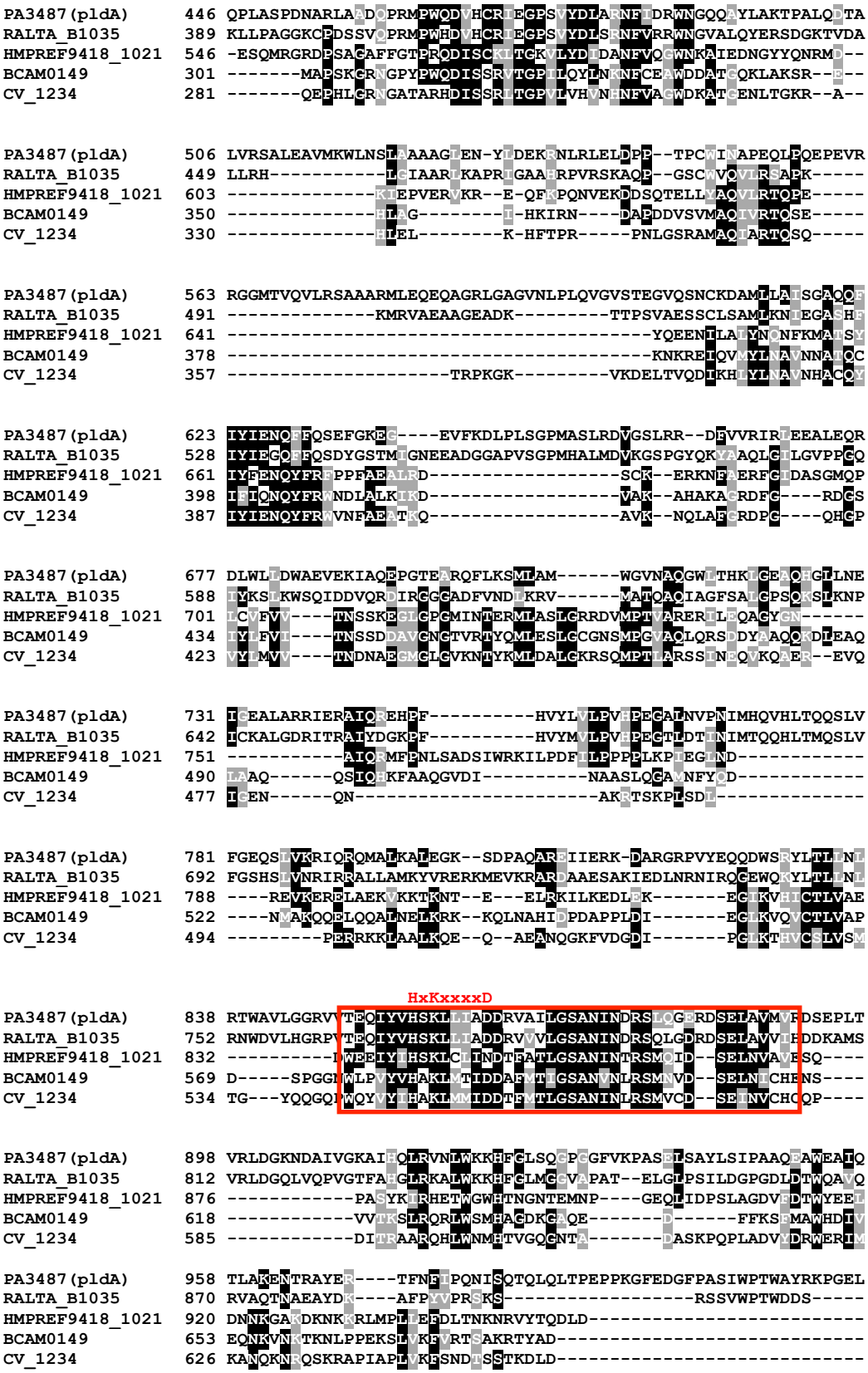

Figure 3.21 Alignment of the product of BCAM0149 with Tle5 family proteins. The amino acid sequence encoded by of BCAM0149 from *B. cenocepacia* J2315 was aligned with the confirmed Tle5 phospholipase T6SS effector encoded by PA3487 in *P. aeruginosa,* and other predicted Tle5 proteins identified in *Cupriavidus taiwanensis* (RALTA_B1035), *N.*

macacae (HMPREF9418_1021) and *C. violaceum* (CV_1234). Black shading indicates identical residues at the corresponding position in 50% of sequences, grey shading indicates similar residues at the corresponding position in 50% of sequences. Conserved catalytic HxKxxxxD motifs are indicated in red above the alignment and the pertinent region of the alignment is enclosed in a red box. The gene locus designations are indicated on the left.

amine in bacterial cell membranes, which was important for inter- and intraspecies competition (Russell et al., 2012). However, the first HxKxxxxD motif of this Tle5 is located further towards the N-terminus of the protein than the first HxKxxxxD motif of the BCAM0149 protein.

The Tli5 immunity protein for the *B. cenocepacia* H111 Tle5 identified by Russell et al. (2013) is homologous to both the BCAM0150 and BCAM0152 encoded proteins in J2315 and homologous to other Tli5 proteins, including those encoded by CV_1235 in *Chromobacterium violaceum* and HMPREF9418_1022 in *Neisseria macacae* (Figure 3.22). Both putative immunity proteins encoded by BCAM0150 and BCAM0152 contain a TPR repeat structural multi-domain, and SEL1 repeat motifs (a TPR subfamily) within this region, which are homologous to regions within other Tli5 immunity proteins. Note that the characterised Tli5 protein in *P. aeruginosa* (PA3488) is not homologous to other candidate Tli5 proteins described here and, moreover, upon a CDD search with the product of PA3488 as a query no TPR repeat domains were identified.

3.4.7 The BCAM2254 cluster

3.4.7.1 Putative RNase-containing Rhs effector encoded by BCAM2253

The BCAM2254 *tssI* cluster encodes a single putative T6SS effector (Figure 3.10G). Using the sequences of the predicted open reading frames neighbouring BCAM2254 as queries in BLASTP searches at least two T6SS-related genes were identified. The product of BCAM2253a is a small 140 amino acid protein containing a DUF1795 domain located at residues 6-136. This domain has been designated as a T6SS accessory protein to Rhs effectors, termed EagR, initially characterised in *S. marcescens* by the protein encoded by SMDB11_2277 located upstream of the *rhs1* effector gene SMDB11_2278 (Diniz and Coulthurst, 2015). EagR is also encoded upstream of other characterised *rhs* effector genes such as RhsA in *D. dadantii* (Koskiniemi et al., 2013). The product of BCAM2253a shows homology to both of these EagR proteins (Figure 3.23).

The gene located downstream of BCAM2253a, BCAM2253, was observed to

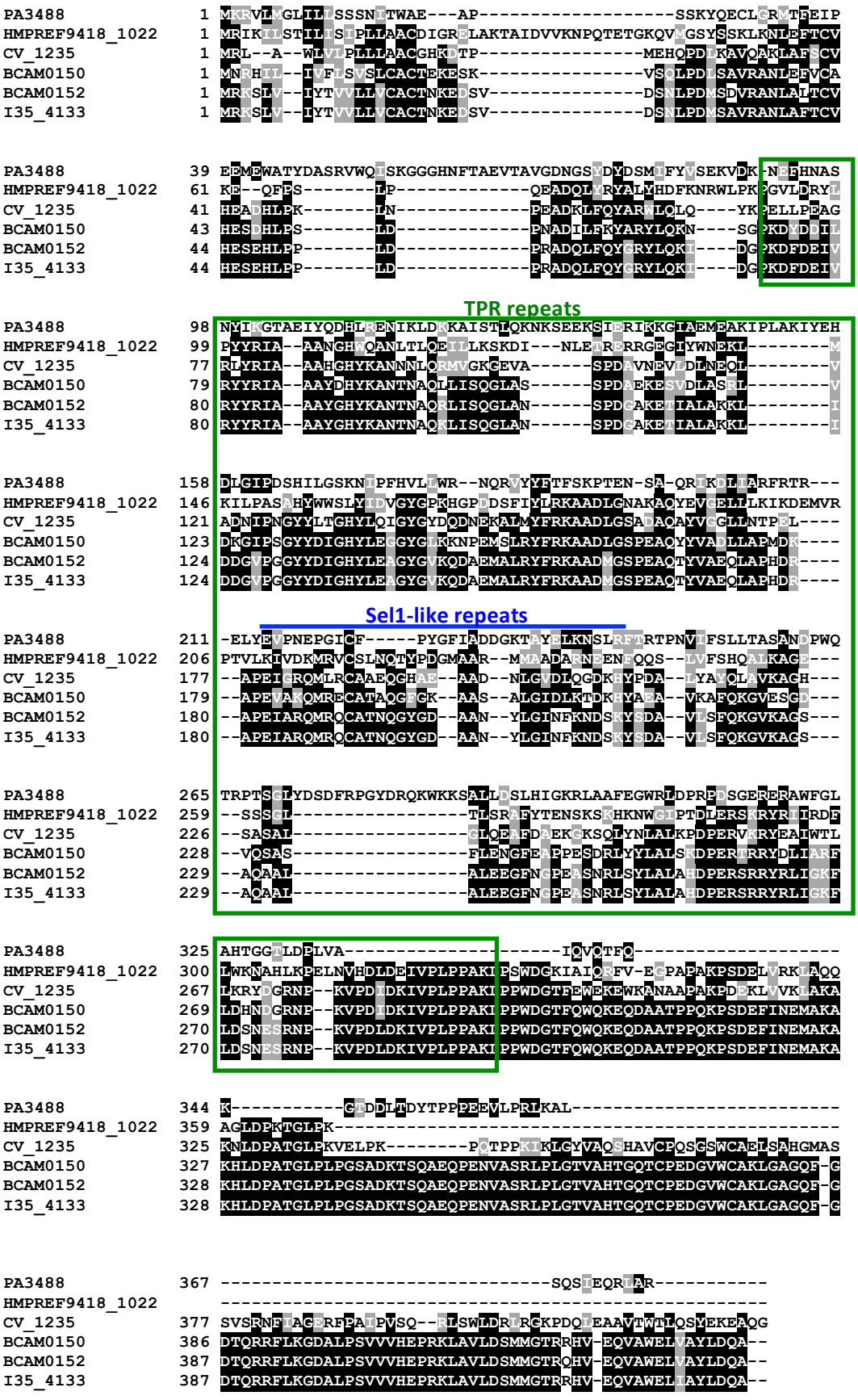
TPR repeats
Sel1-like repeats

Figure 3.22 Alignment of proteins encoded by BCAM0150 and BCAM0152 with Tli5 family orthologues. Amino acid sequences encoded by BCAM0150 and BCAM0152 from *B. cenocepacia* J2315 was aligned with the confirmed Tli5 immunity proteins encoded by PA3488 in *P. aeruginosa,* and other predicted Tli5 proteins identified in *C. violaceum* (CV_1235), *N. macacae* (HMPREF9418_1022) and the BCAM0150 orthologue in *B. cenocepacia* H111 (I35_4133). Black shading indicates identical residues at the corresponding position in 50% of sequences, grey shading indicates similar residues at the corresponding position in 50% of sequences. Predicted TPR repeat multi-domain boxed in green and predicted SEL1 structural motif indicated with a blue overline. The gene locus designations are indicated on the left.

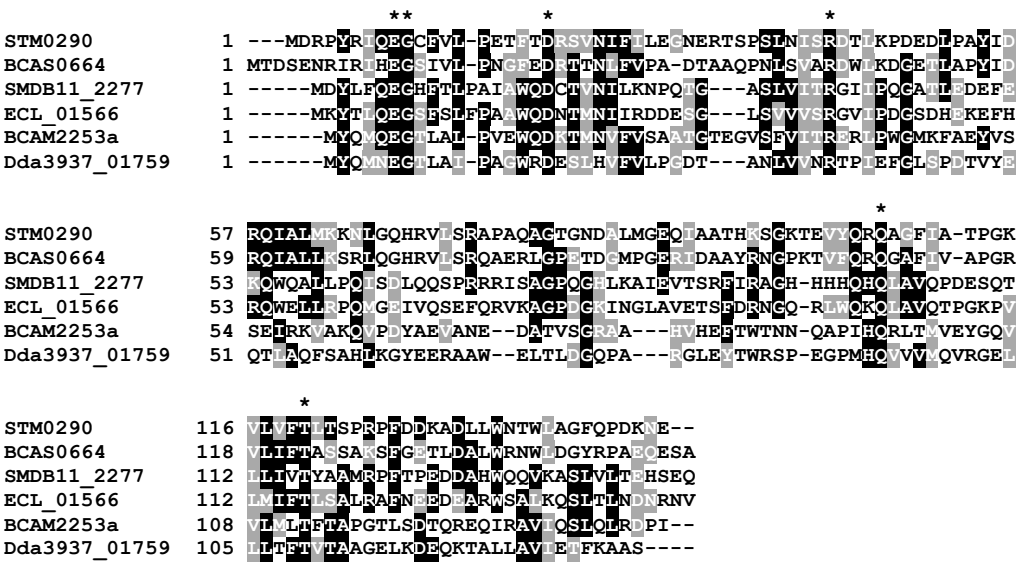

Figure 3.23 Alignment of proteins encoded by BCAM2253a and BCAS0664 with EagR family orthologues. Amino acid sequences encoded by BCAM2253a and BCAS0664 from *B. cenocepacia* J2315 were aligned with the confirmed EagR protein encoded by SMDB11_2277 in *S. marcescens,* and other predicted EagR proteins identified in *S. typhimurium* (STM0290, also known as SciW) *E. cloacae subsp. cloacae* (ECL_01566) and *D. dadantii* (Dda3937_01759). Black shading indicates identical residues at the corresponding position in 50% of sequences, grey shading indicates similar residues at the corresponding position in 50% of sequences. Identical residues in 100% of sequences are indicated with an asterisk. The gene locus designations are indicated on the left.

encode a large 1515 amino acid multi-domain protein. Bioinformatic analysis identified a PAAR_RHS (cd14742) region at residues 204-277, three RHS repeat sequences (pfam05593) at residues 552-587, 759-800, 826-863, a YD_repeat sequence (TIGR01643) at residues 868-909, an RHS repeat-associated core domain (TIGR03696) at residues 1280-1365, and a C-terminal region predicted to contain a RES domain (smart00953), residues 1400-1512, which may function as an RNase (Zhang et al., 2012) (Figure 3.24). All of which are typical of Rhs proteins (Section 1.5.4).

The open reading frame located immediately downstream of BCAM2253, BCAM2252, is unusual in that it potentially starts from a TGG start codon, which would result in the production of a 420 amino acid protein also containing RHS repeat sequences. However, it likely that this is the result of a premature stop codon occurring in a fused BCAM2253-BCAM2252 open reading frame, so is unlikely to give rise to a protein product. Alternatively, it could be an *rhs* vestige that resulted from recombination with another *rhs* that became or gave rise to BCAM2253.

Finally, BCAM2251a encodes a small 132 amino acid protein with no discernible conserved domains when analysed using the amino acid sequence as a query in a BLASTP search. However, it could potentially be the immunity protein for the predicted RNase component of BCAM2253, due to its genetic location downstream of BCAM2253.

3.4.8 The BCAS0667 *tssI* cluster

3.4.8.1 Nuclease Rhs effector encoded by BCAS0663

The final non-*tssI* effector to be discussed is encoded within the BCAS0667 *tssI* gene cluster (Figure 3.10H), which encodes the evolved TssI protein, $TssI_{0667}$ (discussed in Section 3.3.2). BLASTP searches with the protein products of genes located within close proximity to BCAS0667 identified a further DUF1795-containing EagR accessory protein, along with its cognate Rhs effector protein, encoded by BCAS0664 and BCAS0663, respectively. Similar to other EagR proteins, the product

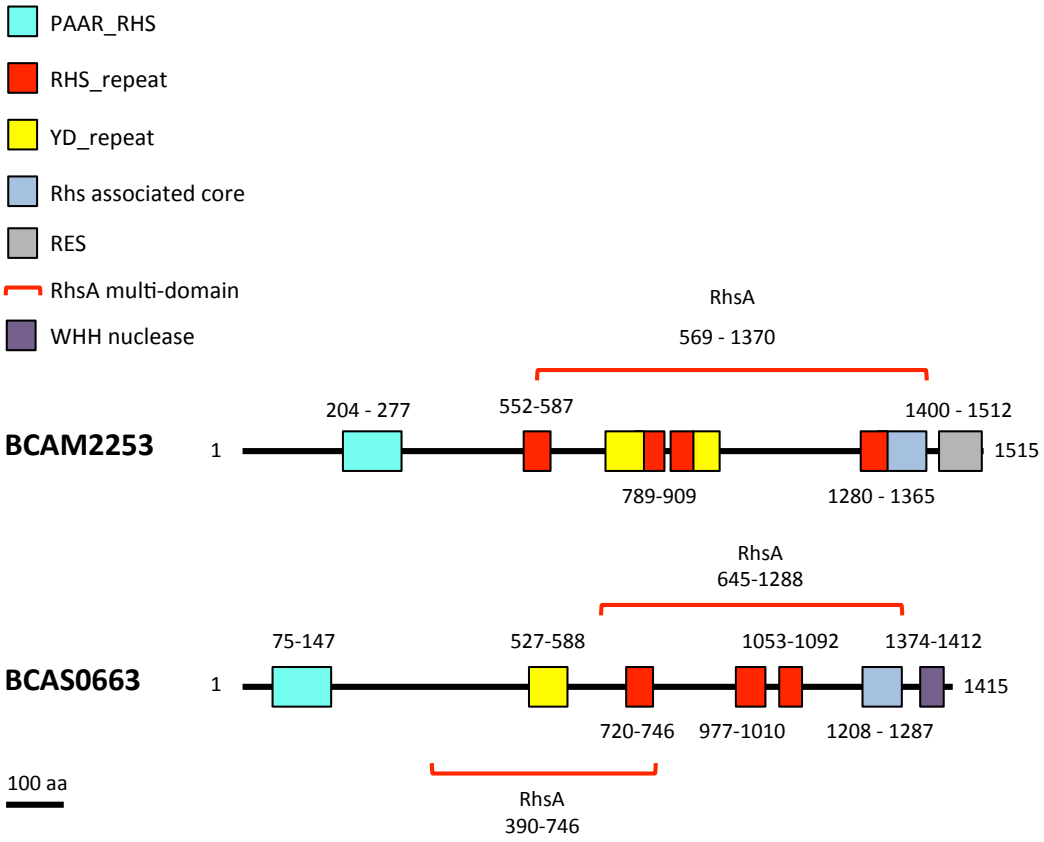

Figure 3.24 Domain organisation of putative T6SS-dependent Rhs effectors encoded by BCAM2253 and BCAS0663 in *B. cenocepacia* J2315. The conserved domains are represented by colour-coded boxes. The key above the figure indicates the identity of each domain. The location of each domain within the amino acid sequence is indicated above or below each box.

of BCAS0664 was predicted to be a small protein of 152 amino acids, with the DUF1795 homology region spanning from residues 12 to 143 (Figure 3.23).

Further analysis of the Rhs protein encoded by BCAS0663 indicated the presence of several conserved domains distributed throughout the protein (Figure 3.24), as defined by the conserved domain database (Marchler-Bauer et al., 2014). These included the typical features of a Rhs protein: a PAAR_RHS domain at residues 75-147; YD repeats between residues 527-588; several RHS_repeat sequences at residues 720-746, 977-1010, 1053-1092 and a RHS repeat-associated core domain at residues 1208-1287. It also has C-terminal domain with homology to a group of nucleases within the HNH/ENDO VII superfamily that contain a conserved WHH domain (pfam14414) (Zhang et al., 2011) (Figure 3.25). This is a colicin-DNase type nuclease which is a member of the His-Metal-finger endonuclease clan (CL0263) as defined by the Pfam database (Finn et al., 2014). It contains a conserved WHH motif at residues 1380-1382, with two additional conserved histidine residues at position 1397 and His1402. The first histidine residue is thought to be involved in metal ion binding, whilst the others are involved in the arrangement of water molecules within the active site to allow water activation and subsequent involvement in a hydrolysis reaction (Zhang et al., 2011).

Two genes, BCAS0662 and BCAS0661c, follow BCAS0663, each of which encodes a small protein, one with a SMI1_KNR4 domain (pfam09346) (SUKH clan) and the other with an Imm-NTF2 domain (pfam15655), respectively. Many proteins that contain these domains are thought to be antitoxin proteins in polymorphic toxin systems in prokaryotes (Zhang et al., 2011; Zhang et al., 2012). Therefore either or both of these proteins could be the immunity protein for the nuclease Rhs effector encoded by BCAS0663.

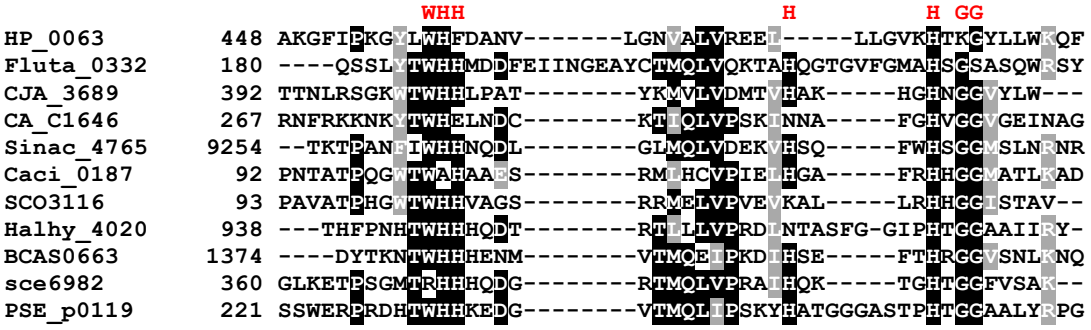

Figure 3.25 Alignment of C-terminal of BCAS0663 with members of the WHH nuclease domain-containing superfamily. The C-terminal amino acid sequence encoded by BCAS0663 (residues 1374-1412) from *B. cenocepacia* J2315 was aligned with the several other WHH nuclease domain-containing proteins from a range of Gram-negative and Gram-positive bacteria. Black shading indicates identical residues at the corresponding position in 50% of sequences, grey shading indicates similar residues at the corresponding position in 50% of sequences. The conserved WHH motif and the catalytically important histidine residues are indicated in red font above the alignment. The gene locus is indicated to the left.

Chapter 4: Role of the type VI secretion system in *Burkholderia cenocepacia*

4.1 Rationale

B. cenocepacia strains generally contain one T6SS gene cluster, the ancestral Burkholderia T6SS that lacks a *tssI* gene, and several TssI-encoding gene clusters, which together give a full complement of the T6SS genes that are required for a functioning system, shown in Figure 3.1. However, little is known regarding the main function of this system in *Bcc*, and the nature of the effectors it utilises.

Observations in another *Burkholderia* species, *B. thailandensis*, found that the first of its five T6SSs, the ancestral T6SS-1 cluster, was, like other better characterised T6SSs in *P. aeruginosa* and *V. cholerae* (Hood et al., 2010; MacIntyre et al., 2010), responsible for providing the bacteria with a fitness advantage over other competing bacterial strains sharing the same environment (Schwarz et al., 2010). It has also been shown that direct attack from a T6SS-bearing bacterium can induce the T6SS to target attacking bacteria, in a 'tit-for-tat' manner (Basler et al., 2013). This attack can also be induced by perturbations of the cell envelope in recipient bacteria by the T4SS pilus of competing bacteria (Ho et al., 2013). As *B. cenocepacia* harbours only a single T6SS, it appears likely that it would play a similar role. Therefore, it was decided it investigate the anti-bacterial role of the T6SS in *B. cenocepacia*.

One T6SS in other *Burkholderia* species has been linked to eukaryotic interactions and virulence, namely the T6SS-5 in the Pseudomallei group of *Burkholderia* (Schell et al., 2007; Shalom et al., 2007; Burtnick et al., 2010; Schwarz et al., 2010; Schwarz et al., 2014; Toesca et al., 2014) (Section 1.2.5.5). *B. cenocepacia* does not encoded a T6SS-5. However, it does have the ability to survive intracellularly within macrophages, persisting in membrane bound vesicles, thus subverting the frontline defence of the innate immune system. In this regard, the T6SS has been shown to be important for actin rearrangements in these infected macrophages, but not for direct vacuole arrest, specifically using a *B. cenocepacia* mutant that hypersecretes TssD (Aubert et al., 2008; Rosales-Reyes et al., 2012a; Rosales-Reyes et al., 2012b). The T6SS in *B. cenocepacia* is also required to initiate pyrin inflammasome activation in infected host cells, which results in a

pro-inflammatory response (Gavrilin et al., 2012). It does this by mediating the deamination of a particular residue in the RhoA GTPase protein, via an unknown mechanism, which leads to an increase in active RhoA (GTP bound), and subsequent downstream effects on the actin cytoskeletal network (Rosales-Reyes et al., 2012b; Xu et al., 2014). Using a hypersecreting TssD mutant, the T6SS was also shown to be important for the ability of *B. cenocepacia* to resist predation by *Dictyostelium discoideum* (Aubert et al., 2008). It was also shown to be a contributor to *in vivo* survival in a rat agar bead lung infection model (Hunt et al., 2004). But further evidence for an anti-eukaryotic role for the T6SS in *B. cenocepacia* is lacking.

To understand whether the T6SS in *B. cenocepacia* plays a dual role in both anti-bacterial and anti-eukaryotic interactions it was decided to determine if the T6SS contributed to virulence in simple eukaryotic infection models, the zebrafish infection model and the *Galleria mellonella* infection model. Previous experiments using the *Galleria* model system and *C. elegans* failed to establish a role for the *B. cenocepacia* T6SS in virulence (Shastri, Schwager, Eberl, Thomas, unpublished observations). However, the *B. cenocepacia* strains employed (H111 and Pc715j) are not particularly virulent in animal model systems. But as the K56-2 strain of *B. cenocepacia* has been demonstrated to be virulent in the zebrafish embryo and *Galleria* models (Seed and Dennis, 2008; Vergunst et al., 2010) it was decided to reinvestigate the role of the *B. cenocepacia* T6SS in interactions with eukaryotes using this strain.

4.2 Construction of T6SS-deficient mutants in *B. cenocepacia* by insertional inactivation

To allow an investigation into the activity and potential role of the T6SS in *B. cenocepacia* it was required to generate a T6SS-deficient mutant. The simplest way to achieve this was by insertional inactivation with an antibiotic resistance cassette.

4.2.1 Insertional inactivation of *tssA* and *tssM* in the *B. cenocepacia* strain K56-2

The K56-2 isolate of *B. cenocepacia* has previously been shown to be more virulent than other isolates in eukaryotic infection models, particularly in a zebrafish embryo infection model (Vergunst et al., 2010) and a *Galleria mellonella* infection model (Seed and Dennis, 2008). Therefore, to investigate whether the T6SS plays any role in the virulence of *B. cenocepacia,* T6SS mutants of the K56-2 strain were required.

Disrupting any of the thirteen core subunit genes in the T6SS cluster (*tssA*-*tssM*) leads to malfunction of the T6SS (Zheng and Leung, 2007; Zheng et al., 2011). *tssM* encodes a membrane protein observed to form a trans-envelope sub complex with other components of the T6SS complex to anchor the complex to the cell membrane (Durand et al., 2015), and the product of *tssA* is an uncharacterised predicted cytosolic protein. *tssA* and *tssM* are located in separate transcriptional units in the *B. cenocepacia* T6SS cluster. Mutant strains of *B. cenocepacia* K56-2 with either a non-functional *tssA* or *tssM* gene were generated by disruption with a gene conferring trimethoprim resistance, *dfr*. This was achieved by conjugating a previously constructed suicide vector, pSHAFT2-*tssM*::Tp(rev) (Shastri, 2011), containing the sequence encoding the cytoplasmic domain fragment of TssM disrupted by *dfr* (in the reverse orientation with respect to *tssM),* and pSHAFT-*tssA*::Tp (Shastri, 2011), containing *tssA* disrupted by *dfr* (in the same orientation with respect to *tssA),* separately into *B. cenocepacia* K56-2. Recombination between regions of homology in the gene fragment contained on the plasmid and on the chromosome of the recipient K56-2 cells results in generation of either single

or double homologous recombinants (Figure 4.1). Both of which are trimethoprim-resistant.

The pSHAFT2 vector backbone contains the *cat* gene (Figure 4.2), conferring resistance to chloramphenicol. This is used to distinguish between single crossover recombinants, in which the vector backbone is integrated into the genome, and double crossover recombinants, in which the vector backbone is not present in the genome. Candidate *tssM* and *tssA* mutants resulting from double crossover recombination were identified by virtue of their resistance to trimethoprim and sensitivity to chloramphenicol. These candidates were then verified by PCR using primers that annealed to genomic DNA just outside of the *tssM*::Tp or *tssA*::Tp homology region contained on the introduced plasmid (outside primers), and primers that annealed within the *tssM*::Tp or *tssA*::Tp homology region (inside primers). Candidate 15 for both mutants was identified as a potential double recombinant, and selected for further colony purification and then rescreened by PCR using the outside annealing primers, to verify insertional inactivation (Figure 4.3). Both candidates proved to be true double recombinants, as the PCR fragments amplified from them were ~650 base pairs (bp) larger than the wild-type (WT) fragment, at approximately 2000 bp, consistent with insertion of the 650 bp trimethoprim-resistance cassette.

4.2.2 Insertional inactivation of *tssM* in the *B. cenocepacia* strain H111

A mutant strain of *B. cenocepacia* H111 with a disrupted *tssM* gene was also generated. To do this, the suicide vector pSHAFT2-*tssM*::Tp(rev) was introduced into *B. cenocepacia* H111 by conjugation. Single crossover recombinants were selected by their acquisition of resistance to trimethoprim. Candidate double crossover recombinants were identified by sensitivity to chloramphenicol and then confirmed by PCR screening using outside and inside primers as described in Section 4.2.1 (Figure 4.4). This confirmed the presence of the trimethoprim resistance cassette in the candidate H111-*tssM*::Tp mutants 1, 2, 4-9, by the amplification of a DNA fragment that was 650 bp larger than that generated by the parental H111 strain.

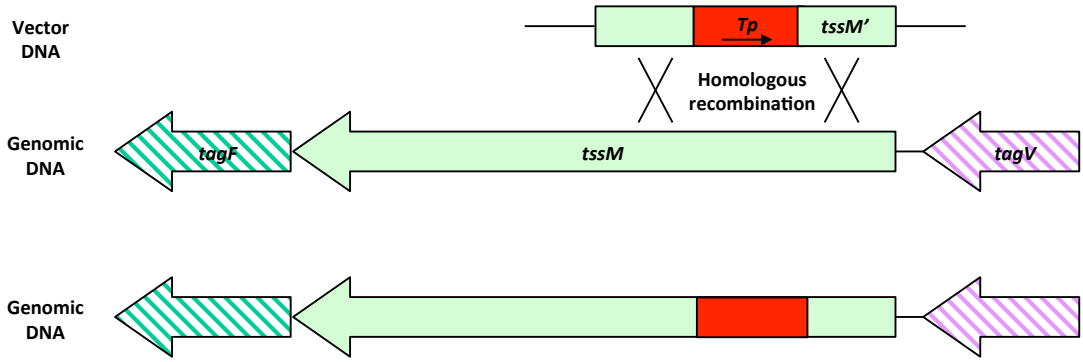

Figure 4.1 Principle of mutant generation in *B. cenocepacia* by insertional inactivation with an antibiotic resistance cassette. A suicide vector is constructed containing the gene of interest, *tssM* in this example, disrupted by an antibiotic resistance cassette (*dfr*, Tp^r). At least 500 bp of homology are required on either side of the inserted cassette. The vector is introduced into the wild-type strain by conjugation or electroporation where homologous recombination events occur between the allele contained within the vector and complementary DNA regions in the genomic DNA. This results in integration of the disrupted allele into the genome by either single or double crossover recombination. In the former, the entire plasmid is integrated into the genome whereas is the latter (shown here) only the mutant allele is transferred to the genome in place of the original wild-type allele. These are selected for resistance to the appropriate antibiotic (conferred by the resistance cassette), trimethoprim in this example. The pSHAFT2 system uses a second antibiotic resistance gene contained within the vector (*cat*, Cm^r) to distinguish between single and double crossover recombinants. Double crossover recombinants are sensitive to chloramphenicol, as they no longer contain the *cat* gene present on the vector backbone.

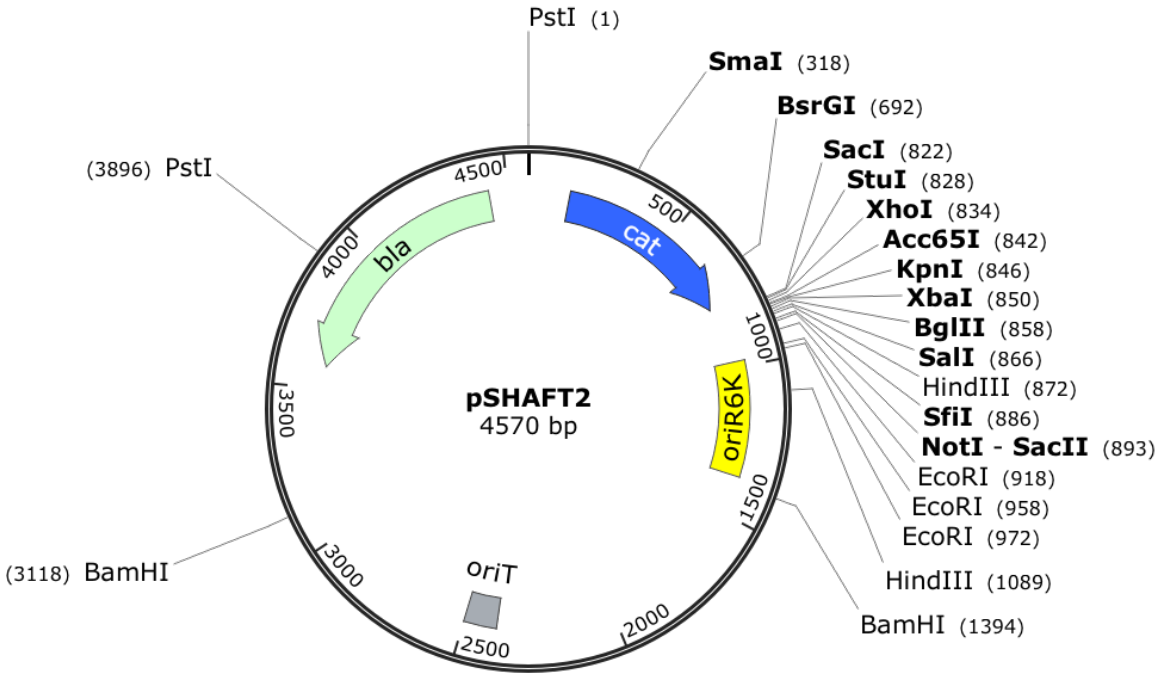

Figure 4.2 Plasmid map of the suicide vector pSHAFT2. Image depicts a map of the 4570 bp suicide vector pSHAFT2, highlighting the presence of the *bla* and *cat* genes, conferring resistance to ampicillin and chloramphenicol, respectively. The RP4 original of transfer, and R6K origin of replication are also indicated, along with important restriction sites. Restriction sites given in bold occur only once in the plasmid DNA sequence.

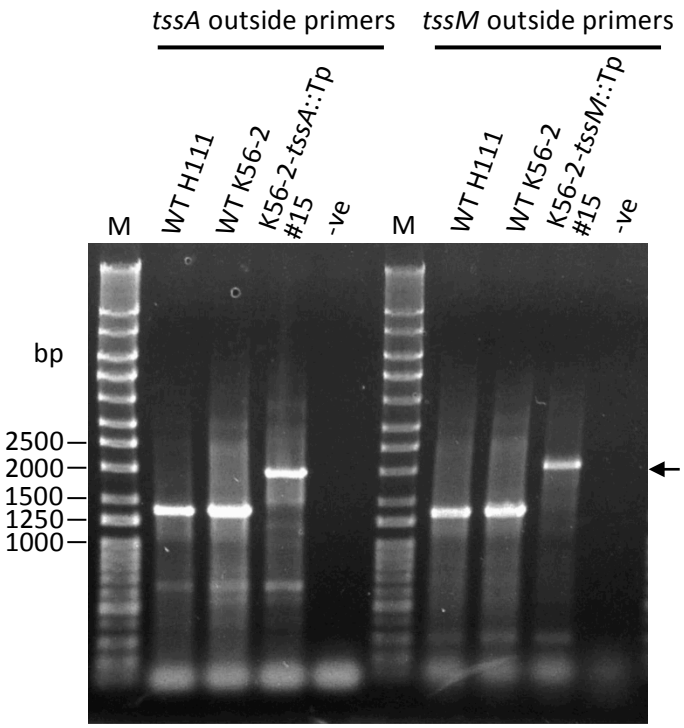

Figure 4.3 Confirmation of insertional inactivation of *tssA* and *tssM* in *B. cenocepacia* K56-2 by PCR screening. *tssA* and *tssM* in *B. cenocepacia* K56-2 were inactivated by homologous recombination with *tssA*::Tp and *tssM*::Tp alleles introduced by the suicide vectors pSHAFT-*tssA*::Tp and pSHAFT2-*tssM*::Tp(rev) respectively. DNA fragments were amplified by PCR from candidate K56-2-*tssA*::Tp and -*tssM*::Tp mutants using outside diagnostic primers and resolved in a 0.8% agarose gel. Wild-type (WT) H111 and K56-2 genomic DNA was used as control templates which gave rise to products of 1400 bp. Mutants resulting from allelic replacement were expected to give rise to DNA fragments 650 bp larger in size, at approximately 2000 bp, indicated by arrow. M, Q-step 4 DNA ladder; -ve, no DNA control.

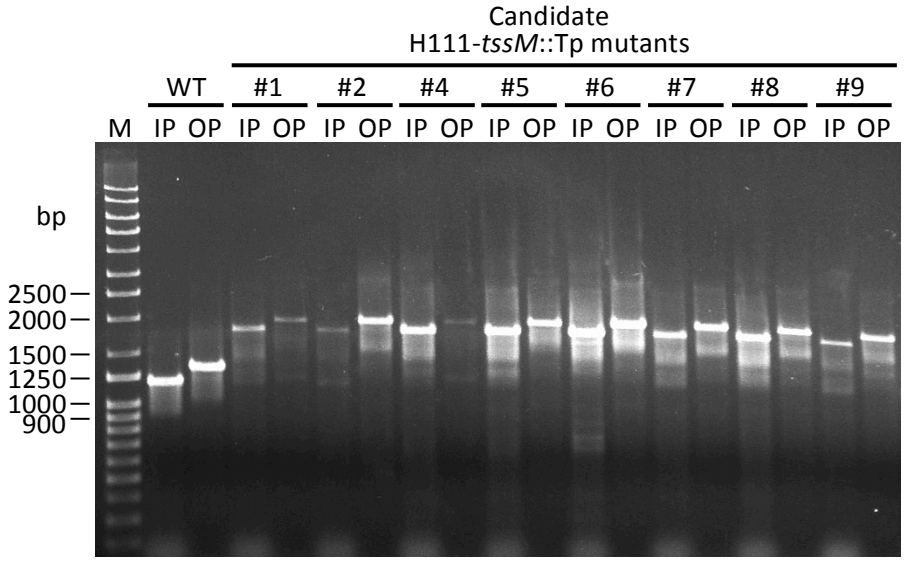

Figure 4.4 Confirmation of insertional inactivation of the *tssM* gene in *B. cenocepacia* H111 by PCR screening. *tssM* in *B. cenocepacia* H111 was inactivated by homologous recombination with a *tssM*::Tp allele introduced on the suicide vector pSHAFT2-*tssM*::Tp(rev). DNA fragments were amplified by PCR from H111-*tssM*::Tp candidates using inside diagnostic primers (IP) and outside primers (OP) and resolved in a 0.8% agarose gel. Wild-type H111 genomic DNA (WT) was used a control template and gave rise to products of 1200 and 1400 bp fragment (IP and OP respectively). Mutants resulting from allelic replacement were expected to give rise to DNA fragments 650 bp larger in size. M, Q-step 4 DNA ladder.

4.3 Construction of a T6SS-deficient mutant in *B. cenocepacia* by in-frame deletion

In general, by disrupting a gene with an antibiotic resistance cassette one has to be aware of potential polar effects to downstream genes located within the same transcriptional unit. In the case of *B. cenocepacia*, which exhibits a high level of intrinsic resistance to many antibiotics commonly used to select for plasmids, construction of a mutant by insertional inactivation with an antibiotic resistance cassette can make subsequence genetic manipulations problematic. Thus it was decided to generate an in-frame deletion mutant of a core T6SS gene in *B. cenocepacia* that lacks an inserted antibiotic resistance cassette, i.e. an unmarked mutant. However, problems regarding the genetic tools needed for generating a mutant of this type first had to be resolved, as discussed below.

4.3.1 Construction of allelic replacement vector pEX18TpTer-*pheS*

A particularly convenient method used to construct markerless mutants by allelic replacement to use a vector containing a counter-selectable marker. Here, initial selection is made for integration of the plasmid into the genome via a homologous recombinant event. In the second step this counter-selectable marker is used to select for a second homologous recombination event that results in excision of the vector (Figure 4.5). This should result in either replacement of the wild-type gene by the mutant allele or reversion back to wild-type.

One such vector developed for use in the *Burkholderia* species is the pEX18-*pheS* vector series (Barrett et al., 2008). This uses incorporation of toxic *p*-chlorophenylalanine (cPhe) into growing polypeptide chains by a mutant version of the α-subunit of phenylalanyl tRNA synthetase (PheS) from *B. pseudomallei*, encoded on the plasmid as a counter-selectable marker. pEX18-*pheS* derivatives, including pEX18Tp-*pheS,* have been successfully used by others to generate deletion mutants in the *Burkholderia* species, including in *B. thailandensis* (Barrett et al., 2008). However, our lab have encountered problems when using pEX18Tp-*pheS* in *B. cenocepacia.* This occurred during initial selection for trimethoprim-

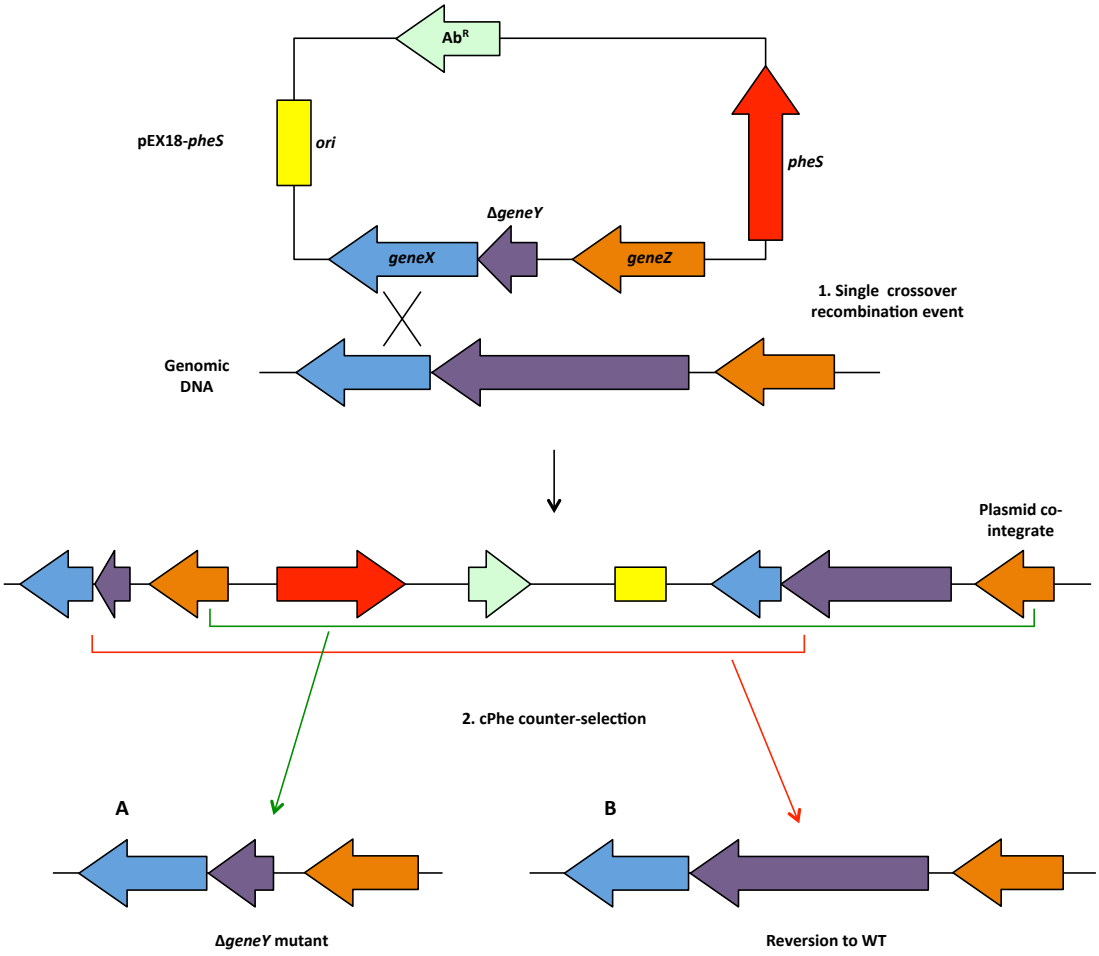

Figure 4.5 Principle of allelic replacement based on cPhe counter-selection. An in-frame deletion allele containing 500 bp homology regions either side of deleted segment is cloned into a pEX18-*pheS* based suicide vector (top row). Upon transfer of the vector to the parental strain, a homologous recombination event occurs (1) between the allele contained in the vector and the corresponding region in the genome. This results in integration of the plasmid into the genome. Single crossover recombinants are grown in the absence of the antibiotic to which the vector specifies resistance to and spontaneous recombinants that result in excision of the plasmid are selected for on M9-glucose plates containing 0.1% cPhe (2). Incorporation of cPhe by the mutated PheS encoded on the vector is toxic to the cell. Excision either results in (A) full integration of the deleted allele or (B) reversion back to wild-type (WT).

resistant single crossover recombinants (V. Eidsvaag, A. Sofoluwe and M.S. Thomas, unpublished observations). Another problem with this vector concerned the effectiveness of the cPhe counter-selection step in H111 (Fazli et al., 2015).

It was noted that other pEX18-*pheS* vectors (such as pEX18Tet-*pheS*) contained their antibiotic resistance gene downstream of and in the same orientation as the *pheS* gene, whereas pEX18Tp-*pheS* did not. Interestingly, pEX18Tet-*pheS* was used effectively in *B. cenocepacia* by the Winans group (Ryan et al., 2013). Therefore, it was rationalised that transcription from the strong P_{S12} promoter used to drive the *pheS* gene was converging with transcription from the reverse orientated *dfr* gene, thus causing down-regulation of *dfr* promoter activity and resulting in an inability to select for trimethoprim-resistance. Therefore, it was decided to re-engineer pEX18Tp-*pheS,* to place the *dfr* gene in the same orientation as *pheS* with the addition of a strong transcriptional terminator to prevent read though transcription into the replication region of the plasmid. To do this, a previously constructed version of the *dfr* gene with the tandem transcription terminators T1 and T2 of the rrnB rRNA operon (rrnBT1T2) located downstream of the stop codon, termed TpTer, was used. A diagrammatic representation of the construction of this modified allelic replacement vector is depicted in Figure 4.6.

First, it was required to remove a rrnBT1T2 region already present in pEX18Tp-*pheS* to prevent possible internal self-homologous recombination between duplicated rrnBT1T2 sequences. To do this, pEX18Tp-*pheS* was digested with AfeI (Eco47III) and BsaI (Eco31I) and 3' overhangs filled-in with T4 DNA polymerase. This generated a 3975 bp linear fragment that was then self-ligated using T4 DNA ligase, to generate the intermediate plasmid pEX18Tp-*pheS*ΔrrnBT1T2.

The *dfr* gene contained within pEX18Tp-*pheS*ΔrrnBT1T2 was removed by digestion with EcoRV and SpeI. The resulting 3516 bp fragment was purified by gel excision and subjected to a fill-in reaction with T4 DNA polymerase. Separately, the TpTer cassette was excised from p34E-TpTer (Shastri, 2011) by NdeI digestion and the 873 bp fragment gel purified and filled in with T4 DNA polymerase. The two

A

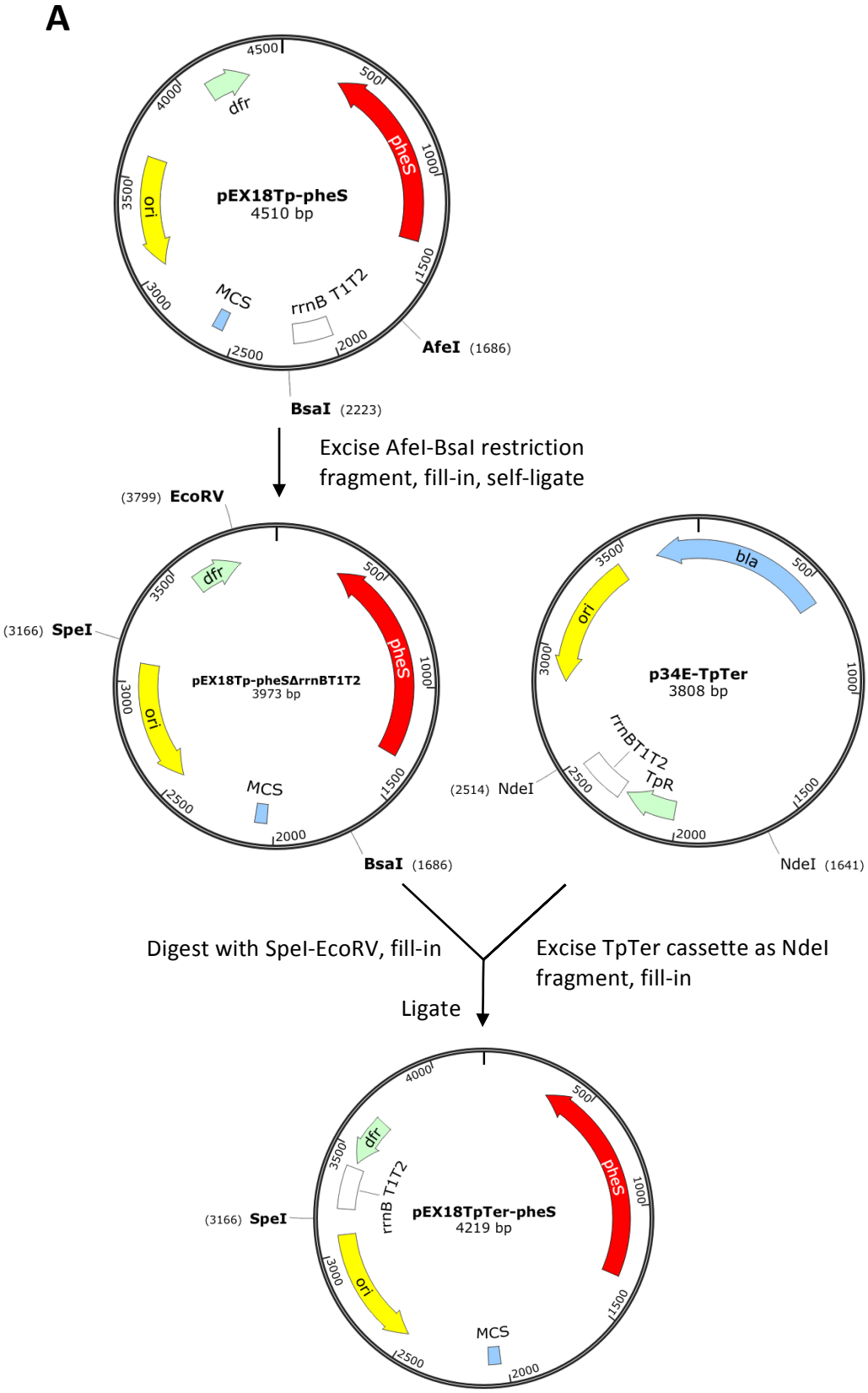
pEX18Tp-pheS
4510 bp
dfr
pheS
ori
MCS
rrnB T1T2
AfeI (1686)
BsaI (2223)
Excise AfeI-BsaI restriction fragment, fill-in, self-ligate
(3799) EcoRV
(3166) SpeI
pEX18Tp-pheSΔrrnBT1T2
3973 bp
BsaI (1686)
p34E-TpTer
3808 bp
bla
rrnBT1T2
TpR
(2514) NdeI
NdeI (1641)
Digest with SpeI-EcoRV, fill-in
Excise TpTer cassette as NdeI fragment, fill-in
Ligate
pEX18TpTer-pheS
4219 bp

B

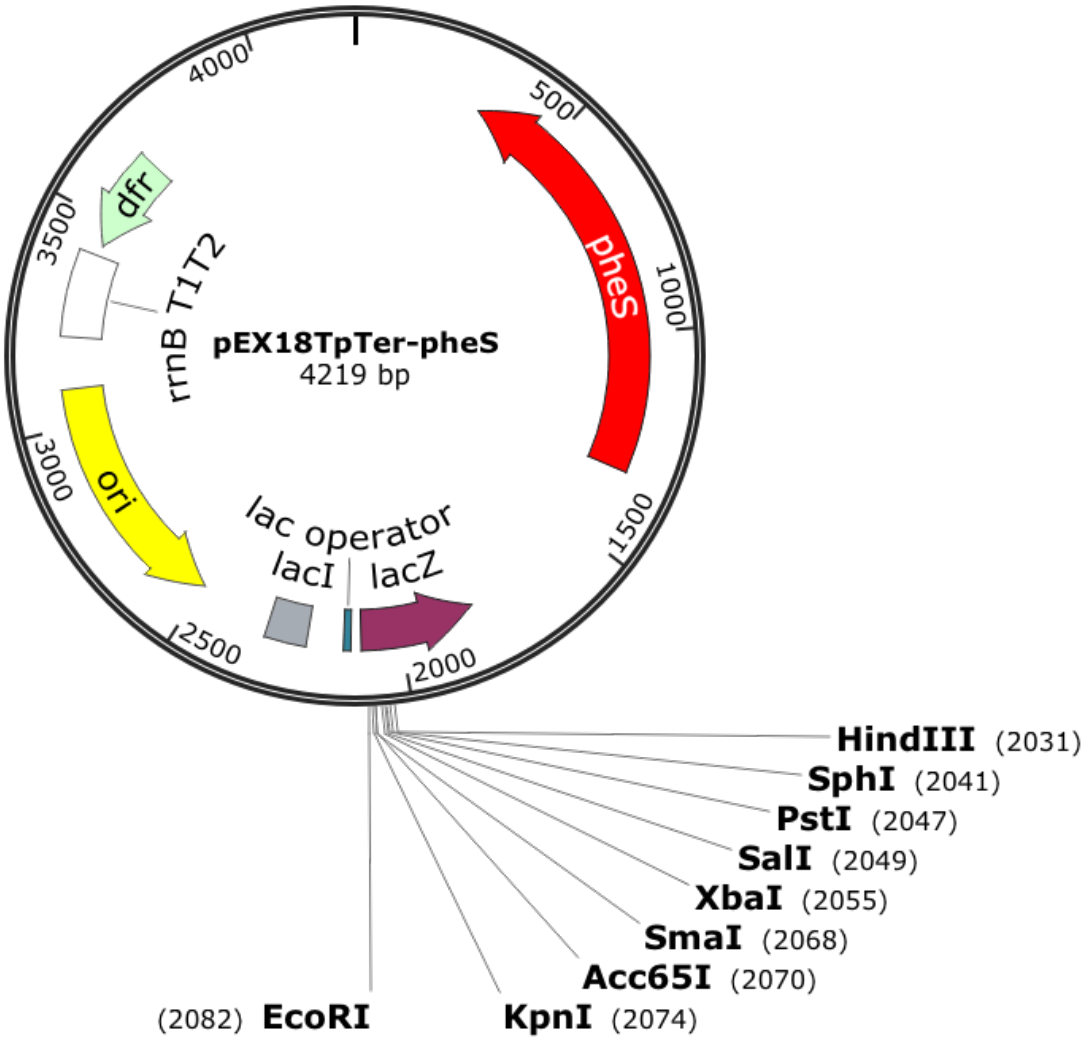

Figure 4.6 Diagrammatic representation of the construction of allelic replacement vector pEX18TpTer-*pheS*. (A) Depicts construction of pEX18TpTer-*pheS*, where pEX18Tp-*pheS* (Top) was digested with AfeI and BsaI to remove the rrnBT1T2 region to give pEX18Tp-*pheS*ΔrrnBT1T2 (middle left). pEX18TpTer-*pheS* was constructed by replacing the SpeI-EcoRV fragment of pEX18Tp-*pheS*ΔrrnBT1T2 with the NdeI TpTer cassette of p34E-TpTer (middle, right), following end-filling of the vector and TpTer DNA fragments. (B) Map for the pEX18TpTer-*pheS* plasmid, highlighting pertinent vector features and restriction sites.

fragments were then ligated together, and following transformation of *E. coli* JM83, transformants were selected for trimethoprim-resistance. Candidate clones were subjected to plasmid isolation and the size of resulting plasmids were analysed following DNA gel electrophoresis (Figure 4.7). Clones of the expected size of 4216 bp were then sequenced using the primers pEX18Tpfor and pEX18Tprev to determine the orientation of the introduced TpTer cassette. Clone 6 contained the TpTer cassette in the desired orientation, i.e. the same orientation as *pheS*. This clone, named pEX18TpTer-*pheS,* was used in all subsequence allelic replacement procedures for generating markerless deletion mutants in *B. cenocepacia*.

4.3.2 Construction of allelic replacement vector pEX18TpTer-*pheS*-Cm

One disadvantage of pEX18Tp-based vectors is that selection for trimethoprim-resistant transformations following ligation of the mutated target gene requires use of Iso-sensitest agar (a nutrient rich medium containing 2% glucose) or minimal salts agar (which generally includes glucose as the carbon source). This is due to the presence of thymine in LB agar and other complex media, which renders the trimethoprim ineffective at standard concentrations (25 μg/mL). It has been observed that the presence of glucose in the selection medium prevents use of the blue-white screening capability of pEX18Tp-derivatives as its catabolite represses the *lacZ* promoter on the vector. To overcome this problem glycerol was employed as a carbon source. However, it was found that this worked more effectively at 30°C, meaning it took 3 days for potential clones to be large enough to be identified and screened, at some inconvenience. Therefore, it was decided to further modify pEX18TpTer-*pheS* to include a different antibiotic selection marker (*cat*) to allow a more convenient selection medium to be used, which permitted quicker identification of recombinant clones by growth on rich medium at 37°C. Figure 4.8 illustrates the construction of this modified vector.

To do this, a previously constructed *cat* cassette that contained a strong synthetic promoter was excised as an EcoRI fragment from p34E-Cm2 and the 889 bp fragment was gel purified. T4 polymerase was then used to fill-in 5' overhangs.

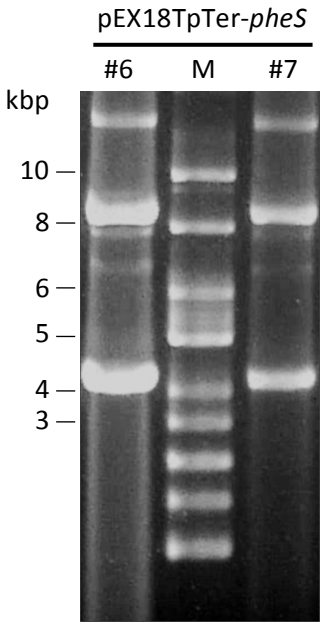

Figure 4.7 Size analysis of candidate pEX18TpTer-*pheS* clones. Transformant colonies containing pEX18TpTer-*pheS* were grown overnight, subjected to plasmid extraction and the resulting plasmids visualised following electrophoresis in a 0.8% agarose gel, to estimate the size of the plasmids, expected to be 4219 bp. Lanes labelled accordingly. M, Supercoiled DNA ladder.

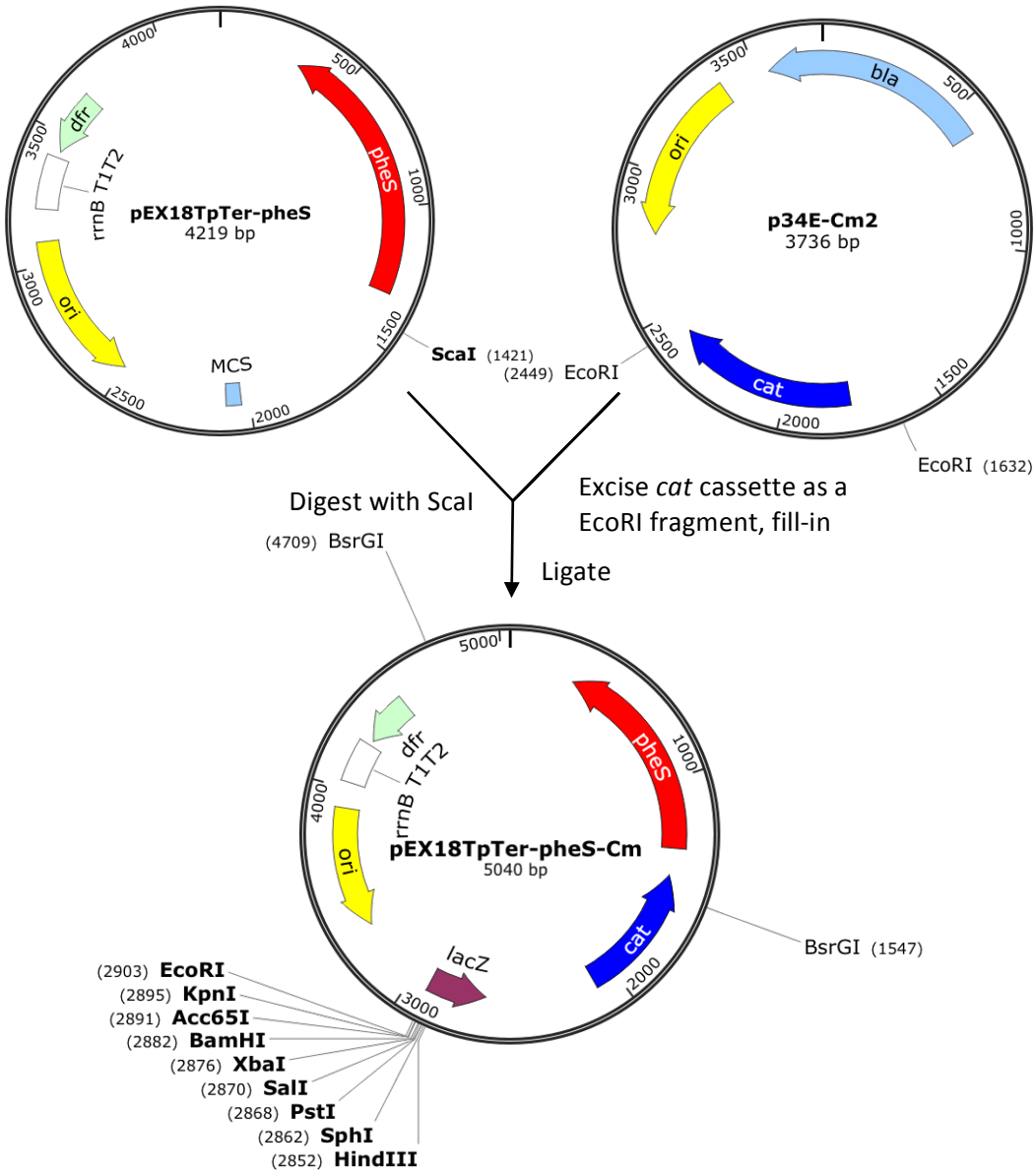

Figure 4.8 Construction of pEX18TpTer-*pheS*-Cm. The *cat* cassette from p34E-Cm2 was excised as an EcoRI fragment (top right), filled-in, and then ligated into the ScaI restriction site of pEX18TpTer-*pheS* (top left), to give a 5040 bp vector, pEX18TpTer-*pheS*-Cm (bottom). The orientation of the *cat* cassette was determined by BsrGI diagnostic restriction digestion. Pertinent vector features and restriction sites are indicated.

Concurrently, pEX18TpTer-*pheS* was digested with the blunt-end generating restriction enzyme ScaI and then blunt-end ligated to the Cm2 cassette. The DNA fragments used for this ligation reaction are shown (Figure 4.9A). Ligation reactions were introduced into *E. coli* JM38 and transformants selected for trimethoprim and chloramphenicol-resistance. Several transformants were subjected to plasmid extraction and the subsequent plasmids were analysed following electrophoresis (Figure 4.9B). Candidates 1 and 13 gave rise to the correct size plasmid, 5040 bp. The orientation of the Cm2 insert was determined by restriction digest with BsrGI. Clone 1 was shown to have the desired orientation of the Cm2 cassette, whereby the strong *cat* promoter would serve to boost transcript of the *pheS* gene, (Figure 4.9C). BsrGI digestion produced fragments of 3162 bp and 1878 bp, indicating the Cm2 cassette was in the same orientation as *pheS*, as required. This modified vector was termed pEX18TpTer-*pheS*-Cm.

4.3.3 Generation of a *tssM* in-frame deletion mutant in *B. cenocepacia* H111

It was decided to generate a *B. cenocepacia* mutant containing an in-frame deletion in the *tssM* gene. For this, a previously generated plasmid containing a mutated *tssM* was used as the source of the Δ*tssM* allele, pBBR1MCS-*tssM*ΔXhoI. This mutant *tssM* allele was generated from pBBR1MCS-1-*tssM* by utilising naturally occurring XhoI sites in *tssM*, which after digestion, excised a large section of the sequence that coded for much of the periplasmic CTD domain, but left the remaining sequence in-frame following self-ligation. In theory, this deletion should render the T6SS inactive, as the periplasmic region of TssM is required to interact with the outer membrane lipoprotein TssJ as part of the TssL-TssM-TssJ membrane core complex that anchors the T6SS to the cell envelope.

To generate an allelic replacement vector for *tssM* deletion mutagenesis, the DNA fragment containing *tssM*ΔXhoI (hereon referred to as Δ*tssM)* was excised from pBBR1MCS-*tssM*ΔXhoI as a XbaI-KpnI restriction fragment and ligated between the same restriction sites in the newly modified vector pEX18TpTer-*pheS* (Section 4.3.1). Following plasmid isolation, two candidate pEX18TpTer-*pheS*-Δ*tssM*

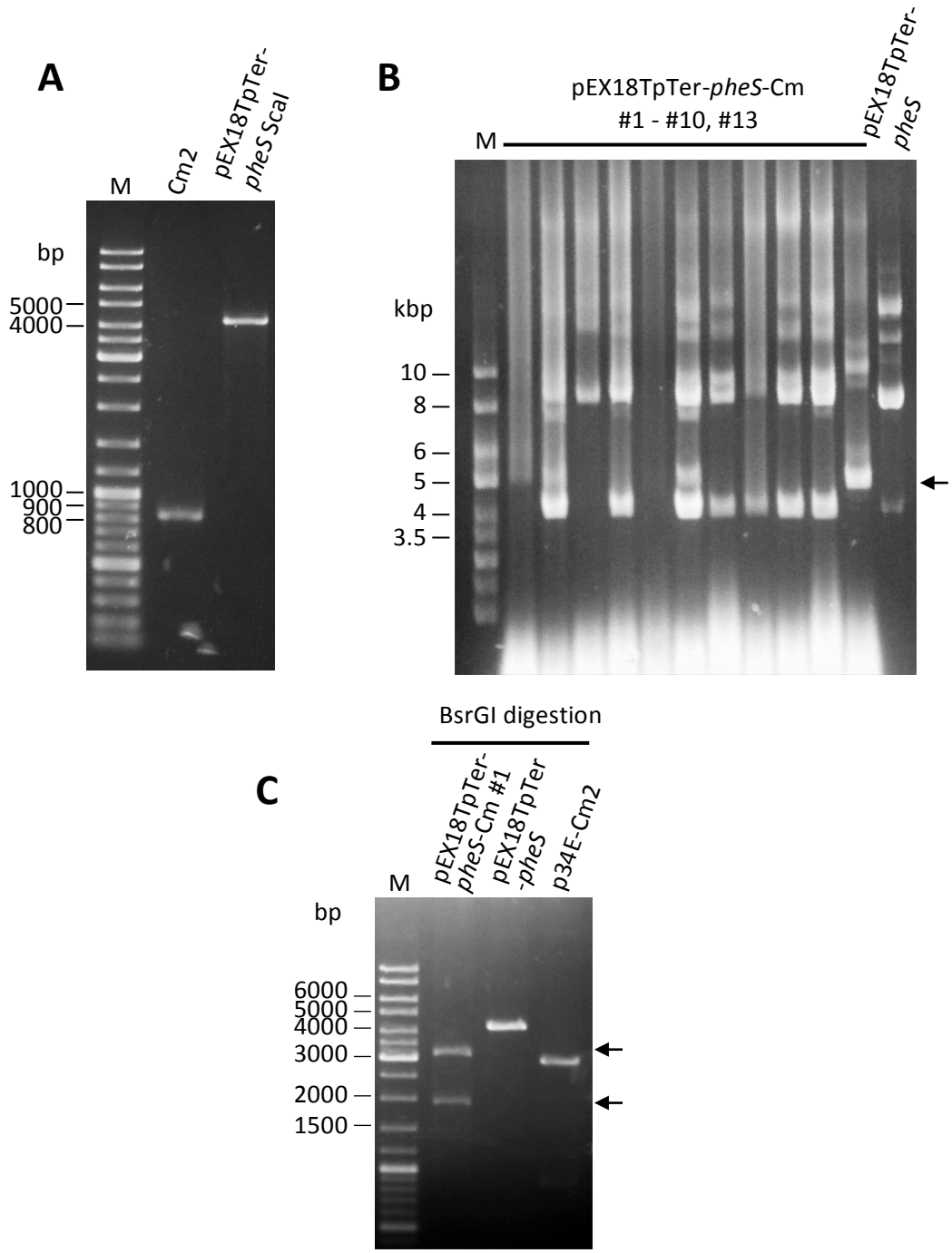

Figure 4.9 Construction of pEX18TpTer-*pheS*-Cm. (A) Restriction fragments of Cm2 excised from p34E-Cm2 with EcoRI and ScaI cut pEX18TpTer-*pheS*, following electrophoresis in a 1.0 % DNA agarose gel. These were used in a ligation reaction to generate the vector pEX18TpTer-*pheS*-Cm. (B) Plasmids were extracted and size determined by electrophoresis in a 0.8 % agarose gel, with an expected size of 5040 bp, as indicated by arrow. M, Supercoiled DNA ladder. (C) Determination of the orientation of the *cat* gene in clone 1 by BsrGI restriction digestion following electrophoresis. Arrows indicate expected fragments of 3162 bp and 1878 bp, for pEX18TpTer-*pheS*-Cm with the *cat* cassette in the desired same orientation as *pheS*. M, GeneRuler DNA ladder mix.

recombinant plasmids (clones 6 and 14) were identified, that gave rise to the expected plasmid size of 6038 bp (Figure 4.10). Both were confirmed by DNA sequencing.

For construction of a Δ*tssM* mutant in *B. cenocepacia* H111, pEX18TpTer-*pheS*-Δ*tssM* was transferred to this strain by conjugation using *E. coli* SM10(λpir) as a donor strain. Single crossover recombination events that occurred between the homologous deletion allele on the plasmid and the wild-type allele in the genome were selected by virtue of the trimethoprim-resistance of the strain, using M9-glucose agar containing trimethoprim. Colonies were screened by PCR using inside primers, iotMfor and iotMrev2, that allowed amplification of the Δ*tssM* allele borne on the plasmid, to verify that they were true co-integrates. Figure 4.11A shows the results of this screen. All colonies gave rise to a DNA fragment of ~1800 bp, corresponding to the size of the Δ*tssM* fragment present on the allelic replacement plasmid.

Co-integrates were then streaked onto M9-glucose without trimethoprim but containing cPhe, to select for a second recombination event that resulted in excision of the vector backbone. Several colonies that grew in the presence of cPhe were re-streaked onto the same medium. After this, candidates were subjected to PCR colony screening using outside primers that annealed to the genomic region outside of the *ΔtssM* fragment, iotMOPfor and tssMrevOP2. The wild-type allele was expected to give rise to a DNA fragment of 4066 bp fragment, whereas the Δ*tssM* allele would generate a 1951 bp DNA fragment. Analysis of the resulting DNA fragments indicated that candidate 5 was a potential Δ*tssM* mutant, whereas the other candidates produced fragments the same size as the wild-type (Figure 4.11B). Candidate 5 were subjected to further colony purification on the same media and then re-screened using the outside *tssM* primers. It was also screened with vector specific primers, pEX18Tpfor and pEX8Tprev to verify the absence of the vector backbone from the genome. All four isolates of candidate #5 gave rise to the correct size Δ*tssM* fragment, and were devoid of the 397 bp pEX18TpTer-*pheS* vector region, indicating they were true H111-Δ*tssM* mutants (Figure 4.11C).

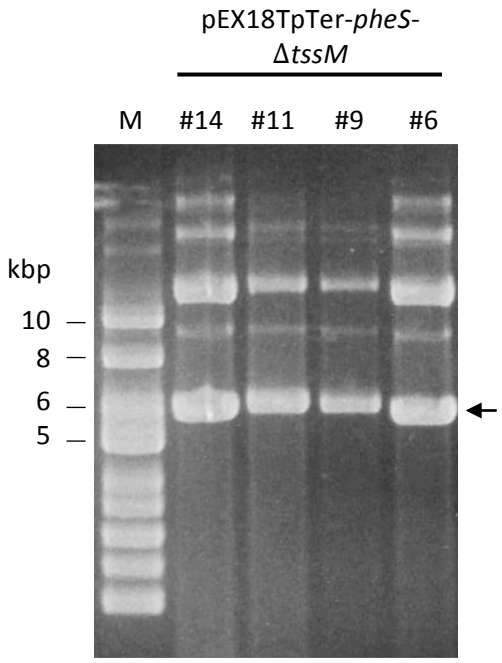

Figure 4.10 Size analysis of candidate pEX18TpTer-*pheS*-Δ*tssM* clones. The *tssM*ΔXhoI allele was transferred from pBBR1MCS-*tssM*ΔXhoI to pEX18TpTer-*pheS* as an XbaI-KpnI restriction fragment. Candidate clones were subjected to plasmid mini-preparation and the resulting plasmids were subjected to electrophoresis in a 0.8% DNA agarose gel. The correct sized clones were expected to give rise to a 6038 bp plasmid, indicated by the arrow. M, Supercoiled DNA ladder.

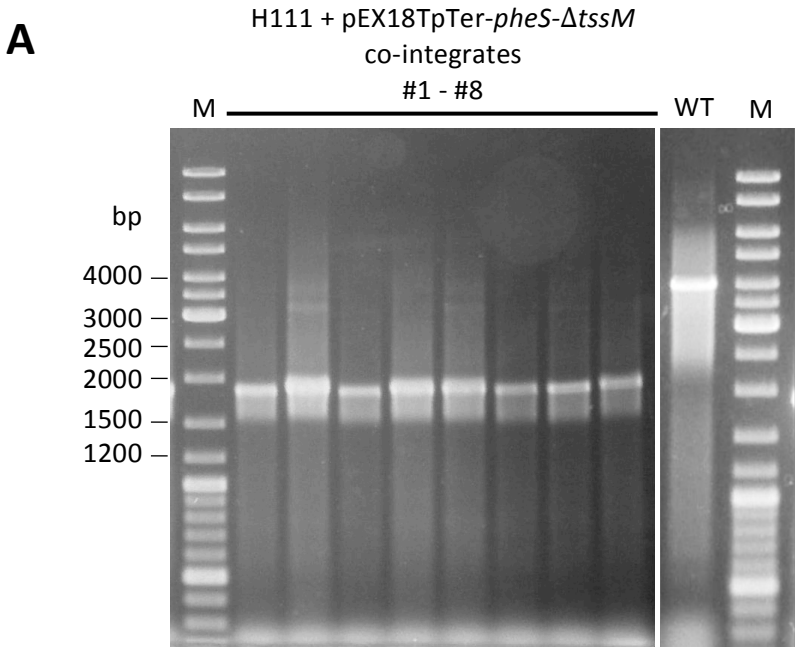
A
H111 + pEX18TpTer-*pheS*-Δ*tssM*
co-integrates
#1 - #8
M
WT
M
bp
4000
3000
2500
2000
1500
1200

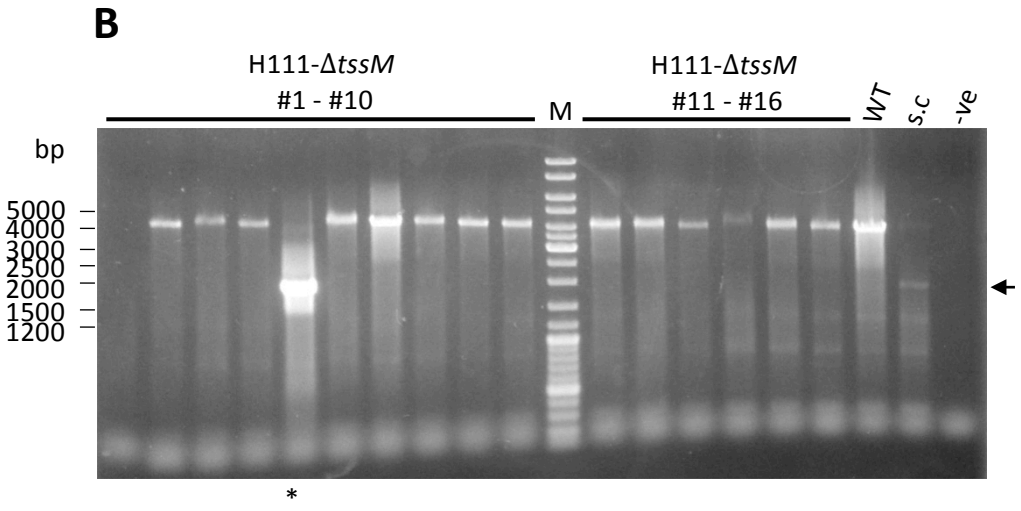
B
H111-Δ*tssM*
#1 - #10
M
H111-Δ*tssM*
#11 - #16
WT
s.c
-ve
bp
5000
4000
3000
2500
2000
1500
1200
*

C

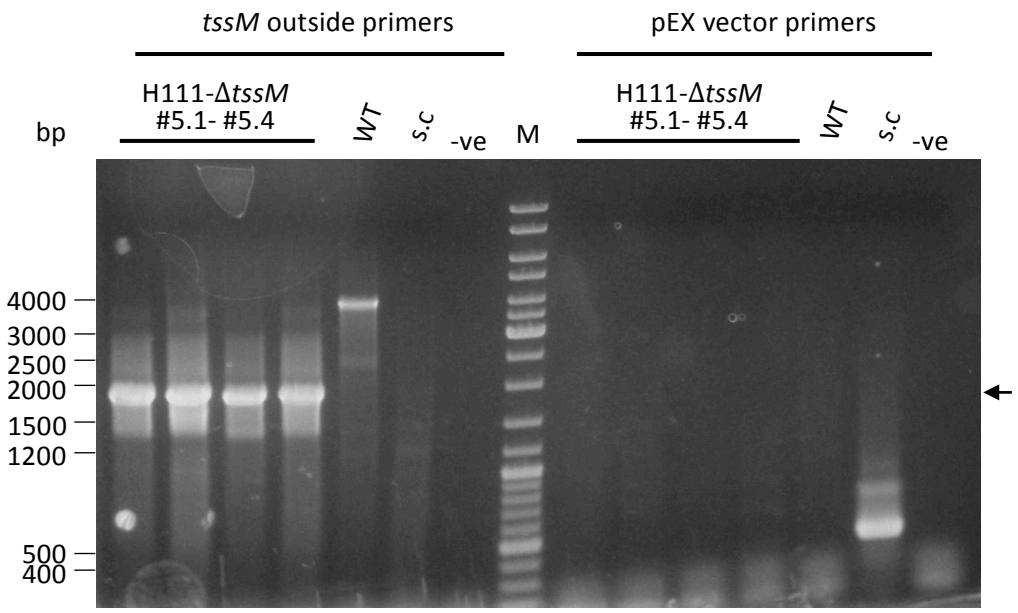

Figure 4.11 Generation of H111-Δ*tssM* mutant by allelic replacement. pEX18TpTer-*pheS*-Δ*tssM* allelic replacement vector was transferred into H111 WT. (A) Recombinants containing an integrated plasmid were verified by PCR screening, using primers iotMfor and iotMrev2 that annealed to the Δ*tssM* fragment contained within the vector, and visualised following electrophoresis in a 0.8% agarose gel. (B) Single crossover recombinants were streaked onto medium containing 0.1% cPhe to selected for a second recombination event, subsequent cPhe resistance colonies were re-streaked on the same medium, and then PCR screened using primers annealing to genomic sequences outside the Δ*tssM* fragment and visualised following electrophoresis in a 0.8% agarose gel. Replacement of the *tssM* gene with Δ*tssM* allele was expected to give rise to a 1951 bp DNA fragment, as indicated by the arrow. (C) Candidate #5 was re-streaked then re-screened using the outside *tssM* primers (left) and screened for absence of the pEX18TpTer-*pheS* backbone using vector specific primers, pEX18Tpfor and pEX18Tprev (right), expected to give rise to a 379 bp fragment if the plasmid is still present. Resulting DNA fragments were visualised following electrophoresis in a 1.0% agarose gel. Arrow indicates the 1951 bp Δ*tssM* allele. M, GeneRuler DNA ladder mix; s.c, single cross over recombinant control; -ve, no DNA control; WT, wild-type control.

4.4 Generation of an anti-TssD polyclonal antibody

TssD is an essential structural protein for the T6SS that is also secreted. The presence of TssD in the culture supernatant is indicative of an active T6SS. A polyclonal rabbit antibody raised against *B. cenocepacia* TssD had been generated previously (Ahmad, 2013) but it was found to be of poor quality. Therefore, it was decided to generate a new anti-TssD antibody to monitor T6SS activity in *B. cenocepacia*.

4.4.1 Construction of a plasmid for overproduction of epitope-tagged TssD for purification by IMAC

To generate sufficient amounts of pure TssD for antibody production a pre-existing T7 promoter based plasmid encoding N-terminally His-tagged TssD was modified. The TssD protein specified by this plasmid, pET14b-His_6.*tssD* contained, in addition to a His-tag and a thrombin cleavage site, four additional amino acids (MRRA) following the epitope tag (Shastri, 2011). pET14b-His_6.*tssD* was digested with NdeI, and re-ligated to excise a 21 bp fragment that encompassed the 4 additional codons and the first three codons of the native *tssD* coding sequence. This generated a 5158 bp plasmid, pHLS22. Transformants containing candidate recombinant plasmids were screened by PCR using primers pETDuet-T7-1for and T7rev (Figure 4.12A) and clones 1 and 15 were selected for plasmid analysis (Figure 4.12B), and confirmed by DNA sequencing.

4.4.2 Overproduction and solubility of His_6.TssD

To determine whether the new plasmid enabled the production of soluble TssD from *E. coli* for purification an initial test expression was undertaken on a small volume-culture. pHLS22 was introduced in BL21(DE3), and protein synthesis in the resulting strain was induced with 1 mM IPTG at 37°C for 4 hours (Section 2.3.1). The resulting cultures were lysed (Section 2.3.2) and samples analysed by SDS-PAGE (Figure 4.13). A protein of approximately 20 kDa was produced in high abundance in cells treated with IPTG and was present in the soluble fraction. As His_6.TssD encoded by this plasmid had an expected molecular mass of 20.1 kDa this

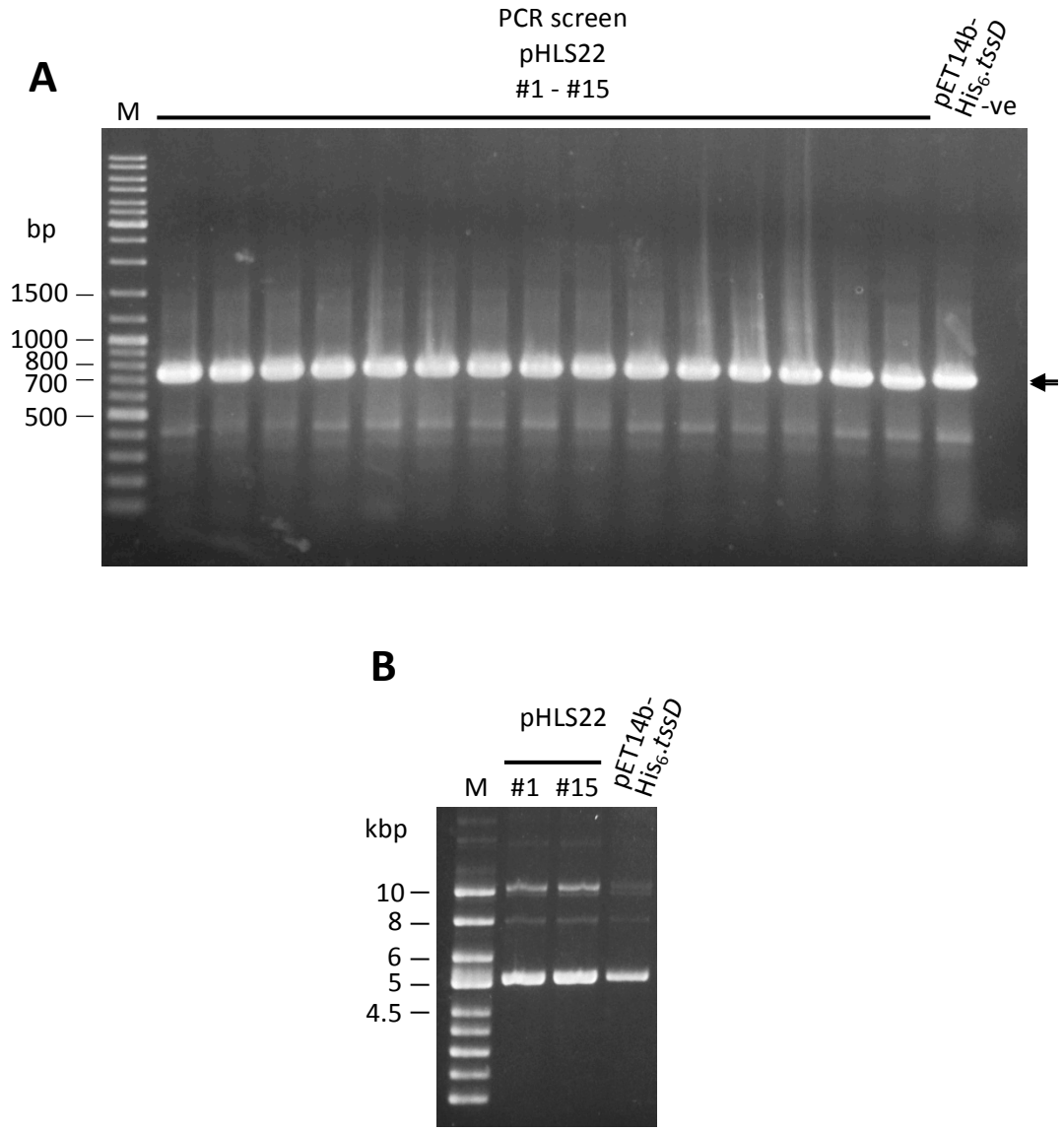

Figure 4.12 Construction of a plasmid for the overproduction of His-tagged TssD. pET14b-His$_6$.*tssD* was digested with NdeI and self-ligated to excise a 21 bp fragment encoding four non-native amino acids and the first three native amino acid of the N-terminus of TssD, generated a plasmid termed pHLS22. (A) Transformants containing candidate pHLS22 clones were identified by colony PCR, using primers pETDuet-T7-1for and T7rev. Positive clones were expected to give rise to a slightly smaller DNA fragment than the pET14-His6.*tssD* control, indicated by the arrows. M, GeneRuler DNA ladder mix. (B) Clones 1 and 15 were selected for mini-prep extracted and analysed by electrophoresis in a 0.8% DNA agarose gel. Positive clones were expected to give rise to a 5158 bp plasmid. M, Supercoiled DNA ladder; -ve, no DNA control.

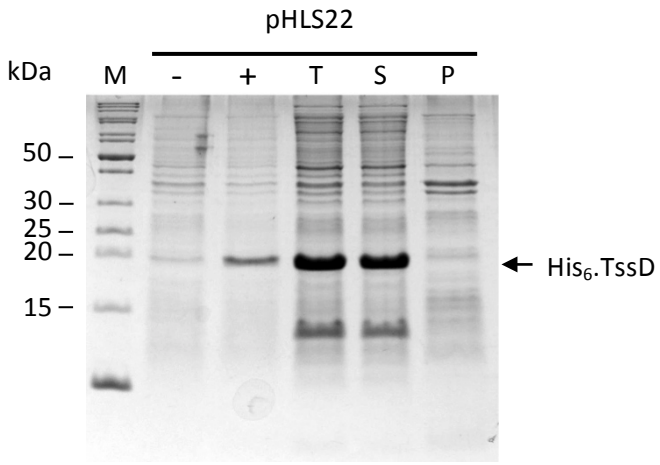

Figure 4.13 Analysis of the overproduction of His_6.TssD from a pET14b-based plasmid in *E. coli*. The expression plasmid pHLS22, specifying the overproduction of His_6.TssD was introduced into BL21(DE3) cells. Liquid cultures were grown to mid-log phase and protein synthesis was induced with 1 mM IPTG for 4 hours at 37°C. Cultures were lysed and sonicated as standard protocol and resulting lysate cleared by centrifugation. Whole cell extracts from uninduced (-) and induced cultures (+), and the total (T), soluble (S) and insoluble (P) protein fractions of the lysate from the induced culture were separated by SDS-PAGE in a 12% SDS-PA gel and stained the Coomassie blue. Samples were loaded as indicated. Labelled arrow indicates the identity of the induced protein, migrating at its expected size. M, EZ-Run *Rec* protein ladder.

suggested that soluble His_6.TssD was successfully produced.

4.4.3 Purification of His_6.TssD for antibody production

To obtain purified TssD, a clarified cell lysate from an induced culture of BL21(DE3) containing the plasmid pHLS22 was first subjected to nickel affinity chromatography (Section 2.3.5). The bound His-tagged protein was eluted by addition of a 10-500 mM imidazole gradient. Protein elution was monitored at A_{280}, which showed that His_6.TssD dissociated from the nickel resin at 225 mM imidazole (Figure 4.14A). Eluted fractions were collected and analysed by SDS-PAGE to determine purity (Figure 4.14B). This indicated that the purest His_6.TssD was present in fractions A13-B10. These fractions were pooled and dialysed against PBS using a 3000 MWCO dialysis membrane for buffer exchange. The resulting dialysed sample was then concentrated using a 10000 MWCO centrifugal concentrator and subjected to further purification by size exclusion chromatography using a Superose 6 10/300 GL column equilibrated in PBS. Eluted fractions were collected and analysed by SDS-PAGE (Figure 4.14D). A protein migrating at approximately 20 kDa was present in high abundance in all fractions. Fractions were then pooled and concentrated using a 10000 MWCO concentrator and the protein concentration determined. An aliquot was then submitted for polyclonal antibody production in rats.

A

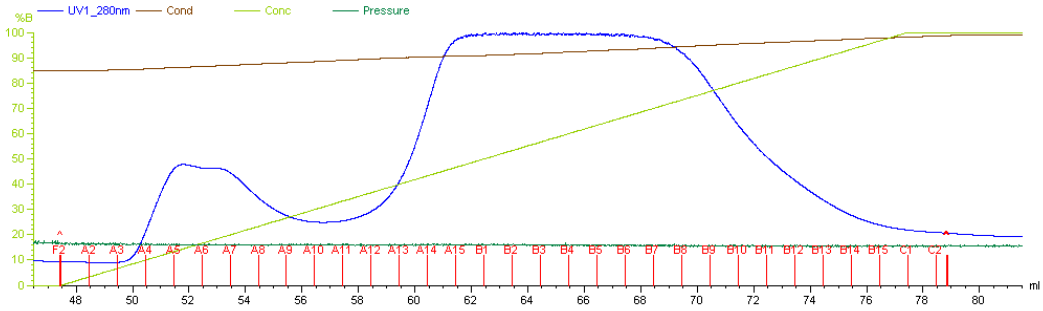
UV1_280nm
Cond
Conc
Pressure
%B
ml

B

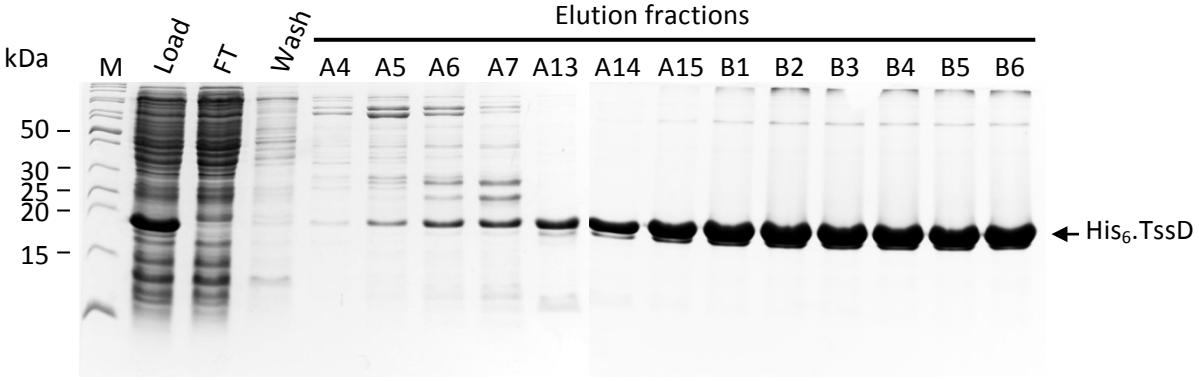
kDa
M
Load
FT
Wash
Elution fractions
A4 A5 A6 A7 A13 A14 A15 B1 B2 B3 B4 B5 B6
50
30
25
20
15
His6.TssD

C

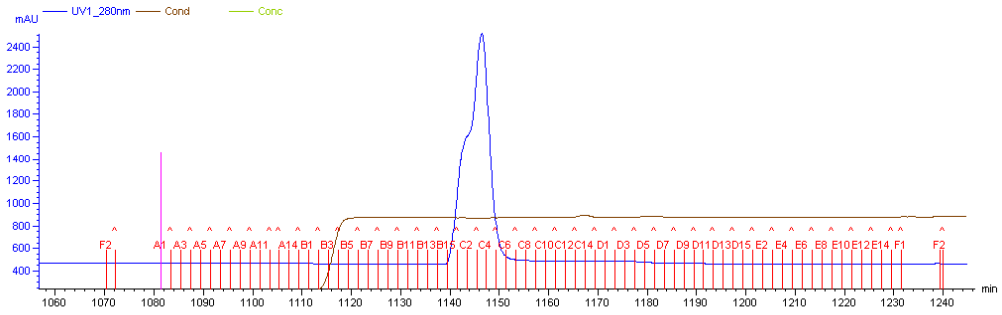
UV1_280nm
Cond
Conc
mAU
min

D

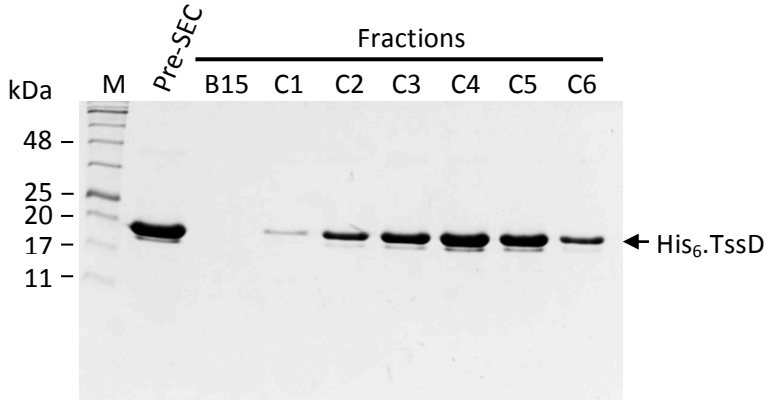

Figure 4.14 Two-step purification of His_6.TssD for antibody production. BL21(DE3)/pHLS22 cells were induced with 1 mM IPTG for 4 hours at 37°C and the resulting lysate loaded onto a 1mL His-Trap nickel affinity column couple to an ÄKTA purifier to bind the His-tagged protein. The column was washed and then bound proteins were eluted by addition of 10-500 mM imidazole gradient. (A) The resulting A_{280} trace of column eluates. (B) Unbound flow-through (FT), wash and imidazole eluted fractions (A7-B6) collected from the nickel column during purification of $His._6$TssD ('load') were analysed on a 15% SDS-PA gel. M, EZ-Run *Rec* protein ladder. Arrow indicates identify of the protein eluted from the column. Pooled fractions were then concentrated (Pre-SEC) and purified further by SEC using a Superose 6 10/200 GL column, with a flow rate of 0.5 mL/min in PBS. (C) A_{280} trace of proteins eluted from the SEC column. (D) Separation of the eluted fractions B15-C6 from the SEC column on a 15% SDS-PA gel. M, BLUeye prestained protein ladder.

4.5 Analysis of T6SS activity in *B. cenocepacia* strains H111, Pc715j and K56-2

In many T6SS-containing bacteria the system is inactive under standard laboratory conditions, making investigating the role of the system and T6SS-dependent effector identification difficult. Therefore, it was vital to first investigate T6SS activity in *B. cenocepacia* to determine what conditions (if any) resulted in activation of the system. This is normally determined by the secretion of a T6SS subunit, TssD, into the culture supernatant. Previous work by our group had observed no phenotypic differences between H111 and Pc715j strains and their *tssA*, *tssK* and *tssM* insertion mutant counterparts in *Dictyostelium* or *C. elegans* models of infections, or in their secreted protein profiles by Coomassie blue staining (Shastri, 2011). However, the effect of inactivation of these genes on T6SS function could not be properly ascertained, as at the time these experiments were conducted, antibodies to TssD (the secreted subunit that is a hallmark of an active T6SS) were not available.

4.5.1 Analysis of T6SS activity in liquid grown cultures

To investigate T6SS activity, extracellular proteins from the culture supernatant of late exponential grown broth cultures of wild-type and T6SS-defective *B. cenocepacia* strains were precipitated by trichloroacetic acid (TCA) in the presence of sodium deoxycholate (DOC) (Section 2.4.1). This method is known to be useful if the protein concentration is very low (1-50 μg) and reproducible precipitation is required (Bensadoun and Weinstein, 1976). Extracellular proteins from *B. cenocepacia* H111, Pc715j and K56-2 T6SS mutants were extracted by this method and concentrated a 1000-fold. Resulting samples were then separated by SDS-PAGE and visualised by Coomassie blue staining to compare protein profiles (Figure 4.15). An 18 kDa protein was clearly present in the culture supernatants of H111 but not present in the culture supernatants of the T6SS mutants thereof. This 18 kDa protein was also present in culture supernatants derived from K56-2 but not in those of K56-2-*tssA*::Tp and -*tssM*::Tp mutants, but in a lower abundance than in

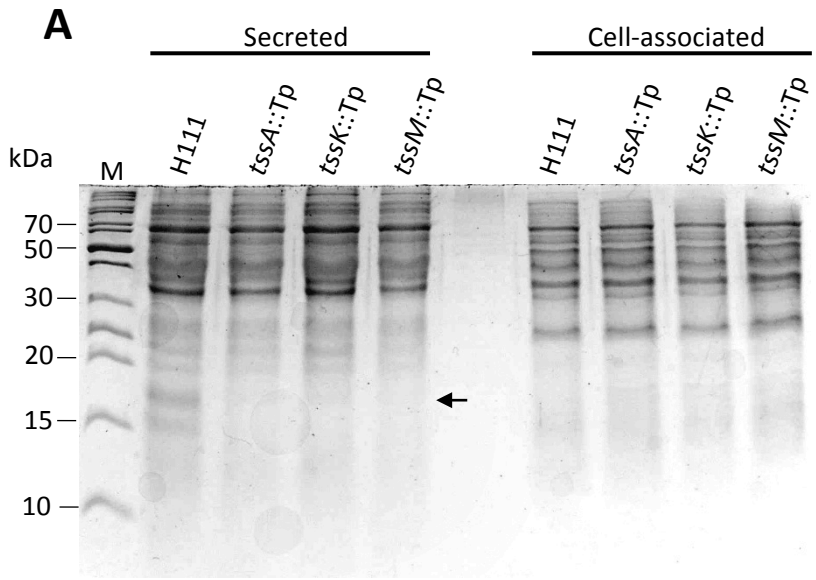
A
Secreted
Cell-associated
kDa
M
H111
tssA::Tp
tssK::Tp
tssM::Tp
H111
tssA::Tp
tssK::Tp
tssM::Tp
70
50
30
20
15
10

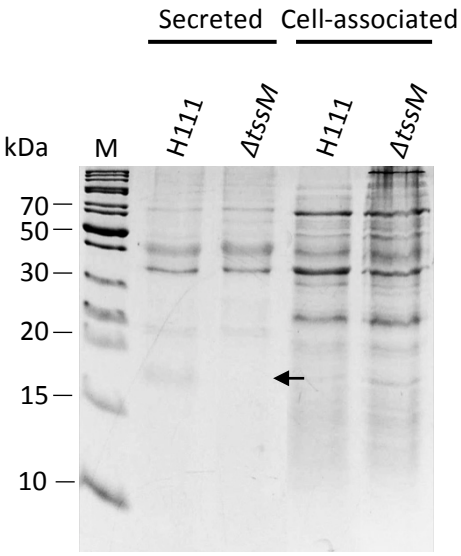
Secreted
Cell-associated
kDa
M
H111
ΔtssM
H111
ΔtssM
70
50
30
20
15
10

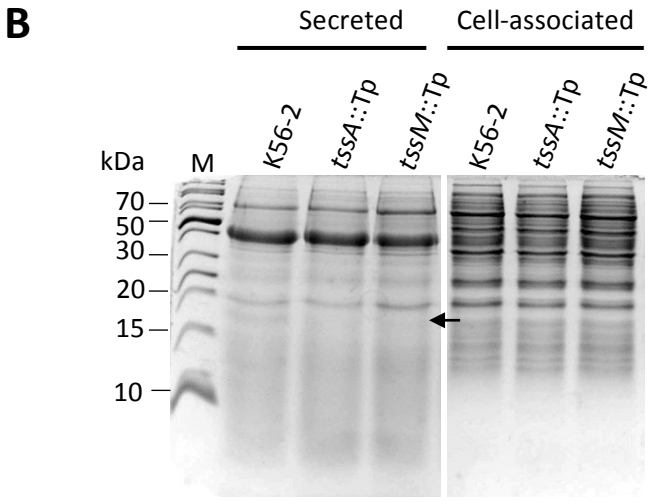
B
Secreted
Cell-associated
kDa
M
K56-2
tssA::Tp
tssM::Tp
K56-2
tssA::Tp
tssM::Tp
70
50
30
20
15
10

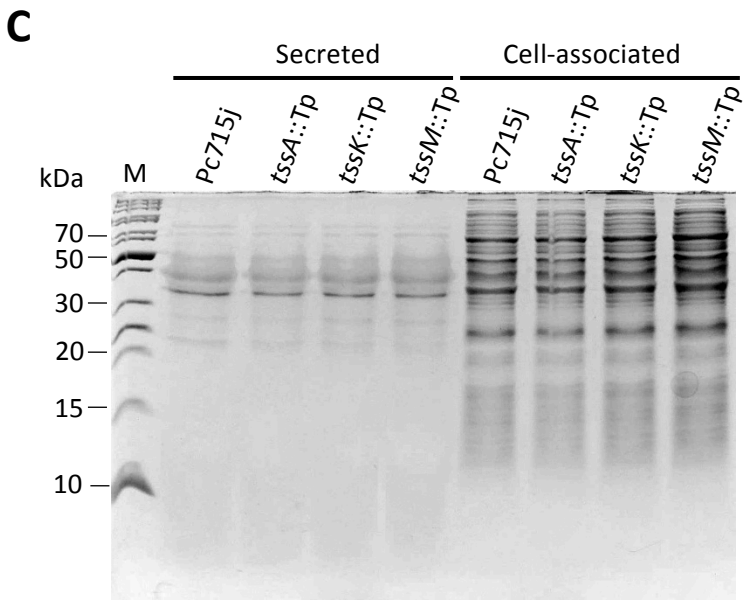

Figure 4.15 Analysis of secreted protein profiles from liquid cultures of *B. cenocepacia* strains H111, K56-2 and Pc715j. Culture supernatants of *B. cenocepacia* strains grown in D-BHI broth were concentrated 1000-fold by DOC-TCA precipitation and analysed by SDS-PAGE. Cell-associated proteins were prepared by concentrating the bacterial cell pellet 20-fold, combined in 1:1 ratio with 2x SDS-sample buffer and then boiled. (A) 15% SDS-PA gel of secreted (left) and cell-associated (right) proteins from *B. cenocepacia* H111 wild-type and corresponding *tssA*::Tp, *tssK*::Tp, *tssM*::Tp (upper) and Δ*tssM* mutants (lower). (B) as (A) but with samples extracted from *B. cenocepacia* K56-2 and *tssA*::Tp and *tssM*::Tp mutants thereof. (C) as (A) and (B) but using samples extracted from *B. cenocepacia* Pc715j and corresponding T6SS mutants. Samples are indicated above the lanes. Arrows indicate expected location of TssD. M, E.Z-Run *Rec* protein ladder.

H111 supernatants. Interestingly, the 18 kDa protein was not present in the supernatants derived from Pc715j. This strain also appeared to have a less extensive range of extracellular proteins present in the culture supernatant in comparison to the H111 and K56-2 strains.

By immunodetection using the custom polyclonal anti-TssD antibody described in Section 4.4, it was found that the 18 kDa protein present in secreted fractions of H111 and K56-2 reacted positively with the antibody, confirming the identity of this protein as TssD (Figure 4.16). However, it was it was not detected in the supernatant derived from Pc715j. Intracellular TssD was also detected in all strains and their T6SS-deficient derivatives indicating that TssD was still being produced in the T6SS mutants but not secreted. Together, this indicates that *B. cenocepacia* H111 and K56-2 have an active T6SS (although perhaps the H111 T6SS is activated to a higher degree) whereas Pc715j does not.

For further confirmation of the identity of this extracellular 18 kDa protein, the secreted protein derived from H111 was excised from an SDS-PA gel, and subjected to in-gel tryptic digestion and protein identification using tandem MS/MS. A database search of the resulting peptide masses and sequences identified TssD in the sample with a score of 334.39, coverage of 85.63% and detection of 5 unique peptides.

4.5.2 Analysis of T6SS activity in bacteria growing on solid medium

To determine whether growth on solid medium (i.e. agar) enhances/induces T6SS activity in *B. cenocepacia,* H111 and Pc715j, and their T6SS mutant derivatives, were grown on solid medium for 24 hours and extracellular proteins collected and concentrated by DOC-TCA precipitation (Section 2.4.2). SDS-PAGE analysis of the resulting samples showed no obvious differences in the secreted protein profile between the wild-type or T6SS mutant for both H111 and Pc715j strains when visualised by Coomassie blue staining (Figure 4.17). A large quantity of a 40 kDa and a 36 kDa protein was present in all samples. The latter is likely to be the T2SS-dependent extracellular metalloproteases ZmpA and/or ZmpB (Corbett et al., 2003; Kooi et al., 2005; Kooi et al., 2006). The 40 kDa secreted protein has also been

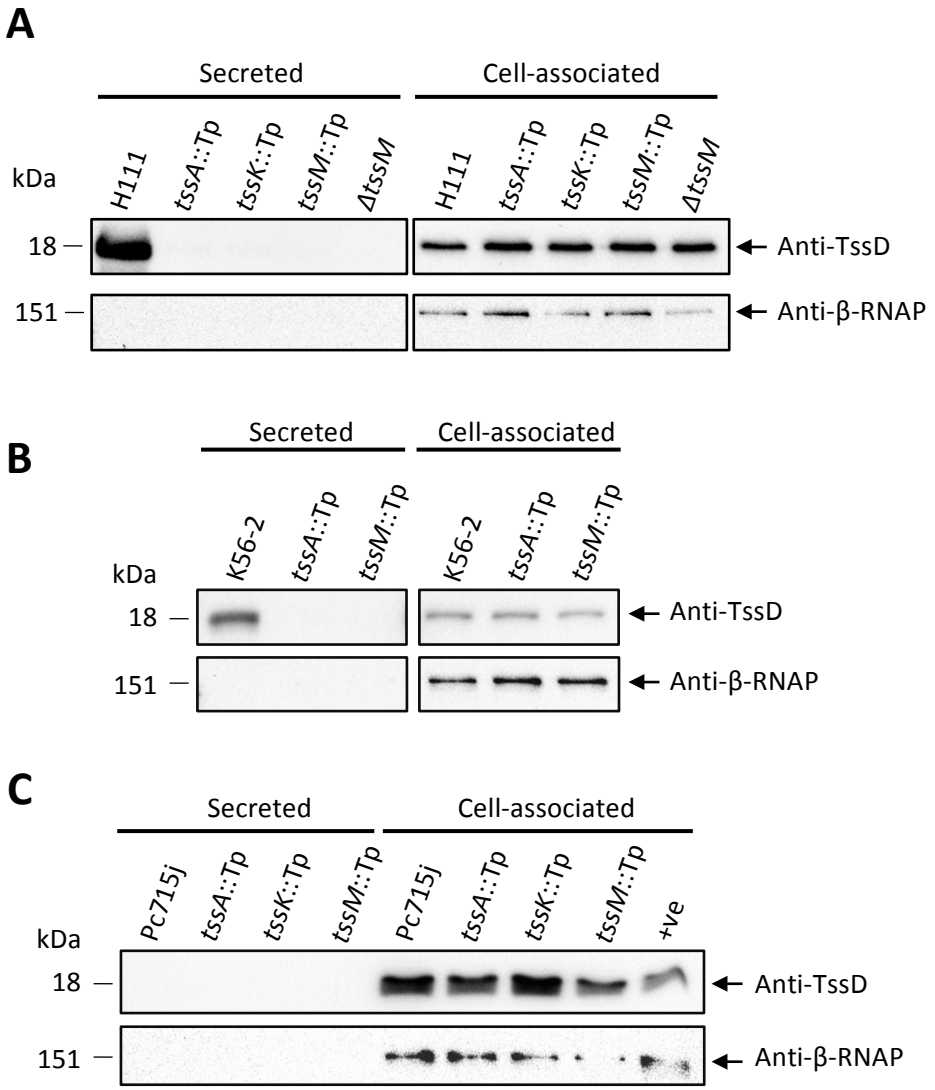

Figure 4.16 Analysis of TssD secretion by *B. cenocepacia* H111, K56-2 and Pc715j. Culture supernatants of wild-type *B. cenocepacia* H111 (A), K56-2 (B) and Pc715j (C) and corresponding T6SS mutants were subjected to DOC-TCA precipitation and concentrated 1000-fold. Cell-associated proteins were prepared by concentrating the bacterial cell pellet 20-fold, combined in 1:1 ratio with 2x SDS-sample buffer and then boiled. Resulting secreted and cell-associated samples were separated by SDS-PAGE, as indicate, and the presence of TssD analysed by anti-TssD western blotting using 1:1000 dilution of a custom polyclonal anti-TssD antibody (top panel in A, B and C). A commercially available anti-β-RNAP antibody was used as an indicator of lysis in preparations (lower panel in A, B and C). Molecular masses of the detected proteins are indicated to the left of each blot. +ve, positive control of H111 cell-associated fraction.

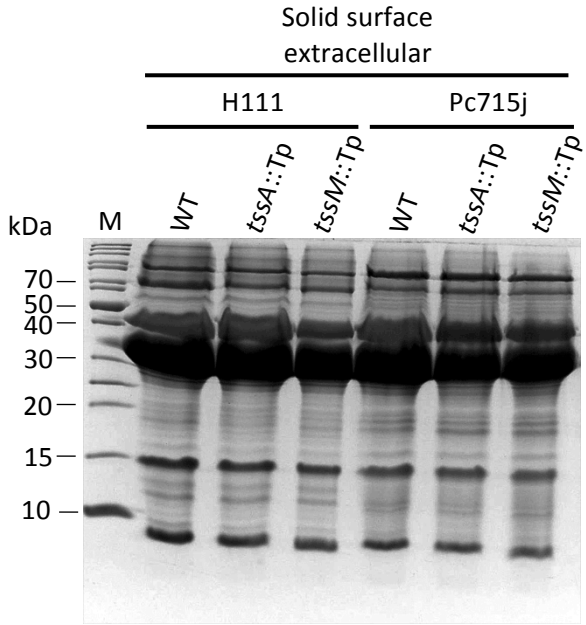

Figure 4.17 Analysis of extracellular protein profiles from *B. cenocepacia* H111 and Pc715j and corresponding T6SS mutants grown on solid medium. *B. cenocepacia* strains were cultured on a dialysis membrane overlaid on solid medium for 24 hours at 37°C, following which the resulting bacterial growth was removed from the membrane and extracellular proteins extracted by DOC-TCA precipitation. Wild-type (WT), *tssA*::Tp, *tssM*::Tp strains of H111 (left) and Pc715j (right) were separated in a 15% SDS-PA gel and visualised by Coomassie blue staining. M, EZ-Run *Rec* protein ladder.

previously observed but its identify remains unclear (Kooi et al., 1994). However, a protein corresponding in size to TssD was not observed. Furthermore, western blotting for TssD indicated that TssD was not present in the extracellular samples for either wild-type strain, or it was at a concentration below the limits of detection (not shown). This result indicated that extracellular protein extraction using this method was less suitable for detection of TssD than liquid growth cultures.

4.5.3 Construction of a *tssA* complementation plasmid pBBR2-*tssA*

For the construction of a *tssA* complementation plasmid with an antibiotic resistance gene that did not confer resistance to chloramphenicol (and was therefore compatible with downstream uses for complementation in experiments described in Section 4.6.2), a previously generated plasmid, pBBR1MCS-1-*tssA,* was used as the source of *tssA*. This plasmid contained the *tssA* gene and its native Shine-Dalgarno sequence under the control of the vector *lac* promoter, but conferred resistance to chloramphenicol. *tssA* was transferred on a BamHI-HindIII restriction fragment from pBBR1MCS-*tssA* into the corresponding restriction sites of pBBR1MCS-2, conferring resistance to kanamycin, to give a 6100 bp plasmid, named pBBR2-*tssA*. Candidate clones were identified by plasmid mini-preparation extraction (Figure 4.18) and clone 2 was confirmed by DNA sequencing.

4.5.4 Construction of *tssM* complementation plasmids, pBBR1-*tssM* and pBBR2-*tssM*

For the genetic complementation of the in-frame H111-Δ*tssM* mutant a broad host-range plasmid was constructed containing the *tssM* coding sequence and its native Shine-Dalgarno sequence upstream of the ATG start codon. To do this a 3999 bp DNA fragment was amplified from H111 genomic DNA using the primers tssMForAcc65I and tssMrevXbaI (Figure 4.19A). The *tssM* fragment was gel purified, digested with XbaI and Acc65I and ligated into the corresponding restriction sites in the vectors pBBR1MCS-1 and pBBR1MCS-2, to give the plasmids pBBR1-*tssM* and pBBR2-*tssM*, respectively. *E. coli* JM83 transformants containing pBBR1MCS-1-based clones were selected by virtue of their chloramphenicol resistance and white

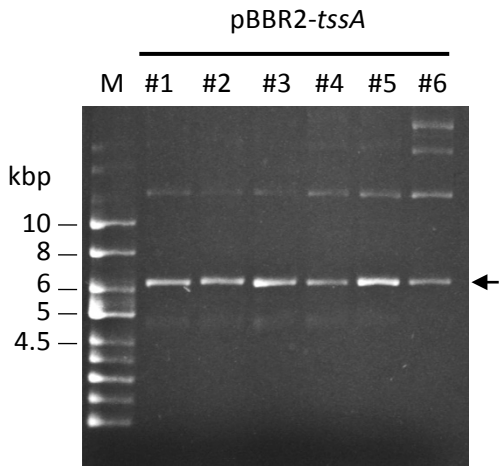

Figure 4.18 Size analysis of candidate pBBR2-*tssA* clones. *tssA* was transferred as a BamHI-HindIII restriction fragment from pBBR1MCS-*tssA* into pBRR1MCS-2. Candidate clones were subjected to plasmid mini-prep extraction and electrophoresis in a 0.8% DNA agarose gel. Arrow indicates the expected plasmid size for pBBR2-*tssM,* at 6100 bp. M, Supercoiled DNA ladder.

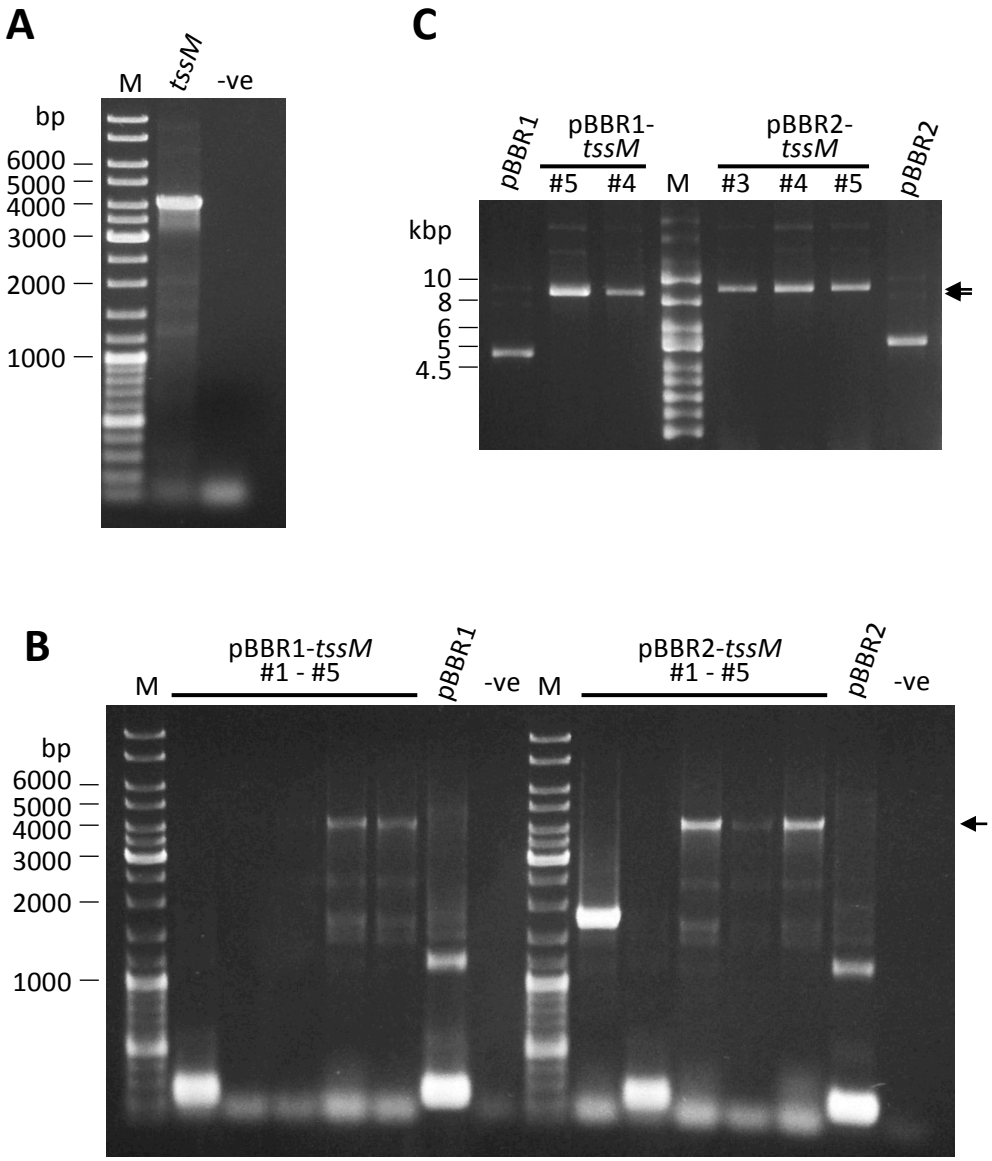

Figure 4.19 Construction of *tssM* complementation plasmids pBBR1-*tssM* and pBBR2-*tssM*. (A) The coding sequence of *tssM* and its native Shine-Dalgarno sequence were amplified on a 3999 bp DNA fragment from H111 genomic DNA and visualised following electrophoresis in 0.8% DNA agarose gel. (B) *tssM* was cloned into pBBR1MCS-1 and pBBR1MCS-2 between the XbaI and Acc65I sites. Positive clones were identified by PCR screening, giving rise to an expected DNA fragment of 4136 bp indicated by the arrow. (C) Candidate clones where then subjected to plasmid minipreparation extraction to determine the plasmid sizes, and visualised following electrophoresis in a 0.8% DNA agarose gel. Plasmids had an expected size of 8613 bp for pBBR1-*tssM* and 9050 bp for pBBR2-*tssM,* indicated by arrows. Lanes as indicated. M, Supercoiled DNA ladder; -ve, no DNA control.

appearance on medium containing IPTG and X-gal, and those containing pBBR1MCS-2-based clones by acquisition of kanamycin resistance. Candidate recombinant plasmids containing *tssM* were identified by PCR screening using the vector primers M13for and M13rev (Figure 4.19B). Candidate pBBR1-*tssM* clones 4 and 5 and candidate pBBR2-*tssM* clones 3, 4 and 5 produced the expected sized product of 4136 bp. These plasmids were isolated to determine their size (Figure 4.19C), and all of them were found to be the expected size of 8613 bp for pBBR1-*tssM* and 9050 bp for pBBR2-*tssM*. Clones pBBR1-*tssM* 5 and pBBR2-*tssM* 3 were confirmed by DNA sequencing.

4.5.5 Complementation of TssD secretion in *tssA* and *tssM*-deficient mutants in *B. cenocepacia* H111

To confirm that the absence of secreted TssD was due to a direct effect of inactivation of the disrupted T6SS genes it was decided to analyse whether TssD secretion could be restored by genetic complementation. To do this, the appropriate complementation plasmid and empty vector were transferred separately into H111 and the *tssA*::Tp and Δ*tssM* T6SS mutants by conjugation, using *E. coli* S17-1(λpir) as a donor. Extracellular proteins present in liquid cultures of the exconjugates were extracted and the presence of TssD was ascertained by anti-TssD western blotting.

Secretion of TssD was restored in the H111-*tssA*::Tp mutant by complementation with pBBR1MCS-*tssA* and pBBR2-*tssA* (Figure 4.20A). Complementation of the *tssA*::Tp mutant by the pBBR1-based plasmid restored TssD secretion to levels similar to that of the wild-type. However, the pBBR2-based plasmid did not. Curiously, it restored TssD secretion only to the levels observed when wild-type H111 contained the pBBR2-*tssA* construct, which for some unknown reason appeared to impair TssD secretion. This inhibition of TssD secretion in the wild-type stain was not observed in the presence of the empty vector.

TssD was detected in the secreted protein fraction of Δ*tssM* harbouring pBBR2-*tssM,* but not in Δ*tssM* containing the empty vector or no plasmid control

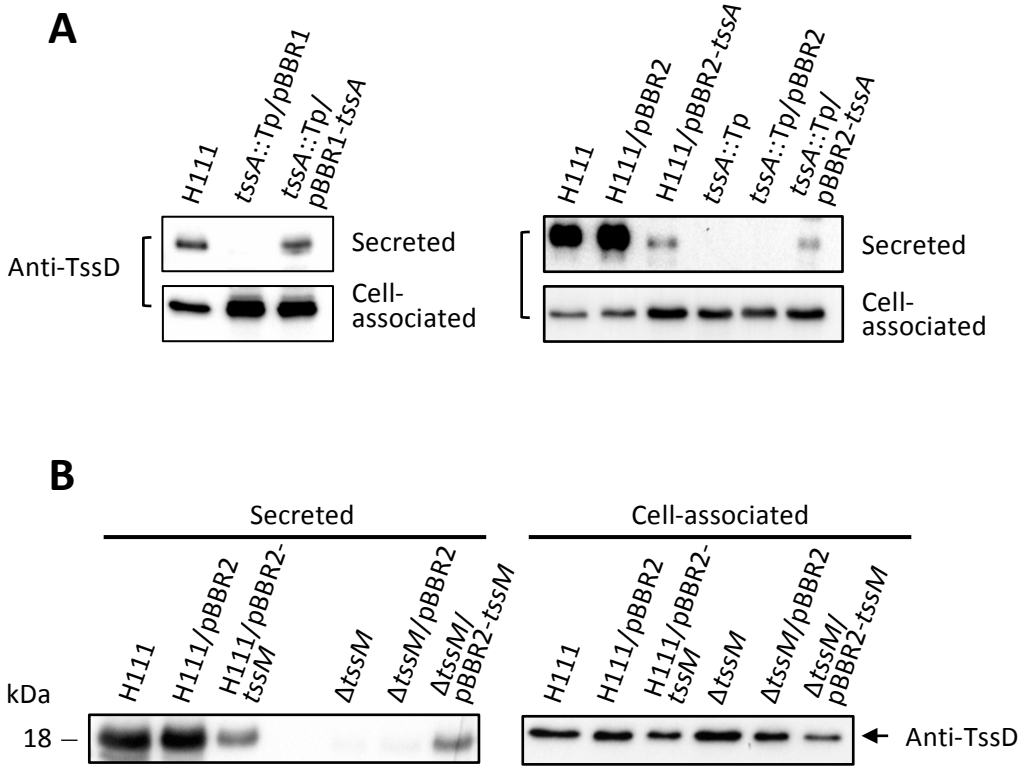

Figure 4.20 Genetic complementation of *B. cenocepacia* H111 *tssA*::Tp and Δ*tssM* mutants. pBBR1-*tssA*, pBBR2-*tssA* and pBBR2-*tssM* complementation plasmids and empty vectors were transferred into H111 and the respective *B. cenocepacia* H111-*tssA*::Tp and H111-Δ*tssM* mutants. Extracellular proteins were then extracted from liquid grown cultures by DOC-TCA precipitation and analysed for the presence of TssD by anti-TssD western blotting. Cell-associated proteins where also analysed. (A) The resulting anti-TssD blots from H111-*tssA*::Tp/pBBR1-*tssA* (left) and H111-*tssA*::Tp/pBBR2-*tssA* (right) complementation. (B) Analysis of TssD secretion following introduction of pBBR2-*tssM* into H111-Δ*tssM*, with secreted samples (left) and cell-associated fractions (right). Molecular masses of detected proteins are indicated on the left of each blot, and arrows with labels describe the antibody used in detection. Lanes as indicated.

(Figure 4.20B). However, this TssD secretion was not restored to wild-type levels, but instead to levels similar to wild-type H111 harbouring the pBBR2-*tssM* plasmid, which mirrored the results obtained with H111-*tssA*::Tp/pBBR2-*tssA* complementation.

4.6 Investigation into the role of the *B. cenocepacia* T6SS in inter-bacterial competition

The main function of T6SSs in other bacteria appears to be in inter-bacterial competition (Section 1.4.2). It is thought that the T6SS can target surrounding bacteria with anti-bacterial effectors to provide a competitive edge. Therefore, it was decided to analyse whether the T6SS in *B. cenocepacia* was also important for interspecies competition.

4.6.1 Analysis of antibiotic susceptibility of several Gram-negative bacteria

In order to help determine which bacterial species and selection conditions would be most appropriate to use in an inter-bacterial competition assay with *B. cenocepacia,* several bacterial species were streaked out onto a range of selection media to determine antibiotic sensitivity and other phenotypic differences. Findings from this screen for *B. cenocepacia* H111, Pc715j, *S. marcescens* Db10, *P. aeruginosa* PAO1, *P. putida* KT2440, *B. thailandensis* E264, *B. lata* 383 and *B. multivorans* C1962 are shown in Table 4.1. This showed for example, that *P. putida* is resistant to chloramphenicol when used at 25 μg/mL but sensitive to tetracycline. Whereas the growth of all *the Burkholderia* strains tested, including *B. cenocepacia* H111 and Pc715j is severely restricted by chloramphenicol at all concentrations tested, but *B. cenocepacia* H111 and Pc715j are resistant to 10 μg/mL tetracycline. Thus indicating that the separate enumeration of *P. putida* and *B. cenocepacia* in a co-culture is possible by growth on these two selective media.

4.6.2 Analysis of *B. cenocepacia* H111 T6SS-mediated bacterial competition with *Pseudomonas putida* KT2440

Studies on other *Burkholderia* spp., namely *B. thailandensis,* indicated that *P. putida* was a strain susceptible to the effects of the T6SS-1 (Schwarz et al., 2010), suggesting it may be a good candidate species to test in an interspecies competition assay with *B. cenocepacia*. *P. putida* had also been previously identified as a

Table 4.1 Analysis of antibiotic sensitivity of selected Gram-negative bacterial strains

	Growth on specific antibiotic selection media[a] (concentration in μg/mL)															
Bacterial strain	**LB**	**LB Ap 50**	**LB Ap 100**	**LB Ap 150**	**LB Km 25**	**LB Km 50**	**LB Km 75**	**LB Km 100**	**LB Tc 10**	**LB Tc 20**	**LB Tc 45**	**LB Cm 12.5**	**LB Cm 25**	**LB Cm 50**	**LB PMB 600**	**Mod BCSA**
B. cenocepacia H111	+	+	+	+	+*R*	+*SR*	-	-	+	+*R*	-	+*SR*	+*SR*	-	+	+*SR*
B. cenocepacia Pc715j	+	+	+	+	+	+	+	+	+	+	+*R*	-	-	-	+	+
S. marcescens Db10	+	+	+*R*	+*SR*	+*R*	+*R*	+*SR*	-	+	+*R*	+*SR*	+*R*	+*R*	+*SR*	+	+*SR*
P. aeruginosa PAO1	+	+	+	+	+	+	+	+*R*	+	+*R*	+SR	+	+	+*R*	-	+*SR*
P. putida KT2440	+	+	+*R*	+*R*	-	-	-	-	-	-	-	+	+	+*R*	+*R*	+*R*
B. thailandensis E264	+	+	+	+*R*	+	+*R*	+*SR*	+*SR*	+*SR*	-	-	+*SR*	-	-	+	+
B. lata 383	+	+*SR*	-	-	+*SR*	-	-	-	+*R*	+*SR*	-	-	-	-	+*SR*	+*R*
B. multivorans C1962	+	+	+	+	+	+	+	+*R*	+*SR*	-	-	+*SR*	-	-	+	+

[a]growth was scored after 40 hours incubation at 37°C. Ap, ampicillin; Km, kanamycin; Tc, tetracycline; Cm, chloramphenicol; PMB, polymyxin B; modified BCSA, *Burkholderia cepacia* Selective Agar without phenol red and crystal violet containing 10 μg/mL gentamicin but no vancomycin.
+, growth; +*R*, growth but restricted; +*SR*, growth but severely restricted; -, no growth.

potential candidate susceptible to the effects of the *B. cenocepacia* T6SS in a long-term co-culture screen, in collaboration with L. Eberl (University of Zurich).

To determine the effect of the T6SS on the competitive fitness of *B. cenocepacia, P. putida* KT2440 was used in a 4-hour co-culture with wild-type *B. cenocepacia* H111 and two different T6SS mutants, *tssA*::Tp and Δ*tssM* (Section 2.9.1). Surviving bacteria were enumerated on two different selection plates, LB agar containing chloramphenicol (25 μg/mL) for *P. putida* and LB agar containing tetracycline (10 μg/mL) for *B. cenocepacia*. The resulting data is shown in Figure 4.21. It was observed that *P. putida* recovery was significantly greater when co-cultured with the *tssA*::Tp mutant than with wild-type H111 by a factor of 57, which was statistically significant with a P value of 0.0067 using a student's t-test. This difference was mirrored with the Δ*tssM* mutant, which resulted in an increase of *P. putida* by a factor of 58 compare to wild-type, which again was statistically significant with a P value of 0.0261. No significant difference was observed between the numbers of *B. cenocepacia* strains recovered for all co-cultures. Together, this data suggests show that the *B. cenocepacia* H111 T6SS is important for interspecies competition under the conditions tested.

B. cenocepacia Pc715j was demonstrated to have an inactive T6SS under standard laboratory conditions (Section 4.5.1). To investigate whether it plays a role in inter-bacterial competition wild-type Pc715j and a corresponding T6SS mutant (715-*tssA*::Tp) were tested in the interspecies competition model. However, no difference was observed between the number of recovered *P. putida* when co-cultured with wild-type Pc715j or a Pc715j T6SS mutant (data not shown).

4.6.3 Analysis of *B. cenocepacia* H111 T6SS-mediated bacterial competition with *Escherichia coli* CC118(λpir)

To determine whether other species could be susceptible to T6SS-mediated attack by *B. cenocepacia* H111, *E. coli* CC118(λpir) was employed as the 'prey' species in the bacterial competition assay, as it is intrinsically resistant to rifampicin, which facilitates its enumeration. LB agar containing tetracycline (10 μg/mL) and LB

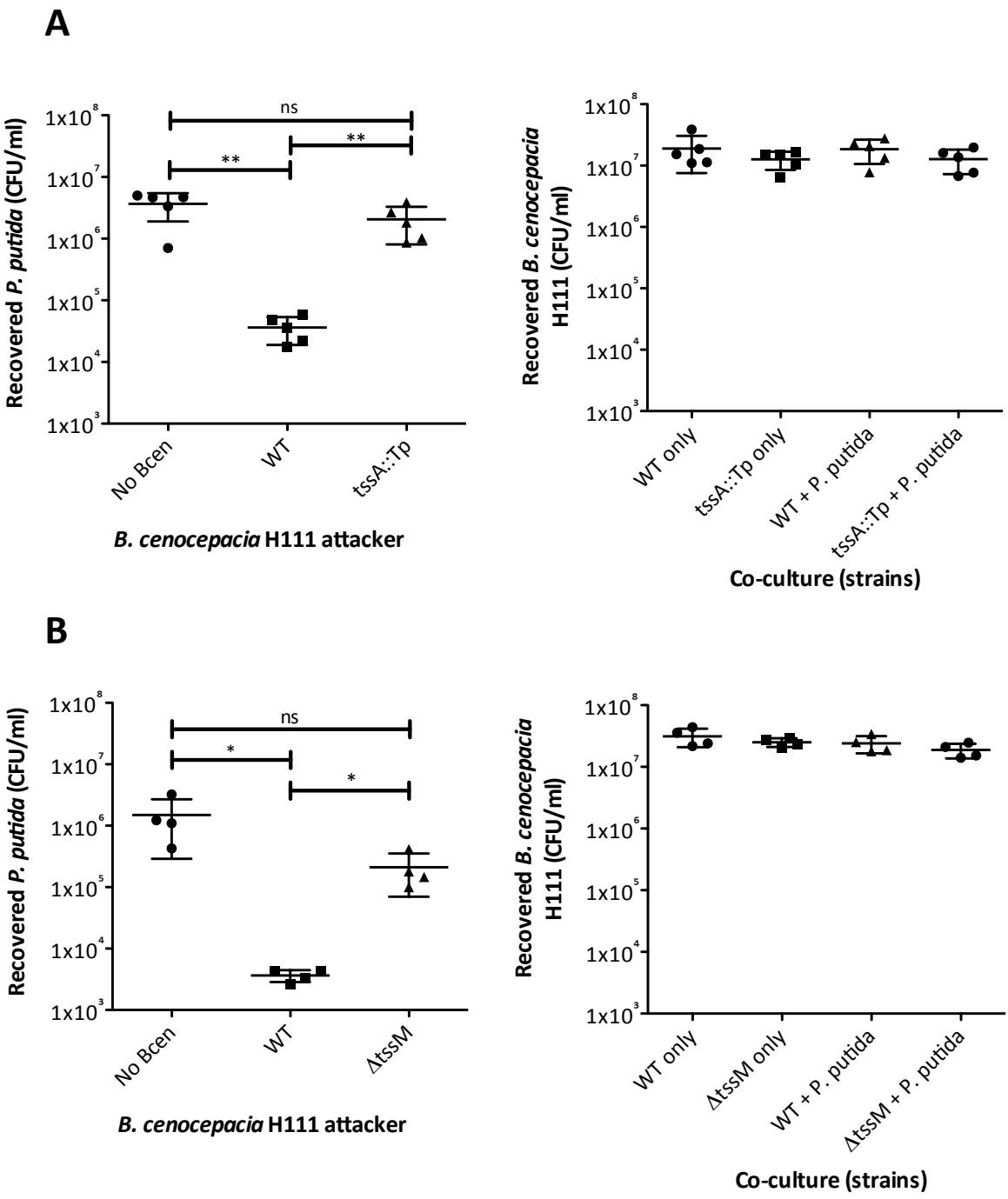

Figure 4.21 Analysis of the contribution of the T6SS to competitive fitness of *B. cenocepacia* H111 against *P. putida*. *B. cenocepacia* H111 and *P. putida* KT2440 were combined in a 5:1 ratio, incubated on solid medium for 4 hours at 30°C. Surviving bacteria were recovered and enumerated on selection plates. (A) Number of recovered *P. putida* after co-culture with H111, H111-*tssA*::Tp or in absence of competing bacteria ('No Bcen') (right) and number of *B. cenocepacia* recovered after each culture. (B) as (A) but using the H111-Δ*tssM* mutant. Statistical analysis by student's t-test, n≥4, p<0.05, error bars = ±SD. *, p<0.05; **, p<0.01; ns, not significant.

agar containing rifampicin (100 μg/mL) were used to select for growth of *B. cenocepacia* and *E. coli* CC118(λpir), respectively. The resulting numbers of surviving *E. coli* and *B. cenocepacia* for each co-culture are shown in Figure 4.22. A similar trend was observed here as that observed when *P. putida* was used as the prey strain (Section 4.6.2). Thus, a significantly greater number of *E. coli* CC118(λpir) bacteria were recovered when co-cultured with the H111-Δ*tssM* T6SS mutant than with wild-type H111, by a factor of 8, which was statistically significant with a P value of <0.0001 using a student's t-test. However, this difference was not as great as the difference seen with *P. putida.*

4.6.4 Analysis of *B. cenocepacia* H111 T6SS-mediated bacterial competition with *Escherichia coli* SM10(λpir)

E. coli SM10(λpir) is a conjugal donor strain that contains an active T4SS system. The T4SS has been shown to induce T6SS activity in some species (Ho et al., 2013). It was decided to employ this strain in the bacterial competition assay above to determine if fitness against *E. coli* could be enhanced in the presence of a T4SS. The number of surviving *E. coli* SM10(λpir) from each co-culture were obtained by differential selection on LB agar containing tetracycline (10 μg/mL) for *B. cenocepacia* growth and Lennox agar containing kanamycin (50 μg/mL) for *E. coli* SM10(λpir). Results shown in Figure 4.23 indicate that a greater number of *E. coli* SM10(λpir) were recovered when co-cultured with the Δ*tssM* T6SS mutant than when co-cultured with wild-type H111 by a factor of 10, which again was statistically significant with a P value of 0.0005. This was a slight, but not significant, enhancement on that seen with the T4SS-deficent *E. coli* strain CC118(λpir), suggesting that presence of a T4SS system under these conditions does not improve the T6SS-dependent fitness advantage of *B. cenocepacia*.

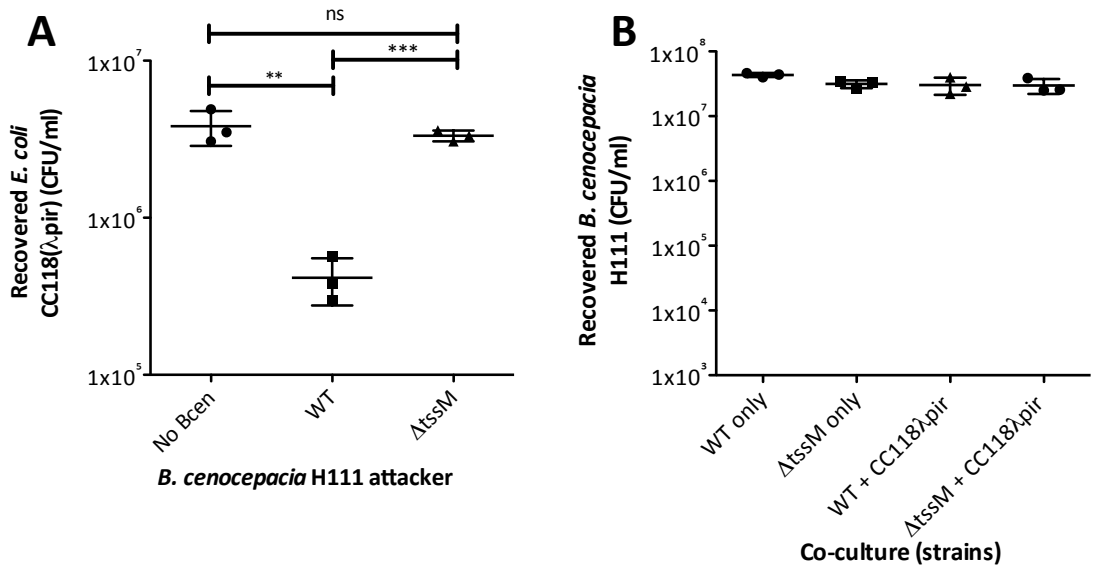

Figure 4.22 Analysis of the contribution of the T6SS to competitive fitness of *B. cenocepacia* H111 against *E. coli* CC118(λpir). *B. cenocepacia* H111 and *E. coli* CC118(λpir) were combined in a 5:1 ratio, incubated on solid medium for 4 hours at 30°C. Surviving bacteria were recovered and enumerated on selection plates. (A) Number of recovered *P. putida* after co-culture with H111, H111-*tssM*::Tp or in absence of competing bacteria ('No Bcen'). (B) Number of *B. cenocepacia* recovered after each culture. Statistical analysis by student's t-test, n=3, p<0.05, error bars = ±SD. **, p<0.01; ***, p<0.001; ns, not significant.

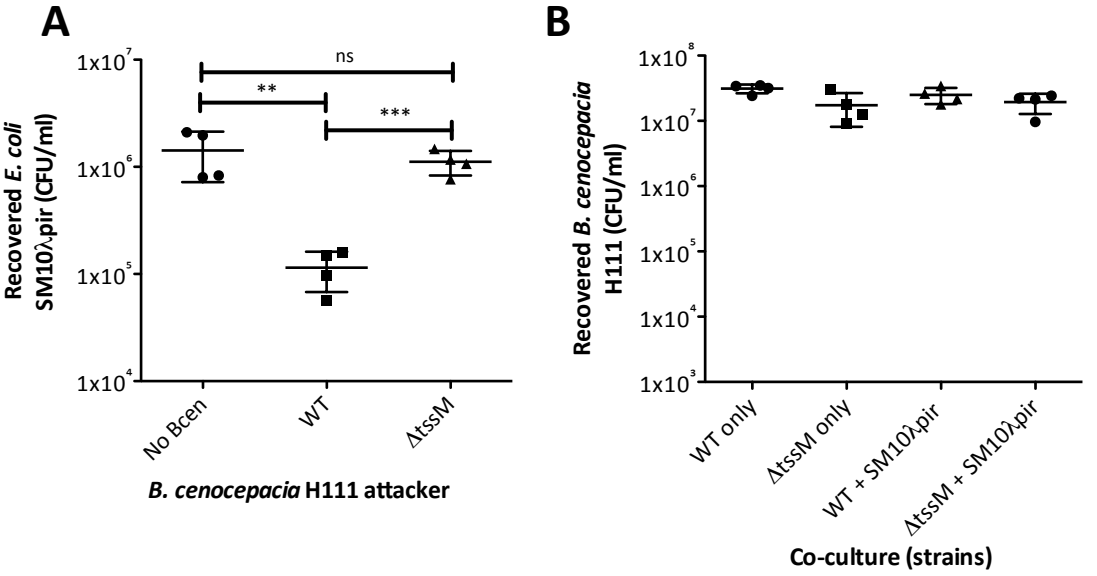

Figure 4.23 Analysis of the contribution of the T6SS to competitive fitness of *B. cenocepacia* H111 against *E. coli* SM10(λpir). *B. cenocepacia* H111 and *E. coli* SM10(λpir) were combined in a 5:1 ratio, incubated on solid medium for 4 hours at 30°C, where upon surviving bacteria were recovered and enumerated on selection plates. (A) Number of recovered *P. putida* after co-culture with H111, H111-*tssM*::Tp or in absence of competing bacteria ('No Bcen') and (B) the number of *B. cenocepacia* recovered after each culture. Statistical analysis by student's t-test, n=3, p<0.05, error bars = ±SD. **, p<0.01; ***, p<0.001; ns, not significant.

4.6.5 Analysis of *B. cenocepacia* T6SS-mediated bacterial competition with *Pseudomonas fluorescens* ATCC 17571

Similar to *B. cenocepacia*, *Pseudomonas fluorescens* is found ubiquitously in the environment. As these two species may have to compete for similar biological niches *P. fluorescens* was tested in the bacterial competition model against wild-type H111 and a T6SS mutant. To do this, a spontaneous rifampicin resistant version of *P. fluorescens* ATCC 17571 was selected (HLS1) and verified as *P. fluorescens* by its ability to fluoresce upon exposure to UV light on King's B agar (Figure 4.24). Use of the *P. fluorescens* rifampicin resistant strain allowed differential selection between *B. cenocepacia* and *P. fluorescens*, by enumerating *B. cenocepacia* recovery on LB agar containing tetracycline (10 μg/mL) *and P. fluorescens* on LB agar containing rifampicin (100 μg/mL). By enumeration of recovered *P. fluorescens*, shown in Figure 4.25, it was observed that when co-cultured with the H111-Δ*tssM* mutant the number of surviving *P. fluorescens* was greater than when co-cultured with wild-type H111, by a factor of 5. This was significant with a P value of 0.0186, but only with an n of 2 for H111-Δ*tssM*. However, there was also a decrease in the number of recovered *P. fluorescens* when cultured alone relative to co-culture with the T6SS mutant, which was significant. Furthermore, when co-cultured with wild-type H111 the number of *P. fluorescens* recovered was similar to the number recovered when. *P. fluorescens* was cultured on its own. Taken together, this indicates that the presence of wild-type *B. cenocepacia* had no determine effect on the fitness of *P. fluorescens*, but co-culturing with a T6SS mutant had a positive effect on the fitness of *P. fluorescens*. A trial experiment using a different *B. cenocepacia* H111 T6SS mutant (*tssA*::Tp) was used in this interspecies competition assay with *P. fluorescens* and a similar trend was seen i.e. co-culturing with a T6SS mutant enhanced the recovery of *P. fluoresces* relative to when it cultured on its own or with the wild-type strain (data not shown). However this was only an n of 1.

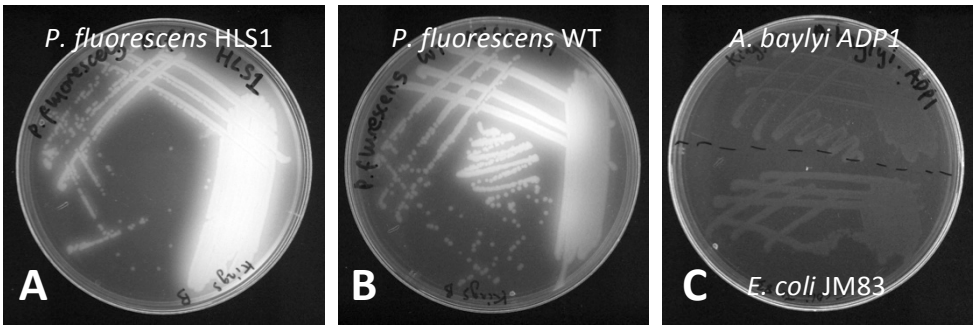

Figure 4.24 Determination of fluorescent phenotype of rifampicin-resistant *P. fluorescens* isolate, HLS1. A spontaneous rifampicin-resistant mutant of *P. fluorescens* was generated, HLS1, and its fluorescent phenotype confirmed by culturing on King's B agar for 48 hours at 25°C. Fluorescence was visualised upon exposure to UV light. (A) *P. fluorescens* HLS1, (B) wild-type (WT) *P. fluorescens* ATCC 17571 and (C) non-fluorescent *A. baylyi* ADP1 and *E. coli* JM83.

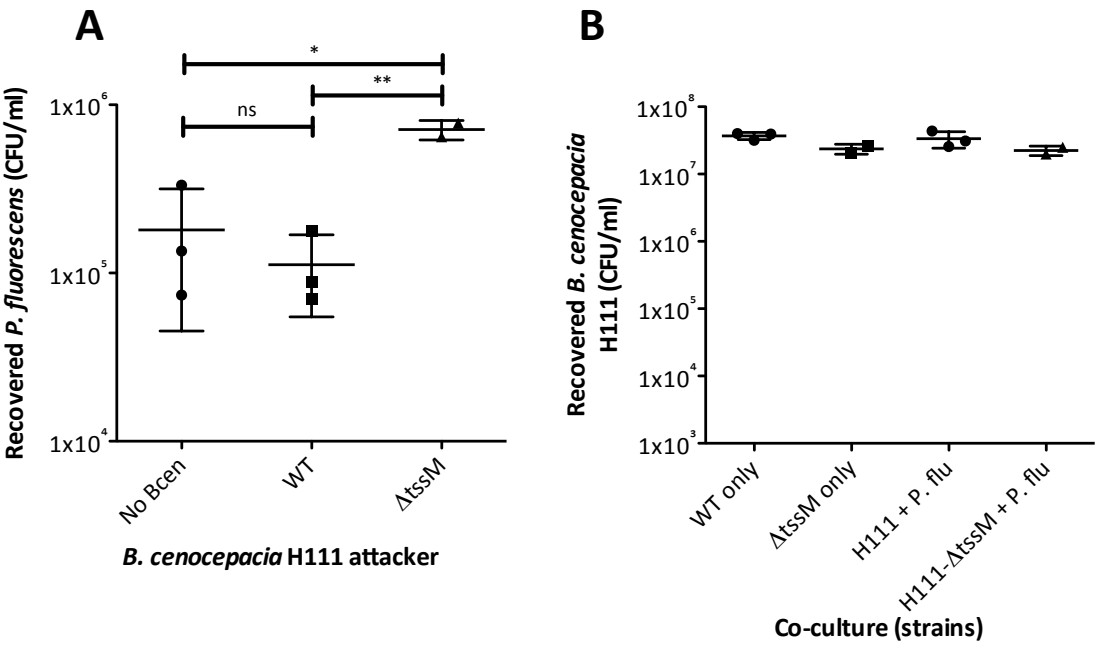

Figure 4.25 Analysis of the contribution of the T6SS to competitive fitness of *B. cenocepacia* H111 against *P. fluorescens.* *B. cenocepacia* H111 and rifampicin resistant *P. fluorescens* HLS1 were combined in a 5:1 ratio, incubated on solid medium for 4 hours at 30°C, where upon surviving bacteria were recovered and enumerated on selection plates. (A) Number of recovered *P. fluorescens* after co-culture with H111, H111-*tssM*::Tp or in absence of competing bacteria ('No Bcen') and (B) shows number of *B. cenocepacia* recovered after each culture. Statistical analysis by student's t-test, n≥2, p<0.05, error bars = ±SD. *, p<0.05; **, p<0.01; ns, not significant.

4.7 Investigation into anti-eukaryotic properties of the *B. cenocepacia* T6SS using eukaryotic infection models

In vivo B. cenocepacia survival in an animal model has been tentatively linked to the T6SS (Section 1.2.5). Therefore, it was decided to determine whether the *B. cenocepacia* T6SS was important for virulence in two different eukaryotic infection models, using a more virulent strain of *B. cenocepacia*, K56-2.

4.7.1 Analysis of the role of the T6SS in the virulence of *B. cenocepacia* in a zebrafish embryo infection model

B. cenocepacia K56-2 and its corresponding T6SS mutants were tested in a zebrafish (*Danio rerio*) embryo infection model in collaboration with A. Vergunst (University of Montpellier). A preliminary experiment found that the parental wild-type strain of *B. cenocepacia* K56-2 used to make initial T6SS mutants had an attenuated virulence in the zebrafish infection model (data not shown). Subsequent to this, it was found that this attenuated wild-type isolate (K56-2^{att}) and corresponding mutants gave a shiny pink colony morphology on Congo red plates. This was consistent with a strain defective in ShvR-related genes encoded on chromosome 3 that correlated with loss of virulence (Bernier et al., 2008; Subramoni et al., 2011). Therefore the *tssA*::Tp and *tssM*::Tp alleles were introduced into a new isolate of wild-type K56-2 (K56-2^{vir}) (Section 4.2.1). This strains and the resulting T6SS mutants were confirmed to have a SHV-positive (red and rough) phenotype on Congo red plates (Table 4.2 and Figure 4.26).

Upon infection of 30 hours post-fertilisation (hpf) embryos with ~100 CFU per embryo of wild-type K56-2^{vir} and its T6SS-deficient derivatives, it was found that infection with either T6SS mutant resulted in no significant difference in embryo survival compared to wild-type (Figure 4.27A). The majority of embryos were killed within 48 hours post-infection for all three strains. Intracellular replication of bacteria were also monitored at 0, 24 and 48 hours post-infection (Figure 4.27B), which again showed no significant difference in the recovered levels of intracellular bacteria: all strains were able to replicate within the embryos. Overall, these results

Table 4.2 Analysis of colony morphology of attenuated and virulent *B. cenocepacia* K56-2 isolates on Congo red agar.

Strain	Colony morphology and colour after Congo red binding[a]
K56-2 WT^{att}	Shiny, pink
K56-2^{att}-*tssA*::Tp	Shiny, pink
K56-2^{att}-*tssM*::Tp	Shiny, pink
K56-2^{vir} WT	Rough, red
K56-2^{vir}-*tssA*::Tp	Rough, red
K56-2^{vir}-*tssM*::Tp	Rough, red

[a] Colony morphology on LB agar containing 0.01% (w/v) Congo red dye after incubation at 37°C for 48 hours.
^{att}, attenuated isolate; ^{vir}, virulent isolate.

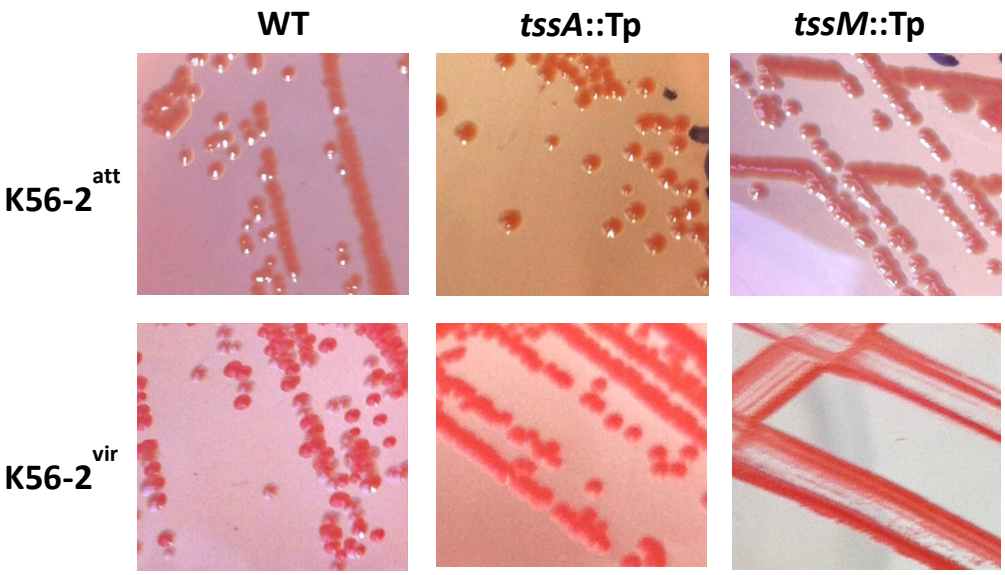

Figure 4.26 Analysis of colony morphology of *B. cenocepacia* K56-2 isolates on Congo red plates. Isolates of *B. cenocepacia* K56-2 were streaked onto LB agar containing 0.01% (w/v) Congo red dye and incubated at 37°C for 48 hours. Colony morphology was scored on their ability to bind Congo red dye, either with high affinity (rough and red phenotype), or lower affinity (shiny and pink), and plates photographed. Top row shows resulting colony morphology of original attenuated *B. cenocepacia* K56-2 wild-type (WT) lab stock (K56-2^{att}) (left), and corresponding *tssA*::Tp (middle) and *tssM*::Tp (right) mutants. Bottom row shows non-attenuated *B. cenocepacia* K56-2 isolate (K56-2^{vir}) and corresponding T6SS mutants generated from this parental strain.

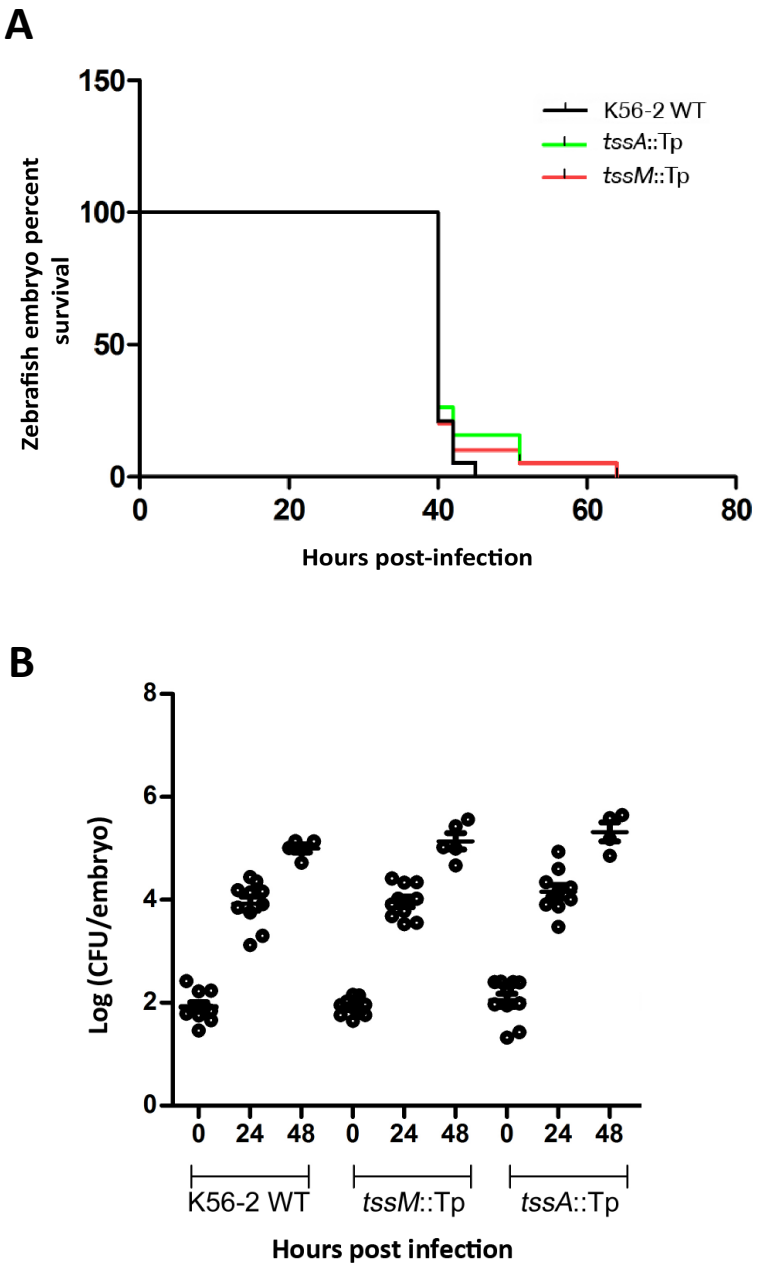

Figure 4.27 Effect of T6SS-inactivation on the virulence of *B. cenocepacia* K56-2 in a zebrafish infection model. 30 hpf zebrafish embryos were infected with wild-type *B. cenocepacia* K56-2^{vir} (WT), *tssA*::Tp or *tssM*::Tp derivatives at ~100 CFU per embryo and embryo survival was monitored over 48 hours. (A) Percentage survival of infected embryos as a function of time for each strain tested, as indicated in the key. (B) Number of bacteria recovered from infected embryos (in CFU/ml) at 0, 24 and 48 hpi. n= 2.

suggest that the T6SS in *B. cenocepacia* is not important for virulence in this model.

4.7.2 Analysis of the role of the T6SS in the virulence of *B. cenocepacia* in the *Galleria mellonella* larvae infection model

Larvae from *Galleria mellonella*, more commonly known as the greater wax moth, have previously been used to model infection by *B. cenocepacia* for evaluating virulence determinants (Seed and Dennis, 2008; Agnoli et al., 2012). Therefore, it was decided to employ this model to investigate whether the *B. cenocepacia* T6SS plays a role in virulence in this alternative infection model.

Preliminary optimisation was undertaken to determine the most appropriate bacterial infection load to use and the infection period. To do this, final instar stage larvae were injected with approx. 4 to 4 x 10^4 CFU/larva of wild-type *B. cenocepacia* K56-2 (K56-2^{vir}) from a mid-log phase liquid culture (Section 2.10.2), and larvae survival was monitor over 48 hours. The initial inoculum was estimated by plating serial dilutions of the normalised culture onto LB agar containing tetracycline. The number of surviving larvae was scored at 18 hours, 24 hours, 40 hours and 48 hours post-infection (hpi). PBS mock-infected and heat-killed K56-2 controls were included. Figure 4.28 shows the resulting percentage larvae survival over time for each infection group, and the data for 24 hpi is presented as a kill curve. Results from this pilot experiment indicated that larvae infected with the highest dose (4 x 10^4 CFU per larva) were the only group to show larvae death at 18 hpi. Larvae killing became rapid between 18 and 24 hours for the both 4 x 10^4 and 4 x 10^3 dose groups. By 48 hours, even a very low inoculum of ~3 CFU resulted in $>$95% death of the larvae. This data showed a good dosage response of bacteria to killing of the larvae, suggesting that 4 x 10^4 CFU per larva and 4 x 10^2 CFU per larva of bacteria were appropriate bacterial loads to use for monitoring larvae survival/death over 24 hours to give a high and low dosage response, respectively.

Following from this, groups of 30 larvae were infected with a high (~4 x 10^4 CFU per larva) and low (~400 CFU per larva) bacterial load of *B. cenocepacia* K56-2 wild-type, *tssA*::Tp or *tssM*::Tp mutants and larvae survival was monitored over 24 hours. Data from 2 independent experiments is shown in Figure 4.29. These results

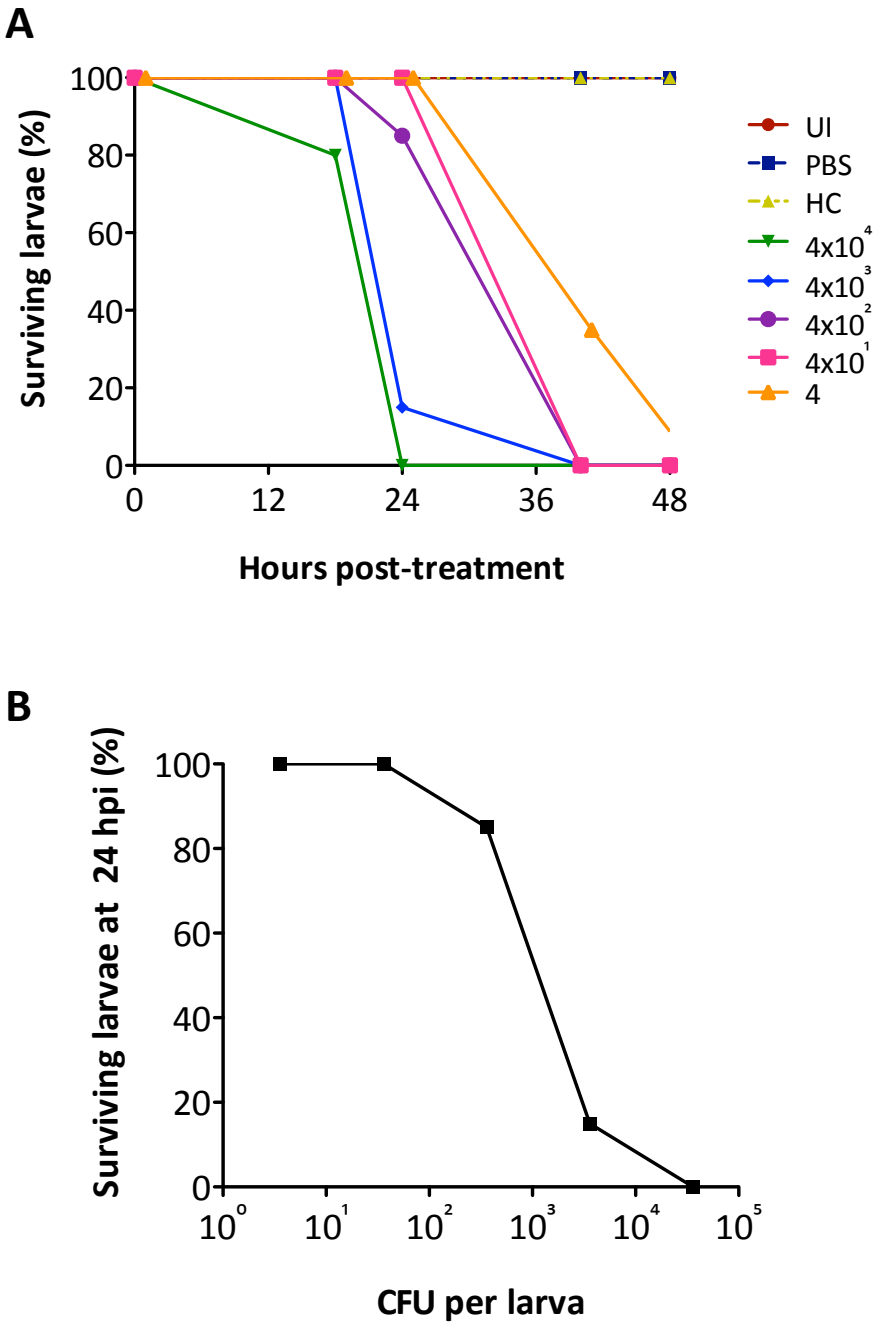

Figure 4.28 Analysis of the effect of initial bacterial inoculum on *Galleria mellonella* larvae survival following infection by *B. cenocepacia* K56-2. Final-instar *G. mellonella* larvae were infected with serial dilutions of *B. cenocepacia* K56-2 and larvae survival was monitored over 48 hours. (A) Percentage larvae survival for each treatment group (n=20 for each group), infected with 4 x 10^4 to 4 CFU per larva, identified in the key to the right. Mock-infected (PBS treated), heat killed K56-2 (HC) and uninfected larvae (UI) were included as controls. (B) A kill curve at 24 hours post-infection for *G. mellonella* infected with varying inocula of *B. cenocepacia* K56-2. n= 1.

A

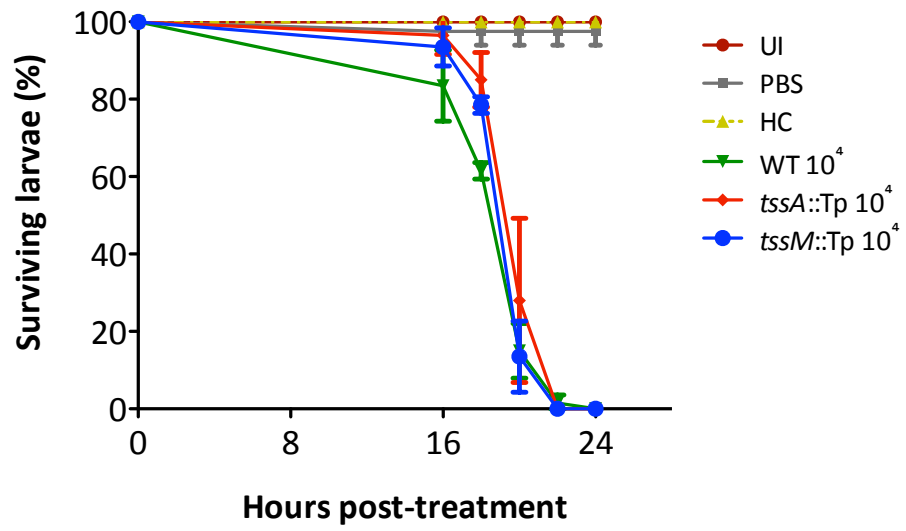
Surviving larvae (%)
100
80
60
40
20
0
0
8
16
24
Hours post-treatment
UI
PBS
HC
WT 10^4
tssA::Tp 10^4
tssM::Tp 10^4

B

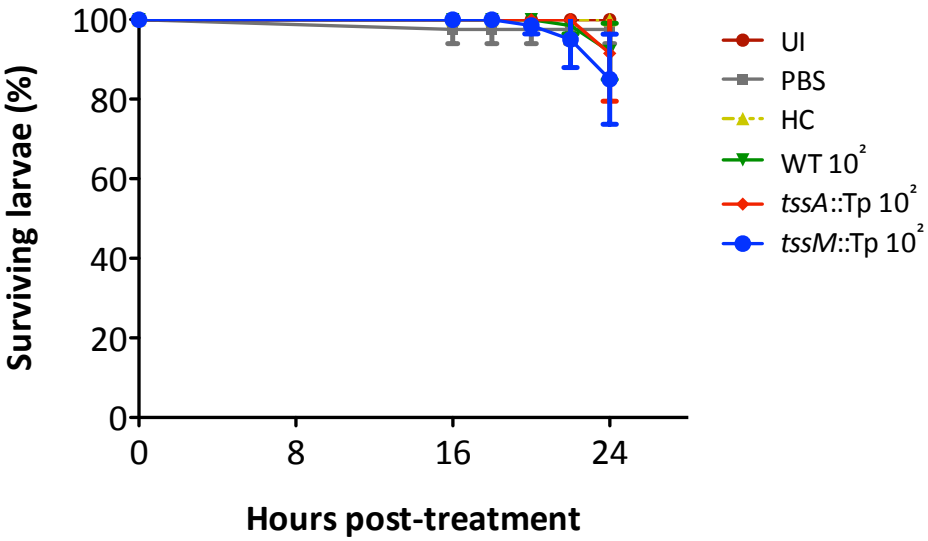
Surviving larvae (%)
100
80
60
40
20
0
0
8
16
24
Hours post-treatment
UI
PBS
HC
WT 10^2
tssA::Tp 10^2
tssM::Tp 10^2

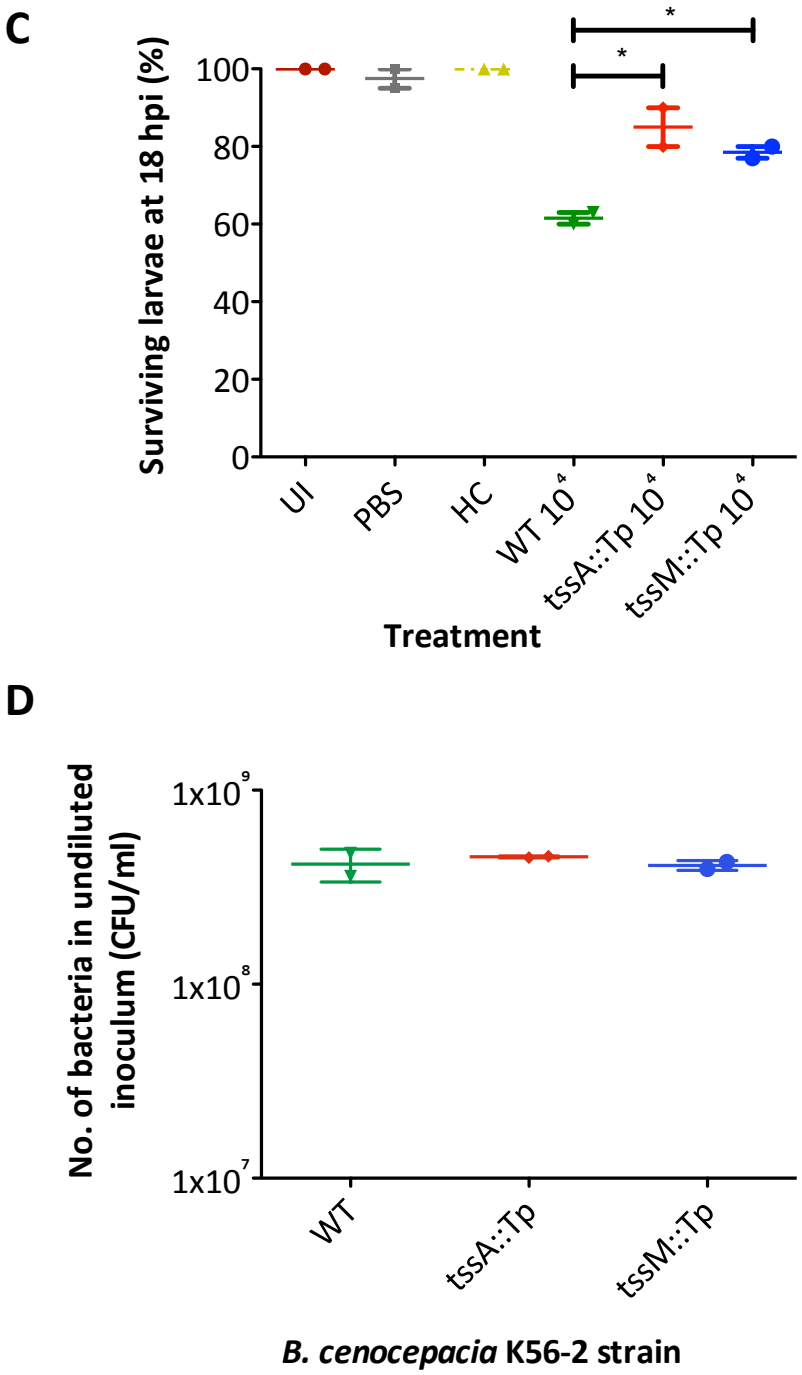

Figure 4.29 Effect of T6SS-inactivation on the virulence of *B. cenocepacia* K56-2 in a *Galleria mellonella* infection model. *G. mellonella* larvae where infected with *B. cenocepacia* K56-2 wild-type, and *tssA*::Tp and *tssM*::Tp mutant derivatives and larval survival monitored over 24 hours. 30 larva per infection group were used. (A) Larval survival over time for larvae infected with a high dose (4 x 10^4CFU per larva) of wild-type, *tssA*::Tp and *tssM*::Tp, as indicated by the key. (B) as (A) but infected with a lower dose of bacteria (4 x 10^2 CFU per larva). (C) Larval surival at 18 hpi in high dose-infected groups. Statistical analysis by student's t-test, where n=2 and $p<0.05$, *, $p<0.05$. UI, uninfected; PBS, mock-infected control group; HC, heat-killed control group. (D) Average calculated CFU/ml of inital bacterial inocula for K56-2 wild-type, *tssA*::Tp and *tssM*::Tp-infected groups over the two experiments.

showed that inactivation of the T6SS resulted in no difference to the overall virulence of *B. cenocepacia* K56-2 in this model as determined at 24 hours with either dose (Figure 4.29A and 4.29B). However, larvae survival was slightly greater when infected with a high dose of either of the T6SS mutants than with a high dose of the wild-type strain, but only at 16 and 18 hpi, with 18 hpi showing the most prominent difference (Figure 4.29C). Thus, an average of 62% larval survival occurred at 18 hpi when infected with wild-type K56-2 in comparison to 85% survival following infection with the *tssA*::Tp mutant and 79% following infection with the *tssM*::Tp mutant, which was statistically significant. However, no difference was observed in the low dose infection groups. This trend was seen in both experiments but it is difficult to draw solid conclusions regarding the role of the T6SS in this due to the limited n number. However, a difference in bacterial inoculum can be ruled out as a cause of the variation in larvae survival in the high dose groups at the 18 hpi time point, as enumeration of the inocula showed similar CFU/mL between wild-type and mutants and between each experiment (Figure 4.29D).

4.8 Discussion

4.8.1 Generation of a genetic tool for in-frame allelic replacement in *B. cenocepacia*

The generation of in-frame deletion mutants in a useful tool for understanding the phenotypic effects of deleting a gene whilst limiting polar effects on genes downstream, which can occur by insertional inactivation, i.e. with an antibiotic resistance cassette. This study generated a new allelic replacement vector, pEX18TpTer-*pheS*, which worked on the principle of conferring trimethoprim resistance for the selection of initial recombinants, and cPhe counter-selection for identification of a second recombination event. This vector is based on pEX18Tp-*pheS,* from the pEX18-*pheS vector* series, which has been successfully used for allelic replacement in *Burkholderia* species other than *B. cenocepacia* (Barrett et al., 2008). Work in our lab had previously observed difficulties in selecting for initial single recombinants by virtue of their trimethoprim-resistance, which was hypothesis to be due to transcription from the strong artificial *pheS* promoter (P_{S12}) converging with transcription from the reverse orientated *dfr* gene, resulting in down-regulation of *dfr* promoter activity. In the study describe here, this was overcome by placing the *dfr* gene in pEX18Tp-*pheS* in the same orientation as *pheS* with the addition of a strong transcriptional terminator.

The plasmid was successfully used to generate an in-frame deletion of the *tssM* gene in *B. cenocepacia* H111. Inactivation of the T6SS in this Δ*tssM* mutant was confirmed by demonstrating that the strain had reduced T6SS activity and T6SS function, i.e. absence of TssD in the culture supernatant, which could be restored by genetic complementation, and reduced competitive fitness in a co-culture, as observed for other T6SS mutants. Thus, indicating in-frame deletion mutagenesis in *B. cenocepacia* was possible using this new allelic replacement vector.

Other methods for generating in-frame deletion mutants in *Burkholderia* species are possible, including sucrose counter-selection using *sacB* (López et al., 2009), and a method based of the yeast homing endonuclease I-SceI (Flannagan et al., 2008). The former is based on the production of levansucrase from *sacB,* which catalyses the hydrolysis of sucrose to produce fructose polymers, this action is

lethal, thus growth on medium containing sucrose is toxic (Steinmetz et al., 1983; Gay et al., 1983). This allows selection of a second recombination event in a similar manner to cPhe counter-selection. However, this approach cannot be taken in all cases, as some *Burkholderia* species posses a *sacB* homologue, and sucrose-sensitivity has been observed to be variable even in strains that do not contain a *sacB* homologue (Essex-Lopresti et al., 2005).

The I-SceI system uses a I-SceI recognition site located in an allelic replacement vector, where once integrated into the genome by a single recombinant event, the site is then cut by the homing endonuclease I-SceI provided in trans by an expression plasmid (Plessis et al., 1992; Posfai et al., 1999). This produces a double stranded DNA break in the genome at the I-SceI recognition site, promoting a second recombinant event to occur via the DNA repair mechanism, resulting in excision of the vector backbone (Posfai et al., 1999). Strains are typically cured of the I-SceI encoding plasmid by counter-selection involving *pheS* expression and cPhe (Fazli et al., 2015) or *sacB* expression and sucrose (Flannagan et al., 2008), encoded within the I-SceI encoding expression plasmid. The strategy used by the vector constructed in this study does not required an additional transformation step for selection of a second recombinant event like that required using the I-SceI system, so in that regards, pEX18TpTer-*pheS* has its advantages.

However, the pEX18TpTer-*pheS* plasmid is not perfect, cPhe counter-selection was still observed to be inefficient in some cases. The reasons for this are unknown, but sensitivity of the system to trace amounts of contaminating phenylalanine may be a contributing factor (Barrett et al., 2008). Furthermore, the mutated *pheS* allele carried on pEX18TpTer-*pheS* is derived from *B. pseudomallei,* not *B. cenocepacia*, which is similar but not identical to the *B. pseudomallei* version, sharing 96% amino acid sequence identify. Hence, the vector may be improved by replacing the *B. pseudomallei pheS* allele with one derived from *B. cenocepacia*, which may overcome the variation in cPhe sensitivity observed.

The plasmid could be improve further still by the introduction of a colour chromogenic marker, such as *gusA,* allowing the insertion and excision of the vector into the genome to be easily distinguished by colour selection on appropriate

medium, e.g. containing X-Gluc. Although, issues regarding the ease of use when cloning in *E. coli* with the pEX18TpTer-*pheS* vector, in regards to growth conditions and media requirements, when selecting for trimethoprim-resistance and using blue/white colony selection, have been improved by the addition of the *cat* cassette, conferring resistance to chloramphenicol, meaning rich medium and a higher incubation temperature can be used for a faster cloning procedure. However, this allelic replacement vector, pEX18TpTer-*pheS*-Cm, has yet to be tested for in-frame mutagenesis in *Burkholderia*.

4.8.2 Differential T6SS activity amongst *B. cenocepacia* strains

The T6SS is typically inactive under standard laboratory conditions, necessitating the use of bacterial strains that have a constitutively active T6SS, either by modification of regulatory genes in the wild-type strain, e.g. the *retS* mutant of *P. aeruginosa* (Mougous et al., 2006), or identification of wild-type isolates that have an active system, such as *cholerae* V52 (Pukatzki et al., 2006), *E. tarda* PPD130/91 (Zheng and Leung, 2007) or *S. marcescens* Db10 (Murdoch et al., 2011), in order to investigate their function. The results presented in this chapter indicate differential activity of the T6SS amongst *B. cenocepacia* strains, where strains H111 and K56-2 both showed constitutive T6SS activity as judged by secretion of TssD in liquid cultures, whereas the Pc715j strain did not show any detectable extracellular TssD. Even the two strains that exhibited constitutive T6SS activity showed differential levels of TssD secretion. These results are consistent with previously published work.

A 2-DE coupled mass spectrometry analysis of total proteins produced by *B. cenocepacia* H111 identified a haemolysin-coregulated protein (later identified as TssD) in its extracellular fraction (Riedel et al., 2006), indicating TssD secretion by H111 under standard laboratory conditions. A functional T6SS in *B. cenocepacia* K56-2 was demonstrated by Aubert and colleagues upon inactivation of a global virulence regulator AtsR, which caused hypersecretion of TssD (Aubert et al., 2008). T6SS-dependent morphological changes were observed in macrophages infected with the hypersecreting strain and the strain had the ability to resist predation by

Dictyostelium discoideum in a T6SS-dependent manner (Aubert et al., 2008). In contrast to the findings here, Aubert and co-workers were only able to detect TssD in liquid supernatants of the hypersecreting Δ*atsR* mutant and not wild-type K56-2. However, this was only analysed using Coomassie blue staining, rather than immuno-detection, and a different precipitation method was employed for the concentration of extracellular proteins. So it may well have been that TssD was present in the wild-type K56-2 isolate used in their study but it went undetected due to the methodology employed.

The constitutive nature of the T6SS in some *B. cenocepacia* strains but not in others coincides with findings in other T6SS-containing bacteria. The *V. cholerae* V52 strain, as mentioned previously has an active T6SS under laboratory conditions, whereas *V. cholerae* N16961 and C6706 strains do not (Pukatzki et al., 2006; Zheng et al., 2010), even though they contain a full complement of the genes required for T6SS activity (Miyata et al., 2010). It was found that the genetic control of T6SS activity in *V. cholerae* was dually negatively regulated by both quorum sensing (via LuxO and HapR regulators) and a global regulator, TsrA, and strains that have a constitutive T6SS (i.e. V52) contain mutations in these key regulators, in particular HapR (Zheng et al., 2010). One can postulate that reasons for the differential activation of the T6SS in *B. cenocepacia* strains may be due to a similar phenomenon.

B. cenocepacia H111 is derived from a non-ET12 lineage and lacks the CciIR QS system encoded on the *B. cenocepacia* island (cci) associated with the ET12 lineage strains of *B. cenocepacia* (Baldwin et al., 2004; O'Grady et al., 2009). The CciIR system was suggested to have a negative regulatory effect on the T6SS cluster (O'Grady et al., 2009). K56-2 is of the ET12 lineage (Varga et al., 2013) and contains the *cci* and thus the CciIR QS system. An MLST analysis performed on Pc715j indicated in was more related to K56-2 that to H111 (M.S. Thomas, unpublished), but it has not had its genome sequenced so it is unknown whether it contains the cci island, and thus the CciIR QS system. However, these two strains differed in T6SS activity also, further complicating the matter, summarised in Figure 4.30. It may be that K56-2 but not Pc715j, has acquired another mutation in an unknown regulator of the T6SS or vice versa, which allows activation/inactivation of the system

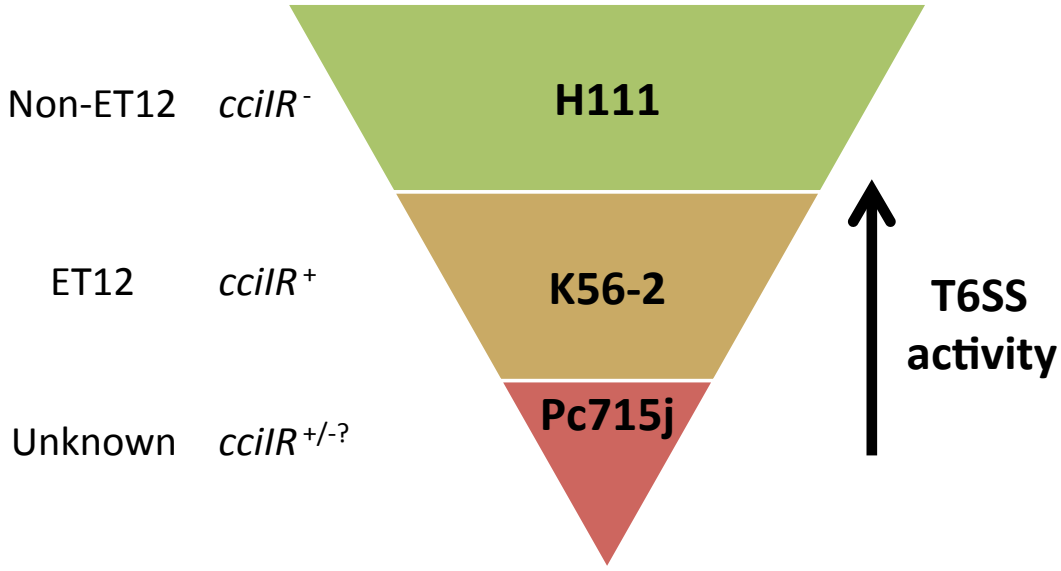

Figure 4.30 Diagrammatic summary of differential T6SS activity amongst *B. cenocepacia* strains. Diagram shows *B. cenocepacia* strains used in this study, H111, K56-2 and Pc715j, ordered relative to their T6SS activity, as accessed by secretion of TssD in the liquid culture supernatants. The presence of the CciIR QS system, a potential negative regulatory mechanism of the T6SS, and the strain lineage is indicated on the left. +, positive; -, negative; -/+?, unknown.

regardless of the presence of the CciIR QS-regulatory system (which may or may not result in the suppression of T6SS activity). But without sequence data available for the Pc715j strain and the unknown T6SS phenotype of CciIR mutants it is difficult to hypothesise what may be causing the difference in the T6SS activity amongst these strains. Nevertheless, the identification of a *B. cenocepacia* strain that exhibits T6SS activity under laboratory conditions was an important step in subsequent evaluation of the role the T6SS in this organism.

4.8.3 Role of the *B. cenocepacia* T6SS in bacterial competition

The role of the T6SS in interspecies and intraspecies bacterial competition has become a prominent feature of the system in a variety of T6SS containing bacteria. Here, there is evidence to support a similar role for the *B. cenocepacia* T6SS in interspecies competition against a variety of bacterial species, including *P. putida* and *E. coli*. Ideally, the loss in competitive edge seen in T6SS mutants needs to be verified by genetic complementation. Plasmids were constructed to test this, but due to lack of time, these experiments were unable to undertaken.

Nevertheless, these findings do coincide with observations of *B. thailandensis*, where its ancestral *Burkholderia* T6SS-1 cluster was found to be important for bacterial competition against *S. proteamaculans, P. fluorescens and P. putida,* where the T6SS was required to prevent *P. putida*-induced stasis of *B. thailandensis* in co-culture (Schwarz et al., 2010).

It was noted that the fitness advantage conferred on *B. cenocepacia* by the T6SS was not as pronounced when using *E. coli* as a competitor in comparison to *P. putida*. This could have been for a multitude of reasons. For example, *P. putida* and *E. coli* may have inherent differences in growth rates, which could, in-turn, affect the co-culture. In addition, or alternatively, *B. cenocepacia* may be able to produce an unknown anti-bacterial effector that is more effective at targeting *P. putida* than *E. coli*. One can also speculate that as *P. putida* contains a T6SS (Bingle et al., 2008; Renzi et al., 2010), this may be further inducing the T6SS in *B. cenocepacia* H111 in a counter-attacking 'T6SS-duelling' manner described recently (Basler et al., 2013). *E. coli* K-12 strains do not possess a T6SS, therefore one can reason that they are

unable to induced a T6SS-mediated attack by *B. cenocepacia* H111 as effectively as a T6SS-proficient strain.

However, the idea that the *B. cenocepacia* T6SS is induced as a response to attack by a competing species is undermined by the observations that the T6SS in *B. cenocepacia* strain Pc715j was unable to provide a competitive advantage in co-culture with *P. putida*. Although, perhaps this is a little unsurprising as the T6SS in Pc715j appeared to be inactive under standard laboratory conditions. Work in *V. cholerae* demonstrated something similar, where a strain with a constitutively active T6SS, V52, exhibited T6SS-dependent interspecies competitive fitness whereas strains, NG16961 and O395, with a silent T6SS did not (MacIntyre et al., 2010). Interestingly, *V. cholerae* does not show 'T6SS-duelling' properties, nor does the T6SS in *S. marcescens* (Gerc et al., 2015). It may be that *B. cenocepacia* does not have this ability either, as indicated by the result of the Pc715j strain.

4.8.4 The *B. cenocepacia* T6SS and eukaryotic virulence

Intracellular survival within phagocytic cells is thought to one of the major virulence determinants employed by *B. cenocepacia* to allow evasion of the immune system and subsequent dissemination throughout the host, where bacteria reside in arrested membrane bound vacuoles, termed BcCVs (Burns et al., 1996; Saini et al., 1999; Martin and Mohr, 2000; Rosales-Reyes et al., 2012b). This feature has been modelled by simple eukaryotic infection models, including a zebrafish embryo infection model (Vergunst et al., 2010) and *in vitro* in eukaryotic cell lines, including macrophages (Rosales-Reyes et al., 2012b), monocytes (Gavrilin et al., 2012), and epithelial cells (Mullen et al., 2007; Mil-Homens et al., 2014). The T6SS of a particular virulent strain of *B. cenocepacia*, K56-2, has been linked to eukaryotic virulence. Mutants lacking an active T6SS were shown to have reduced *in vivo* survival in a rodent lung infection model (Hunt et al., 2004; Aubert et al., 2008) and the causal agent of actin rearrangements in *B. cenocepacia*-infected macrophages, after up-regulation of T6SS through deletion of a global virulence regulator (Aubert et al., 2008; Rosales-Reyes et al., 2012b; Aubert et al., 2012).

However in this study, using two different infection models, the zebrafish

embryo and *G. mellonella* larvae, there was no evidence to suggest an anti-eukaryotic role for the T6SS in *B. cenocepacia* K56-2 in overall virulence. Both models did not exhibit a significant increase in overall survival of the host when infected with T6SS mutants in comparison to the wild-type.

Data from the zebrafish embryo model also indicated that intracellular replication of *B. cenocepacia* was not affected by inactivation of the T6SS, implying that the T6SS mutants were still able to effectively survive within zebrafish embryo macrophages. This is consistent with observations in a macrophage cell line model showing that the T6SS was not responsible for the delayed maturation of *B. cenocepacia* containing vacuoles or for intracellular survival of the bacterium (Rosales-Reyes et al., 2012a; Rosales-Reyes et al., 2012b).

Nonetheless, regarding the *G. mellonella* infection results, there was a slight increase in larval survival at 16 and 18 hpi when inoculated with a high dose of either T6SS mutant, than when compared to infection with the wild-type strain. The experiment was performed twice and showed the same trend, but until this is repeated solid conclusions cannot be drawn from the data. However, it may tentatively suggest that the T6SS is in some way important for early establishment of the infection in this model. Yet the high dose of bacteria required to manifest the difference between wild-type and T6SS mutant infections does place a question mark over the role of the T6SS in this model, as it difficult to see how this would be clinically relevant.

As *B. cenocepacia* K56-2 is able to replicate within *G. mellonella* larvae throughout the infection (Seed and Dennis, 2008), it would be intriguing to investigate whether the T6SS mutants were as effective at intracellular replication as the wild-type in this model. This could account for the higher proportion of larvae surviving at 16 and 18 hpi. The competitive fitness the T6SS provides *B. cenocepacia* in the presence of some other bacterial species could also be a contributing factor to the phenotype seen here, as *G. mellonella* larvae have been shown to contain a microflora of other organisms, particularly in the gut (Bucher, 1963; Bucher and Williams, 1967), linking the two observations made in this study. Work outside the scope of this project would be required to investigate this.

Chapter 5: Design of a system for analysis of the T6SS-dependent secretome of *B. cenocepacia*

5.1 Rationale

One of the main aims in this investigation was to identify the T6SS-dependent effectors of *B. cenocepacia*, as this may provide clues as to the role of this system. One of the approaches to be undertaken involved the use of mass spectrometry, taking a bottom up, shotgun proteomics approach for the analysis of the T6SS-dependent secretome of *B. cenocepacia,* centred on protein identification by tandem MS analysis. This mass spectrometry based discovery approach has been similarly utilised for the identification of effectors of the H1-T6SS of *P. aeruginosa* (Hood et al., 2010), T6SS-1 and T6SS-5 of *B. thailandensis*, (Russell et al., 2012; Schwarz et al., 2014), and other T6SSs such as *S. marcescens* (Fritsch et al., 2013) and a more targeted approach in *V. cholerae* (Miyata et al., 2011). It has also been used for the analysis of the bacterial secretome dependent on other protein secretion systems, including the T2SS-dependent secretome of *B. pseudomallei* (Burtnick et al., 2014).

Such an approach requires conditions for growth of the bacterium that will result in detectable levels of T6SS-dependent effectors. This study has found that the T6SS has differentially activity in three different *B. cenocepacia* strains when growing in broth cultures, as demonstrated by the secretion of the T6SS subunit TssD, which is the hallmark of a functional T6SS. Strains H111 and K56-2, of differing lineages, both have an active T6SS, where TssD secretion was found to be greater in H111 than K56-2, whereas strain Pc715j, which is more closely related to K56-2 than H111 did not exhibit any detectable T6SS activity (Section 4.5.1). Thus, it was decided to utilise the H111 strain as a model organism in order to help identify *B. cenocepacia* T6SS-dependent effectors. However, despite the fact that H111 possesses the most active T6SS under the laboratory conditions employed, TssD was detectable only following 1000-fold concentration of the culture supernatants. To apply the mass spectrometry technique it was deemed necessary to try and establish conditions that would result in a higher level of T6SS activity in this strain.

Several potential regulators of the T6SS in *B. cenocepacia* H111 were identified by bioinformatic analysis, due in part to their homology with characterised T6SS-regulatory proteins in other T6SS-containing bacteria, their

conservation in the ancestral *Burkholderia* T6SS-1 cluster but not in other T6SS clusters, or interesting predicted structures and functional domains (Section 3.1.2). This includes potential post-translational regulators TagF, TagM, and TagX and a orthologue of the hybrid sensor kinase AtsR, involved in a two-component global transcriptional regulatory system characterised in *B. cenocepacia* K56-2 (Aubert et al., 2008; Aubert et al., 2012; Khodai-Kalaki et al., 2013) (Figure 5.1). The work discussed in this chapter centres on the possible role of *tagX*, *tagF* and *atsR* in T6SS regulation in the strain *B. cenocepacia* H111, in particular whether inactivation of these genes leads to up-regulation of T6SS activity.

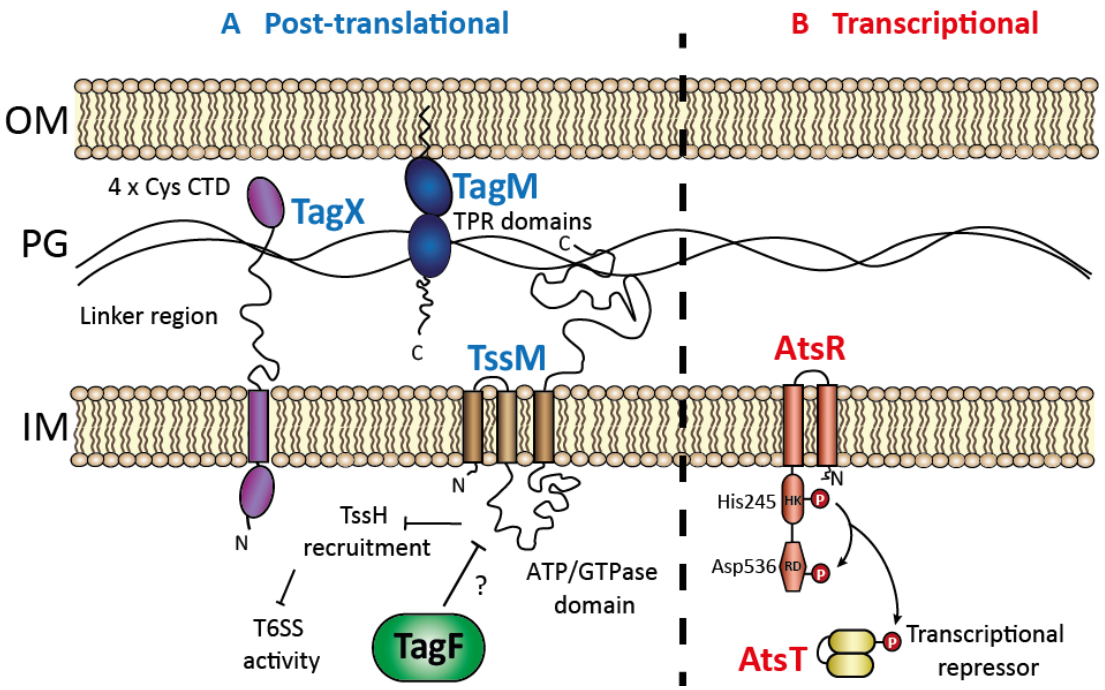

Figure 5.1 Putative regulators of the T6SS in *B. cenocepacia.* (A) TagF, TagM and TagX are candidate post-translational regulators of the T6SS in *B. cenocepacia*. TagF may be a cytoplasmically located negative post-translational regulator, possibly acting against TssM, which results in reduced TssH recruitment to the T6SS complex, reducing TssB/TssC tail sheath disassembly and recycling, leading to a reduction in T6SS activity. TagX is predicted to contain a transmembrane domain, and a long linker region extending into the periplasm with a CTD containing four conserved cysteine residues. This may be involved in iron-sulphur cluster formation and/or disulphide bond oxidation or reduction, which is used to sense an external signal. TagM is an OM-anchored lipoprotein that contains TPR domains that suggests involvement in protein-protein interactions. (B) AtsR acts as a sensor kinase that results in the phosphorylation of the response regulator, AtsT, in a phosphorelay involving autophosphorylation of His245 in its histidine kinase domain and phosphor-transfer to Asp536 in its receiver domain, or to an aspartate residue in AtsT. AtsT is thought to act as a transcriptional repressor to directly or indirectly repress T6SS gene expression. OM, outer membrane; PG, peptidoglycan; IM, inner membrane; RD, receiver domain; HK, histidine kinase.

5.2 Investigation into TagX as a potential regulator of the T6SS in *B. cenocepacia*

Bioinformatic analysis of *Burkholderia* T6SS-1-related/type gene clusters revealed a pair of divergently transcribed genes, *tagX* and *tagV*, that are located upstream of *tssM* in all such clusters that retain the full complement of T6SS subunit genes, i.e. intact clusters (Section 3.1.2). One of these genes, *tagV* (corresponding to BCAL0352 in *B. cenocepacia* J2315 and I35_0343 in strain H111), is likely to be part of the same transcriptional unit as *tssM* (Figure 5.2). In some non-*Burkholderia* species, one or two genes that are associated with *tssI* gene clusters in the genus *Burkholderia* are interposed between *tssM* and *tagV*. *tagV* is predicted to encode a Sec-dependent cytoplasmic membrane-anchored VanY-like D-alanyl-D-alanine carboxypeptidase belonging to the peptidase M15 family. The predicted topology of the transmembrane domain suggests that the C-terminal peptidase domain is located in the periplasmic space of bacteria harbouring T6SS-1, where it would serve as a peptidoglycan hydrolase. The function of this protein is not known but it may play a role in assembly of the T6SS.

tagX (corresponding to BCAL0353 in *B. cenocepacia* J2315 and I35_0344 in strain H111) is located upstream of *tagV* and transcribed in the opposite direction (Figure 5.2). It is expected to be constitute a monocistronic operon based on the presence of a putative Rho-independent transcription termination sequence located 35 bp downstream from the *tagX* stop codon (M. Thomas, personal communication).

Analysis of the predicted coding sequence of *tagX* identified a sequence of 17 amino acids approximately 55 residues from the N-terminus, which are highly conserved in TagX orthologues in the *Burkholderia spp*., and are likely to constitute a transmembrane domain with the N-terminus located within the cytoplasm. The 55 amino acid N-terminal region contains two conserved amino acid sequence motifs (PSLLS and RILAxLEGR) separated by 11-13 amino acids, suggesting that it may constitute a small domain. The putative transmembrane domain is proceeded by a large segment of low complexity with a high alanine and proline content, suggest it acts as an interdomain linker. This is followed by a conserved C-terminal

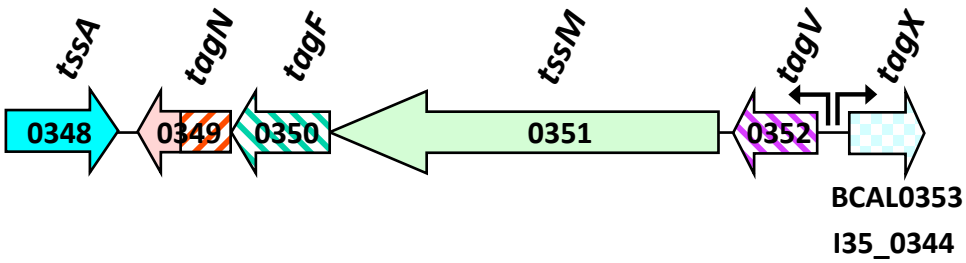

Figure 5.2 Genomic location of *tagX* in *B. cenocepacia*. Diagram showing the location of the *tagX* gene in *B. cenocepacia* J2315 (BCAL0353) and H111 (I35_0344) in relation to other T6SS genes in the T6SS gene cluster. The divergent promoters between *tagY* and *tagV* are also indication. Not to scale.

region of ~40 amino acids containing four cysteine residues (Cys294, Cys305, Cys310, Cys320) in the H111 TagX orthologue) (Figure 5.3). This domain arrangement was likened to the inner membrane-anchored periplasmic protein TonB, which functions as an energy transducer in energy-dependent outer membrane transport processes in Gram-negative bacteria (Figure 5.4) (Noinaj et al., 2010). It was envisaged that the unusual cysteine-rich C-terminal domain of TagX may act as redox or metal ion sensor by oxidation or reduction of thiol groups between pairs of cysteine residues. This may involve formation or collapse of an iron-sulphur cluster.

This led to the hypothesis that TagX may be involved in regulation of the T6SS at a post-translational level. The CTD may sense periplasmic signals related to the T6SS, possibly oxidative stress, either directly caused by outer membrane perturbations from attacking T6SS bacteria or other another environmental origin (Basler et al., 2013), or indirectly via another regulatory component located in the periplasm (such as TagM) or components tethered to the inner leaflet of the outer membrane. This sensed signal may then be transduced to the cytoplasmic NTD facilitating an interaction with unknown regulatory components, which go on to regulate the assembly, disassembly or firing of the T6SS complex.

Therefore, it was decided to generate an insertional *tagX* mutant in *B. cenocepacia* H111 to investigate whether deletion of this gene affected T6SS activity. If inactivation of *tagX* led to an increase in T6SS activity it could be concluded that TagX acts as a negative post-translational regulator of the T6SS, and the mutant would be used to facilitate effector identification. On the other hand, if *tagX* ablation caused a decrease in T6SS activity it could be concluded that TagX serves directly or indirectly to activate T6SS function and it might be possible to hyperstimulate the T6SS by introduction of *tagX* on a multicopy plasmid.

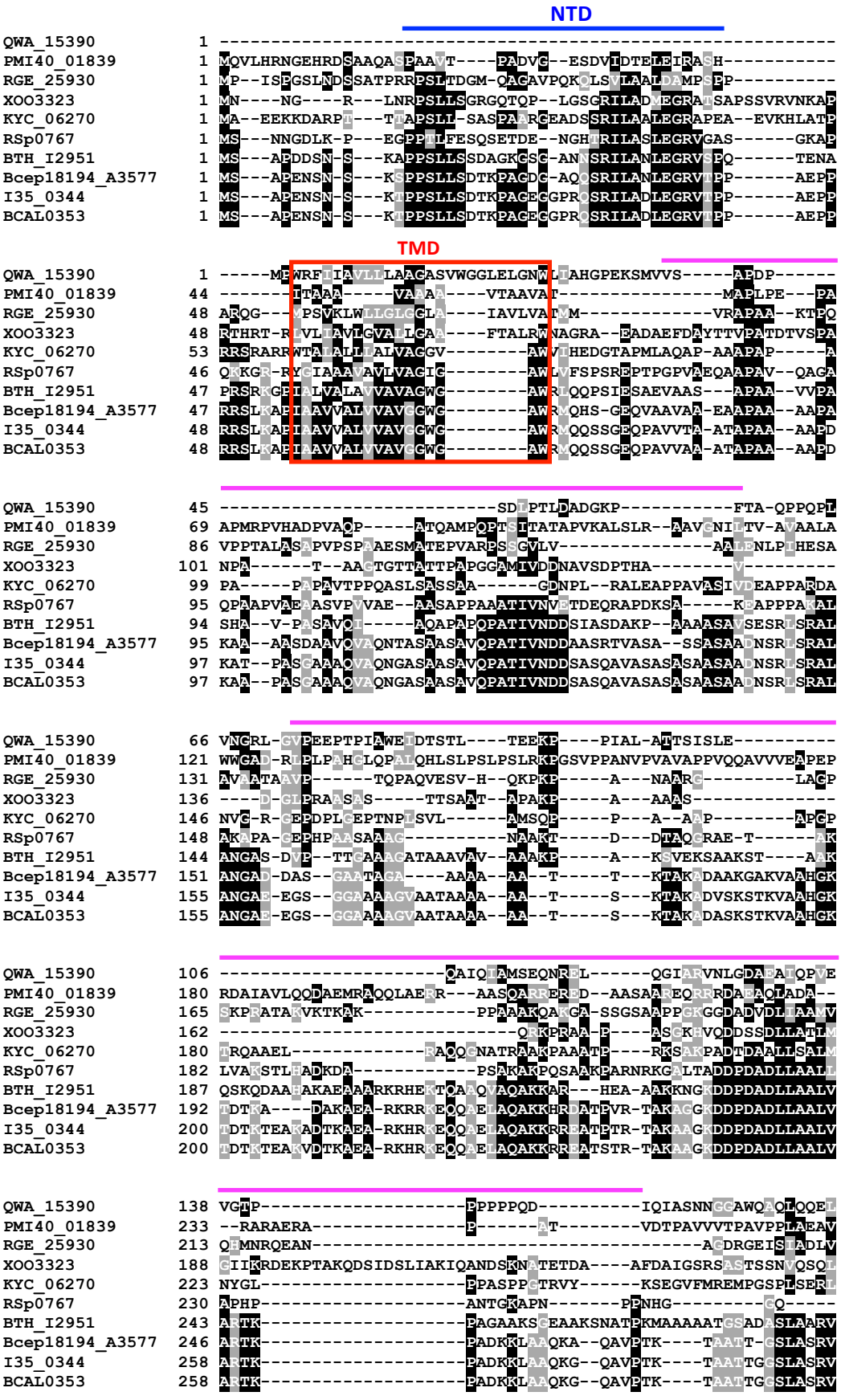
NTD
TMD
QWA_15390
PMI40_01839
RGE_25930
XOO3323
KYC_06270
RSp0767
BTH_I2951
Bcep18194_A3577
I35_0344
BCAL0353

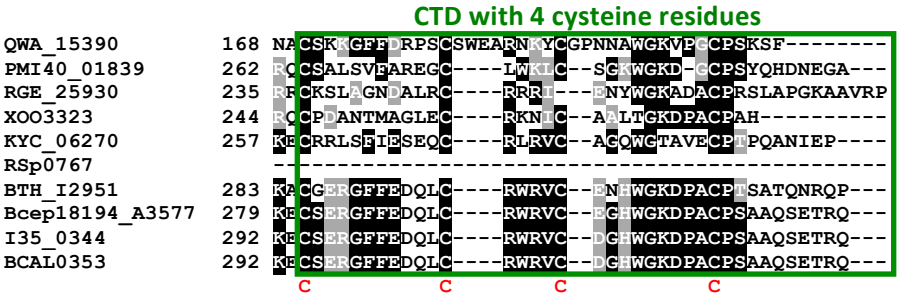

Figure 5.3 Amino acid sequence alignment of the product of BCAL0353 and I35_0344, TagX, with homologous proteins. The amino acid sequences of the putative post-translational regulator, TagX, encoded by BCAL0353 and I35_0344 in *B. cenocepacia* J2315 and H111, respectively, and other homologous proteins, were aligned using Clustal Omega. Black shading indicates identical residues at the corresponding position in 50% of sequences, grey shading indicates similar residues at the corresponding position in 50% of sequences. The putative cytoplasmic N-terminal region is indicated by blue overline, the putative transmembrane domain (TMD) indicated by the red boxed region, and the conserved C-terminal cysteine residues are indicated in red font below the alignment and the pertinent region of the alignment is enclosed in a green box. The region with a high alanine and proline content may correspond to a periplasmic linker region, as indicated by the pink overline. The gene locus designations are indicated on the left.

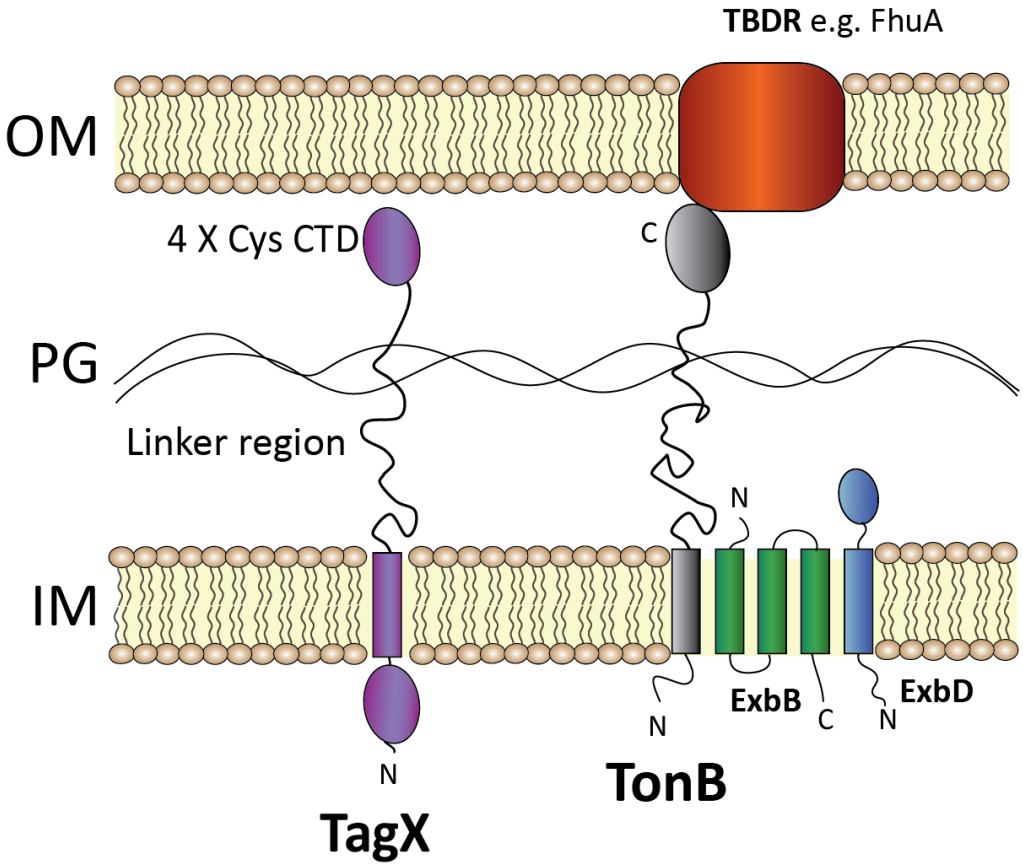

Figure 5.4 Comparison of inferred structural organisation of TagX with that of TonB. TagX is indicated on the left, showing a small cytoplasmic N-terminal domain, transmembrane domain, followed by a periplasmic linker region connected to a cysteine rich C-terminal domain. A similar domain organisation occurs in the energy transducer TonB, depicted on the right, where the periplasmic CTD interacts with an N-terminal periplasmic extension of an TonB-dependent receptors (TBDR) in the outer membrane, facilitating energy-dependent outer membrane transport processes when in a complex with the inner membrane proteins ExbB and ExbD, also illustrated.

5.2.1 Insertional inactivation of *tagX* in *B. cenocepacia* strain H111

For inactivation of the *tagX* gene a gene replacement plasmid was constructed by insertion of the *dfr* cassette (conferring trimethoprim-resistance) into the coding sequence of *tagX,* as depicted in Figure 5.5. To do this, a 1199 bp DNA fragment containing the *tagX* open reading frame (I35_0344 gene locus in *B. cenocepacia* H111) and an additional 105 bp downstream of the TAA stop codon was amplified from H111 genomic DNA by PCR using primers BCAL0353For and BCAL0353Rev and then gel purified (Figure 5.6A). This fragment was then cut with BamHI and XhoI and inserted into the vector pBluescriptII between the corresponding restriction sites to give pBluescriptII-*tagX*, a 4014 bp plasmid (Figure 5.6B). Positive clones were identified by PCR screening using M13 forward and M13 reverse primers and then verified by plasmid extraction and DNA sequencing.

In preparation for *tagX* disruption the *dfr* cassette was released from p34E-Tp using SmaI. Utilising a unique ZraI restriction site in the middle of *tagX*, pBluescriptII-*tagX* was cut with this blunt-end generating enzyme and the SmaI-cut *dfr* cassette was ligated into it. Putative pBluescriptII-*tagX*::Tp transformants were identified by selection on IST agar containing ampicillin and trimethoprim. Plasmid minipreparations from a selection of these colonies resulted in the identification of clones of the expected size of 4654 bp. The orientation of the *dfr* insert in positive pBluescriptII-*tagX*::Tp clones was determined by restriction digestion with BsrGI and BamHI (Figure 5.7). All the clones, except 5, 12-15, produced fragments of 1033 bp and 3621 bp, indicating that the *dfr* coding sequence was in the same orientation as *tagX*, as desired. The *tagX*::Tp insert was then transferred from pBluescriptII-*tagX*::Tp as a XhoI-XbaI fragment into the suicide vector pSHAFT2, where it was cloned between the compatible XbaI and SalI restriction sites, to successfully generate the plasmid pSHAFT2-*tagX*::Tp (Figure 5.8).

For generation of the *B. cenocepacia* insertionally inactivated *tagX* mutant, pSHAFT2-*tagX*::Tp was first introduced into the *E. coli* donor strain S17-1(λpir). This strain was then used to transfer the plasmid into *B. cenocepacia* H111 by conjugation to enable homologous recombination events to occur between the *tagX* sequence contain on the vector and the wild-type *tagX* gene on the genome.

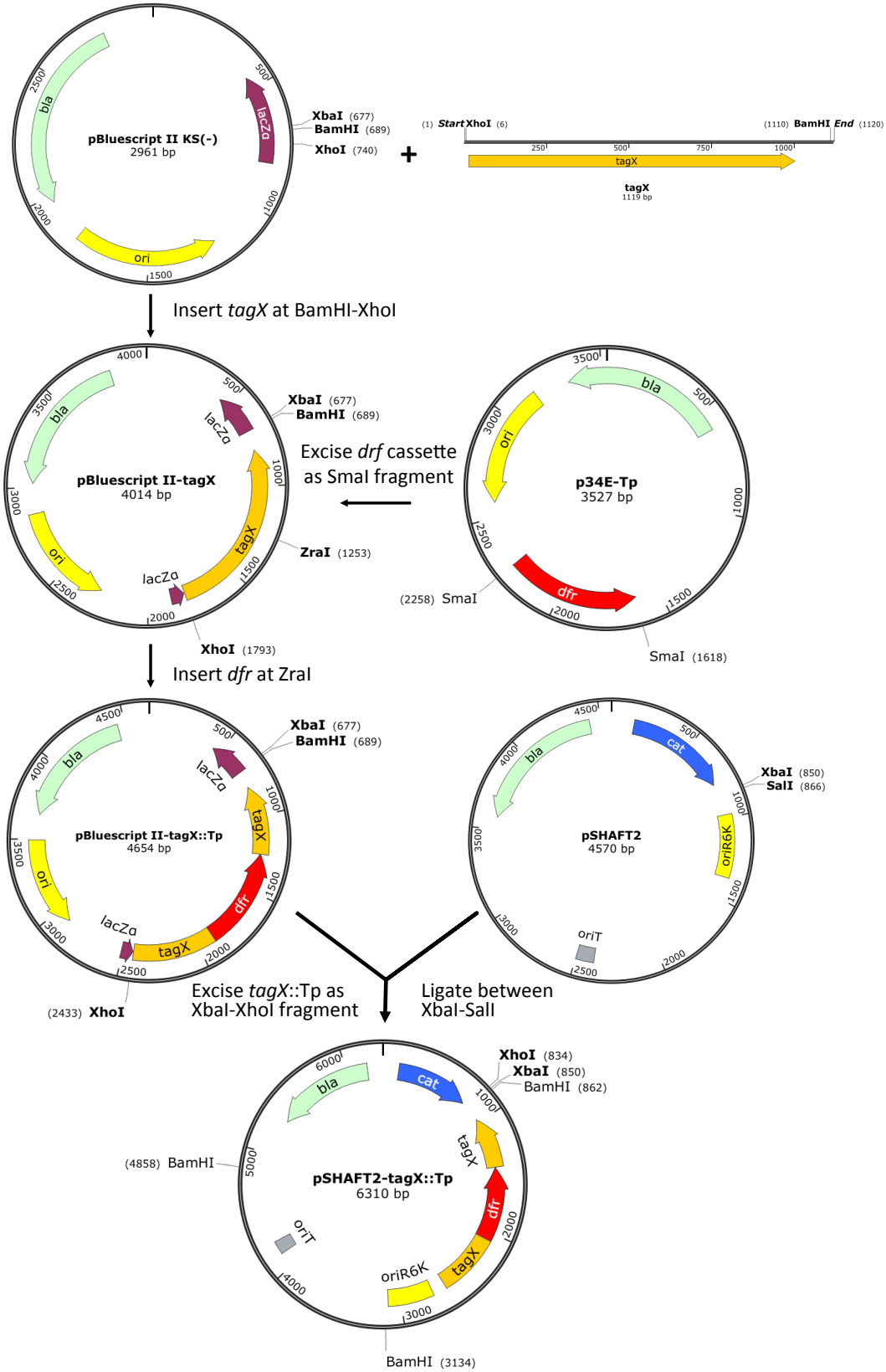

Figure 5.5 Construction of pSHAFT2-*tagX*::Tp for insertional activation. Diagram shows the generation of pSHAFT-*tagX*::Tp. *tagX* was cloned as an XhoI-BamHI fragment into pBluescriptII, then disrupted with a *dfr* cassette excised from p34E-Tp by SmaI and inserted into the ZraI site of *tagX*. The *tagX*::Tp allele was then transferred as an XhoI-XbaI fragment into suicide vector pSHAFT2, ligated between XbaI-SalI, to give pSHAFT2-*tagX*::Tp.

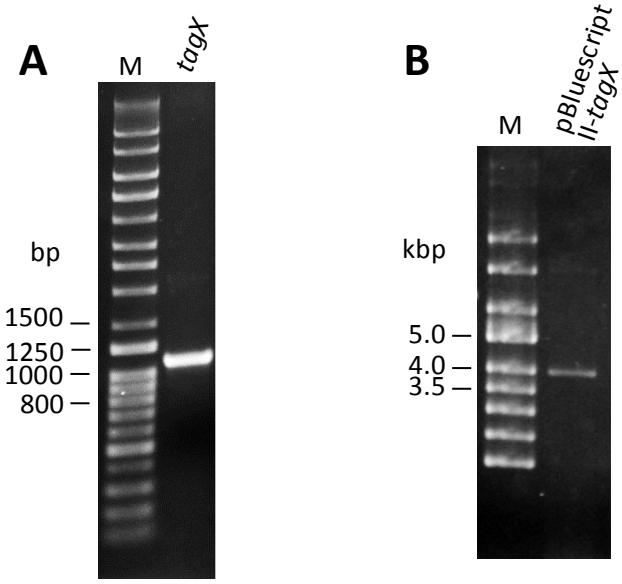

Figure 5.6 Amplification and cloning of *tagX*. (A) Amplification of *tagX* from H111 genomic DNA by PCR, as shown by the presence of a 1119 bp DNA fragment resolved in a 0.8% agarose gel. M, Q-step 4 DNA ladder. *tagX* was then ligated into pBluescript II between the BamHI and XhoI restriction sites. (B) 4014 bp pBluescriptII-*tagX* analysed by electrophoresis in a 0.8% agarose gel. M, Supercoiled DNA ladder.

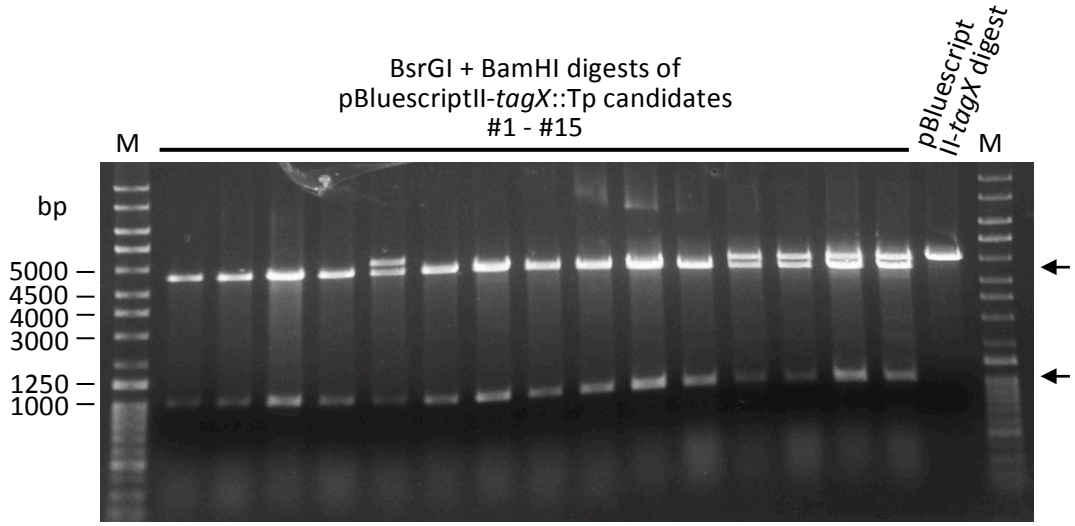

Figure 5.7 Diagnostic restriction digestion of pBluescriptII-*tagX*::Tp to determine the orientation of the *dfr* insert. pBluescriptII-*tagX*::Tp plasmid clones were subjected to double restriction digestion with BsrGI and BamHI to determine the orientation of the *dfr* insert. Resulting fragments were resolved in a 0.8% agarose gel. Arrows indicate the expected fragment sizes (3621 bp and 1033 bp) from plasmids with the *dfr* cassette in the same orientation as *tagX*, as desired. As a control, pBluescriptII-*tagX* was also digested with the same enzymes. M, Q-step 4 DNA ladder.

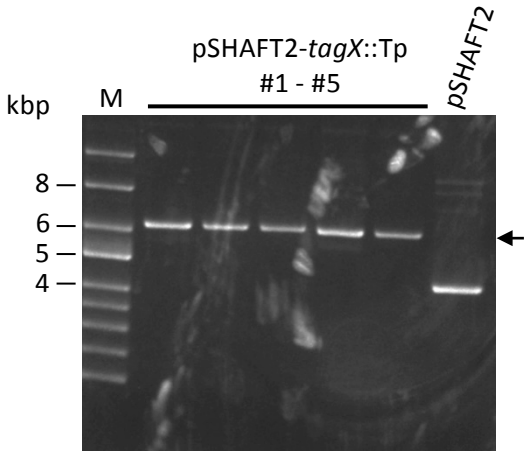

Figure 5.8 Size analysis of pSHAFT2-*tagX*::Tp candidates. The *tagX*::Tp fragment was transferred from pBluescriptII-*tagX*::Tp to the suicide vector pSHAFT2 as an XhoI-XbaI fragment, generating a 6310 bp plasmid, pSHAFT2-*tagX*::Tp. Selected clones were subjected to plasmid minipreparation and resolved in a 0.8% agarose gel. Arrow indicates the expected size of pSHAFT2-*tagX*::Tp. M, Supercoiled DNA ladder.

Recombinants were selected by virtue of their trimethoprim-resistance. pSHAFT2 contains a *cat* gene conferring resistance to chloramphenicol, allowing discrimination between single and double crossover recombinants by challenging trimethoprim-resistant colonies with chloramphenicol. Strains that were sensitive to chloramphenicol but resistant to trimethoprim were identified as potential double crossover recombinants, in which the mutant copy present on the plasmid had replaced the wild-type copy of *tagX*. Chloramphenicol-sensitive candidates were identified and then PCR screened using primer pairs annealing to regions of the genome just outside the *tagX*::Tp homologous region, BCAL0353CompFor-OP and BCAL0353CompRev-OP, and inside primers annealing to the *tagX* homology region, BCAL0353For and BCAL0353Rev. Potential H111-*tagX*::Tp mutants produced DNA fragments of 1900 bp and 1750 bp, respectively, which was an increase of 650 bp in comparison to the DNA fragments derived from the wild-type parent, due insertion of the trimethoprim-resistance cassette (Figure 5.9). Confirmed H111-*tagX*::Tp mutants were then selected for phenotypic analysis in comparison to wild-type H111.

5.2.2 Phenotypic analysis of the H111 *tagX*::Tp mutant

To determine whether disruption *of tagX* caused any differences in protein secretion in comparison to the *B. cenocepacia* wild-type strain, extracellular proteins were extracted from liquid grown cultures (Section 2.4.1). SDS-PAGE analysis demonstrated that the *tagX*::Tp mutant had similar secreted and cell-associated protein profiles as the wild-type strain under the growth conditions tested (Figure 5.10A). Both strains secreted similar levels of TssD as shown by anti-TssD western blotting (Figure 5.10B), indicating that both the wild-type and *tagX* mutant had similar T6SS activity. The cell-associated level of TssD in both strains was also similar. Note, there is a slight but noticeable difference between the observed molecular mass of secreted and intracellular TssD, which may be an artefact of the TCA precipitation method used, as previously observed (Wu et al., 2012; Lin et al., 2013).

Furthermore, by monitoring the optical density (OD_{600}) of broth cultures of

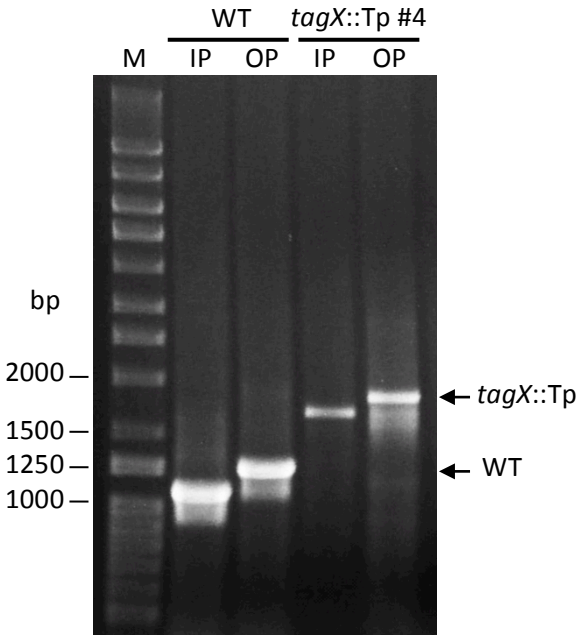

Figure 5.9 PCR verification of insertional inactivation of *tagX* in *B. cenocepacia* H111. The *tagX* gene in H111 was inactivated by homologous recombination with pSHAFT2-*tagX*::Tp. PCR was used to amplify DNA fragments using 'inside' (IP) and 'outside' (OP) primers specific to the *tagX* region from wild-type H111 (WT) and H111-*tagX*::Tp mutant #4 and resolved in a 0.8% agarose gel. Arrows indicate the expected fragment size of OP-generated fragment amplified from the indicated template DNA. M, Q-step 4 DNA ladder.

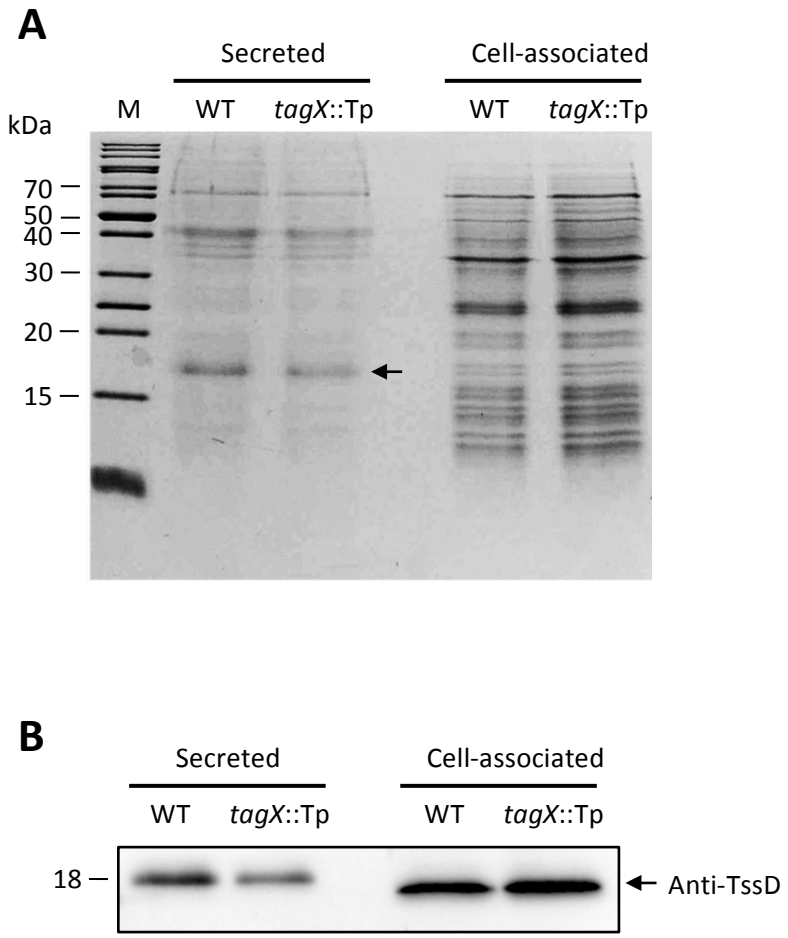

Figure 5.10 Analysis of *tagX* inactivation on T6SS activity. The culture supernatants of *B. cenocepacia* H111 and H111-*tagX*::Tp grown in D-BHI broth were concentrated by DOC-TCA precipitation and analysed by SDS-PAGE and anti-TssD western blotting to investigate T6SS activity. (A) 15% SDS-PA gel of secreted proteins from wild-type H111 (WT) and the *tagX*::Tp mutant (left) and cell-associated proteins (right). Arrow indicates 18 kDa secreted TssD protein. (B) Anti-TssD western blot where secreted (left) and cell-associated (right) TssD was detected using custom polyclonal antibody. M, EZ-Run *Rec* protein ladder.

H111 wild-type and the *tagX* mutant over time, it was observed that the *tagX* mutant had a similar growth rate in comparison to the wild-type strain (Figure 5.11).

Together these findings suggest that TagX does not play a role in the regulation of T6SS activity during growth in nutrient broth. Therefore, this mutant would be of no benefit in effector identification. However, it is still possible that under certain conditions, that have yet to be determined, TagX responds by triggering T6SS firing activity.

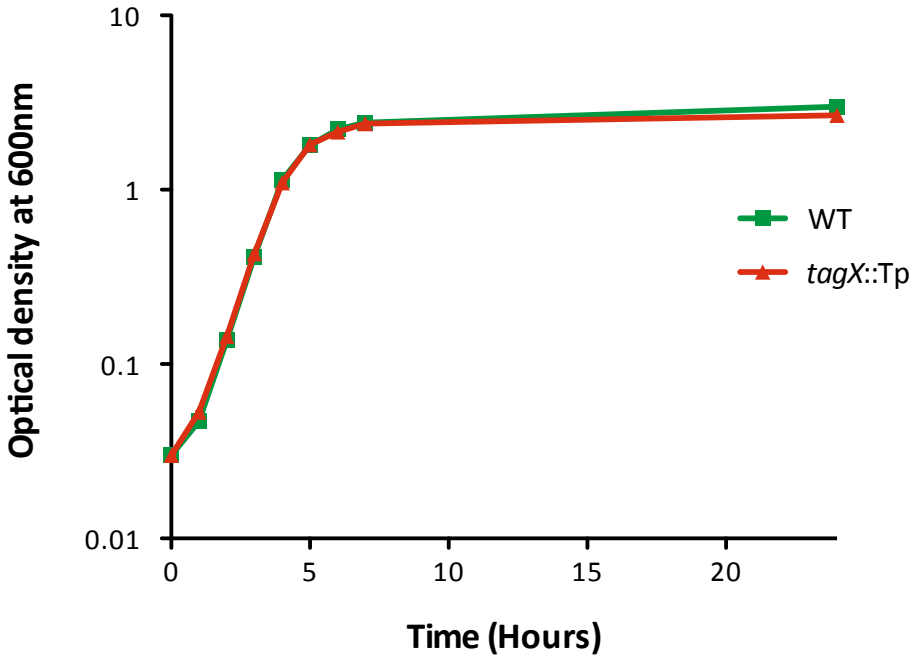

Figure 5.11 Growth rate of the *tagX* insertional inactivation mutant. H111 wild-type (WT) and H111-t*agX*::Tp were grown in 20 mL D-BHI-broth at 37°C and optical densities at OD_{600} were measured at regular intervals. Optical density measurements were plotted on a log scale (y-axis) as a function of time from inoculation (x-axis). Strains are represented by green and red symbols as indicated in the key.

5.3 Investigation into TagF as a potential regulator of T6SS activity in *B. cenocepacia*

As the inactivation of *tagX* did not lead to greater expression of the T6SS in *B. cenocepacia* it was decided to investigate another candidate regulator that had been identified in the *Burkholderia* T6SS-1 gene cluster. This protein was first identified as a homologous protein to the *S. typhimurium* T6SS protein SciT and termed TagF (Shalom et al., 2007). More recently, TagF was identified as a negative post-translational regulator of the *P. aeruginosa* H1-T6SS (Silverman et al., 2011). In *B. cenocepacia* it is encoded by BCAL0350 and I35_0341 in strains J2515 and H111, respectively, which are both located at the same relative position downstream of *tssM,* as is *tagF* in *P. aeruginosa* H1-T6SS (Figure 5.12). Both TagF proteins (from *B. cenocepacia* and *P. aeruginosa*) share a common DUF2094 superfamily domain (COG3913) yet share only 16% overall sequence identify and 25% sequence similarity.

In *P. aeruginosa*, TagF has been demonstrated to be a post-translational negative regulator of the T6SS*,* that acts independently of the characterised Fha1-phosphorylation dependent T6SS activation pathway, the threonine phosphorylation pathway (TPP), which involves the TagQRST-PpkA-Fha1-PppA components (Figure 1.6, Section 1.4.3) (Mougous et al., 2007; Hsu et al., 2009; Silverman et al., 2011; Casabona et al., 2013). In the current model, deletion of TagF is thought to recruit TssH (in complex with unphosphorylated Fha1) to the T6SS apparatus. Thus, meaning the contracted tail sheath-like structure made of TssB/TssC subunits can be disassembled and recycled ready for re-firing of the T6SS.

Intriguingly, the *B. cenocepacia* T6SS cluster does not contain a *fha1* homologue, nor homologues of the Ser/Thr protein kinase PpkA or phosphatase PppA, involved in the TPP T6SS activation pathway. Yet the conserved position of *tagF* in the T6SS cluster of both *B. cenocepacia* and *P. aeruginosa* (and many other T6SSs), directly downstream of *tssM*, could suggest that TagF may be exhibiting a negative regulatory effect on TssM. This in turn could lead to a reduction in TssH recruitment to the T6SS apparatus, which is independent of Fha1 in T6SSs that do not contain a Fha1 homologue. Thus, leading to a reduction in TssB/TssC sheath

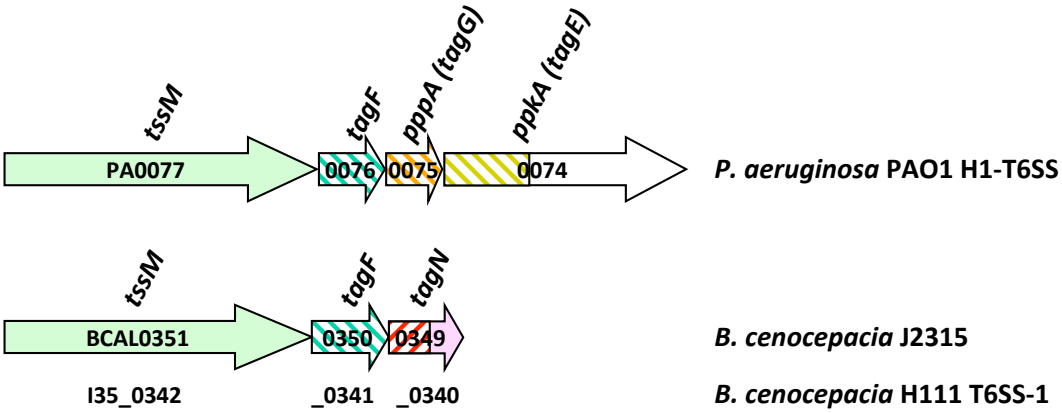

Figure 5.12 Comparison of the *tagF* orthologues in the T6SS clusters of *B. cenocepacia* and *P. aeruginosa*. Image showing the genetic arrangement of *tagF* in the H1-T6SS cluster of *P. aeruginosa* PAO1 in comparison to the *tagF* arrangement in the T6SS-1 cluster in *B. cenocepacia* J2315 and H111. Gene loci are stated within or below the arrows for each gene. Given gene names are indicated above the arrows. Not to scale.

turnover, culminating in a reduction and fine tuning of T6SS activity (Figure 5.1).

To evaluate the role of TagF in the regulation of T6SS activity in *B. cenocepacia* it was decided to analyse a *tagF* null mutant in *B. cenocepacia* H111, to determine whether inactivation of *tagF* resulted in increased T6SS activity, as documented in *P. aeruginosa.*

5.3.1 Effect of a *tagF* null allele on T6SS activity in a spontaneous c3 deficient *B. cenocepacia* H111 mutant

An insertional inactivation mutant of *tagF* was previously constructed by our group (Bull and Thomas, unpublished results) in an isolate of *B. cenocepacia* H111 that was later found to be sensitive to complement-mediate killing (serum-sensitive) and had also lost its entire third chromosome, which was termed H111^{S}. At the time, the phenotypic effect of inactivation of *tagF* was not assessed. Therefore, it decided to first assess the secreted protein profile of the H111^{S}-*tagF*::Km mutant in comparison to its parental strain, H111^{S}. SDS-PAGE analysis of secreted proteins present in broth cultures indicated that a 18 kDa protein was overproduced in the *tagF*::Km mutant in comparison to the parental H111^{S} strain (Figure 5.13). Immuno-detection with an anti-TssD antibody indicated that this overproduced protein was TssD. Densitometric analysis of the difference between secreted TssD in the parental H111^{S} strain to the *tagF*::Km mutant indicated that TssD secretion was increased 1.7-fold in the *tagF*::Km mutant, which as statistically significant with a P value of 0.026. This result implied that deletion of *tagF* was a potential way to stimulate T6SS activity further in *B. cenocepacia*.

Note, that the orientation of the kanamycin-resistance cassette inserted into *tagF* was determined by DNA sequencing and found to the in the same orientation as *tagF*, therefore it is not be expected to exert polar effects on *tagN*, the gene located immediately downstream of *tagF* in the same transcriptional unit.

5.3.2 Effect of a *tagF* null allele on T6SS activity in *B. cenocepacia* H111 wild-type

As the H111^{S} variant did not have a full complement of chromosomes, any

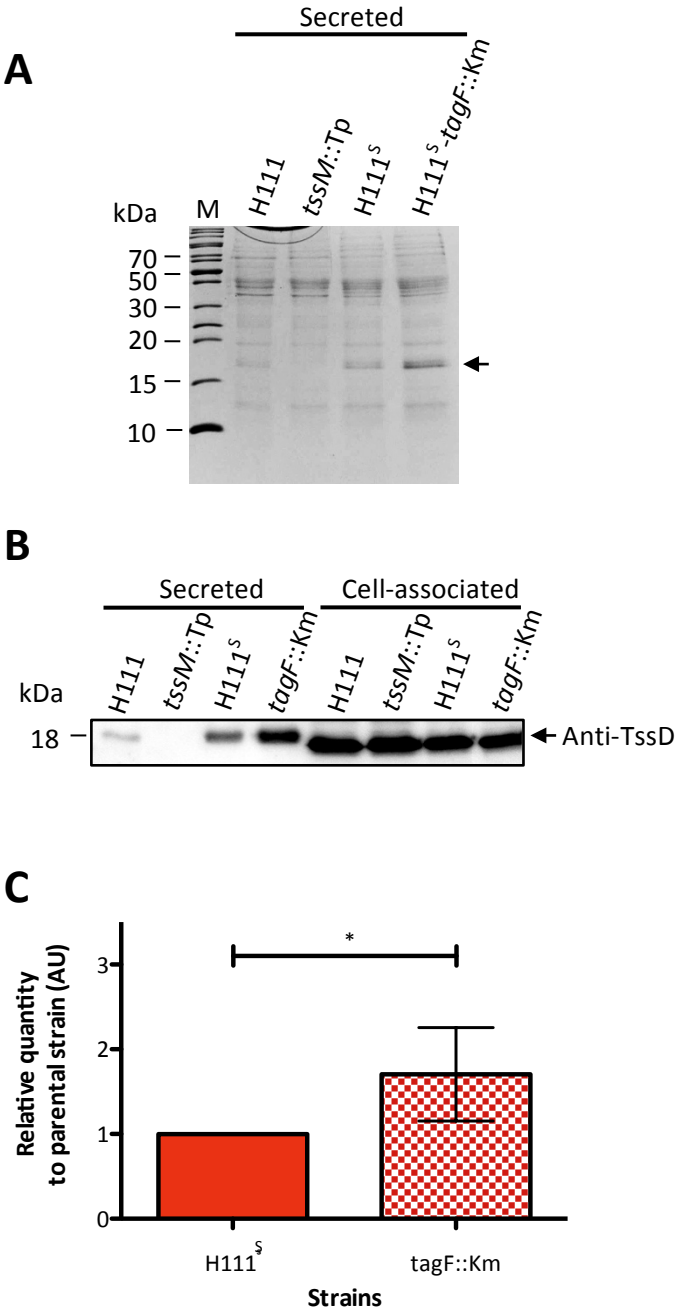

Figure 5.13 Analysis of the effect of *tagF* inactivation on TssD secretion in *B. cenocepacia* H111^S. *tagF* was insertionally inactivated by the kanamycin-resistance cassette. Extracellular proteins were precipitated from liquid culture supernatants of H111 wild-type, a T6SS mutant (*tssM*::Tp), H111^S spontaneous chromosome 3-deficient mutant and H111^S-*tagF*::Km. (A) Profile of extracellular proteins analysed by electrophoresis in a 15% SDS-PA gel and stained with Coomassie blue. (B) Representative anti-TssD western blot of secreted and cell-associated proteins of samples from (A). The size difference between secreted and cell-associated TssD may be due to the TCA precipitation treatment of the secreted proteins. (C) Densitometric analysis of relative difference between secreted TssD in H111^S in comparison to the H111^S-*tagF*::Km strain. Statistical analysis performed using a one sample t-test where $p < 0.05$, $n = 6$. *, $p < 0.05$; AU, arbitrary units.

potential T6SS effector encoded by the third chromosome would be excluded from secretome analysis if this strain were used for a discovery experiment. Therefore, the *tagF* gene of the wild-type *B. cenocepacia* H111, containing a full complement of chromosomes was insertionally inactivated. To do this, a suicide plasmid encoding an insertionally inactivated copy of *tagF* containing the kanamycin-resistance cassette (*nptII*), pSHAFT-*tagF*::Km, was introduced into *B. cenocepacia* H111 and recombinants were selected by acquisition of kanamycin-resistance on Lennox agar. Single and double crossover recombinants were distinguished by virtue of their chloramphenicol-sensitivity (Section 5.2.1), where double crossover recombinants were expected to be kanamycin-resistant but chloramphenicol-sensitive. Candidates were screened by PCR using primers that annealed outside of the *tagF*::Km homology region in the genome, H111tagFfor and H111tagFrev. All kanamycin-resistant candidates that were sensitive to chloramphenicol gave rise to a DNA fragment of the expected sized for the *tagF*::Km allele, i.e. a larger 2500 bp DNA fragment compared the wild-type DNA fragment of 1260 bp, due to the insertion of the *nptII* gene (Figure 5.14A). This indicated successful generation of a H111 *tagF* mutant.

The secretion profile of the H111-*tagF*::Km mutant was compared to that of wild-type H111 to determine whether the overproduction of TssD observed in the $H111^{S}$-*tagF*::Km variant was mirrored in the newly constructed strain with a full complement of chromosomes. Unexpectedly, this was not the case. The level of extracellular TssD in comparison to the wild-type was variable between 5 independent experiments as determined by western blotting (Figure 5.14B) and densitometric analysis (Figure 5.14C). In some cases TssD secretion was the same as the wild-type and in others there was overproduction of TssD even though the same protocol was undertaken. An average 1.8-fold increase of extracellular TssD was observed in the *tagF*::Km mutant in comparison to the wild-type, but the standard deviation of this increase was high, at 1.04, indicating a wide variation in the differences in TssD secretion observed. The irreproducibility of TssD secretion, coupled with observation that T6SS activity was not significantly increased, meant that this strain would not be particularly useful for effector identification.

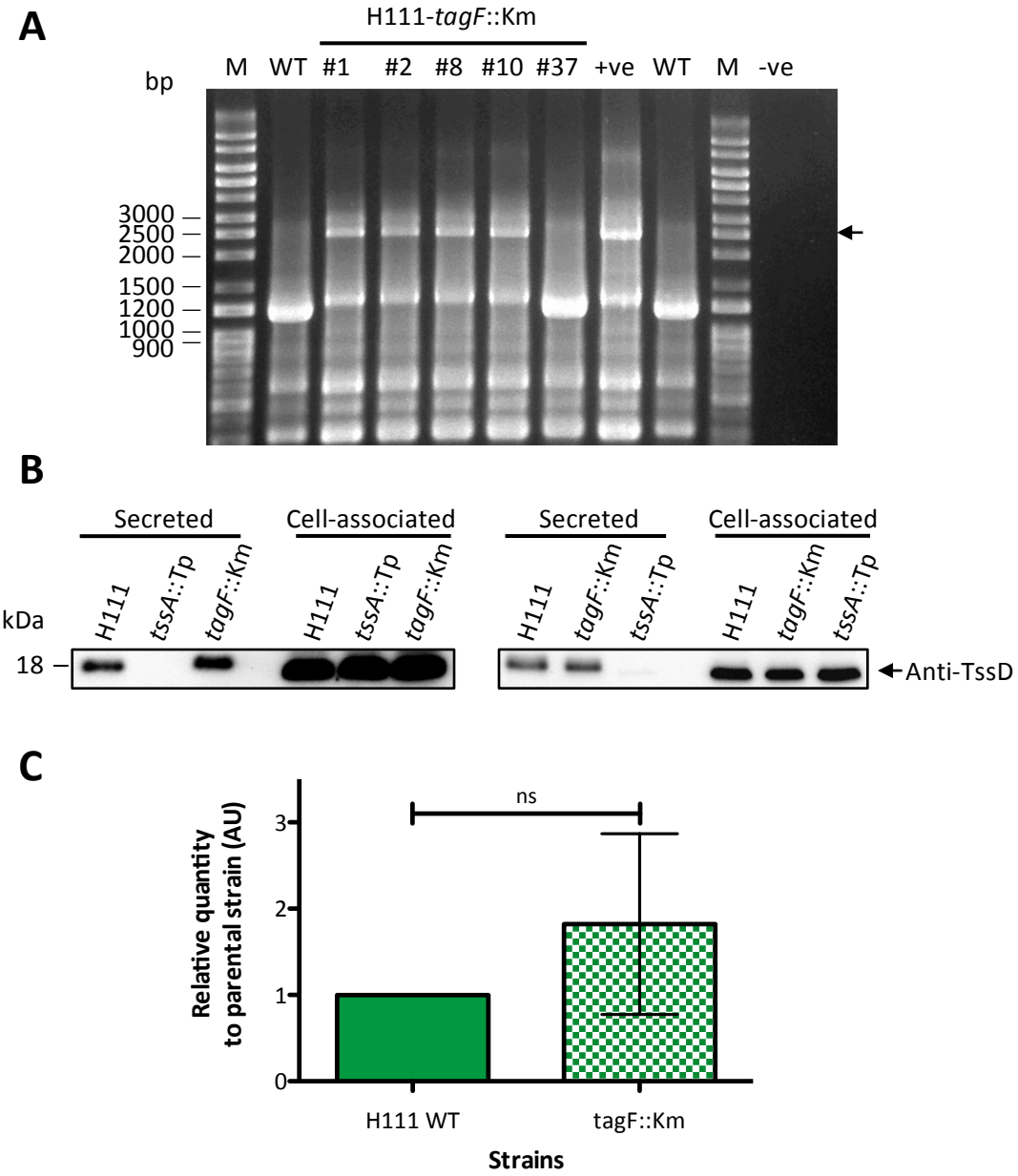

Figure 5.14 Analysis of the effect of *tagF* inactivation on TssD secretion in wild-type *B. cenocepacia* H111. *tagF* was insertionally inactivated by the kanamycin-resistance cassette in wild-type *B. cenocepacia* H111. (A) Mutants were confirmed by PCR using primers that annealed just outside of the *tagF*::Km homologous region on the genome. DNA fragments amplified were analysed following electrophoresis in a 0.8% agarose gel. Mutants were expected to give rise to a DNA fragment of ~2500 bp, indicated by the arrow. Extracellular proteins were precipitated from liquid culture supernatants of H111 wild-type, a T6SS mutant (*tssA*::Tp), and H111-*tagF*::Km. (B) Representative anti-TssD western blots demonstrating variable secretion of TssD from two independent experimental repeats. Cell-associated TssD is also shown, as indicated. The size difference between secreted and cell-associated TssD may be due to TCA precipitation treatment of the secreted protein fraction. (C) Densitometric analysis of relative difference between secreted TssD in H111 wild-type (WT) in comparison to the H111-*tagF*::Km strain. Statistical analysis performed using a one sample t-test where $p < 0.05$, $n = 5$. ns, not significant; AU, arbitrary units; +ve, $H111^{S}$-*tagF*::Km DNA template control; -ve, no DNA control; M, GeneRuler DNA ladder mix.

5.3.3 Effect of a *tagF* null allele on T6SS activity in *B. cenocepacia* H111Δc3

It was thought that H111^S contained an additional lesion(s) other that the loss of c3, as it had been shown to be less virulent than a chromosome 3-deficient strain of H111 that had been genetically manipulated to select for loss of chromosome 3, H111Δc3 (Agnoli et al., 2012). To verify that the more reproducible TssD overproduction observed in the H111^S-*tagF*::Km mutant was due to the lack of chromosome 3, rather than an unlinked genetic lesion, it was decided to construct a *tagF* insertionally inactivated mutant in H111Δc3. H111-Δc3-*tagF*::Km was successfully constructed as described in Section 5.3.2 (Figure 5.15A).

Upon comparison of TssD secretion of the H111Δc3-*tagF*::Km mutant to the parental H111Δc3 strain, it was observed that TssD secretion was slightly increased in the mutant (Figure 5.15B and 5.15C), i.e. a 1.3-fold increase to that of the wild-type, which was significant with a P value of 0.0493 (Figure 5.15D). However, the increase in TssD secretion was not as great as was anticipated, which meant that the usefulness of the H111Δc3-*tagF*::Km for effector identification was limited.

5.3.4 Investigation of the genetic lesion of *B. cenocepacia* H111^S

Evaluation of TssD secretion in the *B. cenocepacia* H111^S-*tagF*::Km and H111Δc3-*tagF*::Km mutants in comparison to their respective parental strains (Section 5.3.2 and 5.3.3) and the inconsistency between them led to the hypothesis that another genetic lesion in the H111^S strain, in combination with insertional inactivation of *tagF,* may be responsible was the reproducible increase in TssD secretion observed in the H111^S-*tagF*::Km mutant. Therefore, it was decided to sequence the entire genome of H111^S and compare it to the *B. cenocepacia* H111 reference genome sequence. This was undertaken in collaboration with the Eberl group, University of Zurich, and the genetic differences between H111 and H111^S were identified by A. Carlier. This analysis indicated over 100 genetic lesions in the H111^S strain, several of which were nucleotide insertions or deletions that produced frame shifts that were likely to result in the production of a truncated

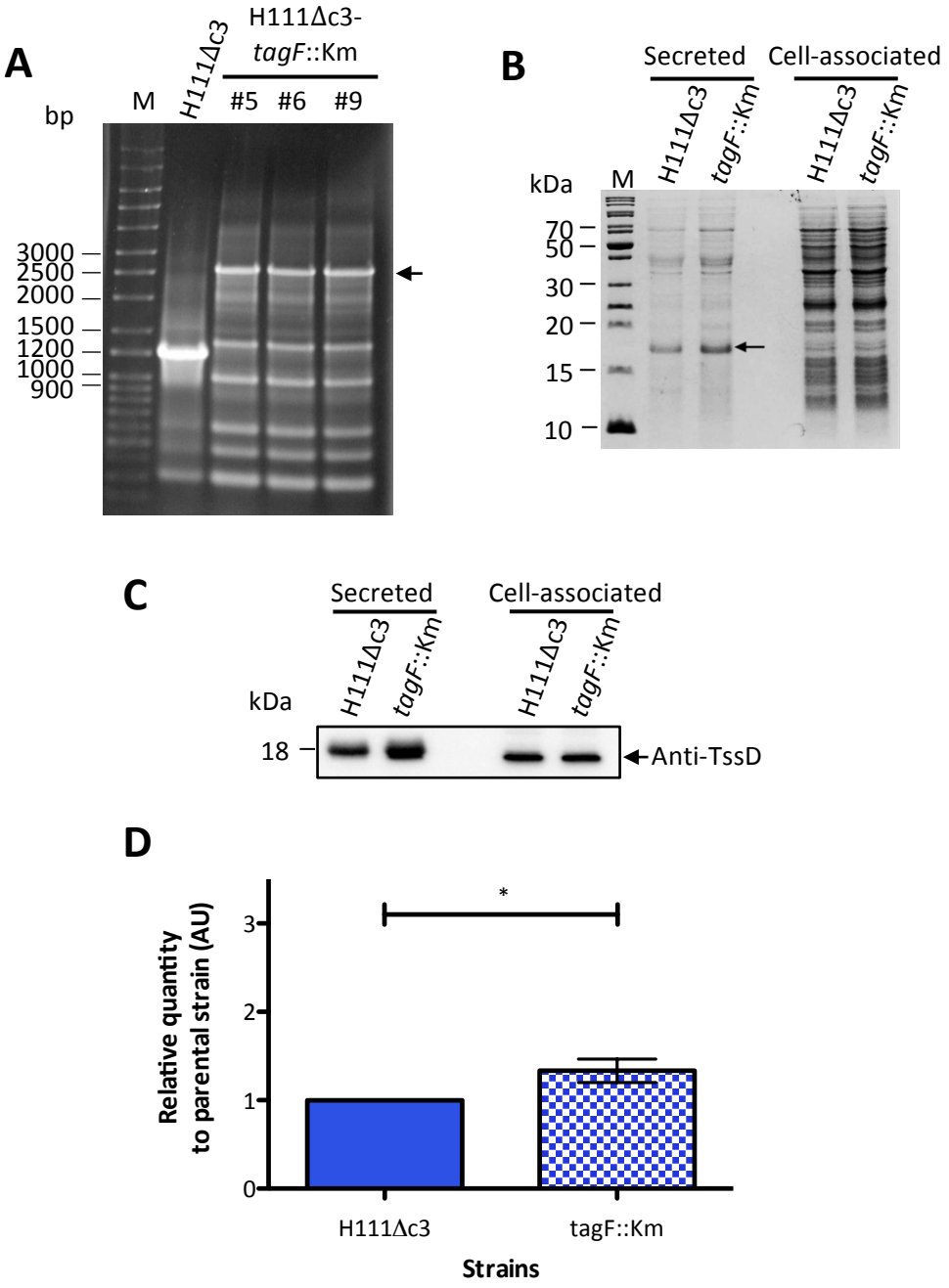

Figure 5.15 Analysis of the effect of *tagF* inactivation on TssD secretion in *B. cenocepacia* H111Δc3. *tagF* was insertionally inactivated by the kanamycin resistance cassette in the chromosome 3 deletion mutant of *B. cenocepacia* H111, H111Δc3. Mutants were confirmed by PCR using primers that annealed just outside of the *tagF*::km homologous region on the genome. DNA fragments amplified were analysed following electrophoresis in a 0.8% agarose gel (A), mutants were expected to give rise to a DNA fragment of ~2500 bp, indicated by arrow. Extracellular proteins were precipitated from liquid culture supernatants of H111Δc3 and H111Δc3-*tagF*::Km. (B) Profile of extracellular and cell-associated proteins as analysed by electrophoresis in a 15% SDS-PA gel and stained with Coomassie blue. (C) Representative anti-TssD western blot of samples from (B). (D) Densitometric analysis of relative difference between secreted TssD in H111Δc3 strain in comparison to H111Δc3-*tagF*::Km strain. n = 3, statistical analysis performed using a one sample t-test where $p < 0.05$, *, $p < 0.05$; AU, arbitrary units; M, GeneRuler DNA ladder mix.

or mistranslated form of the proteins encode by the gene (Table 5.1). This included several frameshift mutations in I35_0136, which encodes the histidine kinase CheA, involved in signal transduction in chemotaxis (Stock et al., 1988). Another such mutation occurred in I35_2333 (*wabR*), which encodes a glycosyl transferase enzyme involved in LPS lipid A core biosynthesis, which resulted in a frameshift mutation at the Arg214 codon, two thirds into the coding sequence of *wabR*. *wabR* mutants have been characterised as having LPS defects, specifically lacking the O-antigen and have a shorter lipid A core than the LPS of the wild-type strain, meaning the mutant is more sensitive to polymyxin B (Ortega et al., 2009). It was previously observed that H111^{S} had a 'rough' colony morphology, suggestive of a defect or loss of O-antigen side chain (M.S. Thomas, unpublished observations). Therefore, the *wabR* mutation was likely to account for these observations and may also account for the serum-sensitivity. However, for this study it was any potential effect that this mutation may have on T6SS activity that was important. In this refrain, it was thought that the *wabR* lesion might increase the sensitive of H111^{S} to external factors that may stimulate the T6SS.

5.3.5 Analysis of polymyxin B on the T6SS activity of *B. cenocepacia* H111

Membrane perturbations have been implicated in the activation of the T6SS, including those caused by an 'attacking' bacterium with an active T6SS (Basler et al., 2013), by the T4SS of another species and by agents capable of binding and disrupting the outer membrane, such as polymyxin B that binds to Mg^{2+}-binding sites in LPS, including those in lipid A (Moore et al., 1986; Ho et al., 2013). It was noted that the H111^{S} strain had a slight increase in TssD secretion in comparison to the wild-type H111 strain (Figure 5.13B). It was hypothesised that the effect of the LPS defect in H111^{S} may be mimicked in the wild-type strain by polymyxin B challenge, resulting in increased activation of the T6SS in this strain, which can be exaggerated by the inactivation of *tagF*. A liquid culture of wild-type H111 was challenged with a subinhibitory concentration of polymyxin B, and the extracellular proteins in the spent culture supernatant were extracted and analysed for the presence of TssD (Figure 5.16). In parallel, a *B. cenocepacia* H111 *waaL* mutant that

Table 5.1 Mutations present in *B. cenocepacia* H111^S that cause significant alterations to the predicted protein product of the mutated gene.

Mapping[a]	Reference Position	Type	Length	Reference	Allele	Coding region change	Amino acid change	Comments[b]
Chromosome 1								
HG938370 mapping	152181	Insertion	1	-	G	CDN58659.1:c.81_82insG	CDN58659.1:p.Ala28fs	Frame shift in I35_0136, which codes for a CheA histidine kinase, part of a chemotaxis operon located just upstream of the flhDC operon.
HG938370 mapping	152243	Insertion	1	-	G	CDN58659.1:c.143_144insG	CDN58659.1:p.Thr48fs	
HG938370 mapping	152248	Insertion	3	-	CCG	CDN58659.1:c.148_149insCCG	CDN58659.1:p.Pro50delinsProAla	
HG938370 mapping	152346	Insertion	1	-	G	CDN58659.1:c.246_247insG	CDN58659.1:p.Gly83fs	
HG938370 mapping	152446	Insertion	1	-	A	CDN58659.1:c.346_347insA	CDN58659.1:p.Pro116fs	
HG938370 mapping	1382473	Insertion	1	-	G	CDN59806.1:c.1327_1328insG	CDN59806.1:p.Arg443fs	Frame shift in I35_1283, codes for putative phosphatase (BCAL1387 homologue)
HG938370 mapping	1382516	Deletion	1	C	-	CDN59806.1:c.1371delC	CDN59806.1:p.Ser457fs	
HG938370 mapping	1382521	Insertion	1	-	G	CDN59806.1:c.1375_1376insG	CDN59806.1:p.*459fs	
HG938370 mapping	1382596	Insertion	1	-	G	CDN59807.1:c.58_59insG	CDN59807.1:p.Arg20fs	Frame shift in I35_1284, codes hypothetical protein.
HG938370 mapping	1382613	Insertion	1	-	G	CDN59807.1:c.75_76insG	CDN59807.1:p.His26fs	
HG938370 mapping	1382627	SNV	1	C	G	CDN59807.1:c.90C>G	CDN59807.1:p.Cys30Trp	
HG938370 mapping	1382633	Deletion	1	C	-	CDN59807.1:c.96delC	CDN59807.1:p.Arg32fs	
HG938370 mapping	1382638	Insertion	1	-	C	CDN59807.1:c.100_101insC	CDN59807.1:p.Ala34fs	
HG938370 mapping	1382654	Insertion	1	-	G	CDN59807.1:c.116_117insG	CDN59807.1:p.Val39fs	
HG938370 mapping	1382720	Insertion	1	-	G	CDN59807.1:c.182_183insG	CDN59807.1:p.Ala61fs	
HG938370 mapping	1382913	Insertion	2	-	GC	CDN59807.1:c.375_376insGC	CDN59807.1:p.Cys126fs	
HG938370 mapping	1382919	Insertion	1	-	G	CDN59807.1:c.381_382insG	CDN59807.1:p.Gly128fs	
HG938370 mapping	1541619	Insertion	1	-	C	CDN59943.1:c.1281_1282insG	CDN59943.1:p.Arg428fs	Frame shift in I35_1420, codes for PE_PGRS family protein, putative lipoprotein (BCAL1523)
HG938370 mapping	2533030	Deletion	10	CGCCAGCGCT	-	CDN60856.1:c.642_651delAGCGCTGGCG	CDN60856.1:p.Arg214fs	Frame shift in I35_2333, codes for WabR, a glycosyl transferase involved in lipid A core biosynthesis. 10nt deletion results in a frame shift at residue 214 (out of 370).
Chromosome 2								
HG938371 mapping	2636236	Insertion	1	-	G	CDN64153.1:c.983_984insG	CDN64153.1:p.Pro328fs	Frame shift in I35_6317, codes for hemagglutinin domain-containing protein (BCAM2418 homologue).
HG938371 mapping	2636252	Insertion	1	-	C	CDN64153.1:c.999_1000insC	CDN64153.1:p.Ser334fs	

[a] GenBank ID for reference sequence used in variant analysis, indicating which chromosome the mutation was mapped to.
[b] Comments indicating name of gene that corresponds to the region mutated, and information regarding function of the protein if known.
Data collection and interpretation courtesy of A. Carlier, Eberl group, University of Zurich.

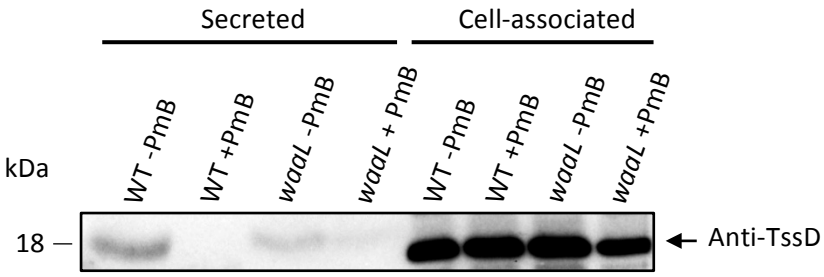

Figure 5.16 Effect of outer membrane alternations on the T6SS activity of *B. cenocepacia* H111. Wild-type H111 (WT) and a *waaL* LPS-defective mutant were grown in LB medium with (+) or without (-) a sub-lethal dose of polymyxin B (600U/mL) (PmB). Extracellular proteins were precipitated from spent culture supernatants and analysed for the presence of TssD by anti-TssD western blotting (left). Cell-associated proteins were also analysed (right). Samples were loaded as indicated. Size difference between secreted and intracellular TssD may be due to TCA precipitation treatment of secreted protein fraction. Labelled arrow indicates detection of TssD, and expected molecular mass of the protein is indicated on the left.

lacked the LPS O-antigen but retained a truncated lipid A core (Ortega et al., 2009) was also screened for T6SS activity and the effect of challenging with polymyxin B (Figure 5.16). Unexpectedly, challenge by polymyxin B appeared to decrease TssD secretion in both wild-type H111 and the *waaL* mutant. Furthermore, secreted TssD was detected in a similar abundance in the culture supernatant from the *waaL* mutant and wild-type, together suggesting that that defects in the LPS or challenge with polymyxin B does not cause an increase in T6SS activity in *B. cenocepacia* H111. Note, however that this experiment was only performed once, so for proper evaluation of the effect of LPS alterations on T6SS activity it needs to be repeated, and other LPS mutants included, including a clean *wabR* that is other isogenic with the wild-type parent, unlike the situation with H111^{S}.

5.3.6 Re-introduction of chromosome 3 into H111^{S}

Although it was not possible to establish the genetic reason why the H111^{S} *tagF* mutant exhibited higher T6SS activity than H111 or H111Δc3 tagF mutants it was decided to re-introduce chromosome 3 (termed pC3 from herein) into the H111^{S}-*tagF*::Km mutant, to return a full complement of chromosomes into the mutant, which would mean any potential effector gene on the third chromosome could now be expressed in a T6SS-proficient background. This was undertaken in collaboration with the Eberl group, University of Zurich by K. Agnoli, using a previously published procedure (Agnoli et al., 2014). The strategy involved re-introduction of pC3 into H111^{S} and then subsequent transfer of the *tagF*::Km allele, rather than direct introduction of pC3 into H111^{S}-*tagF*::Km, as a H111^{S} control strain containing a full complement of chromosomes was also required. To do this, a gene encoded on pC3, *gabD* (I35_7400) was cloned into the suicide vector pSHAFT2. This plasmid was then introduced into H111 wild-type and its integration into chromosome 3, by a single crossover homologous recombination event with the genomic copy of *gabD,* was selected for by the acquisition of chloramphenicol resistance, to generate the strain H111-pC3-*gabD*::pSHAFT2. This strain was then used to mobilise pC3 into a rifampicin-resistant version of H111^{S} by tri-parental mating with the *E. coli* helper strain MM294/pRK2013. H111^{S} exconjugates that had

acquired the mobilised pC3 (pC3-*gabD*::pSHAFT2) were obtained by selection for rifampicin and chloramphenicol-resistance, generating the strain H111^{S}/pC3. To verify that candidate H111^{S}/pC3 strains were indeed derived from H111^{S} and not spontaneous rifampicin-resistant donor H111-pC3-*gabD*::pSHAFT2 strains, candidates were sequenced using primers that amplified a region of the *wabR* gene that contained a segment of 10 nucleotides that were present in wild-type H111 strain and but not in the H111^{S} strain. The integrity of the pC3 insert was also verified by size analysis of specific amplicons that were PCR amplified from the H111^{S}/pC3 candidates (data not shown), and their ability to grow on minimal media containing uracil as a carbon source, as only strains containing chromosome 3 can utilise this for growth.

An insertional inactivation mutant of *tagF* was then constructed in the H111^{S}/pC3 strain. Due to regions of homology between the pSHAFT-*tagF*::Km allelic replacement vector and pSHAFT2 inserted in the mobilised pC3 it was required to clone the *tagF*::Km allele into an alternative suicide vector that lacked regions of homology to pSHAFT2. This was achieved by transferring a ~2200bp DNA fragment encoding *tagF*::Km as a HindIII restriction fragment from pBBR1MCS-*tagF*::Km into the corresponding restriction site of pEX18TpTer-*pheS*, to successfully generate the ~6400 bp plasmid pEX18TpTer-*pheS*-*tagF*::Km (Figure 5.17A). This allelic replacement vector was introduced into H111^{S}/pC3 by conjugation and recombinants containing a chromosomally integrated plasmid were selected for their increased kanamycin-resistance. To identify double crossover recombinants, kanamycin-resistant colonies were checked for sensitivity to trimethoprim (the trimethoprim-resistance marker is contained on the pEX18TpTer-*pheS* vector). H111^{S}-*tagF*::Km/pC3 candidates that were kanamycin-resistant but trimethoprim-sensitive were screened by PCR, as described in Section 5.3.2, and the resulting amplified DNA was analysed by electrophoresis to determine DNA fragment size, verifying the candidates as *tagF*::Km mutants (Figure 5.17B).

The T6SS activity of the H111^{S}-*tagF*::Km/pC3 strain was then investigated by analysis of TssD secretion by western blotting and image quantification (Figure 5.18). This indicated that TssD was more abundant in culture supernatants

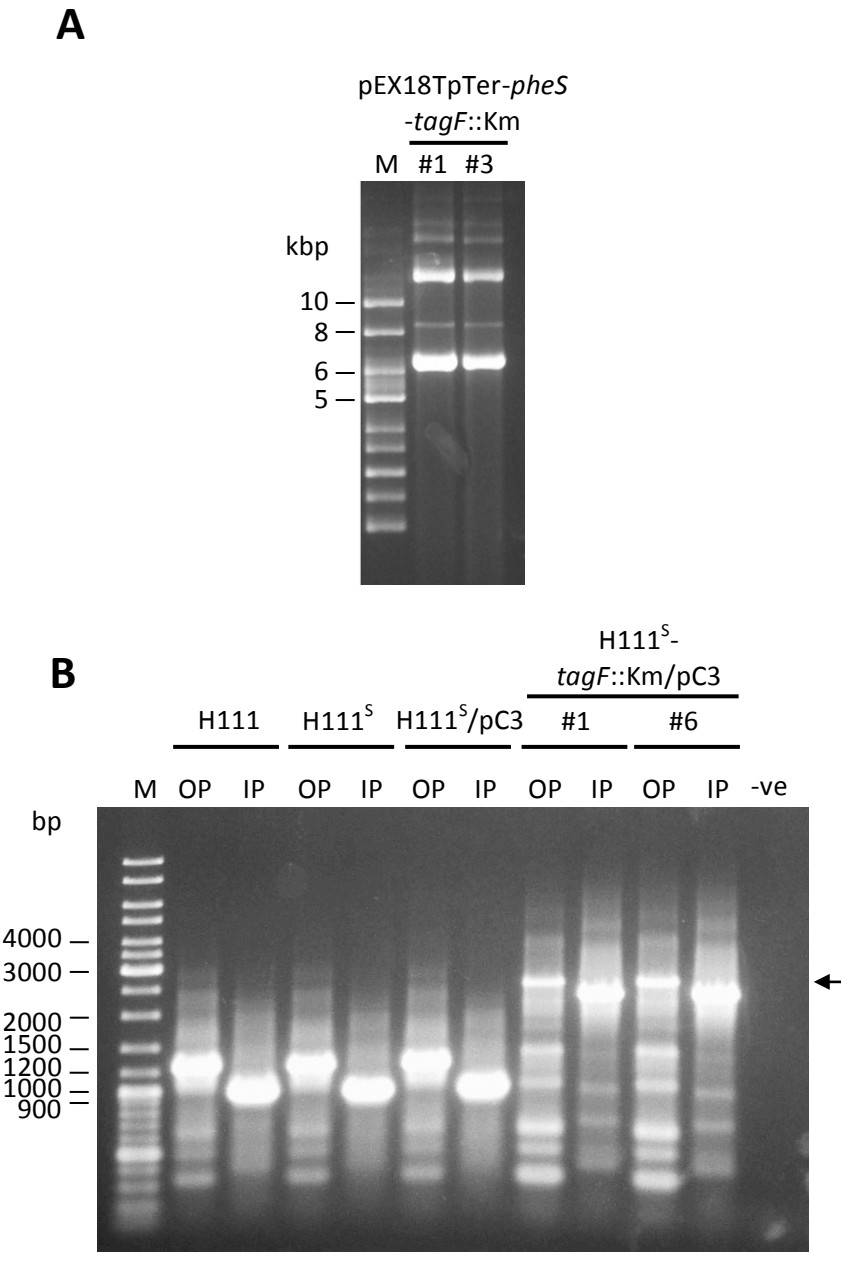

Figure 5.17 Construction of a H111^S-*tagF*::Km/pC3 mutant. Chromosome 3 was re-introduced into H111^S to generate H111^S/pC3. pEX18TpTer-*pheS*-*tagF*::Km (shown in A) was then generated by transferring the *tagF*::Km allele as a HindIII restriction fragment from pBBR1MCS-*tagF*::Km into the corresponding restriction site in pEX18TpTer-*pheS.* pEX18TpTer-*pheS*-*tagF*::Km was used to generate a *tagF* insertional inactivation mutant following its introduction into H111^S/pC3 and selecting for double crossover recombinants. (B) Electrophoretic analysis of DNA fragments from a PCR screen used to verify candidate H111^S-*tagF*::Km/pC3 mutants, using primers that annealed outside (OP) and inside (IP) the *tagF*::Km homologous region. Candidates that amplified a DNA fragment 1260 bp larger than the wild-type strain were considered true mutants, i.e. 2700 bp (indicated by arrow) compared to 1260 bp. Lanes labelled accordingly. M, Supercoiled DNA ladder or GeneRuler DNA ladder mix; -ve, no DNA negative control.

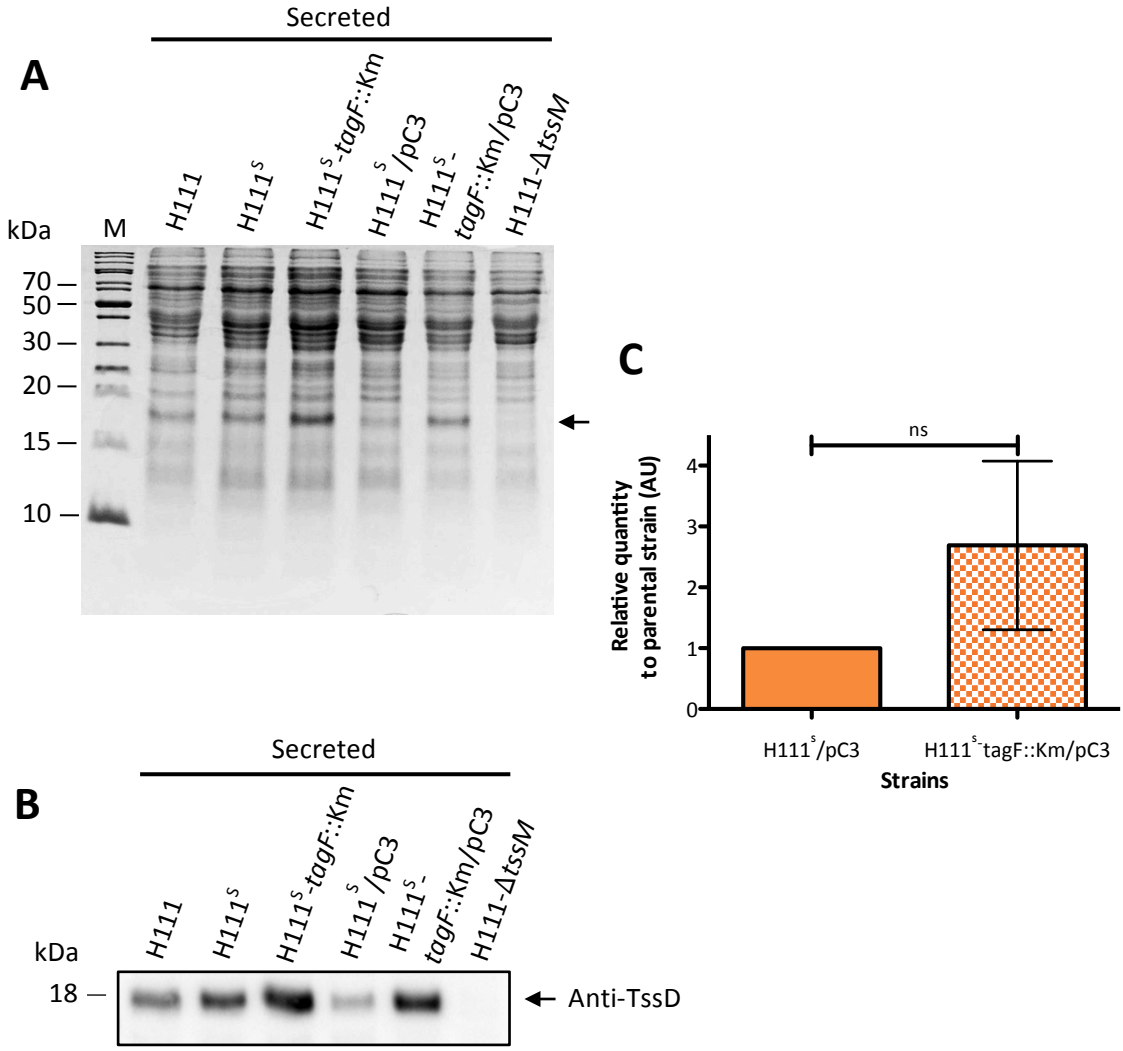

Figure 5.18 Analysis of the effect of *tagF* inactivation on TssD secretion in *B. cenocepacia* H111^S/pC3. *tagF* was insertionally inactivated by the kanamycin resistance cassette in *B. cenocepacia* H111^S/pC3. Extracellular proteins were precipitated from liquid culture supernatants of H111^S/pC3 and H111^S-*tagF*::Km/pC3 and compared to H111^S and H111^S-*tagF*::Km without chromosome 3 and wild-type H111 and a Δ*tssM* mutant. (A) Protein profile of extracellular proteins analysed by electrophoresis in a 15% SDS-PA gel and stained with Coomassie blue. (B) Representative anti-TssD western blot of secreted protein samples from (A). (C) Densitometric analysis of relative difference between secreted TssD in the H111^S/pC3 strain in comparison to the H111^S/pC3-*tagF*::Km strain. Statistical analysis performed using a one sample t-test where p <0.05, n = 2. *, p<0.05; AU, arbitrary units.

derived from in the *tagF*::Km mutant in comparison to the parental H111^{S}/pC3 strain. However, variation in the increase of secreted TssD was observed again between repeat experiments. Therefore, the difference was not statistically significant. Interestingly, it was also observed that TssD secretion in H111^{S}/pC3 was reduced in comparison to the H111^{S} strain lacking chromosome 3. However, as TssD secretion was still unreliable in the H111^{S}-*tagF*::Km/pC3 mutant it was decided to investigate an alternative and potentially more reliable way to increase T6SS expression in *B. cenocepacia*.

5.4 Investigation of the role of AtsR in T6SS-regulation in *B. cenocepacia* H111

Previous work has identified AtsR, a RetS-like inner membrane-anchored hybrid sensor-kinase that acts through the response regulator AtsT, as a transcriptional regulator of T6SS genes in *B. cenocepacia* (Aubert et al., 2008; Khodai-Kalaki et al., 2013). Briefly, the AtsR histidine kinase domain (HK) is auto-phosphorylated upon receiving an unknown signal. A receiver domain located C-terminal to the HK domain can be phosphorylated by phosphate transfer from the phosphorylated His245 residue in the HK domain. Alternatively, the phosphate from His245 can also be transferred to an aspartate residue (Asp208) on the response regulator, AtsT, to modulate its activity as a transcriptional repressor (Khodai-Kalaki et al., 2013) (Figure 5.1). Inactivation of *atsR* (and *atsT*) in K56-2 leads to hypersecretion of TssD into the culture supernatant, and formation of actin protrusions in macrophages infected with this mutant, which otherwise has very little T6SS activity (Aubert et al., 2008; Khodai-Kalaki et al., 2013). The model *B. cenocepacia* strain, H111, contains an *atsR* orthologue that encodes a 606 amino acid protein that is near identical to that of the K56-2 strain, only 8 amino acids are different. The critical phosphorylated residues identified by Aubert and colleagues remain unchanged. Therefore, it was decided to evaluate the effect of deletion of *atsR* in the *B. cenocepacia* H111 strain, which has been shown to have a higher basal level of T6SS activity than the K56-2 strain (Section 4.5.1), as a further increase in T6SS activity in strain H111 may help to facilitate effector identification.

5.4.1 Construction of an allelic replacement vector for deletion of *atsR*

For the generation of an in-frame deletion mutant in *atsR* an allelic replacement vector based on pEX18TpTer-*pheS* was constructed (Figure 5.19). The Δ*atsR* allele used to construct this plasmid was generated by splice overlap extension (SOE) PCR. The principle of SOE-PCR is illustrated in Figure 5.20.

For the generation of the Δ*atsR* DNA fragment, Δ*atsR*-AB DNA fragment was amplified from H111 genomic DNA using primers AtsRForAXbaI and AtsRRevIP-B,

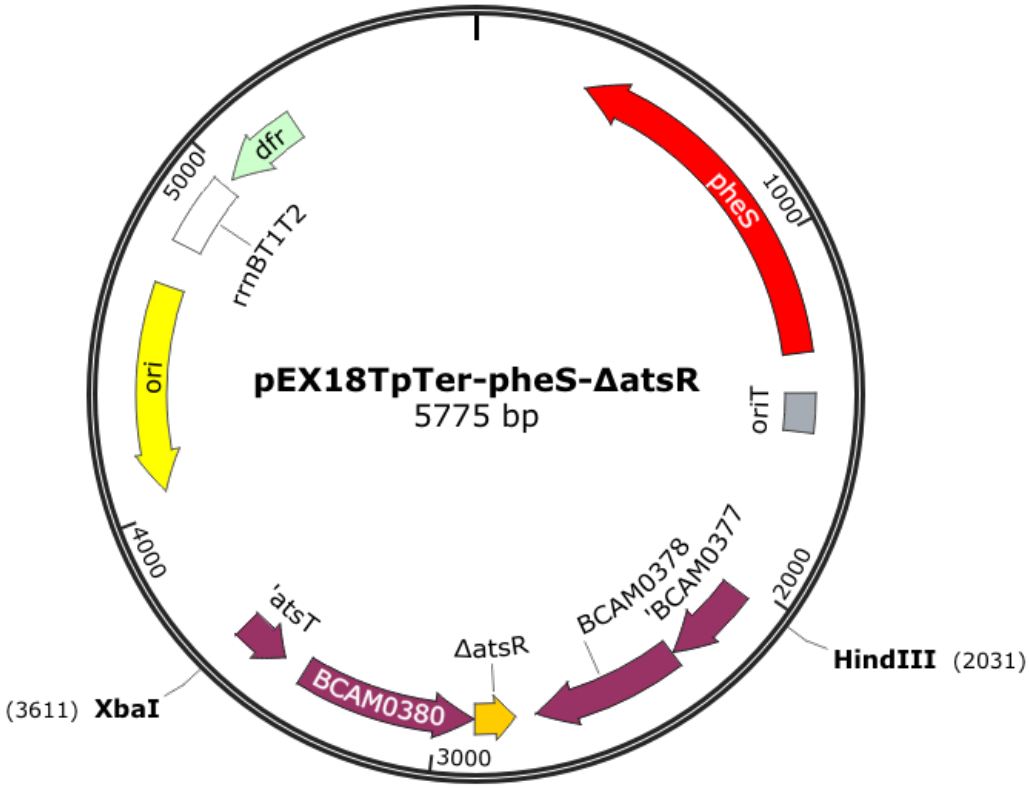

Figure 5.19 Plasmid map for the Δ*atsR* allelic replacement vector pEX18TpTer-*pheS*-Δ*atsR*. Key features such as the *pheS* gene and the Δ*atsR* allele are indicated. Restriction sites XbaI and HindIII used to clone the Δ*atsR* allele into the vector are also indicated.

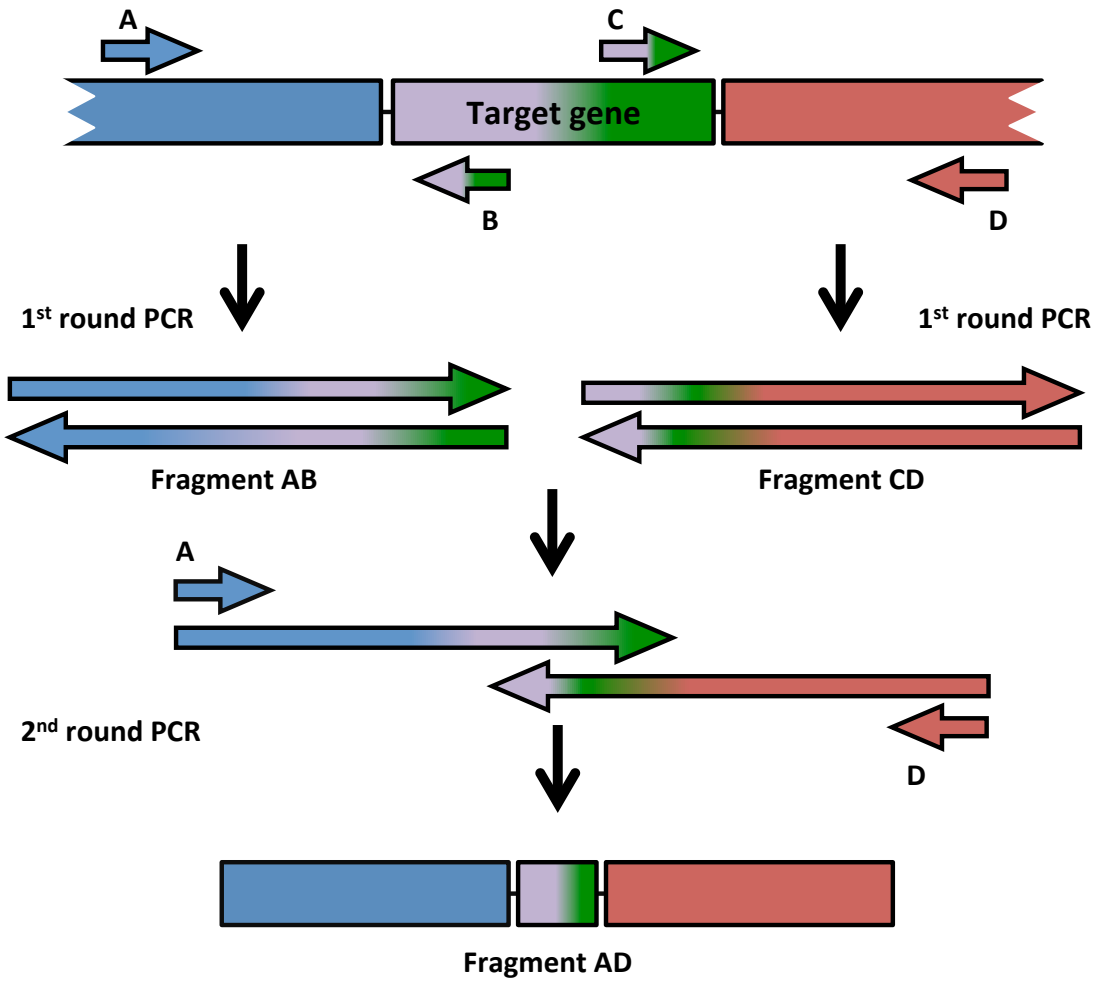

Figure 5.20 Principle of splice overlap extension PCR. Generation of an in-frame deletion allele can be achieved by using splice overlap extension PCR (SOE-PCR) to splice together two DNA fragments either side of the gene that is to be deleted. To do this, each fragment, termed fragment AB and CD, are amplified separately from genomic DNA using primer pairs A and B and C and D in the first round PCR step. Primer A anneals ~500 bp upstream of the target gene and Primer D anneals ~500 bp downstream of target gene. Primers B and C have sequences 5' to the 20 bp annealing region that are complementary to the end of the other fragment that is to be fused. Both primers are therefore complementary along their entire length. Thus, following amplification, amplicon AB contains ~500 bp of DNA corresponding to upstream genomic sequences that flank the target gene followed by the first few codons of the target gene fused to the final few codons of the same gene. Amplicon CD contains the same first few codons of the target gene fused to the final few codons of the same gene followed by ~500 bp of flanking DNA downstream of the target gene. Fragment AB and CD are combined in an equimolar concentration and used as template DNA in a second round PCR step using primer pair A and D. This allows annealing of the overlapping regions common to fragments AB and CD and thus amplification of the spliced AB CD fragments, generating the fragment AD. Primers A and D have 5' extensions which incorporate restriction sites into the product to allow directional cloning of the deletion allele (fragment AD) into an appropriate suicide vector for generating markerless in-frame mutants, such as pEX18TpTer-*pheS*.

and the Δ*atsR*-CD fragment was amplified similarly using primers AtsRForIP-C and AtsRRevDHindIII, generating 801 bp and 789 bp DNA fragments, respectively (Figure 5.21A). Amplicon Δ*atsR*-AB contained 719 bp upstream sequence of *atsR* followed by codons 1-17 of *atsR* fused to the end *atsR* codons 597-605. Amplicon Δ*atsR*-CD contained the last 10 codons of *atsR* (i.e. codons 597-605) proceeded by 737 bp of DNA located downstream of *atsR* in the H111 genome. Fragments Δ*atsR*-AB and Δ*atsR*-CD were then combined in an equal molar ratio and used as the template DNA in a second round of PCR using primers AtsRForAXbaI and AtsRRevDHindIII to splice the two fragments together, to give Δ*atsR*. Several annealing temperatures were tested for this reaction, and all produced a similar low yield of product at the expected size of 1548 bp, but with additional non-specific products at 850 bp and 3000 bp (Figure 5.21B). Therefore, all three PCR products were pooled and the 1548 bp fragment excise by gel excision. This was then cloned into pEX18TpTer-*pheS* as an XbaI-HindIII restriction fragment, to generate pEX18TpTer-*pheS*-Δ*atsR*. Positive clones were identified by PCR screening using vector specific primers M13for and M13revBACTH (Figure 5.21C). Clones 5 and 6 produced a PCR fragment of the expected size of 1691 bp, so were subjected to plasmid minipreparation to evaluate the plasmid sizes (Figure 5.21D). Both produced plasmids of the expected size, 5729 bp, and were confirmed by DNA sequencing.

5.4.2 Generation of an *atsR* deletion mutant in *B. cenocepacia* H111 and K56-2

The allelic replacement vector pEX18TpTer-*pheS*-Δ*atsR* was introduced into *B. cenocepacia* H111 and K56-2 wild-type strains by conjugation to enable recombination between the homologous DNA sequence contained in the vector and the genome, and single crossover recombinants were selected based on their resistance to trimethoprim. Single recombinants were then subjected to cPhe counter-selection on M9 agar containing 0.1% cPhe.

To identify H111 *atsR* mutants, 25 cPhe-resistant colonies were screened with primers AtsRFor-OP and AtsRRev-OP that annealed to genomic DNA outside of

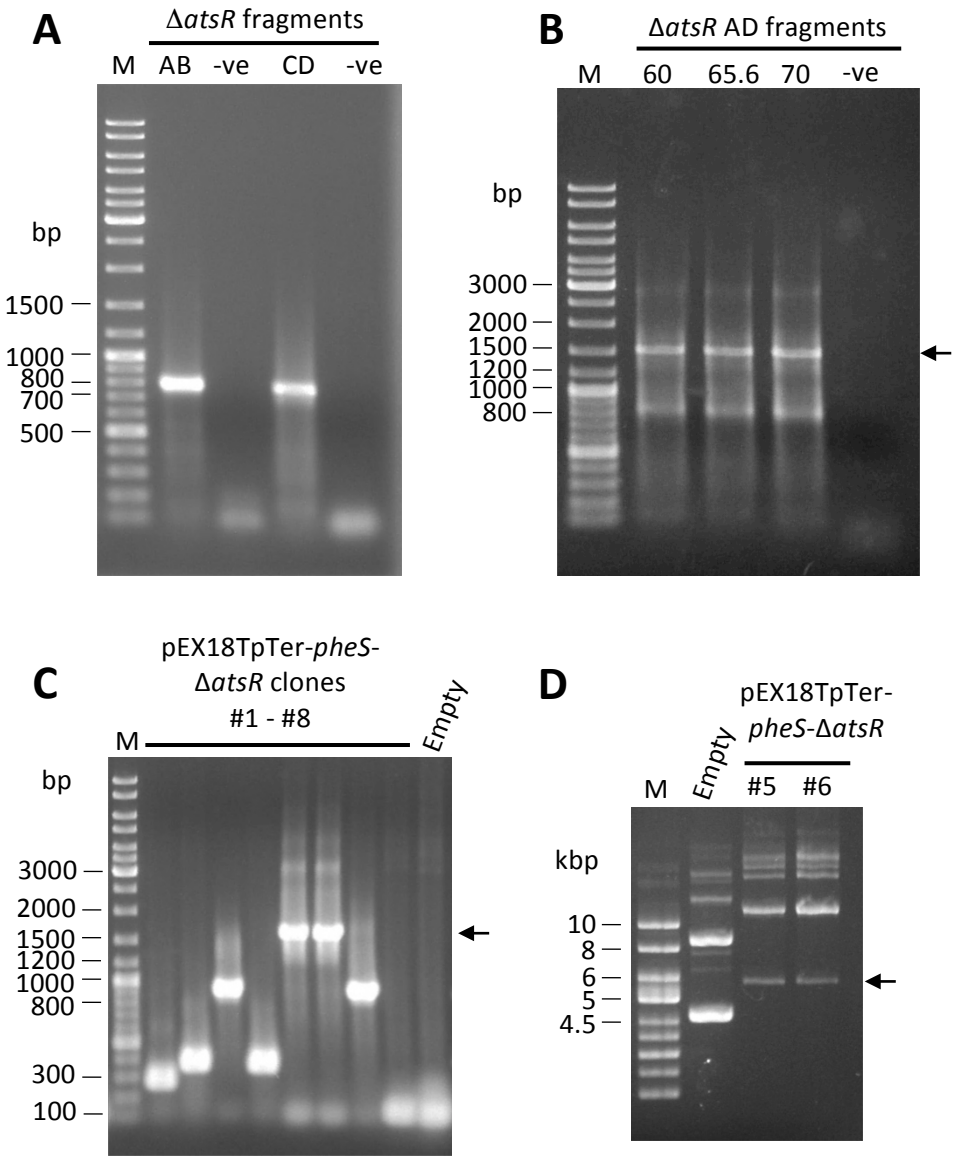

Figure 5.21 Construction of pEX18TpTer-*pheS*-Δ*atsR*. (A) Amplification of Δ*atsR*-AB and -CD fragments as visualised in a 0.8% agarose gel. (B) These where then spliced together in a second PCR reaction using the indicated annealing temperatures, to generate the 1548 bp Δ*atsR* allele as visualised in a 0.8% agarose gel. (C) Δ*atsR* was then ligated into pEX18TpTer-*pheS* and candidate plasmids were screened using vector specific primers, as visualised in a 0.8% agarose gel. Positive clones produced a 1691 bp fragment as indicated by the arrow. (D) Plasmids giving rise to a product of the expected size were subjected to plasmid minipreparation and analysed by electrophoresis in a 0.8% agarose gel. The arrow indicates the expected plasmid size of 5729 bp. M, DNA ladder mix or Supercoiled DNA ladder; -ve, no DNA negative control.

the Δ*atsR* homology region contained within the vector (Figure 5.22A). Δ*atsR* mutants were expected to give rise to a shorter fragment (1734 bp) than the wild-type strain (3471 bp). From this initial screen, candidates 16 and 24 were subjected to colony purification on M9 plates containing cPhe and then rescreened using the outside annealing primers (Figure 5.22B) and vector-specific primers pEX18Tpfor and pEX18Tprev (Figure 5.22C), to indicate the presence or absence of the vector within the genome. Both 16 and 24 contained the correct sized Δ*atsR* fragment but 24 also screened positive for the vector region whereas 16 did not, indicating 16 was a true Δ*atsR* mutant.

For mutagenesis of K56-2, candidates where subjected to the above screening procedure, but trouble-shooting was required to enable amplification of fragments from the *atsR* locus. This included dilution of the template DNA and using a high fidelity DNA polymerase (KOD). Candidate 1 was verified as a true Δ*atsR* mutant (Figure 5.23). Note, the K56-2-Δ*atsR* was made as a control for the H111-Δ*atsR* mutant, to ensure that inactivation of *atsR* in this manner gave the same increase in T6SS as observed previously (Aubert et al., 2008).

5.4.3 Analysis of the T6SS activity of *B. cenocepacia atsR* deletion mutants

To investigate whether the disruption of *atsR* resulted in a sufficient increase in T6SS activity in *B. cenocepacia* to be beneficial in downstream applications, extracellular proteins were precipitated from liquid cultures of both H111-Δ*atsR* and K56-2-Δ*atsR*, and compared to respective parental strains after SDS-PAGE and visualisation with Coomassie blue staining. The resulting analysis indicated an increase in the abundance of an 18 kDa and 15 kDa protein in the secreted fraction of the H111-Δ*atsR* mutant in comparison to wild-type H111 (Figure 5.24A). Similarly, an 18 kDa protein was more abundant in the secreted fraction of K56-2-Δ*atsR* than wild-type K56-2, and this difference was greater than that seen in the H111 strains. Immuno-detection of TssD verified that the over produced 18 kDa protein in both Δ*atsR* mutant strains was TssD (Figure 5.24B). Densitometric quantification of the level of TssD present in the secreted fraction

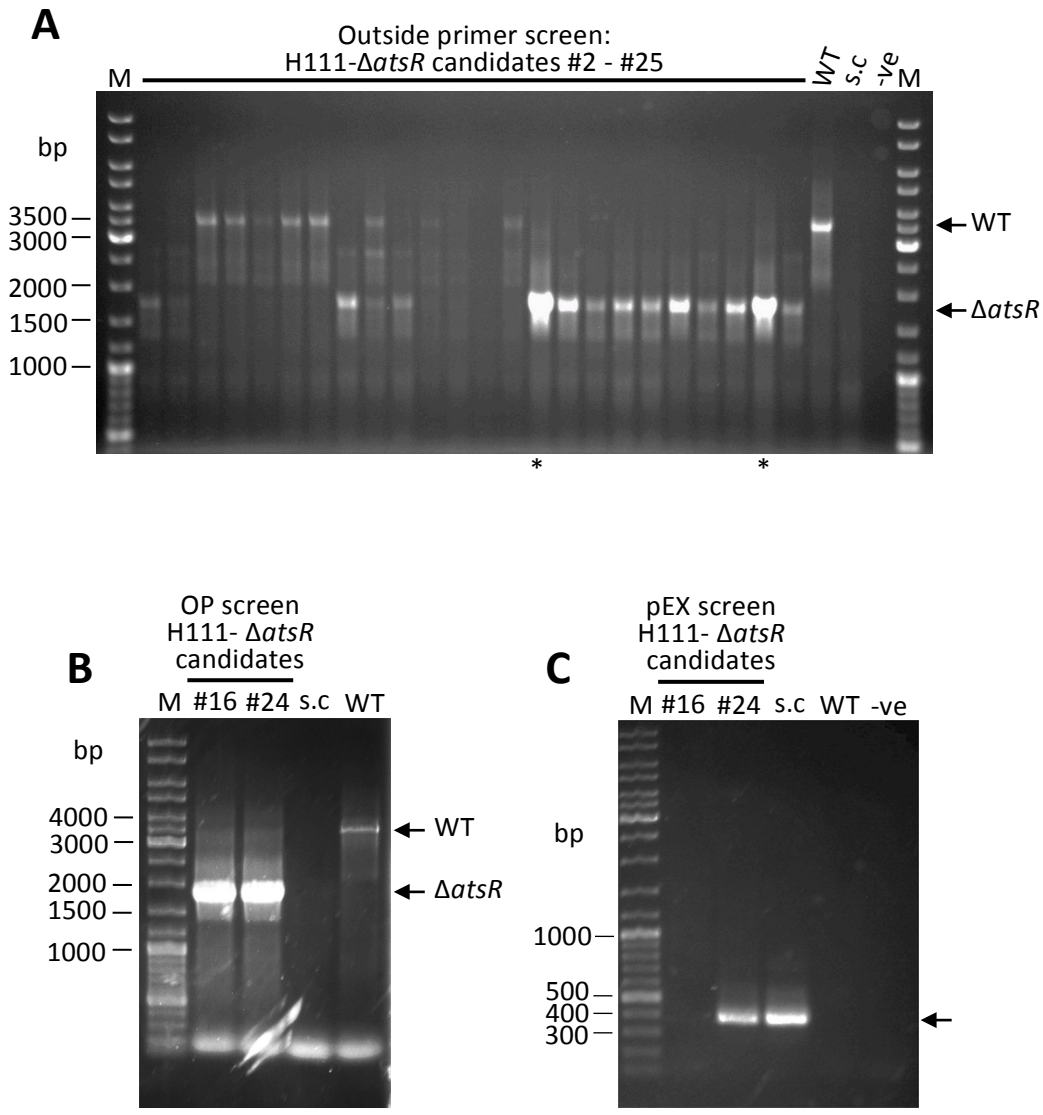

Figure 5.22 Construction of a *B. cenocepacia* H111 Δ*atsR* mutant. (A) Following cPhe counter-selection, candidate H111-Δ*atsR* mutants were screened using outside primers annealing to regions outside of the *atsR* homology region in the genome, and visualised following electrophoresis in a 0.8% agarose gel. The wild-type (WT) was expected to give rise to a 3471 bp DNA fragment and potential mutants a 1734 bp DNA fragment, shown by arrows with indicated labels. Asterisks indicate two candidates subjected to further cPhe counter-selection and colony purification. (B) Rescreen of candidates 16 and 24 with outside primers (OP), as analysed by DNA gel electrophoresis. (C) PCR screen of same candidates with primers specific to the pEX18TpTer-*pheS* vector. Mutants still containing the vector backbone produced a 300 bp DNA fragment, indicated by the arrow. M, GeneRuler DNA ladder mix; s.c, single crossover recombinant control; -ve, no DNA negative control.

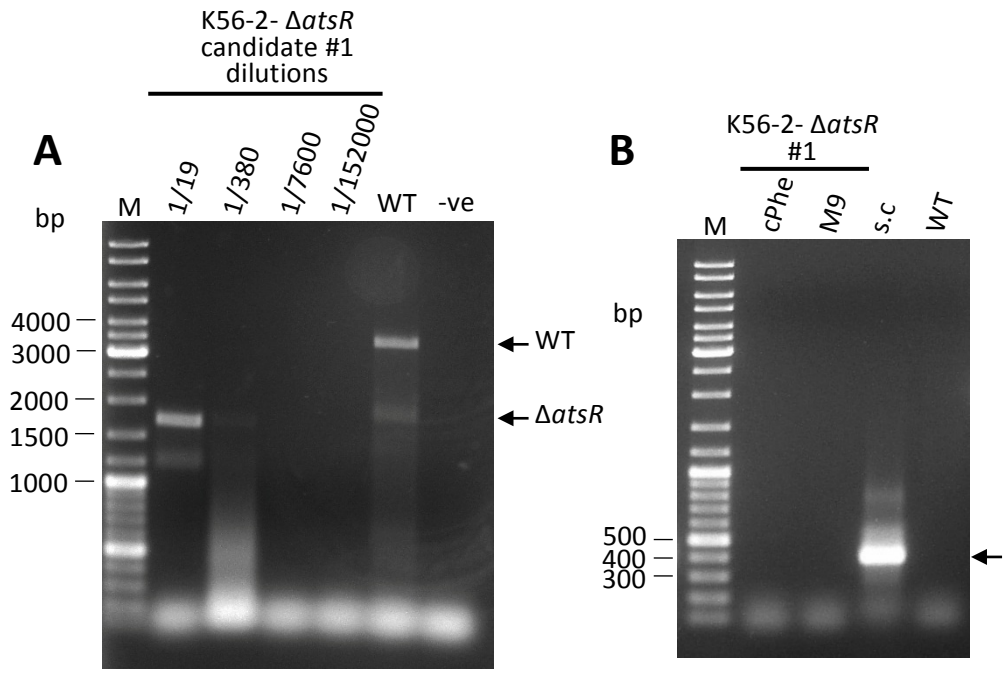

Figure 5.23 Identification of a *B. cenocepacia* K56-2 Δ*atsR* mutant. K56-2 single crossover recombinants containing chromosomally integrated pEX18pTer-*pheS*-Δ*atsR* were counter-selected with cPhe. Candidate H111-Δ*atsR* mutants were screened using outside primers annealing to regions outside of the *atsR* homology region in the genome, using a series of 20-fold serial dilutions of boiled lysate for template DNA for the reaction. (A) 0.8% agarose gel electrophoretic analysis of PCR fragments amplified from candidate K56-2-Δ*atsR* mutant #1. Δ*atsR* (1734 bp) and wild-type (WT) (3471 bp) amplicons are indicated by the labelled arrows. Boiled lysates were made from K56-2-Δ*atsR* candidate #1 after colony purification on minimal agar with (cPhe) and without (M9) cPhe as template DNA. (B) PCR screen of K56-2-Δ*atsR* candidate #1 using pEX18TpTer-*pheS* vector primers, with the template DNA used as indicated above the lanes. Strains still containing the vector backbone were expected to give rise to a 397 bp DNA fragment, indicated by the arrow. M, GeneRuler DNA ladder mix; s.c, single crossover recombinant control; -ve, no DNA negative control.

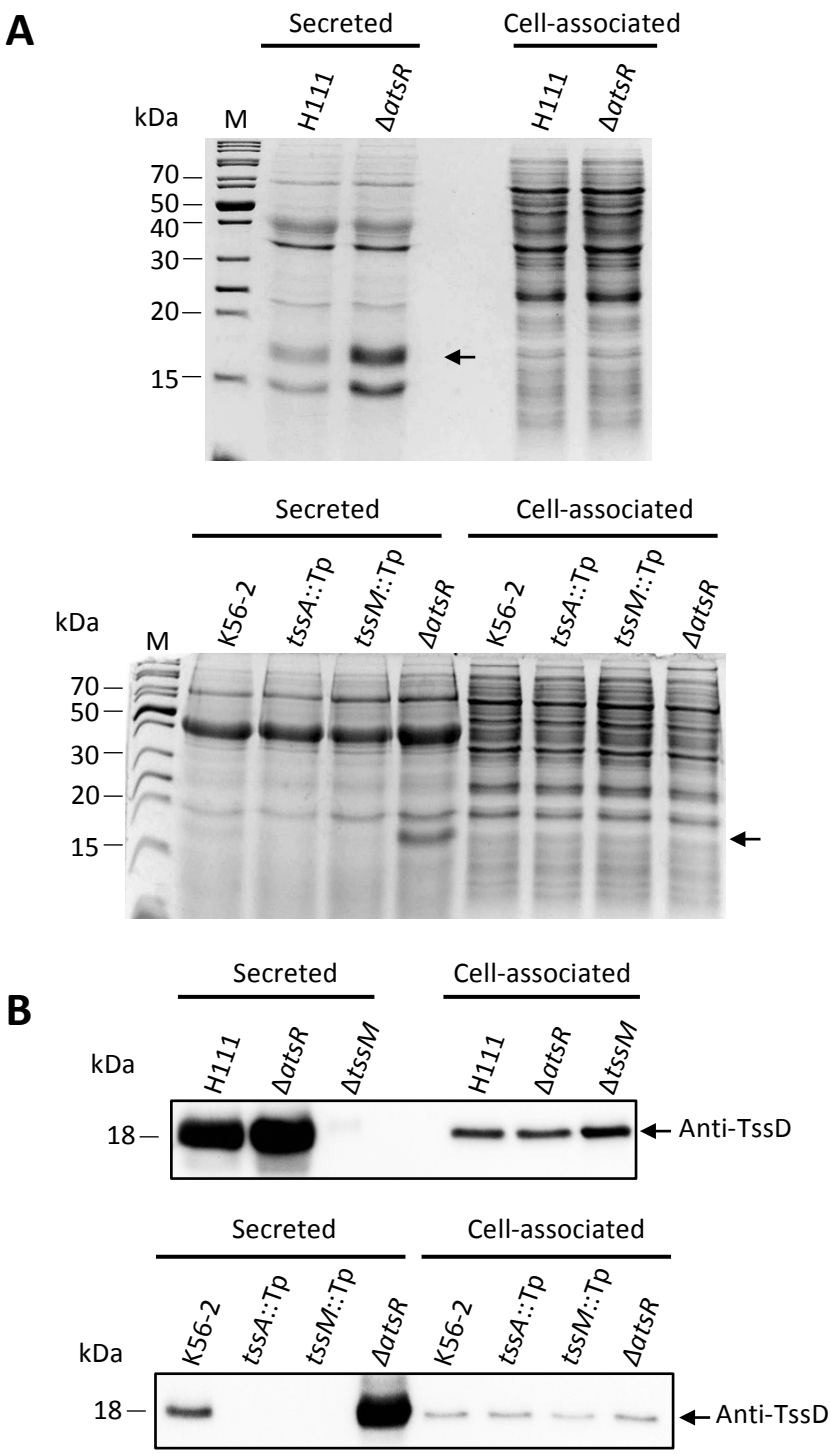

Figure 5.24 Analysis of TssD secretion in *B. cenocepacia* Δ*atsR* mutants. (A) Coomassie-stained 15% SDS-PA gels following electrophoresis of H111 (upper) and K56-2 (lower) extracellular proteins (left) extracted from liquid cultures of respective wild-type, Δ*atsR* and T6SS-deficient mutants (Δ*tssM*, *tssA*::Tp or *tssM*::Tp). Cell-associated proteins are shown on the right. Arrow indicates 18 kDa protein that is more abundant in Δ*atsR* mutants. M, EZ-Run *Rec* protein ladder. (B) Immuno-detection of TssD (indicated by arrow) using a custom anti-TssD antibody in samples from (A), with secreted TssD on the left and cell-associated TssD on the right.

of each strain indicated that deletion of *atsR* in H111 resulted in approx. 1.5-fold increase in the amount of TssD to the wild-type (Figure 5.25A). The difference was greater in the K56-2 background, with *atsR* disruption causing a 4-fold increase in extracellular TssD (Figure 5.25B). However, as these quantifications were only taken from one experiment further repeats would be required to give statistical significance.

As these strains were grown to a similar optical density and the same volume of spent culture medium was precipitated, the results (like those presented in Section 4.5.1) suggest that extracellular TssD is more abundant in wild-type *B. cenocepacia* H111 than in K56-2. Thus, by deleting *atsR* in K56-2 it enabled up-regulation of T6SS activity to levels similar to those seen in wild-type H111. Together this data suggests that removal of the AtsR sensor-kinase from *B. cenocepacia* does not exert as significant effect on T6SS activity in H111 as it does in the K56-2 strain, thus meaning that the H111-Δ*atsR* strain may not be particularly beneficial to use in a secretomics study. However, the results did imply that basal T6SS activity in wild-type H111 may be sufficient for what was required, as it showed similar TssD secretion to the K56-2-Δ*atsR* mutant with an over-activated T6SS.

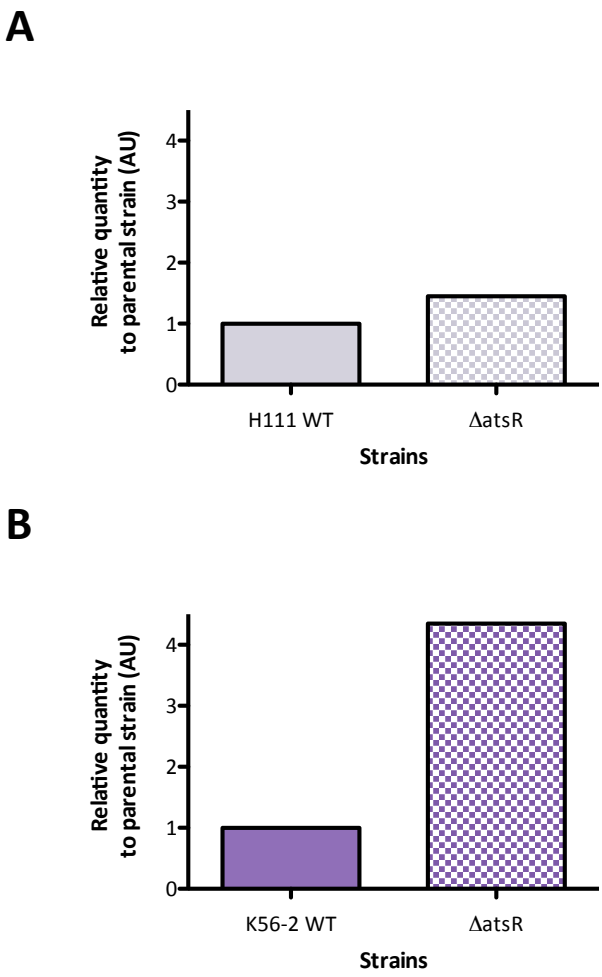

Figure 5.25 Relative quantification of TssD secretion in *B. cenocepacia* Δ*atsR* mutants. Densitometric analysis of anti-TssD western blots using image quantification software, showing quantification of TssD secretion in Δ*atsR* mutants relative to TssD secretion in the respective parental strain. (A) H111 strains, (B) K56-2 strains. n =1.

5.5 Optimising a workflow for a secretome analysis of *B. cenocepacia* by shotgun proteomics

To identify proteins in a complex mixture, bottom-up mass spectrometry techniques can be used. A particularly useful method is the shotgun approach. The basic principle involves a mixture of proteins being digested into peptides by proteolytic enzymes that cut with a low level of specificity, such as trypsin. Trypsin hydrolyses peptide bonds on the C-terminal side of lysine and arginine residues. Peptides are then separated by HPLC and subjected to tandem mass spectrometry. The mass and charge (m/z) of ionised peptides (precursor ion) are determined in the first mass analyser, and then precursor ions are selected for subsequent fragmentation into product ions, which are analysed in the second mass analyser. This generates the m/z of the product ions, and thus generates sequence tags of the precursor ions. This iterative process of precursor ion selection, fragmentation and product ion analysis allows the determination of a peptide's mass and sequence. Thus, the experimentally derived peptide mass data and sequences generated can be compared to an *in silico* tryptic digest of hypothetical proteins from *B. cenocepacia* using a database search, e.g. MASCOT, to identify proteins the peptides correspond to. To help identify T6SS-dependent secreted proteins in *B. cenocepacia* it was decided to try to employ this mass spectrometry analysis technique.

5.5.1 Optimisation of secreted protein extraction from liquid broth cultures

It was found the *B. cenocepacia* strain H111 possessed a functioning T6SS that was active under standard laboratory conditions (Section 4.5). Attempts were made to increase the activity of this system by generating mutants that lacked putative post-translational and confirmed transcriptional regulators of the T6SS, without success. Consequently, it was decided to attempt to analyse the extracellular proteins extracted from wild-type cultures of *B. cenocepacia* H111, and compare them to extracellular proteins extracted from a T6SS mutant. The greater the protein content of samples, the more likely it will be that proteins of

interest will be reliably identified by mass spectrometry. Therefore, it was first required to optimise growth conditions and the extracellular protein extraction procedure from bacterial liquid cultures for an optimal yield of secreted proteins.

First, *B. cenocepacia* H111 was grown in different types of liquid media to determine if this effected extracellular protein production. Growth media, including LB broth and BHI broth, dialysed BHI (D-BHI) broth, and M9 minimal medium containing glycerol and casamino acids or glucose were tested. It was found that upon extraction of extracellular proteins by DOC-TCA precipitation (Section 2.4.3) from BHI and LB broth cultures, components of the media itself interfered with analysis of the extracted proteins by SDS-PAGE, causing smearing and obscuring of proteins below 20 kDa (results not shown). Growth in either minimal medium tested resulted in slow growth of the cultures, but a similar secreted protein profiles was obtained as to those obtained from growth in richer media (results not shown). D-BHI was found to offer the best compromise between rich medium and minimal medium, as the strains still grew at an a convenient rate but there was no interference from the components of the media when analysing the samples by SDS-PAGE (see Section 4.5).

The correlation between the growth phase of the bacteria and extracellular protein production was also investigated to determine if T6SS activity was more active at a particular growth phase. Cultures of *B. cenocepacia* H111 were grown to an OD_{600} of ~0.6 (mid-log), 1.0 (late-log) or as overnight cultures (stationary) and secreted proteins extracted by DOC-TCA precipitation. It was observed that secreted protein profiles were similar between cultures grown to an OD_{600} of 0.6 and 1.0 in terms of the range of proteins produced. But the abundance of proteins was greater in the culture at 1.0 than 0.6 (results not shown), as would be expected, as there is a greater cell density. However, when comparing the secreted proteins extracted from overnight cultures, the secreted protein profile was significantly different (Figure 5.26). There was overproduction of a protein at approximately 32 kDa, and no observable 18 kDa protein corresponding to TssD when compared to log-phase cultures, as analysed by SDS-PAGE. Moreover, extracellular TssD was not detected in secreted protein samples of stationary

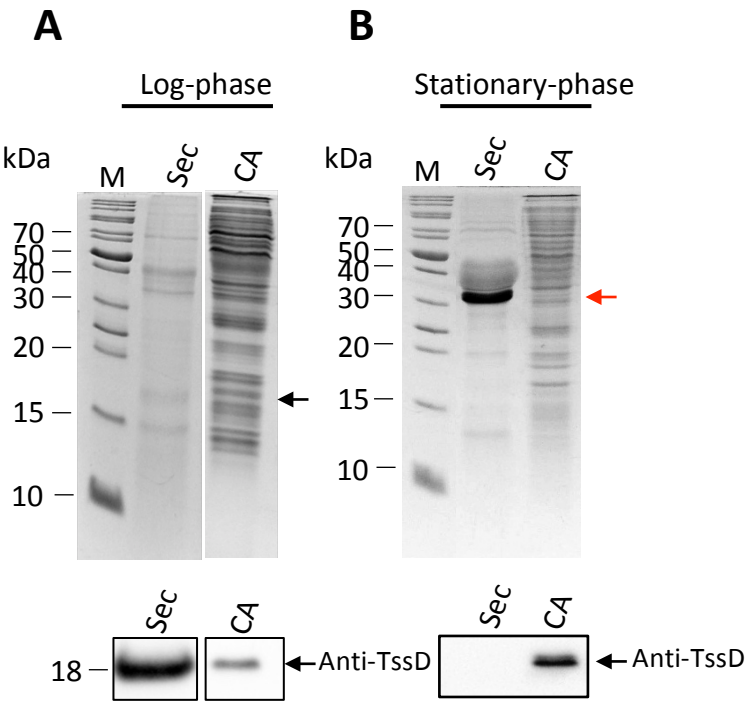

Figure 5.26 Comparison of the secreted protein profile of log phase and stationary phase cultures of *B. cenocepacia* H111. Cultures of *B. cenocepacia* H111 were grown to (A) OD_{600} of 1.0 (late log-phase) and (B) overnight (stationary phase), whereupon culture supernatants were precipitated to extract extracellular proteins (sec), and cell-associated proteins (CA). Samples were subjected to electrophoresis in a 15% SDS-PAGE gel and then stained with Coomassie blue (upper), or electro-blotted onto PVDF and probed with an anti-TssD antibody by western blotting (lower). The black arrow corresponds to TssD, and the red arrow corresponds to an unknown 32 kDa protein. Lanes labelled accordingly. M, EZ-Run *Rec* protein ladder; Sec, secreted proteins; CA, cell-associated.

phase H111 cultures, as ascertained by western blotting, yet cell-associated TssD was still detected (Figure 5.26). This suggests that firing of the T6SS is reduced in stationary phase cultures of *B. cenocepacia* H111.

The main method used for protein precipitation of the spent culture supernatants employed sodium deoxycholate (DOC) and trichloroacetic acetic acid (TCA) in combination, with an acetone wash(s) to remove residual TCA. Alterations to this method were also tried, including using TCA precipitation without the addition of DOC, acetone precipitation alone and concentration of the spent culture supernatants by a 10000 MWCO centrifugal concentrator. However, all of these alternative methods yielded poor results, i.e. little or no protein was visible from samples on an SDS-PA gel stained with Coomassie blue (data not shown). Therefore it was decided to remain with the original precipitation method that employed DOC and TCA.

5.5.2 Optimisation of sample preparation for mass spectrometry

Attempts were made to process extracellular proteins samples extracted from liquid cultures of wild-type *B. cenocepacia* H111 and a T6SS mutant (H111-Δ*tssM*) for mass spectrometry analysis. Here after DOC-TCA precipitation, the final protein pellets were resuspended in solubilisation buffer. After reduction with TCEP and alkylation by MMTS, samples were digested overnight with trypsin. Due to the presence of detergents in the solubilisation buffer, samples were then passed through a HiPPR™ Detergent Removal Spin Column. This was followed by C18 resin purification to remove interfering salts that were also present in the solubilisation buffer. However, following elution from the C18 resin it appeared that a precipitate had formed, an indicator that detergent was still present in the samples. Therefore these samples could not be analysed in their present form. It was then intended to clean the samples up further using strong cation exchange resin (SCX) but due to constraints this was not possible. Therefore unfortunately, no secreted protein preparations could be analysed and interpreted in time for the submission of this thesis.

5.6 Discussion

5.6.1 Role of TagX

This study hypothesised that the product of a conserved gene associated with the ancestral T6SS cluster (T6SS-1), which is found in many *Burkholderia* species and selected β-proteobacteria and ϒ-proteobacteria, might be a putative post-translational regulator of the T6SS, designated as TagX. It was predicted to be an inner membrane protein that contains a periplasmic C-terminal domain with four conserved cysteine residues. This region was postulated to be involved in sensing a periplasmic signal, directly or indirectly through other proteins, such as the outer membrane anchored lipoprotein TagM. This signal could then be transduced to other protein components to regulate the assembly, disassembly or firing of the T6SS complex.

Here, this study sought to determine the role of TagX in T6SS activity by analysing the phenotype of a *tagX* mutant. Unfortunately, it was found that insertional activation of *tagX* exerted no effect on the T6SS activity of *B. cenocepacia* H111, as similar levels of extracellular TssD were detected in the *tagX* mutant as the wild-type strain. Although not the results that were anticipated it does imply that TagX does not down-regulate the T6SS. However, if TagX was to act as a post-translational activator of the T6SS, then an observable difference in T6SS activity may only be observed if the signal to which it is responding to is actually present (i.e. bacteria are being grown under T6SS inducing conditions), rather than the low level constitutive activation conditions observed in *B. cenocepacia* H111. Therefore, a negative result in this experiment does not necessarily eliminate TagX as a T6SS regulator. Indeed, its very strong correlation with the T6SS-1 cluster still suggests some kind of regulatory role.

The T6SS shares a common evolutionary origin to bacteriophage tail-protein complexes (Leiman et al., 2009). Interestingly, GpL of the long non-contractile bacteriophage λ contains a C-terminal domain with four conserved cysteine residues that co-ordinates a Fe-S cluster (Tam et al., 2013), similar to the CTD of TagX. It is required for initial tail tip complex assembly, the distal structure that

interacts with the host cell membrane (Davidson et al., 2012). The Fe-S cluster of GpL may be involved in stabilising the GpL itself, or for transducing confirmation changes (Tam et al., 2013). However, as TagX is not essential for T6SS activity it is unclear if these observations are related in any way.

Investigations into H1-T6SS regulation of *P. aeruginosa* highlighted that null-mutations in several *tag* genes encoding candidate post-translation regulator proteins (TagQ, TagT, and TagS) had no effect on observable TssD levels (Silverman et al., 2011). However, it was later shown that TagQ, TagT and TagS were each required for T6SS-dependent fitness against other bacteria (Casabona et al., 2013). They may do this by sensing and transducing signals received upon attack by another T6SS-containing bacteria in a duelling manner (Basler et al., 2013). Conversely, it is unclear whether the T6SS in *B. cenocepacia* responds in this way, as evidence presented in Section 4 suggests it does not. Yet, an anti-bacterial role for the T6SS in *B. cenocepacia* H111 has been demonstrated (Section 4.6). So in regards to TagX, it is feasible that an observable difference between a *tagX* mutant and the wild-type strain may be only apparent when in a competitive growth environment. This was not tested, as the aim of investigating TagX was to determine if modulation of TagX could be used to enhance T6SS activity for effector identification under normal growth conditions.

To further evaluate the role of TagX in the T6SS of the *Burkholderia* species, either as a regulator or structural protein, it would be rational to investigate whether TagX interacts with other components of the T6SS directly. This could include exploring interactions between the CTD or NTD of TagX with other Tag proteins such as TagM, TagN, TagV or TagF, or structural proteins such as the periplasmic domains TssM or TssJ.

5.6.2 TagF, LPS and chromosome 3 in T6SS regulation

The *Burkholderia* T6SS-1 cluster contains a putative post-translational regulator, homologous to the post-translational repressor TagF (Silverman et al., 2011). TagF in *P. aeruginosa* acts by a poorly understood mechanism independent

from that of the threonine phosphorylation pathway (TPP), but it is thought to converge on the recruitment of TssH in complex with Fha1 to the T6SS complex, but does not require Fha1 to be phosphorylated, like in the TPP (Silverman et al., 2011).

In this study, *tagF* was inactivated by insertion of an antibiotic resistance cassette in several variants of *B. cenocepacia* H111 and the T6SS phenotype of the mutants assessed. A consistent increase in TssD secretion was observed in a *tagF* mutant generated in an isolate of *B. cenocepacia* H111 that was serum-sensitive and had spontaneously lost chromosome 3 ($H111^{S}$). However, when the *tagF* mutant allele was introduced to the wild-type strain there was a high degree of variation in the level of secreted TssD between repeat experiments. It is difficult to understand why this was, but there is a possibility that there were unknown variations between each experiment.

It is plausible that the $H111^{S}$ mutant is more 'leaky' than the wild-type strain, in regards to the integrity of cell membrane, which would result in increased amounts of protein in the extracellular milieu. However, it is difficult to judge this without a control for the amount of total secreted protein present or the precipitation efficiency.

It could be argued that the variation stems from the TCA precipitation procedure, as percentage recovery in protein precipitation by TCA can be variable (Bensadoun and Weinstein, 1976; Manadas et al., 2006). However, the method used in this study included sodium deoxycholate which has been shown to improve the reproducibility and yield of proteins during TCA precipitation significantly (Bensadoun and Weinstein, 1976; Zhou et al., 2006). Moreover, if the precipitation procedure were prone to variation it would lead to inconsistencies in assaying TssD secretion in all strains tested. There is the also the possibility of variation in batches of D-BHI media prepared for each experiment having a knock on effect of the bacteria and T6SS activity. The composition of BHI can vary between lots and manufacturers due to the procedure for preparing this medium (extracts of cow brain and heart).

However, rather than the variation being caused by the experimental procedure, it was initially postulated to be due to the absence of chromosome 3 having a stabilising effect on T6SS up-regulation in the H111^{S}-*tagF* mutant. For example, this could have been due to the removal of an unknown regulator(s) encoded on chromosome 3. Chromosome 3 (or pC3 as it is now referred to) has been shown to be a non-essential megaplasmid that is important for virulence, proteolytic activity, anti-fungal activity and stress tolerance in some species of related *Bcc* bacteria (Agnoli et al., 2012; Agnoli et al., 2014). Though, when a *tagF* mutant was constructed in an isolate of H111 that had been engineered to lose chromosome 3 (H111Δc3) only a marginal increase in TssD secretion was observed. This suggested that further mutations accrued by the H111^{S} isolate may have contributed to the phenotype observed in the H111^{S}-*tagF* mutant, rather than or in addition to deletion of chromosome 3.

Entire genome sequencing of H111^{S} indicated over 100 polymorphisms in the strain, several of them frameshift mutations in open reading frames. A particular frame shift mutation was discovered in the *wabR* gene, likely resulting in a truncated non-functional variant of WabR. WabR is a heptosyltransferase involved in the synthesis of the lipid A core in the LPS of *B. cenocepacia*, such that Δ*wabR* mutants lack O-antigen and have a truncated lipid A core (Ortega et al., 2009). It was reasoned that an impaired outer membrane LPS barrier in the H111^{S} isolate and H111^{S}-*tagF* mutant may have been synergistic or stabilised the TssD hypersecretion phenotype of the *tagF* mutant, by an unknown mechanism. One possibility was that the altered LPS layer allowed greater exposure to an environmental signal that is otherwise dampened down in strains harbouring a functional TagF. It is also possible that the altered LPS layer mimics the signal for T6SS activation in *B. cenocepacia*. To investigate this a different LPS mutant, inactivated in *waaL*, which had a slightly less truncated lipid A core than a *wabR* mutant was analysed. It appeared secretion of TssD in this mutant was similar to the wild-type H111, suggesting that the latter hypothesis was not the case.

It is possible that the combination of the LPS mutation and the absence of chromosome 3 was allowing increased TssD secretion in the *tagF* mutant. To

examine this possibility chromosome 3 was reintroduced into the H111^{S} strain followed by the inactive *tagF* allele, therefore effectively producing a *tagF* and LPS mutant with and without a full complement of chromosomes. The *tagF* mutant in the strain with a reintroduced chromosome 3 still appeared to over produce TssD, however it was not statically significance due to variation in the amount of secreted TssD and lack of experimental repeats due to of time constrains. If the potential link between chromosome 3, *tagF* and LPS were to be fully investigated then a *tagF* mutant should be constructed in a *wabR* mutant that is otherwise identical to the wild-type strain (i.e. lacking the polymorphisms present in H111^{S}). A derivative of this strain should then be constructed lacking chromosome 3, and TssD secretion compared to the *tagF wabR* mutant possessing a full complement of chromosomes. However, it was outside the scope of the project to further investigate this connection. The investigation into *tagF* inactivation did highlight an overall tendency for T6SS activity to be increased, which in itself is intriguing.

5.6.3 Mechanism of TagF regulation

B. cenocepacia does not contain genes homologous to *fha1*, *ppkA* or *pppA* in its T6SS cluster, indicating that, unlike *P. aeruginosa,* it is not regulated by the surface-growth stimulated TPP pathway involving TagQRST-PpkA-Fha1-PppA (Mougous et al., 2007; Hsu et al., 2009; Casabona et al., 2013). Note that *B. cenocepacia* does contain a FHA Ser/Thr protein kinase-encoding locus away from the T6SS cluster, on chromosome 2. However, is it likely to be involved in regulation of bacteriocin production, rather than T6SS regulation, due to the nature of the genes located downstream of the FHA locus. Even though *B. cenocepacia* does not encode Fha1 at the T6SS cluster, evaluation of several *tagF* mutants demonstrated a tendency for increased T6SS activity, as observed in the *P. aeruginosa tagF* mutant. This suggests they may share a TagF-mediated post-translational mechanism, but the *B. cenocepacia* system is unlikely to require complex formation between Fha1 and TssH. The T6SS in *B. cenocepacia* may use another unknown cytosolic subunit in complex with TssH to substitute for the lack of Fha1, which still results in localisation of TssH to the T6SS apparatus for disassembly of the tail tube

sheath and recycling of the TssB/TssC subunits. This is required for re-arming and re-firing of the system (Bönemann et al., 2009; Basler and Mekalanos, 2012). Performing protein-protein interaction studies, such as a two-hybrid analysis, would test this hypothesis.

As the TagF-mediated post-translational regulatory mechanism has not been properly characterised only a speculation on the steps involved can be made. Evaluation of *tagF* orthologues in a T6SS clusters in various Gram-negative bacteria highlight that *tagF* is always located immediately downstream of *tssM* (Figure 5.27). This suggests that as a negative post-translation regulator, TagF may target TssM in some way. The cytoplasmic NTD of most TssM proteins have NTPase activity and contains Walker A (ATP/GTP-binding) and Walker B (ATP/GTP hydrolysis) motifs, including TssM in *B. cenocepacia*. TagF is a predicted cytosolic protein, and it has been noted that where there is no evidence for post-translational regulation of the T6SS, the Walker A motif is absent or is not required, such as in *E. tarda* (Zheng and Leung, 2007; Silverman et al., 2012). This may suggest that TagF directly or indirectly negatively regulates TssM through the ATP/GTPase domain. Conformational changes to TssM upon binding of TagF or another regulator involved in the TagF-mediated pathway may leave the NTPase domain in an inactive conformation, resulting in suppression of T6SS due to reduced recruitment of TssH to the T6SS apparatus (Figure 5.1). However, according to current thinking, this would only be relevant in T6SSs that require this Walker A motif for activity, such as *A. tumefaciens* (Ma et al., 2009).

In contrast to deletion of the *tagF* and *pppA* genes in *P. aeruginosa*, deletion of a *tagF-pppA* fusion (Atu1064) present in the T6SS cluster of *A. tumefaciens* had no effect on TssD secretion (Lin et al., 2014). Yet, when the protein was overexpressed TssD secretion was significantly decreased, suggesting that the fusion protein acts as a repressor (Lin et al., 2014). The reason deletion of the gene did not increase T6SS activity is unclear. This further complicates the post-translational regulatory mechanism of TagF (and PppA).

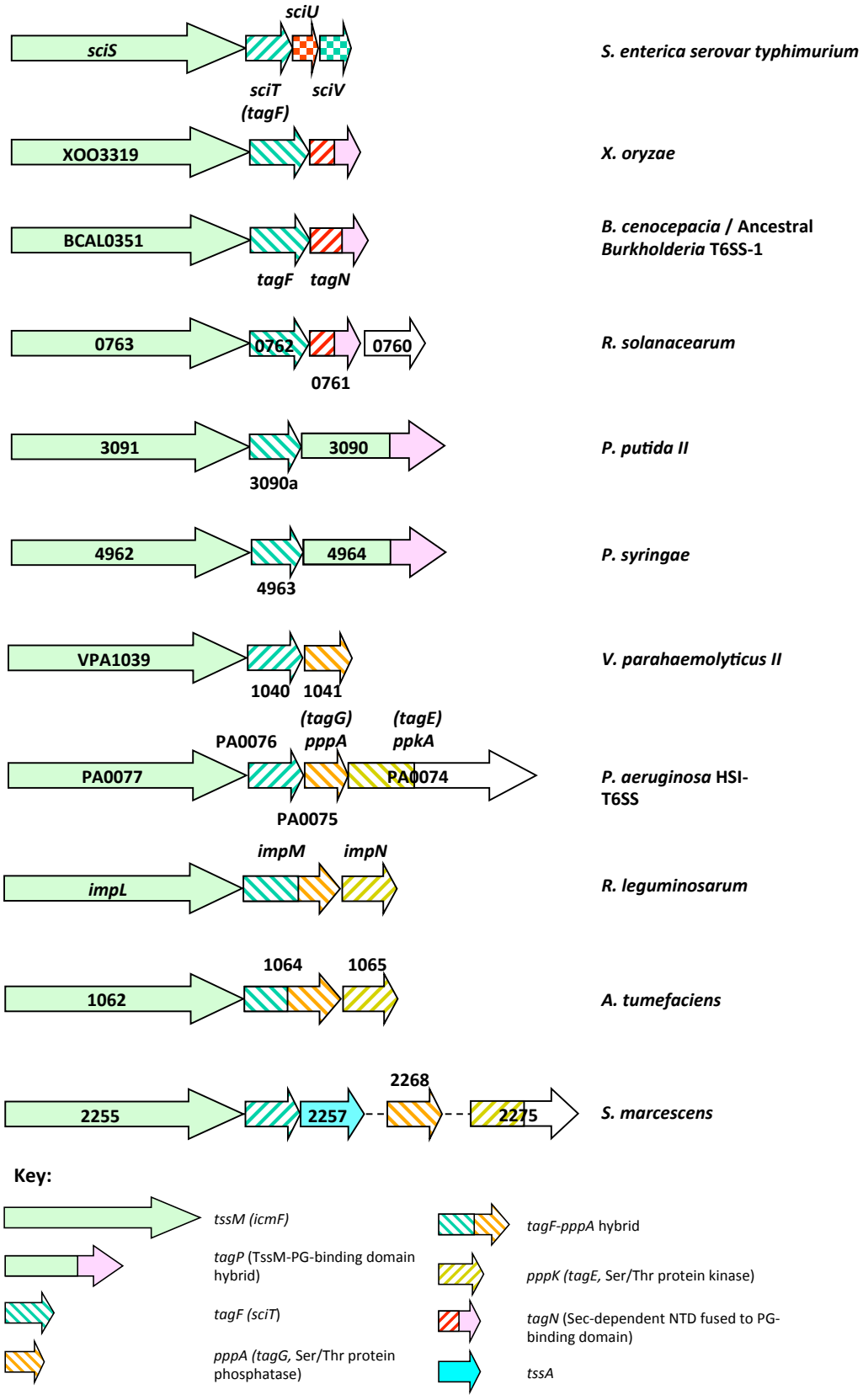

Figure 5.27 Comparison of the genomic location of *tagF* orthologues within T6SS clusters. Image showing the genetic arrangement of *tagF* and surrounding genes in various T6SS clusters. Gene loci are stated within or below the arrows for each gene. Not to scale.

5.6.4 The transcriptional regulator AtsR

B. cenocepacia has a two component regulatory system, AtsR-AtsT, which functions in global transcriptional regulation to exert a variety of downstream effects on the organism. This system negatively regulates the expression of the T6SS system, and other features including motility, biofilm production and protease production, which it does by modulating quorum sensing signalling pathways, CepIR and CciIR, and another mechanism that may involve the orphan LuxR homologue that is independent of AHL, CepR2 (Aubert et al., 2008; Malott et al., 2009; Aubert et al., 2012; Ryan et al., 2013).

In the results presented here, deletion of *atsR* in the H111 strain of *B. cenocepacia* has only a modest stimulatory effect on T6SS activity in comparison to the significant increase in a K56-2-Δ*atsR* mutant. It was previously noted that wild-type H111 exhibited greater basal TssD secretion than K56-2 (Section 4.5.1), which may account for the difference in the effect of deleting *atsR*, i.e. the increase in TssD secretion was not as profound in H111 as the system was already more active to begin with.

Greater basal T6SS activity in H111 could be due to the lack of the CciIR quorum sensing system (Malott et al., 2009). This system has been suggested to negatively regulate the T6SS in *B. cenocepacia*, whereas the CepIR system positively regulates T6SS. This reciprocal relationship is true for many other genes regulated by these two systems (O'Grady et al., 2009). It was observed that all four *cciIR* and *cepIR* genes were up-regulated in a K56-2 Δ*atsR* mutant (Aubert et al., 2012). Therefore, bringing these facts together, a very tentative hypothesis can be generated to try to explain why a profound up-regulation of T6SS activity in H111 was not observed (Figure 5.28).

To begin, in K56-2 the presence of the CciIR system may be restricting basal T6SS activity, which is overridden when the CepRI system is up regulated by deletion of *atsR.* Up-regulation of genes by the CepRI system is thought to be dominant over their down-regulation by the CciIR system, as CepRI acts upstream in the QS signally cascade (O'Grady et al., 2009). Conversely, in H111 where there is

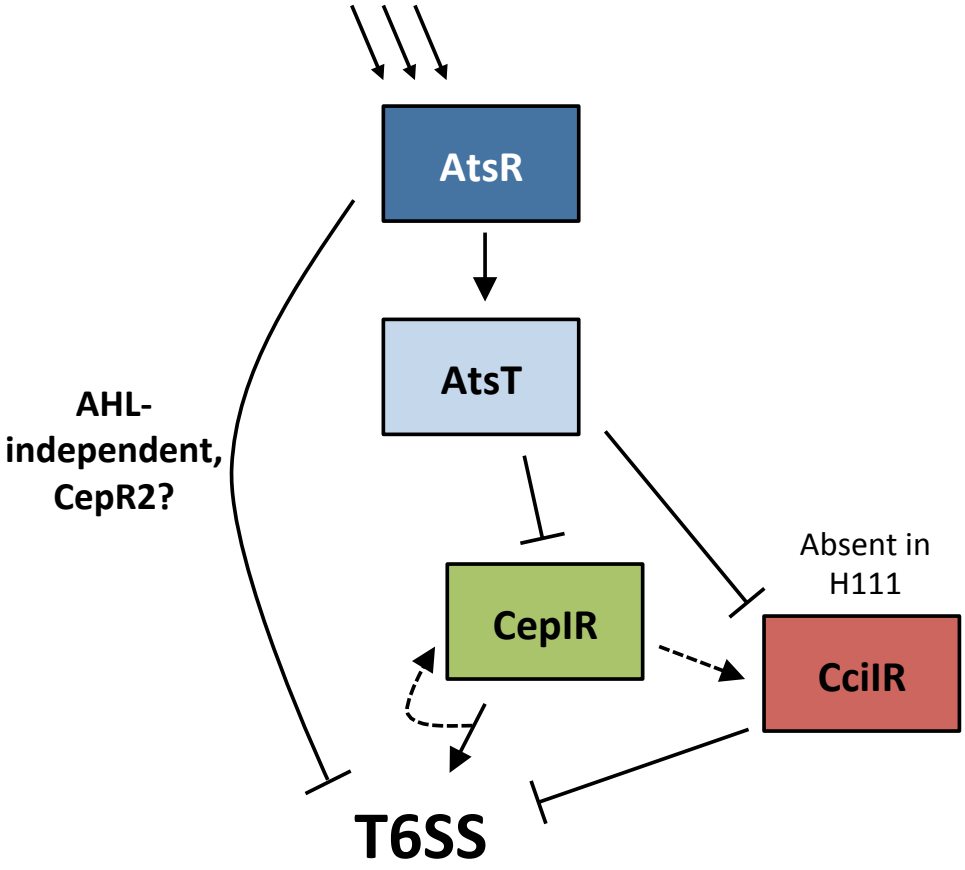

Figure 5.28 Hypothetical model for differential outcome of T6SS activity in *B. cenocepacia* H111 and K56-2 Δ*atsR* mutants. See text for details. Dashed arrows indicate positive feedback of CepIR system, and cross talk between CepIR and CciR (O'Grady et al., 2009; Aubert et al., 2012).

no CciIR to have a negative effect on T6SS expression, deletion of *atsR* may still up-regulate the CepRI system leading to an increase in T6SS activity, but the relative difference in TssD secretion is not as great because the T6SS is more basally active.

There may be a limit to how much T6SS activity is possible, particularly regarding assembly, firing and dissemble of the complex, all of which require significant resources and energy input for the bacterium. Taking this into consideration, it was decided to cease trying to further activate the T6SS in *B. cenocepacia* H111, and instead attempt to identify potential T6SS effectors in the secretome of a simple H111 wild-type strain, comparing it to that of an otherwise isogenic T6SS mutant.

5.6.5 T6SS effector identification by mass spectrometry- problems and solutions

An aim for investigating the regulation of the T6SS in *B. cenocepacia* was to help facilitate effector identification by mass spectrometry. However, there were issues with the compatibility of the extracellular protein preparation method used and downstream processing steps for mass spec analysis that could not be rectified before submission of this thesis. A contributing factor to the incompatibility may have been due to interfering detergents. This could have stemmed from carry over detergents from the precipitation and solubilisation procedures, even though a detergent removal step was undertaken using a commercially available purification kit. This was indicated by the presence of a precipitate during a desalting clean up step with C18 resin. Acidic buffers (trifluoroacetic acid and formic acid) were used in this clean up procedure, so the precipitate formed may have been due to acidification of acid-labile surfactants, such as carry over DOC from the DOC-TCA precipitation.

Possible ways to overcome this could be to acidify the samples before C18 clean up, include an additional purification step, such as using SCX resin, or try an alternative tryptic digestion method that is more compatible with detergent containing samples, such as the Filter Aided Sample Preparation technique (FASP)

(Manza et al., 2005; Wiśniewski et al., 2009). Unfortunately, due to time constraints none of these alternative methods could be undertaken.

Despite initial efforts to try to design a system for the analysis of the secretome of *B. cenocepacia*, including strain manipulation, optimisation of growth conditions, secreted protein extraction and sample preparation, the question regarding the most suitable/optimised workflow for sample preparation of the secretome of *B. cenocepacia* and subsequence MS/MS analysis remains unanswered.

Chapter 6: Characterisation of the putative T6SS effector-immunity protein pair $TanB^{H}$-$TaaB1^{H}$ from *B. cenocepacia* H111

6.1 Rationale

It has been observed that non-TssI T6SS effectors are often encoded adjacent to genes coding for the homologous tail-spike T4 bacteriophage protein, TssI (Koskiniemi et al., 2013; Shneider et al., 2013; Hachani et al., 2014). *B. cenocepacia* J2315 contains several *tssI* gene clusters distributed throughout the genome (Figure 3.10). Bioinformatic analyses of these clusters, presented in Section 3.4, identified at least one putative non-*tssI* effector gene in each *tssI* gene cluster, which was usually located downstream of the *tssI* gene that defined the cluster. The protein encoded by BCAL1298, located within the BCAL1294 *tssI* gene cluster, is one such putative effector (Figure 6.1A). Two proteins encoded by genes located immediately downstream of BCAL1298 (i.e. BCAL1299 and BCAL1300), were identified as candidate BCAL1298 immunity/antitoxins.

BLASTP searches of the genus *Burkholderia* revealed that proteins corresponding to BCAL1298 occur in only a handful of other strains (Section 3.9.2.3) and this did not include other *B. cenocepacia* strains. However, in strain *B. cenocepacia* H111, the ~6.5 Kbp region located downstream of I35_1211 (corresponding to BCAL1297 in J2315) is not annotated as containing any ORFs apart from I35_1212, which corresponds to part of the J2315 BCA1298 ORF. In the H111 annotation, the translation initiation codon of I35_1212 (a rarely used TTG codon) corresponds to the Leu91 codon of the protein encoded by BCAL1299 in J2315. BLASTX analysis of the unannotated region of H111 has shown that ORFs corresponding to BCAL1298, BCAL1299, and BCAL1300 are present downstream of I35_1211 (our unpublished observations). As they are unannotated (or misannotated in the case of I35_1212) these ORFs shall be referred to as BCAL1298H, BCAL1299H and BCAL1300H hereon (Figure 5.1A), where BCAL1299H and BCAL1300H correspond to putative immunity proteins for the product of BCAL1298H.

The proteins encoded by BCAL1298H, BCAL1299H and BCAL1300H are not completely orthologous with their J2315 counterparts. Unlike BCAL1298, which encodes a 'HNH/ENDO VII superfamily nuclease with conserved GH-E residues'

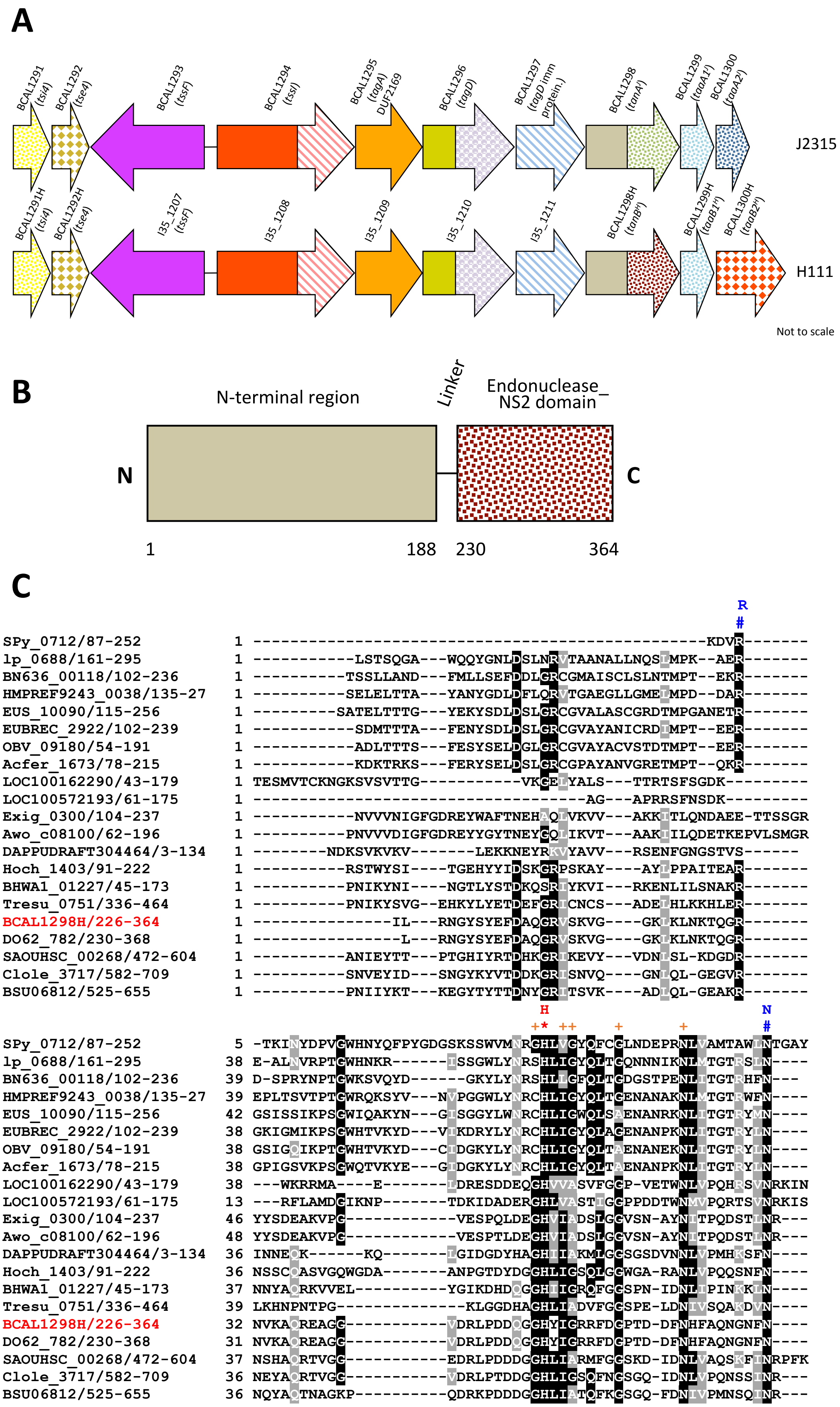

A
BCAL1291 (tsi4)
BCAL1292 (tse4)
BCAL1293 (tssF)
BCAL1294 (tssI)
BCAL1295 (tagA) DUF2169
BCAL1296 (tagD)
BCAL1297 (tagD imm protein.)
BCAL1298 (tanA¹)
BCAL1299 (taaA1¹)
BCAL1300 (taaA2¹)
J2315
BCAL1291H (tsi4)
BCAL1292H (tse4)
I35_1207 (tssF)
I35_1208
I35_1209
I35_1210
I35_1211
BCAL1298H (tanB^H)
BCAL1299H (taaB1^H)
BCAL1300H (taaB2^H)
H111
Not to scale
B
N-terminal region
Linker
Endonuclease_NS2 domain
N
C
1
188
230
364
C
SPy_0712/87-252
lp_0688/161-295
BN636_00118/102-236
HMPREF9243_0038/135-27
EUS_10090/115-256
EUBREC_2922/102-239
OBV_09180/54-191
Acfer_1673/78-215
LOC100162290/43-179
LOC100572193/61-175
Exig_0300/104-237
Awo_c08100/62-196
DAPPUDRAFT304464/3-134
Hoch_1403/91-222
BHWA1_01227/45-173
Tresu_0751/336-464
BCAL1298H/226-364
DO62_782/230-368
SAOUHSC_00268/472-604
Clole_3717/582-709
BSU06812/525-655

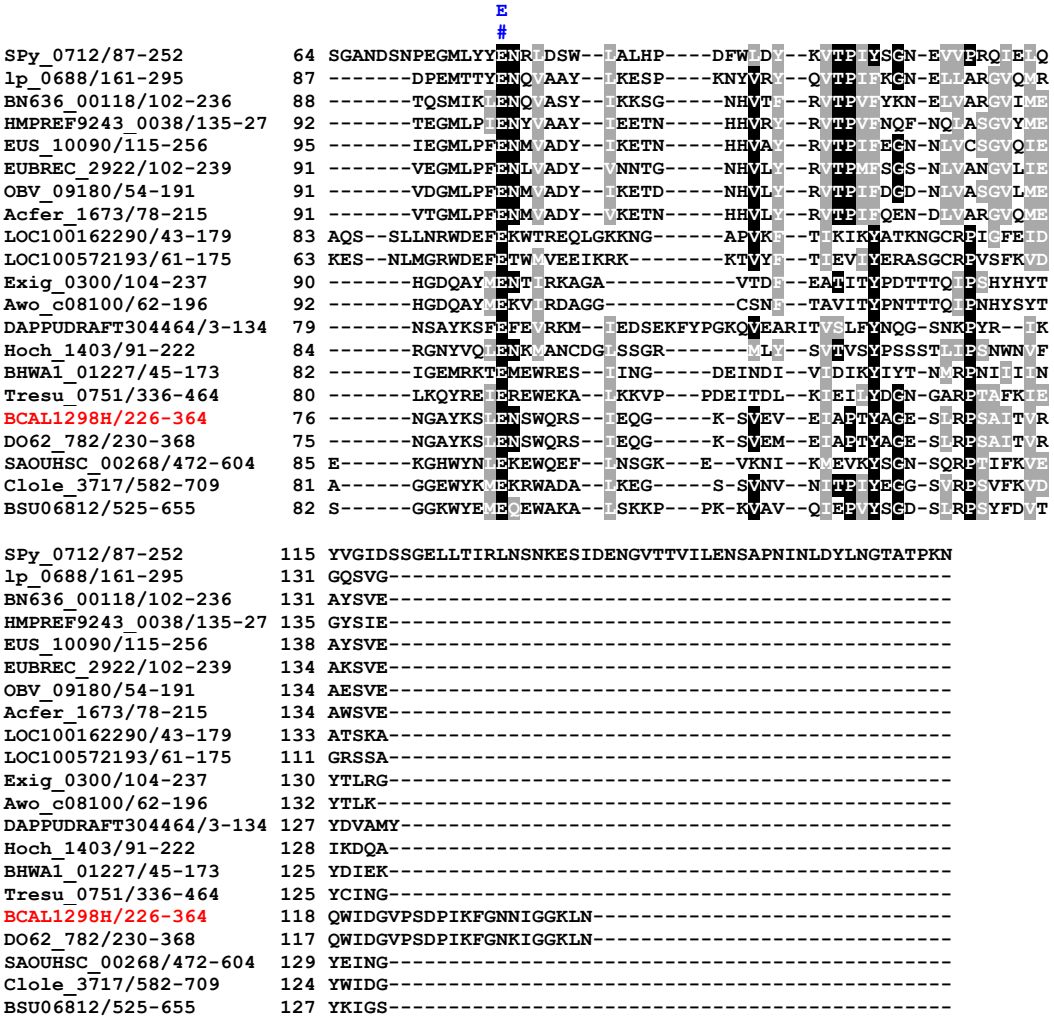

Figure 6.1 Bioinformatic analysis of the product of BCAL1298H from *B. cenocepacia* H111. (A) The labelled BCAL1291-BCAL1300 gene cluster from *B. cenocepacia* J2315 and corresponding cluster in H111, with the addition of unannotated BCAL1291, BCAL1292, BCAL1298, BCAL1299 and BCAL1300 related genes, described using the J2315 nomenclature with H suffix. BCAL1298 and BCAL1298H are drawn with different C-terminal colourings to illustrate the difference in the nuclease domain at the CTD of each encoded protein. Corresponding putative immunity proteins encoded by BCAL1299 and BCAL1300 and BCAL1299H and BCAL1300H are also shown. (B) The domain organisation of the product of BCAL1298H, characteristic feature of the domains are as indicated. (C) An alignment of the C-terminal domain (red font) encoded by BCAL1298H with diverse members of Endonuclease_NS2 domain-containing proteins, including experimentally characterise Spd1 protein from *S. pyogenes* (SPy_0712). Predicted residues important for catalysis (red *), metal iron coordinating (blue #) and other conserved residues within the active site region (orange, +) are shown. Alignment performed using Clustal Omega. Black shading indicates identical residues at the corresponding position in 50% of sequences, grey shading indicates similar residues at the corresponding position in 50% of sequences. The gene loci followed by the corresponding amino acid positions in the full-length protein is indicated on the left, the stated coordinates are relative to this.

domain (pfam14410) at the C-terminus of the protein, amino acid sequence analysis of the product of BCAL1298H identified a predicted DNA/RNA non-specific endonuclease 2 domain (Endonuclease_NS_2, pfam13930) in the C-terminal region of the protein. Yet, the N-terminal regions of the two proteins are virtually identical. This domain arrangement is illustrated in Figure 5.1B.

Interestingly, the two nuclease domains uncovered do however belong to the same domain clan, the His-(ββα)-Metal finger endonuclease (Cl0263), as classified by the Pfam database (Finn et al., 2014). These proteins are defined by a conserved histidine residue and metal binding residues within a (β)βα structural fold (Andreeva et al., 2007).

Due to their predicted enzymatic function and association with *tssI* clusters it was decided to name these proteins T6SS associated nucleases, Tan. It is proposed that this group should encompass T6SS effectors that contain nuclease domains from this defined clan of His-Metal finger endonucleases, including the 'HNH/ENDO VII superfamily nuclease with conserved GH-E residues' of BCAL1298 in J2315 and the 'Endonuclease_NS_2' of BCAL1298H. BCAL1298 will be referred to as a type A Tan (TanA) and BCAL1298H as a type B Tan (TanB) from herein. Furthermore, as an unannotated BCAL1298 gene homologue is found in the *B. cenocepacia* K56-2 strain, an additional superscript to distinguish the orthologues between strains will be included e.g. $TanA^{J}$ and $TanA^{K}$ for J2315 and K56-2, respectively. The protein product of BCAL1298H will thus be referred to as $TanB^{H}$ for completeness. For simplicity in the subsequent sections, the BCAL1298H gene loci will be referred to as $tanB^{H}$ to reflect the protein product that it encodes.

To coincide with naming of the Tan proteins, the putative immunity protein that correspond to them will be designated as T6SS associate antitoxin, Taa, where TaaA corresponds to the immunity protein of TanA and so forth. Due to $TanA^{J}$ and $TanB^{H}$ having two predicted immunity proteins each I will refer to them as $TaaA1^{J}$, $TaaA2^{J}$, $TaaB1^{H}$ and $TaaB2^{H}$, encoded by BCAL1299, BCAL1300, BCAL1299H and BCAL1300H, respectively. Again for simplicity, the genes will thus be referred to in a lower case italicised nomenclature that matches the proteins they encode, e.g.

taaB1^{H} for BCAL1299H. Note, the published Tde-Tdi effector-immunity superfamily defined by Ma and colleagues cannot be defined by the Tan-Taa classification (Ma et al. 2014). The toxin_43 domain (with a conserved HxxD motif) central to their superfamily has an all α-helical arrangement, therefore does not fall under the His-($\beta\beta\alpha$)-Metal finger clan.

An alignment of the C-terminal domain of TanB^{H} with other Endonuclease_NS_2 domain-containing proteins highlights conserved residues that are likely to be important for the function of the enzymatic domain (Figure 5.1C). Included in this alignment is an experimentally characterised Endonuclease_NS_2 containing protein from the Gram-positive bacterium *S. pyogenes*, Spd1. Spd1 was found to required specific Arg90, His121, Asn145 and Glu164 residues for catalysis and coordination/binding of a metal ion (Mg^{2+}), arrange in or around a His-($\beta\beta\alpha$)-Metal finger motif (Korczynska et al., 2012). Like other $\beta\beta\alpha$-Metal nucleases, such as the *Serratia* endonuclease (Nestle and Roberts, 1969; Kühlmann et al., 1999), it is thought to follow the general principle of nucleotide hydrolysis in endonucleases (Friedhoff et al., 1999) (Section 3.4.2.3). These described residues are widely conserved in the Endonuclease_N2_2 domain, including the domain in TanB^{H} (Figure 6.1C). Thus, the corresponding residues identified in TanB^{H}, Arg256, His277, Asn300, and Glu308 are likely to important for catalysis and metal ion coordination. Relatively conserved glycine residues (Gly276 and Gly280), an isoleucine residue (Ile279) and a further asparagine residue (Asn291) may also be important.

Comparison of TanA^{J} and TanB^{H} with the few other *Burkholderia* strains that encode a similar protein showed that the *B. pseudomallei* strain BDD protein (D062_782) has an NTD and CTD that is orthologous with that of TanB^{H} while in the only other *B. pseudomallei* strain to possess a related protein (MSHR7500) the CTD of the putative effector (X976_1941) belongs to the HNH/Endo VII GH-E superfamily, a TanA, yet the NTD is similar. One strain of *B. vietnamiensis* (LMG10929) and many other species outside the genus encode a protein that also has a similar NTD, but it is appended to different toxin domains. This includes an adhesin/haemagglutinin-like CTD in the proteins encoded by AK36_2612 in *B. vietnamiensis* and ROD_20761 in *C. rodentium* (ICC168) (Figure 6.2). The amino acid

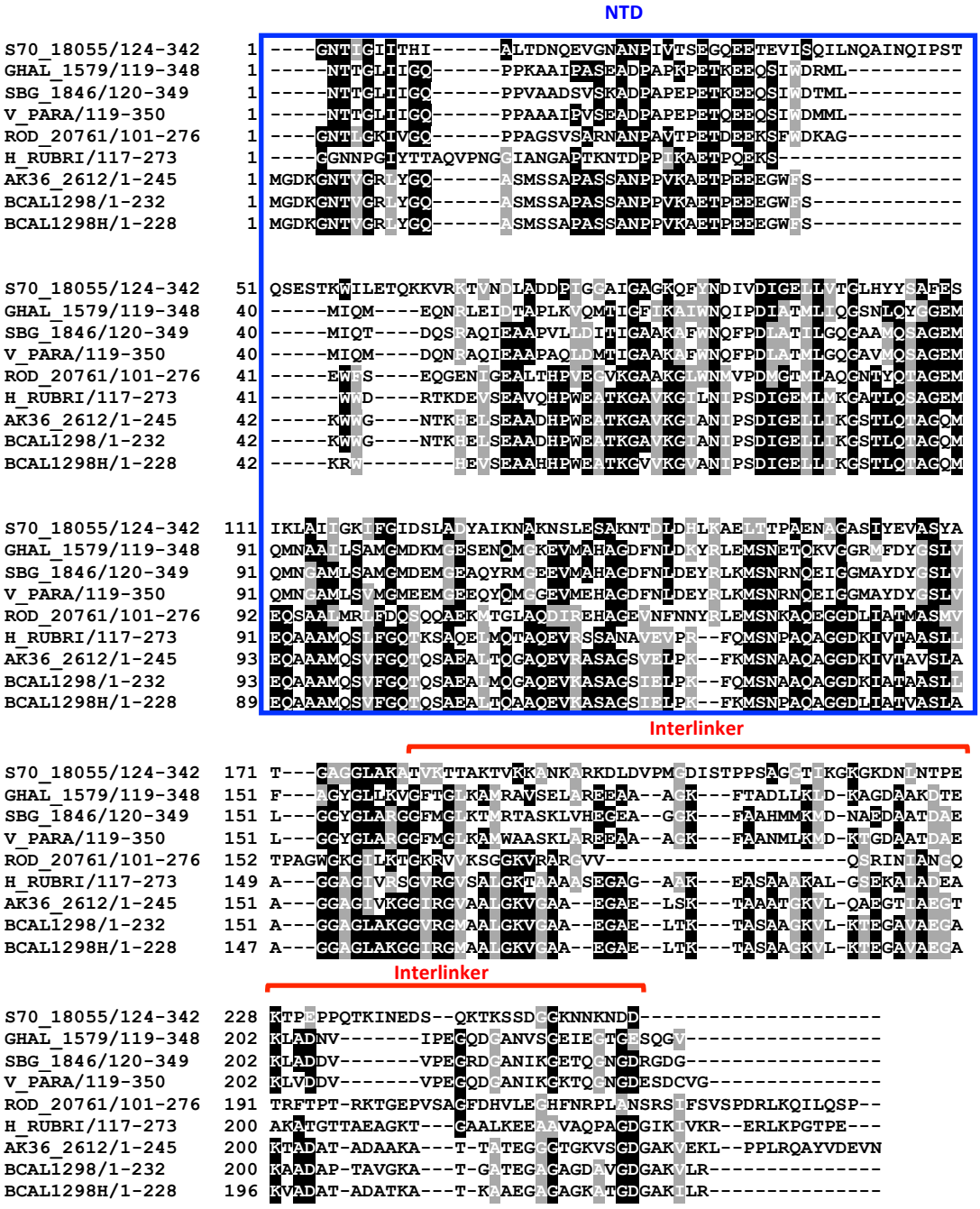

Figure 6.2 Alignment of the N-terminal region of products of BCAL1298 and BCAL1298H with related proteins in other Gram-negative bacteria that are also genetically linked to T6SS genes. BLASTP searches were performed to identify proteins with significant sequence homology towards the N-terminal domain of TanA^{J} and TanB^{H} (blue box), many of which were located within close gene proximity to T6SS genes. A putative interlinker region is indicated in red. The alignment was performed using Clustal Omega. Black shading indicates identical residues at the corresponding position in 50% of sequences, grey shading indicates similar residues at the corresponding position in 50% of sequences. The gene loci followed by the corresponding amino acid positions in the full-length protein is indicated on the left, the stated coordinates are relative to this.

sequence of the NTD also aligned to other uncharacterised Gram-negative bacterial proteins that contain PAAR_4 domains or are annotated as encoding Rhs proteins and are located within *tssI* or T6SS gene clusters.

Interestingly, some of the proteins with homology to the NTD on TanB^{H} are encoded downstream of a DUF2169-containing protein, which is homologous to the T6SS accessory protein (TagA) encoded by BCAL1295 and I35_1209 in *B. cenocepacia* J2315 and H111. Furthermore, a sequence that could possibly serve as an interdomain linker connecting the conserved NTD to the putative effector domain was observed to be located at the C-terminal end of the NTD. The conserved nature of the NTD and the possibility of different toxin domains appended to it is typical of polymorphic toxin families (Zhang et al., 2012), some of which are T6SS-dependent effectors (Jamet and Nassif, 2015).

The putative immunity proteins, TaaA1^{J}, TaaA2^{J} and TaaB1^{H} encoded downstream of both BCAL1298 and BCAL1298H have predicated analogous functions but they vary significantly in sequence and predicted secondary structure, as shown by the amino acid sequence alignment in Figure 6.3A. Both TaaA1^{J} and TaaA2^{J} contain tetratricopeptide repeat structural motifs (TPR) consisting of α-helices that are thought to mediate protein-protein interactions (Section 3.4.2, Figure 3.16) (Blatch and Lässle, 1999). However, TaaB1^{H} aligns well with DUF600-containing proteins (Figure 6.3B). This domain is thought to have a winged helix-turn-helix structure (PDB entry 3i0t and 2ia1).

Whereas TaaA2^{J} is homologous to TaaA1^{J}, the product of BCAL1300H (TaaB2^{H}) is distinct from BCAL1299H (TaaB1^{H}). However, TaaB2^{H} shares some amino acid sequence similarity with other proteins encoded downstream of genes coding putative T6SS-dependent DNase/RNase proteins in other bacteria (Figure 5.3C), including the immunity protein PA0100 located downstream of the experimentally verified nuclease effector PA0099 in *P. aeruginosa* (Hachani et al., 2014), and Atu3638 from *A. tumefaciens*, located downstream of a DNase effector encoded by Atu3640 (Ma et al., 2014). Therefore, TaaB2^{H} may also be an immunity protein for a nuclease-type T6SS effector protein.

A

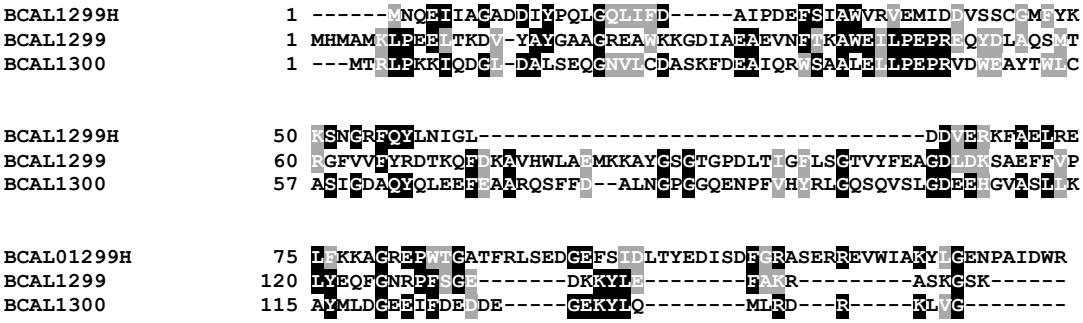
BCAL1299H
BCAL1299
BCAL1300
BCAL01299H

B

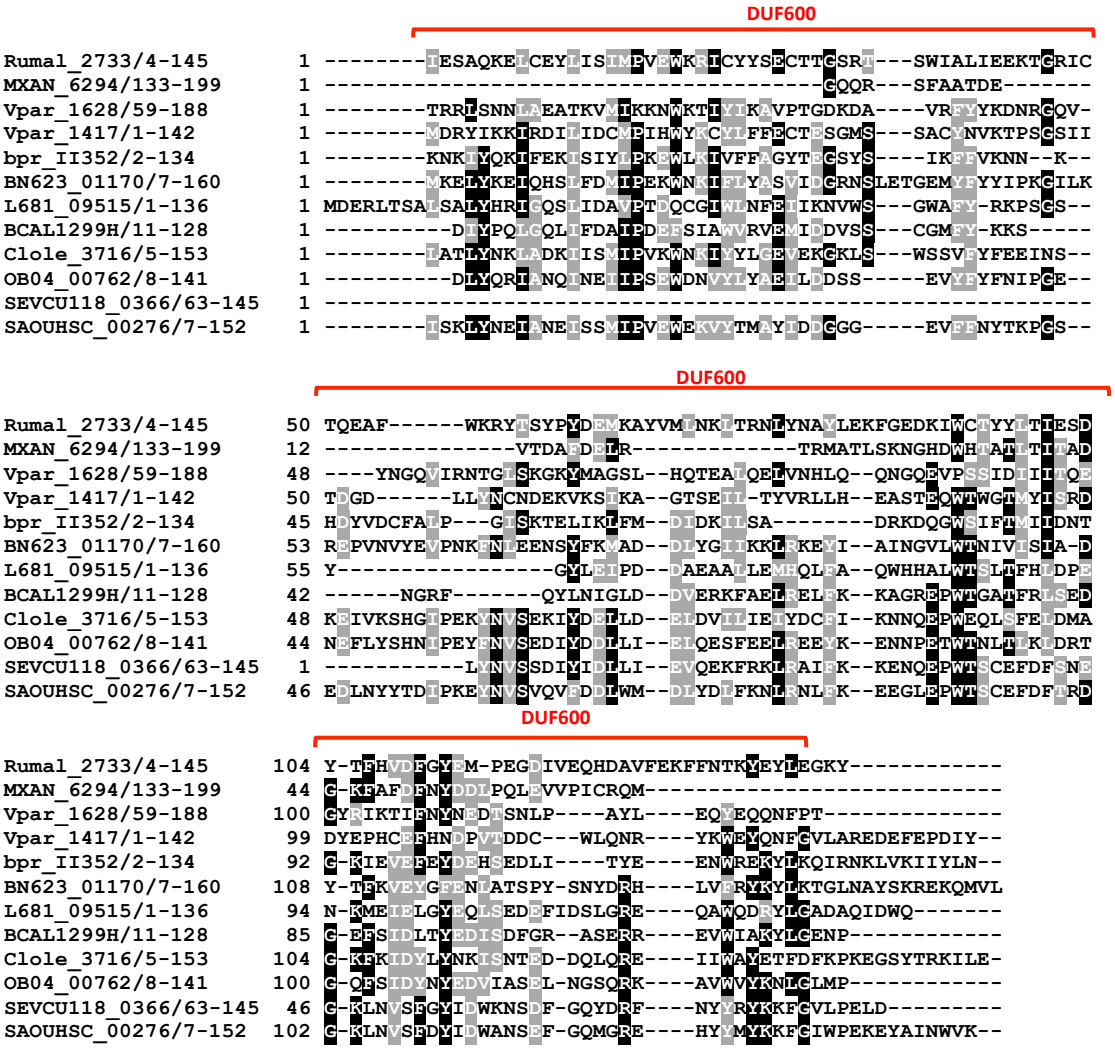
DUF600
DUF600
DUF600
Rumal_2733/4-145
MXAN_6294/133-199
Vpar_1628/59-188
Vpar_1417/1-142
bpr_II352/2-134
BN623_01170/7-160
L681_09515/1-136
BCAL1299H/11-128
Clole_3716/5-153
OB04_00762/8-141
SEVCU118_0366/63-145
SAOUHSC_00276/7-152

C

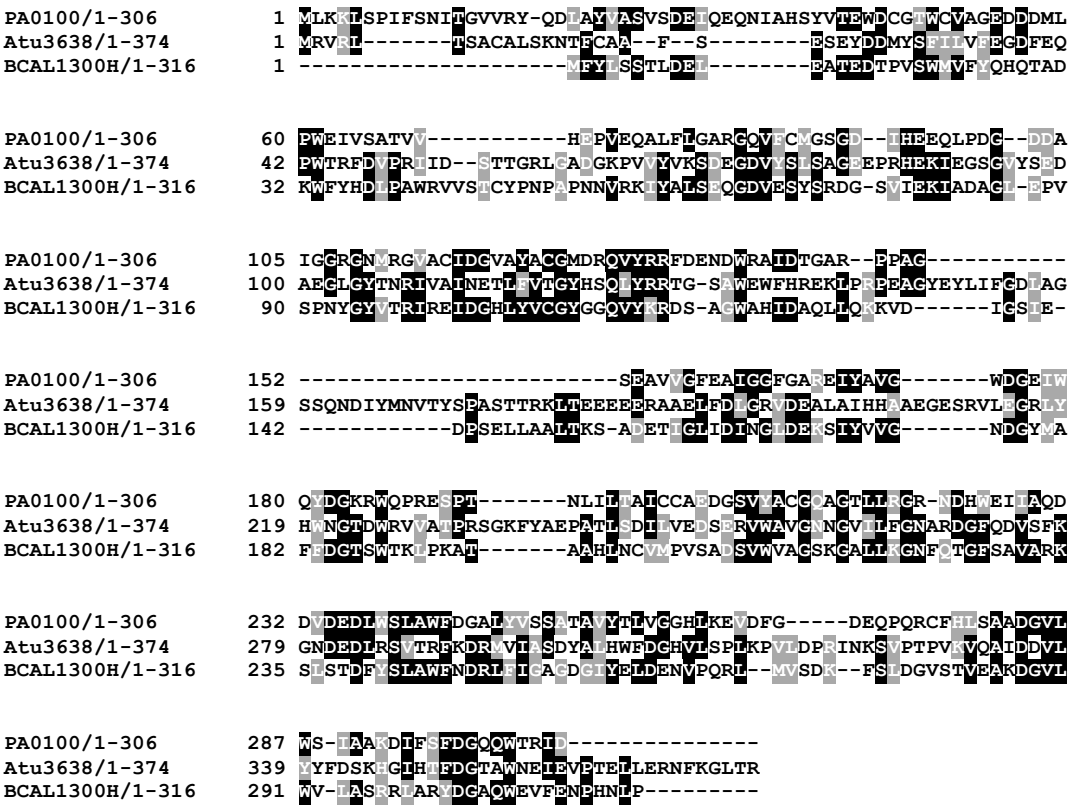

Figure 6.3 Alignments of putative immunity proteins encoded by BCAL1299, BCAL1299H, BCAL1300 and BCAL1300H. (A) Alignment of the products of BCAL1299 (TaaA1^{J}), BCAL1299H (TaaB1^{H}), BCAL1300 (TaaA2^{J}). (B) A BLASTP search was performed to identify proteins with significant sequence homology towards the DUF600 structural motif of the product of BCAL1299H, indicated in red, and the returned sequences were aligned. (C) An alignment of the product of BCAL1300H (TaaB2^{H}) with other putative immunity proteins, PA0100 from *P. aeruginosa* and Atu3638 from *A. tumefaciens* encoded downstream of potential nuclease toxins. Alignments were performed using Clustal Omega. Black shading indicates identical residues at the corresponding position in 50% of sequences, grey shading indicates similar residues at the corresponding position in 50% of sequences. The gene loci followed by the corresponding amino acid positions in the full-length protein is indicated on the left, the stated coordinates are relative to this.

Taking these observations together it was decided to characterise the product of BCAL1298H, $TanB^{H}$: to verify the predicted enzymatic function of the purified protein as a nuclease by *in vitro* methods; to determine the inhibitory role of the candidate immunity proteins $TaaB1^{H}$ and $TaaB2^{H}$ encoded by BCAL1299H and BCAL1300H, and to investigate whether $TanB^{H}$ was secreted, and whether this secretion was T6SS-dependent.

6.2 Cloning of the *tanB^{H}* and *tanB^{H}.CTD* coding regions into a high level expression vector

To facilitate the overproduction and purification of candidate T6SS-dependent effector TanB^{H} and its C-terminal nuclease domain (CTD) for enzymatic studies, it was decided to clone the coding regions of *tanB^{H}* that encoded both the full length protein and the CTD separately into an *E. coli* expression vector, incorporating an N-terminal hexa-histidine-tag for nickel affinity purification. Note that DNA encoding the nuclease component of TanB^{H} will be referred to as *tanB^{H}.CTD,* which encodes the last 139 amino acids of protein.

6.2.1 Cloning of *tanB^{H}* and *tanB^{H}.CTD* in the absence of an immunity protein

First, the coding sequences from *tanB^{H}* and *tanB^{H}.CTD* were amplified from *B. cenocepacia* H111 by PCR using primers BCAL1298ForNtermHisBamHI and BCAL1298RevHindIII for the entire open reading frame and BCAL1298CTDNtermHisForBamHI and BCAL1298RevHindIII for the CTD coding sequence, to generate 1120 bp and 445 bp DNA fragments, respectively. Both DNA fragments were purified (Figure 6.4) and subjected to restriction digestion with BamHI and HindIII. Each DNA fragment was then ligated into pETDuet-1 digested with the same enzymes, that cut within the MCS located downstream of the first T7 promoter, and transformants were selected for on LB agar containing ampicillin. Colonies were screened by colony PCR using vector specific primers pETDuet-T7-1for and pACYCDuet-T7-1rev to identify the desired clones. Unexpectedly, the success rate for the recovery of positive clones was significantly lower than was obtained when cloning other genes into this vector. Moreover, the recombinant clones that were identified, for both the full length and the CTD, contained base pair substitution mutations or deletions resulting in mutants than contained either early stop codons, frame shifts or amino acid changes in regions in or around the predicted active site of the protein (Section 6.1). This indicated that even-though pETDuet-1 has a T7-lac promoter and the LacI repressor, which may dampen read-through transcription originating from vector sequences upstream of the T7

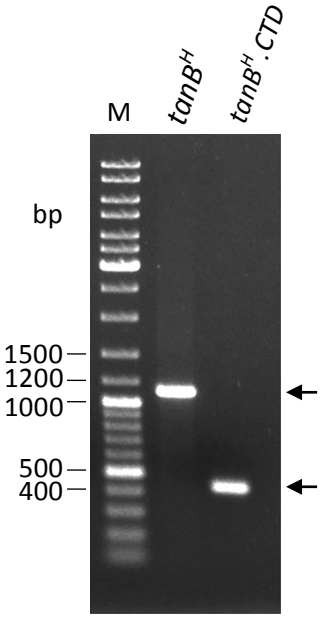

Figure 6.4 Amplification of DNA fragments corresponding to *tanB^H* and *tanB^H.CTD*. Diagram showing electrophoretic analysis of products from the amplification of *tanB^H* and *tanB^H.CTD* from H111 genomic DNA following purification. Arrows indicate 1120 bp and 445 bp fragments for *tanB^H* and *tanB^H.CTD*, respectively. M, GeneRuler DNA ladder mix.

promoter sequences upstream of the T7 promoter (when cloning the gene in a K-12 *E. coli* strain that lacks T7 RNA polymerase), some leaky transcription was still occurring thereby selecting against plasmid clones expressing an intact copy of *tanB*^{H}.

In one of the *tanB*^{H} clones, a single base change in the coding sequence resulted in the substitution of Gly276 (an amino acid residue next to the predicted catalytic His277 residue in the active site of the protein) to a negatively charged aspartate residue. The failure to clone an intact copy of *tanB*^{H}, presumably due to its toxic activity, suggests that the G276D derivative has decreased or abolished nuclease activity, allowing it to act as a negative control for subsequent DNase analysis of purified samples.

6.2.2 Genetic manipulation of pETDuet-1 expression vector

An alternative approach used to facilitate cloning of *tanB*^{H} was to re-engineer the pETDuet-1 vector by inserting a strong reverse-orientated promoter downstream of the second MCS (Figure 6.5). This was postulated to dampen the leaky expression originating from vector sequences located upstream of the MCS due to promoter occlusion (Adhya and Gottesman, 1982). It was decided to employ the promoter of the *dfr* gene (encoding a trimethoprim resistance determinant) as it has been shown to be six times more active than the fully induced *tac* promoter (Lévesque et al., 1994). To do this, the *dfr* gene was excised from the vector p34E-Tp as an EcoRI fragment, filled-in with Klenow fragment and then inserted into pETDuet-1 via a filled in XhoI site, to give pETDuet-Tp. The resulting vector was selected for on IST agar containing ampicillin and trimethoprim. Positive clones giving a plasmid size of approximately 6036 bp were identified by manual plasmid minipreparations (Figure 6.6). Due to the non-directional cloning nature of this approach, the orientation of the inserted *dfr* gene had to be determined by diagnostic restriction digestion with BsrGI (Figure 6.7). Clone #1 produced two fragment sizes of 5413 bp and 623 bp after BsrGI digestion and therefore contained the *dfr* gene in the desired reverse orientation with respect to the T7 promoters on pETDuet-1. Clones producing fragment sizes of 5715 bp and 321 bp contained *dfr* in

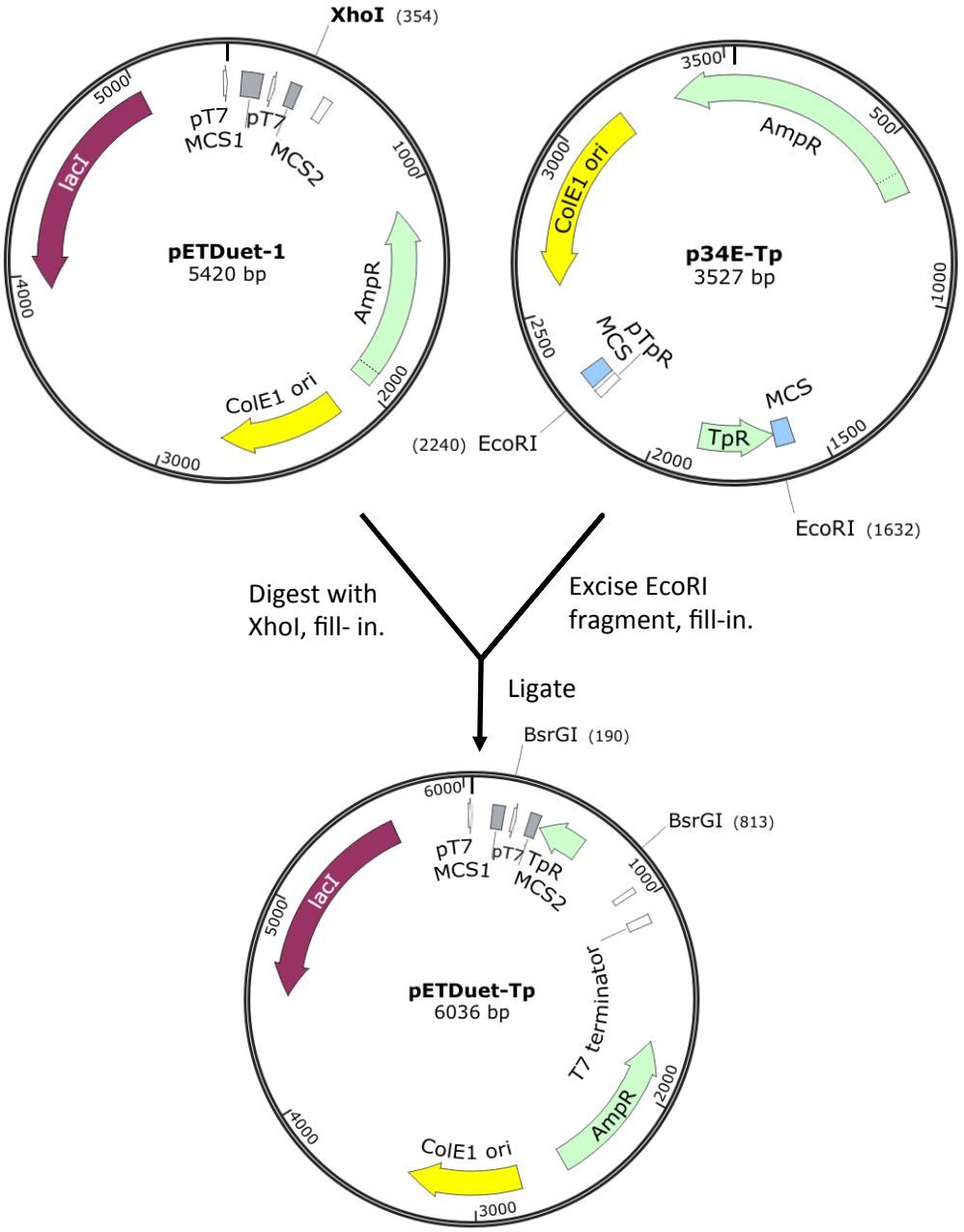

Figure 6.5 Construction of modified expression vector, pETDuet-Tp. The expression vector pETDuet-1 was digested with the restriction enzyme XhoI, and 5' ends filled-in using Klenow fragment. The *dfr* gene (TpR) was excised from p34E-Tp as an EcoRI fragment, filled in with Klenow fragment and ligated into XhoI-cut pETDuet-1 to generate the vector pETDuet-Tp. Clones were selected for trimethoprim and ampicillin resistance. Constructs containing *dfr* in reverse orientation to the T7 promoter were identified by diagnostic restriction digestion with BsrGI.

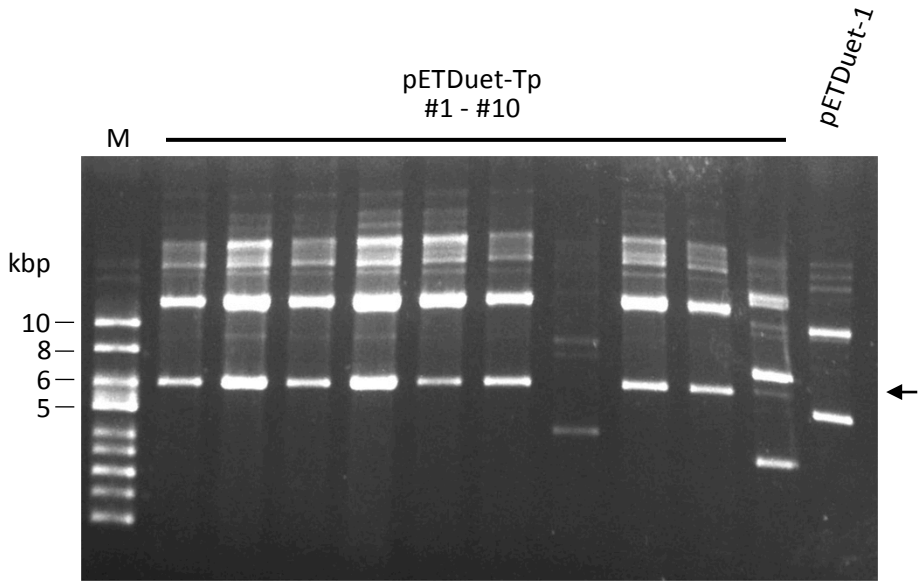

Figure 6.6 Size analysis of pETDuet-Tp candidate clones. Diagram showing plasmid mini-preparations of candidate pETDuet-Tp clones, selected after blunt ligation of *dfr* into pETDuet-Tp, following electrophoresis in a 0.8% agarose gel. M, Supercoiled DNA ladder. Arrow indicates expected plasmid size of pETDuet-Tp (6.04 kbp).

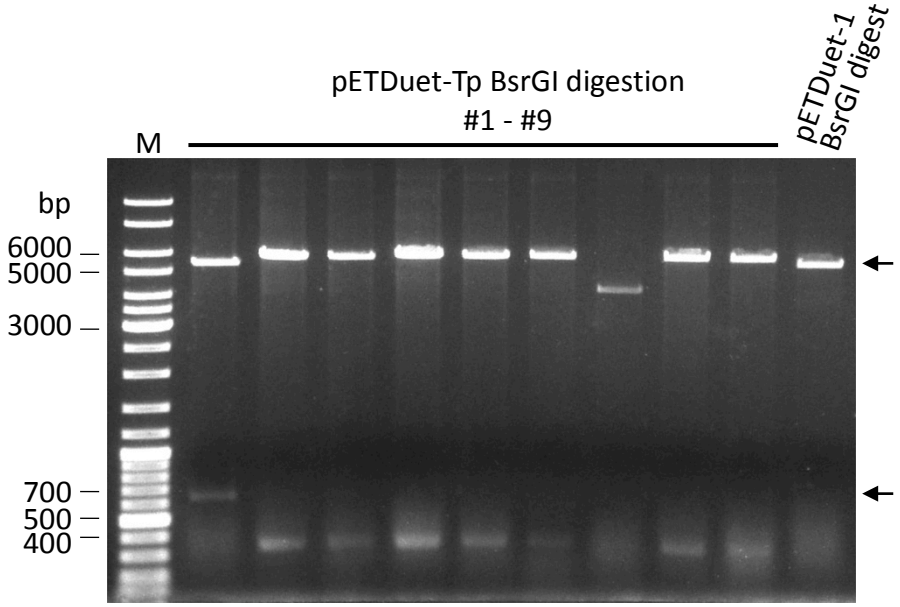

Figure 6.7 Diagnostic restriction digestion of pETDuet-Tp clones. Electrophoretic analysis of DNA fragments from the restriction digestion of candidate pETDuet-Tp clones and with BsrGI. Samples were electrophoresed in a 0.8% agarose gel. Plasmids producing fragment sizes of 5413 bp and 623 bp, indicated by arrows, were considered to contain the correctly orientated *dfr* gene. M, GeneRuler DNA ladder mix.

the incorrect orientation. Cloning of *tanB^{H} and tanB^{H}.CTD* into pETDuet- Tp vector was then attempted as above. Unfortunately, no positive clones were identified.

6.2.3 Cloning the coding sequence of *tanB^{H}* and *tanB^{H}.CTD* in the presence of candidate immunity protein genes *taaB1^{H}* and *taaB2^{H}* in *cis*

Many T6SS-effectors have cognate immunity proteins that are usually encoded directly downstream of the effector. *taaB1^{H}* and *taaB2^{H}* were identified as genes encoding potential TanB^{H} immunity proteins. It was postulated that the presence of the genes of either or both immunity proteins would allow cloning of *tanB^{H}*. Therefore both *taaB1^{H}* and *taaB2^{H}* were amplified separately from *B. cenocepacia* H111 (Figure 6.8), using primers BCAL1299ForNdeI and BCAL1299RevAcc65I, and BCAL1300ForNdeI and BCAL1300RevAcc65I, respectively. DNA fragment sizes of 435 bp for *taaB1^{H}* and 971 bp for *taaB2^{H}* were produced as expected. These fragments were purified, digested with NdeI and Acc65I, and ligated into the second MCS of pETDuet-1 cut with the same restriction enzymes, generating pHLS1 (for *taaB1^{H}*) and pHLS2 (*taaB2^{H}*), with expected sizes of 5790 bp and 6325 bp, respectively. Positive clones were identified by colony PCR using vector-specific primers pACYC-T7-2for and T7rev. Plasmid clones that generated products of the expected size were subjected to plasmid minipreparation extraction, subjected to size analysis (Figure 6.9) and nucleotide sequence analysis for confirmation.

pHLS1 and pHLS2 were then used as recipient plasmids for cloning *tanB^{H}* and *tanB^{H}.CTD* between the BamHI-HindIII restriction sites as described in Section 6.2.1 (Figure 6.10). Desired clones containing *tanB^{H}* and *tanB^{H}.CTD* were only obtained with the pHLS1 recipient plasmid, generating co-expression plasmids pHLS3 (containing *tanB^{H}* and *taaB1^{H}*) and pHLS4 (containing *tanB^{H}.CTD* and *taaB1^{H}*), which suggests TaaB1^{H} is the main immunity protein for TanB^{H}, not TaaB2^{H}.

tanB^{H} was also successfully cloned when inserted into pETDuet-1 as a component of a bicistronic *tanB^{H}-taaB1^{H}* DNA fragment, employing a single T7 promoter. This DNA fragment was amplified from *B. cenocepacia* H111 using

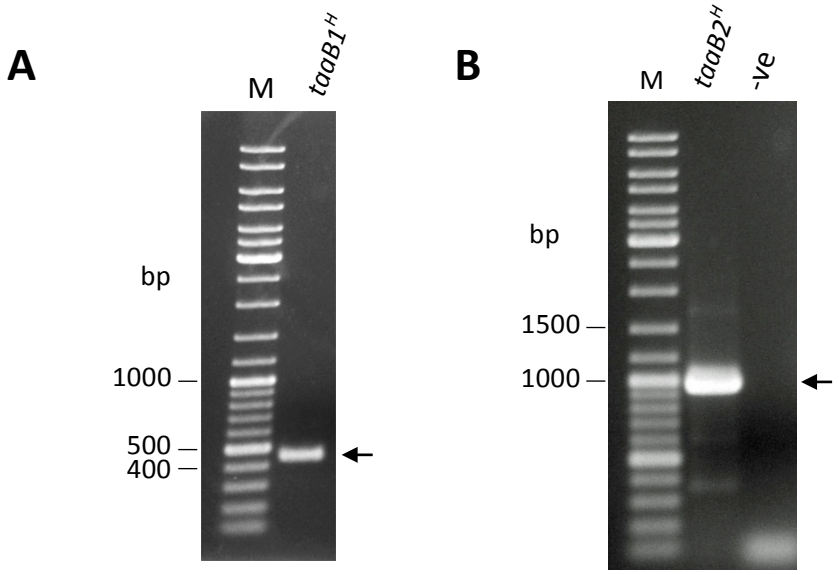

Figure 6.8 Analysis of *taaB1*^{H} and *taaB2*^{H} DNA fragments amplified from *B. cenocepacia* H111. Diagram showing resulting purified DNA fragment from the amplification of (A) *taaB1*^{H} and (B) *taaB2*^{H} from *B. cenocepacia* H111 following electrophoresis in 1.0% agarose gels. Arrow indicates expected fragment sizes of 435 bp for *taaB1*^{H} and 971 bp for *taaB2*^{H}. M, GeneRuler DNA ladder mix; -ve, no DNA negative control.

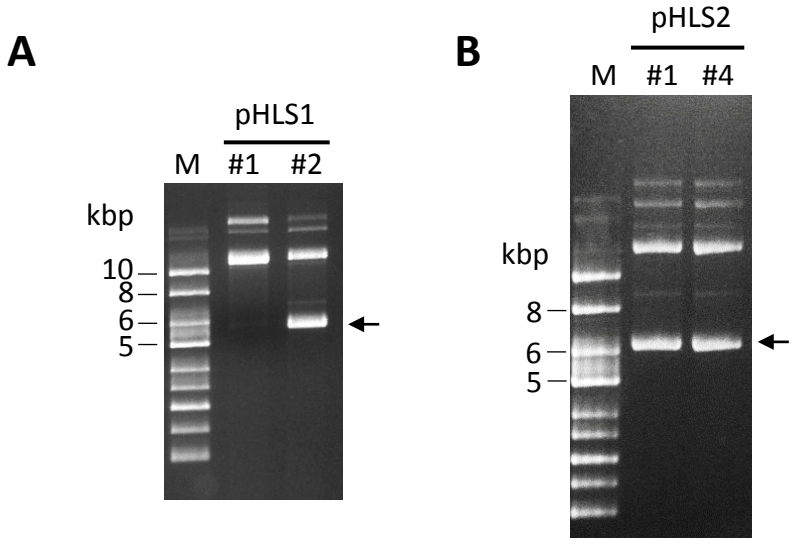

Figure 6.9 Analysis of candidate pHLS1 and pHLS2 plasmids. Diagram showing candidate (A) pHLS1 and (B) pHLS2 plasmid clones following electrophoresis in a 0.8% agarose gel. Arrows indicates 5790 bp pHLS1 plasmid and 6325 bp pHLS2 plasmid. M, Supercoiled DNA ladder.

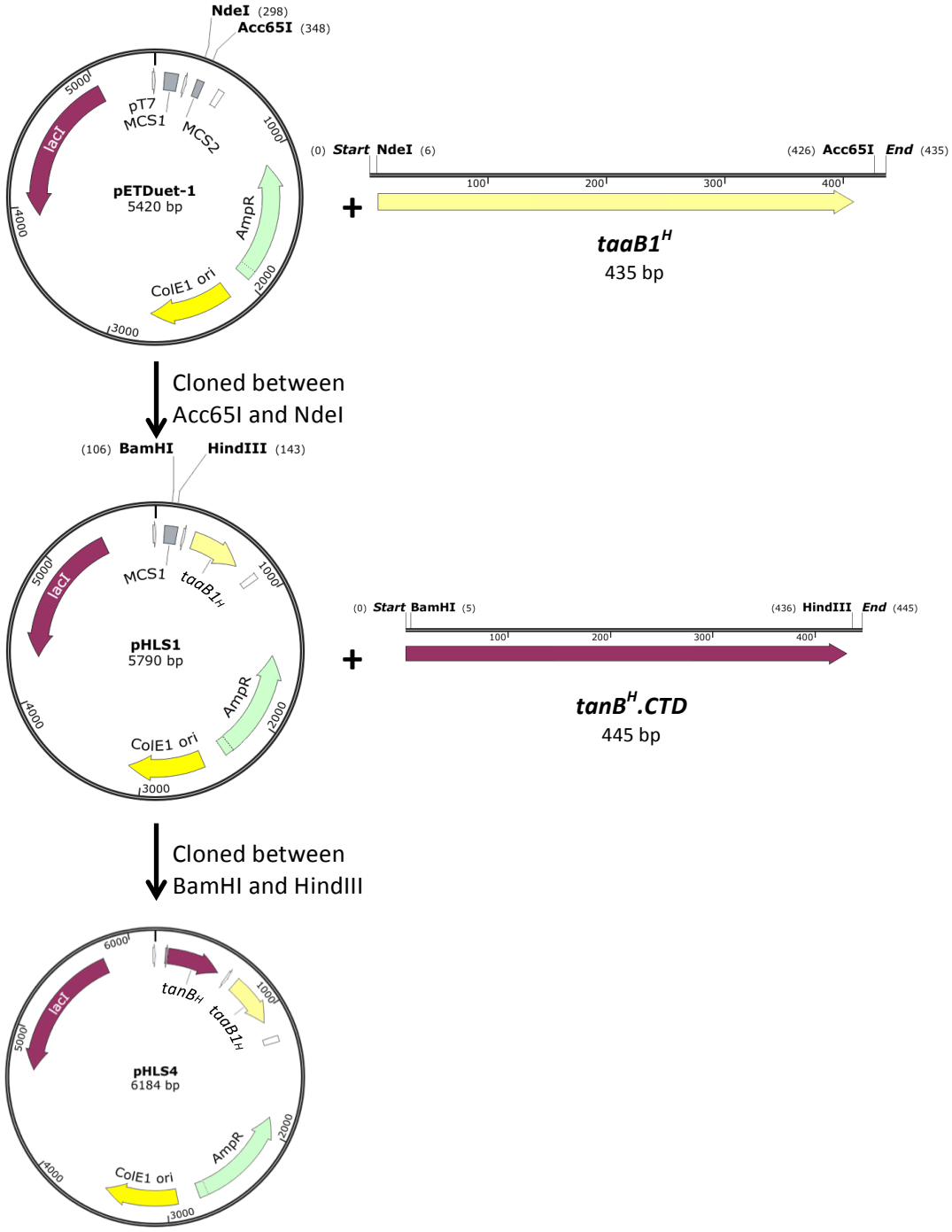

Figure 6.10 Construction of pHLS4 co-expression plasmid. Schematic diagram showing the insertion of *taaB1*^{H} into pETDuet-1 as an NdeI-Acc65I restricted PCR product, to generate the plasmid pHLS1. pHLS1 was then digested with BamHI and HindIII and the PCR amplified *tanB*^{H}*.CTD* DNA fragment inserted as a BamHI-HindIII restriction DNA fragment. Positive clones generated a 6184 bp plasmid, pHLS4.

primers BCAL1298NtermHisForBamHI and BCAL1299RevAcc65I, and inserted between the BamHI and Acc65I restriction sites of pETDuet-1, generating the plasmid pHLS5, with a size of 6711 bp.

6.2.4 Cloning the coding sequencing of *tanB^{H}* and *tanB^{H}.CTD* in the presence of candidate immunity protein gene *taaB1^{H}* in *trans*

It is noteworthy that *tanB^{H}* and *tanB^{H}.CTD* were also successfully cloned into pETDuet-1 when *taaB1^{H}* was present separately on a compatible plasmid under the control of a rhamnose-inducible promoter, pSCrhaB2. To construct this plasmid, a DNA fragment containing the coding region of *taaB1^{H}* was amplified from *B. cenocepacia* H111 (Section 6.2.3) and the resulting DNA fragment was inserted between the NdeI and Acc65I sites of pSCrhaB2, generating a 7929 bp plasmid, termed pHLS6 (Figure 6.11). *E. coli* MC1061 cells containing pHLS6 were then made chemically competent and used as the transformation strain for ligations between pETDuet-1 and PCR amplified *tanB^{H}* and *tanB^{H}.CTD* DNA fragments (Section 6.2.1). IST agar containing ampicillin and trimethoprim was used for selection of transformants. This allowed successful cloning of both *tanB^{H}* and *tanB^{H}.CTD* into pETDuet-1. Interestingly the presence of the pSCrhaB2 inducer, rhamnose, was not required for successful cloning of *tanB^{H}* and *tanB^{H}.CTD*, indicating there was sufficient amounts of the immunity protein generated due to basal expression from pHLS6 to combat the expression of *tanB^{H}* and *tanB^{H}.CTD*.

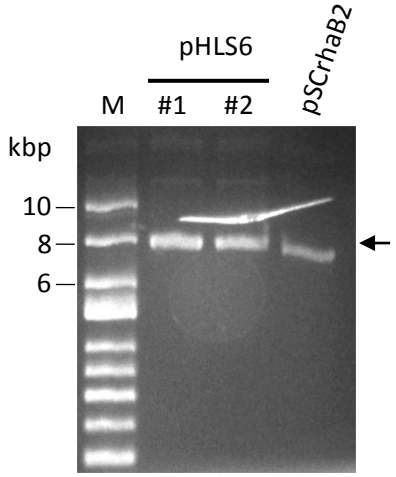

Figure 6.11 Analysis of candidate pHLS6 plasmids. Comparison of the size of candidate pHLS6 plasmids to the empty pSCrhaB2 vector following electrophoresis in a 0.8% DNA agarose gel. Arrow indicates the expected size of pHLS6 plasmid, 7929 bp. M, Supercoiled DNA ladder.

6.3 Purification of TanB^{H} and TanB^{H}.CTD by nickel affinity chromatography

6.3.1 Overproduction of TanB^{H}, TanB^{H}.CTD and TaaB1^{H} in *E. coli*

To determine whether the plasmids generated for overproduction of TanB^{H} and TanB^{H}.CTD, along with TaaB1^{H}, allowed production of the proteins of interest, pHLS3, pHLS4 and pHLS5 were transformed separately into the *E. coli* expression strain BL21(DE3) harbouring pLysS and small volumes of exponentially growing cells were induced with 1 mM IPTG for 4 hours at 30°C (Section 2.3.1). In addition, the plasmid containing only *taaB1^{H}*, pHLS1, was subjected to the same analysis. The expected molecular masses of His-tagged TanB^{H} (His$_6$.TanB^{H}), His$_6$.TanB^{H}.CTD and un-tagged TaaB1^{H} are 39.1 kDa, 16.9 kDa and 15.4 kDa, respectively. SDS-PAGE analysis of total cell proteins harvested from the induced cultures showed that His$_6$.TanB^{H}, His$_6$.TanB^{H}.CTD and TaaB1^{H} were present in the appropriate plasmid-containing cells (Figure 6.12). Proteins migrating with molecular masses corresponding to 40 kDa, 17 kDa and 14.5 kDa were observed. It was noted that there was significantly lower production of His$_6$.TanB^{H} and TaaB1^{H} from the plasmid containing bicistronic *tanB^{H}-taaB1^{H}* (pHLS5) in comparison to the plasmid expressing *tanB^{H}* and *taaB1^{H}* from two separate promoters (pHLS3).

6.3.2 Analysis of solubility of His$_6$.TanB^{H}, His$_6$.TanB^{H}.CTD and TaaB1^{H} recombinant proteins

The solubility of His$_6$.TanB^{H}, His$_6$.TanB^{H}.CTD and TaaB1^{H} were then determined (Section 2.3.2). Following protein overproduction and sonication of harvested cells, similar amounts of His$_6$.TanB^{H}, His$_6$.TanB^{H}.CTD and TaaB1^{H} were present in both the total (i.e. uncleared) cell lysate and the cleared cell lysate (Figure 6.13). This indicated that the majority of overproduced His$_6$.TanB^{H}, His$_6$.TanB^{H}.CTD and TaaB1^{H} were present in the bacterial cytoplasm as soluble proteins rather than as insoluble inclusion bodies.

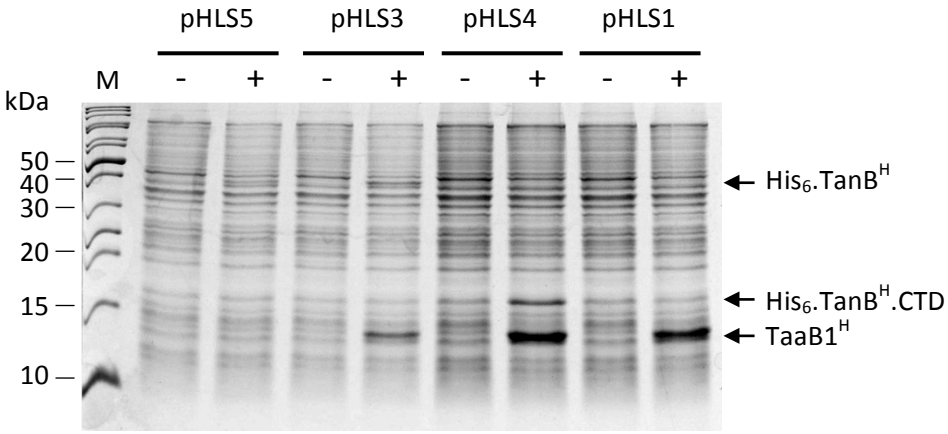

Figure 6.12 Test expression of plasmids containing *tanB^{H}*, *tanB^{H}.CTD* and *taaB1^{H}* for protein overproduction. Plasmids pHLS1 (containing *taaB1^{H}*), pHLS3 (*tanB^{H}* and *taaB1^{H}*), pHLS4 (*tanB^{H}.CTD* and *taaB1^{H}*) and pHLS5 (bicistronic *tanB^{H}-taaB1^{H}*) were introduced into the *E. coli* expression strain BL21(DE3)/pLysS. Strains were then grown at 37°C until an OD_{600} of 0.4 and induced with addition of 1 mM IPTG for 4 hours at 30°C. Uninduced (-) and induced (+) whole cell lysates were analysed by electrophoresis in a 15% SDS-PA gel and stained with Coomassie blue. Labelled arrows indicate the location of proteins of the expected molecular mass for each expression plasmid tested. Lanes labelled accordingly. M, EZ-Run *Rec* protein ladder.

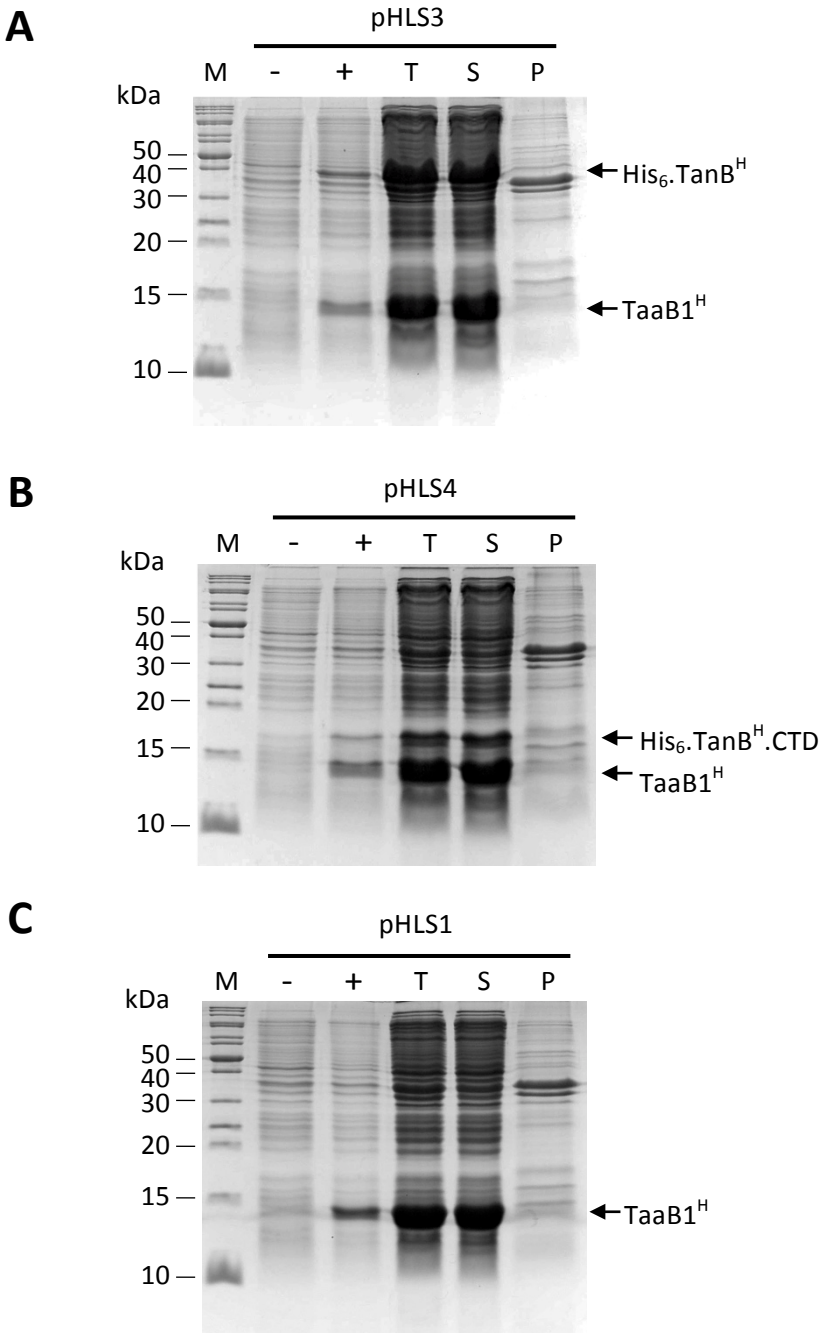

Figure 6.13 Solubility of $His_6.TanB^H$, $His_6.TanB^H.CTD$ and $TaaB1^H$. Cultures of BL21(DE3)/pLysS containing (A) pHLS3 , (B) pHLS4 and (C) pHLS1 were induced with 1 mM IPTG, following which cells were harvested, treated with lysozyme and sodium deoxycholate in the presence of PMSF for 1 hour, followed by 4 rounds of sonication at 30 second intervals and subsequent clearing by centrifugation. This resulted in a non-cleared lysate (T), supernatant (S) and pellet of insoluble material (P). Samples were subjected to SDS-PAGE in a 15% SDS-PA gel followed by staining with Coomassie blue. Labelled arrows indicate presence of overproduced plasmid-encoded protein at the expected molecular mass. Lanes are labelled accordingly. M, EZ-Run *Rec* protein ladder; (-) and (+) indicate whole cell lysate from uninduced and induced cultures, respectively.

6.3.3 Large-scale purification of His_6.$TanB^H$-$TaaB1^H$ and His_6.$TanB^H$.CTD-$TaaB1^H$ complexes by nickel affinity chromatography

Due to the necessity of co-expressing *taaB1*^{H} in order to clone and express intact copies of *tanB*^{H} and *tanB*^{H}*.CTD*, the first step in purification of these proteins meant purification of the proteins in complex with the putative immunity protein, $TaaB1^H$. To do this, large-scale cultures of BL21(DE3)/pLysS cells containing pHLS3 and pHLS4 were induced, and after cell disruption cleared lysates were subjected to immobilised metal-ion affinity chromatography (IMAC) using a HisTrap HP nickel column coupled to an ÄKTA FPLC system (Section 2.3.5). Addition of excess imidazole allows elution of His-tagged proteins that are non-covalently bound to immobilised nickel ions due to competition with the imidazole moiety of the histidine side chain for the nickel ions. Accordingly, a 10-500 mM imidazole gradient was applied to the column to enable elution of the bound His-tagged proteins. Monitoring of the absorbance (A_{280}) of the eluates indicated at which point in the imidazole gradient proteins began to be eluted from the nickel column. Both His_6.$TanB^H$ and His_6.$TanB^H$.CTD were eluted from the column at an imidazole concentration of approximately 150 mM. The purity of fractions collected were then analysed by SDS-PAGE (Figure 6.14). The presence of a 15 kDa protein present in the His_6.$TanB^H$ and His_6.$TanB^H$.CTD eluted fractions indicated that $TaaB1^H$ was also pulled-down in this purification, suggesting that His_6.$TanB^H$ and His_6.$TanB^H$.CTD were directly interacting with $TaaB1^H$ to form complexes. As $TaaB1^H$ did not interact non-specifically with the nickel resin (Section 6.7) it is likely that the co-elution of His_6.$TanB^H$ and His_6.$TanB^H$.CTD and $TaaB1^H$ was due to complex formation rather than non-specific binding of $TaaB1^H$ to the column.

6.3.4 Analysis of the effect of urea on dissociation of the His_6.$TanB^H$-$TaaB1^H$ complex

In order to analyse the enzymatic activity of $TanB^H$ the protein had to be dissociated from the complex formed with $TaaB1^H$. First, denaturation of the purified His_6.$TanB^H$-$TaaB1^H$ complex with 8 M urea and 5 mM DTT was undertaken. The complex was then subjected to further IMAC, using a HisTrap column

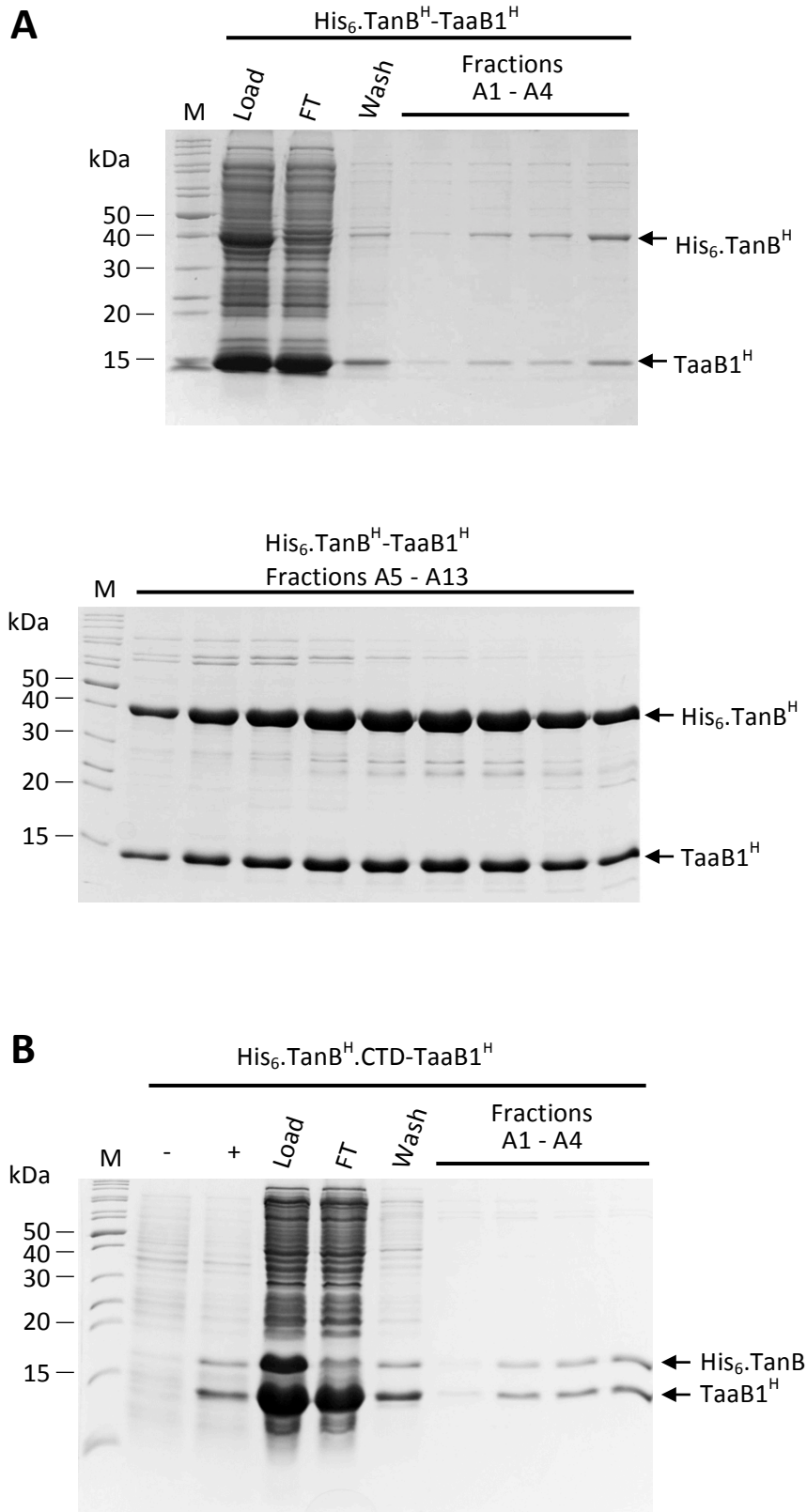
A
His6.TanBH-TaaB1H
M
Load
FT
Wash
Fractions A1 - A4
kDa
50
40
30
20
15
His6.TanBH
TaaB1H
His6.TanBH-TaaB1H
Fractions A5 - A13
M
kDa
50
40
30
20
15
His6.TanBH
TaaB1H
B
His6.TanBH.CTD-TaaB1H
M
-
+
Load
FT
Wash
Fractions A1 - A4
kDa
50
40
30
20
15
His6.TanBH.CTD
TaaB1H

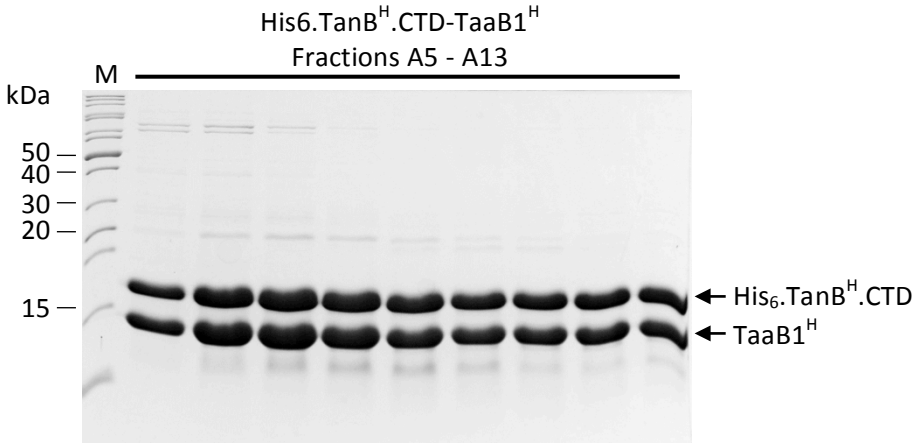

Figure 6.14 Purification of His_6.$TanB^H$ and His_6.$TanB^H$.CTD in complex with $TaaB1^H$ by IMAC. Cleared lysates (load) containing His-tagged proteins were bound to a 1 mL HisTrap nickel column and the flow through (FT) was retained. The column was washed with buffer containing 10 mM imidazole (wash) and then bound proteins were eluted by addition of a 10 to 500mM imidazole gradient using an ÄKTA purifier FPLC system and collected in 13 1mL fractions (A1-A13). SDS-PAGE analysis of the fractions eluted with imidazole during the purification of (A) His_6.$TanB^H$-$TaaB1^H$ and (B) His_6.$TanB^H$.CTD-$TaaB1^H$. 12% and 15% SDS-PA gels were used for the His_6.$TanB^H$-$TaaB1^H$ and His_6.$TanB^H$.CTD-$TaaB1^H$ complexes, respectively and were stained using Coomassie blue. Lanes are labelled accordingly and labelled arrows indicate purified proteins of the expected molecular mass. M, EZ-Run *Rec* protein ladder; (-) and (+) indicate whole cell lysates from uninduced and cultures, respectively,

equilibrated with 8 M urea, 50 mM Tris-HCl pH 7.5, 200 mM NaCl and 20 mM imidazole. Following binding of His_6.$TanB^H$, the column was washed with the same buffer, following which the protein was eluted in the same buffer but containing 150 mM imidazole. Samples of the eluted proteins were then analysed by SDS-PAGE to determine whether $TaaB1^H$ was still present in complex with His_6.$TanB^H$ (Figure 6.15). Presence of a 15 kDa protein alongside His_6.$TanB^H$ in the samples eluted with 150 mM imidazole indicated that $TaaB1^H$ was not dissociated from His_6.$TanB^H$ when treated with 8 M urea, suggesting the two proteins form a tightly bound complex.

6.3.5 Analysis of the effect of pH on dissociation of the His_6.$TanB^H$-$TaaB1^H$ complex in the presence of urea

Due to the observation that the presence of 8 M urea was ineffective at dissociating the His_6.$TanB^H$-$TaaB1^H$ complex an alternative strategy was undertaken. Using batch nickel affinity purification (Section 2.3.4) the His_6.$TanB^H$-$TaaB1^H$ complex was bound to nickel resin in the presence of 8 M urea and sequentially washed with denaturing buffer (8M urea, 50 mM Tris-HCl, 200 mM NaCl, and 20 mM imidazole) with increasing pH (pH 4, pH 6, pH 8 and pH 10). All eluted wash fractions were retained and residual bound proteins were then eluted by boiling the resin in SDS-PAGE sample buffer. Analysis of all samples by SDS-PAGE indicated that $TaaB1^H$ was still co-eluted with His_6.$TanB^H$ following equilibration of the complex with an acidic or alkaline buffer (Figure 6.16). Therefore, the His_6.$TanB^H$-$TaaB1^H$ complex is stable over a wide pH range.

6.3.6 Analysis of the effect of NaCl concentration on dissociation of His_6.$TanB^H$-$TaaB1^H$ complex

The effect of salt concentration on the stability of the His_6.$TanB^H$-$TaaB1^H$ complex was analysed. This was carried out by batch nickel affinity chromatography using sequential washes of the bound complex with a denaturing buffer containing increasing concentrations of NaCl (50 mM, 100 mM, 200 mM, 400 mM, 800 mM and 1 M) followed by a final elution by boiling the resin (Section 2.3.4).

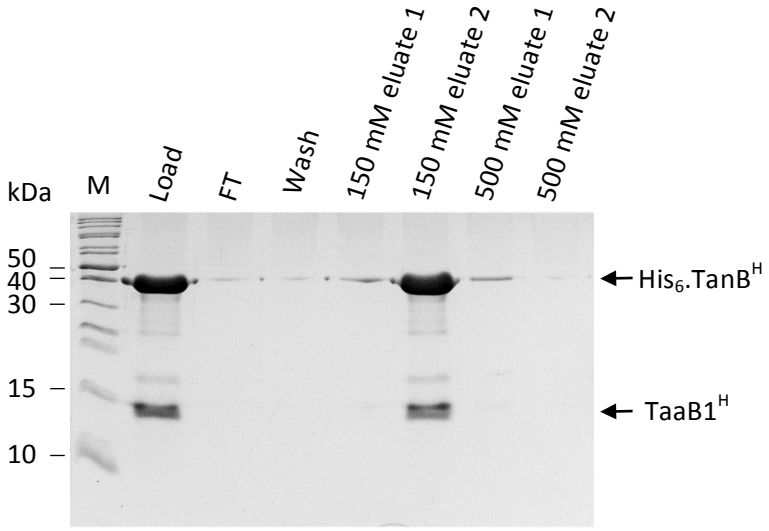

Figure 6.15 Effect of urea on dissociation of the His_6.$TanB^H$-$TaaB1^H$ complex during IMAC. The His_6.$TanB^H$-$TaaB1^H$ complex was purified by IMAC, subjected to buffer exchange into 8 M urea and 5 mM DTT and then loaded onto a His-Trap nickel column (load) equilibrated in 8 M urea, 50 mM Tris-HCl, 200 mM NaCl and 20 mM imidazole. The flow-through (FT) was retained. The column was then washed (wash) with the same buffer, following which bound proteins were eluted with the addition of the same buffer containing 150 mM imidazole. The same buffer containing 500 mM imidazole was then used to elute any proteins that remained bound to the column. Collected samples were then subjected to SDS-PAGE in a 12% SDS-PA gel stained by Coomassie blue. Lanes are labelled accordingly. M, EZ-Run *Rec* protein ladder, labelled arrows indicate purified proteins of the expected molecular mass.

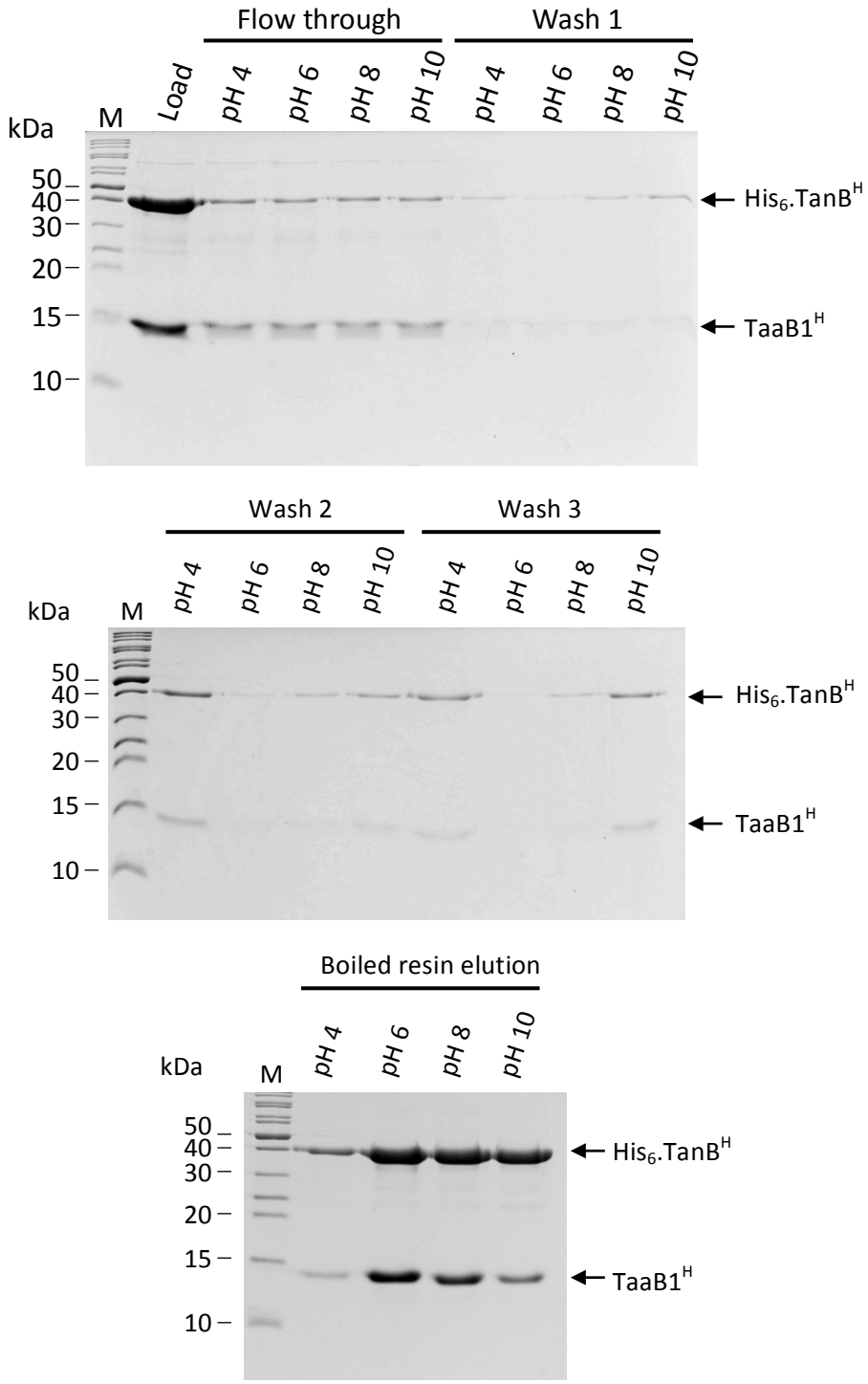

Figure 6.16 Analysis of the effect of pH on dissociation of the His_6.$TanB^H$-$TaaB1^H$ complex by IMAC. The His_6.$TanB^H$-$TaaB1^H$ complex was purified by IMAC, treated with 8 M urea and subsequently bond to nickel resin (load) equilibrated in 8 M urea, 50 mM Tris-HCl, 200 mM NaCl and 20 mM imidazole, and the flow-through was retained. The immobilised complex was then washed sequentially with a buffer with increasing pH (pH 4, 6, 8 or 10) (wash 1-3). Residual bound proteins were eluted by boiling the resin. Each eluted sample was subjected to electrophoresis in a 15% SDS-PA gel and stained by Coomassie blue. Lanes are labelled accordingly. Labelled arrows indicate eluted proteins of the expected molecular masses. M, EZ-Run *Rec* protein ladder.

Analysis of protein samples eluted at each NaCl concentration by SDS-PAGE indicated that TaaB1^{H} was eluted with His$_6$.TanB^{H} and was not dissociated from the complex by altering the NaCl concentration (Figure 6.17).

6.3.7 Analysis of the effect of guanidine hydrochloride on dissociation of the His$_6$.TanB^{H}-TaaB1^{H} complex

Several purification strategies using 8 M urea as a denaturant failed to dissociate the His$_6$.TanB^{H}-TaaB1^{H} complex. Therefore it was decided to analyse the effect of 6 M guanidine hydrochloride (GuHCl) containing 5 mM DTT as a denaturant for uncoupling of the His$_6$.TanB^{H}-TaaB1^{H} complex. A sample of the affinity purified His$_6$.TanB^{H}-TaaB1^{H} complex was subjected to buffer exchange using a 10000 MWCO centrifugal concentrator to give a final buffer composition of 6 M GuHCl, 5 mM DTT, 50 mM Tris-HCl pH 7.5, 200 mM NaCl and 20 mM imidazole. This sample was subjected to IMAC by the batch purification method (Section 2.3.4) in which a buffer containing 6M GuHCl, 5mM DTT, 50mM Tris-HCl pH 7.5, 200 mM NaCl and 20 mM imidazole was used as the wash buffer and protein elution was carried out by the sequential addition of the same buffer containing 150 mM imidazole and 500 mM imidazole. As samples that contain high concentrations of GuHCl are incompatible with SDS-PAGE, a 20 µL aliquot of all samples was subjected to TCA-acetone precipitation and resuspended in 10 µL of 1X SDS-PAGE sample buffer to allow analysis by SDS-PAGE (Figure 6.18). It was observed that that most of the TaaB1^{H} protein was collected in the flow through and accordingly His$_6$.TanB^{H} was present in fractions eluted with high imidazole concentrations, indicating that the His$_6$.TanB^{H}-TaaB1^{H} complex was successfully disrupted by exposure to 6 M GuHCl. Note that the abundance of TaaB1^{H} in the His6.TanB^{H}-TaaB1^{H} complex following treatment with 6 M GuHCl by buffer exchange was less abundant than previously observed. This may have been due to the use of a centrifugal concentrator in the initial buffer exchange stage. Substantial amounts of dissociated TaaB1^{H} may have passed through the nitrocellulose filter membrane during the buffer exchange process rather than being concentrated by it.

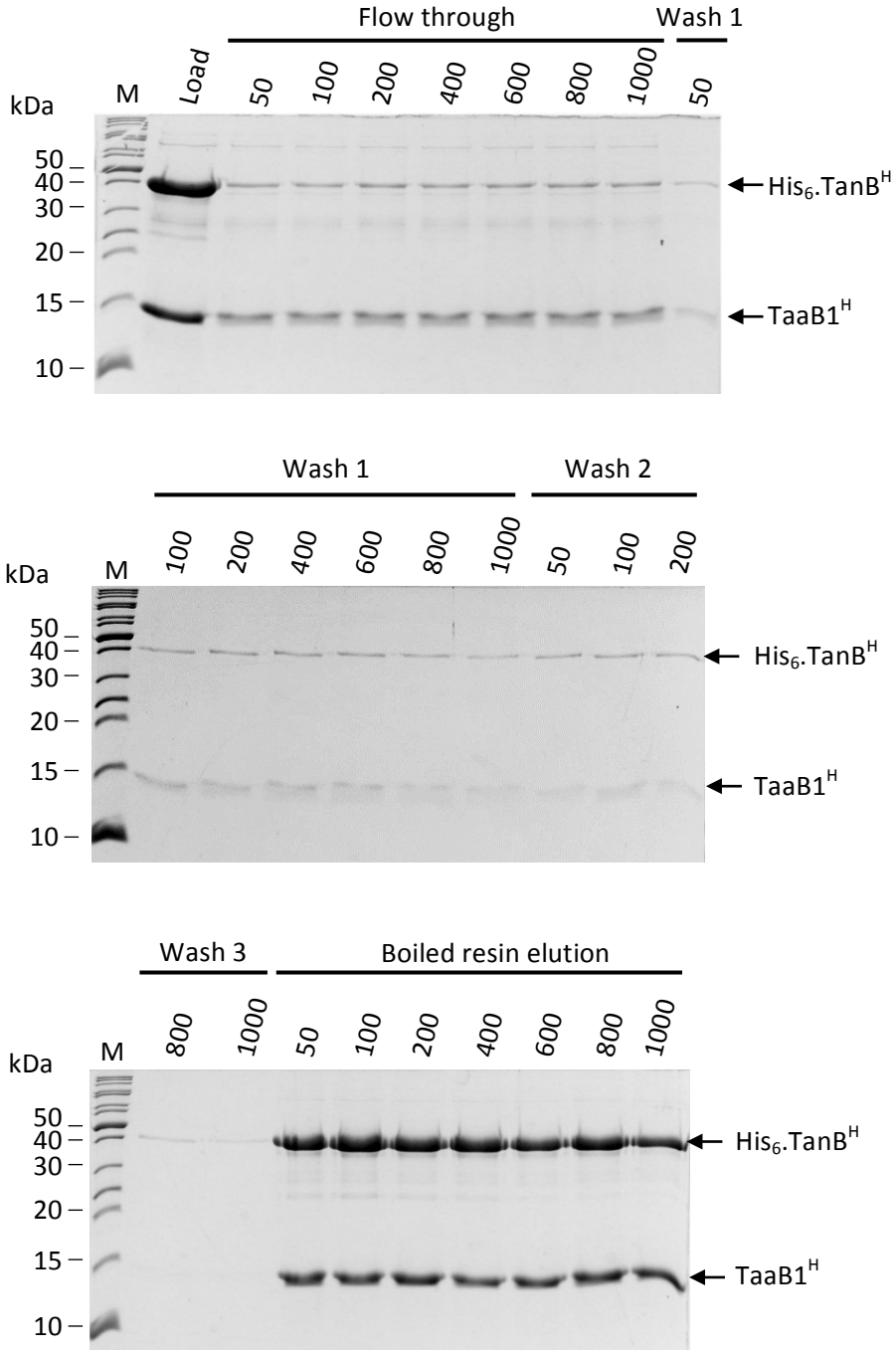

Figure 6.17 Analysis of the effect of NaCl concentration on dissociation of $His_6.TanB^H$-$TaaB1^H$ complex by IMAC. The $His_6.TanB^H$-$TaaB1^H$ complex was purified by IMAC, treated with 8 M urea and subsequently bond to nickel resin (load) equilibrated in 8 M urea, 50 mM Tris-HCl, 200 mM NaCl and 20 mM imidazole, and the flow-through was retained. The immobilised complex was then washed sequentially with buffers containing increasing concentrations of salt (50 mM, 100 mM, 200 mM, 400 mM, 800 mM and 1000 mM) (wash 1-3). Bound proteins were then eluted from the resin by boiling. Samples eluted at each stage were subjected to electrophoretic analysis in a 12% SDS-PA gel and stained with Coomassie blue. Lanes are labelled accordingly. M, EZ-Run *Rec* protein ladder, labelled arrows indicate eluted proteins of the expected molecular mass.

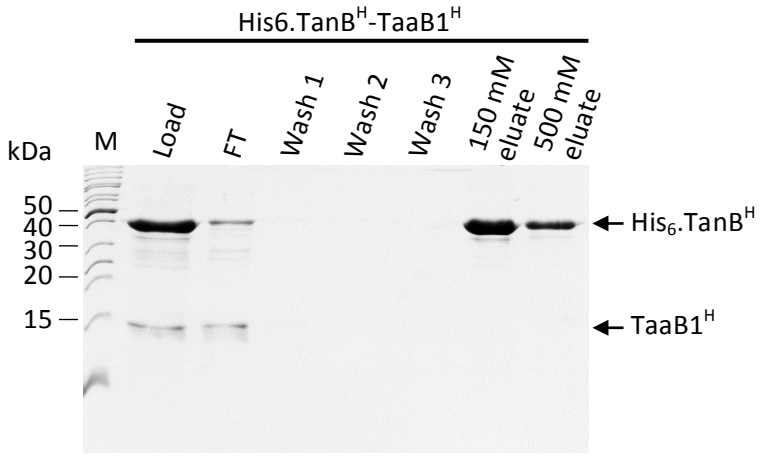

Figure 6.18 Analysis of the effect of guanidine hydrochloride on dissociation of the His_6.TanB^H-TaaB1^H complex by IMAC. The His_6.TanB^H-TaaB1^H complex was purified by IMAC, treated with 6 M GuHCl and 5 mM DTT by buffer exchange using a 10000 MWCO concentrator and then immobilised onto a His-Trap nickel column (load) where the flow-through (FT) was retained. The column was then washed with buffer containing 6 M GuHCl, 50 mM Tris-HCl, 200 mM NaCl and 20 mM imidazole (wash). Following this, bound proteins were eluted with addition of the same buffer containing 150 mM imidazole and 500 mM imidazole. Collected samples were subjected to electrophoresis in a 15% SDS-PA gel and stained with Coomassie blue. Lanes are labelled accordingly. Labelled arrows indicate eluted proteins of the expected molecular mass. M, EZ-Run *Rec* protein ladder.

6.3.8 Large-scale purification of His_6.$TanB^H$ and His_6.$TanB^H$.CTD by IMAC under denaturing conditions

To generate sufficient quantities of purified His_6.$TanB^H$ and His_6.$TanB^H$.CTD for functional analysis, large-scale purification of His_6.$TanB^H$ and His_6.$TanB^H$ from their respective complexes with $TaaB1^H$ was undertaken as described in Section 6.3.7, using a 1 mL HisTrap HP column rather than the batch purification method. Renaturation of His_6.$TanB^H$ and His_6.$TanB^H$.CTD was either performed by in-column renaturation with imidazole elution buffer without denaturants, or post-elution renaturation by overnight dialysis into 50 mM Tris-HCl (pH 7.5). Purified His_6.$TanB^H$ and His_6.$TanB^H$.CTD samples were then concentrated using a 10000 or 3000 MWCO concentrator, respectively, giving a final protein concentration of approximately 1.4 mg/mL. The purity of the samples was determined by SDS-PAGE (Figure 6.19).

6.3.9 Purification of a spontaneous G276D mutant of $TanB^H$

A spontaneous mutant copy of *tanB*^{H} was identified during attempts to clone the gene in the absence of the putative immunity protein-encoding gene *taaB1*^{H}. This mutant contained a single base pair substitution that resulted in the substitution of a glycine codon 276 by an aspartate codon, within the coding sequence of the CTD of $TanB^H$. This residue was near/within the predicted active site of the enzyme, next to a histidine residue identified to be the likely catalytic residue for DNA hydrolysis (His277).

The plasmid expressing the mutant gene, pHLS7, was induced in BL21(DE3)/pLysS for overproduction and purification of the mutated version of the protein by IMAC under non-denaturing conditions (Section 6.3.8), without the use of GuHCl. The resulting purified protein was analysed by SDS-PAGE (Figure 6.19). It was expected that the G276D derivative would have reduced nuclease activity compared to the wild-type protein, as the coding sequence could be cloned in the absence of *taaB1*^{H}, and therefore it could act as a negative control in the analysis of the nuclease activity of $TanB^H$.

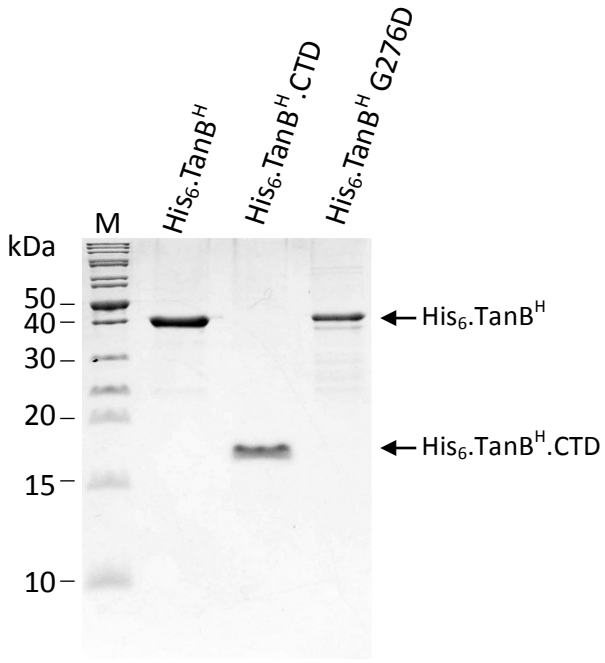

Figure 6.19 Purification of His_6.$TanB^H$, His_6.$TanB^H$.CTD and His_6.$TanB^H$ G276D by IMAC. His_6.$TanB^H$ and His_6.$TanB^H$.CTD were purified in complex with $TaaB1^H$ by native IMAC then treated with 6 M GuHCl and subjected to IMAC under denaturing conditions. Eluted samples were then pooled and dialysed overnight against 50 mM Tris-HCl (pH 7.5) using a 3000 MWCO dialysis membrane. Resulting dialysate was concentrated using a 10000 MWCO centrifugal concentrator and protein purity assessed by SDS-PAGE. The His_6.$TanB^H$ G276D mutant was purified using native IMAC as standard procedure, where the purest fractions were combined, and dialysed against 50 mM Tris-HCl. Lanes as indicated. Labelled arrows indicate eluted proteins of the expected molecular weight. M, EZ-Run *Rec* protein ladder.

6.4 Analysis of DNase activity of TanB^{H} and TanB^{H}.CTD

TanB^{H} contains a predicted non-specific endonuclease domain (Endonuclease_NS_2, pfam13930) at the C-terminus of the protein, so following purification of both the full-length protein and the CTD alone, it was decided to investigate whether these proteins possessed non-specific DNase activity.

6.4.1 Analysis of DNase activity of purified TanB^{H} and TanB^{H}.CTD by DNA zymography

DNase activity can be analysed by the use of DNA substrate polyacrylamide gels, also known as DNA zymography. Here, DNase activity results in the degradation of DNA embedded within the gel, which can be visualised as a non-fluorescent region when the gel is viewed under UV illumination following staining with ethidium bromide. To help determine whether the predicted nuclease TanB^{H} possessed DNase activity, a preliminary DNA zymogram analysis was undertaken on whole cell lysates of induced BL21(DE3)/pLysS cells containing pHLS1, pHLS3 and pHLS4 (Section 2.8.1). Non-fluorescent zones located at the position corresponding to proteins of the same molecular mass of His$_6$.TanB^{H} (40 kDa) and His$_6$.TanB^{H}.CTD (17 kDa) were present on the ethidium bromide stained DNA-substrate gel (Figure 6.20A), suggesting TanB^{H} possessed DNase activity which was located in the CTD. A non-fluorescent region corresponding to the migration of a protein of 25 kDa was also detected in all crude lysate samples irrespective of whether TanB^{H} was induced. This was likely to be an *E. coli* host strain DNase, possibly the periplasmic DNase EndA that has a molecular mass of 25 kDa before processing.

To further confirm the DNase activity of TanB^{H}, affinity purified His$_6$.TanB^{H}, His$_6$.TanB^{H}.CTD and His$_6$.TanB^{H} G276D were subjected to DNA zymography (Figure 6.20B). As expected, non-fluorescent regions, indicative of DNA degradation, were present at the locations corresponding to proteins migrating with the expected molecular masses for both His$_6$.TanB^{H} and His$_6$.TanB^{H}.CTD. Non- fluorescent regions corresponding to proteins of lower molecular masses were also present in the sample of full length His$_6$.TanB^{H}, which may have been due to C-terminal

A

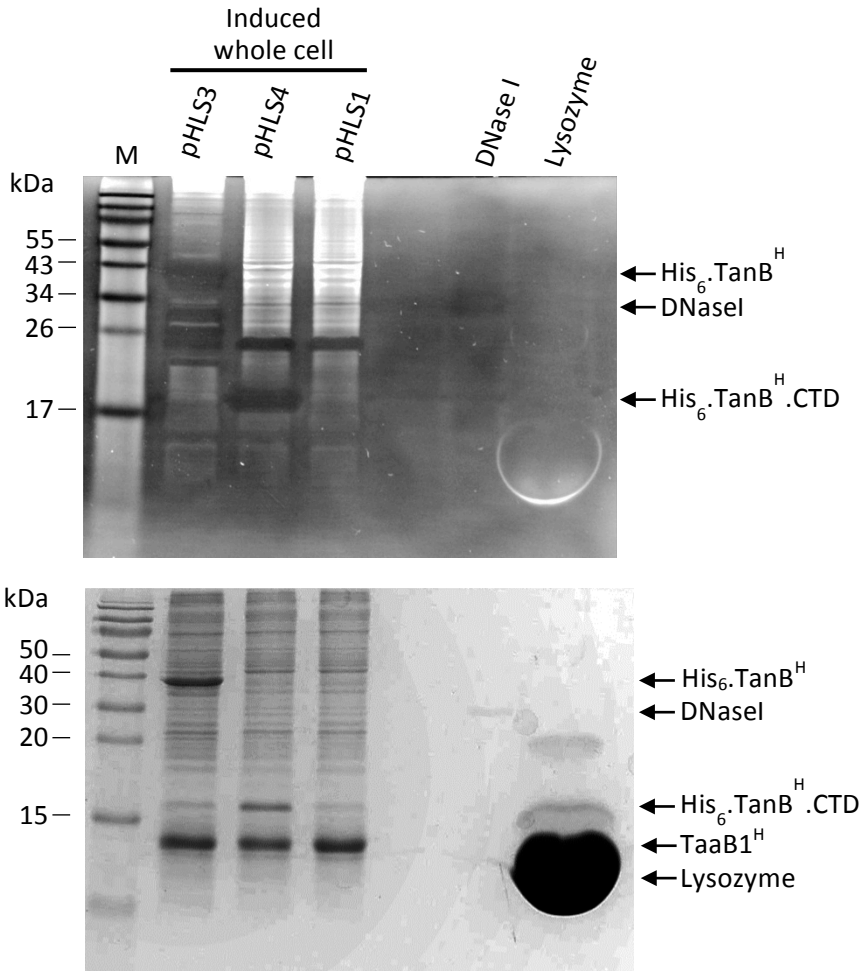
Induced
whole cell
pHLS3
pHLS4
pHLS1
DNase I
Lysozyme
M
kDa
55
43
34
26
17
His6.TanBH
DNaseI
His6.TanBH.CTD
kDa
50
40
30
20
15
His6.TanBH
DNaseI
His6.TanBH.CTD
TaaB1H
Lysozyme

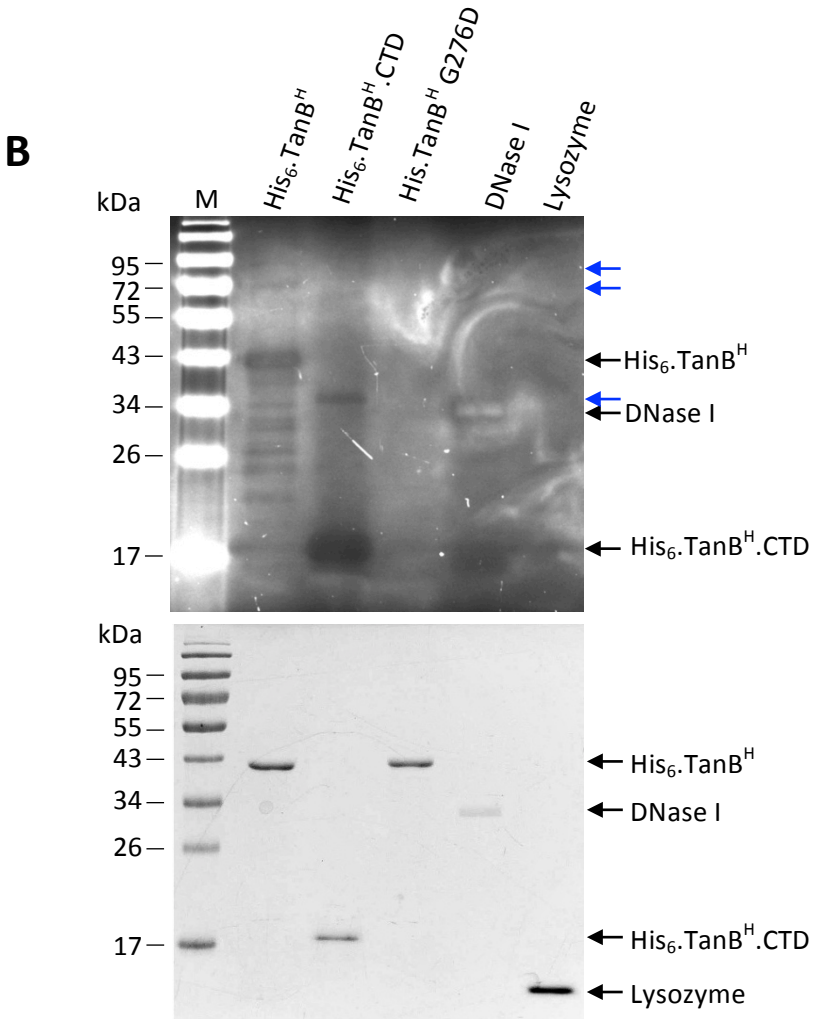

Figure 6.20 Analysis of DNase activity of TanB^H and TanB^H.CTD by DNA zymography. Samples were electrophoresed in 15% SDS-PA substrate gels co-polymerised with 30 µg/mL sheared salmon testis DNA. Gels were sequentially washed in buffer containing 40 mM Tris-HCl (pH 7.6) to remove SDS, and then incubated in renaturation buffer (50 mM Tris-HCl, pH 7.5, 5 mM $MgCl_2$, and 20% 2-propanol). DNase activity was assessed by incubation in reaction buffer (50 mM Tris-HCl, pH 7.5, 5 mM $MgCl_2$, 2 mM $CaCl_2$, and 0.1% Triton X-100) for 37°C for 2 hours, and then visualised by staining of the gel with ethidium bromide solution and imaged by UV illumination. Non-fluorescent bands in the gel indicate DNase activity. (A) DNase activity of induced whole cell lysates of BL21(DE3)/pLysS containing expression plasmid pHLS3, pHLS4 and pHLS1, as indicated (top). Duplicated SDS-PA gel of the DNA-substrate gel stained with Coomassie blue (bottom). Arrows indicate proteins migrating at the expected molecular mass for each protein and equivalent non-fluorescent regions in the DNA-substrate gel. (B) DNase activity of purified His$_6$.TanB^H, His$_6$.TanB^H.CTD, His$_6$.TanB^H G276D mutant (top) and equivalent SDS-PA gel of the DNA substrate gel stained with Coomassie blue (bottom). Arrows indicate proteins migrating at the expected molecular mass for each protein and equivalent non-fluorescent regions in the DNA-substrate gel. Blue arrows indicate non-fluorescent regions migrating at the molecular mass equivalent to dimers complexes. Samples as indicated above the lanes. Purified DNase I, bovine pancreatic (31 kDa) was used as a positive control for DNase activity, and lysozyme, chicken egg white (14.3 kDa) was used as a negative control. M, EZ-Run *Rec* protein ladder (unstained or pre-stained).

degradation products of the protein that retained DNase activity. Non-fluorescent regions were not detected for the His_6.$TanB^H$ G276D mutant, indicating this variant had a substantially decrease DNase activity in comparison to the wild-type protein. Note, non-fluorescent regions corresponding to proteins migrating at a higher molecular mass in both His_6.$TanB^H$ and His_6.$TanB^H$.CTD samples were observed, shown by blue arrows in Figure 6.20. The additional band in the sample of His_6.$TanB^H$.CTD corresponded to a molecular mass of approximately 36 kDa, which is similar to the theoretical molecular mass of a dimeric His_6.$TanB^H$.CTD structure, and the additional bands in the sample of full length His_6.$TanB^H$ corresponded to 72 kDa and 86 kDa, the latter being similar to the theoretical molecular mass of a dimeric His_6.$TanB^H$ structure. As the samples were electrophoresed in system containing SDS in the gel and in the running buffer one would not expected dimer formation. However, the protocol calls for the use of SDS-PAGE sample buffer without a reducing agent, nor are the samples boiled before loading, so there is a possibility of small amounts of multimeric structures (either native or forced) being present in the samples that resist dissociated by SDS.

6.4.2 Analysis of the ability of $TanB^H$ and $TanB^H$.CTD to degrade dsDNA in solution

The ability of $TanB^H$ and $TanB^H$.CTD to degrade linearised double stranded DNA (dsDNA) in solution was analysed (Section 2.8.2). pBluescript II plasmid DNA was linearised by digestion with BamHI, purified and then used to evaluate dsDNA degradation by $TanB^H$. Evaluation of the integrity of the dsDNA after incubation with His_6.$TanB^H$ and His_6.$TanB^H$.CTD indicated that both were able to successfully degrade dsDNA irrespective of the presence of additional $MgCl_2$ or $CaCl_2$ (Figure 6.21).

EDTA is a known inhibitor of nuclease activity due to its ability to chelate divalent cations. To determine whether the DNase activity of $TanB^H$ (via its CTD) required divalent cations, 20 mM EDTA was included in samples with or without $MgCl_2$ and $CaCl_2$. EDTA appeared to reduce DNase activity when in combination with both $TanB^H$ and $TanB^H$.CTD alone, but not when incubated with additional

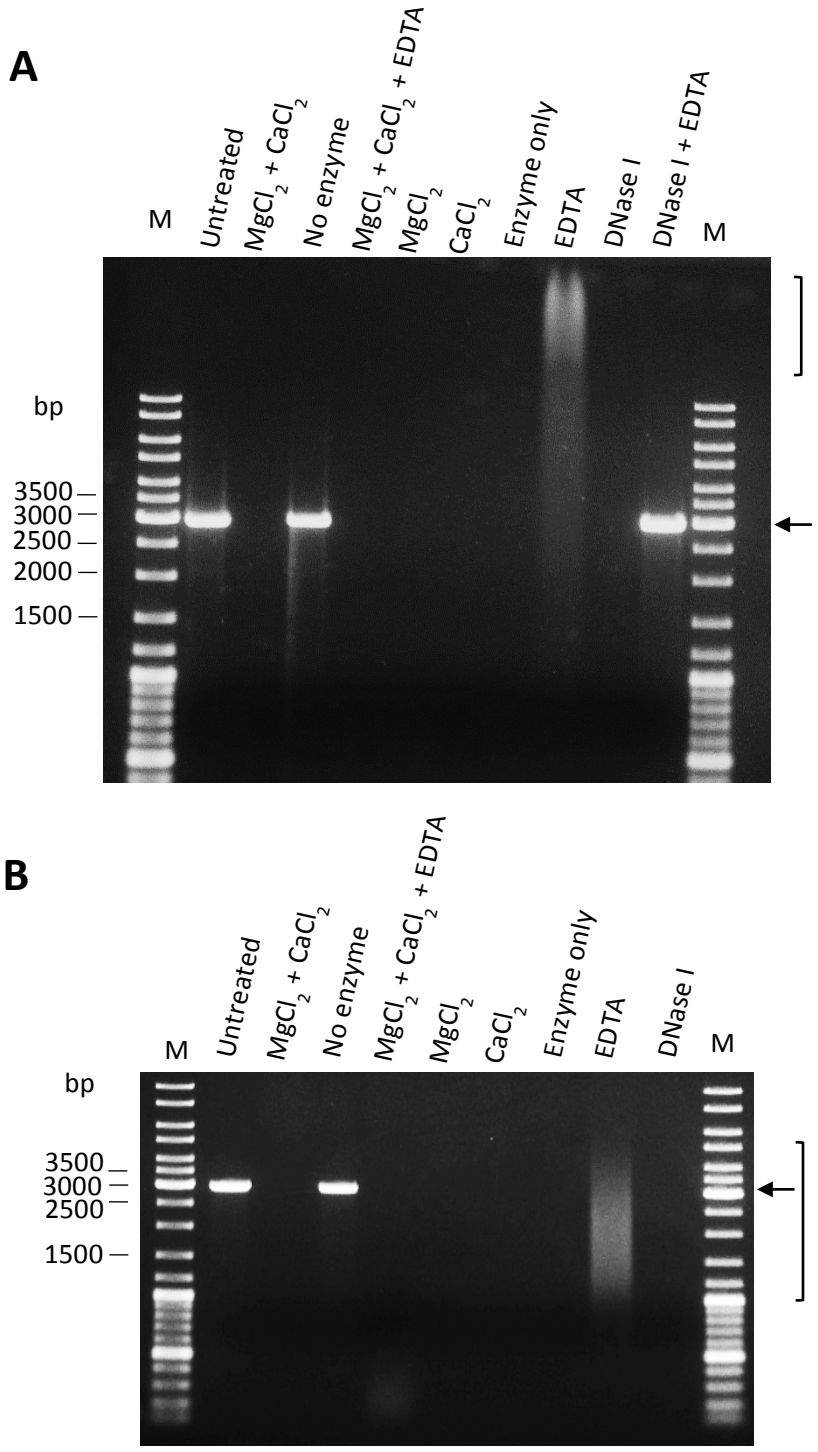

Figure 6.21 In-solution degradation of dsDNA by TanB^{H} and TanB^{H}.CTD. 100 ng dsDNA (pBluescript II (2961bp) linearised by BamHI restriction digestion) was incubated with 2.8 µg purified enzyme in a reaction buffer containing 10 mM Tris-HCl (pH 8.0), with or without 2.5 mM $MgCl_2$, 0.5 mM $CaCl_2$ or 20 mM EDTA in a total reaction volume of 10 µL and incubated at 37°C for 2 hours. DNase I was used as positive control. The integrity of the dsDNA was then determined by DNA gel electrophoresis in a 0.8% agarose DNA and stained with ethidium bromide, after incubation with (A) His_6.TanB^{H} and (B) His_6.TanB^{H}.CTD. Arrows indicate undigested dsDNA, and black lines indicate slower migrating DNA that has been bound by the nuclease due to inhibition of DNase activity by EDTA. M, GeneRuler DNA ladder mix

$MgCl_2$ and $CaCl_2$, as indicated by smearing of the dsDNA (Figure 6.21). The smearing may be due to the association of the nuclease with the DNA, retarding the migration of the DNA in the agarose gel. A greater shift in migration was observed when dsDNA was incubated with full length $TanB^H$ containing EDTA than when incubated the CTD and EDTA. This may indicate that the migration of dsDNA (due to complex formation between $TanB^H$ and the DNA) is perhaps being further retarded by the formation of multimers between $TanB^H$. Together, this indicates that the DNase activity of $TanB^H$ is dependent on divalent cations as the results suggest EDTA was able to chelate any trace divalent cations and prevent DNase activity, but 20 mM EDTA was not enough to chelate the additional $MgCl_2$ and $CaCl_2$ used in the reaction buffer.

6.4.3 Analysis of the ability of $TanB^H$ and $TanB^H$.CTD to degrade supercoiled DNA in solution

The ability of $TanB^H$ and $TanB^H$.CTD to degrade supercoiled pBluescriptII plasmid DNA in-solution was ascertained. 2.8 µg of purified His_6.$TanB^H$ or His_6.$TanB^H$.CTD was combined with pBluescript II in 10 mM Tris-HCl (pH 7.5) reaction buffer with or without potential co-factors $MgCl_2$ and $CaCl_2$, and incubated for 2 hours at 37°C. The integrity of plasmid DNA after incubation was analysed by agarose gel electrophoresis (Figure 6.22). Results showed that both $TanB^H$ and $TanB^H$.CTD were able to degrade supercoiled plasmid DNA irrespective of buffer composition, with or without addition of $MgCl_2$ or $CaCl_2$. Furthermore, plasmid DNA was not degraded when subjected to the above conditions without $TanB^H$ and $TanB^H$.CTD added, indicating that the enzymes were solely responsible for plasmid DNA degradation rather than trace DNase contamination of the reaction buffer. The divalent metal ion-chelating agent, EDTA, inhibited DNase activity of both $TanB^H$ and $TanB^H$.CTD in the reactions containing no additional $MgCl_2$ and $CaCl_2$, similar to that seen in the assessment of the dsDNA activity of $TanB^H$ in Section 6.4.2.

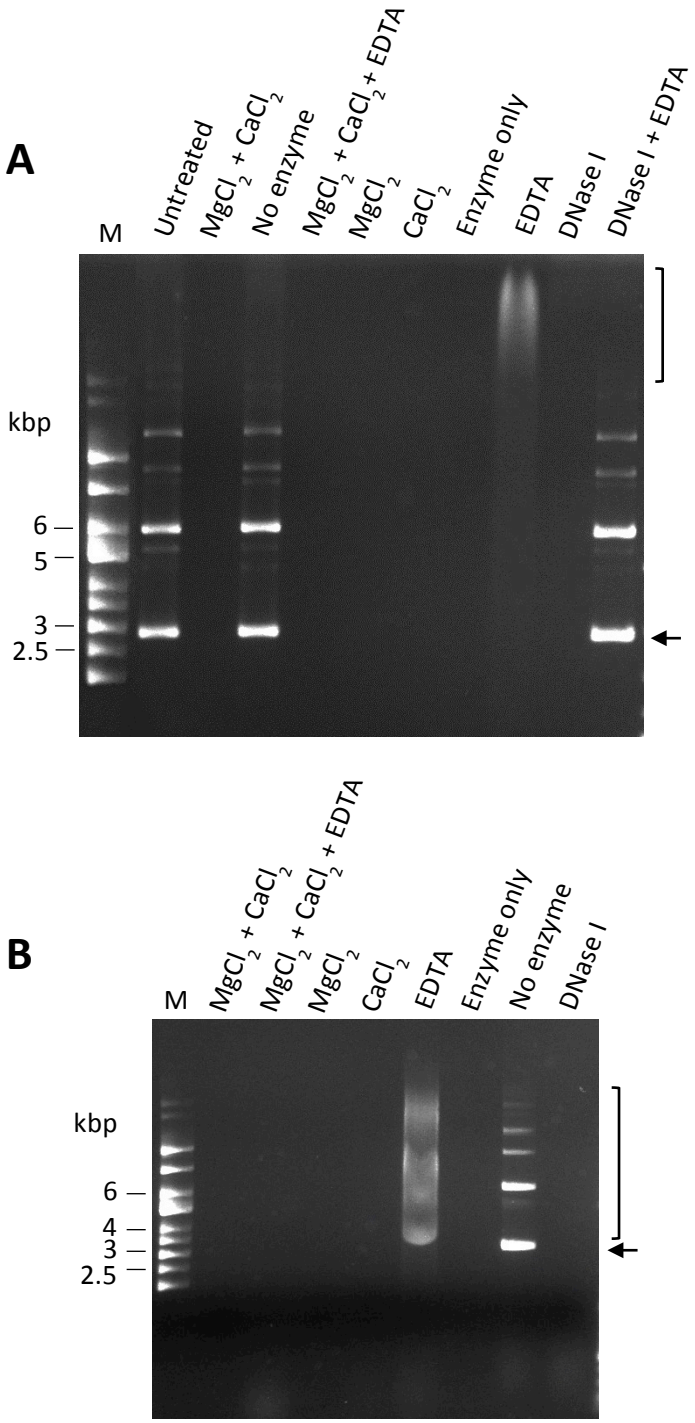

Figure 6.22 In-solution degradation of pBluescript II plasmid DNA by purified TanB^{H} and TanB^{H}.CTD. 100 ng supercoiled plasmid DNA (pBluescriptII) was incubated 2.8 µg purified enzyme in a reaction buffer containing 10 mM Tris-HCl (pH 8.0), with or without 2.5 mM $MgCl_2$, 0.5 mM $CaCl_2$ or 20 mM EDTA in a total reaction volume of 10 µL and incubated at 37°C for 2 hours. DNase I was used as positive control. The integrity of the plasmid DNA was then determined by electrophoresis in a 0.8% agarose gel after incubation with (A) His_6.TanB^{H} and (B) His_6.TanB.CTD. Arrows indicate intact plasmid DNA, and black lines indicate slower migrating DNA that has been bound by the nuclease due to inhibition of DNase activity by EDTA. M, Supercoiled ladder.

6.4.4 Analysis of ability of TanB^{H} and TanB^{H}.CTD to degrade single-stranded DNA in solution

To determine if TanB^{H} and TanB^{H}.CTD were able to degrade single stranded DNA (ssDNA), an in-solution degradation assay was performed (Section 2.8.2), using purified M13mp18 ssDNA as the substrate. Results shown in Figure 6.23 show that both purified TanB^{H} and TanB^{H}.CTD were able to degrade ssDNA irrespective of additional $MgCl_2$ and $CaCl_2$. The presence of 20 mM EDTA was unable to inhibit the DNase activity of TanB^{H} and TanB^{H}.CTD when additional divalent cations were present, but this was not unexpected as similar were observed when tested with dsDNA and supercoiled DNA (Section 6.4.2 and 6.4.3). It is likely that 20 mM EDTA is not enough to chelate the entirety of the Mg^{2+} ions in the reaction buffer.

6.4.5 Analysis of DNase activity of TanB^{H} and TanB^{H}.CTD using DNase test agar

For a rapid and easier determination of the DNase activity of TanB^{H}, DNase test agar was adapted for this purpose. DNase agar plates containing 0.005% (w/v) methyl green, a dye that intercalates high molecular weight DNA to form a coloured complex, were used. When DNA is hydrolysed, unbound dye is released, resulting in decolourisation (Kurnick, 1950; Schreier, 1969; Smith et al., 1969). Affinity purified TanB^{H} and TanB^{H}.CTD in 10 mM Tris-HCl (pH 7.5) were applied to wells bored into DNase test agar plates and incubated at 37°C. After two hours incubation zones of decolourisation began to appear around wells containing both TanB^{H} and TanB^{H}.CTD but not around the negative control well containing only Tris-HCl buffer (**Figure 6.24**A). The diameter of decolourisation became larger over time and was extensive after 16 and 36 hours incubation (**Figure 6.24**B and 6.24C). These results further confirm the DNase activity of TanB^{H} and TanB^{H}.CTD. It was also noted that the diameter of decolourisation for TanB^{H}.CTD was more extensive than that of full length TanB^{H}, which may have been due to a higher molar equivalent of TanB^{H}.CTD being applied to the wells than for TanB^{H}.

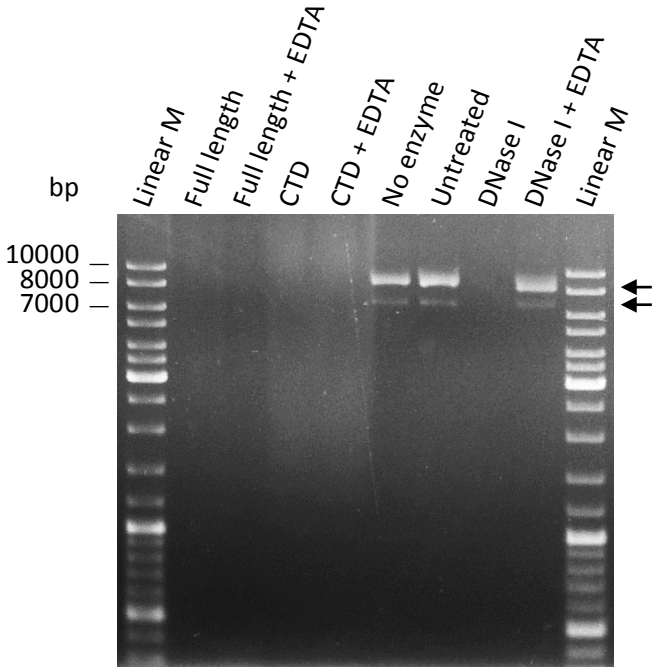

Figure 6.23 Analysis of the degradation of single stranded DNA by TanB^{H} and TanB^{H}.CTD. 250 ng of M13mp18 single-stranded DNA was incubated with 2.8 μg of either TanB^{H} or TanB^{H}.CTD in reaction buffer containing 10 mM Tris-HCl with or without 2.5 mM $MgCl_2$, 0.5 mM $CaCl_2$ and 20 mM EDTA in a total reaction volume of 10 μL for 2 hours at 37°C. DNA integrity was analysed by electrophoresis in a 0.8% agarose gel. Reaction buffer only control, and untreated ssDNA were also included, as well as DNase I positive control. Upper arrow indicates presence of intact circular M13mp18 ssDNA and lower arrow indicates linear M13mp18 ssDNA. Lanes as indicated. M, GeneRuler DNA ladder mix**.**

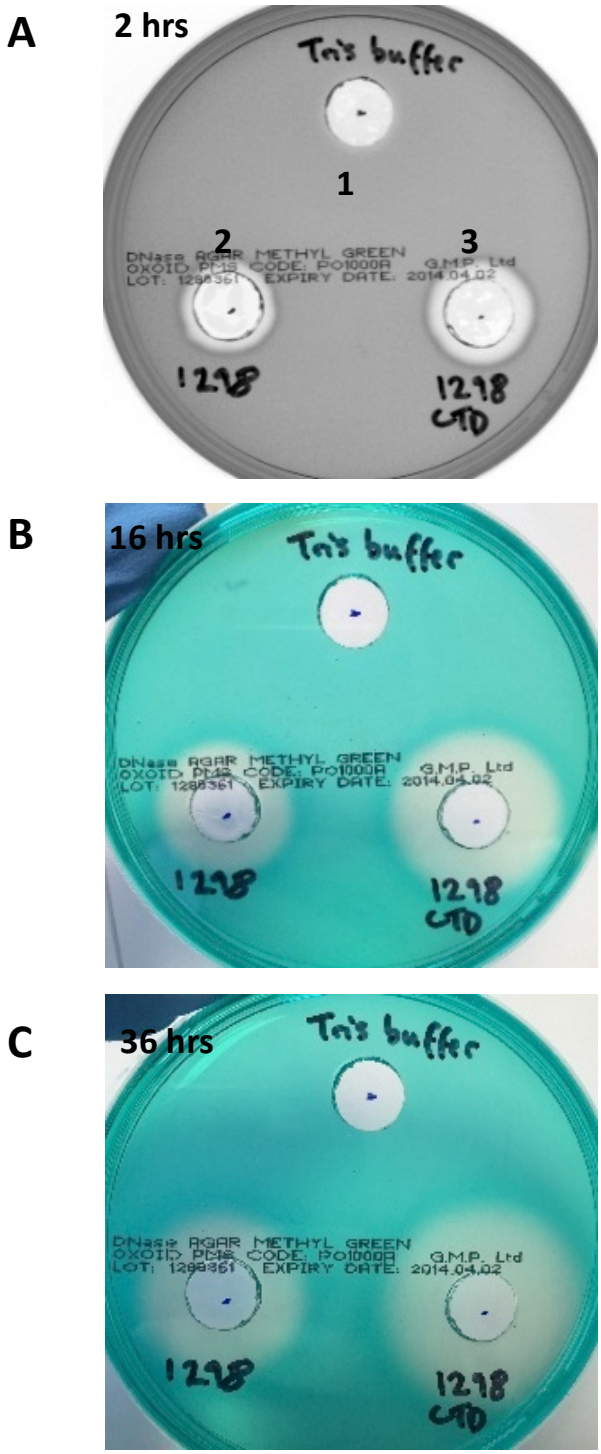

Figure 6.24 Analysis of DNase activity of TanB^{H} and TanB^{H}.CTD using DNase test agar. 2.8 μg purified His$_6$.TanB^{H} (2) and His$_6$.TanB^{H}.CTD (3) in 10 μL of 10 mM Tris buffer (pH 7.5) was applied to wells bored into DNase test agar plates containing 0.005% (w/v) methyl green and incubated at 37°C for 36 hours. Appearance of zones of decolourisation indicating DNase activity was monitored and imaged at (A) 2 hours, (B) 16 hours and (C) 36 hours post-incubation. 10 mM Tris-HCl buffer containing no enzyme was used as a negative control (1). Note, for better clarity of zones of decolourisation at 2 hours post incubation images were taken using a Kodak EDTA imaging system that was only able to capture images in black and white.

6.4.6 Thermo-stability of TanB^{H} and TanB^{H}.CTD DNase activity

Most proteins are susceptible to heat inactivation at 56°C or above. However, thermo-stable enzymes have been described, including the *S. aureus* nuclease, Nuc, which retains DNase activity after heating up to 97°C for 10 minutes (Lachica et al., 1972), as well as a glucose dehydrogenase from a *Burkholderia cepacia* complex spp. that is activate up to 70°C (Sode et al., 1996; Inose et al., 2003). To determine whether the DNase activity of TanB^{H} could tolerate extreme heat, purified samples of TanB^{H} and TanB^{H}.CTD were subjected to boiling in 50 mM Tris-HCl buffer for 10 minutes, and then the DNase activity was compared to that of untreated TanB^{H} and TanB^{H}.CTD by in-solution degradation of plasmid DNA (Section 2.8.2). Analysis of plasmid DNA integrity (Figure 6.25A) indicated that heat-treated TanB^{H} and TanB^{H}.CTD were still able to degrade plasmid DNA suggesting TanB^{H} is thermo-stable.

Analysis of DNase activity on a DNA substrate gel was undertaken to further explore the heat stability of TanB^{H}. Purified TanB^{H} was subjected to heat treatment in non-reducing (without β-mercaptoethanol) and reducing (with β-mercaptoethanol) SDS-PAGE sample buffer and the enzyme activity compared to unheated samples by DNA zymogram analysis (Section 2.8.1). Visualisation of the DNA-substrate gel after ethidium bromide staining indicated non-fluorescent zones at the expected molecular mass for TanB^{H} (40 kDa) in all samples irrespective of heat treatment or presence of β-mercaptoethanol (Figure 6.25B). However, several non-fluorescent zones corresponding to the migration of lower molecular mass proteins (16-18 kDa) were more prominent in the heated TanB^{H} samples, suggesting that heat treatment was having some effect on the stability of the protein, possibly generating more degradation products that still maintained DNase activity.

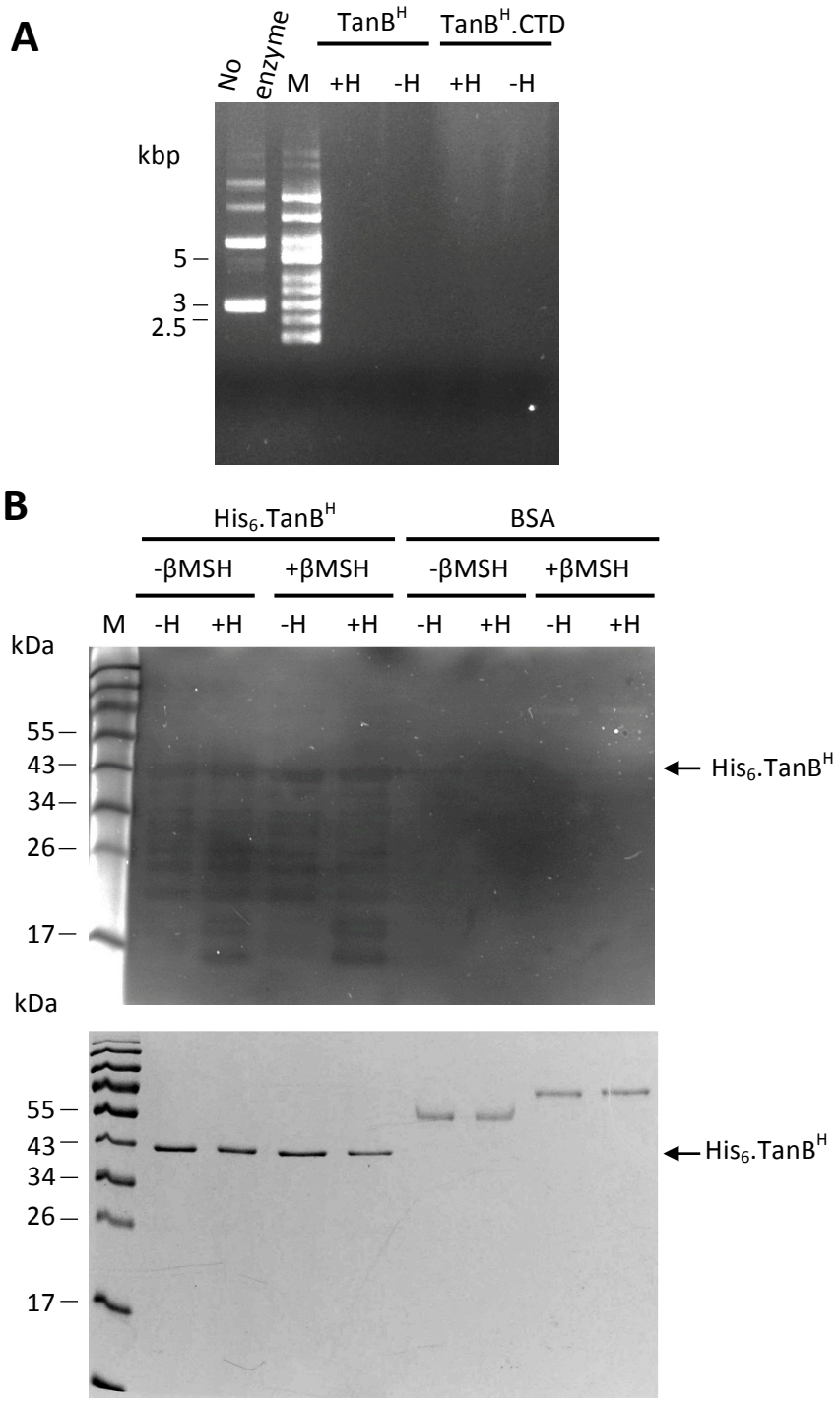

Figure 6.25 Analysis of the DNase activity of TanB^H following heat treatment. 10 μL of purified enzyme was boiled for 10 minutes in 50 mM Tris-HCl (pH 7.5) and the DNase activity determined. (A) Resulting plasmid degradation from in-solution degradation assay using unheated (-H) and heated (+H) samples of His$_6$.TanB^H and His$_6$.TanB^H.CTD. M, Supercoiled DNA ladder. (B) DNA-zymogram analysis (top) of the effect of boiling His$_6$.TanB^H in SDS-PAGE sample buffer with (+βMSH) and without (-βMSH) β-mercaptoethanol as a reducing agent. BSA (right) is used a DNase negative control. Bottom image is a corresponding Coomassie stain of the samples from the DNA-substrate gel. Lanes as indicated. M, EZ-Run *Rec* protein ladder.

6.5 Inhibition of TanB^{H} DNase activity by TaaB1^{H}

It is known that in other T6SS-containing bacteria immunity proteins are encoded adjacent to the gene that encodes their cognate T6SS-effector. Coupling this observation with the results presented in Section 6.2, which demonstrated the inability to clone *tanB^{H}* in the absence of the *taaB1^{H}*, it was decided to investigate whether TaaB1^{H} was able to directly inhibit the enzymatic activity of TanB^{H}.

6.5.1 Purification of TaaB1^{H}

To test the ability of TaaB1^{H} to inhibit TanB^{H}, TaaB1^{H} had to be purified. To do this, the affinity purified His_6.TanB^{H}.CTD-TaaB1^{H} complex was denatured in the presence of 6 M GuHCl and 5 mM DTT, followed by subtractive IMAC. Here, un-complexed His_6.TanB^{H}.CTD was sequestered by passing the solution through a HisTrap nickel column, followed by further washes with denaturing buffer containing 6 M GuHCl, 5 mM DTT, 50 mM Tris-HCl (pH 7.5), 200 mM NaCl, and 20 mM imidazole to remove residual TaaB1^{H}, and then immobilised proteins eluted. SDS-PAGE analysis of samples from each stage of this purification indicated that TaaB1^{H} was present in the flow through and initial wash fractions (data not shown). Therefore, these two fractions were combined and TaaB1^{H} was allowed to refold by removal of buffer denaturants to give a final buffer composition of 50 mM Tris-HCl (pH 7.5). This was achieved by several rounds of concentration and re-suspension using a 10000 MWCO concentrator. TaaB1^{H} purity was analysed by SDS-PAGE (Figure 6.26A) and observed to be >95% pure.

6.5.2 Analysis of the inhibitory effect of TaaB1^{H} on the DNase activity of TanB^{H} and TanB^{H}.CTD

To determine whether TaaB1^{H} was able to inhibit the DNase activity of TanB^{H} and TanB^{H}.CTD, the in-solution DNA degradation assay was employed (Section 2.8.2). Addition of a 2-fold excess of TaaB1^{H} to pBluescript II samples containing purified TanB^{H} or TanB^{H}.CTD resulted in inhibition of DNase activity as judged by the presence of intact plasmid DNA in samples containing TaaB1^{H},

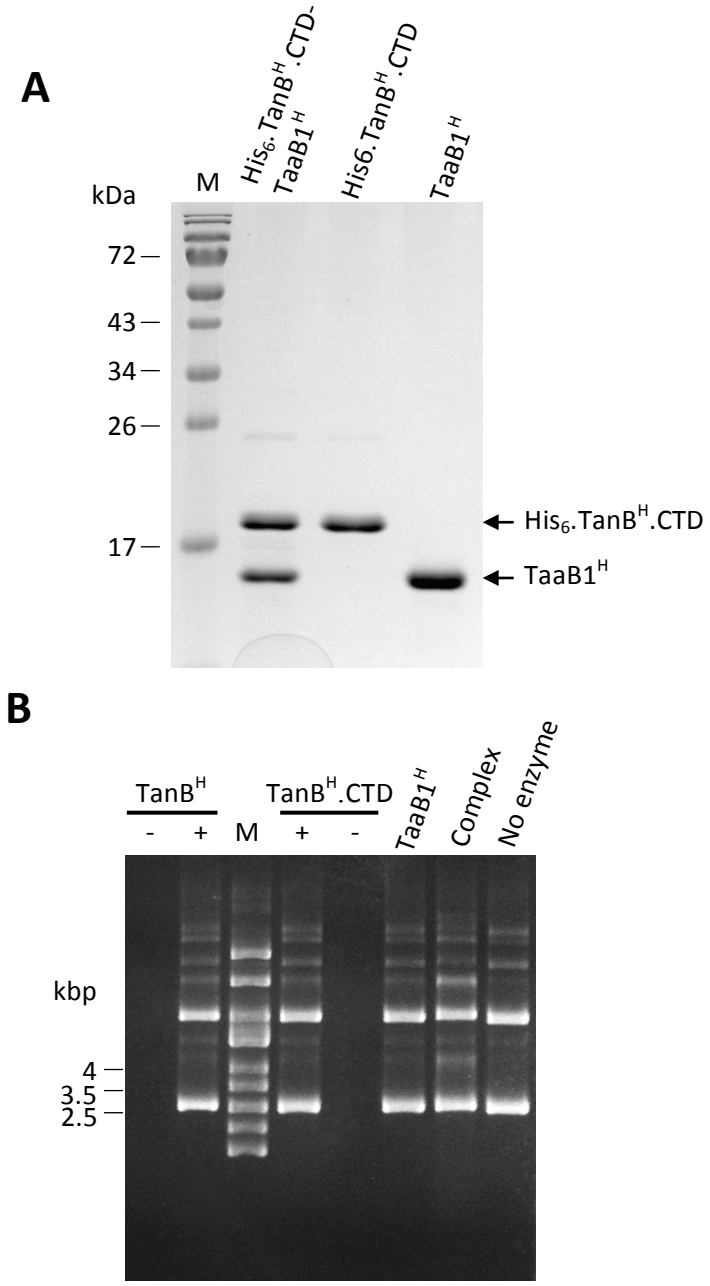

Figure 6.26 Inhibition of DNase activity of TanB^H and TanB^H.CTD by purified TaaB1^H. Affinity purified His.TanB^H.CTD-TaaB1^H complex was denatured using 6 M GuHCl. Free His$_6$.TanB^H.CTD was removed from the dissociated complex by binding to a HisTrap column and washing with 6 M GuHCl-containing buffer. The flow through and wash fractions containing un-tagged free TaaB1^H was retained and subjected to buffer exchange against 50 mM Tris-HCl (pH 7.5) to remove the GuHCl and promote renaturation of TaaB1^H. (A) The purity of the resulting TaaB1^H sample in comparison to the His$_6$.TanB^H-TaaB1^H complex and His$_6$.TanB^H.CTD were analysed in a 15% SDS-PA gel stained with Coomassie blue. Labelled arrows indicate presence of purified proteins. Lanes as indicated. M, EZ-Run *Rec* protein ladder. (B) The inhibition of pBluescript II plasmid DNA degradation by addition of a 2-fold excess of TaaB1^H (+) to His$_6$.TanB^H and His$_6$.TanB^H.CTD. M, GeneRuler DNA ladder mix; Complex, purified His$_6$.TanB^H-TaaB1^H complex.

whereas control reactions that contained only $TanB^{H}$ and $TanB^{H}$.CTD were able to fully degraded plasmid DNA (Figure 6.26B). The inhibitory effect of $TaaB1^{H}$ was further confirmed by analysis of the DNase activity of the purified native His_6.$TanB^{H}$-$TaaB1^{H}$ complex. Addition of this purified complex to plasmid DNA did not cause degradation of the plasmid.

6.6 Investigation of the interaction between TanB^{H}, and TaaB1^{H} by the bacterial adenylate cyclase two-hybrid system

TaaB1^{H} was co-purified during the purification of both TanB^{H} and TanB^{H}.CTD (Section 6.3.3), which indicated a direct physical interaction between the two proteins. Therefore it was decided to further investigate this interaction by use of the bacterial adenylate cyclase two-hybrid system.

6.6.1 Principle of the BACTH assay

The BACTH system was developed to investigate interactions between two proteins of interest (Karimova et al., 1998), Figure 6.27 illustrates the principle of this system. It utilises the observation that the catalytic region of the adenylate cyclase enzyme (CyaA) from *B. pertussis* consists of two complementing fragments, T25 and T18, which have to be in close proximity to allow functional activity of CyaA (Ladant and Ullmann, 1999). Restoration of CyaA functionality by re-association of the two fragments can be monitored by the activation of reporter genes that respond to an increase in the intracellular cyclic-AMP concentration by CyaA. To investigate whether two proteins of interest physically interact, say proteins X and Y, the coding sequences of X and Y are fused in-frame to the coding sequences of T18 and T25, such that N and C-terminal fusion of proteins X and Y to the T18 and T25 fragments are generated. They are made utilising the low copy number BACTH vectors pKT25 and pKNT25 and the compatible high copy-number BACTH vectors pUT18C and pUT18. Gene fusions constructed in pKT25 or pKTN25 and pUT18C or pUT18 are then co-expressed in a Δ*cya* mutant of *E. coli.* If the X and Y moieties interact, T25 and T18 fragments are brought into close proximity, which restores the activity of CyaA and thereby generates cAMP from ATP. cAMP is able to interact with the dimeric cAMP receptor protein CRP to form a CRP.cAMP complex, which acts as an activator of gene transcription. The CRP.cAMP complex can bind to the promoters of many resident operons in *E. coli* resulting in gene activation. This includes promoters controlling the *mal* regulon required for maltose

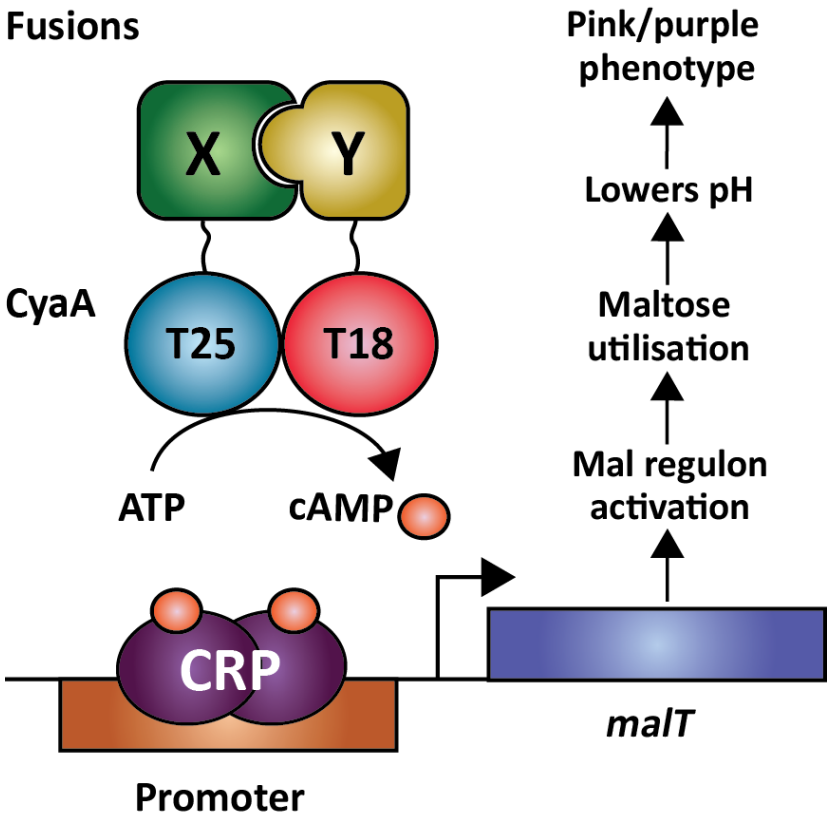

Figure 6.27 Principle of the bacterial adenylate cyclase two-hybrid system. To determine whether two proteins are able to directly interact the bacterial adenylate cyclase two-hybrid system, can be used. See text for further details.

utilisation. CRP.cAMP complex can specifically activate transcription of *malT* that encodes the maltose regulon activator protein, thus leading to activation of other *mal* genes in the *mal* regulon such as *malEFG*, *malK lamB* and *malM* required for maltodextrin uptake (Dippel and Boos, 2005). Maltose utilisation can be distinguished by the use of indicator medium, MacConkey-maltose agar. If maltose is utilised in a fermentation pathway by the bacterium the resulting acid production lowers the pH of the medium. MacConkey agar contains a pH indicator, neutral red, which results in a colour change of the colonies from pale pink to deep purple if there is a decrease in the pH. It has been noticed that the strength of the Cya^+/Mal^+ phenotype resulting from protein-proteins interactions using this system can vary. Table 2.8 in Section 2.7.2 indicates the scoring system used in this analysis to describe the observed Mal phenotypes.

6.6.2 Cloning of the coding sequences of *tanB^H*, *tanB^H.CTD* and *taaB1^H* into the BACTH vectors

Due to the difficulties encountered cloning the coding sequences of *tanB^H* and *tanB^H.CTD* into the pETDuet-1 expression vector (Section 6.2.1), is was hypothesised that it would not be possible to clone wild-type copies of *tanB^H* or *tanB^H*.CTD into the BACTH vectors without the presence of the *taaB1^H* gene encoding its putative immunity protein. To circumvent this, it was decided to utilise a variant of *tanB^H* that encoded a non-toxic TanB^H G276D mutant (Section 6.2.1).

The pHLS7 plasmid was used as template DNA for the amplification of coding sequences of *tanB^H* and *tanB^H.CTD* for insertion into the BACTH vectors. Primer pairs BCAL1298ForNtermHisBamHI and BCAL1298Rev2Acc65I, and BCAL1298ForNtermHisBamHI and BCAL1298RevAcc65I, were used to amplify *tanB^H* for generation of in-frame N- and C-terminal fusions to the T25 and T18 fragments, respectively. Primer pairs BCAL198CTDNtermHisForBamHI and BCAL1298Rev2Acc65I, and BCAL1298CTDNtermHisForBamHI and BCAL1298RevAcc65I were used to amplify *tanB^H.CTD* for generation of in-frame N- and C-terminal fusions to the T25 and T18 fragments, respectively. Primer pairs BCAL1299ForBamHI and BCAL1299Rev2Acc65I, and BCAL1299ForBamHI and

BCAL1299RevAcc65I were used to amplify *taaB1*^{H} for generation of in-frame N- and C-terminal fusions to the T25 and T18 fragments, respectively. PCR generated DNA fragments destined for N-terminal fusion with T25 or T18 lacked a stop codon in the reverse primer, allowing read-through of the amplicon coding sequence into the T18/T25 coding sequence in the vectors. PCR DNA fragments intended for C-terminal fusions incorporated the native stop codon for each gene being amplified.

PCR products resulting from each of the above amplifications were purified, and subjected to restriction digestion with BamHI and Acc65I. Each was then ligated between the corresponding restriction sites of the four BACTH vectors. Transformants harbouring pKT25 and pKTN25 plasmids were selected for using kanamycin and those containing pUT18C and pUT18 derivatives were selected for using ampicillin. Plasmids encoding both N- and C-terminal fusions of TanB^{H} G276D, TanB^{H}.CTD G276D and TaaB1^{H} with both the T25 fragment and the T18 fragment were successfully generated.

6.6.3 Investigation of the interaction between TanB^{H} and TaaB1^{H} by the BACTH system

To determine whether TaaB1^{H} was able to interact with TanB^{H} and its CTD using the BACTH system, pairwise combinations of plasmids encoding N- and C-terminal fusions of T25 and T18 to TanB^{H} G276D, TanB^{H}.CTD G276D and TaaB1^{H} were introduced into *E. coli* BTH101 and the maltose phenotype monitored. Presence of compatible full length T18 and T25 fusions of TanB^{H} G276D or TanB^{H}.CTD G276D with T18 and T25 fusions of TaaB1^{H} resulted in either a strong or very strong Mal^{+} phenotype in all combinations tested (Figure 6.28).

6.6.4 Analysis of self-interaction of TanB^{H}, TanB^{H}.CTD and TaaB1^{H} by the BACTH system

Construction of the TanB^{H} G276D, TanB^{H}.CTD G276D and TaaB1^{H} two-hybrid fusion plasmids also permitted analysis of the ability of each protein to dimerise or oligomerise. To determine whether TanB^{H}, TanB^{H}.CTD or TaaB1^{H} were able to self-interact pairwise combinations of pKT25 and pUT18C or pUT18, and pKNT25 and

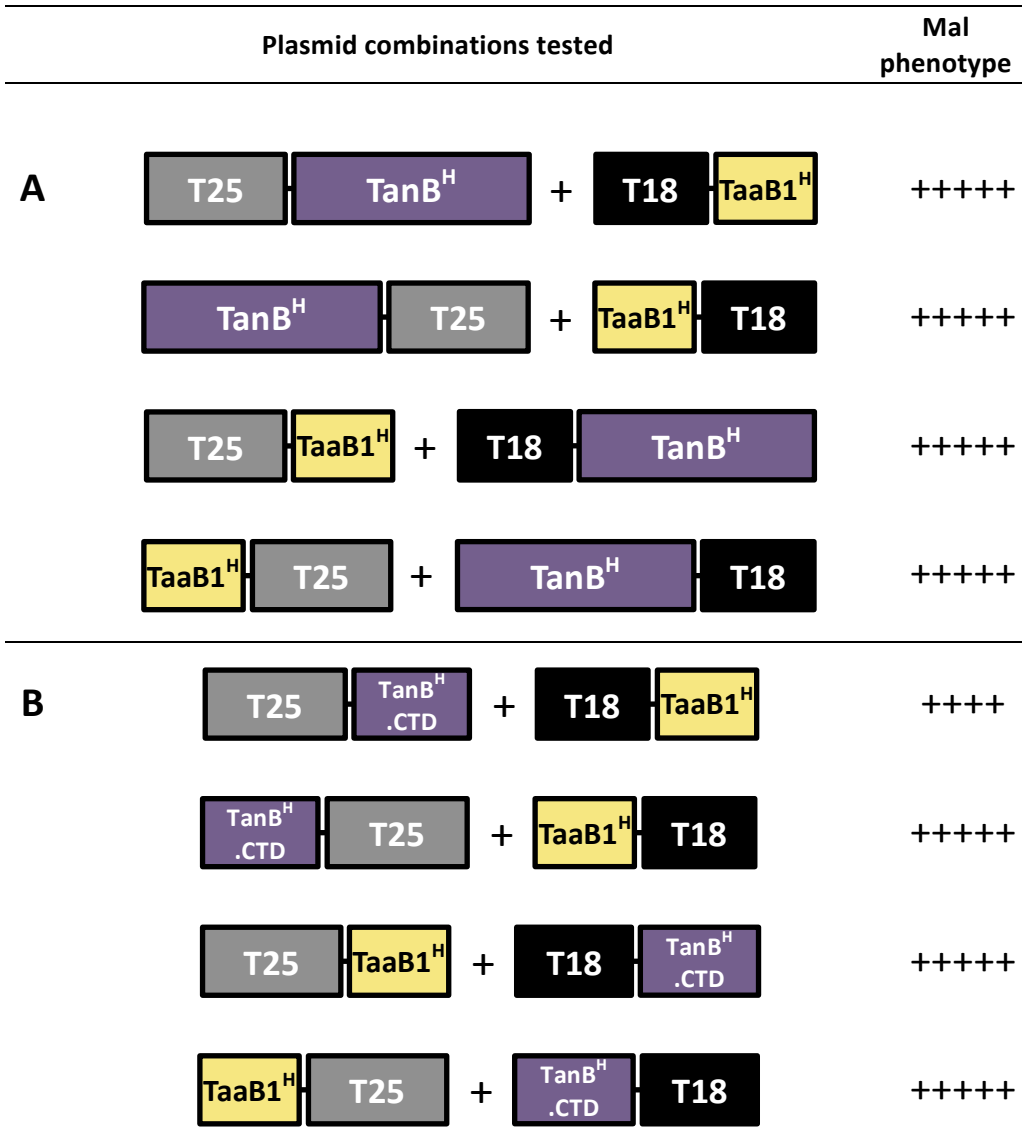

Figure 6.28 Analysis of interactions between TaaB1^H and TanB^H and its C-terminal domain using BACTH assay. Pairwise combinations of plasmids encoding compatible T25/T18 fusions of (A) TanB^H G276D with TaaB1^H and (B) TanB^H.CTD G276D with TaaB1^H were introduced into BTH101 and grown on MacConkey maltose agar containing the antibiotics ampicillin and kanamycin at 30°C, for up to 7 nights. Mal$^+$ phenotype was monitored and scored 72 hours after initial plating. Mal phenotype scored here as: -, negative; ++++, strong, deep purple after 72 hours, as zip control; +++++, very strong, deep purple after 72 hours, stronger than zip control.

pUT18C or pUT18 plasmids, encoding $TanB^{H}$ G276D, $TanB^{H}$.CTD G276D or $TaaB1^{H}$ T25 and T18 fusions, were co-expressed in BTH101 and maltose phenotype monitored by use of MacConkey-maltose media. Figure 6.29 shows the resulting Mal phenotype for each plasmid combination tested. All plasmid combinations tested gave rise to a Mal^{-} phenotype, except one, T25-$TaaB1^{H}$ C-terminal fusion in combination with a N-terminal $TaaB1^{H}$-T18 fusion gave rise to a weak Mal^{+} patchy phenotype after 4 nights incubation. These results suggest full length $TanB^{H}$ or its CTD were unable to self-interacted under the conditions tested. But $TaaB1^{H}$ may be able to interact with itself.

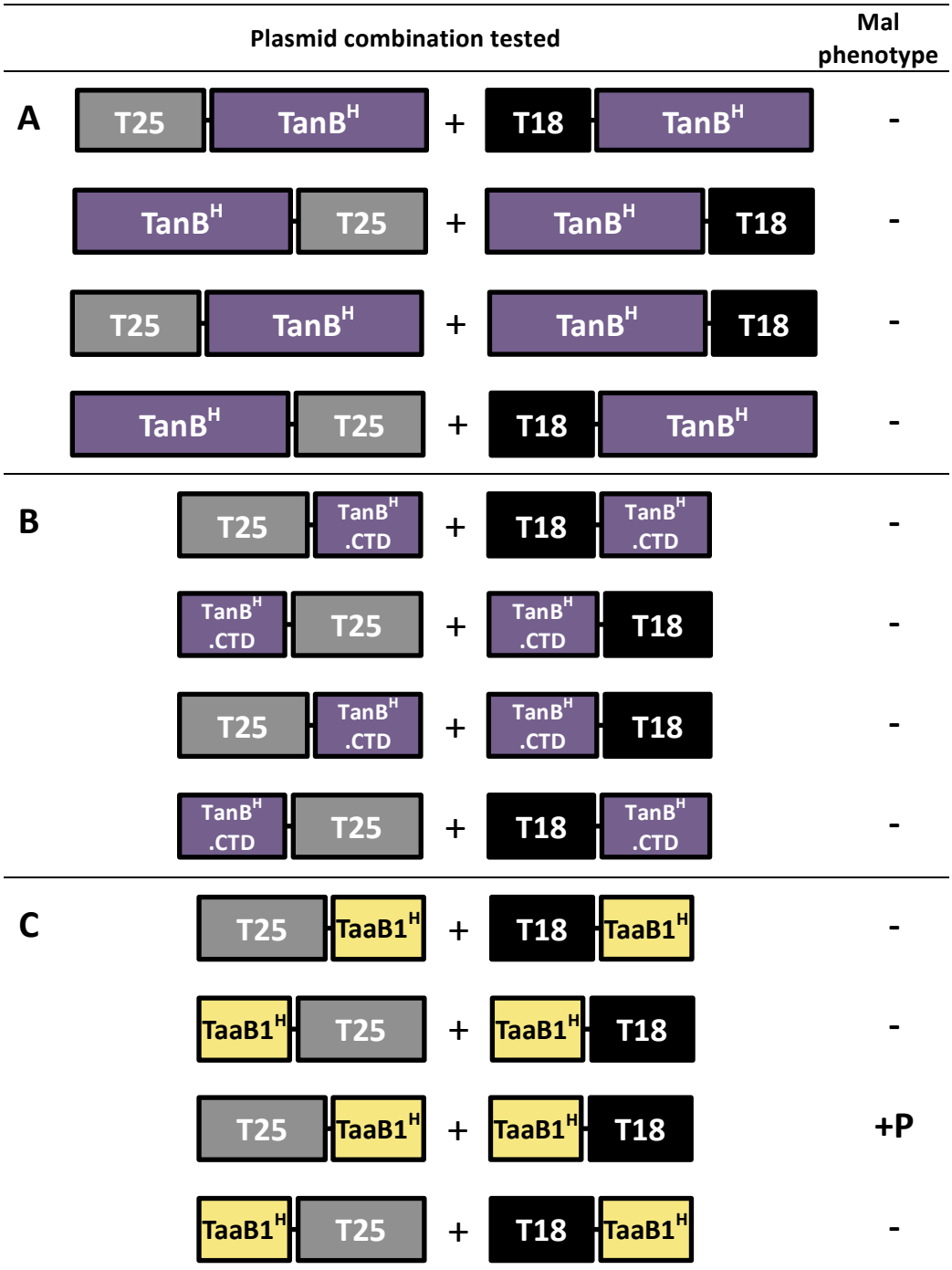

Figure 6.29 Analysis of TanB^H, TanB^H.CTD and TaaB1^H self-interaction by BACTH assay. Pairwise combinations of compatible plasmids encoding T25/T18 fusions of (A) TanB^H G276D, (B) TanB^H.CTD G276D and (C) TaaB1^H were introduced into *E. coli* BTH101, and grown on MacConkey maltose agar containing the antibiotics ampicillin and kanamycin at 30°C for up to 7 nights. Mal phenotype was monitored and scored 72-86 hours after initial plating. Mal phenotype scored here as: -, negative; +, weak, red/pink after 84 hours; P, non-uniform colouration.

6.7 Investigation of interactions between TanB^{H} and TaaB1^{H} by pull-down assays

Co-purification of TaaB1^{H} with His-tagged TanB^{H} and TanB^{H}.CTD (Section 6.3.3) and positive Mal phenotypes in a two-hybrid analysis (Section 6.6) indicated that TanB^{H} was able to directly interact with TaaB1^{H} to form a complex. However, as TaaB1^{H} was not epitope tagged, co-elution of TaaB1^{H} with TanB^{H} could not be verified easily by means of western blotting. Therefore it was decided to add a C-terminal FLAG tag to TaaB1^{H} to allow immuno-detection of both TanB^{H} and TaaB1^{H}.

6.7.1 Construction of plasmids overproducing epitope-tagged TaaB1^{H}

A C-terminal FLAG tag (DYKDDDDK) was added to TaaB1^{H} by way of incorporating the FLAG epitope coding sequencing into the reverse primer used to amplify the coding sequence of *taaB1^{H}*. This primer, termed BCAL1299RevFLAGAcc65I, was used in combination with BCAL1299ForNdeI to amplify the *taaB1^{H}.FLAG* coding sequence from *B. cenocepacia* H111. *taaB1^{H}.FLAG* was inserted into the expression vector pETDuet-1 between the restriction sites NdeI and Acc65I as described in Section 6.2.3, generating the plasmid pHLS8. *tanB^{H}* and *tanB^{H}.CTD* where subsequently amplified and cloned into pHLS8 as BamHI-HindIII restriction digestion fragments as previously described (Section 6.2.1), generating the co-expression plasmids pHLS9 and pHLS10, respectively.

6.7.2 Analysis of the interaction between TanB^{H} and TaaB1^{H} by a pull-down assay

pHLS8, pHLS9 and pHLS10 were introduced separately into the *E. coli* expression strain BL21(DE3)/pLysS for protein over-production. Similar to the results presented in Section 6.3.1-6.3.2, His$_6$.TanB^{H}, His$_6$.TanB^{H}.CTD and TaaB1^{H}.FLAG were all overproduced as soluble proteins following induction of the T7 promoter (results not shown). To determine whether the two epitope tagged proteins directly interacted, the soluble lysates from induced cultures of BL21(DE3)/pLysS harbouring pHLS8, pHLS9 and pHLS10 were subjected to IMAC

using the batch purification method (Section 2.3.4). Samples from each step of the purification were analysed by western blotting, probing with anti-His and anti-FLAG antibodies. Figure 6.30A and 6.30B confirm that both epitope-tagged proteins were present in the load samples when His_6.$TanB^H$ (or His_6.$TanB^H$.CTD) and $TaaB1^H$.FLAG were co-expressed and most of the excess $TaaB1^H$.FLAG was present in the flow-through and wash fractions of these samples. Both His_6.$TanB^H$ or His_6.$TanB^H$.CTD and $TaaB1^H$.FLAG were detected in the imidazole-eluted fraction. $TaaB1^H$.FLAG was unable to bind non-specifically to the nickel resin. Therefore $TanB^H$ and $TaaB1^H$ must physically interact in order for $TaaB1^H$ to be retained on the resin and this interaction occurs through the C-terminal domain of $TanB^H$.

6.7.3 Analysis of the interaction between $TanB^H$ G267D mutant and $TaaB1^H$ by a pull-down assay

The ability of the His_6.$TanB^H$ G276D variant to interact with $TaaB1^H$ was also investigated to determine the usefulness of this mutant, and to infer whether the G276D mutant had a similar overall structure to that of the wild-type $TanB^H$ protein. This was investigated by using a pull down assay (Section 2.7.1). First, the cleared lysate of induced BL21(DE3)/pLysS cells habouring pHLS7 (His_6.$TanB^H$ G276D) was loaded onto nickel affinity resin to allow immobilisation of the His-tagged 'bait' protein. The cleared lysate of induced BL21(DE3)pLysS cells harbouring pHLS1 (overproducing un-tagged $TaaB1^H$) was then applied to the resin containing the anchored $TanB^H$ G276D 'bait' protein. After washing, the column bait:prey complex was then eluted with buffer containing a high concentration of imidazole. His_6.$TanB^H$ G276D and $TaaB1^H$ only controls were included to verify that His_6.$TanB^H$ G27D was able to bind to the nickel resin but $TaaB1^H$ could not. SDS-PAGE analysis of samples resulting from the pull-down assay indicated that $TanB^H$ G276D was able to successfully pull down $TaaB1^H$. The presence of the 15 kDa $TaaB1^H$ protein was observed in the imidazole eluted fraction from resin containing immobilised $TanB^H$ G276D bait protein, but not in the corresponding fraction from the resin that did not contain pre-bound His_6.$TanB^H$ G276D (Figure 6.31). Thus, suggesting that $TanB^H$

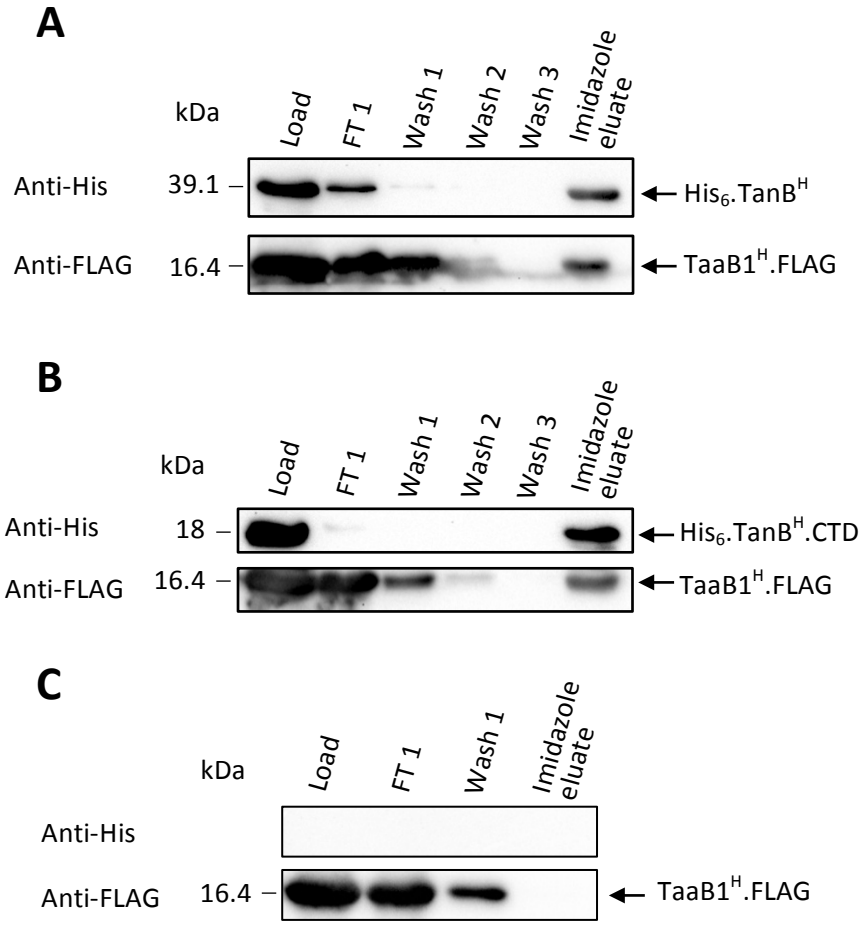

Figure 6.30 Analysis of the interaction between TanB^{H} and TaaB1^{H} by a pull-down assay. His$_6$.TanB^{H} or His$_6$.TanB^{H}.CTD and TaaB1^{H}.FLAG were overproduced together in BL21(DE3)/pLysS cells from pETDuet-1 co-expression derivatives. The resulting lysates from induced cultures were bound to nickel affinity resin, washed and the bound material specifically eluted with 150 mM imidazole. Load, flow-through (FT), wash and imidazole eluate samples from each stage were subjected to SDS-PAGE and electro-blotted onto PVDF membrane. Membranes were probed with anti-His and anti-FLAG antibodies. Images showing resulting blots from (A) His$_6$.TanB^{H} and TaaB1^{H}.FLAG and (B) His$_6$.TanB^{H}.CTD and TaaB1^{H}.FLAG co-expression pull downs and (C) TaaB1^{H} only control. Estimated molecular mass of each protein is indicated to the left, and labelled arrows indicate the detected protein to the right.

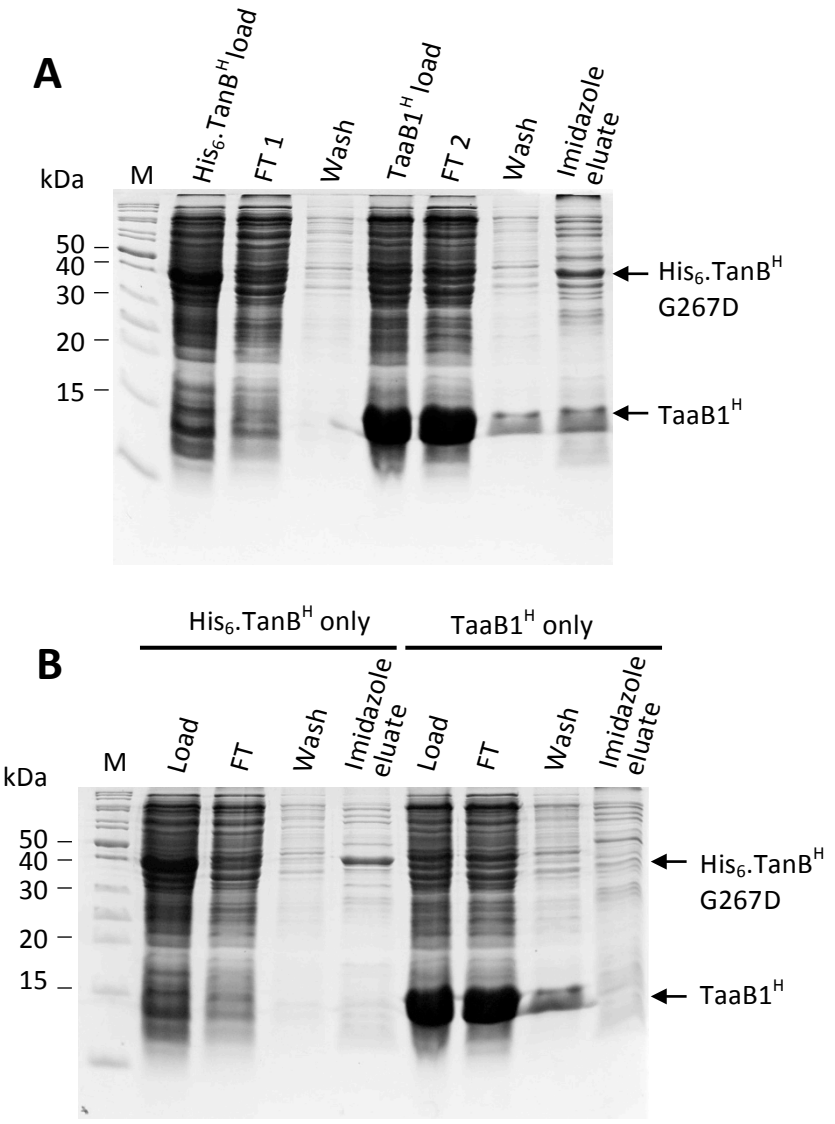

Figure 6.31 Analysis of the interaction between His_6.$TanB^H$ G267D and $TaaB1^H$ by a pull-down assay. His_6.$TanB^H$ G276D mutant and un-tagged $TaaB1^H$ were overproduced separately in BL21(DE3)/pLysS harbouring pHLS7 and pHLS1, respectively. The cleared lysate from induced cultures of overproduced His_6.$TanB^H$ G276D was bound to nickel affinity resin, and washed. Following this the induced cell lysate containing $TaaB1^H$ was added to the resin containing the immobilised His_6.$TanB^H$ G27D, washed and then bound proteins were eluted with a high imidazole buffer. Immobilisation of His_6.$TanB^H$ and $TaaB1^H$ only controls were included. Load flow-through (FT), wash and imidazole eluate samples from each stage were subjected to SDS-PAGE. (A) Coomassie stain of His_6.BCA1298 G276D and $TaaB1^H$ pull down. (B) Coomassie stain of control $TanB^H$ immobilisation (left) and inability of $TaaB1^H$ to bind to the resin (right). Labelled arrows indicate identity of eluted proteins. Lanes as indicated. M, EZ-Run *Rec* protein ladder.

G276D was able to directly interact with TaaB1^{H} to form a complex. This indicated that the G276D mutant possessed sufficient structural similarity to the wild-type protein to facilitate the interaction with TaaB1^{H}.

6.8 Analysis of the oligomeric status of the TanB^{H}-TaaB1^{H} complex

To further characterise the TanB^{H}-TaaB1^{H} complex, the oligomeric status of TanB^{H} and its CTD in complex with TaaB1^{H} was investigated by the use of size exclusion chromatography (SEC).

6.8.1 Estimation of the oligomeric size of the TanB^{H}-TaaB1^{H} complex by size exclusion chromatography

The expected molecular masses of the individual components of the TanB^{H}-TaaB1^{H} complex are 39.1 kDa and 15.4 kDa, respectively. This information was used as a guide to decide the most appropriate SEC column to use for optimal resolution and estimation of the oligomeric status of the complex. As a 1:1 or 2:1 complex would have an estimated molecular mass of 60 kDa or 95 kDa, it was decided that a Superose 12 10/300 column should allow sufficient resolution of the TanB^{H}-TaaB1^{H} complex. First, the Superose 12 10/300 column was calibrated with molecular standards to generate a standard curve (Figure 6.32A). 100 μL of concentrated nickel affinity purified TanB^{H}-TaaB1^{H} complex (prepared as described in Section 6.3.3) was then subjected to gel filtration (Section 2.3.7). It was observed that the TanB^{H}-TaaB1^{H} complex eluted as seven protein peaks, with the majority of the protein present in the third and fourth peaks to be eluted, at 9.5 mL and 10.8 mL, respectively (Figure 6.32B). Comparison with the standard curve indicated that these two major peaks did not lie within the calibration curve limits, as the largest molecular standard used was 149.0 kDa, thus neither could be considered accurate. The third peak (and the first and second) was in-fact outside the exclusion limit of the column. The smaller peaks that eluted later corresponded to proteins of an approximate molecular mass of 37.3 kDa, 8.2 kDa and 7.0 kDa, the former being similar to the estimated molecular mass of monomeric TanB^{H}. The skew of the calibration curve to higher molecular weight proteins may underestimate the molecular weight of the sixth and seventh peak, so either may still correspond to monomeric TaaB1^{H}. Together this data indicated that the TanB^{H}-TaaB1^{H} complex might reside in two different oligomeric states that were larger than expected.

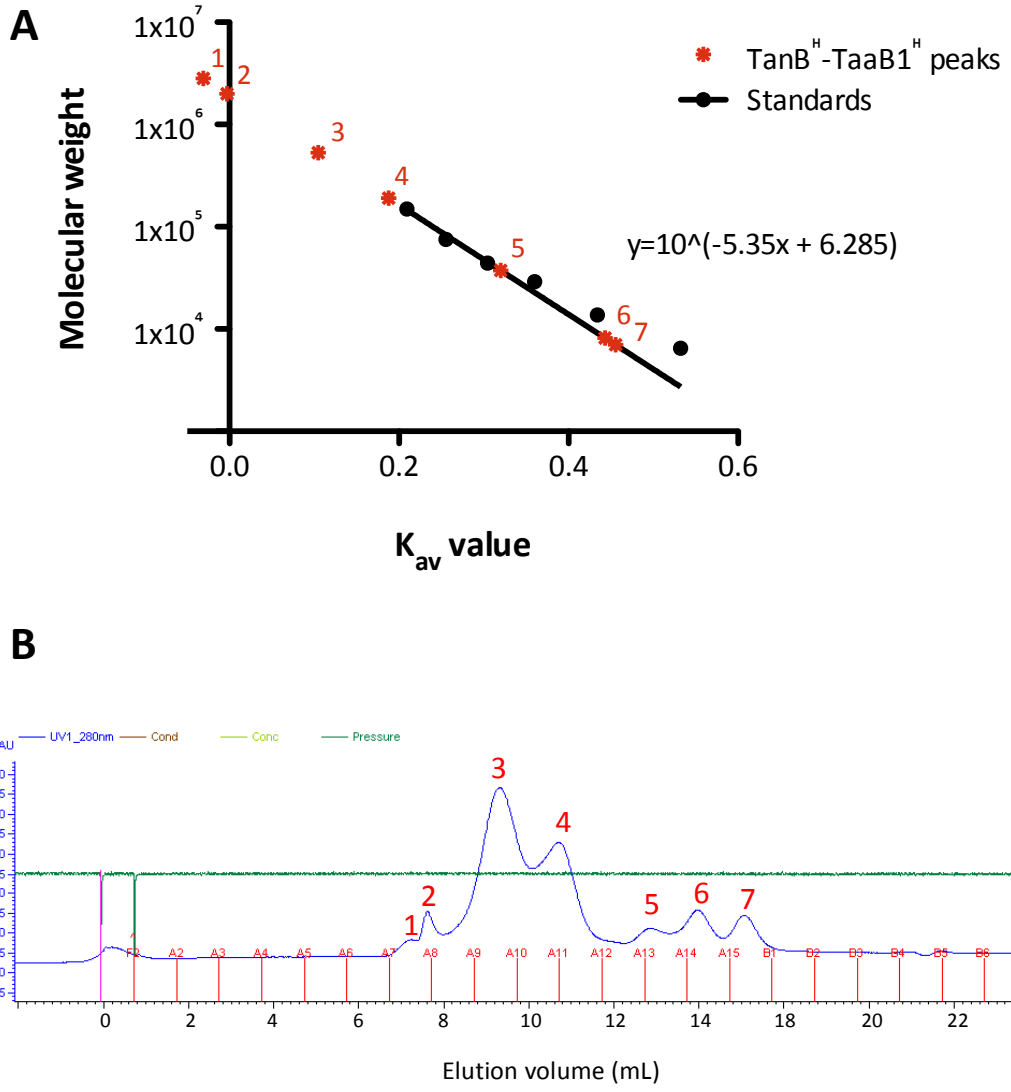

Figure 6.32 Analysis of the His_6.$TanB^H$-$TaaB1^H$ complex by size exclusion chromatography. (A) Calibration curve for the Superose 12 column using proteins of a known molecular weight, where the experimentally defined K_{av} value (x axis) is plotted against molecular weight for each standard (y axis) on a log scale and fitted with a semi-log regression curve, with the equation as indicated. 100 µL of affinity-purified His_6.$TanB^H$-$TaaB1^H$ complex was subjected to SEC using the Superose 12 column with a flow rate of 0.5 mL/min. (B) A_{280} trace (y-axis) of the column eluate after injection of $TanB^H$-$TaaB1^H$ complex. This was used to identify the specific elution volume (x axis) of each protein peak after injection onto the column (pink line, elution volume 0). The number above each peak indicates the order of elution and corresponds to the 'unknown' values plotted on the calibration curve in (A), as indicated in the key.

6.8.2 Estimation of the oligomeric size of the TanB^{H}.CTD-TaaB1^{H} complex by size exclusion chromatography

To determine the oligomeric size of the CTD of TanB^{H} in complex with TaaB1^{H}, nickel affinity purified TanB^{H}.CTD-TaaB1^{H} complex (prepared as described in Section 6.3.3) was subjected to SEC using a Superose 6 10/300 column (Section 2.3.7). This column was deemed appropriate due to the estimated molecular mass of 1:1 complex of 32.3 kDa being within the lower resolution limits of the column, but also as a precautionary measure due to the higher than expected molecular mass values obtained for full length TanB^{H} in complex with TaaB1^{H} using a Superose 12 column (Section 6.8.1). A calibration curve was generated by calibration of the Superose 6 10/300 column with proteins of known molecular masses (Figure 6.33A). The TanB^{H}.CTD-TaaB1^{H} complex was subjected to SEC in triplicate. Proteins were eluted from the column at four specific volumes, as detected by peaks in the A_{280} trace. A minor peak eluting first, followed by a larger peak and then two major peaks (Figure 6.33B). The first peak formed a shoulder on the leading edge of the second peak and corresponded to a protein complex of 93.9 ± 0 kDa (SD). Three subsequent peaks corresponded to an estimated molecular mass of 72.1 ± 2.5 kDa (SD), 52.4 ± 1.2 kDa (SD) and 32.6 ± 0 kDa (SD). All of which lay within the limits of the calibration curve, as shown by the red data points in Figure 6.33A. The theoretical molecular mass of a 1:1 ratio of TanB^{H}.CTD:TaaB1^{H} was calculated to be 32.3 kDa, a 2:1 ratio corresponded to 49.2 kDa, 1:2 ratio corresponded to 47.7 kDa, and a 2:2 ratio corresponded to 64.6 kDa. SDS-PAGE analysis of fractions eluted at each of these corresponding peaks indicated the presence of His$_6$.TanB^{H} and TaaB1^{H} in all four samples (Figure 6.33C). Taken together, this data suggested that the TanB^{H}.CTD-TaaB1^{H} complex may occur in three different stoichiometries, the smallest and most abundant of the three, approximately corresponding to an 1:1 ratio of His$_6$.TanB^{H}.CTD:TaaB1^{H}, and the others potentially being a 1:2, 2:1 or 2:2 complex.

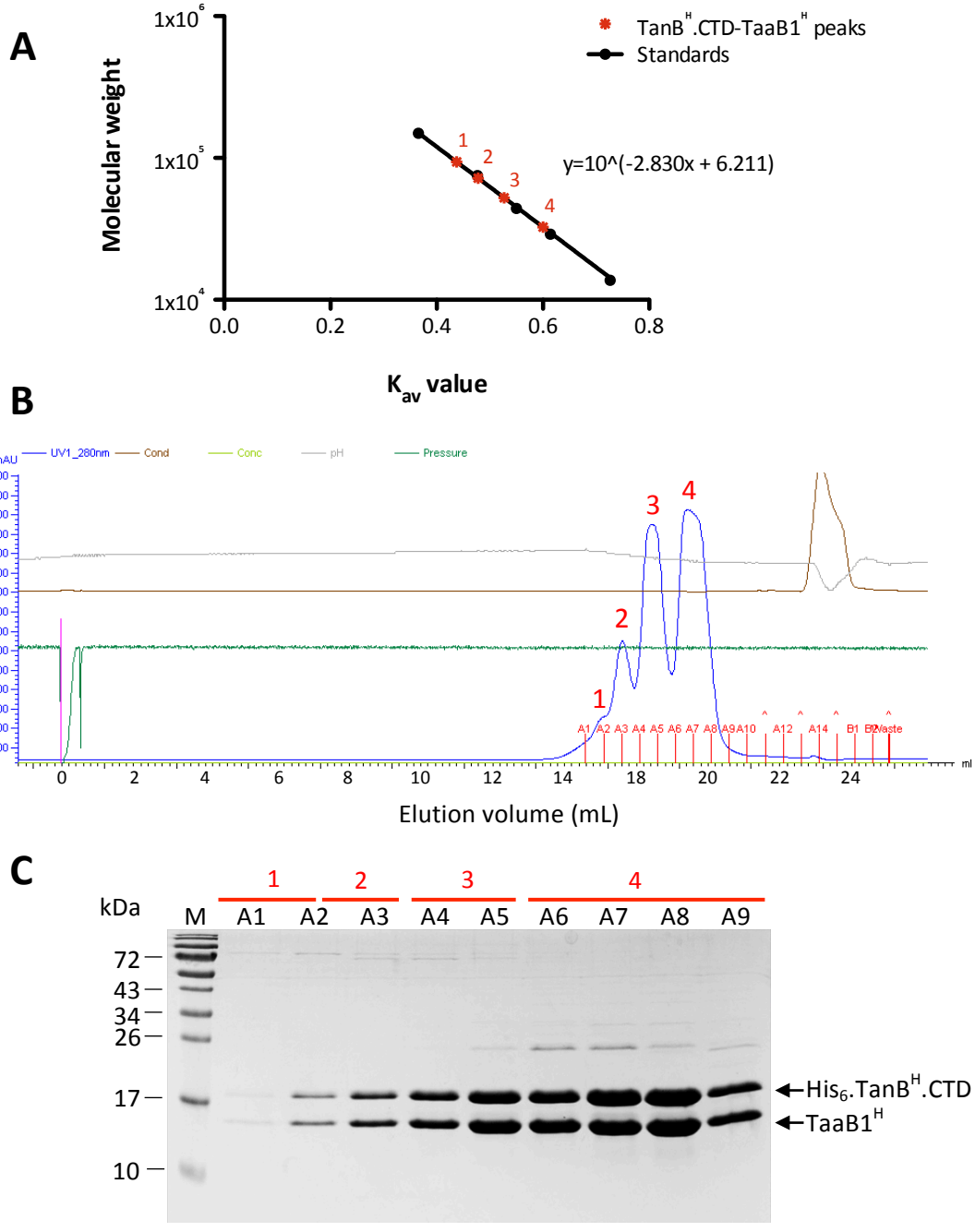

Figure 6.33 Analysis of TanB^{H}.CTD-TaaB1^{H} complex by SEC. 100 µL of affinity-purified His$_6$.TanB^{H}.CTD-TaaB1^{H} complex was subjected to SEC using a Superose 6 column coupled to an ÄKTA purifier FPLC system with a flow rate of 0.5 mL/min. Proteins eluted from the column where collected in 0.5 mL fractions. (A) Calibration curve for the Superose 6 column using proteins of a known molecular weight, depicted as the experimentally defined K_{av} value (x axis) plotted against the molecular weight for each standard (y axis) on a log scale, and fitted with a semi-log regression curve, with the equation as indicated. (B) A280 nm trace following elution of the His$_6$.TanB^{H}.CTD-TaaB1^{H} complex, where fractions (A1-A9) were then analysed by SDS-PAGE (C). Labelled arrows at expected molecular mass indicate the identity of the eluted proteins. Labels 1-4 corresponded to the elution peaks in (B), which also corresponds to the numbered 'unknowns' in (A). M, EZ-Run *Rec* protein ladder.

6.8.3 Estimation of the oligomeric size of $TanB^{H}$.CTD by size exclusion chromatography

To evaluate whether the CTD of $TanB^{H}$ contained an oligomerisation site, allowing multimerisation of the protein, it was decided to estimate the oligomeric size of the CTD of $TanB^{H}$ by SEC. To do this nickel affinity purified His_6.$TanB^{H}$.CTD (prepared as described in Section 6.3.8) was subjected to SEC using a Superose 12 10/300. A standard curve was generated from proteins of known molecular masses (Figure 6.34A) and used to estimate the molecular mass of His_6.$TanB^{H}$.CTD from its average elution volume. By monitoring the A_{280} of the column eluate, a single peak was observed eluting at an average volume of 14 ± 0.07 mL (SD) (Figure 6.34B), which corresponded to a molecular mass of 19.5 ± 0.7 kDa. This value was within the limits of the calibration curve as indicated in Figure 6.34A. As the theoretical molecular mass for recombinant His_6.$TanB^{H}$ is 16.9 kDa, this suggests that His_6.$TanB^{H}$.CTD is likely to occur as a monomer under the conditions tested, hence does not contain an oligomerisation site.

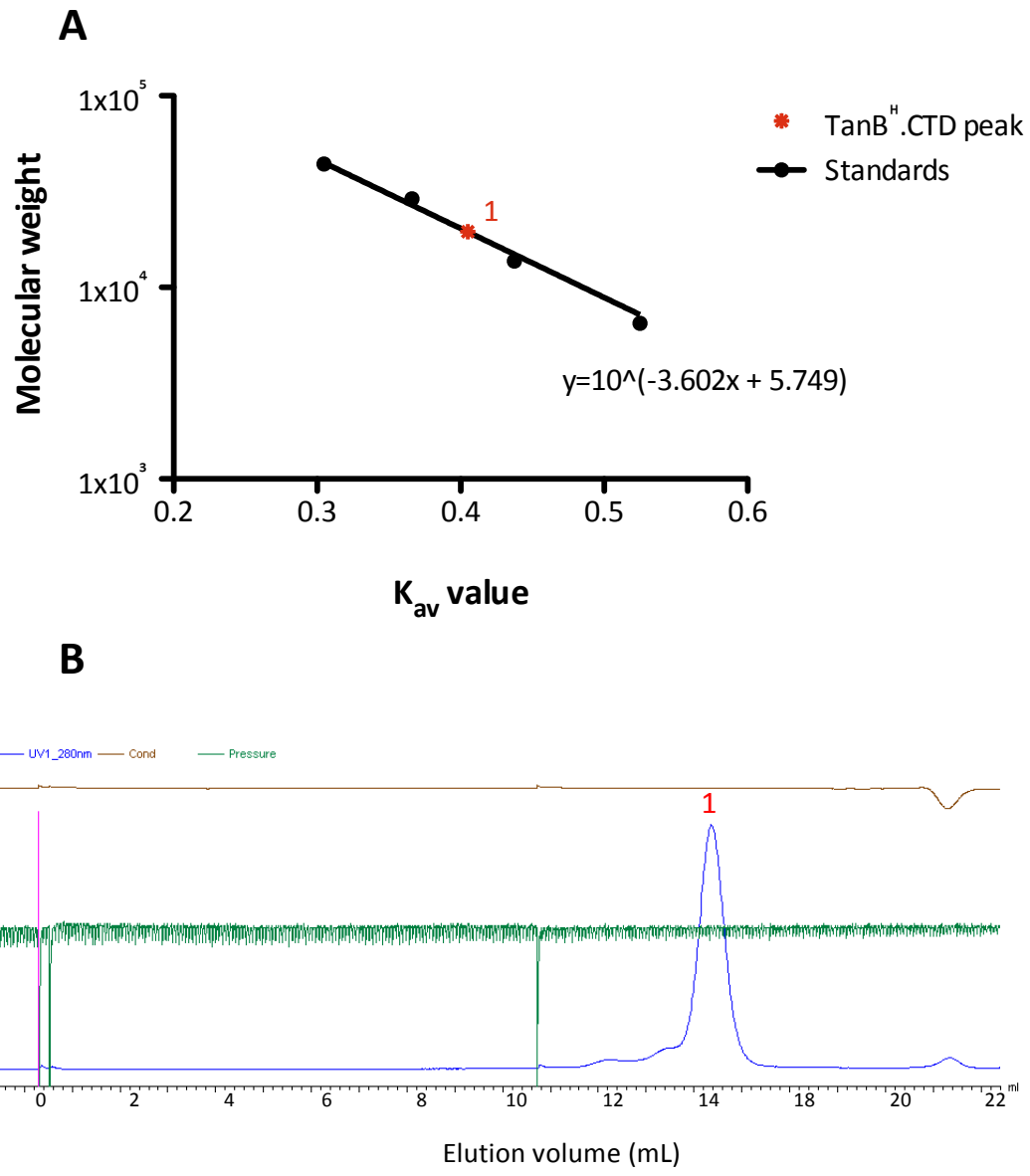

Figure 6.34 Analysis of purified His_6.$TanB^H$.CTD by SEC. 100 µL of purified His_6.$TanB^H$ was subjected to SEC using a Superose 12 10/300 column coupled to an ÄKTA purifier FPLC system with a flow rate of 0.5 mL/min. (A) Calibration curve generated from the elution of protein standards, presented as experimentally determined K_{av} values (x axis) against the known molecular weight (y axis) of each standard, fit with a semi-log regression curve, with the equation as indicated. (B) Representative A_{280} trace for His_6.$TanB^H$.CTD, which eluted as a single peak at a volume of 14 mL following injection onto the column (pink line), labelled as 1. The calculated molecular weight for this peak is plotted in (A).

6.9 Investigation of interactions between TanB^{H} and candidate T6SS accessory proteins

Recent findings, described in detail in Section 1.5, suggest different T6SS-dependent effectors can be secreted by different mechanisms. Some effectors may directly interact with the secreted spike-like TssI subunit, facilitating secretion of the effector (Dong et al., 2013; Whitney et al., 2014). Others may utilise separate adaptor or chaperone proteins to enable secretion of the effector by the T6SS. Current models suggest that T6SS chaperone proteins act as a platform to facilitate the loading of an effector protein onto a cognate TssI protein (Koskiniemi et al., 2013; Shneider et al., 2013; Liang et al., 2015; Unterweger et al., 2015). Therefore it was decided to investigate interactions between the putative T6SS-effector TanB^{H} and other proteins within its gene cluster that may facilitate the secretion of the effector by the T6SS. This included a TssI protein encoded by BCAL1294 (TssI$_{1294}$), and the product of a T6SS accessory gene, *tagA*, that contains a DUF2169 domain. Proteins homologous to *tagA* are also found upstream of other candidate T6SS effectors in T6SS-containing bacteria. Some of these effectors have an N-terminal region homologous to the NTD of TanB^{H} and TanA^{J} (discussed in Section 6.1).

6.9.1 Investigation of interactions between TanB^{H} and TssI$_{1294}$ protein using the BACTH system

Combinations of compatible BACTH plasmids encoding N- and C-terminal fusion of T25 and T18 to TanB^{H} (Section 6.6.2) and TssI$_{1294}$ (Jones, 2012) were introduced into *E. coli* BTH101 and the Mal phenotype was scored as described in Section 2.7.2. Figure 6.35 indicates the combinations tested and the resulting Mal phenotypes. All combinations tested gave rise to a Mal^{-} phenotype, suggesting that TanB^{H} was unable to interact with TssI$_{1294}$ under the conditions tested, or that the interaction was undetectable using this method.

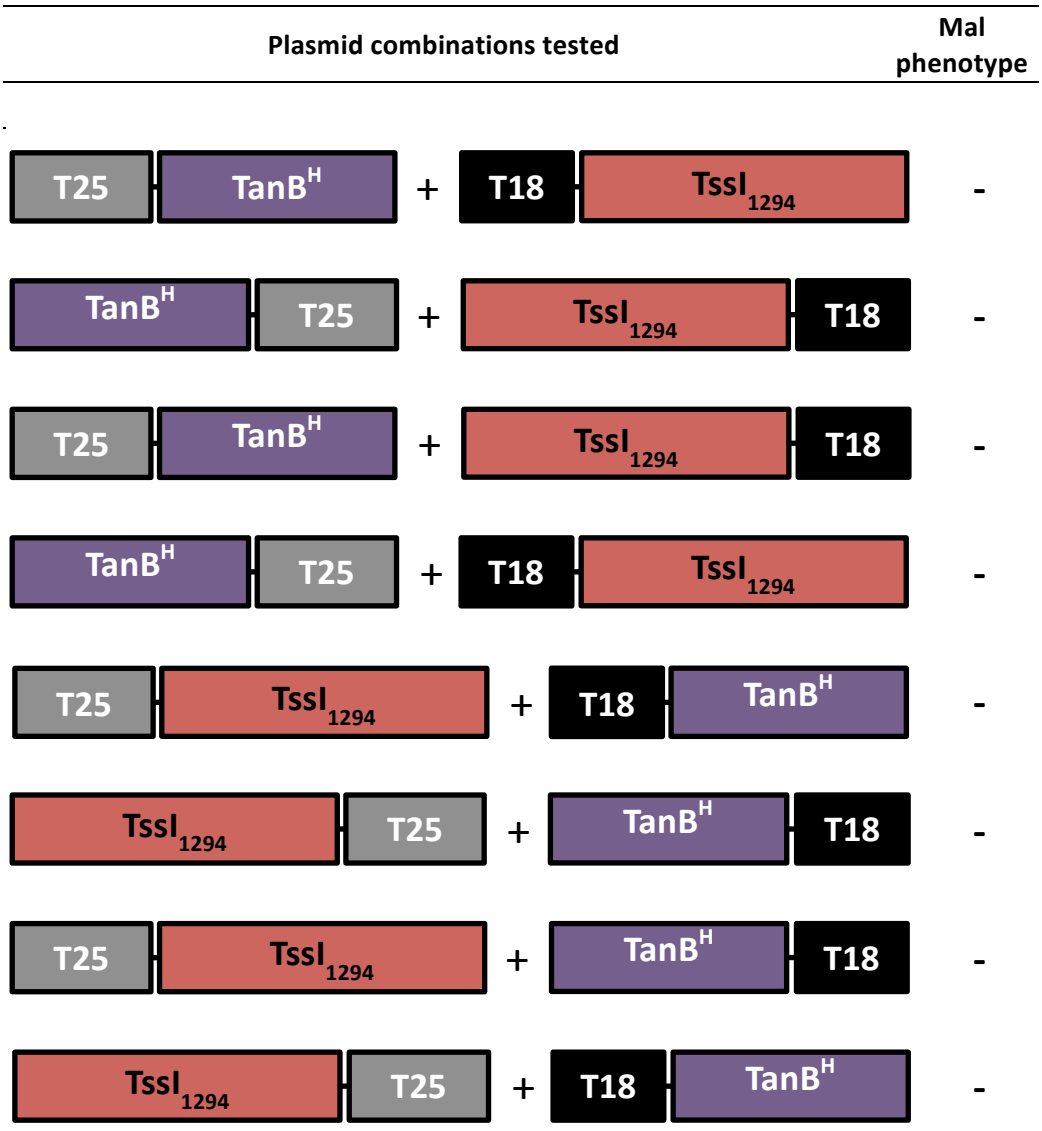

Figure 6.35 Analysis of interactions between TanB^H and TssI$_{1294}$ using the BACTH system. Pairwise combinations of compatible plasmids encoding T25/T18 fusions to TanB^H and TssI$_{1294}$ were introduced into BTH101 and grown on MacConkey maltose agar containing ampicillin and kanamycin for 30°C, for up to 7 nights. Mal phenotype was monitored and scored 72 hours after initial plating. Mal$^+$ phenotype scored here as: -, negative.

6.9.2 Investigation of interactions between $TanB^H$ and TagA using the BACTH system

Combinations of compatible BACTH constructs encoding N- and C-terminal fusions of T25 and T18 to $TanB^H$ (Section 6.6.2) and TagA (Jones, 2012) were introduced into *E. coli* BTH101 and the Mal phenotype scored as described in Section 2.7.2. Figure 6.36 illustrates the resulting Mal phenotypes for each combination tested. Two out of eight possible combinations gave rise to a Mal^+ phenotype after 72 hours incubation: the presence of T25-TagA C-terminal fusion in combination with the T18-$TanB^H$ C-terminal fusion resulted in a weak Mal^+ phenotype and the TagA-T25 N-terminal fusion in combination with T18-$TanB^H$ C-terminal fusion gave rise to a stronger but patchy Mal^+ phenotype. This result strongly suggests that $TanB^H$ is able to interact with TagA.

This result led to further investigations into the interaction between $TanB^H$ and TagA, whereby plasmids encoding T25/T18 fusions to the C-terminal domain of $TanB^H$ ($TanB^H$.CTD) were tested in pairwise combination with the TagA BACTH constructs. All combinations gave rise to a Mal^- phenotypes, suggesting that TagA may interact with the N-terminal region of the $TanB^H$ rather than the CTD.

6.9.3 Investigation of interactions between TagA and DUF2345-containing TssI, $TssI_{0148}$

BACTH results from a previous study (Jones, 2012) suggested that TagA was able to weakly interact with a DUF2345-containing TssI, in $TssI_{0148}$, encoded by BCAM0148. This led to the hypothesis that TagA may act as a T6SS adaptor protein for the secretion of putative effector $TanB^H$ by a TssI protein. Pairwise combinations of compatible BACTH vectors encoding N- and C-terminal fusions to TagA and $TssI_{0148}$ were introduced into *E. coli* BTH101 and the Mal phenotype was monitored. However, in contrast to previous observations, all combinations gave rise to a Mal^- phenotype. Therefore the mechanism by which the putative effector $TanB^H$ may be secreted by the T6SS remains unclear.

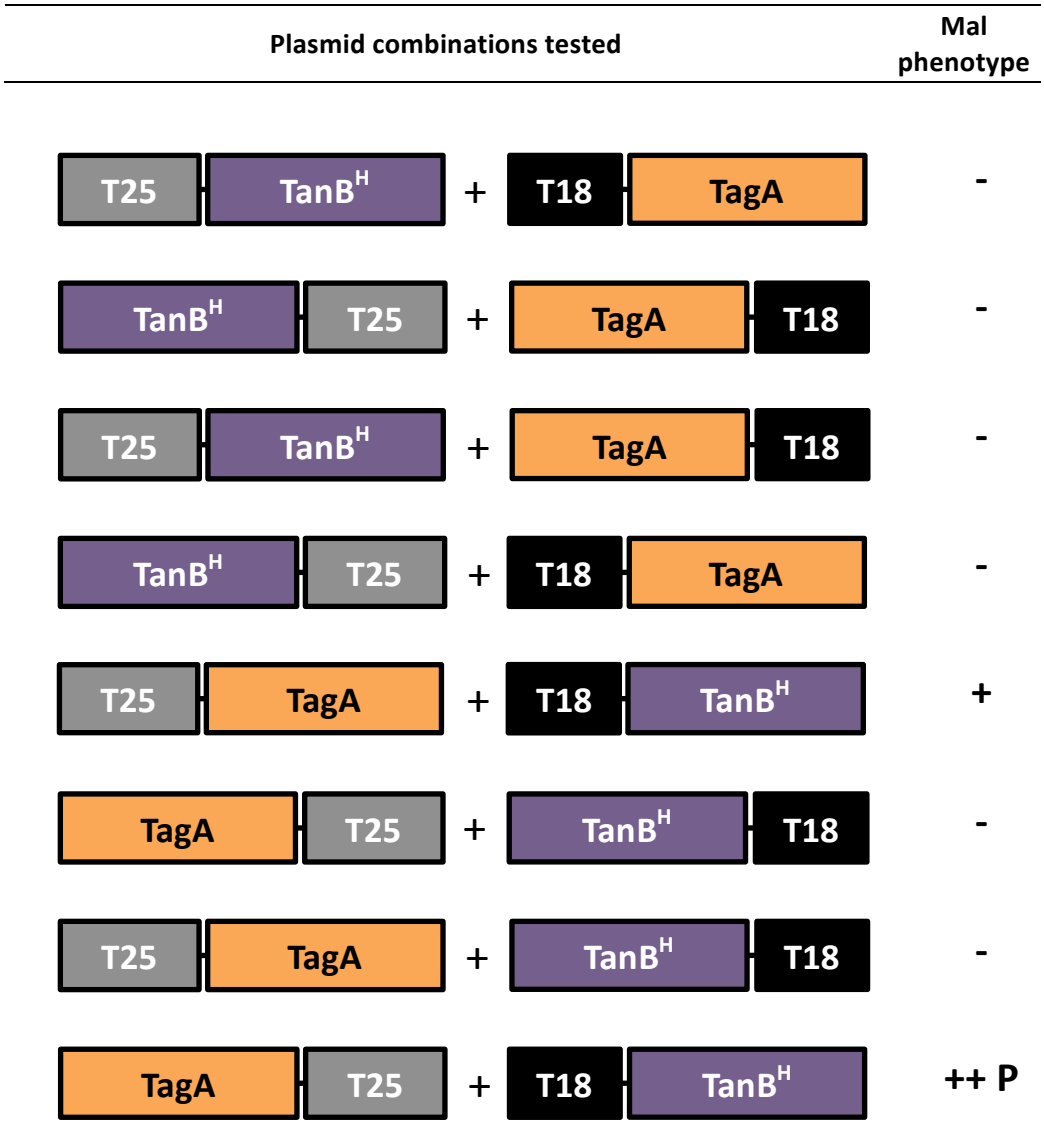

Figure 6.36 Analysis of interactions between TanB^H and TagA by the BACTH system. Pairwise combinations of compatible plasmids encoding T25/T18 fusions to TanB^H and BCAL1295 (TagA) were introduced into BTH101 and grown on MacConkey maltose agar containing ampicillin and kanamycin at 30°C, for up to 7 nights. The Mal$^+$ phenotype was monitored and scored 72-84 hours after initial plating. Mal phenotype scored here as: -, negative; +, weak, red/pink after 84 hours; ++ pink/red after 72 hours; P, non-uniform colouration.

6.10 Investigation of the role of TanB^{H} and TaaB1^{H} *in vivo*

To investigate the function of the putative T6SS effector TanB^{H} and its cognate immunity protein TaaB1^{H} *in vivo* it was decided to introduce in-frame deletions into the *tanB^{H}* open reading frames in the genome of *B. cenocepacia* H111. Although it seemed likely that a *taaB1^{H}* null mutant would be non-viable (based on the inability to clone the intact *tanB^{H}* coding sequence in the absence of *taaB1^{H}*), an equivalent mutant has been attained in *B. cenocepacia* strain K56-2 as part of a random screen looking to identify essential genes in *B. cenocepacia* (Bloodworth et al., 2013). Therefore, it was also decided to attempt to delete *taaB1^{H}*, as a single Δ*taaB1^{H}* mutant and together with the deletion of *tanB^{H}*. Upon deletion of this putative effector-immunity pair the affect on particular phenotypic characteristics of *B. cenocepacia* in comparison to the wild-type strain could then be investigated, in particular the bacterial competition ability of the mutants.

6.10.1 Construction of allelic replacement vectors for construction of *B. cenocepacia* Δ*tanB^{H}*, Δ*taaB1^{H}* and Δ*tanB^{H}-taaB1^{H}* mutants

DNA fragments containing in-frame deletions (Δ) of *tanB^{H}*, *taaB1^{H}* and *tanB^{H}*-Δ*taaB1^{H}* were generated by SOE-PCR. To generate the Δ*tanB^{H}* allele, amplicons Δ*tanB^{H}*-AB and Δ*tanB^{H}*-CD were amplified from *B. cenocepacia* H111. Amplicon Δ*tanB^{H}*-AB contained 573 bp of DNA corresponding to upstream genomic sequences that flanked the *tanB^{H}* gene and codons 1-14 of *tanB^{H}*, fused to the final 7 codons of the same gene. Amplicon Δ*tanB^{H}*-CD contained codons 8-14 of *tanB^{H}* fused to codons 354-365 of the same gene followed by 576 bp of flanking DNA downstream of *tanB^{H}*. Primers BCAL1298ForA and BCAL1298revIP-B were used to generate the amplicon Δ*tanB^{H}*-AB, and primers BCAL1298ForIP-C and BCAL1298revD for amplicon Δ*tanB^{H}*-CD (Figure 6.37A). The amplified DNA fragments were purified, quantified and then combined in 1:1 ratio. A subsequent round of PCR was performed using the two amplicons as a template with primers BCAL1298ForA and BCAL1298revD to generate a 1244 bp Δ*tanB^{H}* DNA fragment, resulting from the fusion of the amplicons Δ*tanB^{H}*-AB and Δ*tanB^{H}*-CD

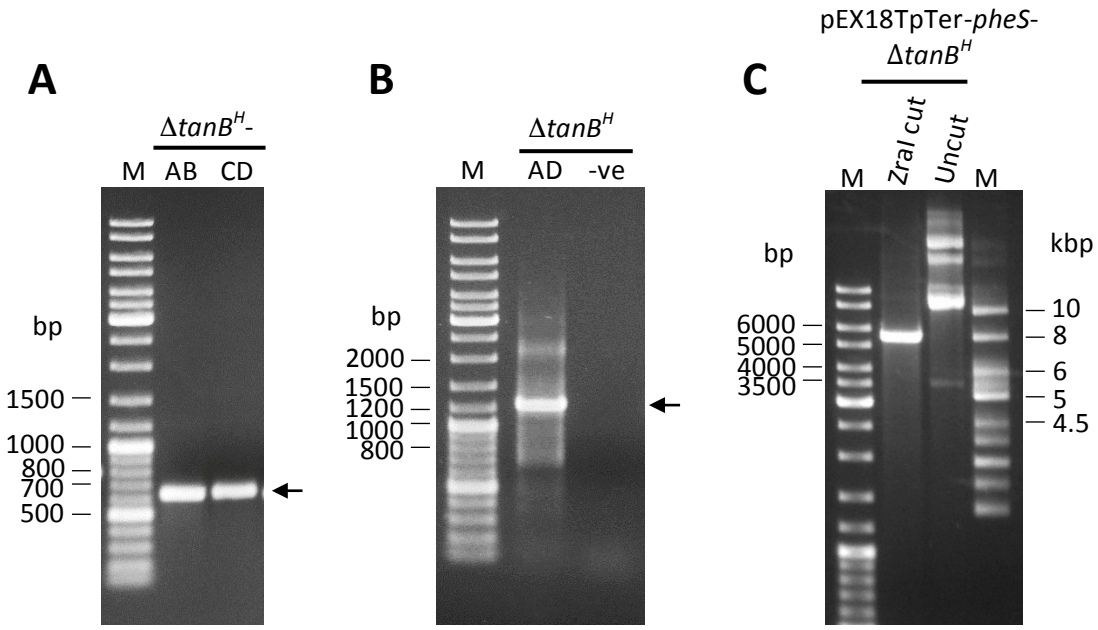

Figure 6.37 Construction of *tanB*^{H} allelic replacement vector, pEX18TpTer-*pheS*-Δ*tanB*^{H}. A DNA fragment containing an in-frame deletion allele of *tanB*^{H} flanked either side by ~500 bp of genome DNA surrounding *tanB*^{H} was generated by SOE-PCR. Fragments AB and CD were amplified from H111 genomic DNA in the first round PCR, as visualised on a 1.0% DNA agarose gel shown in (A). Fragments were then combined in an equal ratio and used as template DNA for the second PCR step using primers annealing to the upstream end of fragment AB and downstream end of fragment CD (primers A and D), to generate a 1244 bp spliced fragment, AD (Δ*tanB*^{H}), as visualised on a 1.0% DNA agarose gel shown in (B). The Δ*tanB*^{H} fragment was then cloned between XbaI and HindIII restriction sites in the allelic replacement vector pEX18TpTer-*pheS*, generating a 5425 bp plasmid. Plasmid minipreparations of a candidate pEX18TpTer-*pheS*-Δ*tanB*^{H} clone was analysed by electroporation and subjected to diagnostic restriction digestion using a unique ZraI restriction site within the region located upstream of *tanB*^{H} in (C). M, DNA ladder mix or supercoiled DNA ladder, arrows indicate DNA fragments of the expected size.

(Figure 6.37B). Δ*tanB*^{H} was digested with XbaI and HindIII, and then ligated between corresponding restriction sites in a modified version of the *Burkholderia* allelic replacement vector pEX18Tp-*pheS*, pEX18TpTer-*pheS* (Section 4.3.1), to generate a 5425 bp plasmid, pEX18TpTer-*pheS*-Δ*tanB*^{H}. Blue white screening was possible for this vector, whereby recombinant clones were identified following growth at 30°C on M9 agar containing trimethoprim and additional supplements. Candidate clones were screened by colony PCR using vector primers M13for and M13revBACTH. Selected positive clones were verified by diagnostic restriction digestion using ZraI, which cuts once within the region located upstream of *tanB*^{H}, thereby linearizing the vector (Figure 6.37C), and further verification by DNA sequencing.

The Δ*tanB*^{H}-*taaB1*^{H} allelic replacement vector, pEX18TpTer-*pheS*-Δ*tanB*^{H}-*taaB1*^{H}, was constructed in an analogous manner. First round amplicons Δ*tanB*^{H}-*taaB1*^{H}-AB and Δ*tanB*^{H}-*taaB1*^{H}-CD were generated by primer pairs BCAL1298ForA and BCAL1298-99revIP-B and BCAL1298-99ForIP-C and BCAL1299RevD, respectively, and then primers BCAL1298ForA and BCAL1299RevD for the second round SOE-PCR. This resulted in the generation of a Δ*tanB*^{H}-*taaB1*^{H} allele that fused the first 14 amino acids of *tanB*^{H} to 13 bp into the 3' UTR region of *taaB1*^{H}, where nucleotides at positions 52-54 correspond to a normally non-functional stop codon that results in termination of the truncated *tanB*^{H} ORF.

The construction of a vector to delete *taaB1*^{H} was attempted, whereby primer pairs BCAL1299ForA and BCAL1299RevIP-B and BCAL1299ForIP-C BCAL1299RevD were used to amplify the DNA fragments Δ*taaB1*^{H}-AB and Δ*taaB1*^{H}-CD. The Δ*taaB1*^{H} DNA fragment was successfully amplified using BCAL1299ForA and BCAL1299RevD in the second SOE-PCR step. However, subsequent cloning of this fragment into pEX18TpTer-*pheS* proved difficult. Several attempts were made but the limited number of candidate clones identified all proved to be incorrect after analysis by diagnostic restriction digestion and DNA sequencing. It appeared the clones contained the correct sequence located downstream of *taaB1*^{H} but incorrect upstream sequences. This region corresponded to the C-terminal coding regions of

tanB^{H}. This fragment also contains a unique EcoRI site. The integrity of the Δ*taaB1*^{H} PCR fragment itself was checked by diagnostic restriction digestion using EcoRI (Figure 6.38). The Δ*taaB1*^{H} amplicon was successfully digested, generating the expected fragment sizes of 1016 bp and 161 bp, but some smearing occurred, indicating the PCR-amplified product may have contained small amounts of incorrect fragments caused by non-specific primer annealing. This indicated that recombinant clones containing the Δ*taaB1*^{H} PCR product were being selected against. No further attempts were made to generate a Δ*taaB1*^{H} allelic replacement vector.

6.10.2 Generation of *tanB*^{H} and *tanB*^{H}-*taaB1*^{H} deletion mutants in *B. cenocepacia* H111 by allelic replacement

To construct Δ*tanB*^{H} and Δ*tanB*^{H}-*taaB1*^{H} mutants in *B. cenocepacia*, allelic replacement constructs pEX18TpTer-pheS-Δ*tanB*^{H} and pEX18TpTer-*pheS*-Δ*tanB*^{H}-*taaB1*^{H} were each introduced into the *E. coli* donor strain, SM10. These donors where then used to transfer in the pEX18TpTer-derivatives into *B. cenocepacia* H111 by conjugation. This allowed homologous single crossover recombination between the deletion allele within the vector and the wild-type allele on the chromosome. Trimethoprim-resistant pEX18TpTer-*pheS*-Δ*tanB*^{H} and pEX18TpTer-*pheS*-Δ*tanB*^{H}-*taaB1*^{H} co-integrate strains were selected on M9-glucose agar containing trimethoprim. Co-integrate strains where purified by streaking onto the same selection medium and checked for plasmid integration by PCR using vector specific primers, pEX18Tpfor and pEX18Tprev. Verified recombinants containing an integrated plasmid were then streaked onto M9-glucose containing 0.1% (w/v) DL-4-chlorophenylalanine (cPhe), for counter-selection of the *pheS* marker. This allowed selection of a second recombination event between the sequence introduced by the integrated vector and homologous sequences on the deleted allele and the chromosome, thus resulting in excision of the vector backbone. This results in the insertion of the entire Δ*tanB*^{H} or Δ*tanB*^{H}-*taaB1*^{H} fragment in place of the wild-type sequences or reversion back to wild-type. As previously encountered in this study, counter-selection using cPhe was found to be inefficient. Candidate

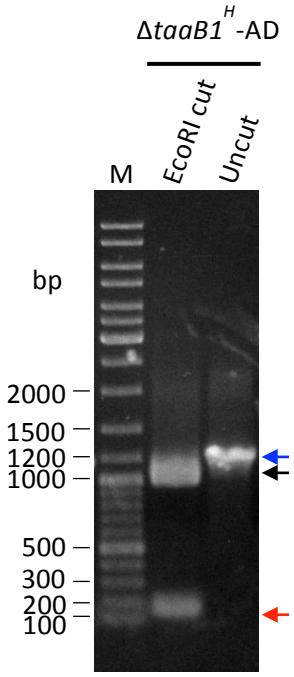

Figure 6.38 Diagnostic restriction digestion of Δ*taaB1*^{H} DNA fragment using EcoRI. Δ*taaB1*^{H} AD amplicon was digested with EcoRI to determine whether the DNA fragment contained the correct flanking sequence upstream of *taaB1*^{H}. Products were analysis by electrophoresis in a 1.0% agarose gel. Expected size fragments of 1016 bp (black arrow) and 161 bp (red arrow) were produced. Uncut Δ*taaB1*^{H} was used as a control (blue arrow). M, GeneRuler DNA ladder mix.

H111-Δ*tanB*^{H} and H111-Δ*tanB*^{H}-*taaB1*^{H} double crossover recombinants were screened using primers BCAL1298ForOP and BCAL1299RevOP that annealed to flanking regions of both deleted alleles. After screening 50-100 cPhe-resistant recombinants for each mutant, several candidate mutants were identified which produced a PCR-generated DNA fragment of the expected size of 1839 bp for Δ*tanB*^{H} and 1375 bp for Δ*tanB*^{H}-*taaB1*^{H}. This was in contrast to the wild-type strain that gave rise to an amplicon of 2856 bp. After subsequent rounds of re-streaking onto M9-glucose cPhe agar and then final colony purification on M9-glucose agar, candidate H111-Δ*tanB*^{H} and H111-Δ*tanB*^{H}-*taaB1*^{H} deletion mutants were PCR screened again using the above primers to verify gene deletion (Figure 6.39A). The candidate mutants were also checked for trimethoprim sensitivity and subjected to a further PCR screen with vector primers pEX18Tpfor and pEX18Tprev (which produced a fragment size of 397 bp if the vector backbone was present). This allowed verification of the excision of the integrated pEX18TpTer-*pheS* vector (Figure 6.39B).

6.10.3 Effect of Δ*tanB*^{H} and Δ*taaB1*^{H}-*taaB1*^{H} null alleles on growth rate in *B. cenocepacia* H111

To determine whether deletion of *tanB*^{H} or *tanB*^{H}-*taaB1*^{H} together affected the growth rate of the strain, wild-type H111, H111-Δ*tanB*^{H} and H111-Δ*tanB*^{H}-*taaB1*^{H} were grown in BHI broth at 37°C and the culture optical densities were monitored over time. The resulting growth curves are shown in Figure 6.40. No statistically significant difference was observed between the growth rate of H111-Δ*tanB*^{H} or H111-*tanB*^{H}-*taaB1*^{H} in comparison to the wild-type strain or a T6SS-inactivated strain, Δ*tssM*.

6.10.4 Effect of Δ*tanB*^{H} and Δ*taaB1*^{H}-*taaB1*^{H} null alleles on T6SS activity in *B. cenocepacia* H111

As TanB^{H} was not predicted to be a core T6SS subunit, inactivation of *tanB*^{H} was not expected to exert an effect on T6SS activity. Accordingly, analysis of

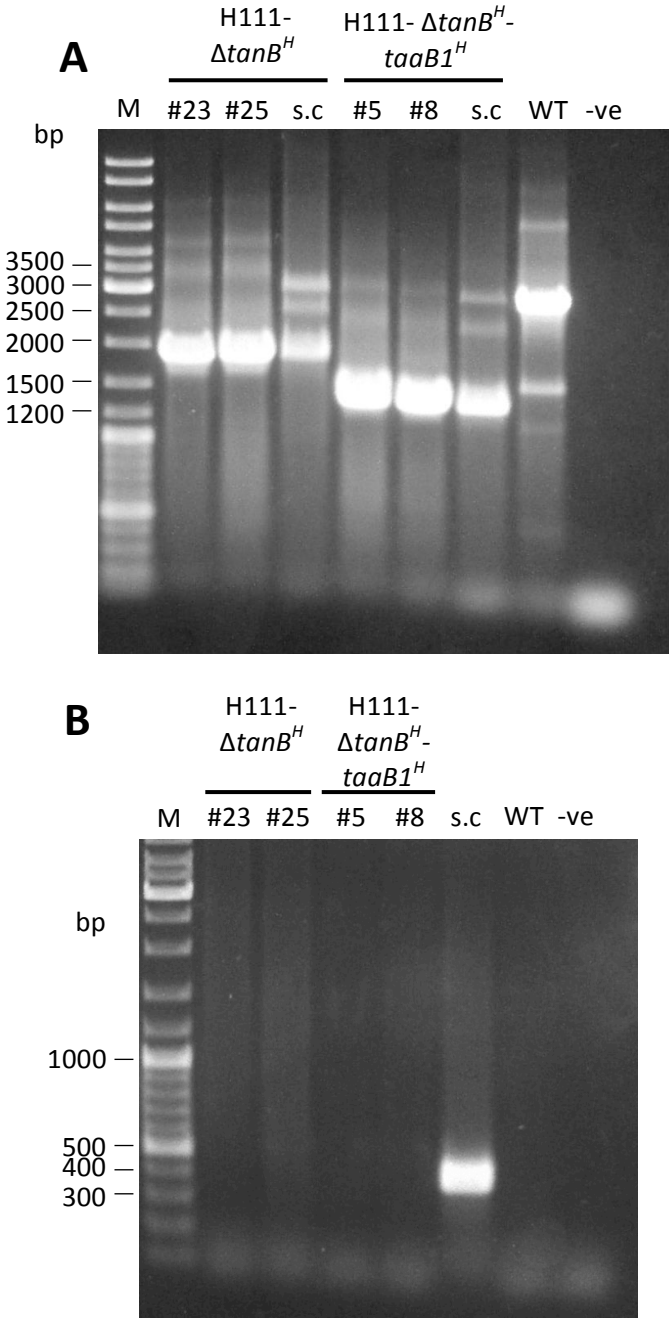

Figure 6.39 Verification of H111-Δ*tanB*^{H} and Δ*tanB*^{H}-*taaB1*^{H} mutants by PCR screening. *B. cenocepacia* H111 derivatives containing allelic replacement vectors pEX18TpTer-*pheS*-Δ*tanB*^{H} and pEX18TpTer-*pheS*-Δ*tanB*^{H}-*taaB1*^{H} integrated at the *tanB*^{H}-*taaB1*^{H} genetic locus, by single cross over recombination, were subjected to counter-selection using medium containing 0.1% cPhe. (A) Resultant cPhe-resistant recombinants were screened by PCR amplification using primers that annealed to genomic DNA just outside of the flanking regions of *tanB*^{H} *and taaB1*^{H}. (B) PCR screening for loss of integrated pEX18TpTer-*pheS*-Δ*tanB*^{H} and pEX18TpTer-*pheS*-Δ*tanB*^{H}-*taaB1*^{H} vectors from candidate H111-Δ*tanB*^{H} and Δ*tanB*^{H}-*taaB1*^{H} mutants using vector specific primers pEX18Tpfor and pEX18Tprev. These primers yielded a 397 bp fragment if the vector was present. Samples as indicated above the lanes. M, GeneRuler DNA ladder mix; s.c, pEX18TpTer-pheS-Δ*tanB*^{H} or Δ*tanB*^{H}-*taaB1*^{H} co-integrate control; WT, wild-type control; -ve, no DNA control.

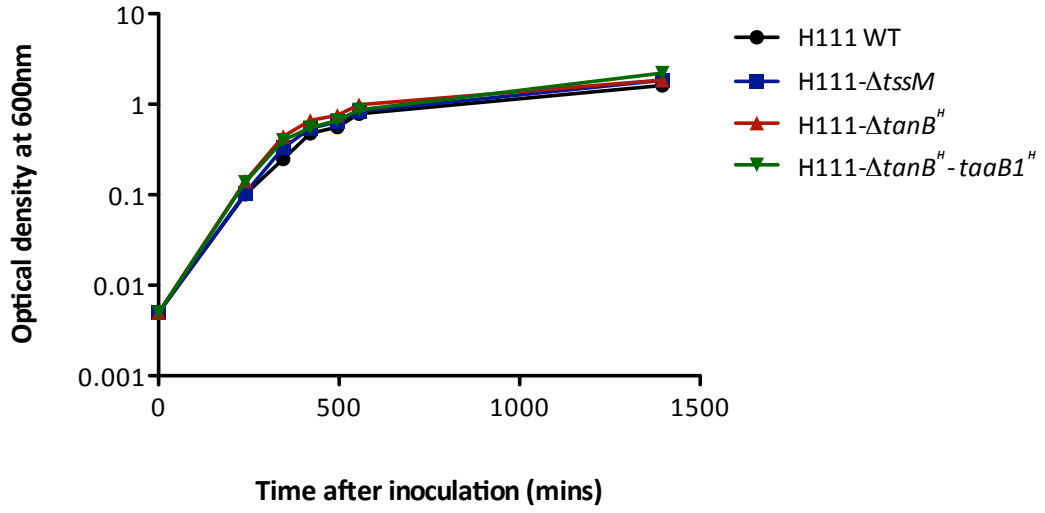

Figure 6.40 Analysis of the growth rates of H111-Δ*tanB*^{H} and Δ*tanB*^{H}-*taaB1*^{H} mutants in comparison to the wild-type strain. Cultures of H111 wild-type (WT), H111-Δ*tssM*, H111-Δ*tanB*^{H} and H111-Δ*tanB*^{H}-*taaB1*^{H} were grown in BHI-broth at 37°C with shaking, and the optical density at 600nm was monitored over time, as indicated. Graph shows resulting optical density (y axis) over time in minutes (x axis).

secreted proteins from H111-Δ*tanB*^{H} and Δ*tanB*^{H}-*taaB1*^{H} in comparison to wild-type H111 and a T6SS mutant *(*Δ*tssM*) indicated the presence of similar levels of secreted TssD from H111 wild-type, H111-Δ*tanB*^{H} and H111-Δ*tanB*^{H}-*taaB1*^{H} strains, but an absence of this protein in the culture supernatants of H111-Δ*tssM*, as detected by a western blot probed with anti-TssD (Figure 6.41). Extracellular levels of the intracellular RNA polymerase β-subunit were determined by western blotting, to indicate the level of lysis occurring in the cultures during growth. This protein was not detected in the culture supernatants of any of the strains tested, it was confined to the intracellular compartment, indicating that only very low level of undetectable lysis was occurring.

6.10.5 Effect of Δ*tanB*^{H} null allele on inter-bacterial competition in *B. cenocepacia* H111

To understand whether TanB^{H} plays a role in the T6SS-dependent competitive advantage *B. cenocepacia* H111 has over some bacterial strains, the H111-Δ*tanB*^{H} mutant strain was employed in a bacterial competition assay with *P. putida* (Section 2.9.1). Control co-cultures using H111 wild-type and a H111 T6SS-deficient mutant (H111-Δ*tssM*) in combination with *P. putida* were also included. Results presented here confirm the previous observation that *B. cenocepacia* results in a decreased titre of viable *P. putida* following co-culture for four hours, and this competition edge is T6SS-dependent (Figure 6.42). However, results obtained following co-culture of the H111-Δ*tanB*^{H} mutant with *P. putida* were inconclusive due to variable recovery of *P. putida* from each competition experiment. The reason for this is not clear.

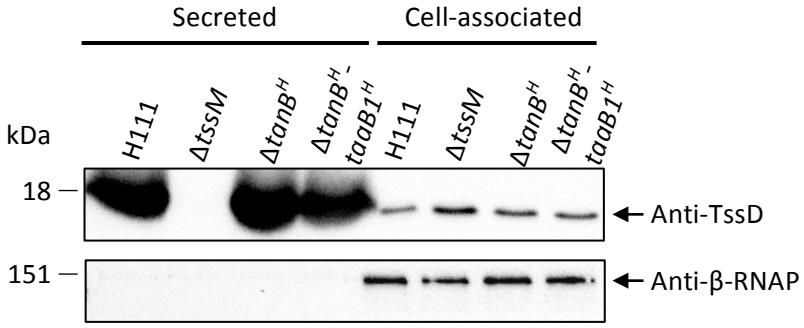

Figure 6.41 Analysis of the effect of *tanB^H* and *tanB^H-taaB1^H* deletion on T6SS activity. Western blot analysis of secreted and cell associated TssD (upper) and β-RNAP (lower) of H111 WT, H111-Δ*tssM*, H111-Δ*tanB*^{H} and H111-Δ*tanB*^{H}*-taaB1^H*, as indicated. Molecular mass (kDa) of each protein is indicated to the left, as verified by a protein ladder.

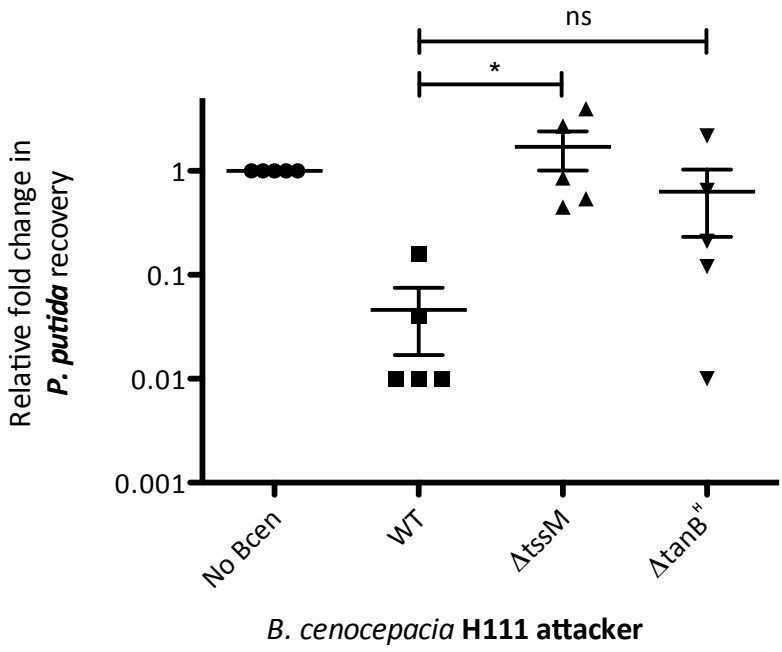

Figure 6.42 Analysis of the competitive ability of H111-Δ*tanB^H* against *P. putida.* H111-Δ*tanB*^{H} was co-cultured with *P. putida* for 4 hours at 30°C on LB agar. The number of surviving *P. putida* was enumerated by growth on appropriate selection plates. *P. putida* co-cultured with H111 WT and H111-Δ*tssM* mutant were used as controls. The graph shows differences in relative fold change in number of *P. putida* recovered (standardised to *P. putida* cultured on its own) (y axis) with different H111 attacker strains (x-axis). Statistical analysis by student's t-test, n= 5, $p<0.05$, error bars = ±SEM.

6.11 Discussion

6.11.1 Characterisation of the DNase activity of TanB^{H}

A range of methods where used to demonstrate the DNase activity of TanB^{H}, including in-solution DNase hydrolysis assays and DNA substrate gels, which attributed the DNase activity of the protein to its C-terminal domain. Results indicated that the DNase activity of the protein was likely to be dependent on a common DNase co-factor Mg^{2+}. TanB^{H} was able to degrade both single and double-stranded linear and supercoiled DNA. These findings are in-line with the predicted endonuclease motif of TanB^{H} belonging to the endonucleases of the $\beta\beta\alpha$-Metal finger clan. Similarly, the experimentally characterised endonuclease Spd1 in *S. pyogenes* and the *S. marcescens* endonuclease both require a Mg^{2+} metal ion for catalysis and are non-specific in the DNA structures they hydrolyse (Nestle and Roberts, 1969; Kühlmann et al., 1999; Korczynska et al., 2012). Furthermore, TanB^{H} was found to be thermostable under the conditions tested, which is similar to the well characterised thermostable unrelated Nuc nuclease found in the Gram-positive bacterium *S. aureus* (Lachica et al., 1972; Kovacevic et al., 1985). Together the data suggests the C-terminal domain of TanB^{H} in *B. cenocepacia* H111 does indeed have nuclease activity, as predicted.

It was also shown that a TanB^{H} variant, mutated to an aspartate residue at Gly276, had diminished DNase activity indicating that this relatively well-conserved glycine residue amongst Endonuclease NS_2 family proteins may be important. However, rather than be involved in catalysis or metal ion coordination, its important feature may be the fact that it is a small neutral amino acid, thus does not interfere with the predicted catalytic histidine residue (His277) next to it. Gly was substituted for an aspartate residue in the spontaneous G276D mutant, which contains a larger, negatively charged side chain, which could potentially interfere with the negatively charged histidine residue, meaning it can no longer function as a base to deprotonate water for the hydrolysis reaction. Further mutagenic studies are required to confirm the true essential residues for the nuclease activity of TanB^{H}.

Some members of the ββα-Metal finger family of endonuclease that TanB^{H} belongs to show RNase activity in addition to DNase activity, including the *Serratia* endonuclease (Friedhoff et al., 1996), colicin E9 of *E. coli* (Pommer et al., 2001) and NucA of *Anabaena spp.* (Meiss et al., 1998), suggesting that TanB^{H} may also posses RNase activity. However, due to time limitations the ability of TanB^{H} and TanB^{H}.CTD to degrade RNA was not tested.

6.11.2 TanB^{H} and TaaB1^{H} as an effector-immunity pair

It was only possible to clone and express the gene encoding TanB^{H} when *E. coli* host cells also encoded its predicted immunity protein, TaaB1^{H}. Failure to clone DNA encoding the putative nuclease without its immunity protein is perhaps not surprising. Being a predicted non-specific endonuclease, TanB^{H} may be expected to degrade most forms of DNA and RNA. Hence, even tiny amounts of expression could result in host cell toxicity due to genomic DNA and RNA degradation. This problem is not exclusive to TanB^{H}; it has been encountered with other nuclease domain-containing proteins from other bacteria. In particular, rearrangement hotspot protein RhsB in the plant pathogen *D. dadantii* contains a C-terminal HNH endonuclease domain that was found to prevent cloning of the entire gene without the ORF encoding its linked immunity protein (Koskiniemi et al., 2013).

Direct inhibition of the enzymatic activity of TanB^{H} caused by TaaB1^{H} was demonstrated by prevention of DNA degradation *in vitro*, illustrated in Figure 6.43. This neutralising quality of immunity proteins is in agreement with other effector-immunity pairs, including the T6SS DNase effector-immunity pair Tde1-Tdi1 (Atu4350-Atu4351) in *A. tumefaciens* (Ma et al., 2014). Here co-expression of the immunity protein Tdi1 restored the viability of *A. tumefaciens* cells overexpressing the toxic Tde1 DNase effector. It is also in line with other ββα-Metal endonucleases, including the *Anabaena* spp. NucA, which has an inhibitor protein NuiA (Muro-Pastor et al., 1997). NuiA is similar to TaaB1^{H} in the respect that it is a small protein, encoded by a gene directly downstream from the gene encoding the NucA nuclease (Muro-Pastor et al., 1997). This pair has been shown to form a strongly associated complex, requiring two points of contact, one of which disrupts

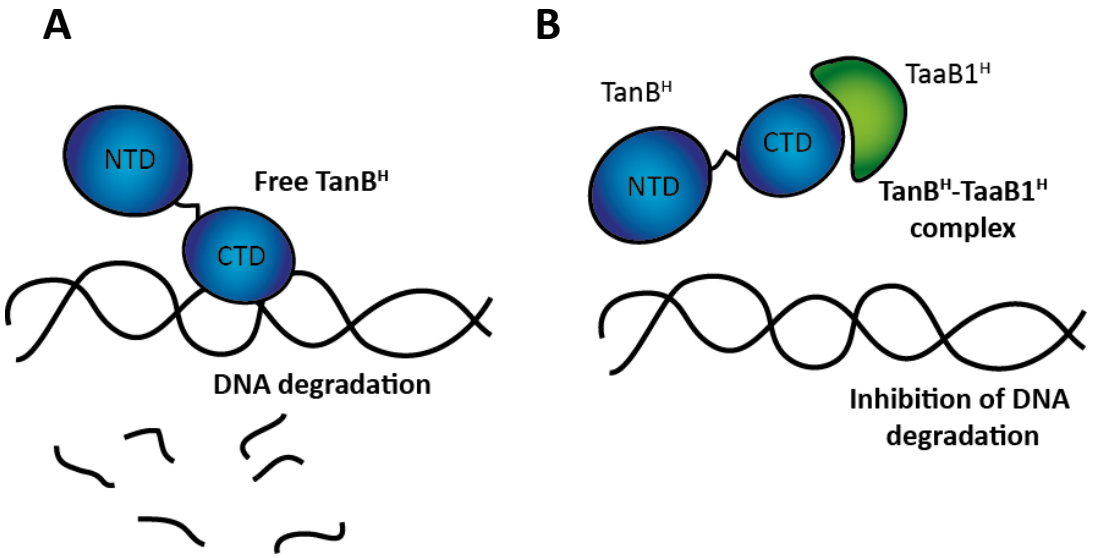

Figure 6.43 Proposed model for inhibition of DNase activity of TanB^{H} by TaaB1^{H}. (A) Free TanB^{H}, both full length and its CTD, can degrade supercoiled DNA, linear dsDNA, ssDNA and short DNA fragments. (B) Upon addition of TaaB1^{H}, a complex is formed that inhibits the DNase activity of TanB^{H}.

the NucA active site through a polar amino acid of NuiA, which coordinates the metal ion. It is, however, unknown whether $TaaB1^H$ acts as an active site or allosteric inhibitor. Further characterisation of the binding and inhibitory properties of $TaaB1^H$ would be beneficial, particularly if $TaaB1^H$ possesses novel binding properties that could be exploited and translated into wider applications.

A direct interaction between $TanB^H$ (or its CTD) and $TaaB1^H$ was demonstrated by use of the BACTH system and by pull-down assays. Neither of these methods allow for a quantitative measurement of the binding affinities. Nevertheless, the interaction between $TanB^H$ and $TaaB1^H$ can be inferred to be a strong one due to the strong denaturing conditions required to dissociate the His_6.$TanB^H$(CTD)-$TaaB1^H$ complex. The use of 8 M urea as a strong denaturant, along with extremes of pH and NaCl concentration, were ineffective at dissociating the complex. Complex dissociation was finally resolved by the use of 6 M GuHCl and DTT.

Characterisation of the interactions between other effector-immunity pairs, such as Tse2-Tsi2, suggest that electrostatic interactions between the effector and immunity protein play a vital role in their strong interaction, specifically via an acid patch of residues on Tsi2 (Li et al., 2012). This general model of acidic immunity proteins and basic effector proteins was also proposed for Ssp-Rap complex formation in *S. marcescens* (English et al., 2012). However, those authors considered complementary shape and protein orientation to be just as significant. The theoretical pI value of the immunity protein $TaaB1^H$ is highly acidic, with a pI of 4.5, whereas the nuclease CTD of $TanB^H$ is basic, with a pI of 9.1. Therefore electrostatic interactions between regions of acidic and basic residue on $TaaB1^H$ and $TanB^H$.CTD, respectively, could also be at play here to facilitate the $TanB^H$-$TaaB1^H$ interaction.

Due to this strong complex association, it is interesting to postulate how the complex might dissociate *in vivo* before its secretion or injection into a target cell. A possible model is that once $TanB^H$ binds to the T6SS secretion apparatus it results in a conformational change that means $TaaB1^H$ is dissociated from $TanB^H$. Or, upon secretion into the periplasm of a target bacteria or exposure to the extracellular

surroundings, a similar conformational change and complex dissociation occurs. Alternatively, TanB^{H} may never be given the chance to target host cell DNA/RNA, where upon translation it is immediately loaded onto the apparatus, or the effector is attached to the apparatus whilst still being translated by the ribosome, in something reminiscent to co-translation translocation.

For TaaB1^{H} to be classed as a bona fide immunity protein, it would have been ideal to determine whether TaaB1^{H} was able to provide protection against TanB^{H} *in vivo*, if in-fact TanB^{H} was injected in a T6SS-dependent manner into surrounding bacterial cells. To address this it was intended to use the H111-Δ*tanB^{H}*-*taaB1^{H}* mutant as the target strain in an intra-species competition experiment, against wild-type H111 and a T6SS-mutant attacker strain to demonstrate T6SS-dependance, and against a Δ*tanB^{H}* mutant to show TanB^{H} is the cognate effector of TaaB1^{H}. However, due to time constraints this experiment was not undertaken.

6.11.3 Stoichiometry of the TanB^{H}-TaaB1^{H} complex

Estimation of the oligomeric status of both the TanB^{H}-TaaB1^{H} and TanB^{H}.CTD-TaaB1^{H} complex by SEC indicated that both complexes potentially existed in at least three oligomeric states. For the TanB^{H}.CTD-TaaB1^{H} complex stoichiometries of at least 1:1 and other higher order state were detected. Structural insights into other T6SS effector-immunity pairs have highlighted that a variety of stoichiometric arrangements are possible between different classes of effector and their cognate immunity proteins.

The *P. aeruginosa* muramidase T6SS-effector Tse3 (Russell et al., 2011) appears to bind in a 1:1 complex with its immunity protein Tsi1 (Li et al., 2013; Wang et al., 2013). In another class of T6SS effector, the Tae4 amidase effectors (Russell et al., 2012), a representative member in *E. cloacae* is thought to bind to its immunity protein Tai4 to form a heterotetramer, made up of a Tai4 homodimer in complex with two Tae4 effector proteins (Zhang et al., 2013). More interestingly, the immunity protein of the cytotoxic effector Tse2 is able to self-interact to form a dimer complex, which in turn interacts with its effector Tse2 (Hood et al., 2010; Li et al., 2012). However, the dimerization of Tsi2 is not strictly required for the Tse2-

Tsi2 interaction, as Tse2 binds at the opposing surface of Tsi2 than the side that is involved in Tsi2 dimerization. Tse2 is a proposed nuclease (Li et al., 2012; Silverman et al., 2013). Together these highlight the diversity in complex formation that is possible between effector-immunity pairs.

On the more general theme of variability in stoichiometries amongst toxin-antitoxin pairs, differing oligomeric states within a complex has also been observed. An *E. coli* ribonuclease toxin, Kid, although not a T6SS-dependent effector, is able to form different stoichiometric complexes with its antitoxin, Kis, which is dependent on the level of Kid available, where different stoichiometric complexes have different affinities for substrate binding (Monti et al., 2007). Taking this previous finding into consideration, it is possible that the different stoichiometric complexes observed for the $TanB^{H}$.CTD-$TaaB1^{H}$ and $TanB^{H}$-$TaaB1^{H}$ complex could be a result of the molar ratios of each unit available in solution.

It important to note, however, that as SEC measures the hydrodynamic volume of proteins through a medium and as a perfect sphere, proteins that are asymmetrical will deviate from this relationship between size and elution volume. Therefore, to gain a more accurate estimation of the molecular weight and oligomeric status of the $TanB^{H}$-$TaaB1^{H}$ complexes, further analysis by methods such as SEC-MALL need to be undertaken.

6.11.4 Investigation into the secretion of $TanB^{H}$

It was postulated that $TanB^{H}$ may be a T6SS-dependent effector based on its genomic location downstream of genes encoding $TssI_{1294}$ and two *tag* genes. Current models of T6SS-effector secretion suggest that particular T6SS-effectors directly or indirectly interact with TssI proteins to allow their export (Dong et al., 2013; Koskiniemi et al., 2013; Shneider et al., 2013; Whitney et al., 2014; Liang et al., 2015; Unterweger et al., 2015). Experimental evidence in *P. aeruginosa* strengthened this notion by demonstrating toxin proteins encoded downstream of three *tssI* genes of the H1-T6SS were required to facilitate TssI-dependent anti-bacterial killing (Hachani et al., 2014). Interestingly, it was found that a toxin that required VgrG1b to exert is anti-bacterial, PA0099, contained a HNH/Endo VII

superfamily nuclease domain at its C-terminus. This study was unable to demonstrate the direct secretion of the putative nuclease effector by the H1-T6SS, but it was implied due to the contribution of PA0099 to VgrG1b-dependent killing.

It was intended to try to detect secretion of TanB^{H} by tandem mass spectroscopy and generate a custom anti-TanB^{H} antibody to be used for immuno-detection. However, due to time constraints neither experiment were undertaken. Although, ectopic expression of a N-terminally His-tagged TanB^{H} in wild-type *B. cenocepacia* and a T6SS mutant was performed as an alternative strategy to try to detect secretion of TanB^{H} (data not shown). However, only small His-tagged degradation products appeared to be presented in the cell culture supernatants after induction in both the wild-type and a T6SS mutant. It is possible that the N-terminal His-tag was interfering with secretion of the effector due to disruption of protein-protein interactions between TanB^{H}.NTD and a T6SS adaptor/chaperone crucial for secretion of the effector, if the NTD functions in this role.

It was intended to exploit the observation that bacteria possessing antibacterial T6SSs can lead to self-killing if co-cultured with mutant strains that lack pertinent effector-immunity protein pairs as a method to determine whether TanB^{H} was a T6SS-dependent effector (Dong et al., 2013; Russell et al., 2013). Thus, the H111-Δ*tanB^{H}-taaB1^{H}* mutant generated in this study would be employed in an intraspecies competition experiment against wild-type *B. cenocepacia* H111, a T6SS-deficient mutant and H111-Δ*tanB^{H}*. If the action of TanB^{H} was dependent on the T6SS then co-culturing of the H111-Δ*tanB^{H}-taaB1^{H}* mutant as 'prey' bacteria with a T6SS-deficient H111 or a Δ*tanB^{H}* mutant as the 'attacker' strain should result in a greater number of recovered prey bacteria, than when co-cultured with the T6SS-proficient wild-type attacker strain. However, this would also be dependent on TanB^{H} having anti-bacterial properties and on TaaB1^{H} being a bona fide immunity protein and expressed under the experimental conditions employed.

6.11.5 Interaction of TanB^{H} with other T6SS associated proteins for secretion

Investigations into interactions between TanB^{H} and other proteins encoded by the BCAL1294-BCAL1300 cluster by two-hybrid analysis suggested TanB^{H} is unable to directly interact with TssI$_{1294}$. However, TanB^{H} was able to interact with TagA (BCAL1295), a product of a T6SS associated gene. This interaction was inferred to occur through the N-terminal region of TanB^{H}, as TanB^{H}.CTD did not demonstrate an interaction with TagA. In light of this, it is surprising that in the two combinations that gave rise to a positive result in the two-hybrid analysis, TanB^{H}.NTD was fused to the T18 fragment and was not free.

It was postulated that that the NTD region of TanB^{H} might be required for the delivery of the toxic CTD, due to the homology of this region with TanA^{J} from *B. cenocepacia* J2315 and other related proteins discussed in Section 5.1. It can be speculated that the CTD nuclease domain may be released from the rest of the protein by proteolytic cleavage of the linker domain. This defines the Tan proteins as a modular polymorphic toxin family (Jamet and Nassif, 2015).

In polymorphic toxin families the conserved N-terminal regions are often related to secretion of the toxin (Jamet and Nassif, 2015). So, as an interaction between TagA and the NTD of TanB^{H} was observed, it may suggest that TagA acts as a T6SS-adaptor protein (depicted in Figure 6.44). TagA may interact with the N-terminal region of TanB^{H} to facilitate the binding of TanB^{H} onto a core T6SS subunit such as TssI (model A in Figure 6.44). This general model has been suggested for secretion of Tle1^{VC} in *V. cholerae*, where Tle1^{VC} interacts with a chaperone protein (TEC/Tap-1) that facilitates its secretion by a TssI protein, but the adaptor is not secreted.

An alternative model for TanB^{H} secretion is the attachment of TanB^{H} onto an additional protein bound to TssI, such as a protein of the PAAR superfamily (Shneider et al., 2013), which is again facilitated by TagA (model B in Figure 6.44). Results from a previous study (Jones, 2012) indicated TagA was able to interact with TssI$_{0148}$ but not with TssI$_{1294}$, the former of the two contains a DUF2345 domain.

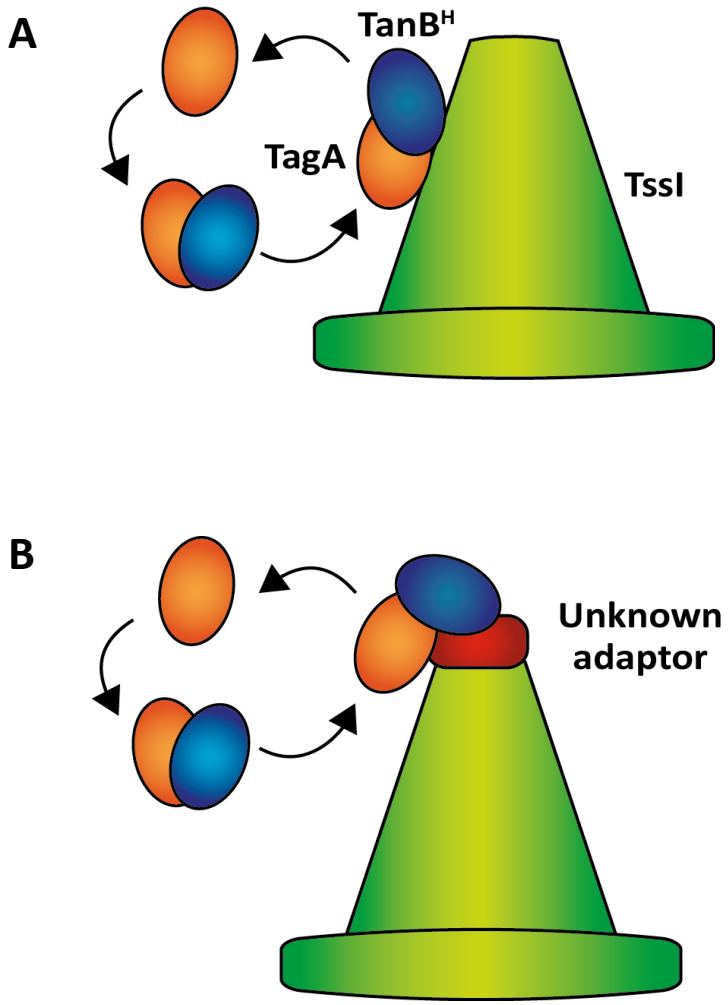

Figure 6.44 Proposed models for secretion of TanB^{H} by the T6SS involving T6SS associated protein TagA. Using the BACTH system, an interaction between TanB^{H} and TagA was detected. Based on this observation and the general model for TssI-mediate effector secretion, two models for secretion of TanB^{H} can be proposed: (A) depicts a model where TagA acts as a chaperone to load TanB^{H} directly onto a TssI subunit for secretion. TagA is removed before secretion. (B) In this model, TagA is again used as a chaperone for TanB^{H}, but this time is loads TanB^{H} indirectly onto a TssI subunit via an additional adaptor protein, such as a PAAR-like protein. TagA is removed before secretion.

However, this study could not repeat these previous findings. Therefore, the identification of the T6SS core component with which TagA interacts with remains unclear. It must be noted, however, that this TagA facilitated $TanB^{H}$ secretion model is solely based on interactions analysed by the BACTH system. Further investigation and validation of these interactions by other methods such pull-down analyses are required.

6.11.6 Translocation of cytotoxic T6SS effectors

Due to the cytoplasmic location of DNA a nuclease effector would need to transverse the inner cell membrane of the target Gram-negative bacterial cell to exert its toxic activity. However, according to current models of T6SS function, effectors are only proposed to be delivered to the periplasmic space (Russell et al., 2014).

Work by Saloman and colleagues identified superfamilies of MIX-effectors, which contained conserved motifs identifying them as putative T6SS-dependent effectors, yet the majority of these effectors were thought to contain transmembrane helices. Therefore, the authors reasoned that these effectors may act in a similar manner to pore-forming proteins, by insertion into the cytoplasmic membrane (Salomon et al., 2014a). Moreover, it is still not clear how the proposed cytotoxic *P. aeruginosa* T6SS nuclease effector, Tse2, is transported into the cytoplasm (Hood et al., 2010; Li et al., 2012). With what little is known concerning the transport of cytotoxic T6SS dependent effectors into the cytoplasm of the target cell it is difficult to predict how $TanB^{H}$ may achieve this, if it is indeed a T6SS-dependent effector.

One method to account for the translocation of a cytotoxic effector could be by self-promoted uptake, in a similar manner to colicin DNase translocation. This involves self-propulsion across the cytoplasmic membrane by electrostatic interactions with the phospholipid bilayer (Mosbahi et al., 2004). Alternatively, the effector may be transported from the periplasm through an inner membrane protein into the target cell cytoplasm. This has recently been suggested as a

mechanism for the translocation of a C-terminal toxin domain of CdiA in a contact-dependent inhibition system (CDI) in *B. pseudomallei* (Koskiniemi et al., 2015). If this were the case for TanB^{H} then the CTD domain may be proteolytically cleaved in the periplasm releasing the small nuclease domain from the remainder of the protein. Concurrently, CdiA proteins in CDI systems have shown to translocate only the C-terminal toxin domain of the protein into the cytoplasm of target bacteria, whilst the N-terminal region remains associated on the cell surface of the target cell (Webb et al., 2013). Overall, investigations outside the scope of this project are needed to fully investigate TanB^{H} as a T6SS-dependent effector.

6.11.7 Role of TanB^{H} and TaaB1^{H} in *B. cenocepacia in vivo*

Prior to this study, the gene homologous to the BCAL1299 locus (*taaA1*^{J}) in J2315 had been identified as being required for the normal growth of *B. cenocepacia* K56-2 in a screen of a conditional growth mutant library, which looked to identify essential genes in *B. cenocepacia* K56-2 (Bloodworth et al., 2013). Insertions of a rhamnose inducible promoter in this gene (and a orthologue of the BCAL1300 gene locus (*taaA2*^{J}) in J2315) led to a slow growth phenotype in the absence of the inducer. Expressed as a percentage of wild-type growth rate, the conditional growth mutants grew at 13% and 16% relative to the wild-type strain, respectively. This in turn suggests that both the putative immunity protein gene(s) and the effector gene itself are expressed under standard laboratory conditions (i.e. nutrient broth at 37°C) in *B. cenocepacia* K56-2. These findings are consistent with the suggestion that the protein encoded by the BCAL1299 gene locus and its related proteins in K56-2 and H111, may act as immunity proteins for their cognate nucleases *in vivo*, and that these putative nucleases have anti-bacterial properties.

Other T6SS-dependent effectors with a nuclease domain have been demonstrated to exhibit anti-bacterial activity and are involved in T6SS-dependent inter- and intra-species competition (Hachani et al., 2014; Ma et al., 2014; Diniz and Coulthurst, 2015). In this study, however, the H111-Δ*tanB*^{H} mutant did not demonstrate a significant decrease in bacterial competition when competing against *P. putida*, a species that is growth restricted or killed in the presence of *B.*

cenocepacia. Although the average number of recovered *P. putida* was higher than when co-cultured with wild-type H111 there was too much variation in the number of recovered prey cells to allow a firm conclusion to be made. Due to time limitations further repeats could not be undertaken. Ideally the experiment should be tested with a different prey strain, such as *E. coli* CC118(λpir) that demonstrates less statistical variation in the bacterial competition assay.

To conclude the functional role of $TanB^{H}$ *in vivo* is still unknown. However, DNase activity for this protein via a non-specific endonuclease domain at its CTD, which is both metal-ion dependent and thermostable, has been demonstrated. Its ability to form a complex with its putative immunity protein $TaaB1^{H}$ was also demonstrated, which leads to inhibition of its toxic effect *in vivo* in *E. coli* and a direct inhibition of DNase activity *in vitro*.

Chapter 7: Investigation of the putative T6SS-dependent effectors $TssI_{0667}$ and Tpe1 from *B. cenocepacia* H111

7.1 Rationale: $TssI_{0667}$

A core structural subunit required for a functional T6SS is the spike-like protein TssI. This protein has distinct homology to the tail spike complex gp27gp5 of the T4 bacteriophage. A bioinformatic survey of putative T6SS effector genes in the *B. cenocepacia* J2315 genome, discussed in Section 3.2, identified eleven different TssI proteins (nine likely to be functional) encoded by loci that are distant from the T6SS gene cluster. BCAS0667, located on the third chromosome, is predicted to encode one such protein, termed $TssI_{0667}$. The orthologous gene of BCAS0667 in the *B. cenocepacia* H111 strain is at the I35_7843 gene loci. The protein product of I35_7843 is near identical to that of the product of BCAS0667, bar several amino acid changes. Bioinformatic analysis of the large $TssI_{0667}$ protein from both BCAS0667 and I35_7843 identified a core gp27gp5-like region located at the N-terminus of the polypeptide that is homologous to other TssI proteins (Jones, 2012). Examples of this type of specialised TssI, containing a C-terminal extension with effector-like function, have been identified and characterised in other T6SS systems and given the term 'evolved TssI' (Section 1.5.1). The secretion of these effector domains have been shown to be T6SS-dependent but they are not an essential component of the T6SS complex itself (Pukatzki et al., 2007; Ma et al., 2009a; Brooks et al., 2013).

Interestingly, bioinformatic analysis of $TssI_{0667}$ identified a C-terminal extension, predicted to contain a phospholipase A_1 (PLA_1) domain, which is connected to the core TssI region via a linker-like region rich in proline residues (Jones, 2012). Figure 7.1 depicts the predicted domain arrangement of $TssI_{0667}$. The PLA_1 domain of $TssI_{0667}$ was found to contain a lipase specific motif, GxSxG, which is also found in an experimentally characterised superfamily of T6SS-dependent phospholipase effectors, Tle (Section 1.5.3 and 3.3.5). This superfamily is further split into five subfamilies, Tle1-Tle5, based on sequence homology of the GxSxG or HxxxxD motif and the flanking regions that surround it (Russell et al., 2012). The CTD of $TssI_{0667}$ is most similar to the Tle2 class of the Tle superfamily, which are also PLA_1 enzymes. However it does not contain the conserved regions that flank the

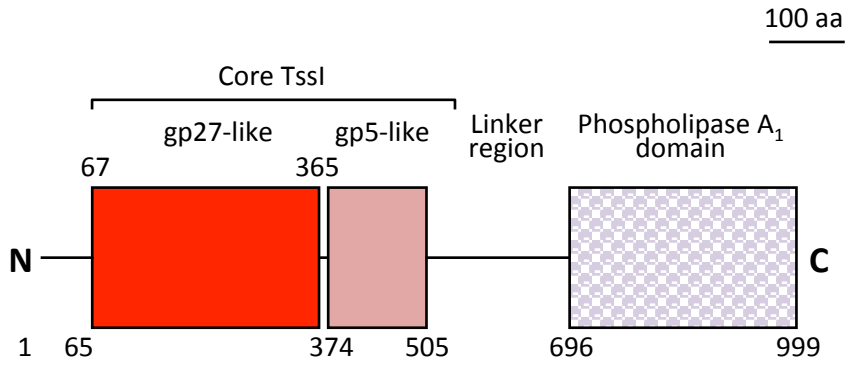

Figure 7.1 Domain organisation of putative T6SS-effector $TssI_{0667}$. Image shows predicted arrangement of protein domains within $TssI_{0667}$. The majority of the protein is comprised of a core TssI region that displays sequence homology to other TssI subunits and to the gp27gp5 tail-spike complex of bacteriophage T4. This is followed by a C-terminal extension with an experimentally verified phospholipase A_1 domain connected via a linker region. Amino acids indicating domain boundaries are shown. Scale as indicated.

GxSxG motif in the Tle2 family (Figure 3.8), therefore it was proposed to create an additional Tle family, Tle6, to encompass the phospholipase domain of $TssI_{0667}$, and other homologous phospholipases such as the protein encoded by BCAL1296, identified as a further putative T6SS-dependent effector located within a *tssI* cluster (Section 3.4.2).

Previous work on the BCAS0667-encoded product has focused on the enzymatic properties of the phospholipase domain (Jones, 2012). Its activity as a phospholipase A_1 was verified and the catalytic residues identified. Intriguingly, the enzyme displayed psychrophilic characteristics *in vitro*, with a temperature optimum for fatty acyl esterase activity at 10°C. However, verification of the protein as a T6SS-dependent effector and an analysis of its role in the lifestyle of *B. cenocepacia* were not carried out. Therefore, the study presented here specifically addresses the hypothesis that $TssI_{0667}$ is a T6SS-dependent secreted effector and investigates its possible role as an effector that can target other bacteria.

Studies carried out on the role of the T6SS in other organisms (Hood et al., 2010; MacIntyre et al., 2010) has suggested the T6SS mainly functions to target other bacteria. For this reason T6SS-effectors have evolved cognate immunity proteins or antitoxins to neutralise anti-bacterial effectors within the producing bacterium and its siblings or closely related strains. Therefore, it was also sought to identify the immunity protein for $TssI_{0667}$ and its Tle6 phospholipase A_1 extension domain and to investigate the complex formed between them. The most likely candidate for the $TssI_{0667}$ immunity protein was a Sec-dependent periplasmic protein encoded directly downstream of BCAS0667, by BCAS0666. Bioinformatic analysis of the protein encoded by BCAS0666 indicated the presence of four ankyrin repeat motifs (Section 3.3.6, Figure 3.9). This motif is thought to form helix-turn-helix structural units, where each repeat unit comes together to form a super helical bundle, shown to be important for facilitating protein-protein interactions. The homologous gene to BCAS0666 in *B. cenocepacia* H111 is represented at the I35_ 7842 loci. This loci is misannotated in the H111 genome, the gene is indicated as starting further downstream than its BCAS0666 orthologue. But inspection of the surrounding DNA sequence indicated a more likely start codon 96 bp upstream,

whether the A base of the ATG start codon is shared by the final A base of the TGA stop codon of I35_7843. Using this upstream start codon results in the generation of a coding sequence, and thus translated protein, that is near identical to that of BCAS0666 and its protein product. Further indication of the product of BCAS0666 (and I35_ 7842) being an immunity protein is its homology to a protein encoded by a gene located immediately downstream of BCAL1296, the product of which is a predicted phospholipase A_1 of the newly created Tle6 family. It was proposed to call this putative immunity protein Tli6, to coincide with the naming of the CTD phospholipase A_1 region of $TssI_{0667}$ as a Tle6 extension domain.

For simplicity, from hereon the gene corresponding to the coding sequence of both BCAS0667 and I35_7843 loci from J2315 and H111, respectively, will be preferred to as BCAS0667, and DNA encoding just the CTD will be preferred to as BCAS0667.CTD. The encoded protein will be referred to as $TssI_{0667}$ and the phospholipase C-terminal extension of $TssI_{0667}$ will be preferred to as a Tle6 extension. A numerical subscript will also be used where appropriate to indicate which amino acids are encoded relative to C-terminal of the protein, i.e. $Tle6_{258}$ is the last C-terminal 258 amino acids of $TssI_{0667}$ corresponding to the phospholipase A_1 Tle6 domain. Accordingly, the gene corresponding to the BCAS0666 and I35_7842 loci will be preferred to as BCAS0666, and protein product as Tli6.

7.2 Analysis of T6SS-dependent secretion of the putative evolved TssI, $TssI_{0667}$, in *B. cenocepacia* H111

7.2.1 Analysis of $TssI_{0667}$ secretion by western blotting

This study found that the H111 strain of *B. cenocepacia* has a basally active T6SS during growth under standard laboratory culture conditions, as demonstrated by the secretion of TssD into the culture supernatant of liquid grown cultures, (Section 4.5). Hence, liquid grown cultures of H111 and a T6SS-deficient mutant were subjected to secreted protein extraction (Section 2.4.1) and assayed for the presence of $TssI_{0667}$ by western blotting, using a custom polyclonal rat antibody raised against the C-terminal domain of $TssI_{0667}$ (R.A. Jones and M.S. Thomas, unpublished results). As controls the secreted T6SS subunit, TssD, and the cytoplasmic β-subunit of the enzyme RNAP were also analysed. $TssI_{0667}$ was detected as a 120 kDa protein present in the secreted samples of H111 wild-type, but not in the secreted proteins from all of the T6SS-deficient mutants tested, including H111-*tssA*::Tp, H111-*tssK*::Tp, H111-*tssM*::Tp and H111-Δ*tssM* mutants, the latter is shown in Figure 7.2. This result strongly suggests that $TssI_{0667}$ is a T6SS-dependent secreted protein. Cell-associated $TssI_{0667}$ was detected in all strains tested, indicating that $TssI_{0667}$ was being produced in the cytoplasm of the T6SS-deficient mutants but not secreted. Accumulation of a possible intracellular $TssI_{0667}$ degradation product was also detected in all cell associated samples, migrating at approximately 26 kDa, which was more abundant in the T6SS-deficient mutants that the wild-type strain (data not shown).

To determine whether secretion of $TssI_{0667}$ could be restored in a T6SS-deficient mutant. Using the *tssA*::Tp mutant as an example, a broad-host range plasmid encoding *tssA* was introduced into the corresponding mutant and secreted proteins extracted and analysed by western blotting. Proteins were probed with anti-$TssI_{0667}$.CTD antibody, and an anti-TssD control antibody. Figure 7.3 shows the restoration of $TssI_{0667}$ secreted by complementation of the H111-*tssA*::Tp mutant with pBBR1-*tssA*. The secretion of TssD was also restored by complementation of this mutant. Cell associated $TssI_{0667}$ was difficult to detect in wild-type and the complemented *tssA*::Tp mutant on this occasion, which may have been due to a

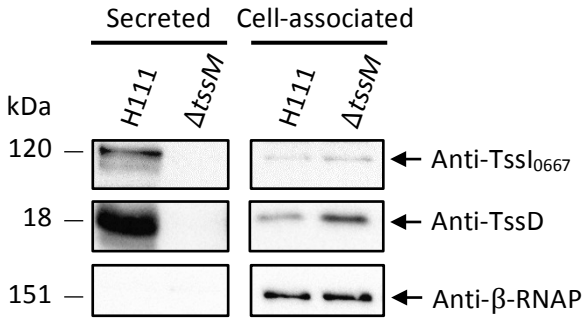

Figure 7.2 Analysis of T6SS-dependent secretion of putative effector TssI$_{0667}$ by *B. cenocepacia* H111. Spent liquid culture supernatants of H111 WT and H111-Δ*tssM* were subjected to DOC-TCA precipitation. The resulting secreted protein samples and cell associated proteins were separated by SDS-PAGE and transferred onto PVDF membrane. Blots were probed with custom polyclonal antibody raised against the CTD region of TssI$_{0667}$ (top panel), custom polyclonal anti-TssD antibody (middle panel) and commercially available anti-β-RNAP antibody as a lysis control (bottom panel). Samples were loaded as indicated above the lanes. Molecular masses of the detected proteins are indicated on the left, as judged by a protein ladder. Arrows with appropriate labels on the right indicate which proteins are being probed for in each blot.

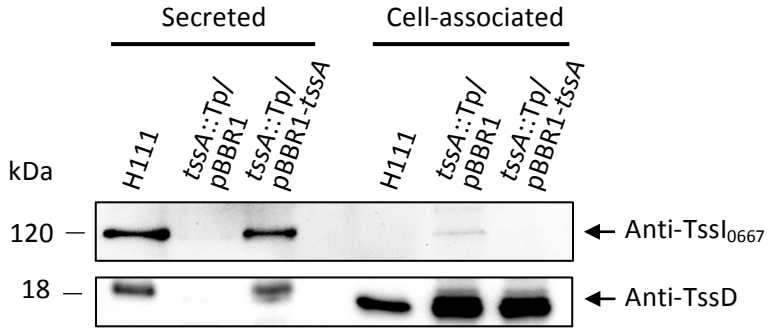

Figure 7.3 Restoration of TssI$_{0667}$ secretion in a T6SS mutant by genetic complementation. Spent culture supernatants of H111 WT and *tssA*::Tp mutant containing pBBR1MCS-1 or pBBR1-*tssA* were subjected to DOC-TCA precipitation. Resulting sample were separated by SDS-PAGE and transferred onto PVDF membrane. Blots were probed with anti-TssI$_{0667}$.CTD antibody (top panel) and anti-TssD antibody (middle panel). Samples were loaded as indicated above the lanes. Molecular masses of the detected proteins are indicated on left, as judged by a protein ladder. Arrows with appropriate labels indicate which protein is being probed for in each blot.

low concentration of cell associated protein being loaded onto the SDS-PA gel.

7.3 Investigation of the role of $TssI_{0667}$ *in vivo*

To allow further verification of the secretion of $TssI_{0667}$ and investigation into its role in *B. cenocepacia* H111 it was decided to generate in-frame deletion H111 mutants containing an in-frame deletion of BCAS0667, either alone or together with a deletion of BCAS0666, encoding its putative immunity protein. Upon deletion of this putative effector-immunity pair, the mutants could then be assessed for phenotypic differences, in particular the ability of the mutants to compete against other bacterial strains.

7.3.1 Construction of allelic replacement vectors for deletion of BCAS0667 and BCAS0667-0666 in *B. cenocepacia* H111

SOE-PCR was used to generate in-frame deletion alleles of both BCAS0667 and BCAS0667-BCAS0666, whereby fragments either side of each region were amplified and splice together to omit the intervening regions, as explained in Section 5.4.1, Figure 5.20. To generate the ΔBCAS0667 allele, DNA fragments either side of BCAS0667 were amplified by PCR from H111 genomic DNA using primers 0667ΔforA and 0667ΔIPrevB to generate a ΔBCAS0667-AB fragment of 672 bp and primers 0667ΔIPforC and 0667ΔrevD to generate a ΔBCAS0667-CD fragment of 635 bp. Each fragment contained overlapping regions complementary to the other fragment to allow splicing of the fragments together by a second PCR step. To do this, ΔBCAS0677-AB and ΔBCAS0667-CD fragments were combined in an equal molar ratio to act as template DNA for a subsequent PCR amplification using primers 0667ΔforA and 0667ΔrevD. This generated a spliced fragment of 1265 bp termed ΔBCAS0667, in which the first 18 codons of the BCAS0667 coding sequence are fused to the last 19 codons of the same sequence, deleting 963 codons in the intervening region. Primers used in this amplification step contained 5' restriction sites, BamHI and HindIII, allowing directional cloning of the ΔBCAS0667 DNA fragment into the *Burkholderia* allelic replacement vector pEX18TpTer-*pheS* at the corresponding restriction sites in the MCS of the vector, generating pEX18TpTer-*pheS*-ΔBCAS0667 of 5440 bp. Clones were selected for trimethoprim-resistance along with blue/white colour screening. Transformant colonies that were white

were screened by PCR using vector specific primers M13for and M13revBACTH to identity positive clones. Plasmids were then isolated from transformants that were positive in the PCR screen and subjected to size analysis by agarose gel electrophoresis (Figure 7.4). Correct sized clones (8, 9 and 10) were confirmed by DNA sequencing.

The ΔBCAS0667-BCAS0666 allele was generated as described above using primer pairs 0667ΔforA and 0667-0666ΔIPRevB and 0667-0666ΔIPforC and 0667-0666ΔrevD, to generate a fragment of 672 bp for ΔBCAS0667-BCAS0666 AB, and a fragment of 665 bp for ΔBCAS0667-BCAS0666 CD. Primers 0667ΔforA and 0666revD were used in the second PCR step, generating the spliced fragment of 1295 bp, ΔBCAS0667-BCAS0666, in which the first 18 codons of the coding sequence of BCAS0667 were fused to last 39 codons of the coding sequence of BCAS0666, deleting 1231 codons in the intervening region, generating a BCAS0667-BCAS0666 in-frame fusion. This was subsequently cloned as a BamHI-HindIII restriction fragment into pEX18TpTer-*pheS* as above, to successfully generate pEX18TpTer-*pheS*-ΔBCAS0667-BCAS0666, of 5470 bp.

7.3.2 Generation of BCAS0667 deletion mutants in *B. cenocepacia* H111

To create an in-frame markerless deletion of BCAS0667 in *B. cenocepacia* H111, the allelic replacement vector pEX18TpTer-*pheS*-ΔBCAS0667 was introduced into the strain H111 by conjugation. This allowed recombination events to occur between the ΔBCAS0667 allele on the vector and the complementary region in H111 genomic DNA. Single crossover recombinants (co-integrates) were selected by virtue of their trimethoprim-resistance on M9-glucose agar containing trimethoprim. Verified co-integrated were then re-streaked onto M9-glucose agar containing 0.1% cPhe to select for a second recombinant event that resulted in excision of the plasmid, leaving behind either the wild-type copy of BCAS0667 or the ΔBCAS0667 allele. Several candidates were PCR screened using primers that annealed upstream of the regions flanking the deleted allele introduced by the pEX18TpTer-*pheS*-ΔBCAS0667 plasmid, termed 0667for-OP and 0667rev-OP. Candidates that amplified a fragment smaller than the wild-type fragment, i.e. 1360

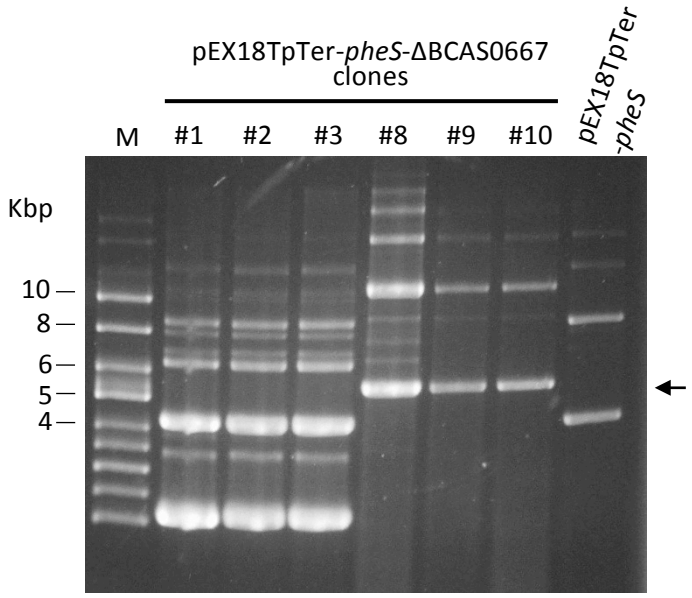

Figure 7.4 Identification of candidate pEX18TpTer-*pheS*-ΔBCAS0667 plasmid by size analysis. Plasmid clones were extracted and visualised following electrophoresis in a 0.8% DNA agarose gel. Desired clones migrated in accordance with their predicted size of 5440 bp (indicated by arrow). M, supercoiled DNA ladder.

bp compared to 4373 bp, were considered as H111-ΔBCAS0667 mutants (Figure 7.5).

Note however, a non-specific band was also generated in the wild-type strain that corresponded to the expected size of the DNA fragment amplified from the ΔBCAS0667 mutants, which was in a greater yield that the wild-type fragment size. This could have given rise to false positive mutants being identified in this initial screen. Candidates 2, 3, 5, 7, 8, 13, 16 and 22 were colony purification by two rounds of re-streaking on the same medium and then final re-streak onto M9-glucose agar. After this, the candidates were re-screened by PCR, again using 0667for-OP and 0667rev-OP outside primers, and also using the 0667ΔForA and 0667ΔRevD inside primers (Figure 7.6A). Excision of the pEX18TpTer-*pheS* plasmid was verified by trimethoprim-sensitivity and by PCR screening using vector specific primers pEX18Tpfor and pEX18Tprev. All candidates were trimethoprim-sensitive and did not amplify the 397 bp vector fragment (Figure 7.6B). Only candidates 2, 3, 5, 8 and 22 gave rise to a DNA fragment corresponding in size to that expected for the presence of the ΔBCAS0667 allele when amplified with the outside primers. Candidate 2 was selected for phenotype studies.

An analogous approach to that described above was undertaken for generation of a H111 mutant that contain a deleted in-frame fusion of BCAS0667 with BCAS0006 (Section 7.3.1). However, problems were encountered with cPhe counter-selection, it appeared to be inefficient. Over 100 cPhe-resistant colonies isolated after the first round of cPhe counter-selection were screened for trimethoprim sensitivity to help identify strains that had excised the pEX18TpTer-*pheS* plasmid. Over 90% of the patched colonies were still trimethoprim-resistant, indicating they still contained the allelic replacement vector integrated into the genome. Several trimethoprim sensitive colonies were eventually found, but after subsequent PCR screening with the outside annealing primers 0667for-OP and 0666rev-OP all candidates were identified as wild-type. This process was repeated, yet no mutants were identified.

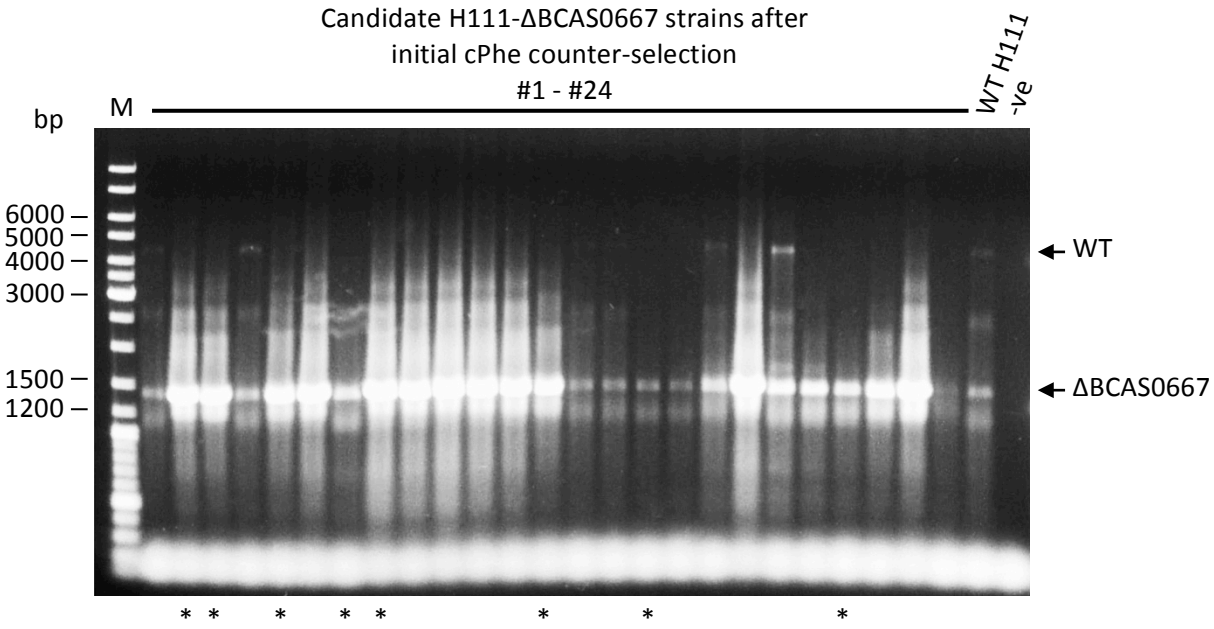

Figure 7.5 Initial PCR screen to identify candidate H111-ΔBCAS0667 mutants. Co-integrates of H111 containing pEX18TpTer-*pheS*-ΔBCAS0667 integrated at the genomic BCAS0667 loci were subjected to counter-selection on M9 agar containing 0.1% cPhe. Selected cPhe-resistant colonies were PCR screened using primers annealing outside of the deleted region to identify recombinants where plasmid excision had resulted in replacement of the wild-type BCAS0667 gene by the ΔBCAS0667 allele. Resulting fragments were visualised following electrophoresis in a 0.8% DNA agarose gel. Mutants were expected to give rise to a fragment smaller than that derived from the wild-type (WT), 1360 bp compared to 4373 bp. *; indicates candidate mutants subjected to further colony purification on the same medium and re-screened. M, GeneRuler DNA ladder mix; arrows indicate expected fragment size amplified from WT (upper arrow) and candidate mutants (lower arrow).

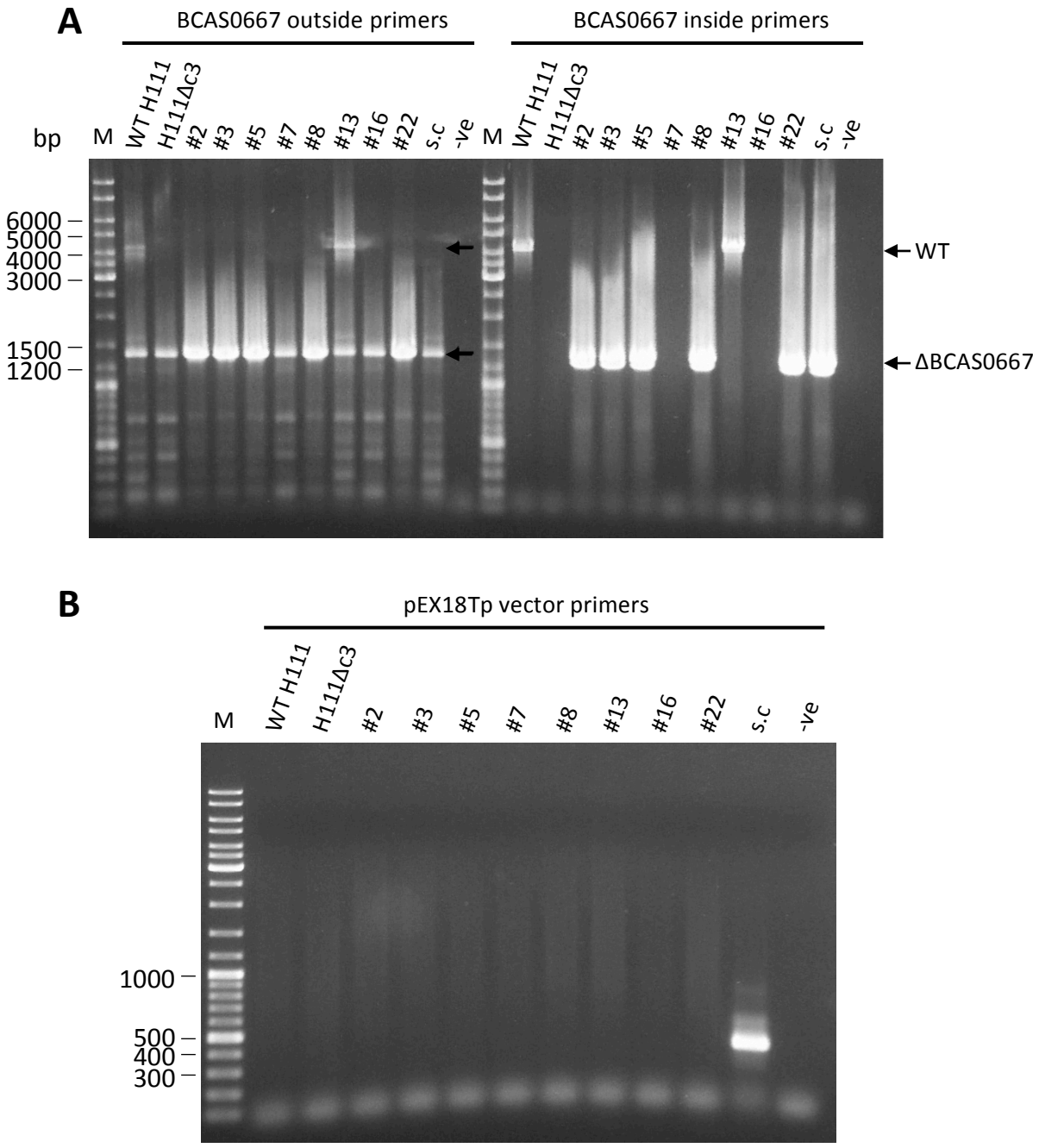

Figure 7.6 Verification of H111-ΔBCAS0667 mutants by PCR screening. Candidate H111-ΔBCAS0667 mutants were PCR screened using pairs of primers that anneal to sequences outside the homologous region of the ΔBCAS0667 allele introduced on pEX18TpTer-*pheS*-ΔBCAS0667, inside primers that anneal to the inserted deletion allele and vector specific primers. (A) DNA agarose gel of fragments amplified using outside and inside primers as indicated, following DNA electrophoresis in a 0.8% agarose gel. The upper arrow indicates expected fragment size amplified from WT and the lower arrow indicates that of a ΔBCAS0667 mutant. (B) Analysis of fragments amplified using vector specific primers. H111 WT, H111Δc3 and a H111 pEX18TpTer-*pheS*-ΔBCAS0667 co-integrate (s.c) were included as controls. M, GeneRuler DNA ladder mix; -ve, no DNA control.

An additional problem was that amplification using the outside primers with wild-type genomic DNA, resulted in non-specific amplification of a fragment of a similar size to that of the expected size for a ΔBCAS0667-0666 mutant (along with the wild-type fragment). Therefore it was sometimes difficult to distinguish between potential mutants and colonies that had reverted back to wild-type. To overcome this problem, primers BCAS0667PLAForNcoI and BCAS0667PLARevXbaI, which annealed to DNA located within the BCAS0667 coding sequence, were used to screen potential mutants. Candidate ΔBCA0667-0666 mutants were revisited and screened using the BCAS0667PLA primers. However, all candidates gave rise to a segment of DNA within the region targeted for deletion, indicating the recombinants were not ΔBCAS0667-0666 mutants (data not shown).

7.3.3 Effect of the deletion of BCAS0667 on the activity of the T6SS in *B. cenocepacia* H111

Ten *tssI* clusters are found within the genome of *B. cenocepacia*, but it is unknown which, if any, of these encoded TssI subunits are strictly required for a functional T6SS in this bacterium. To determine whether deletion of BCAS0667 affected T6SS activity, TssD secretion into the supernatants of cultures of wild-type H111, H111-ΔBCAS0667 and a H111 T6SS-deficient mutant, H111-Δ*tssM*, were analysed by western blotting using a custom polyclonal anti-TssD antibody (Figure 7.7). The level of cell associated TssD in each strain was also determined. The results indicated the presence of similar levels of secreted TssD in the wild-type and ΔBCAS0667 strains, but absence of secreted TssD in the Δ*tssM* mutant. Cell-associated TssD was detected in all strains. These observations indicate that the H111-ΔBCAS0667 mutant possessed a functional T6SS system, and therefore BCAS0667 did not encode a core T6SS subunit.

Secreted samples were also probed with the anti-$TssI_{0667}$.CTD antibody to ensure that deletion of BCAS0667 prevented secretion of the anti-$TssI_{0667}$.CTD reactive protein previously observed in the $TssI_{0667}$ secretion assay shown in Section 7.2.1. $TssI_{0667}$ was detected in the wild-type secreted fraction, but not in the H111-ΔBCAS0667 or Δ*tssM* mutants. Cell associated $TssI_{0667}$ was detected in both wild-

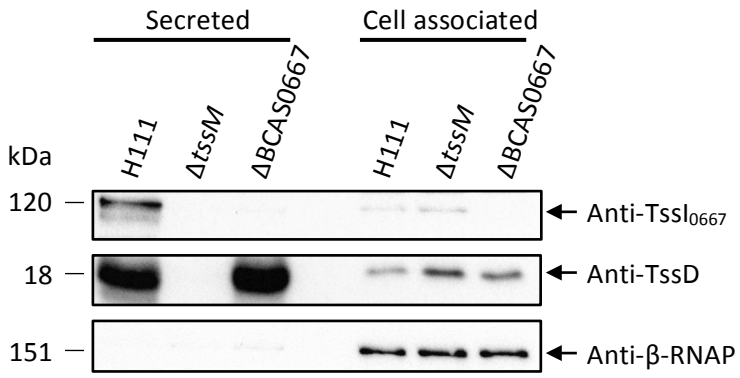

Figure 7.7 Analysis of the effect of deletion of BCAS0667 on T6SS activity in *B. cenocepacia* H111. Secreted proteins were precipitated from liquid grown cultures of wild-type H111, H111-Δ*tssM* and H111-ΔBCAS0667 mutants, concentrated 1000-fold, separated by SDS-PAGE and analysed by western blotting. Image shows resulting western blots probed with anti-$TssI_{0667}$.CTD antibody (upper panel), anti-TssD antibody (middle panel) and anti-β-RNAP antibody (lower panel), as indicated. Molecular masses of probed proteins indicated on the left, as judged by a protein marker.

type and Δ*tssM* strains but absent in the ΔBCAS0667 mutant. These results confirm both the successful deletion of BCAS0667 in the H111-ΔBCAS0667 mutant, and that the custom anti-$TssI_{0667}$.CTD antibody was indeed detecting $TssI_{0667}$, and not an unrelated cross-reacting protein.

An anti-β-RNAP subunit antibody was used as a lysis control to indicate the level of lysis occurring in the cultures during growth. Figure 7.7 shows that this subunit was not detected in the extracellular protein fractions, suggesting undetectable lysis had occurred during growth of the assayed samples.

7.3.4 Effect of the deletion of BCAS0667 on inter-bacterial competition in *B. cenocepacia* H111

Results presented in chapter 4 suggested that the T6SS in *B. cenocepacia* provides this species with a fitness advantage over other bacterial strains in a co-culture, including *P. putida* and *E. coli*, a phenomenon observed in other T6SS-containing bacteria. Therefore it was decided to determine whether the T6SS-dependent secreted effector $TssI_{0667}$ contributed to this fitness. To do this, the H111-ΔBCAS0667 mutant was used as the 'attacker' strain against the 'prey' strain *P. putida* in the bacterial competition assay described in Section 2.9.1. The number of recovered *P. putida* were enumerated and compared to the number of *P. putida* recovered when wild-type H111 and a T6SS-deficient mutant (Δ*tssM*) were used as the 'attacker' strains. Figure 7.8A shows the resulting number of recovered *P. putida* from each co-culture condition, demonstrating that in co-culture with the H111-ΔBCAS0667 mutant, an average fifteen-fold increase in the number of recovered *P. putida* was obtained in comparison to the number recovered when co-cultured with wild-type H111. The average difference between *P. putida* recovered when co-cultured with the Δ*tssM* mutant in comparison to wild-type was greater, by a factor of 58. Levels of recovered *B. cenocepacia* attacker strains were also monitored, and as shown in Figure 7.8B, no significant difference been strains was observed. Together this data suggests that $TssI_{0667}$ makes a partial contribution to the competitive advantage the T6SS confers on *B. cenocepacia* against *P. putida,* suggesting that this effector plays an anti-bacterial role in *B. cenocepacia*.

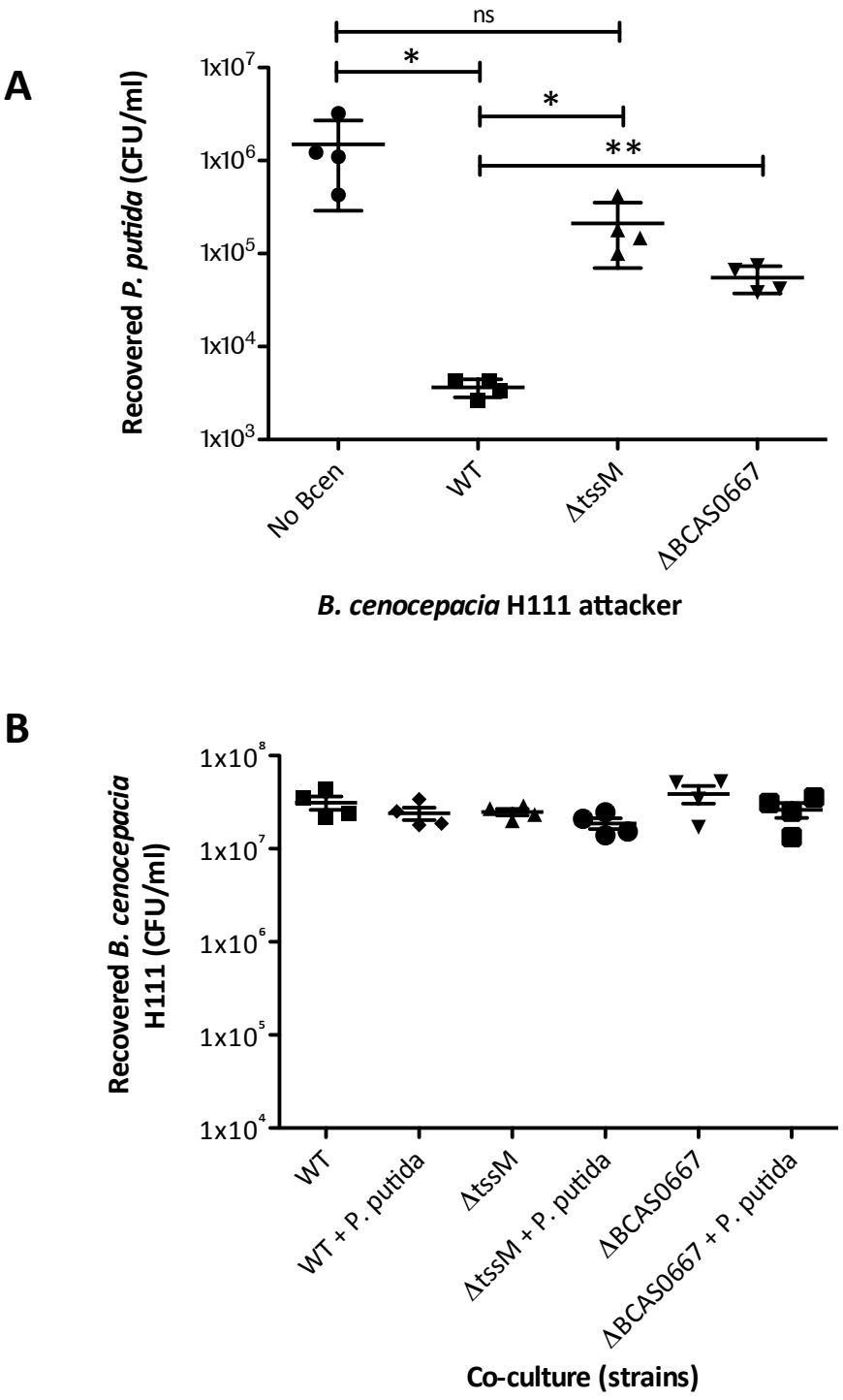

Figure 7.8 Analysis of the contribution of $TssI_{0667}$ to the T6SS-dependent competitive advantage of *B. cenocepacia* H111 against *P. putida*. Wild-type *B. cenocepacia* H111, and corresponding ΔBCAS0667 and Δ*tssM* mutants were co-cultured in a 5:1 ratio against *P. putida* KT2440 and incubated on nitrocellulose membranes on LB agar for 4 hours at 30°C. Surviving bacteria were recovered and enumerated on selection plates. (A) The number of recovered *P. putida* resulting from each co-culture with different *B. cenocepacia* H111 attacker strains, and *P. putida* cultured on its own. (B) The number of recovered *B. cenocepacia* H111 strains resulting from each co-culture, and additional controls where strains were cultured on their own. Statistical analysis by student's t-test where $p<0.05$, n= 4, **; p=0.0012, *; $p<0.05$, ns; not significant, error bars = ±SD.

7.3.5 Construction of a BCAS0667 complementation plasmid

To confirm that the effect of ablation of BCAS0667 on inter-bacterial competition was not due to polar effects of the lesion or an unrelated genetic alteration, a complementation plasmid was constructed. To do this, the coding sequence of BCAS0667 along with a 35 bp sequence directly upstream, encompassing the putative Shine-Dalgarno sequence, was amplified from H111 genomic DNA using the primers BCAS0667ForATG1Acc65I and BCAS0667RevXbaI to generate a DNA fragment of 3088 bp (Figure 7.9A). This fragment was gel purified, and together with the vector pBBR1MCS-2 (named pBBR2 from hereon), were subjected to restriction digest with Acc65I and XbaI (Figure 7.9B). Following this, the two fragments were ligated together, introduced into *E. coli* JM83, and transformants selected for kanamycin-resistance. Positive clones were identified by colony PCR screening using vector primers M13for and M13rev (Figure 7.9C). Clones 1, 2, 4, 7, 11, and 12 gave rise to the correct sized insert of 3224 bp in this screen. Clones 1 and 2 were selected for plasmid isolation and size analysis following electrophoresis (Figure 7.9D). The expected plasmid size for pBBR2-BCAS0667 was 8138 bp, therefore both clones gave rise to plasmids of the desired size. Clone 1 was confirmed by DNA sequencing.

Unfortunately, due to time constraints the effectiveness of pBBR2-BCAS0667 to complement the H111-ΔBCAS0667 mutant was unable to be tested fully. An initial conjugation experiment undertaken to transfer pBBR2-BCAS0667 into wild-type H111 and the ΔBCAS0667 mutant showed that this plasmid exerted a negative effect on the colony growth and morphology. Thus, H111/pBBR2-BCAS0667 colonies were of non-uniform size, some with slightly translucent crateriform morphology when compared to H111/pBBR2. H111-ΔBCAS0667/pBBR2-BCAS0667 colonies had a small, irregular and translucent morphology compared to H111-ΔBCAS0667/pBBR2. Restoration of $TssI_{0667}$ secretion by pBBR2-BCAS0667 was unable to be tested due to time constraints, but the unhealthy appearance of strains containing this plasmid suggest that although it is likely that the plasmid copy of BCAS0667 is being expressed the construct may be too toxic to be useful.

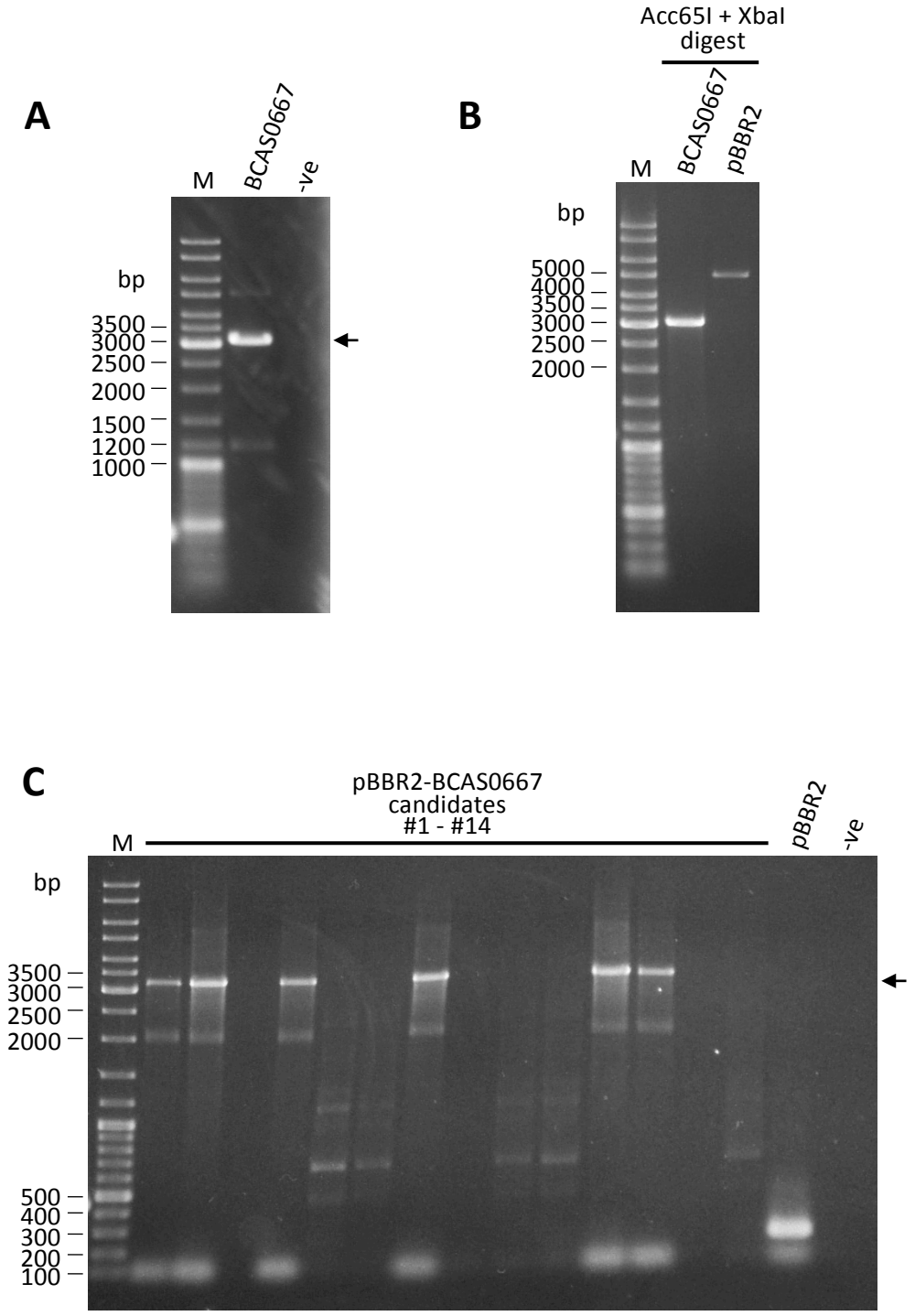
A
M
BCAS0667
-ve
bp
3500
3000
2500
2000
1500
1200
1000
B
Acc65I + XbaI
digest
BCAS0667
pBBR2
M
bp
5000
4000
3500
3000
2500
2000
C
pBBR2-BCAS0667
candidates
#1 - #14
M
pBBR2
-ve
bp
3500
3000
2500
2000
500
400
300
200
100

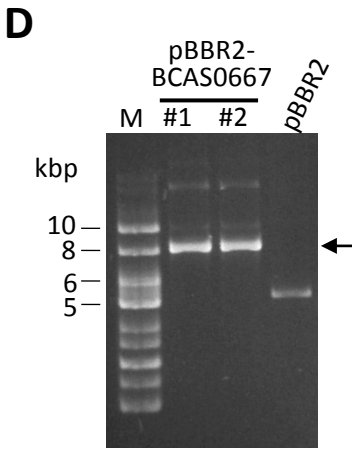

Figure 7.9 Construction of the BCAS0667 complementation vector, pBBR2-BCAS0667. BCAS0667, including its predicted Shine-Dalgarno region, was amplified from H111 genomic DNA and cloned into pBBR1MCS-2 (pBBR2) as an XbaI-Acc65I restriction fragment. (A) Analysis of resulting PCR-amplified BCAS0667 DNA fragment following electrophoresis in 0.8% DNA agarose gel. Arrow indicates expected fragment size of 3088 bp for BCAS0667. (B) BCAS0667 and pBBR2 DNA fragments resulting from XbaI and Acc65I restriction digestion, as indicated. (C) Analysis of PCR colony screen of transformants containing potential pBBR2-BCAS0667 plasmids using vector specific primers, positive clones were expected to amplify a fragment of 3224 bp, as indicated by arrow, and the empty pBBR2 vector was expected to amplify a fragment of 230 bp. (D) Size analysis of candidate pBBR2-BCAS0667 plasmids, arrow indicates expected plasmid size of 8138 bp for pBBR2-BCAS0667. M, GeneRuler DNA ladder mix or supercoiled DNA ladder.

7.4 Characterisation of the anti-bacterial properties of $TssI_{0667}$

Results presented in Section 7.3.4 show that $TssI_{0667}$ was able to contribute to the competitive advantage the T6SS confers upon *B. cenocepacia* when co-cultured with competing bacterial strains, suggesting that $TssI_{0667}$ is an anti-bacterial effector. Therefore it was decided to further investigate the anti-bacterial properties of $TssI_{0667}$ to determine which subcellular location it targeted.

As discussed previously, $TssI_{0667}$ contains a C-terminal extension that was demonstrated in a previous study to have phospholipase A_1 activity, and could be defined as a founding member of a new subfamily of the Tle T6SS-dependent phospholipase effector superfamily, Tle6. Therefore, it was postulated that the anti-bacterial properties associated with this protein might be occurring via the phospholipase activity of the C-terminal extension region, specifically through degradation of the phospholipids in cellular membranes. This should be demonstrable by ectopic expression of DNA encoding the Tle6 domain of $TssI_{0667}$.

7.4.1 Construction of plasmids for periplasmic targeting of the $TssI_{0667}$ Tle6 domain in *E. coli*

To determine whether periplasmic expression of the Tle6 phospholipase domain of $TssI_{0667}$ had an adverse effect on bacterial cell viability, the coding region was cloned in-frame into a pET expression vector that fused a periplasmic localisation signal, the PelB signal sequence, to the N-terminus of the protein in question (Figure 7.10). A previous investigation found that the shortest C-terminal region of $TssI_{0667}$ that retained catalytic activity and was produced as a soluble protein contained amino acids D735 through to the C-terminal H999, inclusive (Jones, 2012). The protein will be termed from hereon $Tle6_{258}$, as it contains the C-terminal 258 amino acids of $TssI_{0667}$ and the corresponding DNA coding region will be referred to as BCAS0667.CTD_{258}.

DNA encoding a slightly longer derivative containing the C-terminal 265 amino acids of $TssI_{0667}$, termed BCAS0667.CTD_{265}, and the BCAS0667.CTD_{258} coding regions were amplified by PCR from H111 genomic DNA, using primer pairs

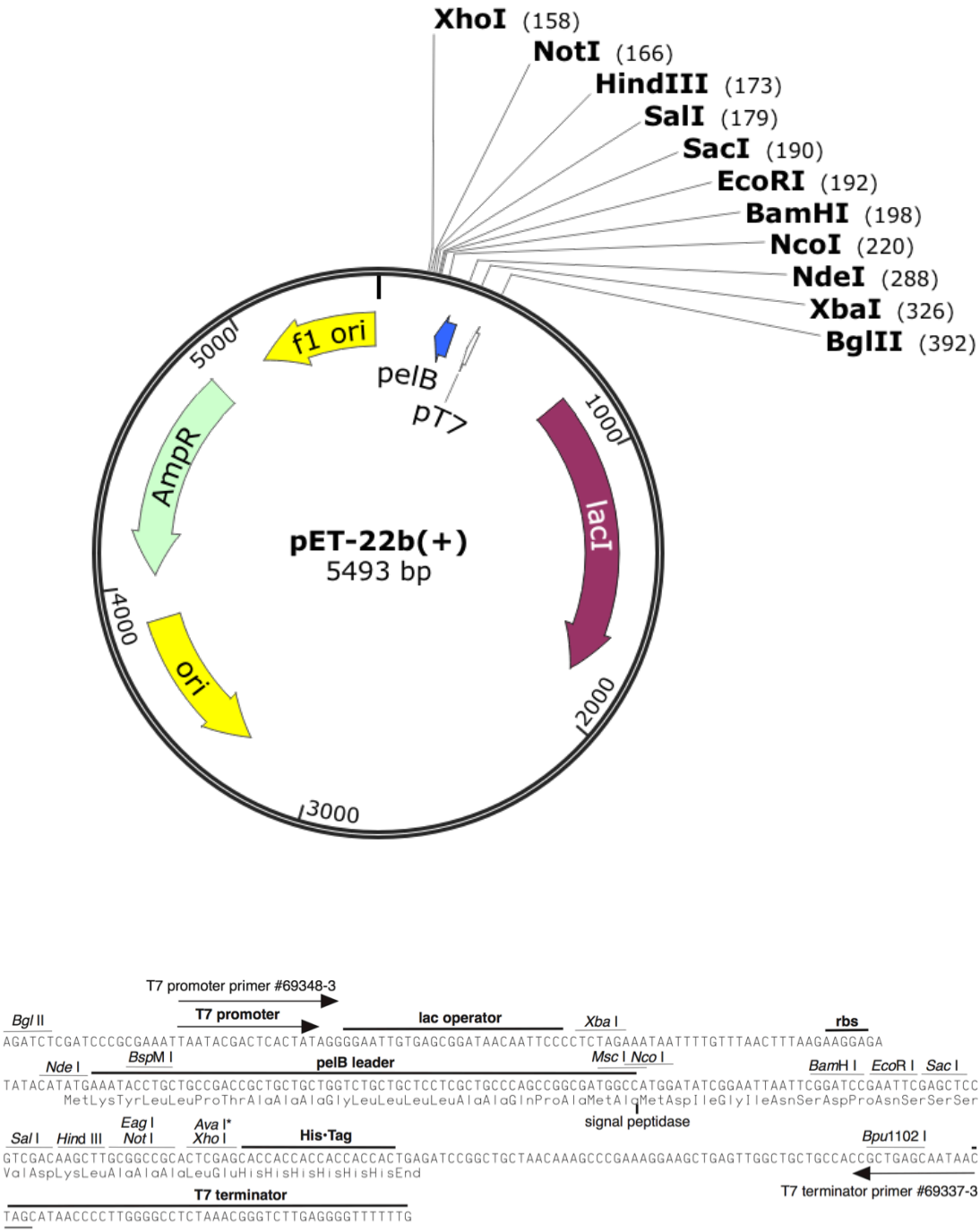

Figure 7.10 Diagrammatic representation of the periplasmic-expression construct pET-22b(+). Image showing a plasmid map of the T7lac periplasmic expression vector pET-22b(+), illustrating the restriction sites in the MCS and the location of the T7 promoter and pelB coding sequence (top). The expression region of the plasmid (bottom) indicates the presence of the coding sequencing for the PelB signal sequence. This sequence allows Sec-dependent targeting of the overproduced protein into the periplasm of host cells if the coding sequence of the protein is inserted in-frame at restriction sites downstream of it. Bottom image is adapted from Novagen data sheet TB038 12/98.

BCAS0667PLAForNcoI and BCAS0667PLARevXhoI, and BCAS0667PLAFor2NcoI and BCAS0667PLARevXhoI, generating DNA fragments of 848 bp and 824 bp, respectively (the latter shown in Figure 7.11A). DNA fragments BCAS0667.CTD$_{265}$ and BCAS0667.CTD$_{258}$ were digested with NcoI and XhoI and ligated between the corresponding restriction sites in the expression vector pET-22b(+), introduced into *E. coli* MC1061 and transformants selected for ampicillin-resistance. This generated 6266 bp and 6245 bp plasmids termed pHLS12 and pHLS13, respectively. Positive clones were identified by colony PCR using vector primers pETDuet-T71for and T7 Rev. Clones that gave rise to the expected DNA fragment size were subjected to plasmid isolation and size analysis following electrophoresis (pHLS13 clones shown in Figure 7.11B), and then confirmed by DNA sequencing.

A pET-22b(+) derivative specifying a catalytically inactive version of the Tle6$_{258}$ domain of TssI$_{0667}$ was also generated to act a negative control in toxicity experiments. A previous study identified three residues in the Tle6 region essential for catalysis, including S879 (numbered from the N-terminus of TssI$_{0667}$) (Jones, 2012). A previously generated plasmid encoding a S879A substitution mutant of Tle6$_{258}$ was used as template DNA in a PCR reaction using the primer pair specified from the coding region of BCAS0667.CTD$_{258}$ described above, to generate the DNA fragment BCAS0667.CTD$_{258}$ S879A (Figure 7.11A). This fragment was then cloned into pET-22b(+) as above, to generate the plasmid pHLS14 (Figure 7.11B). The plasmid was confirmed by DNA sequencing. It is important to note here that the resulting DNA fragments derived from the *B. cenocepacia* Pc715j-based BCAS0667.CTD$_{258}$ S879A was identical to that of H111-derived wild-type BCAS0667.CTD$_{258}$, apart from the relevant the S879A mutation, indicating that the enzymatic Tle6 regions of the TssI$_{0667}$ orthologues in H111 and Pc715j are identical.

7.4.2 Effect of periplasmic production of the TssI$_{0667}$ Tle6 domain on *E. coli*

To understand whether presence of the Tle6 domain of TssI$_{0667}$ in the periplasm of bacteria compromised the viability of the cells, derivatives of this domain were targeted to the periplasm of *E. coli* cells. To do this, expression

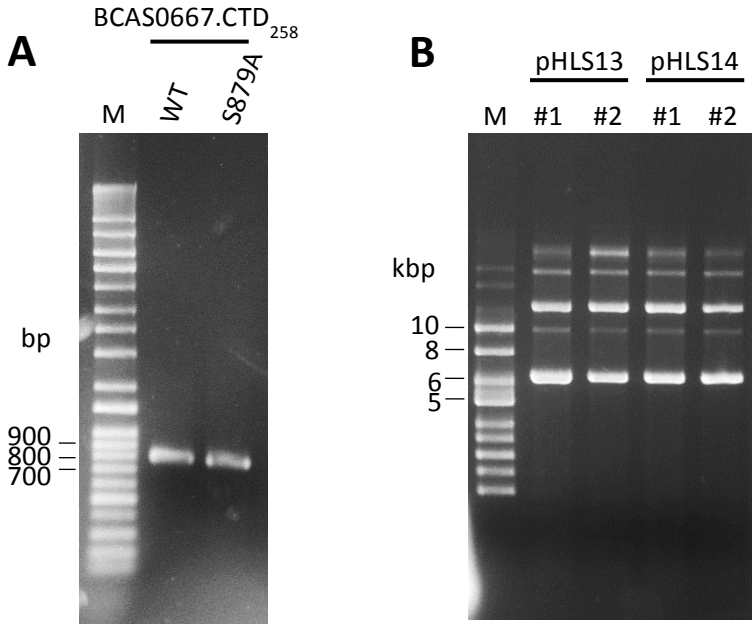

Figure 7.11 Construction of pET-22b(+) plasmids specifying overproduction of periplasmically located $TssI_{0667}$ Tle6 domain derivatives. DNA fragments encoding the C-terminal 258 amino acid of $TssI_{0667}$ were amplified from H111 genomic DNA and a plasmid containing a S789 mutant copy of BCAS0667.CTD_{258} and ligated between the NcoI and XhoI restriction sites of pET-22b(+). (A) PCR-amplified DNA fragments of wild-type BCAS0667.CTD_{258} and a S879A mutant derivative following electrophoresis in a 1.0% DNA agarose gel. (B) Size analysis of candidate pHLS13 and pHLS14 plasmids. M, GeneRuler DNA ladder mix or supercoiled DNA ladder.

vectors pHLS12, pHLS13, and pHLS14 were introduced into *E. coli* expression host cells BL21(DE3)/pLysS. Liquid cultures were grown to mid-log phase and recombinant proteins induced by addition of IPTG. The optical densities (at 600nm) of the cultures were monitored at specific time-points pre- and post-induction to infer the level of lysis occurring in the cultures (Section 2.9.2). Figure 7.12 shows the resulting optical densities recorded after induction of periplasmically targeted $Tle6_{265}$, $Tle6_{258}$ and the $Tle6_{258}$ S879 mutant-derivative of $TssI_{0667}$, from three independent experiments. After induction of $Tle6_{265}$, and the wild-type version of $Tle6_{258}$ there was a significant reduction in the culture optical density in comparison to non-induced cultures and cultures producing catalytically inactive $Tle6_{258}$ S879A, suggesting that lysis was occurring in cells accumulating active periplasmically located Tle6 domains.

To verify production of the proteins from the induced expression plasmids in the cultures described above, crude whole cell extracts of uninduced and induced cultures were subjected to SDS-PAGE and western blot analysis. The resulting Coomassie blue stained gel revealed that no obvious protein corresponding to the Tle6 domains was present in the induced cultures (Figure 7.13A). However, the presence of the correct sized product in the appropriate induced samples was apparent on an anti-$TssI_{0667}$.CTD western blot (Figure 7.13B). The expected molecular mass of each protein was approximately 27 kDa without the signal sequence and 29 kDa with the signal sequence. Proteins were detected at these two expected sizes in the induced cultures, as well as a slightly smaller protein at approximately 26 kDa, which is likely to be a degradation product of Tle6. Interestingly, it appeared that there was greater accumulation of the S879A mutant protein compared to either wild-type Tle6 constructs, strengthening the notion that periplasmically targeted Tle6 is detrimental to the *E. coli* host.

Furthermore, samples of spent culture supernatant were taken at regular intervals from uninduced and induced cultures containing the periplasmic expression plasmids described above and subjected to DOC-TCA precipitation. Analysis of the protein samples by SDS-PAGE highlighted that a greater concentration and range of proteins were present in the supernatants of cultures

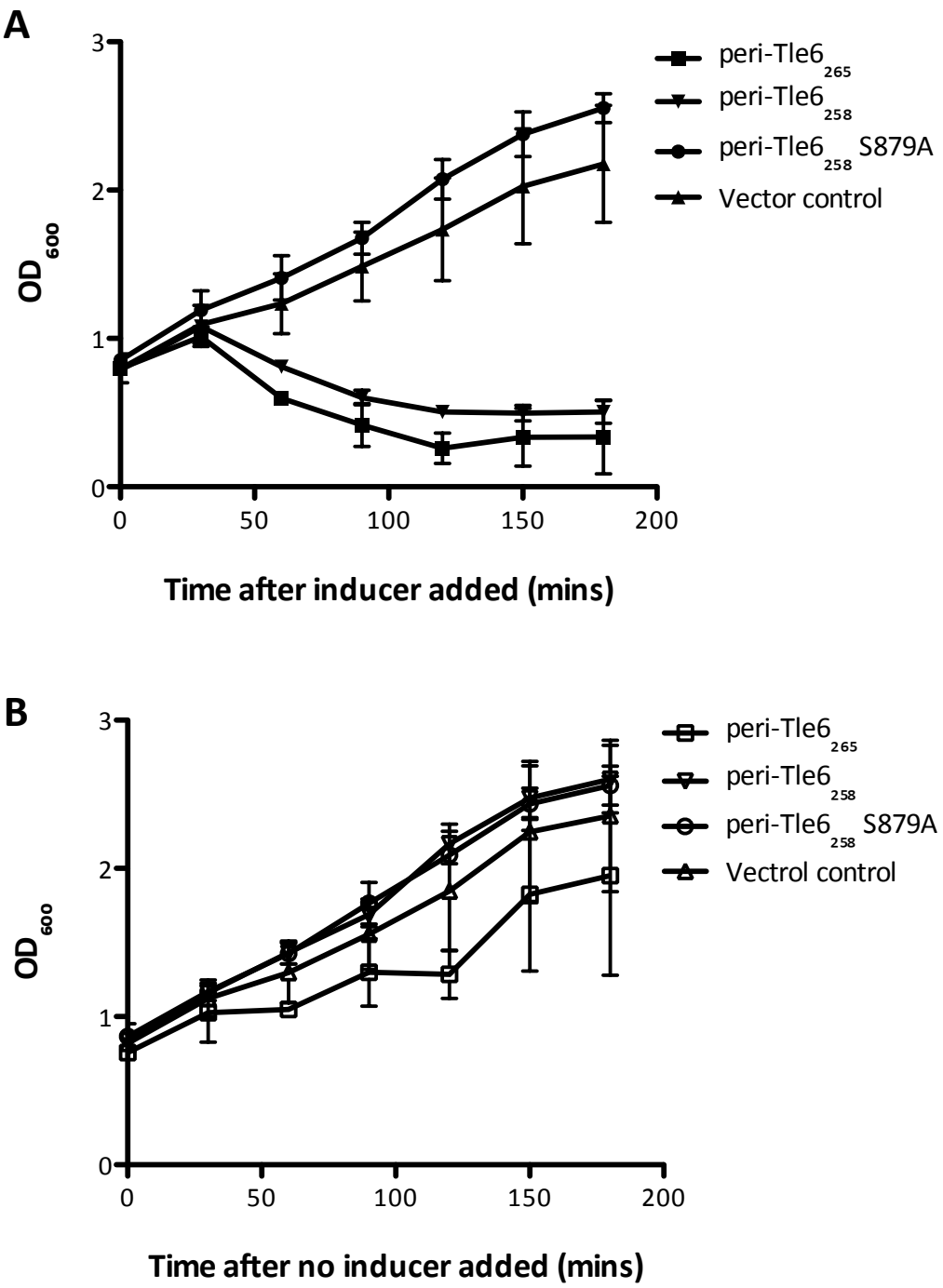

Figure 7.12 Analysis of the effect of periplasmic targeting of the Tle6 domain of $TssI_{0667}$ in *E. coli*. pET22b(+) derivatives specifying overproduction of periplasmically located Tle6 domains of $TssI_{0667}$ were introduced into BL21(DE3)/pLysS, grown in BHI-broth to an OD_{600} of 0.8 and then induced with 1 mM IPTG (final conc.) or left uninduced. Following induction culture optical densities were measured at 30-minute intervals over a 3-hour period. (A) The results of periplasmic targeting of $Tle6_{265}$, $Tle6_{258}$ and $Tle6_{258}$ S879A or empty pET-22b(+) vector, as indicated. (B) The optical densities of corresponding cultures from (A) without the inducer added, as indicated. Points represent average OD_{600} value where n≥3 and error bars = ±SD.

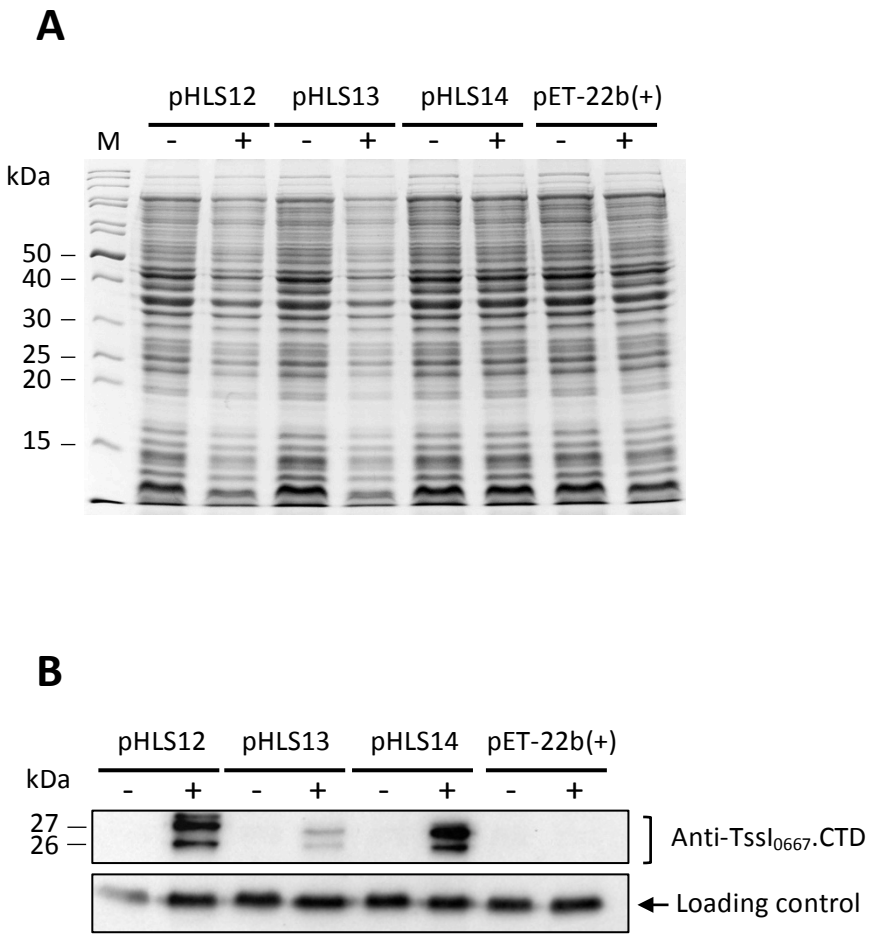

Figure 7.13 Analysis of the cellular abundance of periplasmically targeted Tle6 domain of $TssI_{0667}$. pET22b(+) derivatives specifying overproduction of periplasmically located Tle6 domains of $TssI_{0667}$ were introduced into BL21(DE3)/pLysS and resulting cultures were induced with 1 mM IPTG. (A) SDS-PAGE analysis of uninduced (-) and induced (+) cultures containing pHLS12, encoding $Tle6_{265}$, pHLS13, encoding $Tle6_{258}$ and pHLS14, encoding $Tle6_{258}$ S879A and empty pET-22b(+) vector control, as indicated above the lanes. M, EZ-Run *Rec* protein ladder. (B) Corresponding anti-$TssI_{0667}$.CTD western blot (top panel) of samples in (A) as indicated. A cross-reacting host protein is used as loading control (lower panel) as indicated by labelled arrow. Sizes of detected proteins are indicated on the left, as judged by a protein marker.

following induction of periplasmically targeted Tle6 domain of $TssI_{0667}$ than what was detected in uninduced and vector controls, which increased over the induction period (Figure 7.14). This implied that a significant amount of host cell lysis was occurring, mirroring the observed decreasing culture optical densities.

7.4.3 Effect of intracellular production of the $TssI_{0667}$ Tle6 domain on *E. coli*

To investigate whether cytoplasmic targeting of the Tle6 phospholipase domain of $TssI_{0667}$ exerted an effect on the viability of bacterial cells, previously generated pET-28a-derivatives encoding wild-type and S879A versions of the Tle6 domain of $TssI_{0667}$ (Jones, 2012) were introduced into the *E. coli* expression strain BL21(DE3)/pLysS. Cultures containing the expression plasmids were induced and the culture optical densities monitored (Section 2.9.2). The results indicate that intracellular targeting of either the wild-type or S879 mutant versions of $Tle6_{258}$ had no effect of the growth of *E. coli* cells (Figure 7.15).

Uninduced and induced whole cells lysates of cultures containing the pET-28a-derived expression vectors encoding wild-type and S879A versions of the Tle6 domain of $TssI_{0667}$ described above were also analysed by SDS-PAGE and by anti-$TssI_{0667}$.CTD western blotting to determine whether the desired protein was being produced in the induced cultures. The resulting Coomassie blue stained gel and corresponding western blot shows clear accumulation of a 27 kDa protein in cells containing plasmids specifying both wild-type and S879A versions of the Tle6 domains of $TssI_{0667}$ following induction (Figure 7.16). Therefore, even though a significantly greater amount of $TssI_{0667}$ Tle6 accumulated in the cell than that what occurred following periplasmic targeting, intracellular expression was still not causing cell lysis suggesting that the normal target of the $TssI_{0667}$ Tle6 domain is extracytoplasmic.

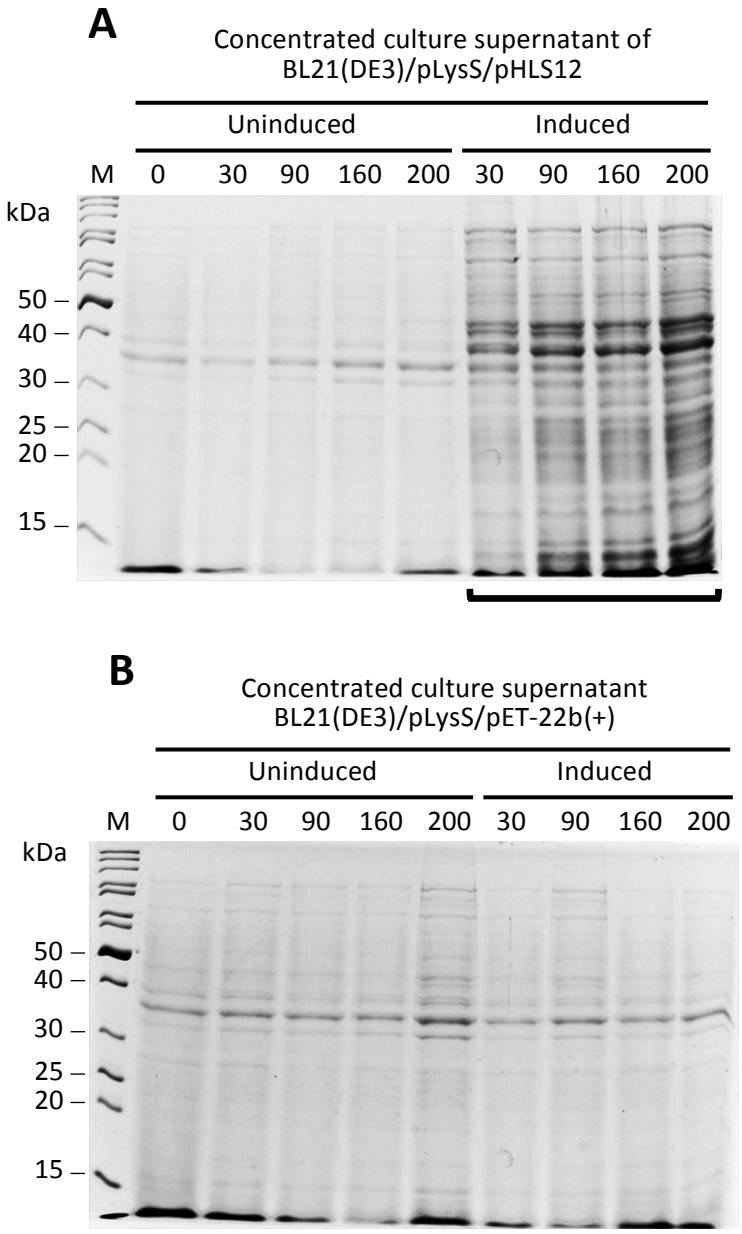

Figure 7.14 Analysis of the protein content of culture supernatants following induction of periplasmically targeted $TssI_{0667}$ Tle6 domain. The spent culture supernatants from BL21(DE)pLysS cells harbouring an expression vector specifying periplasmically targeted $TssI_{0667}$ $Tle6_{265}$ domain, pHLS12, and empty pET-22b(+) vector, were taken at 30, 90, 160 and 200 minutes post-induction, subjected to DOC-TCA precipitation and concentrated 50-fold. Samples were then separated by SDS-PAGE and gels were stained with Coomassie blue. (A) The resulting protein samples from uninduced and induced cultures harbouring pHLS12, encoding $Tle6_{265}$, as indicated. Black underline bracket indicates induced samples with increased protein concentration compared to uninduced samples. (B) as (A) but for cultures containing the empty pET-22b(+) vector. M, EZ-Run *Rec* protein ladder.

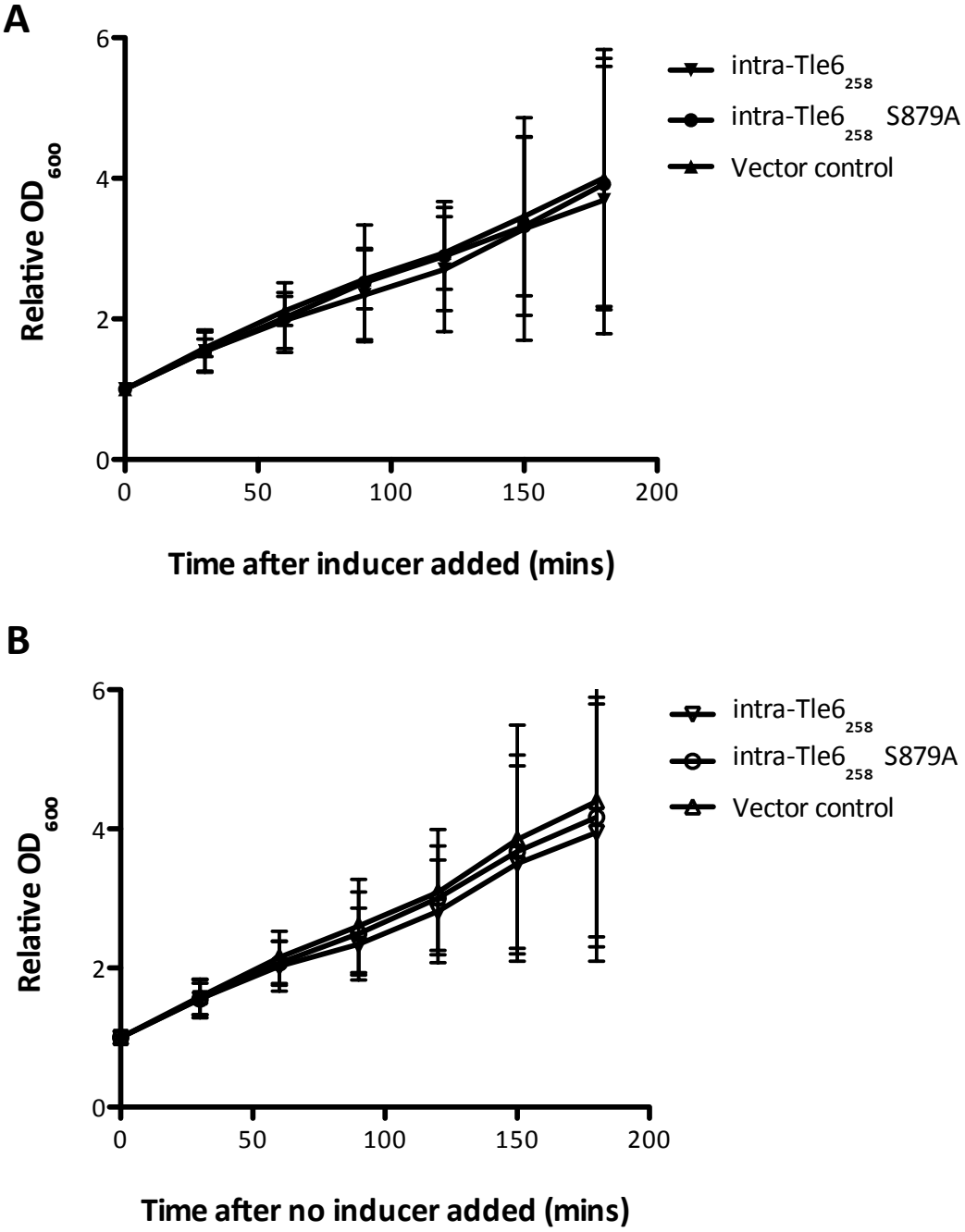

Figure 7.15 Analysis of the effect of cytoplasmic targeting of the Tle6 domain of $TssI_{0667}$ in *E. coli*. pET-28a(+) derivatives specifying overproduction of cytoplasmically located Tle6 domains of $TssI_{0667}$ were introduced into BL21(DE3)/pLysS, grown in BHI-broth to an OD_{600} of 0.8 and then induced with 1 mM IPTG (final conc.) or left uninduced. Following induction culture optical densities were measured at 30-minute intervals over a 3-hour period. (A) The results of cytoplasmic targeting of $Tle6_{258}$ and $Tle6_{258}$ S879A domains of $TssI_{0667}$ or empty pET-28a(+) vector, as indicated. (B) The optical densities of corresponding cultures from (A) without the inducer added, as indicated. Points represent average OD_{600} value where n=3 and error bars = ±SD.

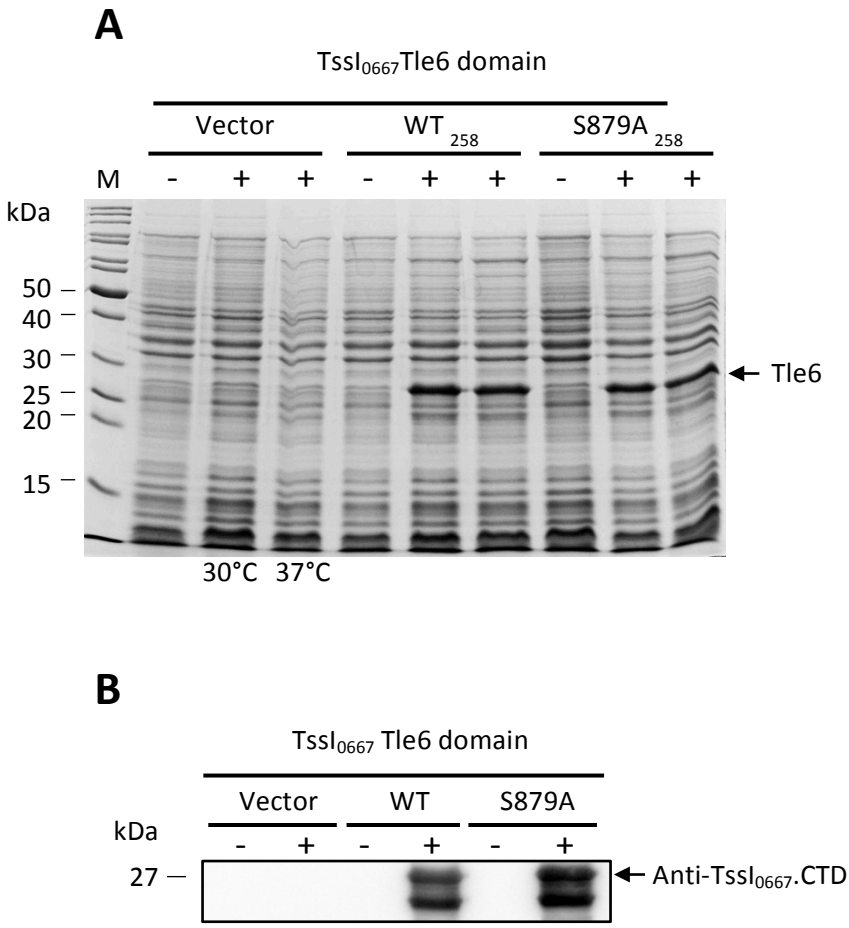

Figure 7.16 Analysis of the cellular abundance of cytoplasmically targeted Tle6 domain of $TssI_{0667}$. pET-28a(+) derivatives specifying overproduction of cytoplasmically located Tle6 domains of $TssI_{0667}$ were introduced into BL21(DE3)/pLysS cells and the resulting cultures were induced with 1 mM IPTG at 30°C or 37°C. (A) SDS-PAGE analysis of uninduced (-) and induced (+) cultures containing plasmids encoding wild-type and S879A versions of $Tle6_{258}$ and empty pET-28a(+) vector control, as indicated above the lanes. M, EZ-Run *Rec* protein ladder. (B) Corresponding anti-$TssI_{0667}$.CTD western blot. Size of detected protein is indicated on the left, as judged by a protein marker. Arrow indicates which of the detected bands corresponds to the correct sized protein using the antibody stated.

7.5 Analysis of Tli6 as a potential immunity protein to the T6SS-dependent effector $TssI_{0667}$

Many T6SS effector have cognate immunity proteins/antitoxins, as discussed in Section 1.5. They are thought to inhibit the toxic activity of the effector protein to prevent self-killing from within and prevent killing of surrounding bacteria of the same species by the toxic effector.

It was hypothesised that BCAS0666 encoded the cognate immunity protein for $TssI_{0667}$, as the gene is situated adjacent to BCAS0667 in the *B. cenocepacia* genome and the protein product, termed Tli6, was predicted to be periplasmically localised due to the presence of an N-terminal Sec-dependent signal peptide and contain ankyrin repeat motifs, known to be important for protein-protein interactions. Therefore it was decided to investigate whether Tli6 was able to inhibit the toxic effect of targeting $TssI_{0667}$ to the periplasmic compartment.

7.5.1 Construction of ColE1-compatible expression plasmid for production of Tli6 in *E. coli*

To facilitate expression of the gene encoding Tli6 with it corresponding effector encoding gene BCAS0667, BCAS0666 was cloned into pSCrhaB2, a rhamnose-inducible pBBR1-based replicon that is compatible with the ColE1-like origin of replication of pET-22b(+). The coding region of BCAS0666 (including the signal peptide coding sequence) was amplified from H111 genomic DNA using the primers BCAS0666ForNdeI and BCAS0666RevXbaI, generating a DNA fragment of 944 bp (Figure 7.17A). The product was then digested with NdeI and XbaI and ligated between the corresponding restriction sites of pSCrhaB2 to generate the plasmid termed pHLS15, with an expected size of 8423 bp. Clones were selected using IST agar containing trimethoprim, and screened by colony PCR using vector primers pSCrhaB2for and pSCrhaB2rev. Candidate clones 1 and 4 were subjected to plasmid isolation and plasmid size analysis following electrophoresis (Figure 7.17B), which were then confirmed by DNA sequencing.

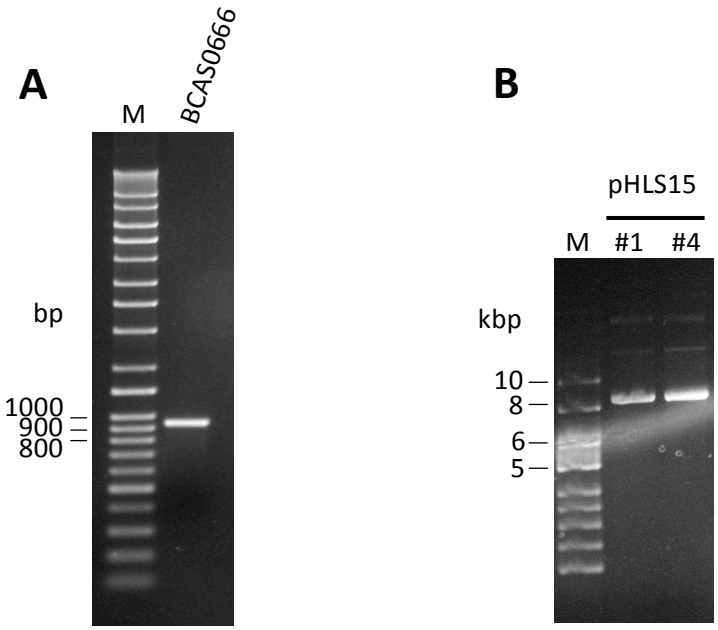

Figure 7.17 Construction of a ColE1-compatible expression vector encoding Tli6. The BCAS0666 coding sequence was amplified from H111 genomic DNA and cloned into the rhamnose-inducible vector pSCrhaB2 between the restriction sites NdeI and XbaI, to give the plasmid termed pHLS15. (A) The 944 bp BCAS0666 fragment amplified by PCR. (B) Size analysis of candidate pHLS15 recombinant plasmids, which had an expected plasmid size of 8423 bp. M, GeneRuler DNA ladder mix or supercoiled DNA ladder.

7.5.2 Effect of co-production of Tli6 and periplasmically targeted $TssI_{0667}$ Tle6 domain on host cell viability

It was decided to investigate whether the presence of Tli6 inhibited the toxic effect of periplasmically targeted Tle6 domain of $TssI_{0667}$ in *E. coli*. To do this, plasmids pHLS15, encoding Tli6, and pHLS13, encoding periplasmically targeted $Tle6_{258}$ domain of $TssI_{0667}$ were co-introduced into the expression strain BL21(DE3)/pLysS. pHLS13 and the empty pSCrhaB2 vector, and pHLS15 and the empty pET-22b(+) vector were also co-introduced as controls. Liquid cultures were simultaneously induced with IPTG and 0.1% rhamnose and the optical density was monitored (Section 7.4.2). Figure 7.18A demonstrates that co-production of Tli6 with the periplasmically located $TssI_{0667}$ Tle6 domain prevented a decrease in the optical density of the culture, unlike the situation when Tle6 is targeted to the periplasmic alone, which occurs following induction of BL21(DE3)/pLysS cells containing pHLS13 and the empty pSCrhaB2 vector. The growths of uninduced cultures harbouring the expression plasmids were similar (Figure 7.18B).

Production of Tli6 was verified by SDS-PAGE analysis of whole cell lysates of cultures described above following induction (Figure 7.18C). The theoretical molecular mass of Tli6 is 31.3 kDa including the Sec-dependent signal sequence, and 28.4 kDa without it. A 30 kDa protein was observed in strains that contained pHLS15 following induction, whereas it was absent from the strain harbouring pSCrhaB2, indicating specific induction of Tli6 synthesis. Intriguingly, there was a faint presence of a protein at approximately 27 kDa in the strain harbouring plasmids encoding both Tli6 and periplasmically target Tli6 domain of $TssI_{0667}$ following induction. This 27 kDa was confirmed to the Tle6 domain of $TssI_{0667}$ by western blotting and probing with an anti-$TssI_{0667}$.CTD antibody (Figure 7.18D). It was observed that when equal amounts of total protein were analysed the $TssI_{0667}$ Tle6 domain accumulated to higher levels in cells co-producing Tli6 than when the Tle6 domain was induced on its own. This is consistent with the idea that complex formation between the two proteins inhibits the toxic action of the Tle6 domain. Hence, more Tle6 can accumulate, as the cells are not being lysed by free active $TssI_{0667}$ Tle6 domain.

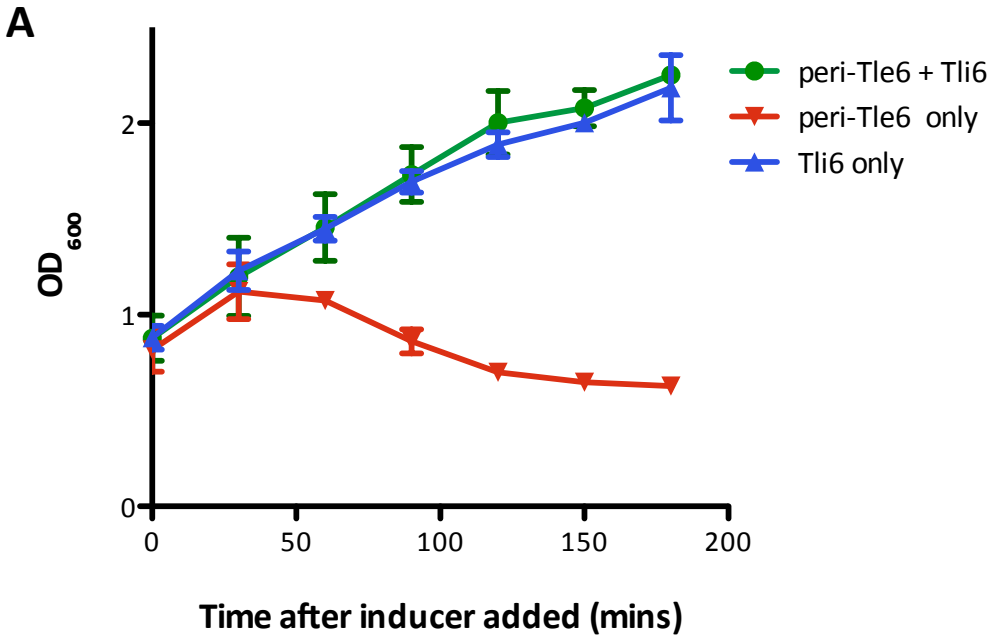
A
peri-Tle6 + Tli6
peri-Tle6 only
Tli6 only
OD 600
0
1
2
0
50
100
150
200
Time after inducer added (mins)

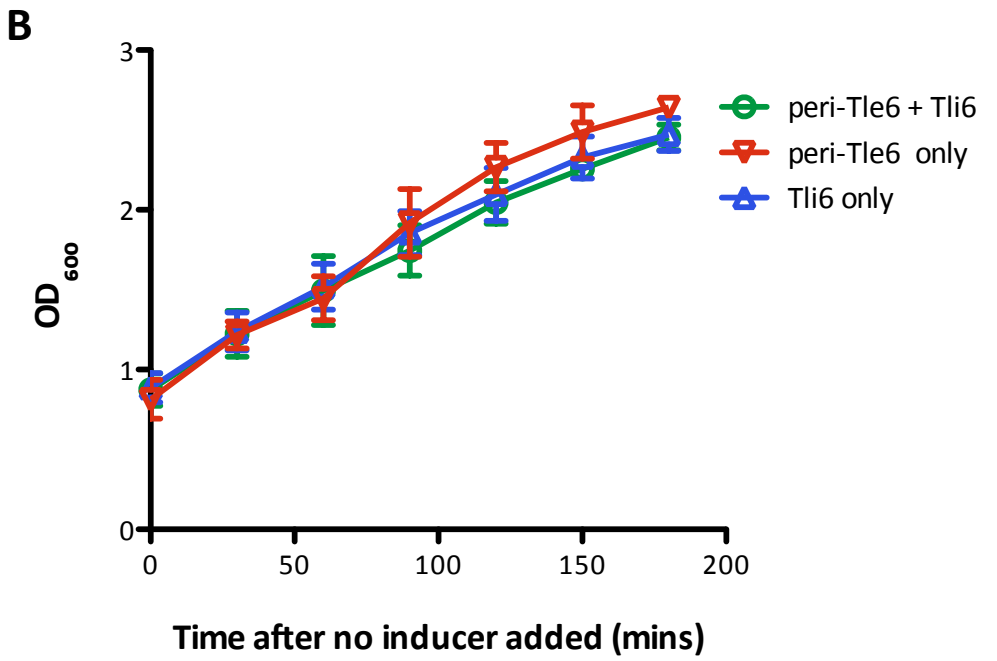
B
peri-Tle6 + Tli6
peri-Tle6 only
Tli6 only
OD 600
0
1
2
3
0
50
100
150
200
Time after no inducer added (mins)

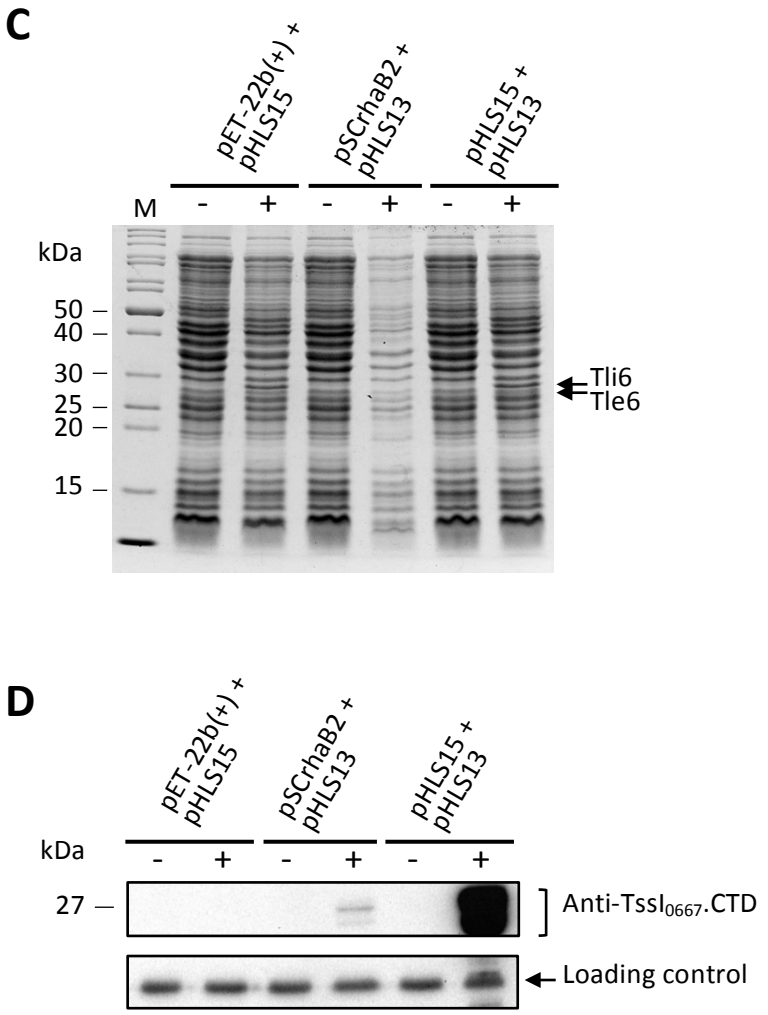

Figure 7.18 Co-production of Tli6 prevents toxicity of periplasmically targeted $TssI_{0667}$ Tle6 domain in *E. coli.* pET-22b(+) and pSCrhaB2 derivatives specifying production of periplasmically located Tle6 domain of $TssI_{0667}$ and Tli6 were introduced into BL21(DE3)/pLysS cells, grown in BHI-broth to an OD_{600} of 0.8 and then induced with 1 mM IPTG and 0.1% rhamnose (final conc.) or left uninduced. pHLS13 encodes periplasmically targeted $TssI_{0667}$ Tl6 domain, and pHLS15 encodes Tli6. Following induction, the culture optical densities were measured at 30-minute intervals over a 3-hour period. Uninduced and induced samples were taken as whole cell lysates and analysed by SDS-PAGE and western blotting. (A) The resulting culture optical densities following induction of periplasmically targeted $TssI_{0667}$ Tle6 domain with or without the production of Tli6, and production of Tli6 alone, as indicated. (B) Optical densities of corresponding cultures from (A) without the inducers added, as indicated. Points represent average OD_{600} value where n=3 and error bars = ±SD. (C) Coomassie blue stained 12% SDS-PA gel of uninduced (-) and induced (+) samples taken from the 3-hour time-point from (A) and (B), as indicated. Labelled arrows indicate presence and identify of induced proteins. (D) Corresponding anti-$TssI_{0667}$.CTD western blot (top panel) of samples in (C). Cross-reactive *E. coli* protein used as loading control. Molecular mass of the detected protein is indicated on the left.

7.6 Characterisation of complex formation between the $TssI_{0667}$ Tle6 domain and Tli6 by pull-down analysis

Experimental results by other groups that demonstrated direct interactions between T6SS-dependent effectors and their cognate immunity protein led to the idea that Tli6 may form a direct complex with $TssI_{0667}$ through the C-terminal Tle6 phospholipase domain of the latter. It was decided to investigate this potential interaction by pull-down analysis.

7.6.1 Construction of plasmids for overproduction of epitope-tagged $TssI_{0667}$ Tle6 domain and Tli6

For immuno-detection of potentially interacting proteins $TssI_{0667}$ Tle6 domain and Tli6 antibodies should be available for both proteins. To facilitate detection of Tli6 it was decided to append a C-terminal triple-FLAG tag to the protein lacking its signal sequence. Although an antibody that specifically recognised the $TssI_{0667}$.CTD (Tle6 domain) was available, it was necessary to append an affinity tag to the N-terminus of this protein for purification. This could also serve as an epitope tag. To do this, the coding sequence of BCAS0667.CTD which encoded the C-terminal 258 amino acids of $TssI_{0667}$ was PCR amplified from the plasmid pHLS13 using the primers BCAS0667PLAForBamHI and BCAS0667PLARevXhoI, generating a DNA fragment of 824 bp. The coding sequence of BCAS0666 encoding mature (i.e. processed) Tli6 was PCR amplified from the plasmid pHLS15 using the forward primer BCAS0666For2NdeI and a long reverse primer that included a 66 bp coding sequence encoding the 3xFLAG peptide sequence, BCAS0666Rev3xFLAGAcc65I, to generate a DNA fragment of 864 bp (Figure 7.19A). The BCAS0667.CTD amplicon was digested with BamHI and XhoI and successfully ligated between the BamHI and SalI restriction sites of the T7lac expression vector pETDuet-1, giving rise to a 6199 bp plasmid termed pHLS16. The BCAS0666.3xFLAG amplicon was digested with NdeI and Acc65I and successfully ligated between the NdeI and Acc65I restriction sites of pETDuet-1, giving rise to pHLS17 with a plasmid size of 6227 bp (Figure 7.19B). Plasmids of the expected size were confirmed by DNA sequencing.

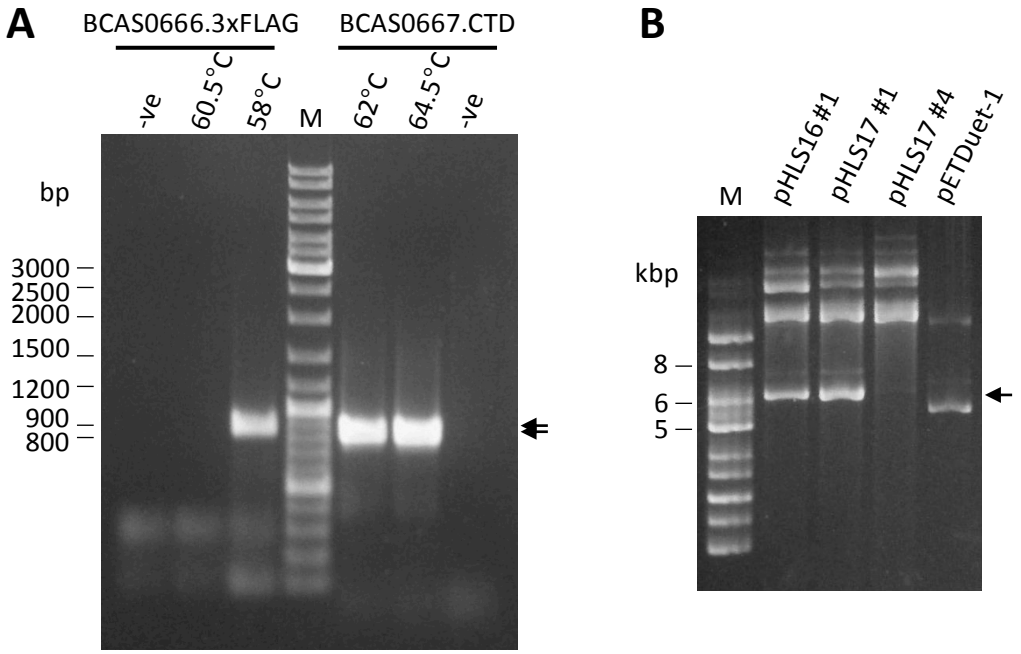

Figure 7.19 Construction of pETDuet-1 based plasmids specifying production of epitope-tagged Tle6 domain of $TssI_{0667}$ and Tli6. The coding sequence of BCAS0667.CTD was amplified from H111 genomic DNA and cloned between the BamHI-SalI restriction sites of pETDuet-1, incorporating an N-terminal His-tag coding sequence provided by the vector. BCAS0666 was amplified from H111 genomic DNA using a reverse primer containing a DNA sequence encoding a 3xFLAG epitope tag, and cloned between the NdeI-Acc65I restriction sites of pETDuet-1. (A) Successful PCR amplification of BCAS0667.CTD and BCAS0666.3xFLAG DNA fragments using the stated annealing temperature, as indicated, visualised following electrophoresis in a 0.8% agarose gel. Upper arrow indicates expected DNA fragment size of BCAS0667.3xFLAG, and lower arrow indicates BCAS0667.CTD DNA fragment. –ve, no DNA negative control; M, GeneRuler DNA ladder mix. (B) Size analysis of candidate pHLS16 and pHLS17 plasmid clones. Arrow indicates approximate size of both plasmids, ~6.2 kbp. M, supercoiled DNA ladder.

A dual expression plasmid was then constructed to direct high-level synthesis of N-terminally His-tagged Tle6 domain of $TssI_{0667}$ and C-terminally 3xFLAG tagged Tli6 from the same plasmid. This was successfully constructed by digesting pHLS16 with NdeI and Acc65I, and ligating in to the BCAS0666.3xFLAG PCR amplified DNA fragment cut with the same restriction enzymes, giving rise to a 7006 bp plasmid, pHLS18.

7.6.2 Overproduction and solubility of His_6.Tle6 domain of $TssI_{0667}$ and Tli6.3xFLAG

It was first required to determine whether the plasmids described above provided sufficient expression for overproduction of soluble protein to be used in a pull-down assay. Therefore constructs pHLS16, pHLS17 and pHLS18 were introduced separately into *E. coli* BL21(DE3)/pLysS, and subjected to a small scale test induction. Strains where induced with 1 mM IPTG at 37°C for 3 hours (Section 2.3.1). Whole cell lysates where then analysed by SDS-PAGE. The expected molecular masses of the His_6.Tle6 domain of $TssI_{0667}$ and Tli6.3xFLAG are 27.8 kDa and 31.2 kDa, respectively. Figure 7.20 shows the resulting SDS-PA gel. The presence of proteins of the expected size can be clearly observed in all induced cultures. The solubility of induced proteins was then determined as described in Section 2.3.2. Both His_6.Tle6 domain of $TssI_{0667}$ and Tli6.3xFLAG were produced as soluble proteins (data not shown).

7.6.3 Analysis of the interaction between $TssI_{0667}$ His_6.Tle6 domain and Tli6.3xFLAG by a pull-down assay

For detection of interactions between the Tle6 phospholipase domain of $TssI_{0667}$ and its putative immunity protein Tli6 a pull-down assay was performed (Section 2.7.1). A cleared lysate containing soluble His_6.Tle6 domain of $TssI_{0667}$ was obtained and this His-tagged bait protein was immobilised onto nickel affinity resin. After subsequent wash steps, a cleared lysate containing soluble Tli6.3xFLAG was used as 'prey' protein and incubated with the immobilised $TssI_{0667}$ Tle6 domain. After further wash steps, bound proteins were eluted from the affinity resin with

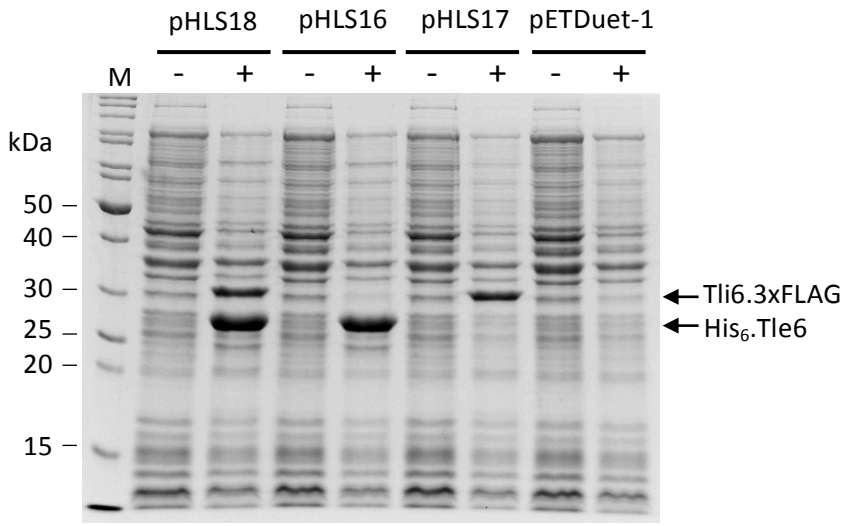

Figure 7.20 Analysis of overproduction of His_6.Tle6 domain of $TssI_{0667}$ and Tli6.3xFLAG from pETDuet-1 based constructs. Expression plasmids pHLS18, specifying the overproduction of both His_6.Tle6 domain of $TssI_{0667}$ and Tli6.3xFLAG, pHLS16, specifying His_6.Tle6 domain of $TssI_{0667}$ alone and pHLS17, specifying Tli6.3xFLAG alone were introduced into BL21(DE3)/pLysS cells separately. Liquid cultures were grown to mid-log phase and induced with 1 mM IPTG for 3 hours at 37°C. Samples of uninduced (-) and induced cells (+) were analysed by SDS-PAGE on a 12% SDS-PA gel. The resulting gel was visualised by Coomassie blue staining, samples were loaded as indicated. M, EZ-Run *Rec* protein ladder, labelled arrows indicate the identity of induced proteins.

addition of a high concentration of imidazole. Samples were fractionated by SDS-PAGE, and analysed by both Coomassie blue staining and western blotting followed by probing with anti-His and anti-FLAG antibodies (Figure 7.21). It was observed that His_6.Tle6 domain of $TssI_{0667}$ was able to bind to the nickel resin and was eluted by the addition of 500 mM imidazole. In agreement with the hypothesis, Tli6.3xFLAG was retained on the nickel resin that was pre-loaded with His_6.Tle6 domain of $TssI_{0667}$ but did not bind to the resin in the absence of the His-tagged Tle6 domain. Upon elution of bound His_6.Tle6 that had retained Tli6.3xFLAG with 500 mM imidazole Tli6.3xFLAG was also co-eluted.

A pull-down of Tli6.3xFLAG with the His_6.Tle6 domain of $TssI_{0667}$ was also performed using a cleared lysate that contained both His_6.Tle6 domain of $TssI_{0667}$ and Tli6.3xFLAG that was obtained following induction of BL21(DE)/pLysS cells containing the co-expression vector pHLS18. Here, the lysate was incubated with nickel affinity resin to allow binding of the His_6.Tle6-Tli6.3xFLAG complex directly to the resin, and then subsequently eluted with 500 mM imidazole. The resulting samples were fractionated by SDS-PAGE and then analysed following Coomassie blue staining (Figure 7.21C) and western blotting (Figure 7.21D), as described above. Similarly, Tli6.3xFLAG was co-eluted from the nickel resin upon imidazole-dependent elution of immobilised His_6.Tle6 domain of $TssI_{0667}$.

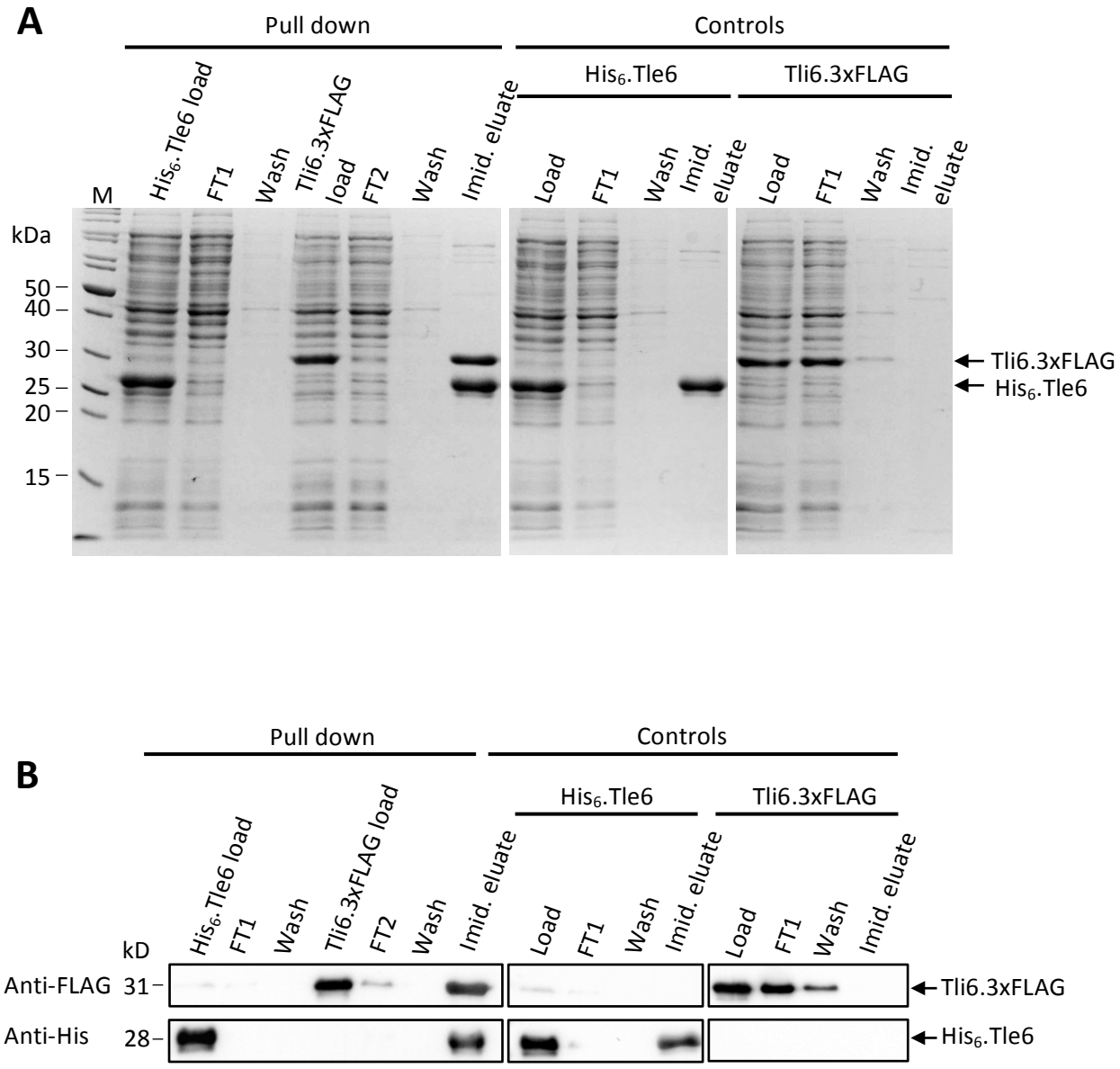
A
Pull down
Controls
His6.Tle6
Tli6.3xFLAG
His6.Tle6 load
FT1
Wash
Tli6.3xFLAG load
FT2
Wash
Imid. eluate
Load
FT1
Wash
Imid. eluate
Load
FT1
Wash
Imid. eluate
M
kDa
50
40
30
25
20
15
Tli6.3xFLAG
His6.Tle6
B
Pull down
Controls
His6.Tle6
Tli6.3xFLAG
His6.Tle6 load
FT1
Wash
Tli6.3xFLAG load
FT2
Wash
Imid. eluate
Load
FT1
Wash
Imid. eluate
Load
FT1
Wash
Imid. eluate
kD
Anti-FLAG
31
Anti-His
28
Tli6.3xFLAG
His6.Tle6

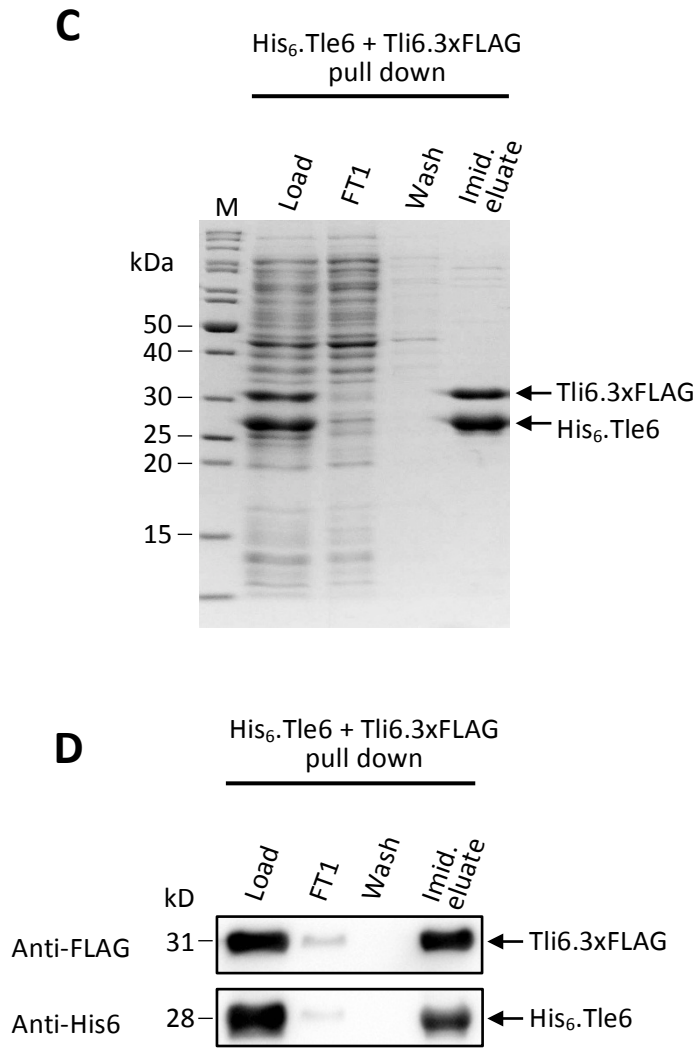

Figure 7.21 Analysis of interaction between the Tle6 domain of $TssI_{0667}$ and Tli6 by pull-down assays. His_6.Tle6 domain of $TssI_{0667}$ and Tli6.3xFLAG were overproduced in BL21(DE3)/pLysS cells harbouring pHLS16 and pHLS17, respectively. The cleared lysate from induced cultures of overproduced His_6.Tle6 was bound to nickel affinity resin, and washed. Following this the induced cell lysate containing Tli6.3xFLAG was added to the resin containing the immobilised His_6.Tle6, washed and then bound proteins were eluted with 500 mM imidazole buffer. Immobilisation of His_6.Tle6 and Tli6.3xFLAG only controls were included. Load flow-through (FT), wash and imidazole eluate samples from each stage were separated by SDS-PAGE and visualised by Coomassie blue staining and by anti-His6 and anti-FLAG western blotting. (A) Resulting Coomassie blue stain of His_6.Tle6 and Tli6 pull down (left) and His_6.Tle6 and Tli6 only controls (right), as indicated. (B) Western blot of samples in (A) following probing with anti-FLAG and anti-His antibodies as indicated. (C) Resulting Coomassie blue stain of samples from pull-down assay that used a lysate containing both His_6.Tle6 domain of $TssI_{0667}$ and Tli6.3xFLAG produced from pHLS18. Samples loaded as indicated above the lanes. (D) Western blot of samples in (C) following probing with anti-FLAG and anti-His antibodies as indicated. Labelled arrows indicate identity of eluted proteins. Molecular masses of detected proteins indicated on right, as judged by a protein ladder. M, EZ-Run *Rec* protein ladder; Imid.,imidazole.

7.7 Analysis of the oligomeric status of the $TssI_{0667}$ Tle6–Tli6 complex

The pull down assay results described in Section 7.6 indicated a direct complex was formed between $TssI_{0667}$ Tle6 domain and the putative immunity protein Tli6. Therefore it was decided to further characterise this complex, particularly in regards to its stoichiometry.

7.7.1 Large-scale purification of $TssI_{0667}$ Tle6-Tli6 complex by IMAC

Larger and purer quantities of the complex formed between the Tle6 domain of $TssI_{0667}$ and Tli6 were required for downstream investigations into the characteristics of the complex. To do this, a previously generated dual expression plasmid (Hedayat and Thomas, unpublished) encoding the C-terminal 267 amino acids of $TssI_{0667}$ with a hexa-histidine tag located at the N-terminus, and an untagged version of Tli6 without its signal sequence was used, termed pSH1. This plasmid was introduced into BL21(DE3)/pLysS cells, and protein synthesis was induced with 1 mM IPTG for 3 hours at 37°C. Protein overproduction and protein solubility of the overproduced proteins were determined following separation by SDS-PAGE and visualisation by Coomassie blue staining (Figure 7.22A). The expected molecular masses of the His_6.Tle6 domain containing the C-terminal 267 amino acids for $TssI_{0667}$ and untagged Tli6 were 28.9 kDa and 28.4 kDa, respectively. Due to the very small size difference between the two proteins it was difficult, but not impossible, to resolve the two proteins by SDS-PAGE. Confirming previous observations both proteins were expressed as soluble proteins in significant quantities.

The soluble lysate containing the two proteins was loaded onto a 1mL His-Trap column and washed (Section 2.3.5). A 10-500 mM imidazole gradient was then applied to the column, and it was observed that the majority of bound material was eluted at a concentration of 75 mM imidazole (data not shown). Fractions containing eluted proteins were analysed by SDS-PAGE to determine protein concentration and purity (Figure 7.22B). Several fractions were pooled,

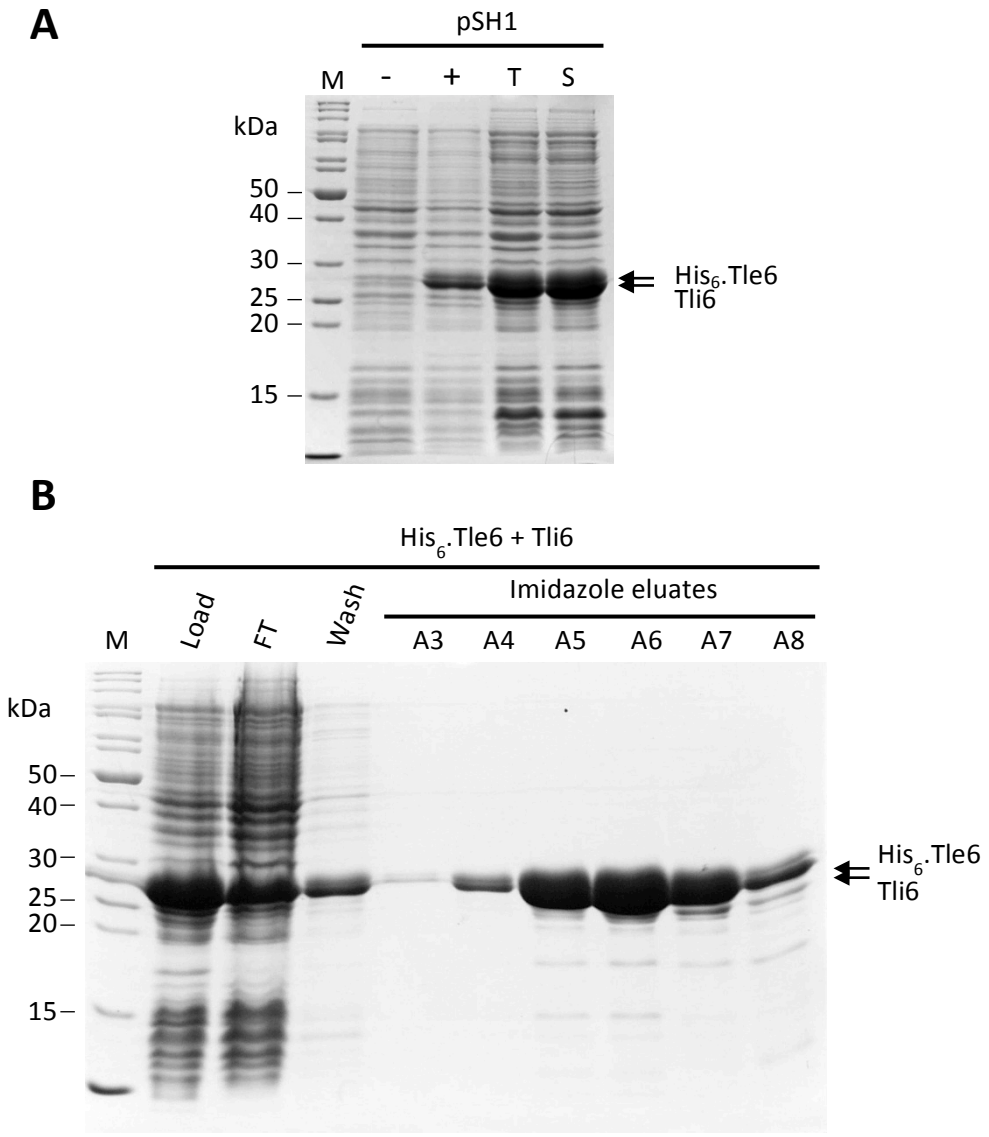

Figure 7.22 Overproduction and purification of His6.Tle6-Tli6 complex by IMAC. pSH1, encoding His_6.Tle6 domain of $Tssl_{0667}$ and untagged Tli6, was introduced into BL21(DE3)/pLysS cells. The strain was grown to mid-log phase in BHI-broth and plasmid encoded protein synthesis was induced with 1 mM IPTG at 37°C for 3 hours, following which cultures were lysed and sonicated as standard procedure. The lysate was then loaded on a 1 mL His-trap column (load), washed (wash) and then bound material eluted by addition of a 10-500 mM imidazole gradient using an ÄKTA FPLC system. (A) Coomassie blue stained 12% SDS-PA gel of cell extracts from uninduced (-) and induced (+) cultures of BL21(DE3)pLysS/pSH1 cells, and the resulting total (T) and soluble protein fractions (S) following lysis. (B) Coomassie blue stained SDS-PA gel of eluted His_6.Tl6-Tli6 samples (A3-A8) following IMAC purification. M, EZ-Run *Rec* protein ladder, arrows indicate identity of induced proteins. Lanes are labelled accordingly.

concentrated and the buffer exchanged to 50 mM Tris-HCl pH 7.5 using a 10000 MWCO centrifugal concentrator, ready to be analysed by size exclusion chromatography, described below.

7.7.2 Estimation of the oligomeric size of the $TssI_{0667}$ Tle6–Tli6 complex by size exclusion chromatography

A sample of the $TssI_{0667}$ His_6.Tle6-Tli6 complex, purified as described in Section 7.7.1 was subjected to size exclusion chromatography to estimate the oligomeric size of the complex. Using a Superose 12 10/300 GL column calibrated with standards of a known molecular weight (Figure 7.23A), 100 μL of the sample was injected onto the column and protein elution was monitored by tracking the A_{280}. This was performed in triplicate. As shown in Figure 7.23B, only one significant peak was detected, eluting at 11.4 mL. By comparing this average elution volume of the peak to the standard curve, the estimated molecular mass of the complex was calculated to be 94.4 ± 0.02 kDa (SD), which was within the limits of the column and the standards used, indicated by red data point in Figure 7.23A. The theoretical molecular mass of a 1:1 complex of the His_6.Tle6 domain of $TssI_{0667}$ to Tli6 is 57.3 kDa, a 1:2 complex is 85.7kDa, a 2:1 complex is 86.2kDa, and a 2:2 complex is 114.6kDa. Therefore the experimental value obtained here, may tentatively suggest that these proteins exist as a 1:2/2:1 His_6.Tle6-Tli6 complex.

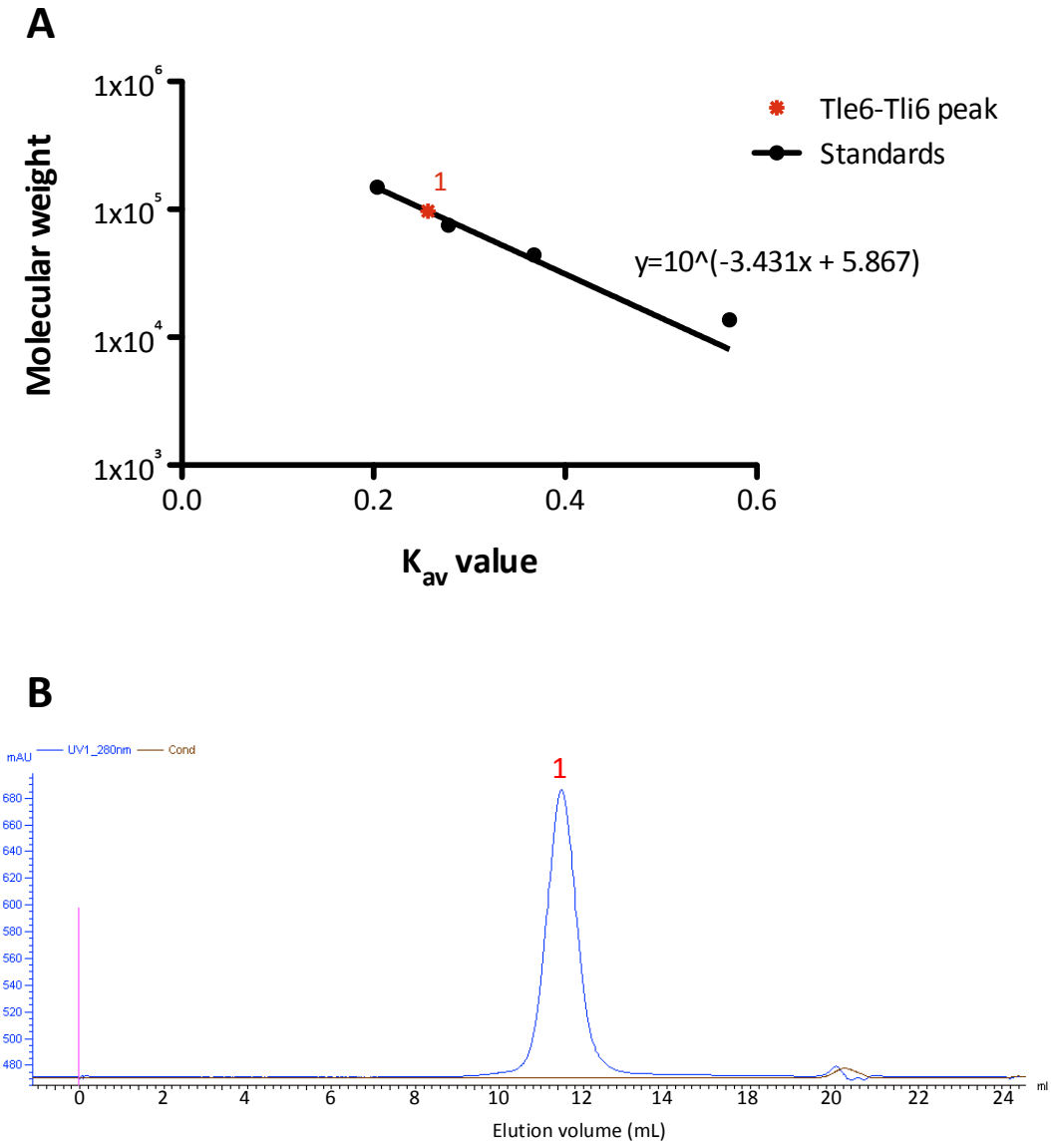

Figure 7.23 Analysis of $TssI_{0667}$ His_6.Tle6-Tle6 complex by SEC. 100 µL of purified $TssI_{0667}$ His_6.Tle6-Tle6 complex was subjected to SEC using a Superose 12 10/300 GL column coupled to an ÄKTA purifier FPLC system with a flow rate of 0.5 mL/min. (A) A calibration curve generated from the elution of protein standards, presented as experimentally determined K_{av} values (x axis) against the known molecular weight (y axis) of each standard, fit with a semi-log regression curve, with the equation as indicated. (B) Representative A_{280} trace for $TssI_{0667}$ His_6.Tle6-Tle6 complex, with a single elution peak at 11.4 mL following injection onto the column (pink line), labelled as 1. The calculated molecular weight for this peak is plotted in (A).

7.8 Characterisation of a putative T6SS-dependent peptidoglycan hydrolase effector encoded by I35_5786

Bioinformatic analysis of genes located downstream of *tssI* orthologues in *B. cenocepacia* J2315 suggested that BCAL1166 encoded a T6SS-dependent effector (Section 3.4.1). This putative effector gene is located downstream of a *tssI* orthologue BCAL1165, which encodes $TssI_{1165}$. The corresponding gene in *B. cenocepacia* H111 that encodes a similar protein to $TssI_{1165}$ is located on chromosome 2, at the locus I35_5787.

Analysis of the gene located directly downstream of this, I35_5786, indicated that its protein product shows homology to the protein encoded by BCAL1166, but they only share 18% sequence identify and 29% sequence similarity. However, both proteins are predicted to contain an N-terminal region containing an M23-like metallo-peptidase domain, which is dispersed in the BCAL1166-encoded product, a conserved domain of unknown function that is shared by both proteins and a C-terminal region containing a lysozyme-like superfamily (cl00222) domain (Figure 7.24). The product of I35_5786 contained a conserved HxH motif found in the M23 family of metallo-peptidases. The first histidine of this motif is the thought to be the active site residue and the latter histidine is required for metal ion binding/coordination, as experimentally defined by the M23 peptidase-containing autolysin protein LytM in *S. aureus* (Odintsov et al., 2004; Firczuk et al., 2005). Additional conserved histidine and aspartate residues in the M23 peptidase-like domain may be also be involved in metal ion co-ordination (Odintsov et al., 2004). The product of BCAL1166 is predicated to contain an additional SH3 domain, thought to be important for protein-protein interactions, and the I35_5787 encoded protein contains an additional DUF domain that is not present in the other protein. Interestingly, the dual feature of a M23 family metallopeptidase domain and a lysozyme-like domain has also been observed in the cell-wall degrading enzyme of bacteriophage ϕ29, the tail protein Gp13 (Xiang et al., 2008).

A BLASTP search of the predicted protein encoded by I35_5786 revealed several homologous proteins were encoded in the genomes of a variety of Gram-

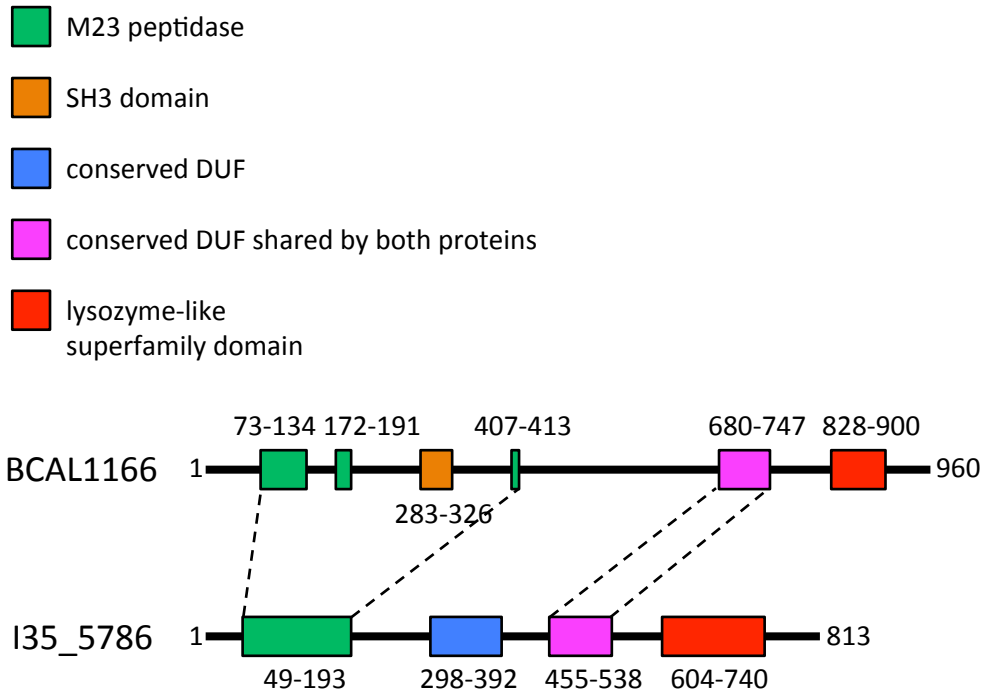

Figure 7.24 Comparison of the domain organisation of proteins encoded by BCAL1166 and I35_5786 in *B. cenocepacia* strains J2315 and H111. A bioinformatic analysis indicated the presence of key domains in the proteins encoded by BCAL1166 in *B. cenocepacia* J2315 and its related gene I35_5786 in *B. cenocepacia* H111, respectively, as indicated by the key on the left. Several domains shared homology between the two proteins, indicated by dashed lines.

negative bacteria, many of which were other *Burkholderia* species, including fellow Bcc member *B. ambifaria,* but it also included several *Yersinia* species, such as *Y. pestis* (not shown). Intriguingly, alignment of these homologous proteins with the proteins encoded by I35_5786 and BCAL1166 indicated that whilst regions of the N-terminus showed some sequence identity, the C-terminal domains were divergent even though all proteins were predicted to contain a lysozyme-like superfamily domain at the C-terminus. Furthermore, it was noted that many of the genes that encoded these related proteins were located downstream from a *tssI* gene, as observed for both I35_5786 and BCAL1166.

As the proteins encoded by BCAL1166 and I35_5786 are predicted to contain M23 peptidase and lysozyme-like domains is it hypothesised that the proteins may specify peptidoglycan hydrolase activity. More precisely, the putative effectors may confer glycoside hydrolase/muramidase activity at their C-terminus via the lysozyme-like domain. This is due to the known substrate specificity of other lysozyme-like proteins, including the Tge effector superfamily (Whitney et al., 2013), which hydrolyse the β-(1,4)-glycosidic bond between *N*-acetylglucosamine and *N*-acetylmuramic acid in the glycan backbone (Figure 1.8, Section 1.5). Second, they may also specify amidase/peptidase activity through their N-terminal M23 peptidase domain, which has been shown to cleave amide bonds in peptidoglycan at peptide cross-links (Firczuk et al., 2005). Due to the predicted muramidase and amidase features of these effectors these proteins shall be designated Tpe1 and Tpe2 (type VI peptidoglycan hydrolase effector) for the protein products of I35_5786 and BCAL1166, respectively. Thus from herein the I35_5786 gene will be referred to as *tpe1*, and subsequently, DNA fragments encoding the N-terminus of *tpe1* will be referred to as *tpe1.NTD* and the C-terminus as *tpe1.CTD.* Note the putative effectors cannot be assigned to either of the current T6SS-dependent superfamilies of peptidoglycan hydrolase effectors, the glycoside hydrolase (Tge) (Whitney et al., 2013) or amidase (Tae) (Russell et al., 2012) superfamilies, as the putative effectors are predicted to contain enzymatic domains that specify both of these activities.

To investigate the enzymatic function and role of the predicted Tpe1 effector

encoded in *B. cenocepacia* H111 it was decided to purify the full-length protein, and the individual N- and C-terminal regions, specifying the predicted M23 peptidase region and the lysozyme-like region, respectively.

7.8.1 Construction of plasmids for overproduction of epitope-tagged Tpe1 derivatives

The coding sequences of full-length *tpe1*, and the N- and C-terminal coding regions of the gene were cloned into the T7lac expression vector pETDuet. To do this, full-length *tpe1* was amplified from H111 genomic DNA using primers BCAL1166ForNtermHisNcoI and BCAL1166CTDRevXhoI, generating a DNA fragment of 2493 bp. The forward primer for this amplification contained the coding sequence of a hexa-histidine tag (encoding the peptide MGSSHHHHHHS) allowing incorporation of this coding sequence into the N-terminus of the coding sequence of *tpe1*. The N-terminal coding sequence, specifying the N-terminal 239 codons of *tpe1*, was amplified using primers BCAL1166NTDForNtermHisBglII and BCAL1166NTDRevHindIII, giving rise to a DNA fragment of 741 bp. The C-terminal coding region, specifying the C-terminal 237 codons of *tpe1* was amplified using primers BCAL1166ForNtermHisNcoI and BCAL1166CTDRevXhoI, giving rise to a DNA fragment of 739 bp.

The PCR product of the full length *tpe1* coding sequence was digested with NcoI and XhoI, and successfully ligated into pETDuet-1 between the NcoI and SalI restriction sites, to generate a plasmid of 7832 bp, termed pHLS19, encoding a N-terminally His-tagged version of Tpe1. The PCR product of the coding sequence of *tpe1.NTD* was digested with BglII and HindIII and cloned between BamHI and HindIII restriction sites in pETDuet-1, to give a 6110 bp plasmid, termed pHLS20. The PCR product of the coding sequence of *tpe1.CTD* was digested with BamHI and XhoI, where it was then ligated into pETDuet-1 cut with BamHI and SalI, generating a 6114 bp plasmid, termed pHLS21. Transformants containing recombinant plasmids of the desired size were identified by PCR colony screening using vector specific primers pETDuet-T7-1for and pACYCDuet-T7-1rev. Following this, plasmids were isolated and subjected to size analysis by agarose gel electrophoresis (Figure 7.25).

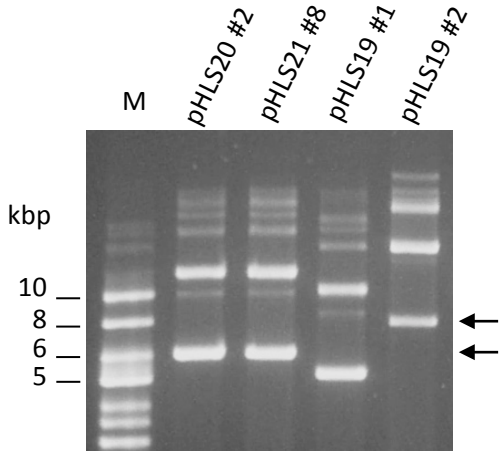

Figure 7.25 Size analysis of pETDuet-1 derivative encoding epitope-tagged Tpe1, Tpe1.NTD and Tpe1.CTD. Transformants containing pHLS19, pHLS20 and pHLS21 were selected for plasmid isolation by mini-preparation, and the resulting plasmids were electrophoresis in 0.8% agarose gel, as indicated. Upper arrow indicates expected size of pHLS19 plasmid, and lower arrow indicates expected size of pHLS20 and pHLS21. M, supercoiled DNA ladder.

7.8.2 Overproduction of epitope-tagged Tpe1, Tpe1.NTD and Tpe1.CTD in *E. coli*

To determine whether the expression plasmids described above allowed the overproduction of sufficient amounts of soluble His_6.Tpe1, His_6.Tpe1.NTD and His_6.Tpe1.CTD proteins for purification, the plasmids pHLS19, pHLS20 and pHLS21 were first introduced into the *E. coli* expression strain BL21(DE3). Cells harbouring the expression plasmids were then subjected to small-scale test inductions at 30°C and 37°C with 1 mM IPTG (Section 2.3.1). SDS-PAGE analysis of the cell lysates from the resulting uninduced and induced cultures demonstrated that proteins at approximate anticipated molecular masses were overproduced in the appropriate cultures following induction (His_6.Tpe1, His_6.Tpe1.NTD, His_6.Tpe1.CTD had expected molecular masses of 92.1 kDa, 28 kDa and 28.1 kDa, respectively) (Figure 7.26).

7.8.3 Solubility of overproduced Tpe1, Tpe1.NTD and Tpe1.CTD in *E. coli*

To determine whether overproduced His_6.Tpe1 and its tagged NTD and CTD derivatives are produced as soluble proteins, induced cultures of BL21(DE3) cells harbouring pHLS19, pHLS20 and pHLS21 were lysed as described in Section 2.3.2, and the total, soluble and insoluble protein fractions were then analysed by SDS-PAGE. The results shown in Figure 7.27 indicated that for cultures grown and induced at 37°C all three overproduced proteins were insoluble, as they were only present in the total and insoluble fractions. To try to improve protein solubility the induction was performed at a lower temperature (30°C) and with a reduced concentration of inducer (100 μM IPTG). However, all three recombinant proteins remained in the insoluble fraction (data not shown).

As Tpe1 contains nine cysteine residues, and it likely to be delivered to the periplasmic compartment of a target cell, it may contain disulphide bonds in its tertiary structure. Therefore, another strategy was undertaken in an attempt to improve protein solubility. This involved the use of a commercially available *E. coli* BL21-derived expression strain that has been engineered to improve folding of proteins containing di-sulphide bonds in the cytoplasm, SHuffle® T7 Express *lysY*

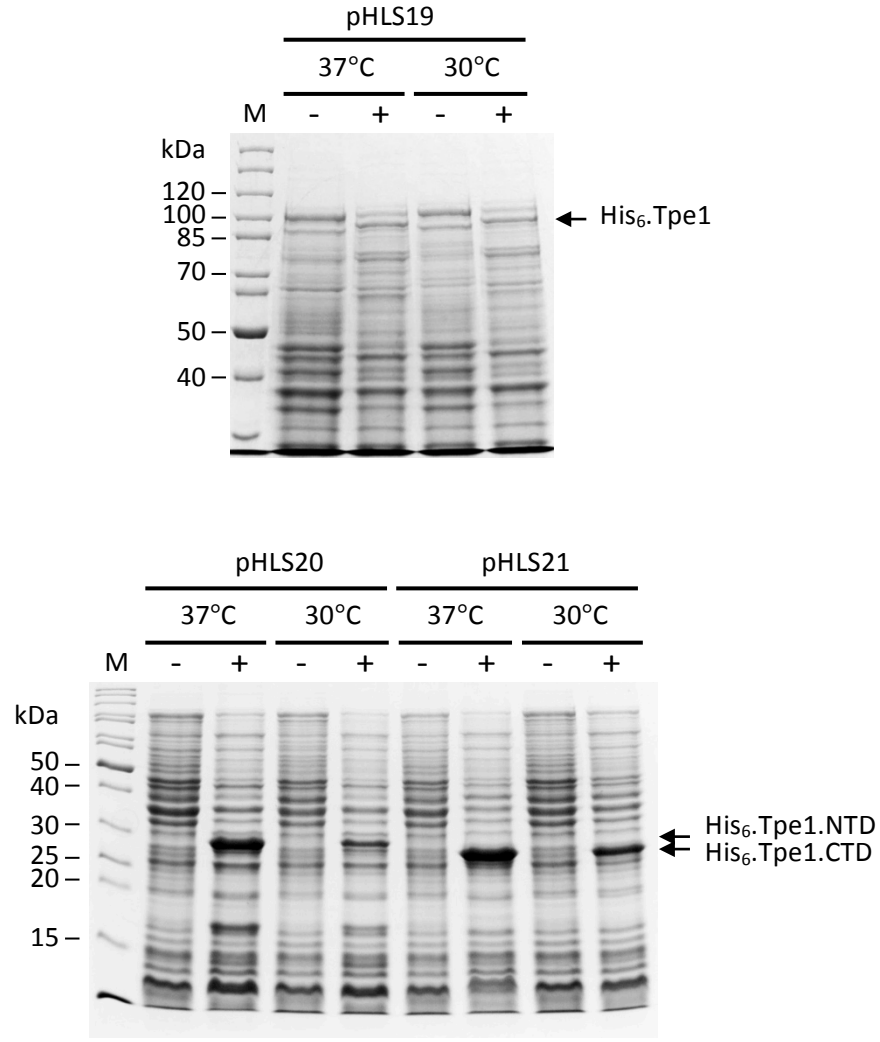

Figure 7.26 Analysis of His_6.Tpe1, His_6.Tpe1.NTD and His_6.Tpe1.CTD overproduction in *E. coli.* pHLS19, pHLS20 and pHLS21 were introduced into BL21(DE3) cells and resulting strains were grown to mid-log growth phase in BHI broth and then plasmid-encoded protein synthesis was induced with 1 mM IPTG at 30°C or 37°C for 3 hours. Image shows SDS-PAGE analysis of lysates from uninduced (-) and induced (+) cultures, as indicated. Labelled arrows indicate the identity of overproduced proteins following induction. M, EZ-Run *Rec* protein ladder.

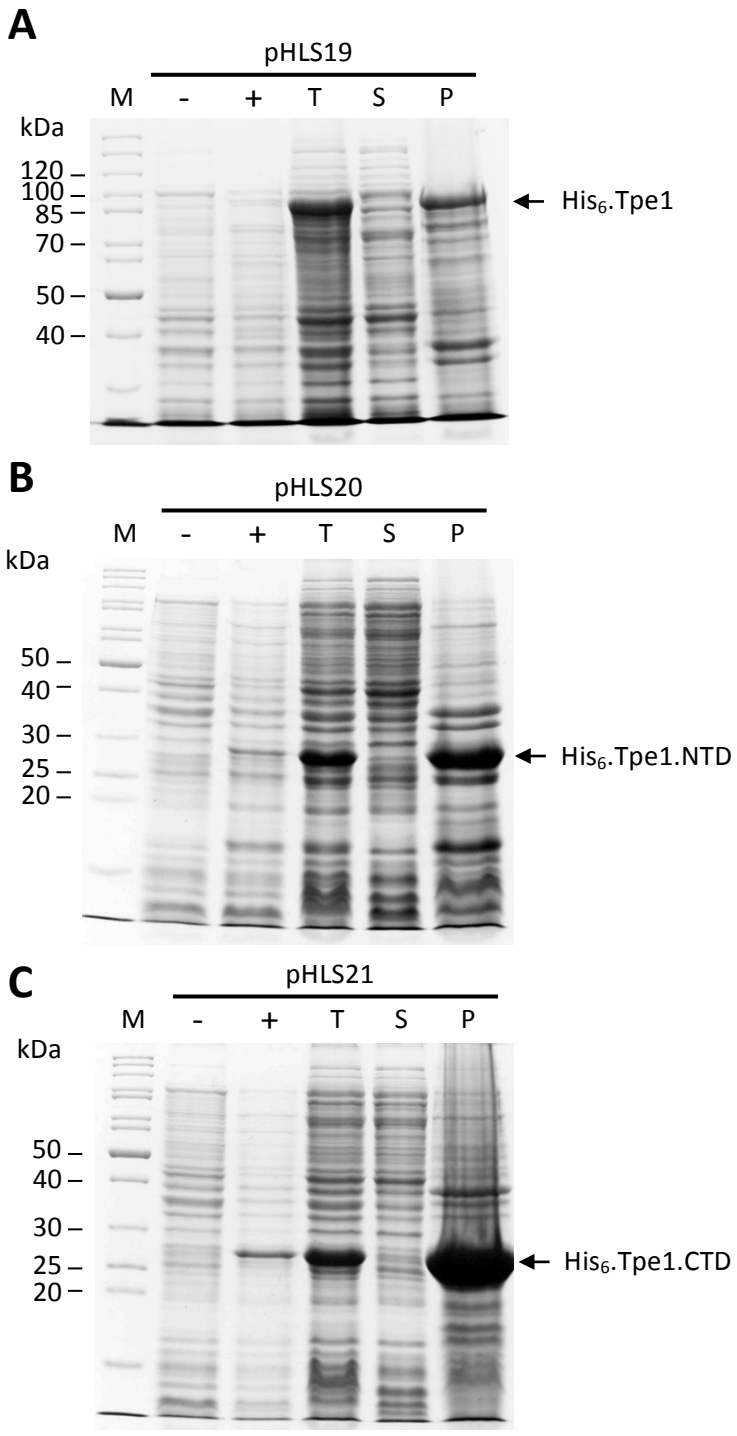

Figure 7.27 Analysis of His_6.Tpe1, His_6.Tpe1.NTD and His_6.Tpe1.CTD solubility following overproduction in BL21(DE3). Cultures of BL21(DE3) cells containing plasmids pHLS19, pHLS20 and pHLS21, specifying overproduction of His_6.Tpe1, His_6.Tpe1.NTD and His_6.Tpe1.CTD, respectively, were induced with 1 mM IPTG at 37°C for 3 hours. Cultures were lysed as standard protocol, and the resulting whole cell extracts, total (T), soluble (S) and insoluble (P) protein fractions from uninduced (-) and induced (+) cultures were separated by SDS-PAGE and the gels stained with Coomassie blue. Images show overproduction of (A) His_6.Tpe1, (B) His_6.Tpe1.NTD and (C) His_6.Tpe1.CTD, as indicated. M, EZ-Run *Rec* protein ladder.

cells. This *E. coli* strain carries nulls mutations in two genes encoding reductase enzymes, *trxB* and *gor*, a gene for the cytoplasmic targeting of disulphide bond isomerase DsbC, and a gene that encodes a suppressor mutant of the peroxidase AhpC that reinstates the viability of the cells (Derman et al., 1993; Ritz, 2001; Lobstein et al., 2012). This set of conditions favours redox enzymes (thioredoxins) to be in an oxidized stated, meaning they confer oxidation activity rather than reductase activity (Stewart et al., 1998), which in turn promotes the oxidation of sulfhydryl groups, generating stable disulphide bonds in the cytoplasm. Unfortunately, use of this expression strain did not improve the solubility of any of the Tpe1 recombinant proteins (Figure 7.28). Other strategies for producing soluble Tpe1 were not tested due to more fruitful areas of this study taking priority. Consequently, no further work was undertaken on this particular candidate effector.

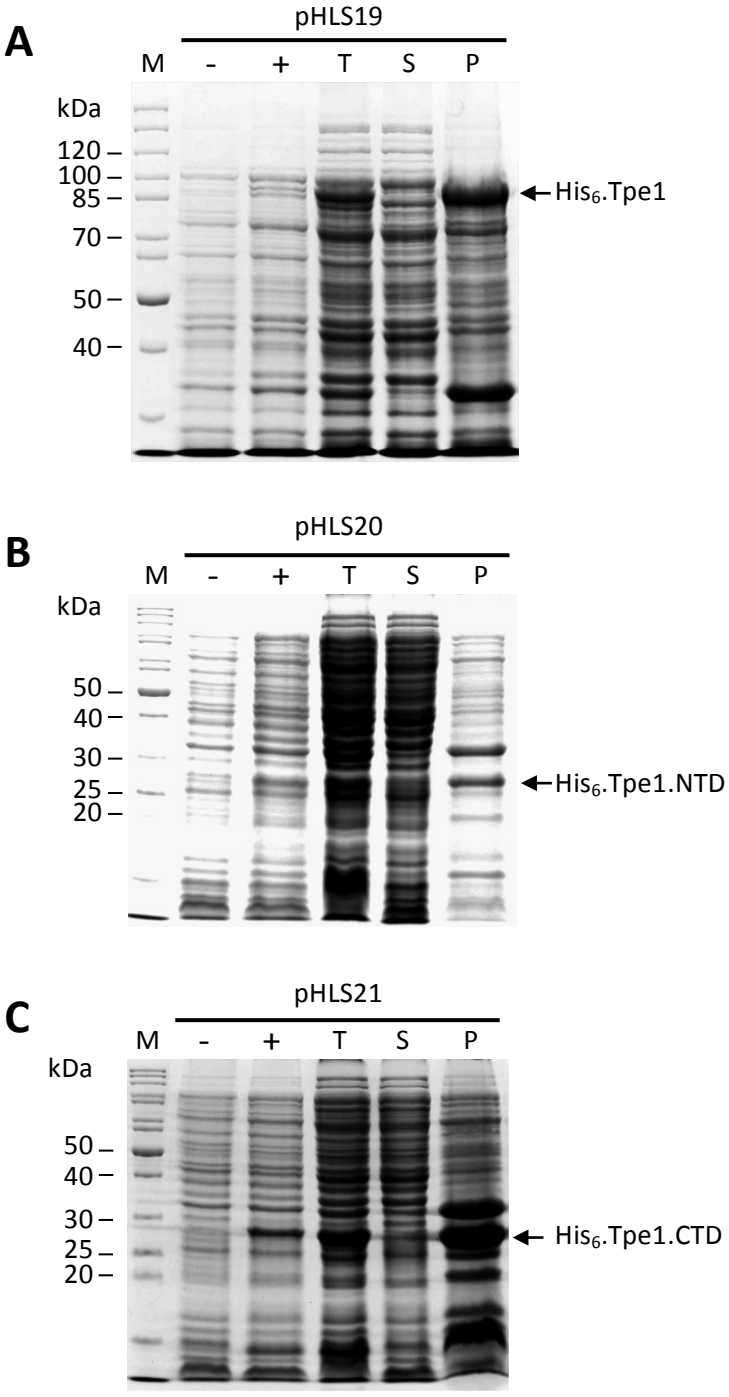

Figure 7.28 Analysis of His_6.Tpe1, His_6.Tpe1.NTD and His_6.Tpe1.CTD solubility following overproduction in SHuffle® T7 Express *lysY*. Cultures of SHuffle® T7 Express *lysY* cells containing plasmids pHLS19, pHLS20 and pHLS21, specifying overproduction of His_6.Tpe1, His_6.Tpe1.NTD and His_6.Tpe1.CTD, respectively, were induced with 1 mM IPTG at 30°C for 3 hours. Cultures were lysed as standard protocol, and the resulting whole cell extracts, total (T), soluble (S) and insoluble (P) protein fractions from uninduced (-) and induced (+) cultures were separated by SDS-PAGE and the gels stained with Coomassie blue. Images show overproduction of (A) His_6.Tpe1, (B) His_6.Tpe1.NTD and (C) His_6.Tpe1.CTD, as indicated. M, EZ-Run *Rec* protein ladder.

7.9 Discussion

7.9.1 $TssI_{0667}$ as an evolved TssI secreted by the *B. cenocepacia* T6SS

Secretion of TssI (VgrG) proteins that contain C-terminal extensions by other bacteria is well documented. Examples include VgrG-5 in the T6SS-5 of *B. thailandensis* and *B. pseudomallei,* which was shown to contained a CTD essential for virulence and membrane fusions between host cells (Burtnick et al., 2011; Schwarz et al., 2014; Toesca et al., 2014). Studies in *V. cholerae* have demonstrated that two of the three TssI subunits encoded within the bacteria possess C-terminal extensions and are secreted by the T6SS. VgrG-1 has a C-terminal actin cross-linking domain (Pukatzki et al., 2007) and VgrG-3 that has a CTD specifying peptidoglycan hydrolase activity (Pukatzki et al., 2007; Dong et al., 2013; Brooks et al., 2013). The putative evolved TssI protein encoded by BCAS0667 in *B. cenocepacia* discussed here has previously been demonstrated to have a C-terminal extension with phospholipase A_1 activity (Jones, 2012). So, consistent with other evolved TssI proteins, T6SS-dependent secretion of $TssI_{0667}$ by *B. cenocepacia* H111 has now been confirmed using immuno-detection. Thus, it is the first confirmed evolved TssI to be characterised with phospholipase activity at its C-terminus.

Unlike some characterised evolved TssI proteins, such as VgrG-1 in *V. cholerae* (Pukatzki et al., 2007), this study found that $TssI_{0667}$ was not essential for T6SS activity as determined by the secretion of TssD in a H111-ΔBCAS0667 mutant. This finding was not surprising, as *B. cenocepacia* encodes ten different TssI subunits encoded within its genome and it is unlikely that all ten are core structural subunits of the system. Furthermore, a very recent observation made by another group, that was published whilst writing this thesis, found that deletion of the ten *tssI* genes in *B. cenocepacia* K56-2 did not have an effect on TssD secretion when deleted individually, but deletion of all ten in the same strain abolished TssD secretion (Aubert et al., 2015). This validates the observation made in this study regarding deletion of the gene encoding $TssI_{0667}$ in H111. Similarly, the VgrG-3 subunit in *V. cholerae* was not essential for T6SS activity, nor were each individual VgrG1a, -b, and -c subunits in *P. aeruginosa* (Hachani et al., 2011).

Another factor regarding the secretion of $TssI_{0667}$ that is yet to be understood is whether the entire polypeptide is transported into the periplasm of the target cell, or whether the C-terminal phospholipase domain alone is released into the periplasm after proteolytic processing of the CTD from the core TssI region. If the latter were the case then this could involve the core TssI region remaining embedded/associated with the outer membrane of the target cell. The presence of a long linker-like region preceding the CTD also suggests this. It is possible that this linker is cleaved to release the phospholipase-specifying CTD of $TssI_{0667}$ into the periplasm. Evidence to support a proteolytically susceptible linker region comes from the presence a smaller anti-$TssI_{0667}$.CTD reactive protein of ~26 kDa (similar in size to the free Tle6 domain) that was present in the cell-associated fraction of *B. cenocepacia* by western blotting (data not shown). This fragment was more prevalent than the full-length $TssI_{0667}$ in the cell associated fraction, particularly in *B. cenocepacia* T6SS-deficient mutants (data not shown).

Evidence of a similar phenomenon of proteolytic cleavage has been suggested for the cytoplasmic delivery of the C-terminal toxin domains of CdiA proteins in the contact dependent inhibition system. It was observed that the entire CdiA protein is first transferred on to the surface of a target cell, where the N-terminal region of CdiA remains associated with the cell surface whilst the C-terminal is then translocated into the cytosol following cleavage, where it has to transverse the entire cell envelope (Webb et al., 2013).

7.9.2 $TssI_{0667}$ as an anti-bacterial effector

Over recent years there has been overwhelming evidence to suggest that the T6SS plays an anti-bacterial role. Superfamilies of T6SS-dependent effectors have been described that are thought to target bacterial cells by a variety of mechanisms, including peptidoglycan hydrolases, such as Tse1 (Tae1) and Tse3 (Tge1) (Hood et al., 2010; Russell et al., 2012), DNases such as Tde1 (Koskiniemi et al., 2013; Ma et al., 2014) as well as phospholipases such as Tle1 (Russell et al., 2013). Here, this study provides evidence to suggest that $TssI_{0667}$ also acts as an anti-bacterial effector, due to a decrease in the ability of a ΔBCAS0667 mutant to

inhibit growth or kill a different co-cultured bacterial strain. It is important to note that it is not known whether $TssI_{0667}$ is causing direct killing of its target or has a bacteriostatic effect.

The anti-bacterial nature of $TssI_{0667}$ was further validated by the observed toxic effect of directing its phospholipase domain (Tle6) to the *E. coli* periplasm, which was specifically related to the phospholipase activity of the protein. Interestingly, intracellular expression of the $TssI_{0667}$ Tle6 domain was not toxic, suggesting that the protein was only able to target the inner leaflet of the outer membrane and/or the outer leaflet of the cytoplasmic membrane of the *E. coli* cell envelope. These findings are consistent with the trans-kingdom phospholipase D effector of the *P. aeruginosa* H3-T6SS, PldB, as this was also observed to be toxic when targeted to the periplasm in *E. coli* but not when directed to the cytoplasm (Jiang et al., 2014). For further evidence of the lytic ability of $TssI_{0667}$ it would be useful to monitor cell viability by additional means, such as monitoring cell membrane integrity or redox potential.

One cannot rule out an additional role for $TssI_{0667}$ as a facilitator for the delivery of other T6SS effectors, as observed for VgrG1a, -b, and -c mediate bacterial killing in *P. aeruginosa*. The killing by each of those VgrG subunits requires a toxin protein encode downstream of the *vgrG* gene (Hachani et al., 2014). Furthermore, VgrG-1 in *V. cholerae* mediates killing by the $Tle1^{VC}$ phospholipase effector (Liang et al., 2015; Unterweger et al., 2015). So, there may be additional effectors that can attach onto $TssI_{0667}$ either directly or indirectly to be translocated into a target cell.

Alternatively, by delivery of $TssI_{0667}$ into the periplasm of competing bacterial cells, this may causes perturbations in either the outer or inner cell membrane that allows the movement of other effectors into to their periplasmic or cytoplasmic target sites. Therefore, the reduction in the competitive ability of the ΔBCAS0667 could well be due to prevention of other unknown anti-bacterial effectors being transported into the bacteria, rather than standalone effects of the phospholipase domain of $TssI_{0667}$. In this regard, it is interesting that predicted T6SS-dependent nuclease effectors, such as that encoded by BCAL1298 and

BCAS0663 in *B. cenocepacia* J2315 are encoded downstream of genes encoding predicted T6SS-dependent phospholipases, BCAL1296 and BCAS0667.

7.9.3 Phospholipase activity of $TssI_{0667}$

Interestingly, the phospholipase domain (Tle6) of $TssI_{0667}$ had been shown to have psychrophilic characteristics, with the optimum temperature for hydrolysis of a fatty acyl ester substrate, 4-nitrophenyl palmitate, of 10°C (Jones, 2012). However, evidence presented in this current study demonstrated a toxic effect of the Tle6 domain at temperatures far above this *in vitro* optimum. For example, periplasmically targeted synthesis of the $TssI_{0667}$ Tle6 domain in *E. coli* was carried out at 30°C. Furthermore, a phenotypic effect on bacterial competition with the ΔBCAS0667 mutant was observed at 30°C. Thus it is difficult to imagine how the psychrophilic characteristics of the Tle6 domain link in with these new findings. It could be argued that the distinct conditions of the periplasm, i.e. an oxidising environment, or presence of unknown additional chaperones or co-factors, may facilitate proper folding of the phospholipase domain of $TssI_{0667}$ to allow its full phospholipase activity to be demonstrated, which is not achieved when the $TssI_{0667}$ Tle6 domain is overproduced and purified from the cytoplasm.

It would be interesting to determine if a more profound effect on the bacterial competition ability of the ΔBCAS0667 mutant and/or lysis caused by periplasmic targeting of the Tle6 domain of $TssI_{0667}$ in *E. coli* is observed when lower incubation temperatures are used, to link in with the psychrophilic characteristics of the phospholipase domain.

7.9.4 Tli6 as an immunity protein to $TssI_{0667}$

Several characteristics of the protein encoded by BCAS0666, termed Tli6, suggested it might be an immunity protein against $TssI_{0667}$, which have been observed with other T6SS-dependent effectors and their cognate immunity proteins. This included the genomic location of BCAS0666 directly downstream of BCAS0667, the predicted periplasmic location of its protein product and the

presence of ankyrin-like repeats throughout the protein that may be involved in protein-protein interactions. This study found that presence of Tli6 in *E. coli* cells prevented the toxic lytic effect of the periplasmically targeted Tle6 phospholipase domain of $TssI_{0667}$ when co-produced, and that the two proteins were able to directly interact to form a stable complex. The latter was demonstrated by pull-down analysis and size exclusion chromatography. These results mirror those that demonstrated TsaB as the antitoxin to the evolved VgrG-3, VgrG-3 (Brooks et al., 2013; Zhang et al., 2014).

It is likely that Tli6 acts as an inhibitor by directly sequestering the $TssI_{0667}$ Tle6 domain, and thereby preventing it from binding to its target substrate, either by masking the catalytic domain or sterically occluding it. By analogy with the charged interaction surface between Tse2 and its immunity protein Tsi2 (Li et al., 2012), one might predict that a difference in surface charge between $TssI_{0667}$ and Tli6 is important for their interaction. The theoretical pI of the Tle6 domain of $TssI_{0667}$ is acidic (5.1), whereas Tli6 has a slightly basic theoretical pI (8.75). However, further investigations are needed to support this idea.

Furthermore, it is also required to confirm the loss of Tle6 phospholipase activity by complex formation with Tli6, which could be achieved by demonstrating direct inhibition of the fatty acyl esterase activity of $TssI_{0667}$ Tle6 domain by the addition of Tli6 *in vitro*.

It is interesting to consider how the immunity function of Tli6 fits in with secretion of $TssI_{0667}$. Does Tli6 prevent self-toxicity of the $TssI_{0667}$ Tl6 domain during transport through the cell envelope? Or is it just required for preventing toxicity to surrounding cells of the same species? Or is it a combination of the two? The former would imply that $TssI_{0667}$ is in complex with Tli6 during secretion. If this were so, the complex would need to dissociate before injection into the surrounding target bacteria. Recent evidence has demonstrated the structure of the purified TssJLM sub-complex. It forms a chamber-like structure that is embedded in the cytoplasmic membrane, transverses the periplasm and is associated with the outer membrane, with a base, arches and tip complex (Durand et al., 2015). This may suggest that when $TssI_{0667}$ is loaded onto the T6SS, it will reside in this chamber

structure and not be exposed to the periplasm of the producing bacterium (Figure 7.29) (Durand et al., 2015). Hence the Tli6 immunity protein would not be required/ associated with $TssI_{0667}$ during secretion of the effector.

For Tli6 to be considered a true immunity protein the ability of this protein to confer direct protection against $TssI_{0667}$ *in vivo* in *B. cenocepacia* will need to be evaluated. This would require the intra-species competition ability of wild-type, ΔBCAS0667 and ΔBCAS0667-BCAS0666 mutants to be assessed. A ΔBCAS0667 mutant was successfully constructed using the pEX18TpTer-*pheS* allelic replacement vector, but unfortunately a ΔBCAS0667-BCAS0666 mutant was unable to be generated using the same system. It appeared that either there was a problem with cPhe counter-selection of single recombinants that was unable to be rectified before submission of this work.

Alternatively, deletion of BCAS0666 may be lethal for some unforeseen reason, even though it was being deleted in combination with the cognate effector gene BCAS0667. If the latter was true then cross-immunity of Tli6 with other potential phospholipases could account for this. There is evidence to suggest some cross-immunity can be provided between different effector-immunity pairs in a peptidoglycan hydrolase effector superfamily, within and between subfamilies and bacterial species (Russell et al., 2012). However, this idea must be taken with caution as cross-immunity does not hold true for all T6SS-effector-immunity modules.

To summarise, the results presented here allow future development of a functional model of the novel evolved TssI protein, $TssI_{0667}$, in *B. cenocepacia*, depicted in Figure 7.30. The model presents $TssI_{0667}$ as a T6SS-dependent secreted protein that acts as an anti-bacterial effector, which likely targets the phospholipid membranes that face the periplasmic space via the phospholipase A_1 activity of its C-terminal extension. In surrounding sibling bacteria, the periplasmic protein Tli6 is able to prevent toxicity of periplasmically located $TssI_{0667}$ if it is injected into it by the T6SS of an attacking sibling. Tli6 does this by a direct interaction with the C-terminal phospholipase domain, forming a stable complex.

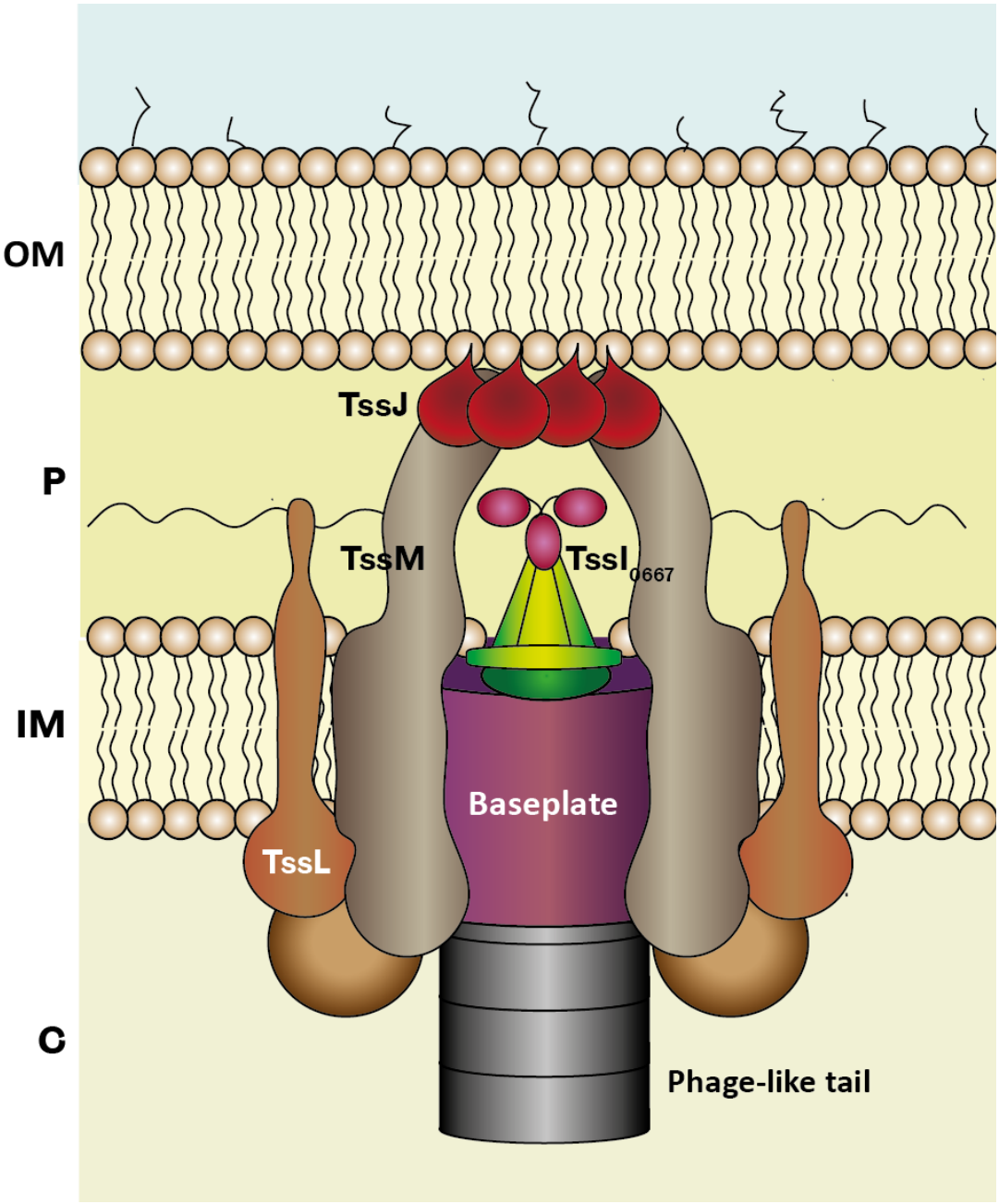

Figure 7.29 Model for shielding of $TssI_{0667}$ in the T6SS chamber. The TssI subunit may reside in a chamber structure created by the TssJLM sub-complex. This would mean that the phospholipase domain of $TssI_{0667}$ would not 'see' the periplasm of the T6SS-containing producer cell. Subunits as indicated by the labels. Individual baseplate and phage-like tail subunits unlabelled for simplicity. C, cytoplasm; IM, inner membrane; P, periplasm; OM, outer membrane.

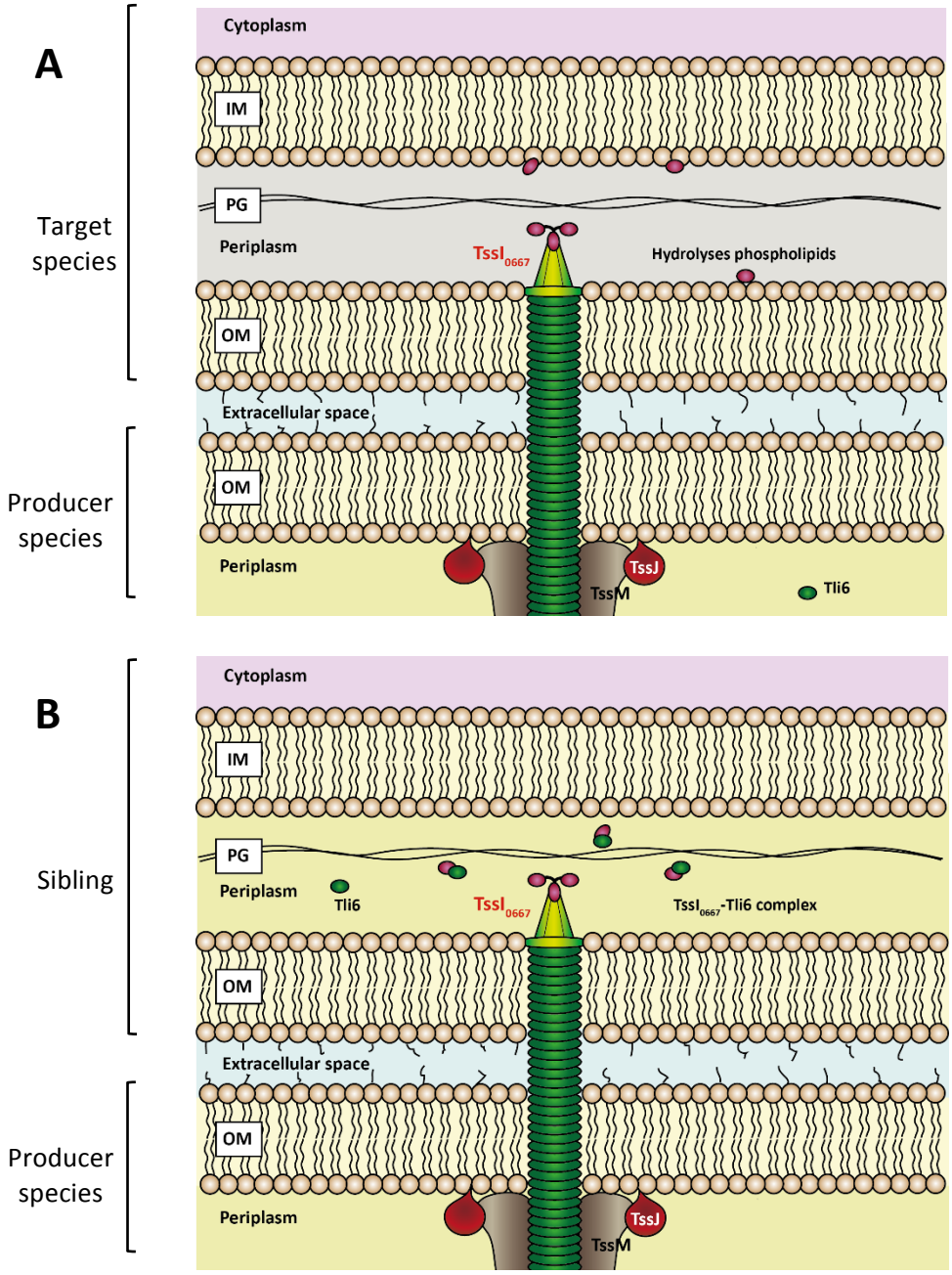

Figure 7.30 Proposed mode of action for the T6SS-dependent evolved TssI, $TssI_{0667}$ in *B. cenocepacia.* Image depicts the trimeric $TssI_{0667}$ subunit with a C-terminal extension domain that specify phospholipase A_1 activity. This subunit is affixed to the tip of a tubular structure in the T6SS complex. It is anticipated that either the core gp27gp5-like region in TssI trimerises with itself or with other TssI subunits. (A) In a co-culture, $TssI_{0667}$ is transported by the T6SS-proficent producer, *B. cenocepacia*, into the periplasm of surrounding target bacteria of a different species. The C-terminal phospholipase domain is able to target cellular membranes facing the periplasmic space, where it hydrolyses phospholipids. This compromises the integrity the cell membrane, resulting in death or bacteriostasis. (B) Protection from the toxic effect of $TssI_{0667}$ is inhibited by complex formation with periplasmic immunity protein Tli6, produced in surrounding sibling cells of the same strain as the producer. IM, inner membrane; OM, outer membrane; PG, peptidoglycan.

$TssI_{0667}$ may be the first evolved TssI to be characterised with phospholipase activity, but many other questions remain to be answered before there is a full understanding of this effector.

7.9.5 Purification of the putative peptidoglycan hydrolase effector Tpe1 and its domains- problems and possible solutions

Characterisation of another candidate T6SS-effector was pursued in this study, Tpe1. This was predicted to contain a M23 peptidase-like domain specifying amidase activity at its N-terminus, and a lysozyme-like domain conferring muramidase activity at its C-terminus. It was encoded by a gene directly downstream of a gene encoding a DUF2345-containing TssI protein. Unfortunately, the purification and characterisation of Tpe1 or its putative enzymatic domains was unable to be undertaken as they were produced as insoluble proteins in *E. coli*.

The insoluble nature of recombinant Tpe1 is in contrast to several T6SS peptidoglycan degrading effectors that have been overproduced and purified, including the amidase effectors Tse1 (Tae1) and Tae2 (Russell et al., 2011; Russell et al., 2012; Ding et al., 2012), further Tae effectors Ssp1 and Ssp2 (Tae4) in *S. marcescens* (English et al., 2012), and muramidase effectors Tse3 (Tge1) and Tge2 (Russell et al., 2011; Li et al., 2013; Whitney et al., 2013; Wang et al., 2013).

Tpe1 contains several cysteine residues so it is possible that for correct folding in the target cell periplasm the polypeptide requires formation of disulphide bridges, which are difficult to achieve in the cytoplasm. This may account for the insolubility of the protein. However, many if not all of characterised peptidoglycan hydrolases stated above also contain cysteine residues thus are also likely to require disulphide bond formation for proper folding. To overcome this many of these effectors were overproduced in *E. coli* expression strains that facilitated cytoplasmic disulphide bond formation. This included the SHuffle® expression host, used in several studies by the same group for production of different peptidoglycan hydrolase effectors (Russell et al., 2011; Russell et al., 2012; Whitney et al., 2013). This expression host was also utilised in this study for the overproduction of Tpe1,

however the recombinant proteins were still insoluble under the conditions tested (1 mM IPTG at 30°C for 3 hours).

The method described in Whitney et al. (2013), which used Shuffle® T7 Express *lysY* cells as the expression host, states induction of protein synthesis from pET expression series-derivatives was performed with 1 mM IPTG for 18 hours at room temperature. Furthermore, several studies that used BL21(DE3) as an expression host for overproduction of these types of effectors (and their immunity proteins) performed the induction with 50 μM IPTG overnight at 16°C (Zhang et al., 2013; Li et al., 2013; Wang et al., 2013). Retrospectively, the induction temperature and duration used for Tpe1 overproduction in both expression hosts tested may have been too short and performed at a too high temperature. Therefore, any future studies involving the overproduction of Tpe1 will need to take this into consideration. Additionally, an alternative solution could be to co-express the gene encoding the putative immunity protein of Tpe1, to determine if that helps improve solubility.

Chapter 8: Final discussion

8.1 General discussion

The overall aim of this study was to identify and characterise novel T6SS-dependent effectors in a *Burkholderia cepacia* complex species, *B. cenocepacia*, to help understand what role the ancestral T6SS plays in this organism and other members of the Bcc. As observed in a related but non-Bcc *Burkholderia* species, *B. thailandensis* (Schwarz et al., 2010), it was shown that selected *B. cenocepacia* strains had a constitutively active T6SS-1 which it used to compete against other bacterial species, including *P. putida* and *E. coli*. This is the first demonstration that T6SS-1 in a Bcc member plays a role in inter-bacterial competition. This observation also further adds to the catalogue of Gram-negative bacteria that use a specific T6SS for bacterial interactions, including but not exclusively, the H1-T6SS in *P. aeruginosa* and the single T6SSs in *V. cholerae*, *A. tumefaciens* and *S. marcescens* (Hood et al., 2010; MacIntyre et al., 2010; Murdoch et al., 2011; Ma et al., 2014). The natural reservoir of *B. cenocepacia* is within the environment, particularly in soil around plant root systems (the rhizosphere), where many other bacteria vie for a foothold. Hence, it is unsurprising that *B. cenocepacia* has evolved a mechanism for competitive fitness against other bacteria, particular if it has to survive in an environment where other microorganisms are competing for the same biological niches.

This study attributed some of the competition advantage the T6SS provides to *B. cenocepacia* on a T6SS-dependent evolved TssI protein, $TssI_{0667}$, with a C-terminal extension that possesses enzymatic activity similar to the anti-bacterial Tle phospholipase superfamily of effectors (Russell et al., 2013). In contrast, this investigation could not assign an anti-bacterial role to a putative T6SS-dependent nuclease effector, $TanB^{H}$, even-though T6SS-dependent nucleases used for inter- or intra-species bacterial competition by *S. marcescens* and *P. aeruginosa* and for bacterial competition *in planta* by *A. tumefaciens* have been described (Hachani et al., 2014; Ma et al., 2014; Diniz and Coulthurst, 2015).

Rather than playing an anti-bacterial role, some T6SSs have been implicated in interactions with eukaryotes. This includes a T6SS cluster encoded in a more

pathogenic *Burkholderia* species *B. pseudomallei* that is required for intracellular survival of the bacteria within a host cell, typically in phagocytes (Shalom et al., 2007; Burtnick et al., 2011). This occurs specifically via the T6SS-5, which is not encoded in Bcc bacteria. Despite this, *B. cenocepacia* and other Bcc bacteria are still able to survival intracellularly within membrane-bound vacuoles (BcCVs) in both professional phagocytes such as macrophages (Saini et al., 1999) and non-professional phagocytes such as epithelial cells (Burns et al., 1996; Sajjan et al., 2006).

The detection of intracellular *B. cenocepacia* is sensed by the cytosolic pyrin inflammasome, which leads to the secretion of pro-inflammatory cytokines following caspase-1 activation, including IL-1β, and thus leads to an inflammatory response. Chronic inflammation in the lungs of CF-patients infected with *B. cenocepacia* is common. Interestingly, it was shown that an active T6SS-1 is required for pyrin inflammasome activation and thus IL-1β secretion in response to intracellular *B. cenocepacia* (Gavrilin et al., 2012). The T6SS-1 induces this response by increasing the amount of active (i.e. GTP-bound) RhoA (Rosales-Reyes et al., 2012b) through deamination of residue Asn21 in the protein (Xu et al., 2014).

There is evidence to suggest that the T6SS-1 is able to puncture the BcCV membrane to release T2SS-dependent effectors from the extracellular milieu of BcCVs into the cytosol, and this event contributes to the activate of the pyrin inflammasome as inferred by IL-β secretion (Rosales-Reyes et al., 2012a). It is currently unknown whether inactivation of the T2SS in *B. cenocepacia* has a direct effect on pyrin activation through deamination of RhoA, but it has been shown to decrease IL-1β secretion similar to that observed upon inactivation of the T6SS (Rosales-Reyes et al., 2012a). If inactivation of the *B. cenocepacia* T2SS did prove to directly affect the deamination of RhoA and in turn affect pyrin inflammasome activation, this would suggest that rather than an effector being secreted directly into the cytosol by the T6SS, T6SS-faciliated leakage of the BcCV contents, including T2SS secreted substrates, into the cytosol may be responsible for inflammasome activation (Rosales-Reyes et al., 2012a).

Although T6SS-1 has been implicated in subverting eukaryotic cells, either directly or indirectly, the results of this study did not demonstrate an obvious role for this system in pathogenicity towards eukaryotic organisms. T6SS-defective mutants all showed a similar overall virulence as the wild-type strain in a zebrafish embryo infection model and a *G. mellonella* larvae model. Both of these organisms are used to model innate immune responses to infection, as they have primitive phagocytic cells and other anti-microbial defences. Taking into consideration the observations regarding T6SS-dependent inflammasome activation and T2SS-dependent IL-1β secretion in phagocytic cells (Rosales-Reyes et al., 2012a; Gavrilin et al., 2012; Xu et al., 2014), one could argue that inactivation of the T6SS may not affect the overall virulence of the bacterium in *vivo*, but the host may show a delayed inflammatory response to strains lacking T6SS-1. A T6SS mutant may still eventually activate the pyrin inflammasome if the toxin that causes this activation is not T6SS-dependent but is able to escape into the cytosol of host cells in a T6SS-independent manner, e.g. T2SS substrate (Rosales-Reyes et al., 2012a). This study did however provide preliminary evidence suggesting T6SS-deficent mutants may have a slight lag-phase in *G. mellonella* larvae killing in comparison to the wild-type strain. This may coincide with a delayed immune response in the larvae.

8.2 Future work

This study has opened up several avenues of investigations that can be further explored in relation to the role of T6SS-1 in Bcc bacteria. First, for firm evidence for the role of the T6SS-1 in bacterial competitive in *B. cenocepacia* the T6SS mutants need to be genetically complemented. The same applies to the observations in the *G. mellonella* larvae infection assays. For further evaluation of the function of T6SS-1 in *B. cenocepacia* it would be interesting to determine (i) whether there are other bacterial species that are more susceptible to the anti-bacterial activity of *B. cenocepacia;* (ii) whether there is a target cell or experimental conditions that can induce T6SS activity in *B. cenocepacia* strains that do not show a constitutively active T6SS-1, such as Pc715j; and (iii) whether T6SS mutants show any difference in their pathogenicity in other innate immune response infection models, such as *C. elegans or D. discoideum*, and plant infection models such as *A. thaliana* or alfalfa seedlings. This may shed light on the observation of T6SS-dependent pyrin inflammasome activation by intracellular *B. cenocepacia* in eukaryotic host cells. It would also be fascinating to investigate whether effectors secreted by other secretion system, such as the T2SS, co-ordinate with the T6SS to leak effectors from BcCVs into the cytosol of infected cells.

It is also intriguing that the *B. cenocepacia* H111 strain shows greater constitutive levels of T6SS expression than other *B. cenocepacia* strains tested in this study and it would be interesting to elucidate the reasons for this phenomenon. One possible reason could be the lack of the CciIR quorum regulatory system in H111, thought to be a negative regulator of T6SS cluster expression. Also in regards to regulation, as this study demonstrated that deletion of *tagF* had a positive effect on T6SS activity in some cases, this could be an additional avenue to explore, particularly because TagF is also found in T6SS gene clusters that do not have a *fha1* homologue. That is, TagF may also function though an alternative pathway that does not involve Fha1 as described for *P. aeruginosa* H1-T6SS.

Moreover, there are numerous paths to be explored regarding both of the

putative effectors and their immunity proteins described in this study. In particular, the verification of both Tli6 and TaaB1^{H} as bona fide immunity proteins to their effector proteins needs to be established by performing intraspecies competition experiments between mutants with and without the effector-immunity pairs.

Furthermore, investigation into the secretion and/or localisation of TanB^{H} by the T6SS is a priority area of investigation, and will be addressed either by direct detection of the protein by immuno-blotting or mass spectrometry methods, or inferred by intraspecies competition assays. Confirmation of the interaction between putative chaperone protein TagA and TanB^{H} would also be beneficial, as well as further exploration of the putative role of TagA as a chaperone by ascertaining whether or not it is able to interact with other core T6SS components.

Overall, it is clear there is significant work still to be carried out to fully understand the role played by the T6SS-1 in *B. cenocepacia* and the effectors it secretes. Nevertheless, this work, and the work of others have begun to uncover potential roles for this secretion system in *B. cenocepacia* and other Bcc bacteria, as well as providing insights into the potential effectors its secretes. A better understanding of these factors is vital to gain awareness into the potential mechanisms Bcc bacteria use, in both pathogenesis and environmental adaptation in their biological niches, which could be exploited in the future.

Appendices

Appendix 1

DNA and protein ladders

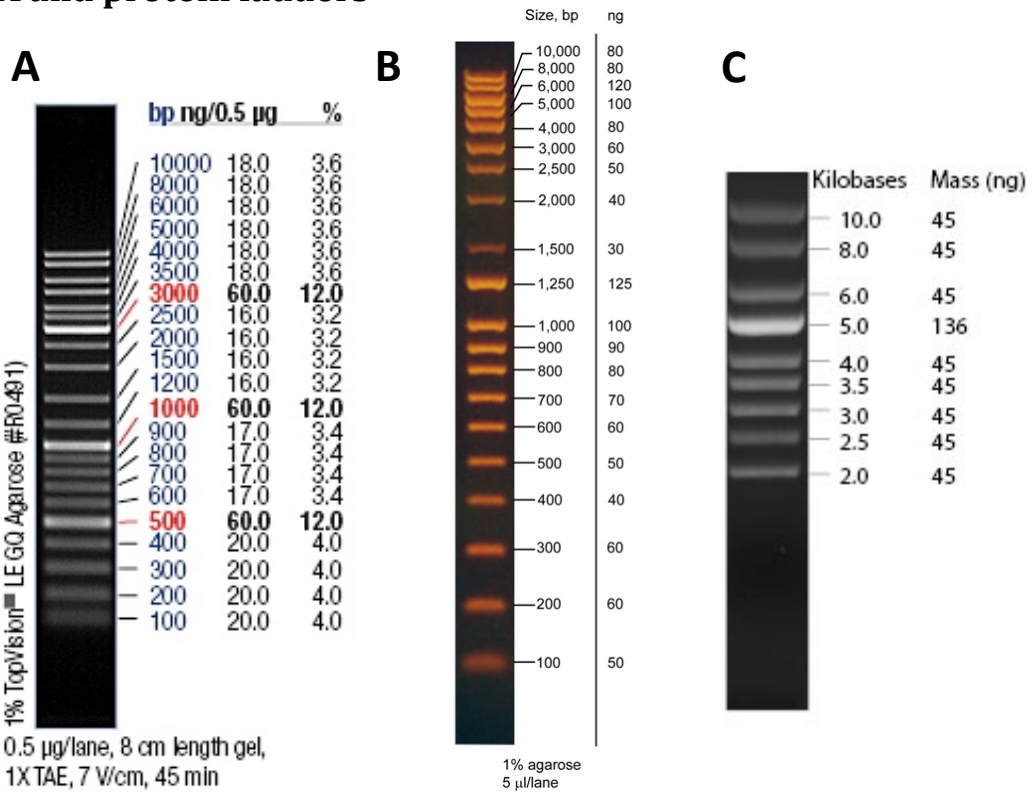

Reference DNA ladders used in this study. Images of DNA ladders supplied by the manufacturer, indicating the fragment sizes in bp or kbp and relative DNA concentration in ng for each DNA fragment, as indicated. (A) GeneRuler DNA ladder mix, (B) Q-Step 4 Quantitative DNA Ladder and (C) Supercoiled DNA ladder.

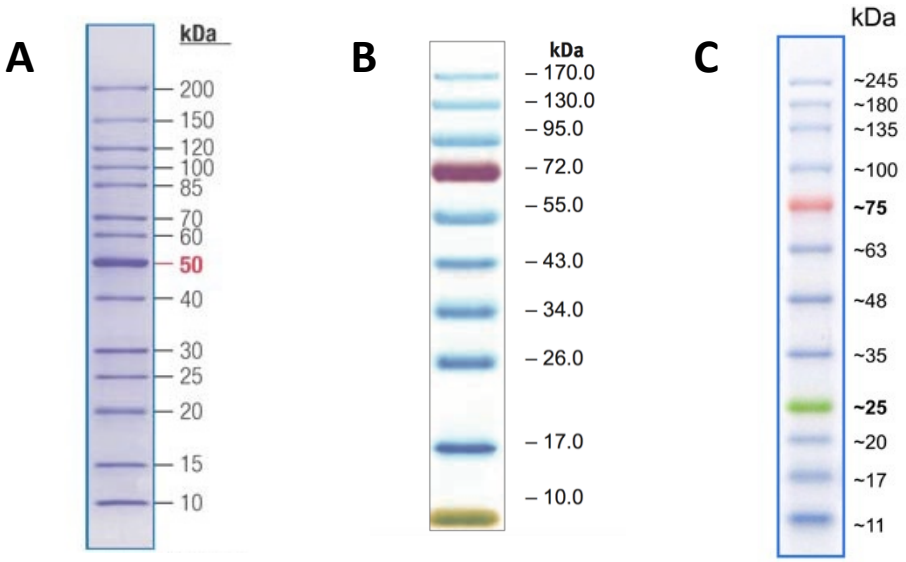

Reference protein ladders used in this study. Images of protein ladders supplied by the manufacturer, indicating the estimated molecular mass of each protein in the ladder following electrophoresis in a 4-20% gradient SDS-PA gel. (A) EZ-Run *Rec* Protein Ladder and (B) EZ-Run Prestained *Rec* Protein Ladder (C) BLUeye Prestained Protein ladder.

Bibliography

ABDALLAH, A.M., GEY VAN PITTIUS, N.C., CHAMPION, P.A.D., COX, J., LUIRINK, J., VANDENBROUCKE-GRAULS, C.M.J.E., APPELMELK, B.J. & BITTER, W., 2007. Type VII secretion--mycobacteria show the way. *Nature Reviews. Microbiology*, 5(11), pp.883–91.

ABE, M. & NAKAZAWA, T., 1994. Characterization of hemolytic and antifungal substance, cepalycin, from Pseudomonas cepacia. *Microbiology and Immunology*, 38(1), pp.1–9.

ABRAHAM, S.N., SUN, D., DALE, J.B. & BEACHEY, E.H., 1988. Conservation of the D-mannose-adhesion protein among type 1 fimbriated members of the family Enterobacteriaceae. *Nature*, 336(6200), pp.682–4.

ADHYA, S. & GOTTESMAN, M., 1982. Promoter occlusion: transcription through a promoter may inhibit its activity. *Cell*, 29(3), pp.939–44.

AGNOLI, K., FRAUENKNECHT, C., FREITAG, R., SCHWAGER, S., JENUL, C., VERGUNST, A., CARLIER, A. & EBERL, L., 2014. The Third Replicon of Members of the Burkholderia cepacia Complex, Plasmid pC3, Plays a Role in Stress Tolerance. *Applied and Environmental Microbiology*, 80(4), pp.1340–8.

AGNOLI, K., SCHWAGER, S., UEHLINGER, S., VERGUNST, A., VITERI, D.F., NGUYEN, D.T., SOKOL, P.A., CARLIER, A. & EBERL, L., 2012. Exposing the third chromosome of Burkholderia cepacia complex strains as a virulence plasmid. *Molecular Microbiology*, 83(2), pp.362–78.

AGODI, A., MAHENTHIRALINGAM, E., BARCHITTA, M., GIANNINÒ, V., SCIACCA, A. & STEFANI, S., 2001. Burkholderia cepacia complex infection in Italian patients with cystic fibrosis: prevalence, epidemiology, and genomovar status. *Journal of Clinical Microbiology*, 39(8), pp.2891–6.

AHMAD, A., 2013. Protein-protein interactions in the bacterial type VI secretion system. Ph.D thesis, The University of Sheffield.

AKEDA, Y. & GALÁN, J.E., 2005. Chaperone release and unfolding of substrates in type III secretion. *Nature*, 437(7060), pp.911–5.

ALAMI, M., LÜKE, I., DEITERMANN, S., EISNER, G., KOCH, H.-G., BRUNNER, J. & MÜLLER, M., 2003. Differential interactions between a twin-arginine signal peptide and its translocase in Escherichia coli. *Molecular Cell*, 12(4), pp.937–46.

ALTING-MEES, M.A. & SHORT, J.M., 1989. pBluescript II: gene mapping vectors. *Nucleic Acids Research*, 17(22), p.9494.

AMÁBILE-CUEVAS, C.F. & DEMPLE, B., 1991. Molecular characterization of the soxRS genes of Escherichia coli: two genes control a superoxide stress regulon. *Nucleic Acids Research*, 19(16), pp.4479–84.

ANDRADE, A. & VALVANO, M.A., 2014. A Burkholderia cenocepacia gene encoding a non-functional tyrosine phosphatase is required for the delayed maturation of the bacteria-containing vacuoles in macrophages. *Microbiology (Reading,*

England), 160(Pt 7), pp.1332–45.

ANDREEVA, A., HOWORTH, D., CHANDONIA, J.-M., BRENNER, S.E., HUBBARD, T.J.P., CHOTHIA, C. & MURZIN, A.G., 2007. Data growth and its impact on the SCOP database: new developments. *Nucleic Acids Research*, 36(Database), pp.D419–D425.

ANGUS, A.A., AGAPAKIS, C.M., FONG, S., YERRAPRAGADA, S., ESTRADA-DE LOS SANTOS, P., YANG, P., SONG, N., KANO, S., CABALLERO-MELLADO, J., DE FARIA, S.M., DAKORA, F.D., WEINSTOCK, G. & HIRSCH, A.M., 2014. Plant-associated symbiotic Burkholderia species lack hallmark strategies required in mammalian pathogenesis. *PloS One*, 9(1), p.e83779.

ARORA, S.K., NEELY, A.N., BLAIR, B., LORY, S. & RAMPHAL, R., 2005. Role of motility and flagellin glycosylation in the pathogenesis of Pseudomonas aeruginosa burn wound infections. *Infection and Immunity*, 73(7), pp.4395–8.

ASCHTGEN, M.-S., BERNARD, C.S., DE BENTZMANN, S., LLOUBÈS, R. & CASCALES, E., 2008. SciN is an outer membrane lipoprotein required for type VI secretion in enteroaggregative Escherichia coli. *Journal of Bacteriology*, 190(22), pp.7523–31.

ASCHTGEN, M.-S., GAVIOLI, M., DESSEN, A., LLOUBÈS, R. & CASCALES, E., 2010a. The SciZ protein anchors the enteroaggregative Escherichia coli Type VI secretion system to the cell wall. *Molecular Microbiology*, 75(4), pp.886–99.

ASCHTGEN, M.-S., THOMAS, M.S. & CASCALES, E., 2010b. Anchoring the type VI secretion system to the peptidoglycan: TssL, TagL, TagP…what else? *Virulence*, 1(6).

AUBERT, D.F., FLANNAGAN, R.S. & VALVANO, M.A., 2008. A novel sensor kinase-response regulator hybrid controls biofilm formation and type VI secretion system activity in Burkholderia cenocepacia. *Infection and Immunity*, 76(5), pp.1979–91.

AUBERT, D.F., HU, S. & VALVANO, M.A., 2015. Quantification of Type VI secretion system activity in macrophages infected with Burkholderia cenocepacia. *Microbiology (Reading, England)*.

AUBERT, D.F., O'GRADY, E.P., HAMAD, M.A., SOKOL, P.A. & VALVANO, M.A., 2012. The Burkholderia cenocepacia sensor kinase hybrid AtsR is a global regulator modulating quorum-sensing signalling. *Environmental Microbiology*.

BAGDASARIAN, M., LURZ, R., RÜCKERT, B., FRANKLIN, F.C.H., BAGDASARIAN, M.M., FREY, J. & TIMMIS, K.N., 1981. Specific-purpose plasmid cloning vectors II. Broad host range, high copy number, RSF 1010-derived vectors, and a host-vector system for gene cloning in Pseudomonas. *Gene*, 16(1-3), pp.237–247.

BAKKES, P.J., JENEWEIN, S., SMITS, S.H.J., HOLLAND, I.B. & SCHMITT, L., 2010. The rate of folding dictates substrate secretion by the Escherichia coli hemolysin type 1 secretion system. *The Journal of Biological Chemistry*, 285(52), pp.40573–80.

BALAKRISHNAN, L., HUGHES, C. & KORONAKIS, V., 2001. Substrate-triggered recruitment of the TolC channel-tunnel during type I export of hemolysin by Escherichia coli. *Journal of Molecular Biology*, 313(3), pp.501–10.

BALDWIN, A., SOKOL, P.A., PARKHILL, J. & MAHENTHIRALINGAM, E., 2004. The Burkholderia cepacia epidemic strain marker is part of a novel genomic island encoding both virulence and metabolism-associated genes in Burkholderia cenocepacia. *Infection and Immunity*, 72(3), pp.1537–47.

BALLY, M., FILLOUX, A., AKRIM, M., BALL, G., LAZDUNSKI, A. & TOMMASSEN, J., 1992. Protein secretion in Pseudomonas aeruginosa: characterization of seven xcp genes and processing of secretory apparatus components by prepilin peptidase. *Molecular Microbiology*, 6(18), pp.2745–2745.

BARDWELL, J.C., MCGOVERN, K. & BECKWITH, J., 1991. Identification of a protein required for disulfide bond formation in vivo. *Cell*, 67(3), pp.581–9.

BARNHART, M.M. & CHAPMAN, M.R., 2006. Curli biogenesis and function. *Annual Review of Microbiology*, 60, pp.131–47.

BARRET, M., EGAN, F., FARGIER, E., MORRISSEY, J.P. & O'GARA, F., 2011. Genomic analysis of the type VI secretion systems in Pseudomonas spp.: novel clusters and putative effectors uncovered. *Microbiology (Reading, England)*, 157(Pt 6), pp.1726–39.

BARRETT, A.R., KANG, Y., INAMASU, K.S., SON, M.S., VUKOVICH, J.M. & HOANG, T.T., 2008. Genetic tools for allelic replacement in Burkholderia species. *Applied and Environmental Microbiology*, 74(14), pp.4498–508.

BASLER, M., HO, B.T. & MEKALANOS, J.J., 2013. Tit-for-Tat: Type VI Secretion System Counterattack during Bacterial Cell-Cell Interactions. *Cell*, 152(4), pp.884–894.

BASLER, M. & MEKALANOS, J.J., 2012. Type 6 secretion dynamics within and between bacterial cells. *Science (New York, N.Y.)*, 337(6096), p.815.

BASLER, M., PILHOFER, M., HENDERSON, G.P., JENSEN, G.J. & MEKALANOS, J.J., 2012. Type VI secretion requires a dynamic contractile phage tail-like structure. *Nature*, 483(7388), pp.182–6.

BELIAEVA, M.I., KAPRANOVA, M.N., VITOL, M.I., GOLUBENKO, I.A. & LESHCHINSKAIA, I.B., 1976. [Nucleic acids utilized as the main source of bacterial nutrition]. *Mikrobiologiia*, 45, pp.420–4.

BENEDIK, M.J. & STRYCH, U., 1998. Serratia marcescens and its extracellular nuclease. *FEMS Microbiology Letters*, 165(1), pp.1–13.

BENSADOUN, A. & WEINSTEIN, D., 1976. Assay of proteins in the presence of interfering materials. *Analytical Biochemistry*, 70(1), pp.241–250.

BERNARD, C.S., BRUNET, Y.R., GUEGUEN, E. & CASCALES, E., 2010. Nooks and crannies in type VI secretion regulation. *Journal of Bacteriology*, 192(15), pp.3850–60.

BERNIER, S.P., NGUYEN, D.T. & SOKOL, P.A., 2008. A LysR-type transcriptional regulator in Burkholderia cenocepacia influences colony morphology and virulence. *Infection and Immunity*, 76(1), pp.38–47.

BIERTÜMPFEL, C., YANG, W. & SUCK, D., 2007. Crystal structure of T4 endonuclease VII resolving a Holliday junction. *Nature*, 449(7162), pp.616–20.

BINGLE, L.E., BAILEY, C.M. & PALLEN, M.J., 2008. Type VI secretion: a beginner's guide. *Current Opinion in Microbiology*, 11(1), pp.3–8.

BLATCH, G.L. & LÄSSLE, M., 1999. The tetratricopeptide repeat: a structural motif mediating protein-protein interactions. *BioEssays : News and Reviews in Molecular, Cellular and Developmental Biology*, 21(11), pp.932–9.

BLOCKER, A., GOUNON, P., LARQUET, E., NIEBUHR, K., CABIAUX, V., PARSOT, C. & SANSONETTI, P., 1999. The tripartite type III secreton of Shigella flexneri inserts IpaB and IpaC into host membranes. *The Journal of Cell Biology*, 147(3), pp.683–93.

BLOKESCH, M. & SCHOOLNIK, G.K., 2008. The extracellular nuclease Dns and its role in natural transformation of Vibrio cholerae. *Journal of Bacteriology*, 190(21), pp.7232–40.

BLONDEL, C.J., JIMÉNEZ, J.C., CONTRERAS, I. & SANTIVIAGO, C.A., 2009. Comparative genomic analysis uncovers 3 novel loci encoding type six secretion systems differentially distributed in Salmonella serotypes. *BMC Genomics*, 10, p.354.

BLOODWORTH, R.A.M., GISLASON, A.S. & CARDONA, S.T., 2013. Burkholderia cenocepacia conditional growth mutant library created by random promoter replacement of essential genes. *MicrobiologyOpen*, 2(2), pp.243–58.

BOLHUIS, A., MATHERS, J.E., THOMAS, J.D., BARRETT, C.M. & ROBINSON, C., 2001. TatB and TatC form a functional and structural unit of the twin-arginine translocase from Escherichia coli. *The Journal of Biological Chemistry*, 276(23), pp.20213–9.

BÖNEMANN, G., PIETROSIUK, A., DIEMAND, A., ZENTGRAF, H. & MOGK, A., 2009. Remodelling of VipA/VipB tubules by ClpV-mediated threading is crucial for type VI protein secretion. *The EMBO Journal*, 28(4), pp.315–25.

BORK, P., 1993. Hundreds of ankyrin-like repeats in functionally diverse proteins: mobile modules that cross phyla horizontally? *Proteins*, 17(4), pp.363–74.

BOWERS, J.H., 1993. Epidemiology of Pythium Damping-off and Aphanomyces Root Rot of Peas After Seed Treatment with Bacterial Agents for Biological Control. *Phytopathology*, 83(12), p.1466.

BRADY, L., BRZOZOWSKI, A.M., DEREWENDA, Z.S., DODSON, E., DODSON, G., TOLLEY, S., TURKENBURG, J.P., CHRISTIANSEN, L., HUGE-JENSEN, B. & NORSKOV, L., 1990. A serine protease triad forms the catalytic centre of a triacylglycerol lipase. *Nature*, 343(6260), pp.767–70.

BRENCIC, A. & LORY, S., 2009. Determination of the regulon and identification of novel mRNA targets of Pseudomonas aeruginosa RsmA. *Molecular Microbiology*, 72(3), pp.612–32.

BROOKS, T.M., UNTERWEGER, D., BACHMANN, V., KOSTIUK, B. & PUKATZKI, S., 2013. Lytic activity of the Vibrio cholerae type VI secretion toxin VgrG-3 is inhibited by the antitoxin TsaB. *The Journal of Biological Chemistry*, 288(11), pp.7618–25.

BROWNING, C., SHNEIDER, M.M., BOWMAN, V.D., SCHWARZER, D. & LEIMAN, P.G., 2012. Phage pierces the host cell membrane with the iron-loaded spike. *Structure*

(London, England : 1993), 20(2), pp.326–39.

BRUNDAGE, L., HENDRICK, J.P., SCHIEBEL, E., DRIESSEN, A.J.M. & WICKNER, W., 1990. The purified E. coli integral membrane protein SecYE is sufficient for reconstitution of SecA-dependent precursor protein translocation. *Cell*, 62(4), pp.649–657.

BRUNET, Y.R., BERNARD, C.S., GAVIOLI, M., LLOUBÈS, R. & CASCALES, E., 2011. An epigenetic switch involving overlapping fur and DNA methylation optimizes expression of a type VI secretion gene cluster. *PLoS Genetics*, 7(7), p.e1002205.

BRUNET, Y.R., HÉNIN, J., CELIA, H. & CASCALES, E., 2014. Type VI secretion and bacteriophage tail tubes share a common assembly pathway. *EMBO Reports*, 15(3), pp.315–21.

BUCHER, G.E., 1963. Survival of populations of Streptococcus faecalis Andrewes and Horder in the gut of Galleria mellonella (Linnaeus) during metamorphosis, and transmission to the filial generation of the host. *Journal of Insect Pathology*, 5, pp.336–343.

BUCHER, G.E. & WILLIAMS, R., 1967. The microbial flora of laboratory cultures of the greater wax moth and its effect on rearing parasites. *Journal of Invertebrate Pathology*, 9(4), pp.467–473.

BURKHOLDER, W., 1950. Sour skin, a bacterial root of onion bulbs. *Phytopathology*, 64, pp.468–75.

BURNS, J.L., JONAS, M., CHI, E.Y., CLARK, D.K., BERGER, A. & GRIFFITH, A., 1996. Invasion of respiratory epithelial cells by Burkholderia (Pseudomonas) cepacia. *Infection and Immunity*, 64(10), pp.4054–9.

BURTNICK, M.N., BRETT, P.J. & DESHAZER, D., 2014. Proteomic analysis of the Burkholderia pseudomallei type II secretome reveals hydrolytic enzymes, novel proteins, and the deubiquitinase TssM. *Infection and Immunity*, 82(8), pp.3214–26.

BURTNICK, M.N., BRETT, P.J., HARDING, S. V, NGUGI, S.A., RIBOT, W.J., CHANTRATITA, N., SCORPIO, A., MILNE, T.S., DEAN, R.E., FRITZ, D.L., PEACOCK, S.J., PRIOR, J.L., ATKINS, T.P. & DESHAZER, D., 2011. The cluster 1 type VI secretion system is a major virulence determinant in Burkholderia pseudomallei. *Infection and Immunity*, 79(4), pp.1512–25.

BURTNICK, M.N., DESHAZER, D., NAIR, V., GHERARDINI, F.C. & BRETT, P.J., 2010. Burkholderia mallei cluster 1 type VI secretion mutants exhibit growth and actin polymerization defects in RAW 264.7 murine macrophages. *Infection and Immunity*, 78(1), pp.88–99.

BUSBY, J.N., PANJIKAR, S., LANDSBERG, M.J., HURST, M.R.H. & LOTT, J.S., 2013. The BC component of ABC toxins is an RHS-repeat-containing protein encapsulation device. *Nature*, 501(7468), pp.547–50.

CARDONA, S.T. & VALVANO, M.A., 2005. An expression vector containing a rhamnose-inducible promoter provides tightly regulated gene expression in Burkholderia cenocepacia. *Plasmid*, 54(3), pp.219–28.

CARLIER, A., AGNOLI, K., PESSI, G., SUPPIGER, A., JENUL, C., SCHMID, N., TÜMMLER, B., PINTO-CARBO, M. & EBERL, L., 2014. Genome Sequence of Burkholderia cenocepacia H111, a Cystic Fibrosis Airway Isolate. *Genome Announcements*, 2(2).

CASABONA, M.G., SILVERMAN, J.M., SALL, K.M., BOYER, F., COUTÉ, Y., POIREL, J., GRUNWALD, D., MOUGOUS, J.D., ELSEN, S. & ATTREE, I., 2013. An ABC transporter and an outer membrane lipoprotein participate in posttranslational activation of type VI secretion in Pseudomonas aeruginosa. *Environmental Microbiology*, 15(2), pp.471–486.

CASADABAN, M.J. & COHEN, S.N., 1980. Analysis of gene control signals by DNA fusion and cloning in Escherichia coli. *Journal of Molecular Biology*, 138(2), pp.179–207.

CASCALES, E., 2008. The type VI secretion toolkit. *EMBO Reports*, 9(8), pp.735–41.

CASCALES, E., BUCHANAN, S.K., DUCHÉ, D., KLEANTHOUS, C., LLOUBÈS, R., POSTLE, K., RILEY, M., SLATIN, S. & CAVARD, D., 2007. Colicin biology. *Microbiology and Molecular Biology Reviews : MMBR*, 71(1), pp.158–229.

CASCALES, E. & CAMBILLAU, C., 2012. Structural biology of type VI secretion systems. *Philosophical Transactions of the Royal Society of London. Series B, Biological Sciences*, 367(1592), pp.1102–11.

CASTANG, S., MCMANUS, H.R., TURNER, K.H. & DOVE, S.L., 2008. H-NS family members function coordinately in an opportunistic pathogen. *Proceedings of the National Academy of Sciences of the United States of America*, 105(48), pp.18947–52.

CHANG, H.K. & ZYLSTRA, G.J., 1998. Novel organization of the genes for phthalate degradation from Burkholderia cepacia DBO1. *Journal of Bacteriology*, 180(24), pp.6529–37.

CHAPMAN, M.R., ROBINSON, L.S., PINKNER, J.S., ROTH, R., HEUSER, J., HAMMAR, M., NORMARK, S. & HULTGREN, S.J., 2002. Role of Escherichia coli curli operons in directing amyloid fiber formation. *Science (New York, N.Y.)*, 295(5556), pp.851–5.

CHENG, H.P. & LESSIE, T.G., 1994. Multiple replicons constituting the genome of Pseudomonas cepacia 17616. *Journal of Bacteriology*, 176(13), pp.4034–42.

CIERI, M. V, MAYER-HAMBLETT, N., GRIFFITH, A. & BURNS, J.L., 2002. Correlation between an in vitro invasion assay and a murine model of Burkholderia cepacia lung infection. *Infection and Immunity*, 70(3), pp.1081–6.

CLEMENS, D.L., GE, P., LEE, B.-Y., HORWITZ, M.A. & ZHOU, Z.H., 2015. Atomic structure of T6SS reveals interlaced array essential to function. *Cell*, 160(5), pp.940–51.

CONWAY, B.-A.D., VENU, V. & SPEERT, D.P., 2002. Biofilm formation and acyl homoserine lactone production in the Burkholderia cepacia complex. *Journal of Bacteriology*, 184(20), pp.5678–85.

CORBETT, C.R., BURTNICK, M.N., KOOI, C., WOODS, D.E. & SOKOL, P.A., 2003. An extracellular zinc metalloprotease gene of Burkholderia cepacia. *Microbiology (Reading, England)*, 149(Pt 8), pp.2263–71.

CORDONNIER, C. & BERNARDI, G., 1965. Localization of E. coli endonuclease I. *Biochemical and Biophysical Research Communications*, 20(5), pp.555–9.

CORNELIS, G.R., 2006. The type III secretion injectisome. *Nature Reviews. Microbiology*, 4(11), pp.811–25.

COSTA, T.R.D., FELISBERTO-RODRIGUES, C., MEIR, A., PREVOST, M.S., REDZEJ, A., TROKTER, M. & WAKSMAN, G., 2015. Secretion systems in Gram-negative bacteria: structural and mechanistic insights. *Nature Reviews Microbiology*, 13(6), pp.343–359.

CÔTÉ, J. & RUIZ-CARRILLO, A., 1993. Primers for mitochondrial DNA replication generated by endonuclease G. *Science (New York, N.Y.)*, 261(5122), pp.765–9.

COUTTE, L., ANTOINE, R., DROBECQ, H., LOCHT, C. & JACOB-DUBUISSON, F., 2001. Subtilisin-like autotransporter serves as maturation protease in a bacterial secretion pathway. *The EMBO Journal*, 20(18), pp.5040–8.

CULLINANE, M., GONG, L., LI, X., LAZAR-ADLER, N., TRA, T., WOLVETANG, E., PRESCOTT, M., BOYCE, J.D., DEVENISH, R.J. & ADLER, B., 2008. Stimulation of autophagy suppresses the intracellular survival of Burkholderia pseudomallei in mammalian cell lines. *Autophagy*, 4(6), pp.744–53.

DABNEY-SMITH, C., MORI, H. & CLINE, K., 2006. Oligomers of Tha4 organize at the thylakoid Tat translocase during protein transport. *The Journal of Biological Chemistry*, 281(9), pp.5476–83.

DALBEY, R.E. & WICKNER, W., 1985. Leader peptidase catalyzes the release of exported proteins from the outer surface of the Escherichia coli plasma membrane. *The Journal of Biological Chemistry*, 260(29), pp.15925–31.

DAVIDSON, A.R., CARDARELLI, L., PELL, L.G., RADFORD, D.R. & MAXWELL, K.L., 2012. Long noncontractile tail machines of bacteriophages. *Advances in Experimental Medicine and Biology*, 726, pp.115–42.

DAVIS, L.H., OTTO, E. & BENNETT, V., 1991. Specific 33-residue repeat(s) of erythrocyte ankyrin associate with the anion exchanger. *The Journal of Biological Chemistry*, 266(17), pp.11163–9.

DECOIN, V., BARBEY, C., BERGEAU, D., LATOUR, X., FEUILLOLEY, M.G.J., ORANGE, N. & MERIEAU, A., 2014. A type VI secretion system is involved in Pseudomonas fluorescens bacterial competition. *PloS One*, 9(2), p.e89411.

DELEPELAIRE, P., 2004. Type I secretion in gram-negative bacteria. *Biochimica et Biophysica Acta*, 1694(1-3), pp.149–61.

DERMAN, A.I., PRINZ, W.A., BELIN, D. & BECKWITH, J., 1993. Mutations that allow disulfide bond formation in the cytoplasm of Escherichia coli. *Science (New York, N.Y.)*, 262(5140), pp.1744–7.

DESAI, M., BÜHLER, T., WELLER, P.H. & BROWN, M.R., 1998. Increasing resistance of planktonic and biofilm cultures of Burkholderia cepacia to ciprofloxacin and ceftazidime during exponential growth. *The Journal of Antimicrobial Chemotherapy*, 42(2), pp.153–60.

DeShazer, D. & Woods, D.E., 1996. Broad-host-range cloning and cassette vectors based on the R388 trimethoprim resistance gene. *BioTechniques*, 20(5), pp.762–4.

Desvaux, M., Hébraud, M., Talon, R. & Henderson, I.R., 2009. Secretion and subcellular localizations of bacterial proteins: a semantic awareness issue. *Trends in Microbiology*, 17(4), pp.139–45.

Ding, H. & Demple, B., 2000. Direct nitric oxide signal transduction via nitrosylation of iron-sulfur centers in the SoxR transcription activator. *Proceedings of the National Academy of Sciences of the United States of America*, 97(10), pp.5146–50.

Ding, J., Wang, W., Feng, H., Zhang, Y. & Wang, D.-C., 2012. Structural insights into the Pseudomonas aeruginosa type VI virulence effector Tse1 bacteriolysis and self-protection mechanisms. *The Journal of Biological Chemistry*, 287(32), pp.26911–20.

Diniz, J.A. & Coulthurst, S.J., 2015. Intraspecies Competition in Serratia marcescens Is Mediated by Type VI-Secreted Rhs Effectors and a Conserved Effector-Associated Accessory Protein. *Journal of Bacteriology*, 197(14), pp.2350–60.

Dippel, R. & Boos, W., 2005. The maltodextrin system of Escherichia coli: metabolism and transport. *Journal of Bacteriology*, 187(24), pp.8322–31.

Dodson, G., 1998. Catalytic triads and their relatives. *Trends in Biochemical Sciences*, 23(9), pp.347–352.

Dong, T.G., Dong, S., Catalano, C., Moore, R., Liang, X. & Mekalanos, J.J., 2015. Generation of reactive oxygen species by lethal attacks from competing microbes. *Proceedings of the National Academy of Sciences of the United States of America*, 112(7), pp.2181–6.

Dong, T.G., Ho, B.T., Yoder-Himes, D.R. & Mekalanos, J.J., 2013. Identification of T6SS-dependent effector and immunity proteins by Tn-seq in Vibrio cholerae. *Proceedings of the National Academy of Sciences of the United States of America*, 110(7), pp.2623–8.

Douville, K., Leonard, M., Brundage, L., Nishiyama, K., Tokuda, H., Mizushima, S. & Wickner, W., 1994. Band 1 subunit of Escherichia coli preportein translocase and integral membrane export factor P12 are the same protein. *J. Biol. Chem.*, 269(29), pp.18705–18707.

Drevinek, P. & Mahenthiralingam, E., 2010. Burkholderia cenocepacia in cystic fibrosis: epidemiology and molecular mechanisms of virulence. *Clinical Microbiology and Infection : The Official Publication of the European Society of Clinical Microbiology and Infectious Diseases*, 16(7), pp.821–30.

Dudley, E.G., Thomson, N.R., Parkhill, J., Morin, N.P. & Nataro, J.P., 2006. Proteomic and microarray characterization of the AggR regulon identifies a pheU pathogenicity island in enteroaggregative Escherichia coli. *Molecular Microbiology*, 61(5), pp.1267–82.

DURAND, E., CAMBILLAU, C., CASCALES, E. & JOURNET, L., 2014. VgrG, Tae, Tle, and beyond: the versatile arsenal of Type VI secretion effectors. *Trends in Microbiology*, 22(9), pp.498–507.

DURAND, E., NGUYEN, V.S., ZOUED, A., LOGGER, L., PÉHAU-ARNAUDET, G., ASCHTGEN, M.-S., SPINELLI, S., DESMYTER, A., BARDIAUX, B., DUJEANCOURT, A., ROUSSEL, A., CAMBILLAU, C., CASCALES, E. & FRONZES, R., 2015. Biogenesis and structure of a type VI secretion membrane core complex. *Nature*, 523(7562), pp.555–60.

DURAND, E., ZOUED, A., SPINELLI, S., WATSON, P.J.H., ASCHTGEN, M.-S., JOURNET, L., CAMBILLAU, C. & CASCALES, E., 2012. Structural characterization and oligomerization of the TssL protein, a component shared by bacterial type VI and type IVb secretion systems. *The Journal of Biological Chemistry*, 287(17), pp.14157–68.

ENGLISH, G., BYRON, O., CIANFANELLI, F.R., PRESCOTT, A.R. & COULTHURST, S.J., 2014. Biochemical analysis of TssK, a core component of the bacterial Type VI secretion system, reveals distinct oligomeric states of TssK and identifies a TssK-TssFG sub-complex. *The Biochemical Journal*.

ENGLISH, G., TRUNK, K., RAO, V. A, SRIKANNATHASAN, V., HUNTER, W.N. & COULTHURST, S.J., 2012. New secreted toxins and immunity proteins encoded within the Type VI secretion system gene cluster of Serratia marcescens. *Molecular Microbiology*, 86(September), pp.921–936.

ENOS-BERLAGE, J.L., GUVENER, Z.T., KEENAN, C.E. & MCCARTER, L.L., 2005. Genetic determinants of biofilm development of opaque and translucent Vibrio parahaemolyticus. *Molecular Microbiology*, 55(4), pp.1160–82.

ESSEX-LOPRESTI, A.E., BODDEY, J.A., THOMAS, R., SMITH, M.P., HARTLEY, M.G., ATKINS, T., BROWN, N.F., TSANG, C.H., PEAK, I.R.A., HILL, J., BEACHAM, I.R. & TITBALL, R.W., 2005. A type IV pilin, PilA, Contributes To Adherence of Burkholderia pseudomallei and virulence in vivo. *Infection and Immunity*, 73(2), pp.1260–4.

FAZLI, M., HARRISON, J.J., GAMBINO, M., GIVSKOV, M. & TOLKER-NIELSEN, T., 2015. In-Frame and Unmarked Gene Deletions in Burkholderia cenocepacia via an Allelic Exchange System Compatible with Gateway Technology. *Applied and Environmental Microbiology*, 81(11), pp.3623–3630.

FAZLI, M., MCCARTHY, Y., GIVSKOV, M., RYAN, R.P. & TOLKER-NIELSEN, T., 2013. The exopolysaccharide gene cluster Bcam1330-Bcam1341 is involved in Burkholderia cenocepacia biofilm formation, and its expression is regulated by c-di-GMP and Bcam1349. *MicrobiologyOpen*, 2(1), pp.105–22.

FAZLI, M., O'CONNELL, A., NILSSON, M., NIEHAUS, K., DOW, J.M., GIVSKOV, M., RYAN, R.P. & TOLKER-NIELSEN, T., 2011. The CRP/FNR family protein Bcam1349 is a c-di-GMP effector that regulates biofilm formation in the respiratory pathogen Burkholderia cenocepacia. *Molecular Microbiology*, 82(2), pp.327–41.

FELISBERTO-RODRIGUES, C., DURAND, E., ASCHTGEN, M.-S., BLANGY, S., ORTIZ-LOMBARDIA, M., DOUZI, B., CAMBILLAU, C. & CASCALES, E., 2011. Towards a structural comprehension of bacterial type VI secretion systems: characterization of the

TssJ-TssM complex of an Escherichia coli pathovar. *PLoS Pathogens*, 7(11), p.e1002386.

FERREIRA, A.S., SILVA, I.N., FERNANDES, F., PILKINGTON, R., CALLAGHAN, M., MCCLEAN, S. & MOREIRA, L.M., 2015. The tyrosine kinase BceF and the phosphotyrosine phosphatase BceD of Burkholderia contaminans are required for efficient invasion and epithelial disruption of a cystic fibrosis lung epithelial cell line. *Infection and Immunity*, 83(2), pp.812–21.

FINN, R.D., BATEMAN, A., CLEMENTS, J., COGGILL, P., EBERHARDT, R.Y., EDDY, S.R., HEGER, A., HETHERINGTON, K., HOLM, L., MISTRY, J., SONNHAMMER, E.L.L., TATE, J. & PUNTA, M., 2014. Pfam: the protein families database. *Nucleic Acids Research*, 42(Database issue), pp.D222–30.

FIRCZUK, M., MUCHA, A. & BOCHTLER, M., 2005. Crystal structures of active LytM. *Journal of Molecular Biology*, 354(3), pp.578–90.

FLANNAGAN, R.S., LINN, T. & VALVANO, M.A., 2008. A system for the construction of targeted unmarked gene deletions in the genus Burkholderia. *Environmental Microbiology*, 10(6), pp.1652–60.

FLYG, C., KENNE, K. & BOMAN, H.G., 1980. Insect pathogenic properties of Serratia marcescens: phage-resistant mutants with a decreased resistance to Cecropia immunity and a decreased virulence to Drosophila. *Journal of General Microbiology*, 120(1), pp.173–81.

FOCARETA, T. & MANNING, P.A., 1991. Distinguishing between the extracellular DNases of Vibrio cholerae and development of a transformation system. *Molecular Microbiology*, 5(10), pp.2547–2555.

FRIEDHOFF, P., FRANKE, I., MEISS, G., WENDE, W., KRAUSE, K.L. & PINGOUD, A., 1999. A similar active site for non-specific and specific endonucleases. *Nature Structural Biology*, 6(2), pp.112–3.

FRIEDHOFF, P., MEISS, G., KOLMES, B., PIEPER, U., GIMADUTDINOW, O., URBANKE, C. & PINGOUD, A., 1996. Kinetic analysis of the cleavage of natural and synthetic substrates by the Serratia nuclease. *European Journal of Biochemistry / FEBS*, 241(2), pp.572–80.

FRITSCH, M.J., TRUNK, K., ALCOFORADO DINIZ, J., GUO, M., TROST, M. & COULTHURST, S.J., 2013. Proteomic identification of novel secreted anti-bacterial toxins of the Serratia marcescens Type VI secretion system. *Molecular & Cellular Proteomics : MCP*.

GAVÍN, R., RABAAN, A.A., MERINO, S., TOMÁS, J.M., GRYLLOS, I. & SHAW, J.G., 2002. Lateral flagella of Aeromonas species are essential for epithelial cell adherence and biofilm formation. *Molecular Microbiology*, 43(2), pp.383–97.

GAVRILIN, M.A., ABDELAZIZ, D.H.A., MOSTAFA, M., ABDULRAHMAN, B.A., GRANDHI, J., AKHTER, A., ABU KHWEEK, A., AUBERT, D.F., VALVANO, M.A., WEWERS, M.D. & AMER, A.O., 2012. Activation of the pyrin inflammasome by intracellular Burkholderia cenocepacia. *Journal of Immunology (Baltimore, Md. : 1950)*, 188(7), pp.3469–77.

GAY, P., LE COQ, D., STEINMETZ, M., FERRARI, E. & HOCH, J.A., 1983. Cloning structural gene sacB, which codes for exoenzyme levansucrase of Bacillus subtilis: expression of the gene in Escherichia coli. *Journal of Bacteriology*, 153(3), pp.1424–31.

GEORGATSOS, J.G. & LASKOWSKI, M., 1962. Purification of an endonuclease from the venom of Bothrops atrox. *Biochemistry*, 1, pp.288–95.

GERC, A.J., DIEPOLD, A., TRUNK, K., PORTER, M., RICKMAN, C., ARMITAGE, J.P., STANLEY-WALL, N.R. & COULTHURST, S.J., 2015. Visualization of the Serratia Type VI Secretion System Reveals Unprovoked Attacks and Dynamic Assembly. *Cell Reports*, 12(12), pp.2131–2142.

GILSON, L., MAHANTY, H.K. & KOLTER, R., 1987. Four plasmid genes are required for colicin V synthesis, export, and immunity. *Journal of Bacteriology*, 169(6), pp.2466–70.

GILSON, L., MAHANTY, H.K. & KOLTER, R., 1990. Genetic analysis of an MDR-like export system: the secretion of colicin V. *The EMBO Journal*, 9(12), pp.3875–84.

GIRAUD-PANIS, M.J. & LILLEY, D.M., 1996. T4 endonuclease VII. Importance of a histidine-aspartate cluster within the zinc-binding domain. *The Journal of Biological Chemistry*, 271(51), pp.33148–55.

GIVSKOV, M. & MOLIN, S., 1993. Secretion of Serratia liquefaciens phospholipase from Escherichia coli. *Molecular Microbiology*, 8(2), pp.229–42.

GIVSKOV, M., OLSEN, L. & MOLIN, S., 1988. Cloning and expression in Escherichia coli of the gene for extracellular phospholipase A1 from Serratia liquefaciens. *Journal of Bacteriology*, 170(12), pp.5855–62.

GLEW, M.D., VEITH, P.D., CHEN, D., SEERS, C.A., CHEN, Y.-Y. & REYNOLDS, E.C., 2014. Blue native-PAGE analysis of membrane protein complexes in Porphyromonas gingivalis. *Journal of Proteomics*, 110, pp.72–92.

GOLZ, S., CHRISTOPH, A., BIRKENKAMP-DEMTRÖDER, K. & KEMPER, B., 1997. Identification of amino acids of endonuclease VII essential for binding and cleavage of cruciform DNA. *European Journal of Biochemistry / FEBS*, 245(3), pp.573–80.

GOODMAN, A.L., KULASEKARA, B., RIETSCH, A., BOYD, D., SMITH, R.S. & LORY, S., 2004. A signaling network reciprocally regulates genes associated with acute infection and chronic persistence in Pseudomonas aeruginosa. *Developmental Cell*, 7(5), pp.745–54.

GORINA, S. & PAVLETICH, N.P., 1996. Structure of the p53 tumor suppressor bound to the ankyrin and SH3 domains of 53BP2. *Science (New York, N.Y.)*, 274(5289), pp.1001–5.

GOYAL, P., KRASTEVA, P. V, VAN GERVEN, N., GUBELLINI, F., VAN DEN BROECK, I., TROUPIOTIS-TSAÏLAKI, A., JONCKHEERE, W., PÉHAU-ARNAUDET, G., PINKNER, J.S., CHAPMAN, M.R., HULTGREN, S.J., HOWORKA, S., FRONZES, R. & REMAUT, H., 2014. Structural and mechanistic insights into the bacterial amyloid secretion channel CsgG. *Nature*, 516(7530), pp.250–3.

GREENBERG, J.T., MONACH, P., CHOU, J.H., JOSEPHY, P.D. & DEMPLE, B., 1990. Positive control of a global antioxidant defense regulon activated by superoxide-generating agents in Escherichia coli. *Proceedings of the National Academy of Sciences of the United States of America*, 87(16), pp.6181–5.

GRUSS, F., ZÄHRINGER, F., JAKOB, R.P., BURMANN, B.M., HILLER, S. & MAIER, T., 2013. The structural basis of autotransporter translocation by TamA. *Nature Structural & Molecular Biology*, 20(11), pp.1318–20.

GUERRY, P., EWING, C.P., SCHIRM, M., LORENZO, M., KELLY, J., PATTARINI, D., MAJAM, G., THIBAULT, P. & LOGAN, S., 2006. Changes in flagellin glycosylation affect Campylobacter autoagglutination and virulence. *Molecular Microbiology*, 60(2), pp.299–311.

GUO, L., 1997. Regulation of Lipid A Modifications by Salmonella typhimurium Virulence Genes phoP-phoQ. *Science*, 276(5310), pp.250–253.

HAAS, G.H. DE, DAEMEN, F.J.M. & DEENEN, L.L.M. VAN, 1962. Positional Specificity of Phosphatide Acyl Hydrolase (Phospholipase A). *Nature*, 196(4849), pp.68–68.

HACHANI, A., ALLSOPP, L.P., ODUKO, Y. & FILLOUX, A., 2014. The VgrG proteins are "à la carte" delivery systems for bacterial type VI effectors. *The Journal of Biological Chemistry*, 289(25), pp.17872–84.

HACHANI, A., LOSSI, N.S., HAMILTON, A., JONES, C., BLEVES, S., ALBESA-JOVÉ, D. & FILLOUX, A., 2011. Type VI secretion system in Pseudomonas aeruginosa: secretion and multimerization of VgrG proteins. *The Journal of Biological Chemistry*, 286(14), pp.12317–27.

HÅKANSSON, S., SCHESSER, K., PERSSON, C., GALYOV, E.E., ROSQVIST, R., HOMBLÉ, F. & WOLF-WATZ, H., 1996. The YopB protein of Yersinia pseudotuberculosis is essential for the translocation of Yop effector proteins across the target cell plasma membrane and displays a contact-dependent membrane disrupting activity. *The EMBO Journal*, 15(21), pp.5812–23.

HAMAD, M.A., DI LORENZO, F., MOLINARO, A. & VALVANO, M.A., 2012. Aminoarabinose is essential for lipopolysaccharide export and intrinsic antimicrobial peptide resistance in Burkholderia cenocepacia(†). *Molecular Microbiology*, 85(5), pp.962–74.

HAMMER, N.D., SCHMIDT, J.C. & CHAPMAN, M.R., 2007. The curli nucleator protein, CsgB, contains an amyloidogenic domain that directs CsgA polymerization. *Proceedings of the National Academy of Sciences of the United States of America*, 104(30), pp.12494–9.

HANAHAN, D., 1983. Studies on transformation of Escherichia coli with plasmids. *Journal of Molecular Biology*, 166(4), pp.557–80.

HANUSZKIEWICZ, A., PITTOCK, P., HUMPHRIES, F., MOLL, H., ROSALES, A.R., MOLINARO, A., MOYNAGH, P.N., LAJOIE, G.A. & VALVANO, M.A., 2014. Identification of the flagellin glycosylation system in Burkholderia cenocepacia and the contribution of glycosylated flagellin to evasion of human innate immune responses. *The Journal of Biological Chemistry*, 289(27), pp.19231–44.

HARTL, F.-U., LECKER, S., SCHIEBEL, E., HENDRICK, J.P. & WICKNER, W., 1990. The binding cascade of SecB to SecA to SecYE mediates preprotein targeting to the E. coli plasma membrane. *Cell*, 63(2), pp.269–279.

HATIC, S.O., PICKING, W.L., YOUNG, B.M., YOUNG, G.M. & PICKING, W.D., 2002. Purification and characterization of two active derivatives of recombinant YplA, a secreted phospholipase from Yersinia entercolitica. *Biochemical and Biophysical Research Communications*, 292(2), pp.463–7.

HEDSTROM, L., 2002. Serine protease mechanism and specificity. *Chemical Reviews*, 102(12), pp.4501–24.

HENDERSON, I.R., NAVARRO-GARCIA, F., DESVAUX, M., FERNANDEZ, R.C. & ALA'ALDEEN, D., 2004. Type V protein secretion pathway: the autotransporter story. *Microbiology and Molecular Biology Reviews : MMBR*, 68(4), pp.692–744.

HERRERO, M., DE LORENZO, V. & TIMMIS, K.N., 1990. Transposon vectors containing non-antibiotic resistance selection markers for cloning and stable chromosomal insertion of foreign genes in gram-negative bacteria. *Journal of Bacteriology*, 172(11), pp.6557–67.

HO, B.T., BASLER, M. & MEKALANOS, J.J., 2013. Type 6 Secretion System-Mediated Immunity to Type 4 Secretion System-Mediated Gene Transfer. *Science*, 342(6155), pp.250–253.

HOBSON, R., GOULD, I. & GOVAN, J., 1995. Burkholderia (Pseudomonas) cepacia as a cause of brain abscesses secondary to chronic suppurative otitis media. *European Journal of Clinical Microbiology & Infectious Diseases*, 14(10), pp.908–911.

HOLDEN, M.T.G. ET AL., 2004. Genomic plasticity of the causative agent of melioidosis, Burkholderia pseudomallei. *Proceedings of the National Academy of Sciences of the United States of America*, 101(39), pp.14240–5.

HOLDEN, M.T.G. ET AL., 2009. The genome of Burkholderia cenocepacia J2315, an epidemic pathogen of cystic fibrosis patients. *Journal of Bacteriology*, 191(1), pp.261–77.

HOLLOWAY, B.W., 1955. Genetic Recombination in Pseudomonas aeruginosa. *Journal of General Microbiology*, 13(3), pp.572–581.

HOOD, R.D., SINGH, P., HSU, F., GÜVENER, T., CARL, M.A., TRINIDAD, R.R.S., SILVERMAN, J.M., OHLSON, B.B., HICKS, K.G., PLEMEL, R.L., LI, M., SCHWARZ, S., WANG, W.Y., MERZ, A.J., GOODLETT, D.R. & MOUGOUS, J.D., 2010. A type VI secretion system of Pseudomonas aeruginosa targets a toxin to bacteria. *Cell Host & Microbe*, 7(1), pp.25–37.

HSU, F., SCHWARZ, S. & MOUGOUS, J.D., 2009. TagR promotes PpkA-catalysed type VI secretion activation in Pseudomonas aeruginosa. *Molecular Microbiology*, 72(5), pp.1111–25.

HUBER, B., RIEDEL, K., KÖTHE, M., GIVSKOV, M., MOLIN, S. & EBERL, L., 2002. Genetic analysis of functions involved in the late stages of biofilm development in

Burkholderia cepacia H111. *Molecular Microbiology*, 46(2), pp.411–26.

HUECK, C.J., 1998. Type III protein secretion systems in bacterial pathogens of animals and plants. *Microbiology and Molecular Biology Reviews : MMBR*, 62(2), pp.379–433.

HUNT, T.A., KOOI, C., SOKOL, P.A. & VALVANO, M.A., 2004. Identification of Burkholderia cenocepacia genes required for bacterial survival in vivo. *Infection and Immunity*, 72(7), pp.4010–22.

HUTCHISON, M.L., POXTON, I.R. & GOVAN, J.R., 1998. Burkholderia cepacia produces a hemolysin that is capable of inducing apoptosis and degranulation of mammalian phagocytes. *Infection and Immunity*, 66(5), pp.2033–9.

IEVA, R. & BERNSTEIN, H.D., 2009. Interaction of an autotransporter passenger domain with BamA during its translocation across the bacterial outer membrane. *Proceedings of the National Academy of Sciences of the United States of America*, 106(45), pp.19120–5.

ILANGOVAN, A., CONNERY, S. & WAKSMAN, G., 2015. Structural biology of the Gram-negative bacterial conjugation systems. *Trends in Microbiology*, 23(5), pp.301–10.

INOSE, K., FUJIKAWA, M., YAMAZAKI, T., KOJIMA, K. & SODE, K., 2003. Cloning and expression of the gene encoding catalytic subunit of thermostable glucose dehydrogenase from Burkholderia cepacia in Escherichia coli. *Biochimica et Biophysica Acta*, 1645(2), pp.133–8.

ISHIKAWA, T., ROMPIKUNTAL, P.K., LINDMARK, B., MILTON, D.L. & WAI, S.N., 2009. Quorum sensing regulation of the two hcp alleles in Vibrio cholerae O1 strains. *PloS One*, 4(8), p.e6734.

ISHIKAWA, T., SABHARWAL, D., BRÖMS, J., MILTON, D.L., SJÖSTEDT, A., UHLIN, B.E. & WAI, S.N., 2012. Pathoadaptive conditional regulation of the type VI secretion system in Vibrio cholerae O1 strains. *Infection and Immunity*, 80(2), pp.575–84.

ISLES, A., MACLUSKY, I., COREY, M., GOLD, R., PROBER, C., FLEMING, P. & LEVISON, H., 1984. Pseudomonas cepacia infection in cystic fibrosis: an emerging problem. *The Journal of Pediatrics*, 104(2), pp.206–10.

JAMET, A. & NASSIF, X., 2015. New players in the toxin field: polymorphic toxin systems in bacteria. *mBio*, 6(3), pp.e00285–15.

JEKEL, M. & WACKERNAGEL, W., 1995. The periplasmic endonuclease I of Escherichia coli has amino-acid sequence homology to the extracellular DNases of Vibrio cholerae and Aeromonas hydrophila. *Gene*, 154(1), pp.55–9.

JESSEN, O., 1965. Pseudomonas aeruginosa and other green fluorescent pseudomonads: a taxonomic study, Munksgaard.

JIANG, F., WATERFIELD, N.R., YANG, J., YANG, G. & JIN, Q., 2014. A Pseudomonas aeruginosa Type VI Secretion Phospholipase D Effector Targets Both Prokaryotic and Eukaryotic Cells. *Cell Host & Microbe*, 15(5), pp.600–10.

JONES, C.H., PINKNER, J.S., ROTH, R., HEUSER, J., NICHOLES, A. V., ABRAHAM, S.N. & HULTGREN, S.J., 1995. FimH adhesin of type 1 pili is assembled into a fibrillar tip structure in the Enterobacteriaceae. *Proceedings of the National Academy of Sciences*, 92(6), pp.2081–2085.

JONES, R.A., 2012. Characterisation of Putative Type VI Secretion System Effector Proteins from Burkholderia cenocepacia. Ph.D thesis, The University of Sheffield.

JUNI, E. & JANIK, A., 1969. Transformation of Acinetobacter calco-aceticus (Bacterium anitratum). *Journal of Bacteriology*, 98(1), pp.281–8.

KANAMARU, S., LEIMAN, P.G., KOSTYUCHENKO, V.A., CHIPMAN, P.R., MESYANZHINOV, V. V, ARISAKA, F. & ROSSMANN, M.G., 2002. Structure of the cell-puncturing device of bacteriophage T4. *Nature*, 415(6871), pp.553–7.

KANG, Y., CARLSON, R., THARPE, W. & SCHELL, M.A., 1998. Characterization of genes involved in biosynthesis of a novel antibiotic from Burkholderia cepacia BC11 and their role in biological control of Rhizoctonia solani. *Applied and Environmental Microbiology*, 64(10), pp.3939–47.

KANONENBERG, K., SCHWARZ, C.K.W. & SCHMITT, L., 2013. Type I secretion systems - a story of appendices. *Research in Microbiology*, 164(6), pp.596–604.

KAPITEIN, N., BÖNEMANN, G., PIETROSIUK, A., SEYFFER, F., HAUSSER, I., LOCKER, J.K. & MOGK, A., 2013. ClpV recycles VipA/VipB tubules and prevents non-productive tubule formation to ensure efficient type VI protein secretion. *Molecular Microbiology*, 87(5), pp.1013–28.

KARIMOVA, G., PIDOUX, J., ULLMANN, A. & LADANT, D., 1998. A bacterial two-hybrid system based on a reconstituted signal transduction pathway. *Proceedings of the National Academy of Sciences of the United States of America*, 95(10), pp.5752–6.

KEITH, K.E., HYNES, D.W., SHOLDICE, J.E. & VALVANO, M.A., 2009. Delayed association of the NADPH oxidase complex with macrophage vacuoles containing the opportunistic pathogen Burkholderia cenocepacia. *Microbiology*, 155(4), pp.1004–1015.

KHODAI-KALAKI, M., ANDRADE, A., FATHY MOHAMED, Y. & VALVANO, M.A., 2015. Burkholderia cenocepacia Lipopolysaccharide Modification and Flagellin Glycosylation Affect Virulence but Not Innate Immune Recognition in Plants. *mBio*, 6(3), p.e00679.

KHODAI-KALAKI, M., AUBERT, D.F. & VALVANO, M.A., 2013. Characterization of the AtsR phosphorelay pathway and identification of its response regulator in Burkholderia cenocepacia. *The Journal of Biological Chemistry*.

KIKUCHI, T., MIZUNOE, Y., TAKADE, A., NAITO, S. & YOSHIDA, S., 2005. Curli fibers are required for development of biofilm architecture in Escherichia coli K-12 and enhance bacterial adherence to human uroepithelial cells. *Microbiology and Immunology*, 49(9), pp.875–84.

KIM, K.K., SONG, H.K., SHIN, D.H., HWANG, K.Y. & SUH, S.W., 1997. The crystal structure of a triacylglycerol lipase from Pseudomonas cepacia reveals a highly open conformation in the absence of a bound inhibitor. *Structure*, 5(2), pp.173–185.

KLEMM, P. & CHRISTIANSEN, G., 1990. The fimD gene required for cell surface localization of Escherichia coli type 1 fimbriae. *Molecular & General Genetics : MGG*, 220(2), pp.334–8.

KOHL, A., BINZ, H.K., FORRER, P., STUMPP, M.T., PLÜCKTHUN, A. & GRÜTTER, M.G., 2003. Designed to be stable: crystal structure of a consensus ankyrin repeat protein. *Proceedings of the National Academy of Sciences of the United States of America*, 100(4), pp.1700–5.

KOOI, C., CORBETT, C.R. & SOKOL, P.A., 2005. Functional analysis of the Burkholderia cenocepacia ZmpA metalloprotease. *Journal of Bacteriology*, 187(13), pp.4421–9.

KOOI, C., COX, A., DARLING, P. & SOKOL, P.A., 1994. Neutralizing monoclonal antibodies to an extracellular Pseudomonas cepacia protease. *Infection and Immunity*, 62(7), pp.2811–7.

KOOI, C., SUBSIN, B., CHEN, R., POHORELIC, B. & SOKOL, P.A., 2006. Burkholderia cenocepacia ZmpB is a broad-specificity zinc metalloprotease involved in virulence. *Infection and Immunity*, 74(7), pp.4083–93.

KORCZYNSKA, J.E., TURKENBURG, J.P. & TAYLOR, E.J., 2012. The structural characterization of a prophage-encoded extracellular DNase from Streptococcus pyogenes. *Nucleic Acids Research*, 40(2), pp.928–38.

KORENNYKH, A. V, PLANTINGA, M.J., CORRELL, C.C. & PICCIRILLI, J.A., 2007. Linkage between substrate recognition and catalysis during cleavage of sarcin/ricin loop RNA by restrictocin. *Biochemistry*, 46(44), pp.12744–56.

KORONAKIS, V., SHARFF, A., KORONAKIS, E., LUISI, B. & HUGHES, C., 2000. Crystal structure of the bacterial membrane protein TolC central to multidrug efflux and protein export. *Nature*, 405(6789), pp.914–9.

KOROTKOV, K. V, SANDKVIST, M. & HOL, W.G.J., 2012. The type II secretion system: biogenesis, molecular architecture and mechanism. *Nature Reviews. Microbiology*, 10(5), pp.336–51.

KOSKINIEMI, S., GARZA-SÁNCHEZ, F., EDMAN, N., CHAUDHURI, S., POOLE, S.J., MANOIL, C., HAYES, C.S. & LOW, D.A., 2015. Genetic analysis of the CDI pathway from Burkholderia pseudomallei 1026b. *PloS One*, 10(3), p.e0120265.

KOSKINIEMI, S., LAMOUREUX, J.G., NIKOLAKAKIS, K.C., T'KINT DE ROODENBEKE, C., KAPLAN, M.D., LOW, D.A. & HAYES, C.S., 2013. Rhs proteins from diverse bacteria mediate intercellular competition. *Proceedings of the National Academy of Sciences*.

KOSTYUCHENKO, V.A., LEIMAN, P.G., CHIPMAN, P.R., KANAMARU, S., VAN RAAIJ, M.J., ARISAKA, F., MESYANZHINOV, V. V & ROSSMANN, M.G., 2003. Three-dimensional structure of bacteriophage T4 baseplate. *Nature Structural Biology*, 10(9), pp.688–93.

KOTRANGE, S., KOPP, B., AKHTER, A., ABDELAZIZ, D., ABU KHWEEK, A., CAUTION, K.,

ABDULRAHMAN, B., WEWERS, M.D., MCCOY, K., MARSH, C., LOUTET, S.A., ORTEGA, X., VALVANO, M.A. & AMER, A.O., 2011. Burkholderia cenocepacia O polysaccharide chain contributes to caspase-1-dependent IL-1beta production in macrophages. *Journal of Leukocyte Biology*, 89(3), pp.481–8.

KOVACEVIC, S., VEAL, L.E., HSIUNG, H.M. & MILLER, J.R., 1985. Secretion of staphylococcal nuclease by Bacillus subtilis. *Journal of Bacteriology*, 162(2), pp.521–8.

KOVACH, M.E., ELZER, P.H., HILL, D.S., ROBERTSON, G.T., FARRIS, M.A., ROOP, R.M. & PETERSON, K.M., 1995. Four new derivatives of the broad-host-range cloning vector pBBR1MCS, carrying different antibiotic-resistance cassettes. *Gene*, 166(1), pp.175–6.

KOVACH, M.E., PHILLIPS, R.W., ELZER, P.H., ROOP, R.M. & PETERSON, K.M., 1994. pBBR1MCS: a broad-host-range cloning vector. *BioTechniques*, 16(5), pp.800–2.

KUDRYASHEV, M., WANG, R.Y.-R., BRACKMANN, M., SCHERER, S., MAIER, T., BAKER, D., DIMAIO, F., STAHLBERG, H., EGELMAN, E.H. & BASLER, M., 2015. Structure of the type VI secretion system contractile sheath. *Cell*, 160(5), pp.952–62.

KÜHLMANN, U.C., MOORE, G.R., JAMES, R., KLEANTHOUS, C. & HEMMINGS, A.M., 1999. Structural parsimony in endonuclease active sites: should the number of homing endonuclease families be redefined? *FEBS Letters*, 463(1-2), pp.1–2.

KURNICK, N.B., 1950. The determination of desoxyribonuclease activity by methyl green; application to serum. *Archives of Biochemistry*, 29(1), pp.41–53.

LACHICA, R. V, HOEPRICH, P.D. & RIEMANN, H.P., 1972. Tolerance of staphylococcal thermonuclease to stress. *Applied Microbiology*, 23(5), pp.994–7.

LADANT, D. & ULLMANN, A., 1999. Bordatella pertussis adenylate cyclase: a toxin with multiple talents. *Trends in Microbiology*, 7(4), pp.172–6.

LAEMMLI, U.K., 1970. Cleavage of structural proteins during the assembly of the head of bacteriophage T4. *Nature*, 227(5259), pp.680–5.

LAMBETH, J.D., 2004. NOX enzymes and the biology of reactive oxygen. *Nature Reviews. Immunology*, 4(3), pp.181–9.

LAMOTHE, J., HUYNH, K.K., GRINSTEIN, S. & VALVANO, M.A., 2007. Intracellular survival of Burkholderia cenocepacia in macrophages is associated with a delay in the maturation of bacteria-containing vacuoles. *Cellular Microbiology*, 9(1), pp.40–53.

LEAKE, M.C., GREENE, N.P., GODUN, R.M., GRANJON, T., BUCHANAN, G., CHEN, S., BERRY, R.M., PALMER, T. & BERKS, B.C., 2008. Variable stoichiometry of the TatA component of the twin-arginine protein transport system observed by in vivo single-molecule imaging. *Proceedings of the National Academy of Sciences of the United States of America*, 105(40), pp.15376–81.

LEIMAN, P.G., BASLER, M., RAMAGOPAL, U.A., BONANNO, J.B., SAUDER, J.M., PUKATZKI, S., BURLEY, S.K., ALMO, S.C. & MEKALANOS, J.J., 2009. Type VI secretion apparatus and phage tail-associated protein complexes share a common evolutionary origin.

Proceedings of the National Academy of Sciences of the United States of America, 106(11), pp.4154–9.

LEROUX, M., DE LEON, J. A, KUWADA, N.J., RUSSELL, A.B., PINTO-SANTINI, D., HOOD, R.D., AGNELLO, D.M., ROBERTSON, S.M., WIGGINS, P. A & MOUGOUS, J.D., 2012. Quantitative single-cell characterization of bacterial interactions reveals type VI secretion is a double-edged sword. *Proceedings of the National Academy of Sciences of the United States of America*, pp.1–6.

LÉVESQUE, C., BRASSARD, S., LAPOINTE, J. & ROY, P.H., 1994. Diversity and relative strength of tandem promoters for the antibiotic-resistance genes of several integrons. *Gene*, 142(1), pp.49–54.

LI, L., ZHANG, W., LIU, Q., GAO, Y., GAO, Y., WANG, Y., WANG, D.Z., LI, Z. & WANG, T., 2013. Structural Insights on the Bacteriolytic and Self-protection Mechanism of Muramidase Effector Tse3 in Pseudomonas aeruginosa. *The Journal of Biological Chemistry*.

LI, M., LE TRONG, I., CARL, M.A., LARSON, E.T., CHOU, S., DE LEON, J.A., DOVE, S.L., STENKAMP, R.E. & MOUGOUS, J.D., 2012. Structural basis for type VI secretion effector recognition by a cognate immunity protein. *PLoS Pathogens*, 8(4), p.e1002613.

LIANG, X., MOORE, R., WILTON, M., WONG, M.J.Q., LAM, L. & DONG, T.G., 2015. Identification of divergent type VI secretion effectors using a conserved chaperone domain. *Proceedings of the National Academy of Sciences*, p.201505317.

LILL, R., 2009. Function and biogenesis of iron-sulphur proteins. *Nature*, 460(7257), pp.831–8.

LILLINGTON, J., GEIBEL, S. & WAKSMAN, G., 2014. Biogenesis and adhesion of type 1 and P pili. *Biochimica et Biophysica Acta*, 1840(9), pp.2783–93.

LIM, J., LEE, T.-H., NAHM, B.H., CHOI, Y. DO, KIM, M. & HWANG, I., 2009. Complete genome sequence of Burkholderia glumae BGR1. *Journal of Bacteriology*, 191(11), pp.3758–9.

LIN, J.-S., MA, L.-S. & LAI, E.-M., 2013. Systematic dissection of the agrobacterium type VI secretion system reveals machinery and secreted components for subcomplex formation. *PloS One*, 8(7), p.e67647.

LIN, J.-S., WU, H.-H., HSU, P.-H., MA, L.-S., PANG, Y.-Y., TSAI, M.-D. & LAI, E.-M., 2014. Fha Interaction with Phosphothreonine of TssL Activates Type VI Secretion in Agrobacterium tumefaciens. J. D. Mougous, ed. *PLoS Pathogens*, 10(3), p.e1003991.

LINDBERG, F., TENNENT, J.M., HULTGREN, S.J., LUND, B. & NORMARK, S., 1989. PapD, a periplasmic transport protein in P-pilus biogenesis. *Journal of Bacteriology*, 171(11), pp.6052–8.

LLOSA, M., BOLLAND, S. & DE LA CRUZ, F., 1994. Genetic organization of the conjugal DNA processing region of the IncW plasmid R388. *Journal of Molecular Biology*, 235(2), pp.448–64.

LOBSTEIN, J., EMRICH, C.A., JEANS, C., FAULKNER, M., RIGGS, P. & BERKMEN, M., 2012. SHuffle, a novel Escherichia coli protein expression strain capable of correctly folding disulfide bonded proteins in its cytoplasm. *Microbial Cell Factories*, 11, p.56.

LÓPEZ, C.M., RHOLL, D.A., TRUNCK, L.A. & SCHWEIZER, H.P., 2009. Versatile dual-technology system for markerless allele replacement in Burkholderia pseudomallei. *Applied and Environmental Microbiology*, 75(20), pp.6496–503.

LOVGREN, A., ZHANG, M., ENGSTROM, A., DALHAMMAR, G. & LANDEN, R., 1990. Molecular characterization of immune inhibitor A, a secreted virulence protease from Bacillus thuringiensis. *Molecular Microbiology*, 4(12), pp.2137–2146.

LOW, H.H., GUBELLINI, F., RIVERA-CALZADA, A., BRAUN, N., CONNERY, S., DUJEANCOURT, A., LU, F., REDZEJ, A., FRONZES, R., ORLOVA, E. V. & WAKSMAN, G., 2014. Structure of a type IV secretion system. *Nature*, 508(7497), pp.550–553.

MA, A.T., MCAULEY, S., PUKATZKI, S. & MEKALANOS, J.J., 2009a. Translocation of a Vibrio cholerae type VI secretion effector requires bacterial endocytosis by host cells. *Cell Host & Microbe*, 5(3), pp.234–43.

MA, L.-S., HACHANI, A., LIN, J.-S., FILLOUX, A. & LAI, E.-M., 2014. Agrobacterium tumefaciens Deploys a Superfamily of Type VI Secretion DNase Effectors as Weapons for Interbacterial Competition In Planta. *Cell Host & Microbe*, pp.1–11.

MA, L.-S., LIN, J.-S. & LAI, E.-M., 2009b. An IcmF family protein, ImpLM, is an integral inner membrane protein interacting with ImpKL, and its walker a motif is required for type VI secretion system-mediated Hcp secretion in Agrobacterium tumefaciens. *Journal of Bacteriology*, 191(13), pp.4316–29.

MA, L.-S., NARBERHAUS, F. & LAI, E.-M., 2012. IcmF family protein TssM exhibits ATPase activity and energizes type VI secretion. *The Journal of Biological Chemistry*, 287(19), pp.15610–21.

MACINTYRE, D.L., MIYATA, S.T., KITAOKA, M. & PUKATZKI, S., 2010. The Vibrio cholerae type VI secretion system displays antimicrobial properties. *Proceedings of the National Academy of Sciences of the United States of America*, 107(45), pp.19520–4.

MACKMAN, N., NICAUD, J.M., GRAY, L. & HOLLAND, I.B., 1985. Identification of polypeptides required for the export of haemolysin 2001 from E. coli. *Molecular & General Genetics : MGG*, 201(3), pp.529–36.

MACKMAN, N., NICAUD, J.M., GRAY, L. & HOLLAND, I.B., 1986. Secretion of haemolysin by Escherichia coli. *Current Topics in Microbiology and Immunology*, 125, pp.159–81.

MAHENTHIRALINGAM, E., BISCHOF, J., BYRNE, S.K., RADOMSKI, C., DAVIES, J.E., AV-GAY, Y. & VANDAMME, P., 2000a. DNA-Based diagnostic approaches for identification of Burkholderia cepacia complex, Burkholderia vietnamiensis, Burkholderia multivorans, Burkholderia stabilis, and Burkholderia cepacia genomovars I and III. *Journal of Clinical Microbiology*, 38(9), pp.3165–73.

MAHENTHIRALINGAM, E., COENYE, T., CHUNG, J.W., SPEERT, D.P., GOVAN, J.R.W., TAYLOR, P. & VANDAMME, P., 2000b. Diagnostically and experimentally useful panel of strains from the Burkholderia cepacia complex. *Journal of Clinical …*, 38(2), pp.910–913.

MAHENTHIRALINGAM, E., SIMPSON, D.A. & SPEERT, D.P., 1997. Identification and characterization of a novel DNA marker associated with epidemic Burkholderia cepacia strains recovered from patients with cystic fibrosis. *Journal of Clinical Microbiology*, 35(4), pp.808–16.

MAHENTHIRALINGAM, E., URBAN, T. A & GOLDBERG, J.B., 2005. The multifarious, multireplicon Burkholderia cepacia complex. *Nature Reviews. Microbiology*, 3(2), pp.144–56.

MAHILLON, J. & CHANDLER, M., 1998. Insertion sequences. *Microbiology and Molecular Biology Reviews : MMBR*, 62(3), pp.725–74.

MALOTT, R.J., O'GRADY, E.P., TOLLER, J., INHÜLSEN, S., EBERL, L. & SOKOL, P.A., 2009. A Burkholderia cenocepacia orphan LuxR homolog is involved in quorum-sensing regulation. *Journal of Bacteriology*, 191(8), pp.2447–60.

MANADAS, B.J., VOUGAS, K., FOUNTOULAKIS, M. & DUARTE, C.B., 2006. Sample sonication after trichloroacetic acid precipitation increases protein recovery from cultured hippocampal neurons, and improves resolution and reproducibility in two-dimensional gel electrophoresis. *Electrophoresis*, 27(9), pp.1825–31.

MANZA, L.L., STAMER, S.L., HAM, A.-J.L., CODREANU, S.G. & LIEBLER, D.C., 2005. Sample preparation and digestion for proteomic analyses using spin filters. *Proteomics*, 5(7), pp.1742–5.

MARCHLER-BAUER, A. ET AL., 2014. CDD: NCBI's conserved domain database. *Nucleic Acids Research*, 43(Database issue), pp.D222–6.

MARLOVITS, T.C., KUBORI, T., SUKHAN, A., THOMAS, D.R., GALÁN, J.E. & UNGER, V.M., 2004. Structural insights into the assembly of the type III secretion needle complex. *Science (New York, N.Y.)*, 306(5698), pp.1040–2.

MARTIN, D.W. & MOHR, C.D., 2000. Invasion and intracellular survival of Burkholderia cepacia. *Infection and Immunity*, 68(1), pp.24–9.

MARTINA, P., BETTIOL, M., VESCINA, C., MONTANARO, P., MANNINO, M.C., PRIETO, C.I., VAY, C., NAUMANN, D., SCHMITT, J., YANTORNO, O., LAGARES, A. & BOSCH, A., 2013. Genetic diversity of Burkholderia contaminans isolates from cystic fibrosis patients in Argentina. *Journal of Clinical Microbiology*, 51(1), pp.339–44.

MAZAR, J. & COTTER, P.A., 2007. New insight into the molecular mechanisms of two-partner secretion. *Trends in Microbiology*, 15(11), pp.508–15.

MCKEON, S., MCCLEAN, S. & CALLAGHAN, M., 2010. Macrophage responses to CF pathogens: JNK MAP kinase signaling by Burkholderia cepacia complex lipopolysaccharide. *FEMS Immunology and Medical Microbiology*, 60(1), pp.36–43.

MCKEVITT, A.I., BAJAKSOUZIAN, S., KLINGER, J.D. & WOODS, D.E., 1989. Purification and

characterization of an extracellular protease from Pseudomonas cepacia. *Infection and Immunity*, 57(3), pp.771–8.

MEDINA-PASCUAL, M.J., VALDEZATE, S., CARRASCO, G., VILLALÓN, P., GARRIDO, N. & SAÉZ-NIETO, J.A., 2015. Increase in isolation of Burkholderia contaminans from Spanish patients with cystic fibrosis. *Clinical Microbiology and Infection : The Official Publication of the European Society of Clinical Microbiology and Infectious Diseases*, 21(2), pp.150–6.

MEISS, G., FRANKE, I., GIMADUTDINOW, O., URBANKE, C. & PINGOUD, A., 1998. Biochemical characterization of Anabaena sp. strain PCC 7120 non-specific nuclease NucA and its inhibitor NuiA. *European Journal of Biochemistry / FEBS*, 251(3), pp.924–34.

MIL-HOMENS, D. & FIALHO, A.M., 2011. Trimeric autotransporter adhesins in members of the Burkholderia cepacia complex: a multifunctional family of proteins implicated in virulence. *Frontiers in Cellular and Infection Microbiology*, 1, p.13.

MIL-HOMENS, D. & FIALHO, A.M., 2012. A BCAM0223 mutant of Burkholderia cenocepacia is deficient in hemagglutination, serum resistance, adhesion to epithelial cells and virulence. *PloS One*, 7(7), p.e41747.

MIL-HOMENS, D., LEÇA, M.I., FERNANDES, F., PINTO, S.N. & FIALHO, A.M., 2014. Characterization of BCAM0224, a multifunctional trimeric autotransporter from the human pathogen Burkholderia cenocepacia. *Journal of Bacteriology*, 196(11), pp.1968–79.

MIL-HOMENS, D., ROCHA, E.P.C. & FIALHO, A.M., 2010. Genome-wide analysis of DNA repeats in Burkholderia cenocepacia J2315 identifies a novel adhesin-like gene unique to epidemic-associated strains of the ET-12 lineage. *Microbiology (Reading, England)*, 156(Pt 4), pp.1084–96.

MILES, A.A., MISRA, S.S. & IRWIN, J.O., 1938. The estimation of the bactericidal power of the blood. *The Journal of Hygiene*, 38(6), pp.732–49.

MIYATA, S.T., KITAOKA, M., BROOKS, T.M., MCAULEY, S.B. & PUKATZKI, S., 2011. Vibrio cholerae requires the type VI secretion system virulence factor VasX to kill Dictyostelium discoideum. *Infection and Immunity*, 79(7), pp.2941–9.

MIYATA, S.T., KITAOKA, M., WIETESKA, L., FRECH, C., CHEN, N. & PUKATZKI, S., 2010. The Vibrio Cholerae Type VI Secretion System: Evaluating its Role in the Human Disease Cholera. *Frontiers in Microbiology*, 1, p.117.

MIYATA, S.T., UNTERWEGER, D., RUDKO, S.P. & PUKATZKI, S., 2013. Dual expression profile of type VI secretion system immunity genes protects pandemic Vibrio cholerae. *PLoS Pathogens*, 9(12), p.e1003752.

MOFFATT, B.A. & STUDIER, F.W., 1987. T7 lysozyme inhibits transcription by T7 RNA polymerase. *Cell*, 49(2), pp.221–7.

MONTI, M.C., HERNÁNDEZ-ARRIAGA, A.M., KAMPHUIS, M.B., LÓPEZ-VILLAREJO, J., HECK, A.J.R., BOELENS, R., DÍAZ-OREJAS, R. & VAN DEN HEUVEL, R.H.H., 2007. Interactions of Kid-

Kis toxin-antitoxin complexes with the parD operator-promoter region of plasmid R1 are piloted by the Kis antitoxin and tuned by the stoichiometry of Kid-Kis oligomers. *Nucleic Acids Research*, 35(5), pp.1737–49.

MOORE, R.A., BATES, N.C. & HANCOCK, R.E., 1986. Interaction of polycationic antibiotics with Pseudomonas aeruginosa lipopolysaccharide and lipid A studied by using dansyl-polymyxin. *Antimicrobial Agents and Chemotherapy*, 29(3), pp.496–500.

MORI, H. & CLINE, K., 2002. A twin arginine signal peptide and the pH gradient trigger reversible assembly of the thylakoid [Delta]pH/Tat translocase. *The Journal of Cell Biology*, 157(2), pp.205–10.

MOSBAHI, K., WALKER, D., LEA, E., MOORE, G.R., JAMES, R. & KLEANTHOUS, C., 2004. Destabilization of the colicin E9 Endonuclease domain by interaction with negatively charged phospholipids: implications for colicin translocation into bacteria. *The Journal of Biological Chemistry*, 279(21), pp.22145–51.

MOTA, L.J., JOURNET, L., SORG, I., AGRAIN, C. & CORNELIS, G.R., 2005. Bacterial injectisomes: needle length does matter. *Science (New York, N.Y.)*, 307(5713), p.1278.

MOUGOUS, J.D., CUFF, M.E., RAUNSER, S., SHEN, A., ZHOU, M., GIFFORD, C.A., GOODMAN, A.L., JOACHIMIAK, G., ORDOÑEZ, C.L., LORY, S., WALZ, T., JOACHIMIAK, A. & MEKALANOS, J.J., 2006. A virulence locus of Pseudomonas aeruginosa encodes a protein secretion apparatus. *Science (New York, N.Y.)*, 312(5779), pp.1526–30.

MOUGOUS, J.D., GIFFORD, C.A., RAMSDELL, T.L. & MEKALANOS, J.J., 2007. Threonine phosphorylation post-translationally regulates protein secretion in Pseudomonas aeruginosa. *Nature Cell Biology*, 9(7), pp.797–803.

MUELLER, C.A., BROZ, P. & CORNELIS, G.R., 2008. The type III secretion system tip complex and translocon. *Molecular Microbiology*, 68(5), pp.1085–95.

MUELLER, C.A., BROZ, P., MÜLLER, S.A., RINGLER, P., ERNE-BRAND, F., SORG, I., KUHN, M., ENGEL, A. & CORNELIS, G.R., 2005. The V-antigen of Yersinia forms a distinct structure at the tip of injectisome needles. *Science (New York, N.Y.)*, 310(5748), pp.674–6.

MULLEN, T., CALLAGHAN, M. & MCCLEAN, S., 2010. Invasion of Burkholderia cepacia complex isolates into lung epithelial cells involves glycolipid receptors. *Microbial Pathogenesis*, 49(6), pp.381–7.

MULLEN, T., MARKEY, K., MURPHY, P., MCCLEAN, S. & CALLAGHAN, M., 2007. Role of lipase in Burkholderia cepacia complex (Bcc) invasion of lung epithelial cells. *European Journal of Clinical Microbiology & Infectious Diseases : Official Publication of the European Society of Clinical Microbiology*, 26(12), pp.869–77.

MULVEY, M.A., LOPEZ-BOADO, Y.S., WILSON, C.L., ROTH, R., PARKS, W.C., HEUSER, J. & HULTGREN, S.J., 1998. Induction and evasion of host defenses by type 1-piliated uropathogenic Escherichia coli. *Science (New York, N.Y.)*, 282(5393), pp.1494–7.

MURDOCH, S.L., TRUNK, K., ENGLISH, G., FRITSCH, M.J., POURKARIMI, E. & COULTHURST, S.J., 2011. The opportunistic pathogen Serratia marcescens utilizes type VI secretion to target bacterial competitors. *Journal of Bacteriology*, 193(21), pp.6057–69.

MURO-PASTOR, A.M., HERRERO, A. & FLORES, E., 1997. The nuiA gene from Anabaena sp. encoding an inhibitor of the NucA sugar-non-specific nuclease. *Journal of Molecular Biology*, 268(3), pp.589–98.

NACAMULLI, C., BEVIVINO, A., DALMASTRI, C., TABACCHIONI, S. & CHIARINI, L., 2006. Perturbation of maize rhizosphere microflora following seed bacterization with Burkholderia cepacia MCI 7. *FEMS Microbiology Ecology*, 23(3), pp.183–193.

NAKAYAMA, K., 2015. *Porphyromonas gingivalis* and related bacteria: from colonial pigmentation to the type IX secretion system and gliding motility. *Journal of Periodontal Research*, 50(1), pp.1–8.

NAKAYAMA, K., KADOWAKI, T., OKAMOTO, K. & YAMAMOTO, K., 1995. Construction and characterization of arginine-specific cysteine proteinase (Arg-gingipain)-deficient mutants of Porphyromonas gingivalis. Evidence for significant contribution of Arg-gingipain to virulence. *The Journal of Biological Chemistry*, 270(40), pp.23619–26.

NAKAZAWA, T., YAMADA, Y. & ISHIBASHI, M., 1987. Characterization of hemolysin in extracellular products of Pseudomonas cepacia. *J. Clin. Microbiol.*, 25(2), pp.195–198.

NATALE, P., BRÜSER, T. & DRIESSEN, A.J.M., 2008. Sec- and Tat-mediated protein secretion across the bacterial cytoplasmic membrane--distinct translocases and mechanisms. *Biochimica et Biophysica Acta*, 1778(9), pp.1735–56.

NELSON, S.S., GLOCKA, P.P., AGARWAL, S., GRIMM, D.P. & MCBRIDE, M.J., 2007. Flavobacterium johnsoniae SprA is a cell surface protein involved in gliding motility. *Journal of Bacteriology*, 189(19), pp.7145–50.

NENNINGER, A.A., ROBINSON, L.S., HAMMER, N.D., EPSTEIN, E.A., BADTKE, M.P., HULTGREN, S.J. & CHAPMAN, M.R., 2011. CsgE is a curli secretion specificity factor that prevents amyloid fibre aggregation. *Molecular Microbiology*, 81(2), pp.486–99.

NESTLE, M. & ROBERTS, W.K., 1969. An Extracellular Nuclease from Serratia marcescens. I. PURIFICATION AND SOME PROPERTIES OF THE ENZYME. *J. Biol. Chem.*, 244(19), pp.5213–5218.

NGUYEN, K.-A., ZYLICZ, J., SZCZESNY, P., SROKA, A., HUNTER, N. & POTEMPA, J., 2009. Verification of a topology model of PorT as an integral outer-membrane protein in Porphyromonas gingivalis. *Microbiology (Reading, England)*, 155(Pt 2), pp.328–37.

NICAUD, J.M., MACKMAN, N., GRAY, L. & HOLLAND, I.B., 1985. Regulation of haemolysin synthesis in E. coli determined by HLY genes of human origin. *Molecular & General Genetics : MGG*, 199(1), pp.111–6.

NISHIYAMA, K., HANADA, M. & TOKUDA, H., 1994. Disruption of the gene encoding p12

(SecG) reveals the direct involvement and important function of SecG in the protein translocation of Escherichia coli at low temperature. *The EMBO Journal*, 13(14), pp.3272–7.

NOBLE, M.E., CLEASBY, A., JOHNSON, L.N., EGMOND, M.R. & FRENKEN, L.G., 1993. The crystal structure of triacylglycerol lipase from Pseudomonas glumae reveals a partially redundant catalytic aspartate. *FEBS Letters*, 331(1-2), pp.123–8.

NOINAJ, N., GUILLIER, M., BARNARD, T.J. & BUCHANAN, S.K., 2010. TonB-dependent transporters: regulation, structure, and function. *Annual Review of Microbiology*, 64, pp.43–60.

NOINAJ, N., KUSZAK, A.J., GUMBART, J.C., LUKACIK, P., CHANG, H., EASLEY, N.C., LITHGOW, T. & BUCHANAN, S.K., 2013. Structural insight into the biogenesis of β-barrel membrane proteins. *Nature*, 501(7467), pp.385–90.

NUMMILA, K., KILPELÄINEN, I., ZÄHRINGER, U., VAARA, M. & HELANDER, I.M., 1995. Lipopolysaccharides of polymyxin B-resistant mutants of Escherichia coli are extensively substituted by 2-aminoethyl pyrophosphate and contain aminoarabinose in lipid A. *Molecular Microbiology*, 16(2), pp.271–8.

NUNOSHIBA, T., HIDALGO, E., AMÁBILE CUEVAS, C.F. & DEMPLE, B., 1992. Two-stage control of an oxidative stress regulon: the Escherichia coli SoxR protein triggers redox-inducible expression of the soxS regulatory gene. *Journal of Bacteriology*, 174(19), pp.6054–60.

O'GRADY, E.P., VITERI, D.F., MALOTT, R.J. & SOKOL, P.A., 2009. Reciprocal regulation by the CepIR and CciIR quorum sensing systems in Burkholderia cenocepacia. *BMC Genomics*, 10(1), p.441.

O'TOOLE, G., KAPLAN, H.B. & KOLTER, R., 2000. Biofilm formation as microbial development. *Annual Review of Microbiology*, 54, pp.49–79.

ODINTSOV, S.G., SABALA, I., MARCYJANIAK, M. & BOCHTLER, M., 2004. Latent LytM at 1.3A resolution. *Journal of Molecular Biology*, 335(3), pp.775–85.

OLLIS, D.L., CHEAH, E., CYGLER, M., DIJKSTRA, B., FROLOW, F., FRANKEN, S.M., HAREL, M., REMINGTON, S.J., SILMAN, I. & SCHRAG, J., 1992. The alpha/beta hydrolase fold. *Protein Engineering*, 5(3), pp.197–211.

OLSÉN, A., ARNQVIST, A., HAMMAR, M., SUKUPOLVI, S. & NORMARK, S., 1993. The RpoS Sigma factor relieves H-NS-mediated transcriptional repression of csgA, the subunit gene of fibronectin-binding curli in Escherichia coli. *Molecular Microbiology*, 7(4), pp.523–536.

OLSÉN, A., JONSSON, A. & NORMARK, S., 1989. Fibronectin binding mediated by a novel class of surface organelles on Escherichia coli. *Nature*, 338(6217), pp.652–5.

ORTEGA, X., SILIPO, A., SALDÍAS, M.S., BATES, C.C., MOLINARO, A. & VALVANO, M.A., 2009. Biosynthesis and structure of the Burkholderia cenocepacia K56-2 lipopolysaccharide core oligosaccharide: truncation of the core oligosaccharide leads to increased binding and sensitivity to polymyxin B. *The Journal of Biological Chemistry*, 284(32), pp.21738–51.

ORTEGA, X.P., CARDONA, S.T., BROWN, A.R., LOUTET, S.A., FLANNAGAN, R.S., CAMPOPIANO, D.J., GOVAN, J.R.W. & VALVANO, M.A., 2007. A Putative Gene Cluster for Aminoarabinose Biosynthesis Is Essential for Burkholderia cenocepacia Viability. *Journal of Bacteriology*, 189(9), pp.3639–3644.

PALMER, T. & BERKS, B.C., 2012. The twin-arginine translocation (Tat) protein export pathway. *Nature Reviews. Microbiology*, 10(7), pp.483–96.

PARKE, J. & GURIAN-SHERMAN, D., 2001. Diversity of the Burkholderia cepacia complex and implications for risk assessment of biological control strains. *Annual Review of Phytopathology*, 39, pp.225–58.

PAVLOVA, O., PETERSON, J.H., IEVA, R. & BERNSTEIN, H.D., 2013. Mechanistic link between β barrel assembly and the initiation of autotransporter secretion. *Proceedings of the National Academy of Sciences of the United States of America*, 110(10), pp.E938–47.

PELL, L.G., KANELIS, V., DONALDSON, L.W., HOWELL, P.L. & DAVIDSON, A.R., 2009. The phage lambda major tail protein structure reveals a common evolution for long-tailed phages and the type VI bacterial secretion system. *Proceedings of the National Academy of Sciences of the United States of America*, 106(11), pp.4160–5.

PIETROSIUK, A., LENHERR, E.D., FALK, S., BÖNEMANN, G., KOPP, J., ZENTGRAF, H., SINNING, I. & MOGK, A., 2011. Molecular basis for the unique role of the AAA+ chaperone ClpV in type VI protein secretion. *The Journal of Biological Chemistry*, 286(34), pp.30010–21.

PLESSIS, A., PERRIN, A., HABER, J.E. & DUJON, B., 1992. Site-specific recombination determined by I-SceI, a mitochondrial group I intron-encoded endonuclease expressed in the yeast nucleus. *Genetics*, 130(3), pp.451–60.

POHLNER, J., HALTER, R., BEYREUTHER, K. & MEYER, T.F., 1987. Gene structure and extracellular secretion of Neisseria gonorrhoeae IgA protease. *Nature*, 325(6103), pp.458–62.

POMMER, A.J., CAL, S., KEEBLE, A.H., WALKER, D., EVANS, S.J., KÜHLMANN, U.C., COOPER, A., CONNOLLY, B.A., HEMMINGS, A.M., MOORE, G.R., JAMES, R. & KLEANTHOUS, C., 2001. Mechanism and cleavage specificity of the H-N-H endonuclease colicin E9. *Journal of Molecular Biology*, 314(4), pp.735–49.

POOLE, S.J., DINER, E.J., AOKI, S.K., BRAATEN, B.A., T'KINT DE ROODENBEKE, C., LOW, D.A. & HAYES, C.S., 2011. Identification of functional toxin/immunity genes linked to contact-dependent growth inhibition (CDI) and rearrangement hotspot (Rhs) systems. M. Achtman, ed. *PLoS Genetics*, 7(8), p.e1002217.

POSFAI, G., KOLISNYCHENKO, V., BERECZKI, Z. & BLATTNER, F.R., 1999. Markerless gene replacement in Escherichia coli stimulated by a double-strand break in the chromosome. *Nucleic Acids Research*, 27(22), pp.4409–4415.

PUGSLEY, A.P., 1993. The complete general secretory pathway in gram-negative bacteria. *Microbiological Reviews*, 57(1), pp.50–108.

PUKATZKI, S., MA, A.T., REVEL, A.T., STURTEVANT, D. & MEKALANOS, J.J., 2007. Type VI

secretion system translocates a phage tail spike-like protein into target cells where it cross-links actin. *Proceedings of the National Academy of Sciences of the United States of America*, 104(39), pp.15508–13.

PUKATZKI, S., MA, A.T., STURTEVANT, D., KRASTINS, B., SARRACINO, D., NELSON, W.C., HEIDELBERG, J.F. & MEKALANOS, J.J., 2006. Identification of a conserved bacterial protein secretion system in Vibrio cholerae using the Dictyostelium host model system. *Proceedings of the National Academy of Sciences of the United States of America*, 103(5), pp.1528–33.

PUKATZKI, S., MCAULEY, S.B. & MIYATA, S.T., 2009. The type VI secretion system: translocation of effectors and effector-domains. *Current Opinion in Microbiology*, 12(1), pp.11–7.

RADICS, J., KÖNIGSMAIER, L. & MARLOVITS, T.C., 2014. Structure of a pathogenic type 3 secretion system in action. *Nature Structural & Molecular Biology*, 21(1), pp.82–7.

RENZI, F., RESCALLI, E., GALLI, E. & BERTONI, G., 2010. Identification of genes regulated by the MvaT-like paralogues TurA and TurB of Pseudomonas putida KT2440. *Environmental Microbiology*, 12(1), pp.254–63.

RICHMOND, G.S. & SMITH, T.K., 2007. A novel phospholipase from Trypanosoma brucei. *Molecular Microbiology*, 63(4), pp.1078–1095.

RICHMOND, G.S. & SMITH, T.K., 2011. Phospholipases A 1. *International Journal of Molecular Sciences*, 12(1), pp.588–612.

RIEDEL, K., CARRANZA, P., GEHRIG, P., POTTHAST, F. & EBERL, L., 2006. Towards the proteome of Burkholderia cenocepacia H111: setting up a 2-DE reference map. *Proteomics*, 6(1), pp.207–16.

RITZ, D., 2001. Conversion of a Peroxiredoxin into a Disulfide Reductase by a Triplet Repeat Expansion. *Science*, 294(5540), pp.158–160.

RÖMLING, U., FIEDLER, B., BOSSHAMMER, J., GROTHUES, D., GREIPEL, J., VON DER HARDT, H. & TÜMMLER, B., 1994. Epidemiology of chronic Pseudomonas aeruginosa infections in cystic fibrosis. *The Journal of Infectious Diseases*, 170(6), pp.1616–21.

ROSALES-REYES, R., AUBERT, D.F., TOLMAN, J.S., AMER, A.O. & VALVANO, M.A., 2012a. Burkholderia cenocepacia type VI secretion system mediates escape of type II secreted proteins into the cytoplasm of infected macrophages. *PloS One*, 7(7), p.e41726.

ROSALES-REYES, R., SKELDON, A.M., AUBERT, D.F. & VALVANO, M. A, 2012b. The Type VI secretion system of Burkholderia cenocepacia affects multiple Rho family GTPases disrupting the actin cytoskeleton and the assembly of NADPH oxidase complex in macrophages. *Cellular Microbiology*, 14(2), pp.255–73.

RUIZ-PEREZ, F., HENDERSON, I.R., LEYTON, D.L., ROSSITER, A.E., ZHANG, Y. & NATARO, J.P., 2009. Roles of periplasmic chaperone proteins in the biogenesis of serine protease autotransporters of Enterobacteriaceae. *Journal of Bacteriology*,

191(21), pp.6571–83.

RUSSELL, A.B., HOOD, R.D., BUI, N.K., LEROUX, M., VOLLMER, W. & MOUGOUS, J.D., 2011. Type VI secretion delivers bacteriolytic effectors to target cells. *Nature*, 475(7356), pp.343–7.

RUSSELL, A.B., LEROUX, M., HATHAZI, K., AGNELLO, D.M., ISHIKAWA, T., WIGGINS, P.A., WAI, S.N. & MOUGOUS, J.D., 2013. Diverse type VI secretion phospholipases are functionally plastic antibacterial effectors. *Nature*, 496(7446), pp.508–12.

RUSSELL, A.B., PETERSON, S.B. & MOUGOUS, J.D., 2014. Type VI secretion system effectors: poisons with a purpose. *Nature Reviews Microbiology*, 12(2), pp.137–148.

RUSSELL, A.B., SINGH, P., BRITTNACHER, M., BUI, N.K., HOOD, R.D., CARL, M.A., AGNELLO, D.M., SCHWARZ, S., GOODLETT, D.R., VOLLMER, W. & MOUGOUS, J.D., 2012. A widespread bacterial type VI secretion effector superfamily identified using a heuristic approach. *Cell Host & Microbe*, 11(5), pp.538–49.

RYAN, G.T., WEI, Y. & WINANS, S.C., 2013. A LuxR-type repressor of Burkholderia cenocepacia inhibits transcription via antiactivation and is inactivated by its cognate acylhomoserine lactone. *Molecular Microbiology*, 87(1), pp.94–111.

RYAN, R.P., MCCARTHY, Y., WATT, S.A., NIEHAUS, K. & DOW, J.M., 2009. Intraspecies signaling involving the diffusible signal factor BDSF (cis-2-dodecenoic acid) influences virulence in Burkholderia cenocepacia. *Journal of Bacteriology*, 191(15), pp.5013–9.

SAIKI, K. & KONISHI, K., 2007. Identification of a Porphyromonas gingivalis Novel Protein Sov Required for the Secretion of Gingipains. *Microbiology and Immunology*, 51(5), pp.483–491.

SAINI, L.S., GALSWORTHY, S.B., JOHN, M.A. & VALVANO, M.A., 1999. Intracellular survival of Burkholderia cepacia complex isolates in the presence of macrophage cell activation. *Microbiology (Reading, England)*, 145 (Pt 1, pp.3465–75.

SAJJAN, U.S., YANG, J.H., HERSHENSON, M.B. & LIPUMA, J.J., 2006. Intracellular trafficking and replication of Burkholderia cenocepacia in human cystic fibrosis airway epithelial cells. *Cellular Microbiology*, 8(9), pp.1456–66.

SALOMON, D., GONZALEZ, H., UPDEGRAFF, B.L. & ORTH, K., 2013. Vibrio parahaemolyticus type VI secretion system 1 is activated in marine conditions to target bacteria, and is differentially regulated from system 2. *PloS One*, 8(4), p.e61086.

SALOMON, D., KINCH, L.N., TRUDGIAN, D.C., GUO, X., KLIMKO, J. A, GRISHIN, N. V, MIRZAEI, H. & ORTH, K., 2014a. Marker for type VI secretion system effectors. *Proceedings of the National Academy of Sciences of the United States of America*, 1(15).

SALOMON, D., KLIMKO, J.A. & ORTH, K., 2014b. H-NS regulates the Vibrio parahaemolyticus type VI secretion system 1. *Microbiology (Reading, England)*, pp.mic.0.080028–0–.

SANA, T.G., BAUMANN, C., MERDES, A., SOSCIA, C., RATTEI, T., HACHANI, A., JONES, C., BENNETT, K.L., FILLOUX, A., SUPERTI-FURGA, G., VOULHOUX, R. & BLEVES, S., 2015.

Internalization of Pseudomonas aeruginosa Strain PAO1 into Epithelial Cells Is Promoted by Interaction of a T6SS Effector with the Microtubule Network. *mBio*, 6(3), pp.e00712–15–.

SANA, T.G., HACHANI, A., BUCIOR, I., SOSCIA, C., GARVIS, S., TERMINE, E., ENGEL, J., FILLOUX, A. & BLEVES, S., 2012. The second type VI secretion system of Pseudomonas aeruginosa strain PAO1 is regulated by quorum sensing and Fur and modulates internalization in epithelial cells. *The Journal of Biological Chemistry*, 287(32), pp.27095–105.

SANDKVIST, M., MICHEL, L.O., HOUGH, L.P., MORALES, V.M., BAGDASARIAN, M., KOOMEY, M. & DIRITA, V.J., 1997. General secretion pathway (eps) genes required for toxin secretion and outer membrane biogenesis in Vibrio cholerae. *Journal of Bacteriology*, 179(22), pp.6994–7003.

SARGENT, F., BOGSCH, E.G., STANLEY, N.R., WEXLER, M., ROBINSON, C., BERKS, B.C. & PALMER, T., 1998. Overlapping functions of components of a bacterial Sec-independent protein export pathway. *The EMBO Journal*, 17(13), pp.3640–50.

SATO, K., NAITO, M., YUKITAKE, H., HIRAKAWA, H., SHOJI, M., MCBRIDE, M.J., RHODES, R.G. & NAKAYAMA, K., 2010. A protein secretion system linked to bacteroidete gliding motility and pathogenesis. *Proceedings of the National Academy of Sciences of the United States of America*, 107(1), pp.276–81.

SATO, K., YUKITAKE, H., NARITA, Y., SHOJI, M., NAITO, M. & NAKAYAMA, K., 2013. Identification of Porphyromonas gingivalis proteins secreted by the Por secretion system. *FEMS Microbiology Letters*, 338(1), pp.68–76.

SCHELL, M.A., ULRICH, R.L., RIBOT, W.J., BRUEGGEMANN, E.E., HINES, H.B., CHEN, D., LIPSCOMB, L., KIM, H.S., MRÁZEK, J., NIERMAN, W.C. & DESHAZER, D., 2007. Type VI secretion is a major virulence determinant in Burkholderia mallei. *Molecular Microbiology*, 64(6), pp.1466–85.

SCHMIEL, D.H., WAGAR, E., KARAMANOU, L., WEEKS, D. & MILLER, V.L., 1998. Phospholipase A of Yersinia enterocolitica contributes to pathogenesis in a mouse model. *Infection and Immunity*, 66(8), pp.3941–51.

SCHOLZ, S.R., KORN, C., BUJNICKI, J.M., GIMADUTDINOW, O., PINGOUD, A. & MEISS, G., 2003. Experimental evidence for a beta beta alpha-Me-finger nuclease motif to represent the active site of the caspase-activated DNase. *Biochemistry*, 42(31), pp.9288–94.

SCHREIER, J.B., 1969. Modification of deoxyribonuclease test medium for rapid identification of Serratia marcescens. *American Journal of Clinical Pathology*, 51(6), pp.711–6.

SCHWAB, U., LEIGH, M., RIBEIRO, C., YANKASKAS, J., BURNS, K., GILLIGAN, P., SOKOL, P. & BOUCHER, R., 2002. Patterns of epithelial cell invasion by different species of the Burkholderia cepacia complex in well-differentiated human airway epithelia. *Infection and Immunity*, 70(8), pp.4547–55.

SCHWARZ, S., SINGH, P., ROBERTSON, J.D., LEROUX, M., SKERRETT, S.J., GOODLETT, D.R., EOIN WEST, T. & MOUGOUS, J.D., 2014. VgrG-5 is a Burkholderia type VI secretion

system-exported protein required for multinucleated giant cell formation and virulence. *Infection and Immunity*, 82(4), pp.1445–1452.

SCHWARZ, S., WEST, T.E., BOYER, F., CHIANG, W.-C., CARL, M.A., HOOD, R.D., ROHMER, L., TOLKER-NIELSEN, T., SKERRETT, S.J. & MOUGOUS, J.D., 2010. Burkholderia type VI secretion systems have distinct roles in eukaryotic and bacterial cell interactions. *PLoS Pathogens*, 6(8), p.e1001068.

SEED, K.D. & DENNIS, J.J., 2008. Development of Galleria mellonella as an alternative infection model for the Burkholderia cepacia complex. *Infection and Immunity*, 76(3), pp.1267–75.

SELKRIG, J. ET AL., 2012. Discovery of an archetypal protein transport system in bacterial outer membranes. *Nature Structural & Molecular Biology*, 19(5), pp.506–10, S1.

SEPER, A., FENGLER, V.H.I., ROIER, S., WOLINSKI, H., KOHLWEIN, S.D., BISHOP, A.L., CAMILLI, A., REIDL, J. & SCHILD, S., 2011. Extracellular nucleases and extracellular DNA play important roles in Vibrio cholerae biofilm formation. *Molecular Microbiology*, 82(4), pp.1015–37.

SETTLES, A.M., 1997. Sec-Independent Protein Translocation by the Maize Hcf106 Protein. *Science*, 278(5342), pp.1467–1470.

SHALOM, G., SHAW, J.G. & THOMAS, M.S., 2007. In vivo expression technology identifies a type VI secretion system locus in Burkholderia pseudomallei that is induced upon invasion of macrophages. *Microbiology (Reading, England)*, 153(Pt 8), pp.2689–99.

SHASTRI, S., 2011. Characterisation of the type VI secretion system of Burkholderia cenocepacia. Ph.D thesis, The University of Sheffield.

SHIMUTA, K., OHNISHI, M., IYODA, S., GOTOH, N., KOIZUMI, N. & WATANABE, H., 2009. The hemolytic and cytolytic activities of Serratia marcescens phospholipase A (PhlA) depend on lysophospholipid production by PhlA. *BMC Microbiology*, 9, p.261.

SHNEIDER, M.M., BUTH, S. A., HO, B.T., BASLER, M., MEKALANOS, J.J. & LEIMAN, P.G., 2013. PAAR-repeat proteins sharpen and diversify the type VI secretion system spike. *Nature*.

SHRIVASTAVA, A., JOHNSTON, J.J., VAN BAAREN, J.M. & MCBRIDE, M.J., 2013. Flavobacterium johnsoniae GldK, GldL, GldM, and SprA are required for secretion of the cell surface gliding motility adhesins SprB and RemA. *Journal of Bacteriology*, 195(14), pp.3201–12.

SILVERMAN, J.M., AGNELLO, D.M., ZHENG, H., ANDREWS, B.T., LI, M., CATALANO, C.E., GONEN, T. & MOUGOUS, J.D., 2013. Haemolysin Coregulated Protein Is an Exported Receptor and Chaperone of Type VI Secretion Substrates. *Molecular Cell*, pp.1–10.

SILVERMAN, J.M., AUSTIN, L.S., HSU, F., HICKS, K.G., HOOD, R.D. & MOUGOUS, J.D., 2011. Separate inputs modulate phosphorylation-dependent and -independent type

VI secretion activation. *Molecular Microbiology*, 82(5), pp.1277–90.

SILVERMAN, J.M., BRUNET, Y.R., CASCALES, E. & MOUGOUS, J.D., 2012. Structure and regulation of the type VI secretion system. *Annual Review of Microbiology*, 66, pp.453–72.

SIMON, R., PRIEFER, U. & PÜHLER, A., 1983. A Broad Host Range Mobilization System for In Vivo Genetic Engineering: Transposon Mutagenesis in Gram Negative Bacteria. *Bio/Technology*, 1(9), pp.784–791.

DE SMET, B., MAYO, M., PEETERS, C., ZLOSNIK, J.E.A., SPILKER, T., HIRD, T.J., LIPUMA, J.J., KIDD, T.J., KAESTLI, M., GINTHER, J.L., WAGNER, D.M., KEIM, P., BELL, S.C., JACOBS, J.A., CURRIE, B.J. & VANDAMME, P., 2015. Burkholderia stagnalis sp. nov. and Burkholderia territorii sp. nov., two novel Burkholderia cepacia complex species from environmental and human sources. *International Journal of Systematic and Evolutionary Microbiology*, 65(7), pp.2265–71.

SMITH, M.D., WUTHIEKANUN, V., WALSH, A.L. & WHITE, N.J., 1995. Quantitative recovery of Burkholderia pseudomallei from soil in Thailand. *Transactions of the Royal Society of Tropical Medicine and Hygiene*, 89(5), pp.488–90.

SMITH, P.B., HANCOCK, G.A. & RHODEN, D.L., 1969. Improved medium for detecting deoxyribonuclease-producing bacteria. *Applied Microbiology*, 18(6), pp.991–3.

SODE, K., TSUGAWA, W., YAMAZAKI, T., WATANABE, M., OGASAWARA, N. & TANAKA, M., 1996. A novel thermostable glucose dehydrogenase varying temperature properties by altering its quaternary structures. *Enzyme and Microbial Technology*, 19(2), pp.82–85.

SOKOL, P.A., SAJJAN, U., VISSER, M.B., GINGUES, S., FORSTNER, J. & KOOI, C., 2003. The CepIR quorum-sensing system contributes to the virulence of Burkholderia cenocepacia respiratory infections. *Microbiology (Reading, England)*, 149(Pt 12), pp.3649–58.

SONG, J.K., KIM, M.K. & RHEE, J.S., 1999. Cloning and expression of the gene encoding phospholipase A1 from Serratia sp. MK1 in Escherichia coli. *Journal of Biotechnology*, 72(1-2), pp.103–14.

DE SOYZA, A., MEACHERY, G., HESTER, K.L.M., NICHOLSON, A., PARRY, G., TOCEWICZ, K., PILLAY, T., CLARK, S., LORDAN, J.L., SCHUELER, S., FISHER, A.J., DARK, J.H., GOULD, F.K. & CORRIS, P.A., 2010. Lung transplantation for patients with cystic fibrosis and Burkholderia cepacia complex infection: a single-center experience. *The Journal of Heart and Lung Transplantation : The Official Publication of the International Society for Heart Transplantation*, 29(12), pp.1395–404.

STANIER, R.Y., PALLERONI, N.J. & DOUDOROFF, M., 1966. The aerobic pseudomonads: a taxonomic study. *Journal of General Microbiology*, 43(2), pp.159–271.

STEINMETZ, M., LE COQ, D., DJEMIA, H.B. & GAY, P., 1983. [Genetic analysis of sacB, the structural gene of a secreted enzyme, levansucrase of Bacillus subtilis Marburg]. *Molecular & General Genetics : MGG*, 191(1), pp.138–44.

STEWART, E.J., ASLUND, F. & BECKWITH, J., 1998. Disulfide bond formation in the

Escherichia coli cytoplasm: an in vivo role reversal for the thioredoxins. *The EMBO Journal*, 17(19), pp.5543–50.

STOCK, A., CHEN, T., WELSH, D. & STOCK, J., 1988. CheA protein, a central regulator of bacterial chemotaxis, belongs to a family of proteins that control gene expression in response to changing environmental conditions. *Proceedings of the National Academy of Sciences of the United States of America*, 85(5), pp.1403–1407.

STUDIER, F.W. & MOFFATT, B.A., 1986. Use of bacteriophage T7 RNA polymerase to direct selective high-level expression of cloned genes. *Journal of Molecular Biology*, 189(1), pp.113–30.

SUAREZ, G., SIERRA, J.C., EROVA, T.E., SHA, J., HORNEMAN, A.J. & CHOPRA, A.K., 2010. A type VI secretion system effector protein, VgrG1, from Aeromonas hydrophila that induces host cell toxicity by ADP ribosylation of actin. *Journal of Bacteriology*, 192(1), pp.155–68.

SUBRAMONI, S., NGUYEN, D.T. & SOKOL, P.A., 2011. Burkholderia cenocepacia ShvR-regulated genes that influence colony morphology, biofilm formation, and virulence. *Infection and Immunity*, 79(8), pp.2984–97.

TABEI, S.M.B., HITCHEN, P.G., DAY-WILLIAMS, M.J., MERINO, S., VART, R., PANG, P.-C., HORSBURGH, G.J., VICHES, S., WILHELMS, M., TOMÁS, J.M., DELL, A. & SHAW, J.G., 2009. An Aeromonas caviae genomic island is required for both O-antigen lipopolysaccharide biosynthesis and flagellin glycosylation. *Journal of Bacteriology*, 191(8), pp.2851–63.

TAM, W., PELL, L.G., BONA, D., TSAI, A., DAI, X.X., EDWARDS, A.M., HENDRIX, R.W., MAXWELL, K.L. & DAVIDSON, A.R., 2013. Tail Tip Proteins Related to Bacteriophage λ gpL Coordinate an Iron-Sulfur Cluster. *Journal of Molecular Biology*, 425(14), pp.2450–62.

THANASSI, D.G., SAULINO, E.T., LOMBARDO, M.-J., ROTH, R., HEUSER, J. & HULTGREN, S.J., 1998. The PapC usher forms an oligomeric channel: Implications for pilus biogenesis across the outer membrane. *Proceedings of the National Academy of Sciences*, 95(6), pp.3146–3151.

THOMSON, E.L.S. & DENNIS, J.J., 2012. A Burkholderia cepacia complex non-ribosomal peptide-synthesized toxin is hemolytic and required for full virulence. *Virulence*, 3(3), pp.286–98.

TOESCA, I.J., FRENCH, C.T. & MILLER, J.F., 2014. The Type VI secretion system spike protein VgrG5 mediates membrane fusion during intercellular spread by pseudomallei group Burkholderia species. *Infection and Immunity*, 82(4), pp.1436–44.

TOLMAN, J.S. & VALVANO, M. A, 2012. Global changes in gene expression by the opportunistic pathogen Burkholderia cenocepacia in response to internalization by murine macrophages. *BMC Genomics*, 13(1), p.63.

TOMLIN, K.L., MALOTT, R.J., RAMAGE, G., STOREY, D.G., SOKOL, P.A. & CERI, H., 2005. Quorum-sensing mutations affect attachment and stability of Burkholderia

cenocepacia biofilms. *Applied and Environmental Microbiology*, 71(9), pp.5208–18.

UNTERWEGER, D., KOSTIUK, B., ÖTJENGERDES, R., WILTON, A., DIAZ-SATIZABAL, L. & PUKATZKI, S., 2015. Chimeric adaptor proteins translocate diverse type VI secretion system effectors in Vibrio cholerae. *The EMBO Journal*.

UNTERWEGER, D., MIYATA, S.T., BACHMANN, V., BROOKS, T.M., MULLINS, T., KOSTIUK, B., PROVENZANO, D. & PUKATZKI, S., 2014. The Vibrio cholerae type VI secretion system employs diverse effector modules for intraspecific competition. *Nature Communications*, 5, p.3549.

VANDAMME, HOLMES, B., COENYE, T., GORIS, J., MAHENTHIRALINGAM, E., LIPUMA, J.J. & GOVAN, J.R.W., 2003. Burkholderia cenocepacia sp. nov.--a new twist to an old story. *Research in Microbiology*, 154(2), pp.91–6.

VANDAMME, P., HOLMES, B., VANCANNEYT, M., COENYE, T., HOSTE, B., COOPMAN, R., REVETS, H., LAUWERS, S., GILLIS, M., KERSTERS, K. & GOVAN, J.R., 1997. Occurrence of multiple genomovars of Burkholderia cepacia in cystic fibrosis patients and proposal of Burkholderia multivorans sp. nov. *International Journal of Systematic Bacteriology*, 47(4), pp.1188–200.

VARGA, J.J., LOSADA, L., ZELAZNY, A.M., KIM, M., MCCORRISON, J., BRINKAC, L., SAMPAIO, E.P., GREENBERG, D.E., SINGH, I., HEINER, C., ASHBY, M., NIERMAN, W.C., HOLLAND, S.M. & GOLDBERG, J.B., 2013. Draft Genome Sequences of Burkholderia cenocepacia ET12 Lineage Strains K56-2 and BC7. *Genome Announcements*, 1(5).

VASIL, M.L., KRIEG, D.P., KUHNS, J.S., OGLE, J.W., SHORTRIDGE, V.D., OSTROFF, R.M. & VASIL, A.I., 1990. Molecular analysis of hemolytic and phospholipase C activities of Pseudomonas cepacia. *Infect. Immun.*, 58(12), pp.4020–4029.

VERGUNST, A.C., MEIJER, A.H., RENSHAW, S.A. & O'CALLAGHAN, D., 2010. Burkholderia cenocepacia creates an intramacrophage replication niche in zebrafish embryos, followed by bacterial dissemination and establishment of systemic infection. *Infection and Immunity*, 78(4), pp.1495–508.

VIALLARD, V., POIRIER, I., COURNOYER, B., HAURAT, J., WIEBKIN, S., OPHEL-KELLER, K. & BALANDREAU, J., 1998. Burkholderia graminis sp. nov., a rhizospheric Burkholderia species, and reassessment of [Pseudomonas] phenazinium, [Pseudomonas] pyrrocinia and [Pseudomonas] glathei as Burkholderia. *International Journal of Systematic Bacteriology*, 48 Pt 2, pp.549–63.

VINCENT, R.D., HOFMANN, T.J. & ZASSENHAUS, H.P., 1988. Sequence and expression of NUC1, the gene encoding the mitochondrial nuclease in Saccharomyces cerevisiae. *Nucleic Acids Research*, 16(8), pp.3297–312.

VOLLMER, W., BLANOT, D. & DE PEDRO, M.A., 2008. Peptidoglycan structure and architecture. *FEMS Microbiol Rev*, 32(2), pp.149–167.

VOULHOUX, R., BALL, G., IZE, B., VASIL, M.L., LAZDUNSKI, A., WU, L.F. & FILLOUX, A., 2001. Involvement of the twin-arginine translocation system in protein secretion via the type II pathway. *The EMBO Journal*, 20(23), pp.6735–41.

WANDERSMAN, C. & DELEPELAIRE, P., 1990. TolC, an Escherichia coli outer membrane protein required for hemolysin secretion. *Proceedings of the National Academy of Sciences of the United States of America*, 87(12), pp.4776–80.

WANG, T., DING, J., ZHANG, Y., WANG, D.-C. & LIU, W., 2013. Complex structure of type VI peptidoglycan muramidase effector and a cognate immunity protein. *Acta Crystallographica. Section D, Biological Crystallography*, 69(Pt 10), pp.1889–900.

WANG, Y.D., ZHAO, S. & HILL, C.W., 1998. Rhs elements comprise three subfamilies which diverged prior to acquisition by Escherichia coli. *Journal of Bacteriology*, 180(16), pp.4102–10.

WEBB, J.S., NIKOLAKAKIS, K.C., WILLETT, J.L.E., AOKI, S.K., HAYES, C.S. & LOW, D.A., 2013. Delivery of CdiA nuclease toxins into target cells during contact-dependent growth inhibition. *PloS One*, 8(2), p.e57609.

WEBER, B., CROXATTO, A., CHEN, C. & MILTON, D.L., 2008. RpoS induces expression of the Vibrio anguillarum quorum-sensing regulator VanT. *Microbiology (Reading, England)*, 154(Pt 3), pp.767–80.

WHITNEY, J.C., BECK, C.M., GOO, Y.A., RUSSELL, A.B., HARDING, B., DE LEON, J.A., CUNNINGHAM, D.A., TRAN, B.Q., LOW, D.A., GOODLETT, D.R., HAYES, C.S. & MOUGOUS, J.D., 2014. Genetically distinct pathways guide effector export through the type VI secretion system. *Molecular Microbiology*.

WHITNEY, J.C., CHOU, S., RUSSELL, A.B., BIBOY, J., GARDINER, T.E., FERRIN, M.A., BRITTNACHER, M., VOLLMER, W. & MOUGOUS, J.D., 2013. Identification, structure, and function of a novel type VI secretion peptidoglycan glycoside hydrolase effector-immunity pair. *The Journal of Biological Chemistry*, 288(37), pp.26616–24.

WILHELMS, M., FULTON, K.M., TWINE, S.M., TOMÁS, J.M. & MERINO, S., 2012. Differential glycosylation of polar and lateral flagellins in Aeromonas hydrophila AH-3. *The Journal of Biological Chemistry*, 287(33), pp.27851–62.

WINANS, S.C. & WALKER, G.C., 1983. Genetic localization and characterization of a pKM101-coded endonuclease. *J. Bacteriol.*, 154(3), pp.1117–1125.

WINKLER, F.K., D'ARCY, A. & HUNZIKER, W., 1990. Structure of human pancreatic lipase. *Nature*, 343(6260), pp.771–4.

WIŚNIEWSKI, J.R., ZOUGMAN, A., NAGARAJ, N. & MANN, M., 2009. Universal sample preparation method for proteome analysis. *Nature Methods*, 6(5), pp.359–62.

WOODS, D.E., CRYZ, S.J., FRIEDMAN, R.L. & IGLEWSKI, B.H., 1982. Contribution of toxin A and elastase to virulence of Pseudomonas aeruginosa in chronic lung infections of rats. *Infect. Immun.*, 36(3), pp.1223–1228.

WRETLIND, B., BJÖRKLIND, A. & PAVLOVSKIS, O.R., 1987. Role of exotoxin A and elastase in the pathogenicity of Pseudomonas aeruginosa strain PAO experimental mouse burn infection. *Microbial Pathogenesis*, 2(6), pp.397–404.

WRIGHT, G.D., MOLINAS, C., ARTHUR, M., COURVALIN, P. & WALSH, C.T., 1992. Characterization of vanY, a DD-carboxypeptidase from vancomycin-resistant

Enterococcus faecium BM4147. *Antimicrobial Agents and Chemotherapy*, 36(7), pp.1514–8.

WU, C.-F., LIN, J.-S., SHAW, G.-C. & LAI, E.-M., 2012. Acid-induced type VI secretion system is regulated by ExoR-ChvG/ChvI signaling cascade in Agrobacterium tumefaciens. *PLoS Pathogens*, 8(9), p.e1002938.

WU, T., MALINVERNI, J., RUIZ, N., KIM, S., SILHAVY, T.J. & KAHNE, D., 2005. Identification of a multicomponent complex required for outer membrane biogenesis in Escherichia coli. *Cell*, 121(2), pp.235–45.

XIANG, Y., MORAIS, M.C., COHEN, D.N., BOWMAN, V.D., ANDERSON, D.L. & ROSSMANN, M.G., 2008. Crystal and cryoEM structural studies of a cell wall degrading enzyme in the bacteriophage phi29 tail. *Proceedings of the National Academy of Sciences of the United States of America*, 105(28), pp.9552–7.

XU, H., YANG, J., GAO, W., LI, L., LI, P., ZHANG, L., GONG, Y.-N., PENG, X., XI, J.J., CHEN, S., WANG, F. & SHAO, F., 2014. Innate immune sensing of bacterial modifications of Rho GTPases by the Pyrin inflammasome. *Nature*, 513(7517), pp.237–41.

YABUUCHI, E., KOSAKO, Y., OYAIZU, H., YANO, I., HOTTA, H., HASHIMOTO, Y., EZAKI, T. & ARAKAWA, M., 1992. Proposal of Burkholderia gen. nov. and transfer of seven species of the genus Pseudomonas homology group II to the new genus, with the type species Burkholderia cepacia (Palleroni and Holmes 1981) comb. nov. *Microbiology and Immunology*, 36(12), pp.1251–75.

YAHR, T.L. & WICKNER, W.T., 2001. Functional reconstitution of bacterial Tat translocation in vitro. *The EMBO Journal*, 20(10), pp.2472–9.

YAMAGUCHI, Y., PARK, J.-H. & INOUYE, M., 2011. Toxin-antitoxin systems in bacteria and archaea. *Annual Review of Genetics*, 45, pp.61–79.

YANISCH-PERRON, C., VIEIRA, J. & MESSING, J., 1985. Improved M13 phage cloning vectors and host strains: nucleotide sequences of the M13mp18 and pUC19 vectors. *Gene*, 33(1), pp.103–19.

YOSHIHISA, H., ZENJI, S., FUKUSHI, H., KATSUHIRO, K., HARUHISA, S. & TAKAHITO, S., 1989. Production of antibiotics by Pseudomonas cepacia as an agent for biological control of soilborne plant pathogens. *Soil Biology and Biochemistry*, 21(5), pp.723–728.

YOUNG, G.M., SCHMIEL, D.H. & MILLER, V.L., 1999. A new pathway for the secretion of virulence factors by bacteria: the flagellar export apparatus functions as a protein-secretion system. *Proceedings of the National Academy of Sciences of the United States of America*, 96(11), pp.6456–61.

YU, Y., KIM, H.S., CHUA, H.H., LIN, C.H., SIM, S.H., LIN, D., DERR, A., ENGELS, R., DESHAZER, D., BIRREN, B., NIERMAN, W.C. & TAN, P., 2006. Genomic patterns of pathogen evolution revealed by comparison of Burkholderia pseudomallei, the causative agent of melioidosis, to avirulent Burkholderia thailandensis. *BMC Microbiology*, 6(1), p.46.

ZHANG, D., IYER, L.M. & ARAVIND, L., 2011. A novel immunity system for bacterial

nucleic acid degrading toxins and its recruitment in various eukaryotic and DNA viral systems. *Nucleic Acids Research*, 39(11), pp.4532–52.

ZHANG, D., DE SOUZA, R.F., ANANTHARAMAN, V., IYER, L.M. & ARAVIND, L., 2012. Polymorphic toxin systems: Comprehensive characterization of trafficking modes, processing, mechanisms of action, immunity and ecology using comparative genomics. *Biology Direct*, 7, p.18.

ZHANG, H., GAO, Z.-Q., WANG, W.-J., LIU, G.-F., XU, J.-H., SU, X.-D. & DONG, Y.-H., 2013. Structure of the type VI effector-immunity complex (Tae4-Tai4) provides novel insights into the inhibition mechanism of the effector by its immunity protein. *The Journal of Biological Chemistry*, 288(8), pp.5928–39.

ZHANG, J., ZHANG, H., GAO, Z., HU, H., DONG, C. & DONG, Y.-H., 2014. Structural basis for recognition of the type VI spike protein VgrG3 by a cognate immunity protein. *FEBS Letters*, 588(10), pp.1891–8.

ZHENG, J., HO, B. & MEKALANOS, J.J., 2011. Genetic analysis of anti-amoebae and anti-bacterial activities of the type VI secretion system in Vibrio cholerae. *PloS One*, 6(8), p.e23876.

ZHENG, J. & LEUNG, K.Y., 2007. Dissection of a type VI secretion system in Edwardsiella tarda. *Molecular Microbiology*, 66(5), pp.1192–206.

ZHENG, J., SHIN, O.S., CAMERON, D.E. & MEKALANOS, J.J., 2010. Quorum sensing and a global regulator TsrA control expression of type VI secretion and virulence in Vibrio cholerae. *Proceedings of the National Academy of Sciences of the United States of America*, 107(49), pp.21128–33.

ZHOU, J., ZHOU, T., CAO, R., LIU, Z., SHEN, J., CHEN, P., WANG, X. & LIANG, S., 2006. Evaluation of the application of sodium deoxycholate to proteomic analysis of rat hippocampal plasma membrane. *Journal of Proteome Research*, 5(10), pp.2547–53.

ZLOSNIK, J.E.A., ZHOU, G., BRANT, R., HENRY, D.A., HIRD, T.J., MAHENTHIRALINGAM, E., CHILVERS, M.A., WILCOX, P. & SPEERT, D.P., 2015. Burkholderia species infections in patients with cystic fibrosis in British Columbia, Canada. 30 years' experience. *Annals of the American Thoracic Society*, 12(1), pp.70–8.

ZOUED, A., BRUNET, Y.R., DURAND, E., ASCHTGEN, M.-S., LOGGER, L., DOUZI, B., JOURNET, L., CAMBILLAU, C. & CASCALES, E., 2014. Architecture and assembly of the Type VI secretion system. *Biochimica et Biophysica Acta*, 1843(8), pp.1664–73.

ZOUED, A., DURAND, E., BEBEACUA, C., BRUNET, Y.R., DOUZI, B., CAMBILLAU, C., CASCALES, E. & JOURNET, L., 2013. TssK is a trimeric cytoplasmic protein interacting with components of both phage-like and membrane anchoring complexes of the Type VI secretion system. *The Journal of Biological Chemistry*.